PURINERGIC SIGNALLING INVOLVEMENT IN THE REGULATION OF THE HUMAN PLACENTAL VASCULATURE



University of Nottingham
UK | CHINA | MALAYSIA

PURINERGIC SIGNALLING INVOLVEMENT IN THE REGULATION OF THE HUMAN PLACENTAL VASCULATURE

Paul Fodor

Thesis submitted to the University of Nottingham for the degree of Doctor of Philosophy in Physiology and Pharmacology
March 2021

Table of Contents

Abstract **12**

Abbreviations **14**

CHAPTER 1 ..... **18**

INTRODUCTION **18**

1.1 THE HUMAN PLACENTA 19
1.1.1 Placental development *26*
1.1.2 Cardiovascular adaptations to human pregnancy *28*
1.1.3 The development of the human placental vasculature *29*
1.1.4 Regulation of blood vascular permeability in the human placenta *30*
1.1.5 Resistance arteries in the human placenta *32*
1.1.6 Structure of blood vessel walls *33*
1.1.7 Mechanisms of blood flow regulation in the placenta *34*
1.1.8 Pregnancy related disorders *35*
1.1.9 Endothelial adhesion molecules in diabetes *41*
1.1.10 The human placental endothelium *44*
1.2 OVERVIEW OF PURINERGIC RECEPTORS 46
1.3 THE DUAL CONTROL OF HUMAN VASCULAR TONE BY ENDOTHELIAL CELLS AND PERIVASCULAR NERVES 58
1.3.1 Endothelial cells involvement in the management of vascular tone *61*
1.4 THE HUMAN P2X7 RECEPTOR 70
1.4.1 Structure and function of the P2X7 receptor *71*
1.4.2 Distribution of the P2X7 receptor *72*
1.4.3 The permeability of the P2X7 receptor *74*
1.4.4 Gating of the P2X7 receptor *75*
1.4.5 P2X7 receptor-dependent signalling pathways *76*
1.5 THE ROLE OF P2X7 RECEPTOR IN INFLAMMATION 78
1.5.1 The inflammasome *79*
1.5.2 The P2X7 receptor involvement in DAMPs and PAMPs associated switch for the initiation of immune responses *84*
1.6 THE ROLE OF NUCLEOTIDES IN HUMAN PLACENTAL VASCULAR TONE REGULATION ... 87
1.7 HYPOTHESIS AND AIMS 91

CHAPTER 2 ..... **93**

MATERIALS AND METHODS **93**

2.1 PATIENT RECRUITMENT 94
2.2 INCLUSION AND EXCLUSION CRITERIA 94
2.3 HUMAN TISSUE COLLECTION 96
2.4 ISOLATION OF PLACENTAL ARTERIES 97
2.5 WIRE MYOGRAPHY 98
2.5.1 Data analysis *102*
2.6 WESTERN BLOTTING 103
2.6.1 Collection of placental tissue and PBMC cells *103*
2.6.2 Control tissue and cells *104*
2.6.3 Tissue and primary cell homogenisation *104*
2.6.4 Protein determination *112*

2.6.5 IgG immunodepletion from trophoblast, SVA and myometrium tissue... 113
2.6.6 SDS PAGE Electrophoresis and electroblotting..... 115
2.6.7 Blocking, control peptide blocking and antibody application 116
2.6.8 β Actin measurement 117
2.6.9 Secondary antibody and data analysis..... 117
2.7 STIMULATION OF TROPHOBLAST TISSUE WITH D-GLUCOSE 118
2.7.1 Stimulation of CPA, SVA and trophoblast tissue with LPS, ATP and BzATP 120
2.8 ISOLATION OF PBMC 121
2.9 ENZYME LINKED IMMUNOSORBENT ASSAY (ELISA)..... 122
2.10 LACTATE DEHYDROGENASE (LDH) ASSAY 123
2.11 CONFOCAL AND WIDE FIELD MICROSCOPY..... 124
2.12 MRNA ANALYSIS AND RT-QPCR 126
2.13 DISSOCIATION OF HUMAN PLACENTAL VASCULAR SMOOTH MUSCLE CELLS ORIGINATING FROM CHORIONIC PLATE ARTERY (CPA) 128
2.14 ISOLATION AND CULTURE OF CHORIONIC PLATE ARTERY SMOOTH MUSCLE CELLS (CPA-SMC) FROM TERM HEALTHY, GESTATIONAL AND TYPE 1 DIABETES MELLITUS HUMAN PLACENTA SAMPLES..... 130
2.15 CALCULATION OF PRIMARY SMOOTH MUSCLE CELLS POPULATION DOUBLING TIME 133
2.16 SURVEYING THE EXPRESSION OF HUMAN PLACENTA SMOOTH MUSCLE CELL MYOFILAMENTOUS PROTEIN A-SMOOTH MUSCLE ACTIN 135
2.17 STIMULATION OF CPA-SMC WITH ATP, BZATP AND A740003..... 136
2.18 IMMUNOHISTOCHEMISTRY..... 138
2.19 HUMAN UMBILICAL VEIN ENDOTHELIAL CELLS ISOLATION..... 140
2.20 CALCULATION OF HUVEC CELLS POPULATION DOUBLING TIME 142
2.21 PERMEABILITY STUDIES..... 142
2.21.1 Initial transwell cell culture studies to investigate the adherence capability of CPA-SMC and HUVEC on polyester membrane inserts..... 142
2.21.2 Investigating the capability of $3x10^4$ chorionic plate artery smooth muscle cells to adhere to 6.5mm transwell with 0.4μm pore size polycarbonate membrane inserts..... 144
2.21.3 Optimisation of CPA-SMC seeding density on 6.5mm diameter polycarbonate transwell polyester inserts 145
2.21.4 Optimisation of HUVEC seeding density on 6.5mm diameter transwell polyester inserts 145
2.21.5 Investigating the capacity of $1x10^5$ HUVEC cells to adhere to 12mm membrane diameter 0.4μm pore size polyethylene terephthalate (PET) membrane inserts..... 147
2.21.6 Characterisation of CPA-SMC phenotype cultured in HUVEC media.. 148
2.21.7 Preliminary permeability studies to investigate the barrier integrity of cultured human CPA-SMC and HUVEC on transwell polyester membrane inserts 149
2.21.8 Characterising the optimised cell culture conditions of HUVEC and CPA-SMC for undertaking permeability and endothelial junction formation studies 151
2.21.9 Tracer leakage permeability studies of HUVEC and CPA-SMC 153
2.21.10 Post-permeability studies of endothelial junctional integrity..... 156
2.21.11 Investigating the potential membrane double labelling of isolated primary cells with PKH26 and PKH67 for studying the properties of trans-endothelial migration of CPA-SMC across HUVEC monolayers 160

2.22 IMMUNOPHENOTYPING OF ISOLATED HUMAN PRIMARY SMOOTH MUSCLE CELLS ORIGINATING FROM THE CHORIONIC PLATE ARTERY 161

CHAPTER 3 167

INVESTIGATING THE EXPRESSION OF THE P2X7 RECEPTOR IN THE VASCULATURE OF THE HUMAN PLACENTA 167

3.1 INTRODUCTION 168
3.1.1 P2X7 receptor involvement in the pathogenesis of type 2 diabetes from a microvascular complication point of view 168
3.1.2 P2X and P2Y receptor expression in the human placenta 170
3.2 HYPOTHESIS AND AIMS 176
3.3 RESULTS 178
3.3.1 Two P2X7 receptor bands were identified at approximately 74kDa and circa 97kDa in the second pellet of CPA, SVA and trophoblast tissue lysates 178
3.3.2 P2X7 receptor specific bands were identified in the second pellet fraction of SVA, trophoblast tissue and myometrium tissue lysates which have been successfully immunodepleted of IgG originating from 3 healthy placental samples 185
3.3.3 The NLRP3 inflammasome expression in the second supernatant of fourth order CPA, SVA and choriodecidua tissue lysates highlighted the presence of 4 isoforms at approximately 79kDa, 107kDa, 171kDa and 222kDa 211
3.3.4 Stimulated human trophoblast tissue with ATP, LPS+ATP and LPS+BzATP does not significantly alter the relative protein expression levels of three NLRP3 inflammasome isoforms 224
3.3.5 D-glucose stimulation of trophoblast tissue for 4, 24 and 48 hours does not significantly alter the relative P2X7 receptor protein expression levels 226
3.3.6 The relative P2X7 receptor, NLRP3 inflammasome and procaspase-1 protein expression levels in stem villous artery do not significantly alter between healthy (N=8) and preeclamptic (N=8) placental samples 242
3.3.7 Investigating the relative mRNA expression levels of the P2X7 receptor, NLRP3 inflammasome and caspase-1 in stem villous arteries originating from 2 healthy and 2 preeclamptic placental samples 257
3.3.8 LPS+ATP stimulation elicited the highest IL-1β release from CPA, SVA and trophoblast tissue originating from 10 healthy placental samples 259
3.3.9 Human chorionic plate artery smooth muscle cells isolated using an enzymatic digestion method are positive for α-actin, P2X7 receptor and vimentin but not CD31 265
3.3.10 Chorionic plate artery smooth muscle cells isolated using the tissue explant method are positive for the P2X7 receptor and vimentin and negative for the NLRP3 inflammasome 270
3.3.11 Stimulation of chorionic plate artery smooth muscle cells with 100μM ATP for 4 hours gives rise to a localised increase in the P2X7 receptor density (punctuate staining) that is clustered around the nuclear membrane 273
3.3.12 Stimulation of human chorionic plate artery smooth muscle cells with 1mM, 5mM or 10mM ATP for 4 hours gave rise to the formation of numerous P2X7 receptor clusters evenly distributed on the primary placental cell body 281
3.3.13 Immunohistochemical expression of the P2X7 receptor in isolated sections of human placental villous tissue showed that the syncytiotrophoblast layer and fetal capillaries stained positive for the purinergic receptor 286

3.3.14 Immunohistochemical expression of the P2X7 receptor in isolated sections of human placenta chorionic plate artery showed that the endothelial cells stained positive for the purinergic receptor 296
3.4 DISCUSSION 299

CHAPTER 4 318

INVESTIGATING THE EFFECTS OF PURINERGIC AGONISTS AND ANTAGONISTS ON ISOLATED HUMAN PLACENTAL BLOOD VESSELS USING WIRE MYOGRAPHY 318

4.1 INTRODUCTION 319
4.2 HYPOTHESIS AND AIMS 322
4.3 RESULTS 324
4.3.1 Sodium nitroprusside dihydrate caused an effective vasorelaxation response in preconstricted chorionic plate arteries whereas riluzole elicited a limited vasoactive modulator capacity in adjacent human placental artery preparations of a healthy patient 324
4.3.2 The endothelium-independent dilator riluzole caused a limited vasorelaxation effect in preconstricted chorionic plate arteries of a healthy pregnancy case 327
4.3.3 The potent and selective P2X7 receptor antagonist A740003 may elicit a significant reduction of U46619-induced vasoactive effects in isolated chorionic plate arteries of healthy placental samples 328
4.3.4 The P2X7 receptor antagonist A740003 elicited a desensitization effect of ATP-induced vasoconstriction in the second and fourth order chorionic plate arteries of healthy placental samples 337
4.3.5 Adenosine 5'-triphosphate concentration response curves were notably displaced downwards in subsequent nucleotide challenges of second order CPA's in the presence and absence of A740003 345
4.3.6 Repeated cumulative additions of ATP gave rise to a progressively reduced vasomotor response in the presence and absence of the P2X7 receptor antagonist A740003 349
4.3.7 Adenosine 5'-triphosphate gives rise to spontaneous progressively attenuated contractions of human placental chorionic plate artery preparations with increasing nucleotide cumulative concentrations in the presence and absence of the P2X7 receptor antagonist A740003 359
4.3.8 Three consecutive additions of ATP gave rise to a progressively reduced vasomotor response which ultimately resulted in a maximal vasoconstriction effect that reached below 3% of the U46619 standard 366
4.3.9 The 30mM KPSS-induced elevation in the human placental chorionic plate artery resting basal tone increased the efficacy of the first ATP stimulation by more than 38% at a nucleotide concentration of 10^{-3}M and by more than 27% at an ATP concentration of $3.3*10^{-3}$M 372
4.3.10 The 30mM KPSS preimposed tone did not increase the efficacy of three consecutive additions of 10^{-2}M ATP in isolated resistance human chorionic plate artery preparations originating from two healthy patients 376
4.3.11 The 40mM KPSS-induced elevation in the resting basal tone did not significantly alter the efficacy of the first and second ATP stimulations in isolated chorionic plate arteries originating from three healthy patients 377

4.3.12 The P2X7 receptor agonist BzATP gave rise to a substantially reduced vasoconstriction effect of less than 25% of the U46619 standard characterised by an almost flat concentration response curve 382
4.3.13 A 30mM KPSS-induced elevation in the resting basal tone caused a substantially reduced spontaneous BzATP maximal vasoconstriction effect of less than 6% of the U46619 standard 385
4.3.14 A 50mM KPSS-induced rise in the chorionic plate artery resting basal tone caused a progressively reduced vasomotor response initiated by the exogenous application of BzATP 388
4.3.15 Elevated chorionic plate artery resting basal tone using 70mM KPSS notably decreases the BzATP-induced vasoconstriction responses below 6% of the U46619 standard 393
4.4 DISCUSSION 397

CHAPTER 5 412

ESTABLISHMENT OF AN *IN VITRO* MODEL OF HUMAN PLACENTAL CHORIONIC VESSEL 412

5.1 INTRODUCTION 413
5.1.1 Molecular regulation of endothelial permeability 418
5.1.2 Investigating human feto-placental endothelial junction formation and barrier integrity using macromolecular permeability studies 422
5.2 HYPOTHESIS 427
5.3 RESULTS 428
5.3.1 Human placenta chorionic plate artery smooth muscle cells can be isolated and grown to a high confluency using the tissue explant technique 428
5.3.2 The morphology of human umbilical vein endothelial cells is characterised by a cobblestone appearance with dark large size nuclei inside the primary cells 444
5.3.3 Isolated human placenta chorionic plate artery smooth muscle cells seeded at a density of $3x10^4$ cells on 6.5mm diameter 0.4µm pore size polycarbonate membrane inserts highlight a limited adhesion and proliferation capacity 446
5.3.4 In vitro validation studies suggest that the cell seeding density of $1x10^4$ human placenta chorionic plate artery smooth muscle cells on 6.5mm diameter 0.4µm pore size polycarbonate membrane insert prevents the formation of nodular cultures for at least 48 hours 451
5.3.5 Isolated human umbilical vein endothelial cells seeded at a density of $2x10^4$ cells on 6.5mm diameter 0.4µm pore size polycarbonate membrane insert did attach and proliferate but did not form a monolayer for the first 48 hours in culture conditions 457
5.3.6 The cell seeding density of $1x10^5$ human umbilical vein endothelial cells on 12mm diameter 0.4µm pore size polyethylene terephthalate membrane insert did not give rise to the establishment of a monolayer after 48 hours in culture conditions 460
5.3.7 Human placenta chorionic plate artery smooth muscle cells can survive and proliferate in complete endothelial cell media for at least 120 hours without significant changes in the primary cell morphology 461
5.3.8 Human umbilical vein endothelial cells seeded on transwell inserts showed a reduced staining for α smooth muscle actin compared to chorionic plate artery smooth muscle cells which was mainly immunolocalised on the plasma membrane 463

5.3.9 There were no statistically significant differences in terms of tracer leakage levels between the coculture of human placenta chorionic plate artery smooth muscle cells with human umbilical vein endothelial cells and monoculture of primary endothelial cells at the same timepoints during the 120 minutes long permeability assay 466
5.3.10 Immunolocalization studies involving monocultures and cocultures of primary endothelial and smooth muscle cells showed VE-Cadherin staining as a thin or at parts thick uninterrupted or discontinuous line positioned at the paracellular overlapping regionsbetween tightly arranged adjacent human umbilical vein endothelial cells 472
5.3.11 Successful membrane labelling of human umbilical vein endothelial cells with PKH67 and human placenta chorionic plate artery smooth muscle cells with PKH26 revealed further potential opportunities of studying the trans-endothelial migration properties of smooth muscle cells across confluent primary endothelial cell monolayers 488
5.4 DISCUSSION 491
5.4.1 Isolation, culture and characterisation of human placenta chorionic plate artery smooth muscle cells 491
5.4.2 Isolation, culture and characterisation of human umbilical vein endothelial cells 495
5.4.3 Permeability of CPA-SMC and HUVEC coculture model 496
5.4.4 Immunocytochemistry studies of endothelial junction formation in the mono- and co-culture of HUVEC with CPA-SMC cells 502
5.5 CONCLUSIONS 504
CHAPTER 6 505
GENERAL DISCUSSION 505
6.1 THE MOST IMPORTANT FINDINGS OF THE CURRENT STUDY 515
6.2 LIMITATIONS OF THE CURRENT STUDY 516
6.3 FUTURE RESEARCH 519
6.4 CONCLUSION 520
REFERENCES 521
APPENDICES 582

Declaration

I declare that this PhD Thesis in Physiology and Pharmacology is the result of my own work based on research that was carried out at the Academic division of Obstetrics and Gynaecology, Derby Medical School and Queen's Medical Centre, University of Nottingham during the period of 30th September 2016 to 31st March 2021.

Paul Fodor

31st March 2021

Publications

Fodor Paul, Benjamin White, Raheela Khan, Inflammation – The role of ATP in preeclampsia (2019), *Journal of Microcirculation*, Volume 27, Issue 1, e12585, Available at: https://onlinelibrary.wiley.com/doi/abs/10.1111/micc.12585

Abstract

Pregnancy involves a physiological series of actions which necessitate a coordinated transformation involving numerous organ systems. The human placenta supports and protects the growing fetus by facilitating an adequate oxygen and selective nutrient transfer to the fetus whilst functioning as a selective barrier. This notably vascularised fetal organ lacks neuronal innervation, therefore the regulation of the blood flow is adjusted via released vasoactive mediators within the local microcirculation. The role of adenosine 5'-triphosphate (ATP) and associated nucleotides in the control of systemic vascular tone has attracted much attention over the past few decades. However, few studies have assessed the role of purines at the level of the fetoplacental circulation. Here, extracellular nucleotides and their corresponding receptors may act as paracrine and autocrine signals in regulating the microvascular contractility of the low resistance placental blood vessels, potentially involving the P2X7-NLRP3-IL-1β pathway. The hypothesis of this investigation was that purinergic receptor agonists as well as danger associated molecular patterns (DAMPs) such as D-glucose and pathogen associated molecular patterns (PAMPs) for instance lipopolysaccharide (LPS) regulate the blood flow at the level of the chorionic plate and stem villous vasculature of the human placenta via their interaction with the endothelial and smooth muscle cells. This process is mainly achieved by involving the P2X7 receptor in the autoregulation of the blood flow and vessel tone which is altered by DAMPs, PAMPs and inflammation.

Human placental collected after written informed consent, from healthy pregnancies (N) and those complicated by preeclampsia (PE) and gestational diabetes mellitus (GDM) were used. All healthy and GDM were from elective Caesarean section at term (≥37 weeks). PE placenta samples fell within 33 and 39 weeks of gestation. The P2X7 receptor, Nod-like receptor protein-3 (NLRP3) inflammasome and procaspase-1 protein expression levels in stem villous artery lysates (N=8, PE=8 patients) were assessed using western blotting. No statistically significant differences in the relative P2X7 receptor levels were found between the two study groups using a Mann Whitney test (P=0.3823). The relative NLRP3 inflammasome levels did not significantly differ between the two study groups in the case of both 74kDa isoform (unpaired T-test) and 92kDa isoform (Mann Whitney test). The relative procaspase-1 levels between healthy and PE groups did not significantly differ (P=0.8785); Mann Whitney test. Chorionic plate artery (CPA), stem villous artery (SVA) and trophoblast tissue originating from N=10 healthy patients were incubated with RPMI media (control) with added antibiotics (4h), 10mM ATP (4h), 10μg/mL LPS (3.5h) + 10mM ATP (0.5h) and 10μg/mL LPS (3.5h) + 300μM 3'-O-(4-Benzoyl)benzoyl ATP (BzATP) (0.5h) and the released levels of IL-1β, IL-6 and IL-18 were measured using enzyme-linked immunosorbent assay. LPS+ATP condition induced the highest secretion of IL-1β in all tissue types studied. There were no statistically significant differences in IL-18 levels between control vs. ATP, control vs LPS+ATP and control vs LPS+BzATP in CPA, SVA and trophoblast tissue. The P2X7 receptor protein expression (N=3) in trophoblast tissue lysates incubated with 0, 5.5, 10, 20 and 30mM D-glucose for 4 and 48 hours was also assessed using western blotting. No statistically significant differences in P2X7 receptor levels were found between the 0h control and the D-glucose different concentrations at both timepoints using Dunnett's T3 multiple comparison tests. IL-1β release also showed no statistically significant differences

between the D-glucose groups (Dunn's multiple comparison tests). However, the measured LDH levels in the same media were notably decreased in 20mM and 30mM D-glucose subgroups at 48 hours and showed multiple statistically significant differences between 5.5mM vs. 20mM (*P=0.0101), 5.5mM vs. 30mM (*P=0.0254) and between 0mM vs. 20mM (*P=0.0395) D-glucose treated trophoblast tissue using the same statistical test.

The functional responses of resistance sized CPA's (≤520μm) were investigated using wire myography. The vasoactive effects of ATP (10^{-5}M to 10^{-2}M) in the presence and absence of the P2X7 receptor antagonist A740003 (10^{-6}M) were investigated using resistance chorionic plate arteries (n=5) originating from N=5 placental samples. ATP gave rise to spontaneous concentration-dependent vasoconstriction responses in the absence of A740003. Addition of A740003 with subsequent ATP stimulation elicited a notably downward shifted concentration response curve implying a marked loss of ATP efficacy. The exogenous application of BzATP on isolated CPA's originating from healthy patients elicited a weak vasoconstriction response characterised by a particularly low efficacy of less than 25% of the U46619 standard. The absence of robust and reproducible responses to BzATP of isolated human placental chorionic plate arteries are due to the lack of involvement of the P2X7 receptor in the contractility of these blood vessels.

This study also provides evidence of a completely established *in vitro* model of a human chorionic vessel via the formation of a human umbilical vein endothelial cells (HUVEC) monolayer on transwell membrane inserts for the duration of 48 hours post-seeding followed by the coculture of HUVEC with chorionic plate artery smooth muscle cells (CPA-SMC) for a further 26 hours prior to the start of the permeability assay. The permeability data highlighted that CPA-SMC's do not significantly alter the tightness of the bilayer compared to monoculture of HUVEC cells during all timepoints of the tracer leakage assay.

The P2X7 receptor and CD31 immunolocalization in placental villous tissue originating from N=12 healthy and N=6 diet managed GDM patients was investigated using immunohistochemistry. There was a significant downregulation of the P2X7 receptor surface expression in GDM vascular profiles (double labelled with CD31) compared to normal (**P=0.0063); Mann-Whitney test. The correlation between P2X7 downregulation and the endothelial monolayer permeability remains to be elucidated.

In conclusion, these studies suggest that extracellular ATP may act on various P2X receptors giving rise to a local constriction of superficial placental blood vessels denoting that circulating nucleotides are particularly involved in the regulation of the feto-placental blood flow. These results suggest that the CPA-SMC's were unable to induce a notable alteration in the vascular permeability levels of established HUVEC monolayers which may denote that during the coculture of both primary cell types, a limited EC-SMC cross talk regarding vascular permeability took place. Further *in vitro* studies are necessary to fully understand the complicated interplay between isolated primary cells in co-culture conditions and to elucidate the potential involvement of multiple purinergic signalling pathways in the regulation of the human placental barrier function including the role of the P2X7 receptor in controlling the vascular permeability at the level of the chorionic plate arteries.

Abbreviations

- 8-SPT 8-(p-sulfophenyl)theophylline
- A_1 adenosine receptor
- A_2 adenosine receptor
- A_{2A} adenosine receptor
- A_{2B} adenosine receptor
- ACTH adrenocorticotropic hormone
- ADP adenosine 5'-diphosphate
- ADPβF adenosine 5'-O-(2-fluoro)-diphosphate
- ADPβS adenosine 5'-O-(2-thio)-diphosphate
- AEP active effective pressure
- AIM2 absent in melanoma 2
- AMP adenosine monophosphate
- AMPK adenosine monophosphate stimulated protein kinase
- APNEA N-[2-(4-aminophenil)ethyl]adenosine
- ATP adenosine 5'-triphosphate
- ATPyS adenosine 5'-O-(3-thyotriphosphate)
- AP alkaline phosphatase
- BMI body mass index
- BREC bovine retinal endothelial cells
- BzATP 3'-O-(4-benzoyl)benzoyl adenosine 5'-triphosphate
- Ca^{2+} calcium ion
- cAMP cyclic adenosine monophosphate
- CD-73 Ecto-5’-nucleotidase
- CGS21680 carbon modified N-ethylcarboxamidoadenosine analogue
- CHO Chinese hamster ovary
- CNS central nervous system
- CO cardiac output
- CPA coronary plate artery
- CPA's coronary plate arteries
- CRF corticotropin releasing factor
- CSAIDs Cytokine suppressive anti-inflammatory drugs
- CSC 8-(3-chlorostyryl)caffeine
- CXCR4 receptor for cytokines involved in chemotaxis
- CYP1 Cytochrome P450 family 1
- CYP1A1 Cytochrome P450 family 1 subfamily A member 1
- CYP1B1 Cytochrome P450 family 1 subfamily B member 1
- DAMP's Danger-associated molecular patterns
- DMSO Dimethyl sulfoxide

- DPMA N6-(2(3,5-dimethoxyphenyl)-2-(2-methylphenyl)ethyl)-adenosine
- DPSPX 1,3-dipropyl-8-sulfophenylxanthine
- eATP extracellular adenosine 5'-triphosphate
- DRG dorsal root ganglion
- EC_{50} 50% maximal effective concentration
- EC_{80} 80% maximal effective concentration
- EC_{90} 90% maximal effective concentration
- EC's endothelial cells
- EDHF endothelium derived hyperpolarising factor
- EGF epidermal growth factor
- EMT epithelial mesenchymal transition
- E-NTPDases ectonucleotidase 5'-triphosphate diphosphohydrolases
- EV's extracellular vesicles
- EVT extravillous trophoblast
- EVTs extravillous trophoblasts
- FGF fibroblast growth factor
- GnRH gonadotropin releasing hormone
- GRK2 G protein coupled receptor kinase 2
- hCG human chorionic gonadotropin
- HSP heat shock protein
- hGH human growth hormone
- hGH-V human growth hormone V
- HLA human leukocyte antigen
- HLA-C human leukocyte antigen-C
- HLA-E human leukocyte antigen-E
- HLA-G human leukocyte antigen-G
- HDGF hepatoma derived growth factor
- HMC-1 human mast cell line
- HPA hypothalamic pituitary adrenal
- hPL human placental lactogen
- HPV hypoxic pulmonary vasoconstriction
- HUVEC human umbilical vein endothelial cell
- I-ABOPX 3-(3-iodo-4-aminobenzyl)-8-(4-oxyacetate)phenyl-1-propylxanthine
- IB-MECA 6-carboxymethyl-5,9-dihydro-9-methyl-2-phenyl-[1,2,4]-triazolo[5,1-a][2,7]naphthydrine
- IGF-1 insulin like growth factor 1
- IGF-2 insulin like growth factor 2
- IL17 interleukin-17
- IL1α interleukin-1α
- IL1β interleukin-1β

- IL-6 interleukin-6
- IL-1β interleukin-1β
- IP3 inositol 1,4,5-triphosphate
- IUGR intrauterine growth restriction
- K+ potassium ion
- KAR's killer activatory receptors
- KIR's killer inhibitory receptors
- KPSS high potassium physiological solution
- lgG immunoglobulin G
- LH luteinizing hormone
- MCP-1 monocyte chemoattractant protein-1
- MHC major histocompatibility complex
- MI medically indicated
- mRNA messenger ribonucleic acid
- MSU monosodium urate
- NA noradrenaline
- NADPH nicotinamide adenine dinucleotide phosphate
- NECA N-ethylcarboxamidoadenosine
- NG-108-15 neuroblastoma x glioma hybrid cell line
- NKG2 natural killer cell group 2
- NO nitric oxide
- NOS nitric oxide synthase
- PAMP's pathogen-associated molecular patterns
- PE Preeclampsia
- PKC protein kinase C
- PLA2 phospholipase A2
- PLC phospholipase C
- PRR pattern recognition receptor
- pO2 partial pressure of oxygen
- pCO2 partial pressure of carbon dioxide
- PPADS pyridoxalphosphate-6-azophenyl-2',4'-disulfonic acid
- PSS physiological salt solution
- PTB preterm birth
- RBL-2H3 rat basophilic leukemia mast cell line
- ROS reactive oxygen species
- SMC's smooth muscle cells
- STBM's syncytiotrophoblast microparticles
- STZ Streptozotocin
- tcf-DNA total cell-free deoxyribonucleic acid
- TLR Toll-like receptor

- TM transmembrane
- UDP uridine 5'-diphosphate
- uNK uterine natural killer
- Up4A uridine adenosine tetraphosphate
- UTP uridine 5'-triphosphate
- WHO World Health Organisation
- VEGF vascular endothelial growth factor
- VSM vascular smooth muscle
- ZM241385 4-(2-[7-amino-2-(2-furyl)[1,2,4]-triazolo [2,3-α] [1,3,5] triazin-5-yl-amino]ethyl)phenol

CHAPTER 1

INTRODUCTION

1.1 The human placenta

Pregnancy is a physiological process which involves a synchronised physiological adjustment of various maternal organ systems [1]. Mammalian pregnancy relies on the placenta which is a transient organ originating from the fetus. The term ‘’placenta’’ derives from the Greek word ‘’plakoenta’’ which means a flat object [2]. In humans, the entire development of the placenta and fetus starts after attachment and interstitial implantation of the blastocyst into the endometrial mucosa [3]. This process can be subdivided into two main stages: firstly, proximal apposition and secondly adherence of the trophoblast cells forming the blastocyst to the epithelial cells present on the surface of the endometrial parenchyma. This attachment phase gives rise to multiple structural adjustments at the level of both endometrial epithelium and the surrounding stromal tissue, which in turn elicits the formation of the maternal constituent of the placenta [4]. In terms of its function, the organ acts as a selective barrier and gatekeeper between the mother and the fetus, as well as the only site of gas and nutrient exchange between the two.

The macroscopic characteristics of the delivered human placenta highlight in the majority of cases a circular to elliptical, discoid flat organ. The typical diameter of the placenta is 22 cm with a regular thickness in the epicentre of the organ of 2.5 cm and a common weight of approximately 470g [5]. The umbilical cord insertion point and the placental aspect are considered as important structural characteristics. In most cases, the umbilical cord attaches to the fetal side of the placenta in a central point, but there are exceptions such as eccentric, marginal, velamentous or vasa previa. The umbilical vein transfers oxygenated blood towards the fetus while the two umbilical arteries carry deoxygenated blood towards the maternal circulation. The placental shape can also display multiple abnormal variations such as placenta duplex, placenta zonaria,

placenta bilobata, placenta succenturiata or placenta membranacea. The fetal surface which reveals the amniotic cavity possesses a shiny aspect due to the undamaged amniotic epithelial lining and exposes the chorionic plate along with the chorionic vessels [5]. The chorionic arteries and veins divide in a star-like arrangement from the point of the umbilical cord insertion towards the placental margin. At the point of chorionic arterial and venous crossing, the branches of arteries generally overlap the veins at a location closer to the amnion. In the proximity of chorionic vessels with an increased internal diameter, the chorionic plate displays an opaque presentation due to a significant accumulation of collagen fibers. The surface area of the chorionic plate situated in between the chorionic vessels generally possesses a translucent appearance, highlighted by a distinct lilac colour as the intervillous maternal blood shines through. The chorionic plate gives rise to approximately 60 to 70 villous stems, with each one further subdividing into a single villous tree [5]. The maternal surface of the placenta is particularly opaque and exposes the basal plate which consists of a blend of decidual and trophoblastic cells which are directly exposed to the maternal blood. A partial arrangement of placental septa projecting towards the intervillous territory separate the basal plate into 10 to 40 relatively raised areas termed maternal cotyledons [5]. [Figure 1 shows the anatomy of human term placenta on both fetal (A) and maternal (B) sides, as well as the umbilical cord (C). Figure 2 shows a scheme replicating the anatomical structure of the human term placenta in cross section by highlighting the key architecture of the fetal and maternal surfaces of the organ. Figure 3 denotes the branching of the placental villous tree, from the point of umbilical insertion into the chorionic plate to the end of the terminal villi. Figures 4 and 5 indicate the angioarchitecture of the mature intermediate villous and terminal villi.]

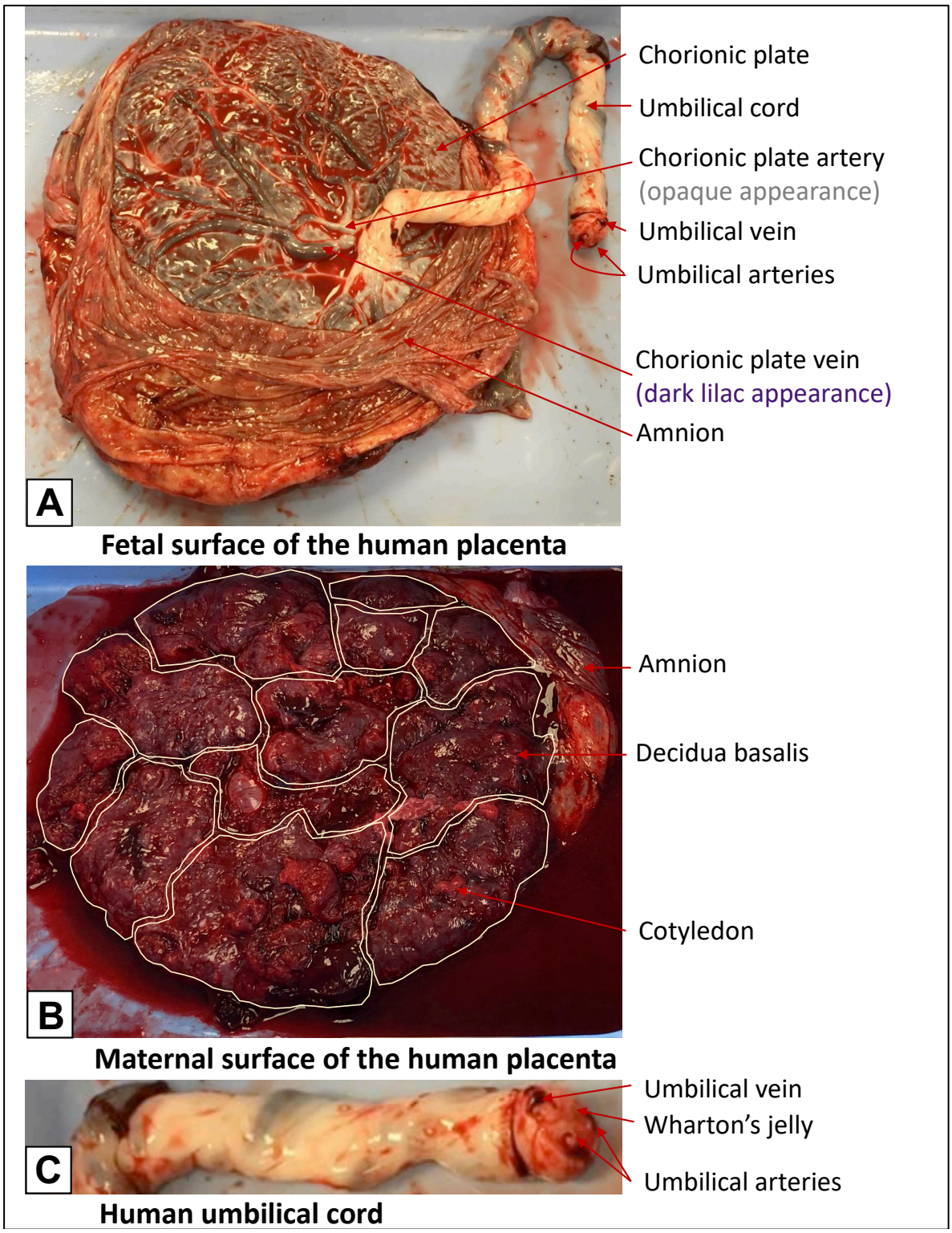


***Figure 1**. This figure highlights the anatomy of a newly delivered mature human term placenta **A.** Shows the fetal surface of the placenta with the slightly eccentric insertion of the umbilical cord and the branching of the chorionic plate arteries (opaque presentation) and chorionic plate veins (dark lilac aspect) **B.** Highlights the maternal surface of the placenta partitioned into 12 maternal cotyledons of variable size (emphasized in pale yellow) which are separated by a discontinued network of indentations **C.** Indicates the appearance of the umbilical cord by pointing out its two umbilical arteries, one umbilical vein and the Wharton's jelly. The original images in this figure were acquired by Paul Fodor.*

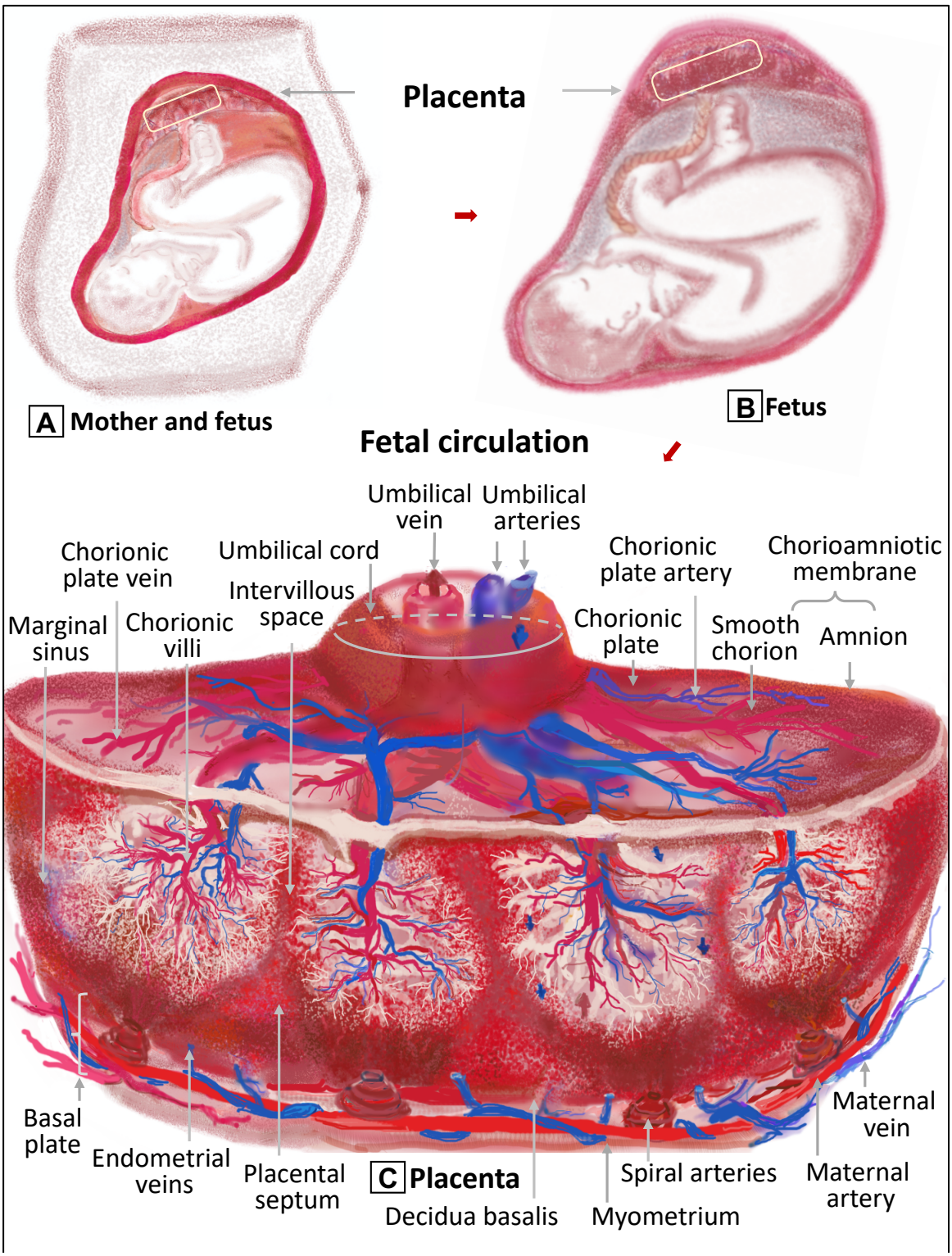


***Figure 2**. This scheme shows the anatomy of the: **A**. pregnant mother with the developing fetus before parturition **B**. fully grown fetus and the placenta with the umbilical cord **C**. human term placenta in cross-section highlighting the chorionic plate, basal plate and the intervillous space. The chorionic villi accommodating the fetal blood vessels emerge from the chorionic plate and project towards the intervillous space. This region contains the maternal blood entering the placenta via the spiral arteries and collected back into the maternal circulation through the endometrial veins. This figure has been hand drawn by Paul Fodor using Autodesk SketchBook software version 8.7.0.*

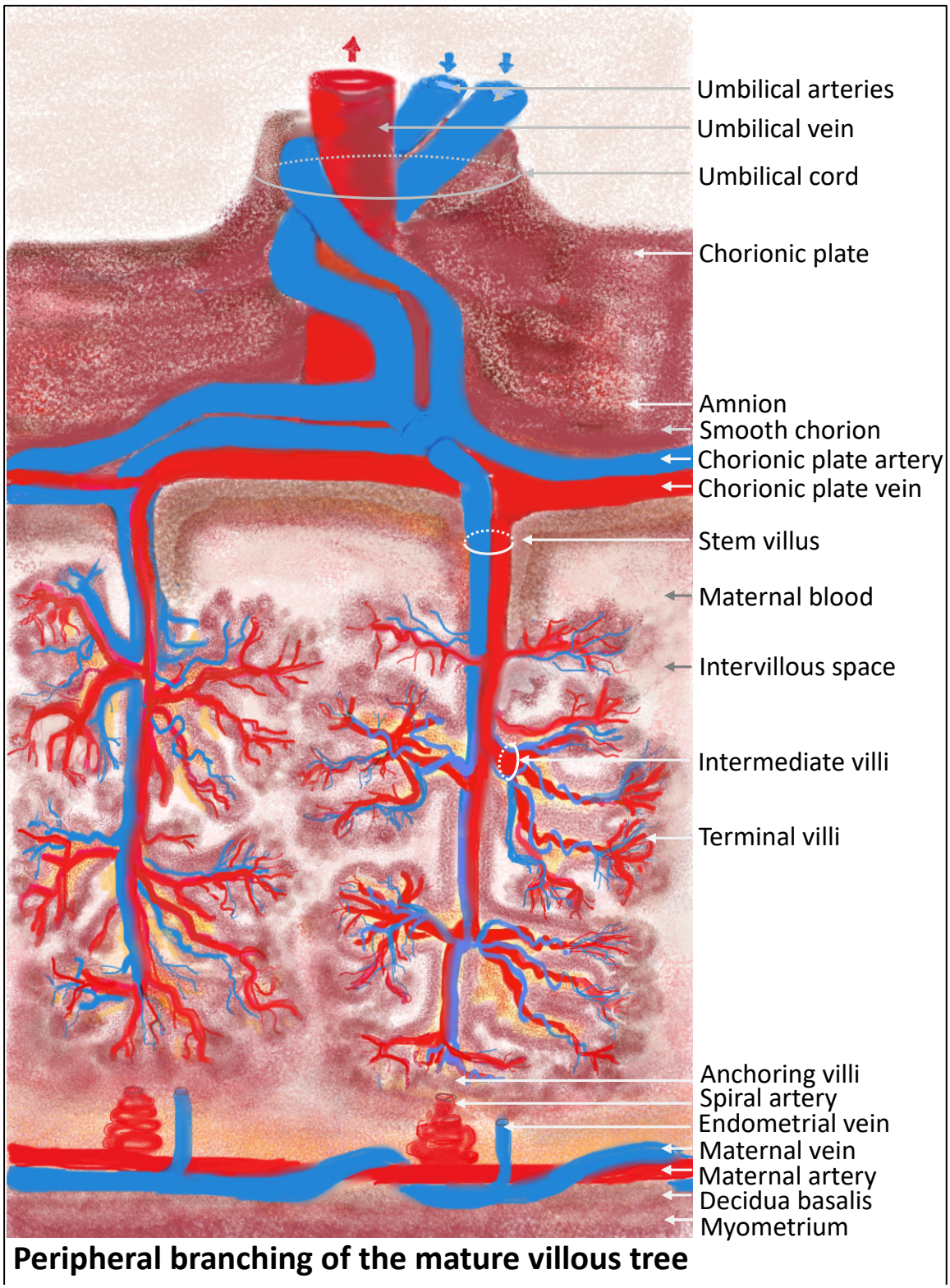


Figure 3. *This scheme shows the morphology of the placental villous structures of the human term placenta in cross section. The emerging branches of the mature villous tree float free into the maternal blood lacunae in discrete maternal lakes. These ramifications consist of a stem villous which branches to form a mature intermediate villous and ultimately giving rise to the terminal villi. The syncytiotrophoblast layer covers the surface of the villous tree which separates the fetal and the maternal blood. This figure has been hand drawn by Paul Fodor using Autodesk SketchBook software version 8.7.0.*

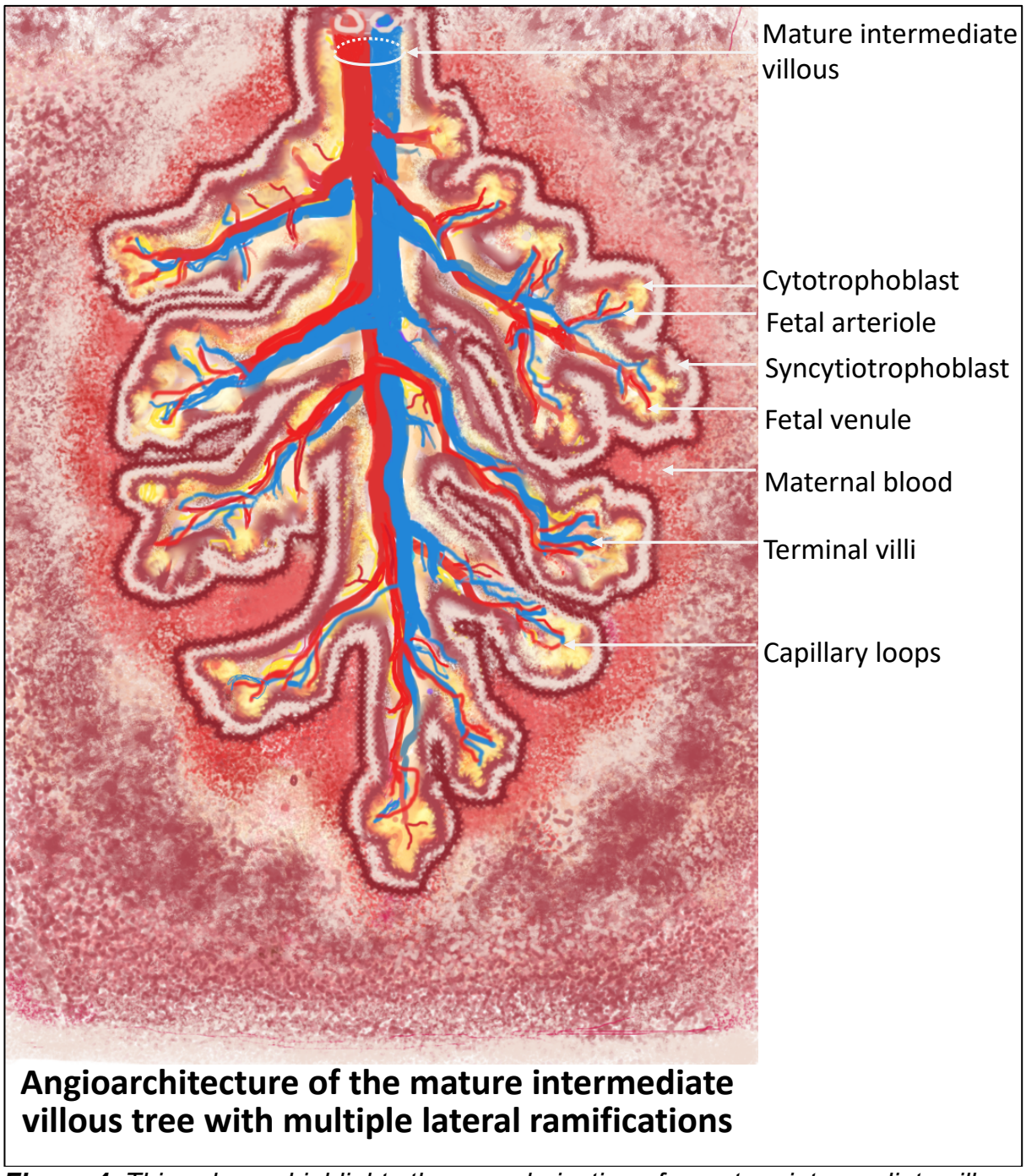


Figure 4. *This scheme highlights the vascularisation of a mature intermediate villous possessing numerous side branches described as terminal villi. The most peripheral bifurcations of the stem villi branch or extend to form the mature intermediate villi. These villi give rise to one or two small arterioles usually consisting of only endothelial cells with the occasional surrounding of smooth muscle cells. The peripheral ends of the arterioles continue to form the capillaries via a marked decrease in their internal diameter and the absence of smooth muscle cells. Furthermore, the mature intermediate villi branch to form one or two venules positioned more superficially in the villous stroma compared to the arterioles which are situated particularly central. The postcapillary venule does not possess any smooth muscle cells and their structure is almost entirely surrounded by pericytes. This figure has been hand drawn by Paul Fodor using Autodesk SketchBook software version 8.7.0.*

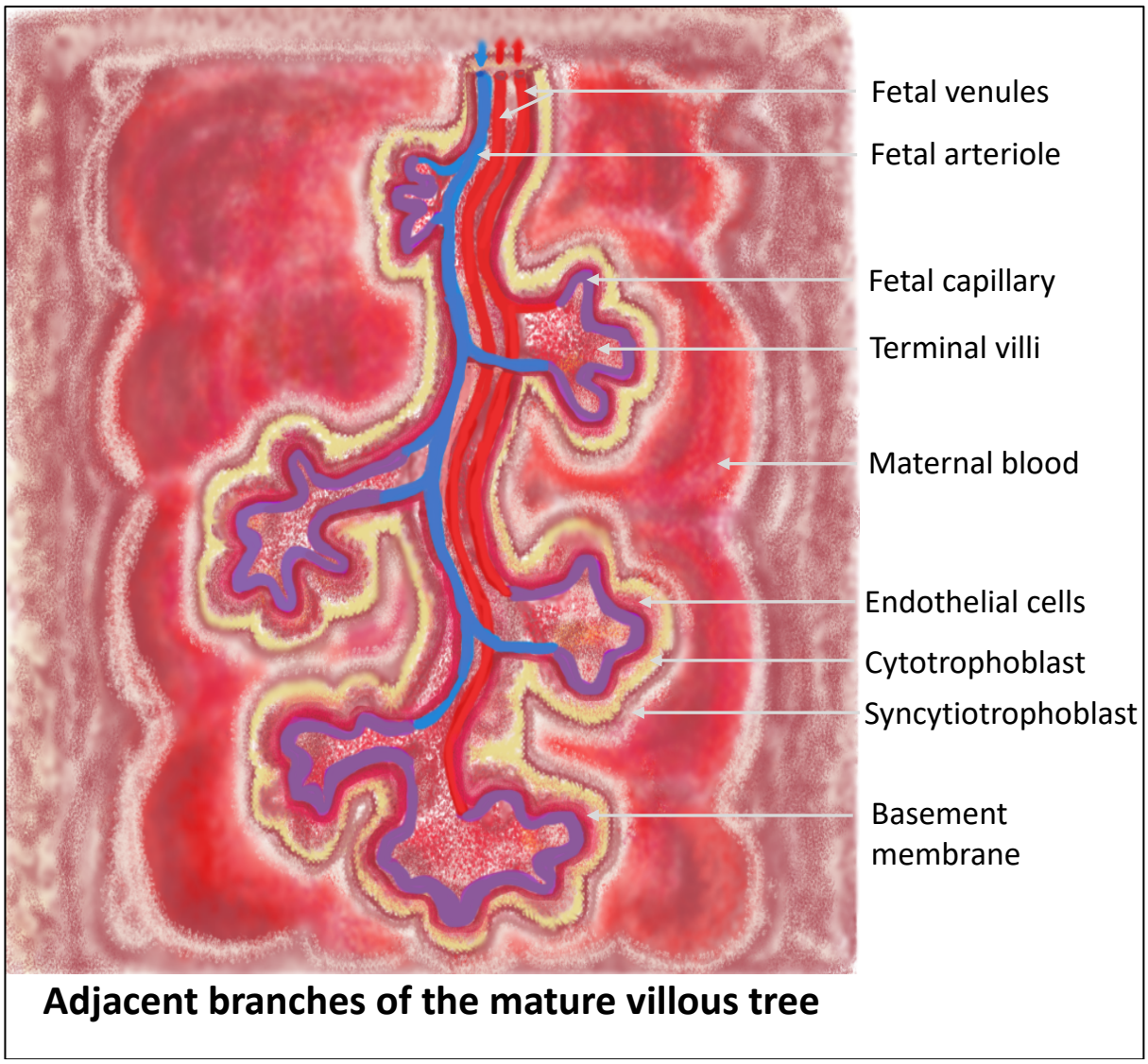


Figure 5. *This scheme shows the distribution of the fetal vessels in an accumulation of terminal villi originating from a completely developed mature intermediate villous. The remarkably intricate coil organisation of the terminal fetal capillaries possesses the property of being serially connected to adjacent capillary loops. The fetal blood exiting a terminal arteriole and arriving at the terminal capillaries ordinarily flows through the capillary coils of 3-5 terminal villi ahead of gaining access to the postcapillary venule. Distinct dilatations termed sinusoids significantly decrease the blood flow impedance. Blue colour signifies arteries or arterioles; dark lilac colour denotes fetal villous capillaries and sinusoids; red colour suggests fetal veins and venules. This figure has been hand drawn by Paul Fodor using Autodesk SketchBook software version 8.7.0.*

1.1.1 Placental development

During the course of every gestation period, the placenta and the correlated extraembryonic covering layers originate from the zygote, therefore possess the equivalent genetic profile of the developing fetus. The fertilised ovum evolves into the blastocyst during the first five days postconception. The blastocyst consists of three main structures: the embryonic inner cell mass, a cavity containing fluid and the trophectoderm, which is part of the surface of the blastocyst and later during the pregnancy becomes the placenta [2,6]. The trophectoderm evolves to form the trophoblast which constitutes the outermost coating of the placenta, as well as giving rise to a discrete invasive population of extravillous trophoblast cells. The extraembryonic mesoderm generates the villous foundation of the developing placenta, consisting of the extensive vascular ramifications, fibroblasts and macrophage cells [7]. The trophectoderm bilayer is composed of two main types of trophoblasts: the cytotrophoblast stem cells and their evolved and fused form establishing the syncytial layer called the syncytiotrophoblast. This covering is a fully differentiated tissue and its proliferation is accomplished via the merging and unification of the fundamental mononuclear predecessor cytotrophoblast cells residing on the basement membrane. The indicated coupling process is particularly intricate and has not been fully elucidated yet, although it may potentially require the withdrawal of the cytotrophoblast cells from the cell cycle, the development of multiple gap junctions with the adjacent syncytiotrophoblast tissue, as well as the release of phosphatidylserine into the extracellular space [8,9].

At the beginning of pregnancy, the blastocyst becomes anchored to the maternal decidua and at about 10 to 12 days after conception, the structure becomes surrounded by a layer of syncytiotrophoblasts [10]. For the duration of pregnancy, the

syncytiotrophoblast layer is always covered with blood originating from the mother. Twelve days after implantation, the cytotrophoblasts divide and invade into the lacunar zone [11]. Usually, about two days after the penetration, these cells may divide laterally to cover the perilacunar space to give rise to the well-known cytotrophoblastic shell [2]. These changes in the early development of the implanted embryo arise in hypoxic circumstances with a partial pressure of oxygen of less than 15mmHg, which in turn stimulates cell division [12]. The oxygen tension must be tightly regulated in order to give rise to a normal placenta and pregnancy. On the other side, the cytotrophoblasts escaping the shell evolve to form the extravillous trophoblasts (EVTs). These cells are highly predominant for the course of the first trimester of the gestation period and originate from the apex of the anchoring villi connecting the chorionic villi to the endometrium [7]. Their aim is to bind the maternal decidua to the placenta and to remodel the lumens of the spiral arteries using a mechanism characteristic of the epithelial-mesenchymal transition (EMT) [7,13–15]. This transformation requires a gradual decrease of smooth muscle cell population located at the level of the spiral arteries potentially via a programmed cell death mechanism or differentiation and their substitution with a passive, vaguely defined fibrinoid coating [16,17]. In this case, the cellular signalling pathways involved have not been fully elucidated yet, although a few groups have suggested a potential early stage endocrine priming succeeded by a follow-up stage entirely reliant on the participation of the extravillous trophoblast cells [18,19]. Inadequate remodelling of the spiral arteries has been strongly associated with preeclampsia, as the developing insufficient perfusion leads to oxidative stress and in turn the secretion of angiogenic mediators and pro-inflammatory cytokines from the syncytiotrophoblast layer, ultimately activating the endothelium of the pregnant mother [20].

The interstitial extravillous trophoblasts invade both the decidua, as well as the inner maternal myometrium with the aim to remodel approximately 100-150 spiral arteries [21]. Usually between 10-12 weeks of pregnancy, the EVT plugs start to deplete which gives rise to a well oxygenated utero-placental vasculature. This process continues until about week 20 to 22 during pregnancy in the myometrial part of the maternal vessels, giving rise to an increased-flow, low-resistance circulation which guides the maternal blood to the intervillous space [22–24]. At about week 24 during the gestation period, a change between conductance stem villi to gas and nutrient exchange terminal villi is taking place. This change is marked by the development of villi covered with a thin layer of syncytiotrophoblast called vasculo-syncytial membrane [25]. As a result, this transformation facilitates the transport of oxygen and carbon dioxide between the mother and the fetus. During the third trimester, the synthesis of terminal villi happens exponentially. The placental growth is also dominated by a rise in non-branching blood vessel formation of the mature intermediate villi [26].

1.1.2 Cardiovascular adaptations to human pregnancy

Many significant adjustments occur in the maternal cardiovascular system during pregnancy, particularly at about week 12-16 of the gestation period. Some of these changes cause an increase in size of the uterus, resulting in the diaphragm being pushed towards the cranial direction and a displacement of the heart upwards and laterally. According to Abbas and colleagues (2005), pregnancy is characterised by a high volume and a low-resistance state, which is dominated by an increase of 22% in cardiac output (CO) before 8 weeks of gestation [27]. The CO gradually increases for the duration of pregnancy, reaching a plateau phase (30-40% elevation) by the end of the second trimester. This rise is dominated mainly by an increase in the stroke output (30%) and to some extent by the elevation of the heart rate by 10-15

beats every minute [28]. For the duration of pregnancy, the myocardial contractility is elevated, which is strongly related to the elongated myocardial muscle fibres. Towards the end of the pregnancy, the cardiac output starts to decline when the mother lies in a supine position. This is due to the compression of inferior vena cava by the expanded uterus, which interferes with the venous return to the heart [29].

During the gestation period, a marked vasorelaxation effect takes place, especially in the systemic blood vessels as well as the maternal kidneys [30]. These changes start from approximately 5 weeks of pregnancy and support the formation of the uteroplacental vasculature [31]. Towards the end of the first trimester of pregnancy, the vasorelaxation of the kidneys gives rise to a 50% elevation in the renal plasma flow, as well as the glomerular filtration rate, resulting in a reduction of serum urea, creatinine and uric acid levels [32].

1.1.3 The development of the human placental vasculature

Angiogenesis and vasculogenesis are decisive when it comes to physiological development of the human placenta. The mechanism involved in vasculogenesis is accomplished by the *de novo* synthesis of blood vessels, which originates from mesenchymal stem cells. Following differentiation of these stem cells, they give rise to hemangiogenic stem cells, which can further differentiate into hemangioblastic stem cells and finally resulting in the generation of angioblastic cells. According to Arroyo and Winn (2008), these cells finally evolve to give rise to endothelial cells [33]. On the other side, angiogenesis is a process by which additional vessels are generated from the existing ones [34].

One of the most important characteristics of the fetal and maternal vascular systems is they do not connect. In humans, although the evolution of the vasculature is tightly coordinated, the process happens independently [33,35]. The growth of the

placental vasculature starts during the early stages of the gestation and is maintained for the duration of pregnancy. This growth is characterised by a significant elevation in the rate of blood flow to different parts of the placenta, in both the umbilical and uterine vasculature. The purpose of this rise is to accomplish the constant growth of metabolic requirement of the developing fetus [36].

Branching angiogenesis usually starts at day 21 post implantation and is marked by a gradual increase of the villous vasculature. This period is also dominated by an expansion of the fetal capillaries [36]. After 6 weeks of fetal development, basal lamina starts to grow in the placental capillaries, giving rise to a web-like anastomosis of the capillaries inside the functional tissue of tinier villi. However, in the bigger villi, most of the capillaries are positioned at a superficial level, just under the trophoblast coating the villous surface [37].

The 15th week of gestation marks a significant change of the principal enlarged villi in terms of the tunica adventitia which fuses, giving rise to a fibrosed functional mesh right in the middle of the villous [36]. The non-branching angiogenesis occurs approximately from week 26 of fetal development and is marked by a vascular angiogenesis change dominated by the generation of the specialised villi responsible for the gas transfer.

1.1.4 Regulation of blood vascular permeability in the human placenta

The barrier created by the human placenta represents a complicated and constantly changing environment which supports the transfer of various solutes, hormone production as well as creating a wall for the purposes of guarding the fetus and the mother for the duration of the gestation period [38]. Furthermore, the placental

barrier comprises of a delicate coating with multiple nuclei termed syncytiotrophoblast accompanied by fetal capillary endothelial cells and also a fluctuating number of cytotrophoblasts, proteins of extracellular matrix and various immune cells [39,40]. The integrated syncytiotrophoblast barrier is in direct contact with the maternal blood and the fetal capillaries in particular the endothelial cells comprising them delimitate the blood vessels inside the chorionic villi that hold the blood originating from the fetus and sit embedded in the mesoderm [39,40]. Similar to other healthy barriers around the human body, the placental barrier has an important clinical usefulness to the extent of regulating the transfer of crucial nutrients and also to allow or prevent the passage of various drugs or compounds from the circulation of the mother into the fetus.

Some of the cellular processes participating in the trans-syncytiotrophoblastic exchange comprise of: passive diffusion that is regulated by Fick's law and could happen to nearly any substances with a molecular weight not exceeding 500 Da and facilitated diffusion happening in cases of passive movement through the syncytiotrophoblast layer according to a concentration gradient with the help of molecular carriers such as FATPs in the case of fatty acids or GLUTs promoting the transport of glucose. Other methods of movement include active transport which happens in an opposite direction to the concentration gradient needing energy which may be provided via hydrolysis of adenosine 5'-triphosphate for instance Ca^{2+}, protons [41,42] or using co-transporters for instance sodium coupled neutral amino acid transporter (SNAT) family for moving amino acids across the trophoblast barrier [43]. Further cellular mechanisms include pinocytosis and phagocytosis in its multiple kinds [44] granting the ability to the syncytiotrophoblast to engulf and transport macromolecules via different processes. An excellent representative case is the transport of low density lipoprotein through receptor-moderated endocytosis [45].

Furthermore, transcytosis which is a separate cellular system of receptor-moderated endocytosis enables the movement of high molecular weight molecules for instance maternal IgG [46] from the apical to the basal membrane of the syncytiotrophoblast finally releasing the immunoglobulin into the fetal circulation.

1.1.5 Resistance arteries in the human placenta

The regulation of vascular tone present in the fetoplacental interphase has not been fully understood yet. As the placenta lacks innervation [47], the fetoplacental vascular tone is thought to be regulated by either paracrine or autocrine vasoactive substances or by alterations in the villous resistance circulation of the intrinsic smooth muscle tone [48,49]. Therefore, the physiological pattern of blood flow through the fetoplacental circulation could be deeply disturbed in the case of various pathological conditions. Moreover, very little is known about which locally synthetized substances are crucial for regulating the vascular tone of the placental vasculature [50,51].

It is very important to distinguish the resistance arteries of the placenta with the passive conduit-type arteries. Although for wire myography purposes of studying the functional aspect of resistance arteries from the placenta, different journal articles have set an independent cut off value for the diameter of the isolated vessels, there are two main considerations to be analysed [52].

The umbilical arteries branch to give rise to chorionic plate arteries (CPA's) on the fetal side of the placenta. Nugent and colleagues (2013) have described these arteries as possessing attributes of a resistance circulation, with an internal diameter of less than 300 μm [51]. They are thought to be involved in the modulation of vascular tone particularly in the fetoplacental circulation. A similar internal diameter characterising a resistance vein from the chorionic plate has been stated in another study by Cabrera and colleagues in 2016 highlighting the optimal diameter for

isometric force measurements was 310 μM [47]. Many other studies have addressed the resistance circulation from the coronary plate of the placenta as isolating arteries with an internal diameter of less than 500 μM [50,53,54]. In another study, the chorionic plate arteries were defined as having an internal diameter of less than 400 μM [55]. Therefore, although the range of the internal diameter varies, for the purposes of isometric tension assessments, most of the CPA's have been classed as less than approximately 500μM in diameter.

Another way of defining these resistance arteries which only few studies have considered was the location of CPA's on the fetal part of the placenta. To expand on this, Ali and colleagues (2014) have stated that in the isolation of the coronary plate arteries, the fourth order branch of the main umbilical artery was used in the study [53]. This further classification of a resistance artery was very important for the inclusion-exclusion criteria of studying the isometric force measurements of CPA's.

1.1.6 Structure of blood vessel walls

The wall of blood vessels is composed of three different layers which surround the main cavity containing the blood called the vessel lumen. The first innermost layer is called tunica intima. The most important feature of this layer is that it contains the endothelium. This is a simple squamous epithelium in direct contact with blood. Its flat cells come in direct contact with each other forming a smooth surface resulting in a reduced friction as blood passes through the lumen of the vessel [56].

The middle layer is called tunica media and is composed of mainly smooth muscle cells (SMCs) arranged in a circular way and elastin. In order to regulate the body's needs, either vasoconstriction (decrease in the lumen diameter due to the contraction of smooth muscle cells) or vasodilation (increase in the lumen diameter as a result of relaxation of SMCs) can be elicited [57].

Lastly, the outermost layer of the blood vessel is called tunica adventitia. This layer consists of lightly woven collagen fibers with the purpose of supporting and strengthening the vessel. The tunica adventitia is in direct contact with nerve fibers [58].

1.1.7 Mechanisms of blood flow regulation in the placenta

The maintenance of vascular tone at the interphase between the mother and the fetus is not known [49]. A decisive regulator of vascular tone giving rise to vasodilation or in other words tissue reperfusion of most organs is tissue hypoxia. However, an exception to this is the lung, where similarly to the fetoplacental vasculature, the vascular resistance is reduced. As a result, the link between oxygen delivery to tissue and blood flow resistance is achieved in the lung by hypoxic pulmonary vasoconstriction (HPV) [54].

A crucial physiological mediator which induces vasorelaxation in the human fetoplacental blood vessels is nitric oxide [59]. Furthermore, nitric oxide signalling is fundamental for the control of a suitable blood perfusion to the developing fetus for the course of the gestation period. Karuse *et al*, (2013) have shown that decreased nitric oxide production is closely linked to fetal growth restriction [60]. Beside nitric oxide, other important vasorelaxant mediators acting at the level of the umbilical vessels, the chorionic plate and villous vasculature are PGI_2 and adrenomedullin, with endothelin-1 mainly vasodilating the umbilical blood vessels and atrial natriuretic peptide possessing a vasorelaxant property at the level of the villous tree [61–64].

HPV acts by activating the vascular smooth muscle (VSM) in conjunction with the endothelium in the absence of any neuronal signalling. Also, HPV response can be initiated in isolated smooth muscle cells originating from the pulmonary arteries via the activation of Ca^{2+} activated and voltage-dependent K^+ channels [65]. As a point of

view of endothelium activation involved in this process, hypoxia is detected in pulmonary arteries via the action of endothelin-1 and nitric oxide (NO) [66,67].

A matching mechanism of action in response to hypoxia has been proposed in the fetoplacental interphase in humans giving rise to vasoconstriction. To expand on this, it has been postulated that the general understanding of the management of vascular tone in the fetal side of the placenta (chorionic plate) has been generated particularly from isolated and perfused cotyledons originating from this organ [54]. It has been reported that using perfusion myography studies, by decreasing the pO_2, a slight vasoconstriction was initiated in vessels isolated from the chorionic plate as compared to a reduction of pCO_2 or pH. An increased vasoconstriction response has been noted in ring-mounted chorionic plate vessels with a wider diameter (more than 1mm) which may suggest that the constriction response could be dependent on the size of the blood vessel when it comes to reducing the pO_2 [54,68,69]. In other words, the hypoxic stress applied to the perfused cotyledons could be crucial, as fetal-acidosis and hypoxia do not elicit vasoconstriction when compared to hypoxia of the pregnant mother [54].

The work undertaken by Hampl and colleagues in 2002 highlights that the fetoplacental vasoconstriction elicited by hypoxia could be also initiated by a change in the voltage dependent K^+ channels [69].

1.1.8 Pregnancy related disorders

1.1.8.1 Gestational diabetes mellitus

Gestational diabetes mellitus (GDM) is nowadays the most frequent pregnancy disorder and the preponderance of undetected elevated blood glucose and also overt diabetes especially in adolescent females is rising [70]. Some of the principal GDM risk causes include obese or overweight mother, family history of type 2 diabetes, previous

history of gestational diabetes, increased maternal age during the gestation period and maternal ethnicity [71]. In terms of diagnosis of the disorder, an oral glucose tolerance test (OGTT) is usually undertaken, although a non-fasting glucose challenge test is performed in a few areas of the world to pre-evaluate patients prior to performing a complete OGTT [72]. The principal treatments for gestational diabetes mellitus are elevated physical exercise and dietary adjustment with insulin being used in cases where physiological glucose levels are not obtained [73]. In a few regions around the world, oral hypoglycaemic compounds are also prescribed namely metformin and glibenclamide [74]. The management of GDM enhances pregnancy outcomes via decreasing supplementary fetal development and adipose tissue as well as gestation-connected high blood pressure diseases [75]. Furthermore, gestational diabetes mellitus elevates the predisposition to lasting complications for instance defective glucose turnover, cardiovascular disease and obesity taking place in both mother and child [76,77].

1.1.8.2 Preeclampsia (PE)

Preeclampsia has been considered one of the most important health problems related to human pregnancy [78]. The condition is described by maternal hypertension, endothelial cell dysfunction, decreased utero-placental blood flow, elevated platelet aggregation accompanied by proteinuria and sometimes edema [79]. Moreover, the disorder has been characterised by a failure in chronological spiral artery remodelling in the early stages of pregnancy [80,81]. It has been also pointed out that the replacement of smooth muscle and vascular endothelial cells by fetal trophoblasts is prevented, which in turn causes a non-adequate gas and nutrient exchange between the mother and the fetus [82]. Some of the risk factors associated with PE include the following: a history of the condition, advanced maternal age, first pregnancy, obesity

or even hypertension. Preeclampsia is diagnosed by an elevated resting blood pressure with increased proteins in the urine. The systolic pressure is ≥140 mmHg and the diastolic pressure should be ≥90mmHg. Proteinuria is accepted as ≥0.3g of protein in a 24 hours urine sample or 3+ protein when using a urine dipstick [83]. Lastly, the only treatment of preeclampsia is fetus delivery. Also, it is important to treat the hypertension aspect of the disease with different β-blockers or calcium channel blockers [83].

Figure 6 highlights the possible role of adenosine 5'-triphosphate to the pathogenesis of preeclampsia by showing the anatomical structure of the placenta in cross-section and by emphasizing the potential stimulation of the purinergic P2X7 receptor present on the endothelial and immune cells by the nucleotide, which may ultimately result in endothelial cell dysfunction [84–86]. Figure 7 shows the anatomy of the placental villous tree in cross section, as well as the release of danger associated molecular patterns for instance syncytiotrophoblast microparticles (STBM's), extracellular vesicles (EV's) and total cell-free deoxyribonucleic acid (tcf-DNA) into the extracellular space in the case of preeclamptic patients, potentially resulting in endothelial and immune cell activation [87–89].

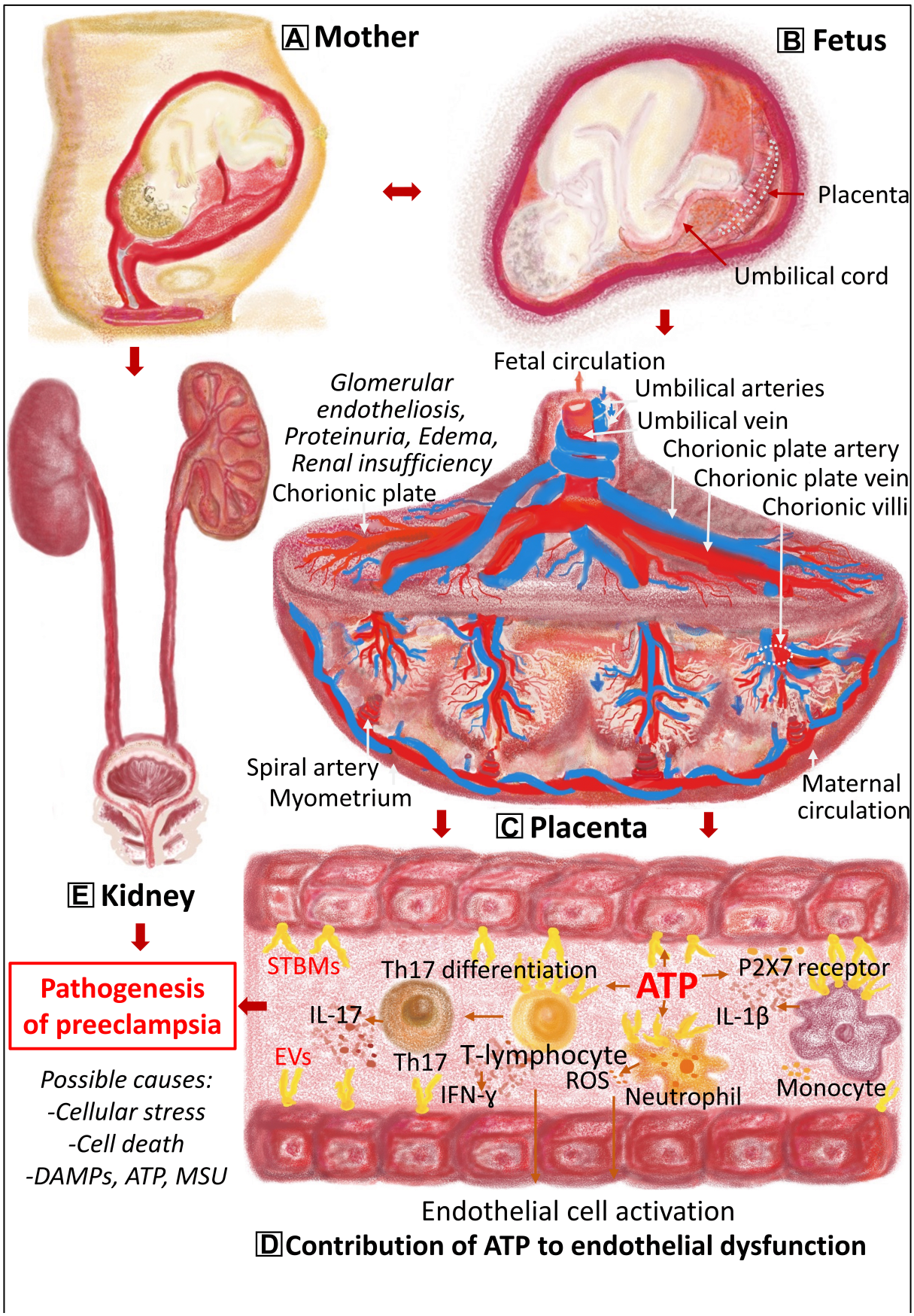


Figure 6. *This scheme shows the potential mechanism of ATP involvement in the pathogenesis of preeclampsia* ***A****. Pregnant mother with the growing fetus* ***B****. Fully developed fetus and the placenta with the umbilical cord* ***C****. Human term placenta*

highlighting the key angioarchitecture of the chorionic plate and the mature villous tree ***D****. Extracellular adenosine 5'-triphosphate is capable of stimulating the endothelial cells present in the fetal or maternal blood vessels, as well as activating circulating neutrophils, T-lymphocytes and monocytes. Elevated circulating levels of eATP could arise due to the action of other danger associated molecular patterns being released into the maternal blood vessels for instance syncytiotrophoblast microparticles (STBM's), extracellular vehicles (EV's) and monosodium urate (MSU) crystals, which could further circulate into the systemic vasculature promoting the release of pro-inflammatory mediators for the duration of pregnancy. The stimulation of the P2X7 receptors expressed on the endothelial cells gives rise to the release of interleukin-6 (IL-6), monocyte chemoattractant protein-1 (MCP-1), vascular cell adhesion molecule-1, IL-8 and intracellular adhesion molecule-1. Extracellular ATP also activates granulocytes and monocytes resulting in the excretion of reactive oxygen species (ROS), IL-6, macrophage inflammatory protein 2-α and IL-1β. This nucleotide also stimulates the P2X7 receptor present on T-lymphocytes resulting in the differentiation of Th17 cells and the release of interferon-γ in the extracellular space.* ***E****. Severe endothelial cell dysfunction in the glomerulus accompanied by significant changes in terms of podocyte associated protein levels in the kidney gives rise to glomerular endotheliosis, proteinuria, edema and renal insufficiency which are strongly associated with the pathogenesis of preeclampsia. Therefore, in preeclamptic patients, extracellular ATP stimulation of endothelial and circulating immune cells could further encourage the establishment of a pro-inflammatory state during the gestation period. This figure has been hand drawn by Paul Fodor using Autodesk SketchBook software version 8.7.0. The scheme in panel D has been taken from Spaans et al (2014)* [85].

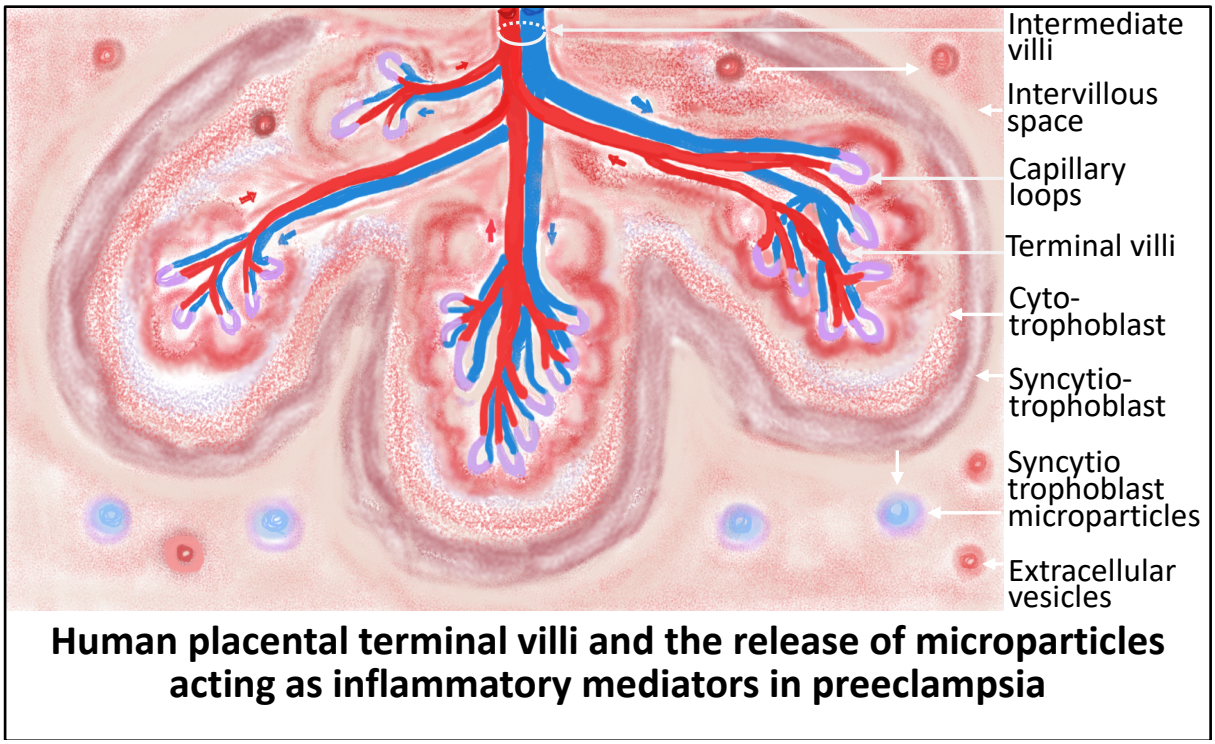


Figure 7. *This scheme shows the anatomical cross-sectional structure of the intermediate and terminal villi in the context of pre-eclampsia. Due to persistent elevated blood pressure in the circulation of the mother, syncytiotrophoblast microparticles (STBM), extracellular vesicles (EV) and total cell-free deoxyribonucleic*

acid (tcf-DNA) become released into the maternal circulation from the syncytiotrophoblast layer covering the terminal villi. These extracellular debris travels through the circulation of the mother causing the release of ATP from stimulated endothelial cells as well as monocytes particularly at the level of the feto-maternal interface. In the case of preeclamptic patients, STBM particles are able to stimulate platelets, which further causes the release vast quantities of adenosine 5'-triphosphate that activates the P2X7 receptor expressed on multiple types of immune cells, ultimately giving rise to uncontrolled assembly of the pyrin domain-containing protein 3 (NLRP3) inflammasome and the release of pro-inflammatory cytokines. This figure has been hand drawn by Paul Fodor using Autodesk SketchBook software version 8.7.0 and is adapted from Sargent et al (2006) [89].

1.1.8.3 Intrauterine growth restriction (IUGR)

IUGR is characterised by the inability of the fetus to accomplish its complete growth capability. The condition influences about 9% of all pregnancies. Intrauterine growth restriction is the second principal cause of fetal mortality after pre-term birth [90]. Furthermore, excluding the perinatal complications, the newborns are thought to be at a high risk of acquiring both developmental or chronic neurological diseases for example systemic hypertension, stroke, coronary heart disease or even non-insulin dependent diabetes mellitus.

The mechanisms by which IUGR arises in the pregnant women are poorly understood, although some of the potential risk factors involved in the generation of the disorder have been elucidated for example: malnutrition, tobacco, alcohol, maternal diseases (renal insufficiency, systemic arterial hypertension) [90].

The aetiology of IUGR is relatively vague with an emphasis to a maternal, fetal or even placental origin. The disease is strongly dominated by placental insufficiency, a term that describes a malfunction of the fetal-maternal interface exchange of nutrients and gasses [91]. In terms of treatment of the disease, there is currently no effective way of preventing or treating the disease. However, there are approaches to decrease the risk factors of IUGR by trying to alter the mother's health behaviour.

1.1.9 Endothelial adhesion molecules in diabetes

Occludin is a tight junctional mediator which has been proved to be significantly reduced in the paracellular junctions particularly in streptozotocin (STZ)-induced diabetic rats in the retinal endothelial cells, the results corresponding also with elevated periods of leakiness [92]. In primary bovine retinal endothelial cells (BREC), vascular endothelial growth factor encouraged occludin phosphorylation.

However, chemical inhibitors of protein kinase C family of serine-threonine kinases action have blocked the VEGF-induced elevation of occludin phosphorylation which was evaluated by 2D gel electrophoresis analysis and also partly blocked in the monolayer permeability assessed with 70-kDa dextran [93]. Moreover, matrix metalloproteases (MMPs) are catalysts belonging to the endopeptidase classification which are participating in the cleavage of extracellular receptors. MMP-9 and MMP-2 function and expression are especially elevated in diabetes and their participation in the deterioration of occludin in cultured BREC's has also been documented [94]. Furthermore, a study by Babawale and colleagues in 2000 has demonstrated that occludin expression is decreased in large conduit blood vessels belonging to the placenta notably in gestational diabetic patients [95].

Endothelial cells (EC's) belonging to the retina of STZ-induced diabetic rats present a reduction of vascular endothelial cadherin expression, which is inversely proportional with vascular leakiness [96]. The study also suggested this phenomenon happens as a result of an elevated expression of MMP's, which interact with VE-cadherin from the extracellular compartment. Furthermore, in blood vessels originating from type 1 diabetic placental specimens, endothelial cells possess a change in junctional occupancy of important adhesion factors for instance β-catenin and VE-cadherin in more than 50% of the vasculature [97]. In addition, this study further showed

that perivascular cells and the endothelium have elevated levels of vascular endothelium growth factor – A and that the fetoplacental blood vessels express an elevated permeability to big macromolecules (76kDa) which are even higher in molecular weight than circulating albumin. This study also confirmed using western blotting that the decrease in expression of β-catenin and VE-cadherin was as a result of phosphorylation and not due to a decrease of junctional proteins [97].

A further research study presented data on measurable quantities of vascular endothelium growth factor from 210 specimens of ocular fluid taken from 164 patients subjected to intraocular surgery [98]. A high preponderance was found in 69 positive VEGF fluids out of 136 samples originating from subjects with diabetic retinopathy, 29 of 38 fluids from volunteers with neovascularisation of the iris and 3 of 4 samples from volunteers with ischemic obstruction of the central retinal vein, suggesting that VEGF is a crucial component regulating active intraocular neovascularisation [98]. Moreover, beside the retina, vascular endothelial growth factor and its corresponding receptors have been suggested to be elevated in the renal glomeruli originating from streptozotocin-caused diabetic rats [99]. Also, another study confirmed the presence of elevated concentrations of VEGF specifically in the microvessels originating from the cochlea belonging to STZ-induced diabetic rats [100]. The elevated concentration of vascular endothelial growth factor in the placenta is further supported by high vascular permeability and also modifications in junctional proteins [95,97].

Further studies have suggested that elevated angiogenesis present in the fetoplacental vasculature can be found in a lot of cases of human type 1 diabetic placental samples [97,101–103]. Moreover, one of these studies from Mayhew undertaken in 2002 has highlighted using stereological results that even in appropriately-managed type 1 diabetic placental samples, there was an elevated angiogenesis which

happened largely via mechanisms of lengthwise development [97,102]. Vascular endothelial growth factor-A concentrations have also been found in placental samples originating from type 1 diabetic patients, with VEGF being located in the trophoblast layer found in intermediate and terminal stem villi tissue, as well as the endothelium compared to healthy pregnancies where it is located only on the terminal villous tissue [97]. As a mechanism of action point of view, *in vitro* angiogenesis taking place in the endothelial cells originating from the umbilical cord and the human placenta has been correlated with external inclusion of vascular endothelial growth factor and modified turnover of β-catenin and VE-cadherin [104,105].

Furthermore, hyperglycaemia in the maternal and potentially fetal circulation may have a significant effect on the mechanisms involved in the control of placental vascular permeability. When considering diabetes as a metabolic disorder *per se*, the elevation of glucose in the circulation gives rise to numerous consequences affecting the adjacent blood vessel wall and the surrounding tissues. Increased blood glucose concentrations have been proposed to have a straightforward consequence on the vasculature favouring, encouraging and supporting inflammation [106,107], angiogenesis [108,109], constriction [110,111], coagulation [110,112,113] and permeability [114,115].

Another cause supporting the malfunction of the placental circulation is increased insulin concentrations in the fetal vasculature. This happens during the second and third trimesters of the gestation period when the insulin receptor becomes expressed on the luminal area belonging to the capillaries of the fetus [116,117].

1.1.10 The human placental endothelium

The endothelium plays a key role in vascular physiology by coordinating vasomotor tone, modulating cellular exchange of nutrients, regulation of pro- and anti-coagulant factors and angiogenesis. It is important to point out that the endothelial cells could change their phenotype in accordance with their location in the human body, highlighting the heterogeneity of these cells. When it comes to the placenta, as an interesting fact, the vascular endothelium grows to a size of 550 km in length or it could cover a surface of 15 m^2 just before the labour [118]. Surprisingly, at the level of the stem villous and chorionic plate vessels, it has been pointed out that the gene expression profile is different between arterial and venous endothelial cells. To expand on this, placental venous endothelial cells have been shown to express genes linked to lipid metabolism. As a result, these endothelial cells could have a phenotype which is directly involved in the increased nutrient carriage to the fetus.

On the other side, microarray data suggests that the genes associated with placental arterial endothelial cells are closely related to signal transduction and further molecular cascade events linked to vascular endothelial growth factor A (VEGF) signalling [118].

The fetal endothelium and the external syncytial barrier play a crucial role in providing a continuous resistance to the movement of hydrophilic substances in a bilateral manner from the mother to the fetus. As a result, the integrity of the feto-maternal endothelial barrier has a pivotal importance when it comes to fetal development [119]. The human placental barrier is a structure composed of multiple layers consisting of basal membrane, endothelial cells (EC), cytotrophoblasts and syncytiotrophoblasts for the duration of the first trimester of pregnancy. As the gestation period progresses, the placental barrier of the mature placenta becomes

composed of EC, basal membrane and the syncytiotrophoblast [120]. Furthermore, the transport across the placental barrier is regulated by passive diffusion, facilitated diffusion, pinocytosis and active transport [121].

The endothelium of the human placenta is continuous and has well-defined cell-cell junctions preventing the motion of large molecular weight hydrophilic compounds (>65 kDa) alongside the paracellular junction [122,123]. Furthermore, adherens junctions are considered key modulators of paracellular permeability, particularly in the capillaries of the placenta, as well as transmembrane adhesion substances for instance vascular endothelial (VE)- cadherin. Elevated paracellular permeability may result via the phosphorylation of VE-cadherin that gives rise to breakage of the homophylic binding. This process leads to a loss in terms of interaction to peri-junctional actin followed by movement across the endothelial cells of adherens junction domains and finally giving rise to elevated growth of paracellular cleft size. Moreover, binding of VEGF-A to VEGFR2 has been demonstrated to increase the phosphorylation of VE-Cadherin at position Tyr-731 and Tyr-685 giving rise to elevated permeability to hydrophilic substances [124].

The human placenta possesses the pro-angiogenic and pro-permeability VEGF-A_{165}a and also the anti-angiogenic VEGF-A_{165}b, as well as placental growth factor (PIGF) and their corresponding receptors namely VEGFR2, VEGFR1, neuropilin-1 and also soluble Flt-1 (sFlt-1). In terms of growth factors secreted by this organ, there is a differential expression during the gestation period and also in pregnancies with complications. The most elevated expression of vascular endothelial growth factor A takes place during the first trimester of the pregnancy when *de novo* synthesis of placental vessels happens [125]. Also, a high expression of VEGF-A in the final trimester is predominantly found in the terminal villi close to the fetal capillaries

where the feto-maternal exchange takes place [126]. Furthermore, in pregnancies complicated by gestational diabetes for example, increased expression of VEGF-A accompanied by a deficit in the levels of junctional VE-cadherin and elevated vascular permeability have been reported [97]. On the other hand, in the case of pre-eclamptic patients, an emphasis has been placed on trophoblast derived factors, potentially syncytiotrophoblast microparticles having an impact on decreasing the function of the placental barrier and modifying the VE-cadherin localisation *in vitro* [127]. When it comes to VEGF-A_{165}b, the antiangiogenic splice variant expression in term placental samples has been considerably lower with reference to total VEGF levels. Furthermore, in pre-eclamptic patients, VEGF-A_{165}b expression has been shown to be further decreased [128]. However, the implication of VEGF splice variants in the adjustment placental vascular permeability has not yet been identified.

1.2 Overview of purinergic receptors

Purinergic signalling defined as nucleotides acting as signalling mediators outside of cells was initially suggested by Burnstock in 1972 [129]. In spite of this, the notion was not widely acknowledged prior to the early 1990's after which multiple pyrimidine and purine receptor subclasses were cloned and vigorously described comprising of 4 subtypes of P1 (adenosine) receptors, 7 subtypes of P2X ion channel pores and 8 subtypes of P2Y purinoceptors that are G-protein coupled [130]. Initial research was primarily focused on the pharmacology, biochemistry and physiology of purinergic signalling [131]. Adenosine 5'triphosphate (ATP) is a cotransmitter alongside other signalling mediators at the level of the central and peripheral nervous systems. Furthermore, purines are important extracellular transmitters which have a crucial influence on non-neuronal cells for instance inflammatory, secretory, endocrine, exocrine, immune, musculo-skeletal and epithelial cells [132]. Purinergic signalling is

fast in neuro-transmission and -modulation and also prolonged in migration, differentiation, apoptosis, proliferation and healing [133].

Adenosine regulates its responses via binding to 4 G-protein-coupled receptors (AR) namely A_1, A_{2A}, A_{2B} and A_3 which are present at the level of multiple tissues and cell types [134]. The expression of adenosine receptors has been illustrated for instance in the cerebral cortex by inspecting the targeted antagonism of adenosine-induced cyclic adenosine monophosphate build-up initiated by methylxanthines such as theophylline and caffeine [135]. The knowledge that adenosine receptors are involved in the pathophysiology of multiple human disorders have motivated scientists to investigate new compounds acting on the P1 purinoceptors [136]. Ongoing research gave rise to the discovery of multiple crucial compounds for instance antagonists, agonists or partial agonists, enzyme modulators and allosteric enhancers that possess numerous properties [137]. However, there are only few commercially available clinically approved adenosinergic compounds that have been discovered due to the intricacy of adenosine receptor signalling pathways. Beside adenosine, some AR-mediated compounds on the market include an A_{2A} adenosine receptor agonist (Regadenoson) that is administrated during imaging of the coronary artery but also an A_{2A} adenosine receptor antagonist used in the therapy of Parkinson's disorder that is solely prescribed in Japan namely Istradefylline. Furthermore, a particular attention has been allocated to investigating the discovery of novel A_3 adenosine receptor agonists which have demonstrated promising capabilities in the treatment of important disorders such as autoimmune conditions and cancer [134].

The expression of adenosine receptors varies in different tissues with intracellular actions depending on the effector coupling. All 4 adenosine receptors have been thoroughly characterised, cloned and pharmacologically investigated.

These purinoceptors possess a shared structure containing a principal domain that spans the plasmalemma 7 times in which each helix is between 20-27 amino acids long and connected by 3 extracellular and 3 intracellular domains [138]. The N-terminus located at the level of the extracellular space comprises of one or more glycosylation sites and the carboxyl terminus positioned in the intracellular space contains sites for palmitoylation and phosphorylation therefore possessing an important function in cellular mechanisms involving internalisation and desensitization [139].

Adenosine receptors are expressed at the level of the cardiovascular, nervous, gastrointestinal, respiratory, immune and urogenital systems but also in joints, eyes, bone and skin [137] – a vast distribution which suggests their complex implication in the regulation of cardiac, neuronal, renal and metabolic systems [140]. Every single adenosine receptor is uniquely distributed in various tissues and cells and may give rise to physiological effects that are mediated through certain secondary signalling mediators as illustrated in table 1 and figure 8. Moreover, A_1 and A_3 adenosine receptor signals are arbitrated via G_i and G_o subclasses of G protein family which result in a decrease in adenylate cyclase action and cyclic adenosine monophosphate abundance. On the other hand, A_{2A} and A_{2B} adenosine receptors are linked to G_s proteins which activate adenylate cyclase and elevate cyclic adenosine monophosphate levels giving rise to the stimulation of multiple regulators [139].

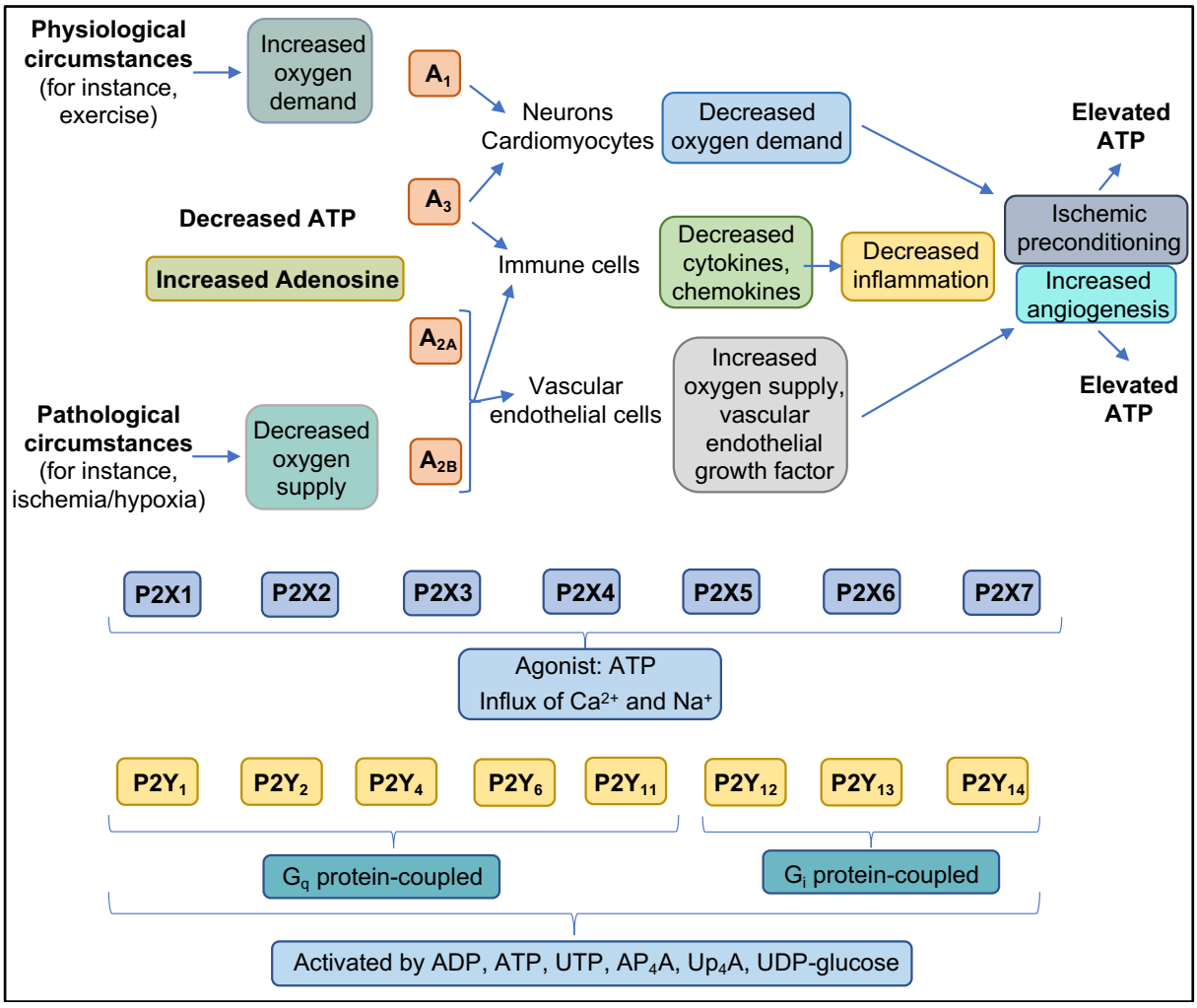


***Figure 8**. This figure shows some of the physiological functions of adenosine via its binding to A_1, A_{2A}, A_{2B} and A_3 adenosine receptors. The purine nucleoside acts as a critical local tissue function regulator by stimulating adenosine receptors which gives rise to a diminished inflammation and oxygen requirement, elevated oxygen perfusion and blood vessel synthesis from existing vasculature but also ischemic preconditioning. The circulating agonists which stimulate P2X and P2Y receptors are also illustrated. This figure was taken from Borea et al (2018)* [141] *and now includes the P2X and P2Y receptors showed in Ralevic and Dunn (2015)* [142] *(hand drawn by Paul Fodor using Microsoft PowerPoint software version 16.53).*

Name	A_1	A_{2A}	A_{2B}	A_3
G protein coupling	$G_{i/o}$	G_S	$G_SG_{q/11}$	$G_iG_{q/11}$
Effector system	Decreased adenylyl cyclase	Increased adenylyl cyclase	Increased adenylyl cyclase	Decreased adenylyl cyclase
	Increased Phospholipase C	Increased mitogen-activated protein kinase	Increased Phospholipase C	Increased Phospholipase C
	Increased K^+		Increased mitogen-activated protein kinase	Elevated phosphoinositide 3-kinase
	Elevated phosphoinositide 3-kinase			Increased mitogen-activated protein kinase
	Elevated mitogen-activated protein kinase			
Adenosine affinity	1-10nM	30nM	1000nM	100nM
Agonists	CCPA	CGS21680	NECA	Cl-IB-MECA
	R-PIA	UK-432,097	BAY60-6583	IB-MECA
	CPA	HE-NECA	R-PIA	MRS5698
	IB-MECA	NECA	IB-MECA	NECA
	NECA	R-PIA		R-PIA
				CGS21680
Antagonists	PSB36	SCH442416	PSB-603	MRE3008F20
	KW-3902	ZM241385	ZM241385	MRS1523
	DPCPX	SCH58261	MRS 1754	DPCPX
	Caffeine	DPCPX	DPCPX	ZM241385
	Theophylline	Caffeine	Caffeine	Caffeine
		Theophylline	Theophylline	Theophylline
Positive allosteric modulators	T62			LUF6000
	TRR469			

Table 1. *This table shows the types and mechanism of action of adenosine receptors. Adapted from Borea et al (2018)* [141].

The established 7 mammalian receptor subcategories (P2X1-7) constitute cationic pores gated by adenosine 5'-triphosphate. Three subunits give rise to a receptor pore with each subunit being formed of a polypeptide chain comprising of 2 membrane spanning domains (TM1 and TM2), an N-terminus, a C-terminus both positioned intracellularly and a substantial extracellular domain which extends 70Å above the membrane plane. The agonist-binding site is positioned at the cross-section of 2 adjacent subunits. The intracellular region expands less compared to the extracellular region and comprises of the "cytoplasmic cap" which is a particularly convoluted domain that contains multiple β-sheets. An exception is the P2X7 receptor which possesses 2 supplementary regions at the C-terminal end namely the cysteine-rich C-cys terminal and the cytoplasmic ballast [143]. There are currently no available selective agonists acting at P2X receptor subcategories, however medicinal chemistry provided a plethora of subtype-selective antagonists accompanied by negative and positive allosteric modulators [144,145]. Furthermore, selective antagonists as well as knockout mice have aided to determine the implication of P2X receptors in various disorders for instance hearing loss (P2X2), male infertility (P2X1), pain (P2X3), inflammatory bone decay (P2X5), neuropathic pain (P2X4) and lastly defective immune responses (P2X7) [146].

In terms of the general structure of P2X purinoceptors, there are 27 high-resolution P2X receptor conformations which have been elucidated over the last 10 years all sourced from truncated subunits, with the exception of the P2X7 receptor for which the entire-length conformation has been determined [146].

The mammalian P2X receptors give rise to heterotrimeric or homotrimeric pores with individual channels hosting 3 adenosine 5'-triphosphate binding pockets. Table 2 outlines the pharmacological (antagonist and agonist potencies) and

molecular attributes of all 7 P2X receptor subcategories. Adenosine 5'-triphosphate has considerable different potencies at each of the purinergic P2X receptor subcategories. The nucleotide is active at concentrations from low micromolar to under micromolar spectrum, with the P2X7 receptor being a special case which necessitates adenosine 5'-triphosphate levels in the hundred micromolar spectrum for stimulation [146].

In terms of P2X receptor agonists, ATPγS and 2-Methylthio-ATP possess a pharmacological signature comparable to adenosine 5'-triphosphate with both ATP analogues being more metabolically stable. Moreover, α,β-Methylene adenosine 5'-triphosphate is particularly potent at P2X1 and P2X3 purinoceptors and has a slightly lower potency at P2X4 receptors, with a further decreased potency at the P2X7 receptor. Also, β,γ-methylene adenosine 5'-triphosphate is particularly potent at P2X1 receptor and has lower potencies at all other P2X receptor subtypes. Furthermore, 2'(3')-*O*-(4-benzoylbenzoyl) adenosine 5'-triphosphate (BzATP) is occasionally characterised as a P2X7 receptor selective agonist. However, the compound is the most potent at P2X1 receptors and then at P2X3 receptors. In spite of this, as the compound is ten times more potent than ATP at the P2X7 purinoceptor, it is commonly applied to stimulate the cationic channel in order to prevent elevated, cytotoxic levels of adenosine 5'-triphosphate [146].

Considering non-selective P2X receptor antagonists, a few fairly potent compounds include Reactive blue 2, suramin, PPADS and iso-PPADS. Furthermore, the ATP analogue TNP-ATP is particularly potent (with decreased nanomolar IC_{50} values) at P2X3 and P2X1 receptors and has a low potency at P2X4 and P2X2 receptors [147]. Obrecht and colleagues (2019) have highlighted that aurintricarboxylic

acid is a potent suppressor of nucleases by non-competitively blocking both P2X3 and P2X1 purinoceptors [148].

In the case of positive allosteric modulators of P2X purinoceptors, ivermectin a central nervous system penetrant macrocyclic lactone has been utilised in both human and veterinary medicine as an anti-parasitic compound that binds to multiple ion pores as well as functioning as an positive allosteric modulator at P2X4 purinoceptors at concentrations ranging from 100nM up to 3μM [149,150]. Moreover, at 3μM the compound is active at human P2X7 receptors but not rat and mouse [151]. Also, MRS2219 is a selective potentiator of ATP-induced reactions at the level of recombinant P2X1 receptors (EC_{50} of 5.9μM) present in *Xenopus laevis* oocytes [152]. A further compound acting at the P2X2 receptor as a positive allosteric modulator (EC_{50} = 489nM) is PSB-10129 which gives rise to an elevation of approximately 3-fold in the maximal adenosine 5'-triphosphate-elicited current [153].

					NC-IUPHAR subunit nomenclature						
					P2X1	P2X2	P2X3	P2X4	P2X5	P2X6	P2X7
Molecular properties				Gene name	P2RX1	P2RX2	P2RX3	P2RX4	P2RX5	P2RX6	P2RX7
				Human chromosome location	17p13.3	12q24.33	11q12.1	12q24.32	17p13.3	22q11.21	12q24.31
				Protein length (amino acids)	399	471	397	388	444	441	595
				C tail length	41	113	56	29	82	87	240
				Membrane expression	Good	Good	Good	Good	Poor	Usually no expression	Good
				Desensitization (complete in)	Fast (<1s)	Slow (>20s)	Fast (<1s)	Slow (>20s)	Slow (>20s)	N.A.	Slow (>20s)
				Activation dependant endocytosis	Yes	No	N.A.	Yes	N.A.	N.A.	N.A.
Pharmacology	Agonists (EC_{50} values [μM])			ATP	0.56-0.70	2-8	0.5-1	1-10	0.44-10	12	100 (r)
				2-MeSATP	0.07-1	1	0.35	0.29	0.5-10	9	178
				ATPγS	2.3	1.5 (r)	0.7	2.3 (r)	0.5	1.3 (r)	138
				α,β-MeATP	0.1-1	>300	0.74	0.81	160 to >300	>100	>300
				β,γ-MeATP	2	>300	>300 (r)	>300	11.8 (r)	N.A.	N.A.
				BzATP	0.002	0.75	0.08	0.5	6-40	25	5
	Antagonists	Non-selective antagonists		Suramin	1-2	10	3	>300	2-3	N.A.	>300
				PPADS	1	1	1	>500	3	>100	10-50
				RB-2	30 (r)	0.4-0.5	N.A.	N.A.	18.3 (r)	N.A.	N.A.
		Nucleotide derived antagonists		TNP-ATP	0.006	1-2	0.001	1.5-15	0.45 (r)	N.A.	>30
				2',3'-O-Benzylidene-ATP	0.002	5.5	0.08	0.49	40	25	52
				DT-0111	N.A.	N.A.	0.3 (P2X2/3)	N.A.	N.A.	N.A.	N.A.
		Non-nucleotide derived antagonists	P2X1 receptor antagonists	PSB-2001	0.019	>10	>10	0.156	N.A.	N.A.	0.175
				PSB-2014	0.0231	>10	>10	0.209	N.A.	N.A.	0.196
				PSB-2013	0.058	>10	>10	0.049	N.A.	N.A.	0.177
			P2X2 Receptor antagonists	NF770	1	0.019	0.08	>100	N.A.	N.A.	>100
				PSB-10211	N.A.	0.09 (r)	N.A.	N.A.	N.A.	N.A.	N.A.
				PSB-1011	0.42 (r)	0.08 (r)	0.49 (r)	>10 (r)	N.A.	N.A.	>10 (r)
			P2X3 Receptor antagonists	A-317491	>10	>100	0.1	>100	N.A.	>100	>100
				Gefapixant	>10	0.100-0.250 (P2X2/3)	0.03	>10	>10 (r)	N.A.	>10
				AF-353	>10	>10	0.006	N.A.	>10	N.A.	>10
			P2X4 Receptor antagonists	5-BDBD	>10 (r)	>10 (r)	>10 (r)	0.35-0.5	N.A.	N.A.	>10 (r)
				NP-1815-PX	>30	7.3	>30 (r)	0.26	N.A.	N.A.	>30
				PSB-12054	6.5	>10	>10	0.19	N.A.	N.A.	>10
			P2X7 Receptor antagonists	A-438079	>100	>100	>100	>100	N.A.	>100	0.06-0.5
				A-804598	>100	>100	>100	>100	N.A.	>100	0.010 (h,r,m)
				A-740003	>100	>100	>100	>100	N.A.	>100	0.04-0.05
	Positive allosteric modulators			Ivermectin	N.A.	>30	>30	0.25	N.A.	N.A.	>30 (r,m)
				MRS2219	5.9 (r)	>100 (r)	>100 (r)	>100 (r)	N.A.	N.A.	N.A.
				PSB-10129	N.A.	0.489	N.A.	N.A.	N.A.	N.A.	N.A.
	Modulatory Cations			Zn^{2+}	N.A.	Increase EC_{50}=7μM	N.A.	Increase 2μM	N.A.	N.A.	N.A.
				H^{+}	Decrease pKa 6.3	Increase pKa 7.3	Decrease pKa 6.0	Decrease pKa 6.8	N.A.	N.A.	Decrease pKa 6.1
Physiology and pathophysiology				Major cellular expression	Smooth muscle	Neurons	Pain-sensing neurons	Neurons, microglia	Skeletal muscle	Broad expression	Immune cells
				Major role	Neuroeffector transmission	Taste, hearing	Pain, bladder reflexes, taste	Vascular remodelling, neuropathic pain	Inflammatory bone loss	N.A.	Inflammation, neurodegenerative disorders
				Model native cell type	Vas deferens, myocytes	SCG, myenteric plexus neurons	Small DRG neurons	Macrophages	Skeletal myocytes	N.A.	Monocytes, macrophages, microglia
				KO available	Yes	Yes	Yes	Yes	Yes	Yes	Yes

Table 2. *This table highlights the pharmacology and molecular properties of recombinant homomeric P2X receptors. The pharmacological values are related to homotrimeric receptors unless otherwise stated. "h" suggests human unless noted "r" denotes rat, "m" illustrates mouse, "N.A." highlights not available, DRG stands for dorsal root ganglion, KO indicates knockout, NC-IUPHAR represents International Union of Basic and Clinical Pharmacology Committee on Receptor Nomenclature and Drug Classification, SCG underlines superior cervical ganglion. The table has been adapted from Illes et al (2021) [146].*

In total, 8 G-protein coupled P2Y purinoceptor subtypes may become stimulated by circulating mononucleotides for instance adenosine 5'-diphosphate, adenosine 5'-triphosphate, uridine diphosphate or uridine triphosphate, by dinucleotides for instance diadenosine tetraphosphate or diuridine tetraphosphate and by nucleotide sugars for instance uridine 5'-diphosphoglucose [154]. Selective antagonists and agonists are crucial in investigating the function of P2Y purinoceptor subcategories from the perspective of physiology and pathophysiology [155]. For each of the P2Y purinoceptors, the structure-function connection was established with a high degree of accuracy via chemical approaches. In the majority of investigations, recombinant receptor proteins were utilized in the assessment of the acquired data [154]. Table 3 highlights the properties of human P2Y purinoceptors and principal agonist and antagonist compounds.

Important phylogenetic investigations and consequential characterisation of the developmental history of the G-protein coupled receptor (GPCR) superfamily showed multiple crucial divisions of GPCR's namely the adhesion/secretin-, rhodopsin- and glutamate-like metabotropic receptor subclasses [156]. Taking into consideration the amino acid arrangement correlations, P2Y purinoceptors are part of the rhodopsin-like receptor division, particularly to the δ subclass within this division. Furthermore, the δ subclass does not comprise only of the P2Y purinoceptors but also of hydroxycarboxylic acids, lipids and peptides [154].

The phylogenetic connection of P2Y purinoceptors subclassifies them into 2 main subdivisions which are closely related to their favoured G protein pairing. The first group includes $P2Y_1$, $P2Y_2$, $P2Y_4$, $P2Y_6$ and $P2Y_{11}$ purinoceptors which are G_q-paired $P2Y_1$ receptor-like and the second group includes $P2Y_{12}$, $P2Y_{13}$ and $P2Y_{14}$ purinoceptors which are G_i-paired $P2Y_{12}$ receptor-like [154].

The cellular origins of nucleotide agonists acting at the level of P2Y purinoceptors consist of endocytosis, lysis during cellular injury, co-transmission and excretion via pannexin 1 hemichannels [157]. Furthermore, the individual P2Y purinoceptors are corelated with numerous G proteins as well as signalling cascades (as it was demonstrated in the case of the $P2Y_1$ purinoceptor) which comprise of both G protein- dependent and -independent for instance β-arrestin pathways [158]. A few of these P2Y purinoceptors are further linked to $G_{12/13}$ ($P2Y_2$ and $P2Y_6$) or G_s ($P2Y_{11}$) proteins. Moreover, the P2Y purinoceptors coordinate mitogen-activated protein kinase signalling cascades and therefore may influence cell division and metabolism [159].

Structural investigations of P2Y purinoceptors have provided substantial advances in the pharmacology field over the last decade. During 2014 and 2015, 5 configurations of 2 important receptors namely $P2Y_1$ and $P2Y_{12}$ from 2 subfamilies were resolved [160–162]. These configurations via which the purinoceptors are visualised interacting with various compounds that alter their chemical composition and binding location give crucial observations into compound identification and stimulation of P2Y purinoceptors [154].

The P2Y purinoceptors are expressed in the brain particularly in the vasculature, glial cells and neurons. Furthermore, endothelial $P2Y_1$, $P2Y_2$, $P2Y_4$ and $P2Y_6$ purinoceptors give rise to vasorelaxation. However, smooth muscle $P2Y_2$, $P2Y_4$ and $P2Y_6$ purinoceptor stimulation results in vasocontraction. In the case of the pancreas, $P2Y_1$ and $P2Y_6$ purinoceptors activate while $P2Y_{13}$ receptors supress insulin release. Antagonists of $P2Y_{12}$ purinoceptors prevent the formation of blood clots. Furthermore, P2Y receptor agonists usually promote inflammation while antagonists could subsequently ameliorate inflammatory disorders [154].

Group	Subclassification, gene symbol, chromosome	Principal G protein coupling; expression	Compound Agonist/Antagonist	pEC_{50}, pIC_{50} or pK_i	Other interactions, Subtype
$P2Y_1$-like	$P2Y_1$, P2RY1, 3q25.2	G_q; heart, platelets, intestine, skeletal muscle, brain	ADP	5.09	$P2Y_{12,13}$
			2-MeSADP	5.6	$P2Y_{12,13}$
			MRS2365	9.4	Selective
			ADPβS	5.62	$P2Y_{12}$
			MRS2500[a]	9.02	Selective
	$P2Y_2$, P2RY2, 11q13.4	Gq, G_i; immune, endocrine and reproductive systems, cardiac and skeletal muscle, lung, intestine	UTP	7.22	$P2Y_4$
			MRS2698	8.1	Selective
			ATP	7.07	$P2Y_{4,11}$ + others
			Ap_4A	6.1	$P2Y_{12}$ and others
			Up_4U	6.68	$P2Y_4$ (6.89), $P2Y_6$ (5.94)
	$P2Y_4$, P2RY4, Xq13.1	G_q, G_i; placenta, prostate, brain, fat, intestine, lung, heart	UTP	6.26	$P2Y_2$
			GTP	5.18	Nonselective
			MRS4062	7.64	Selective
			ATP[b]	6.15	$P2Y_{2,11}$ +others
			PSB-16133	6.63	Selective
	$P2Y_6$, P2RY6, 11q13.4	G_q; spleen, lung, heart, kidney, placenta	UDP	6.28	$P2Y_{14}$ (6.80)
			Up_3U	6.57	$P2Y_2$ (5.88), $P2Y_4$ (6.06)
			MRS2957	7.92	$P2Y_2$ (6.77), $P2Y_4$ (6.10)
			PSB-0474	7.15	Selective
			MRS2693	7.83	Selective
	$P2Y_{11}$, P2RY11, 19p13.2	G_qG_s; intestine, spleen, immunocytes	ATP	4.77	$P2Y_{2,4}$ +others
			ATPγS	4.62	$P2Y_{2,4}$ +others
			AR-C67085	8.5	$P2Y_{12}$
			Sp-α-borano-ATP	6.47	$P2Y_1$ (5.92)
			NF546[c]	6.27	Selective
$P2Y_{12}$-like	$P2Y_{12}$, P2RY12, q25.1	G_i; brain, platelets, immunocytes	ADP[a]	7.22	$P2Y_{1,13}$
			2-MeSADP	8.3	$P2Y_{1,13}$
			Ap_4A	6	$P2Y_4$ (5.9), $P2Y_{13}$ (6.7)
			PSB-0739	9.8	Selective
			AZ11931285[a]	9	Selective
	$P2Y_{13}$, P2RY13, 3q25.1	G_i; spleen, myeloid cells, brain	ADP	7.94	$P2Y_{1,12}$
			2-MeSADP	7.72	$P2Y_{1,12}$
			MRS2211	5.97	Selective
	$P2Y_{14}$. P2RY14, 3q25.1	G_i, Immune and endocrine system, intestine, brain, muscle, lung, pancreas, kidney	UDP[a]	6.8	$P2Y_6$
			UDP-glucose[a]	6.45	$P2Y_2$
			MRS2690	7.31	Selective
			MRS2802	7.2	Selective
			MRS2905	8.7	Selective

Table 3. *This table shows the characteristics of human P2Y purinoceptors and principal agonists and antagonists. "a" denotes used as a radioligand when labelled with [^{3}H], [^{32}P], [^{33}P] or [^{125}I]. "b" suggests ATP acts as an antagonist at human $P2Y_4$ receptor but an agonist at mouse or rat $P2Y_4$ receptor. "c" suggests NF546 stimulates the $P2Y_{11}$ receptor even if it belongs to a structural class of antagonists. This table has been adapted from Jacobson et al (2020)[154].*

1.3 The dual control of human vascular tone by endothelial cells and perivascular nerves

Over the last few decades, the vascular tone was understood to be regulated via two opposing mechanisms specifically by sympathetic noradrenergic nerves, possessing the property to constrict blood vessels and by parasympathetic cholinergic nerves (although most blood vessels do not possess this innervation) with the main function implicated in vasorelaxation. Nevertheless, following the identification of important advancements in terms of cotransmission by Burnstock in 1976 [163], and about endothelium-derived relaxing factor(s) by Furchgott in 1984 [164], a better understanding of the dual management of vascular tone by multiple mediators released from endothelial cells and cotransmitters released from perivascular nerves was established [165–170]. Furthermore, endothelium-dependent vasorelaxation is primarily achieved via fluctuations in Ca^{2+} levels inside the endothelial cells as a result of a mechanical perturbation for instance plasmalemma elongation or shear pressure or intracellular agonists such as adenosine 5'-triphosphate, bradykinin or reactive oxygen species [171]. One crucial process of cell-cell interaction is regulated by the liberation of autocrine or paracrine messengers. In this case, prostaglandins, nitric oxide and adenosine 5'-triphosphate are particularly acknowledged as paracrine or autocrine mediators which are involved in multiple roles that regulate vascular function such as maintenance of vasomotor tone, platelet accumulation, smooth muscle growth, leucocyte infiltration and vascular permeability [172].

Figure 9 shows the involvement of purines and pyrimidines in the management of vascular tone via the involvement of P2 purinoceptors.

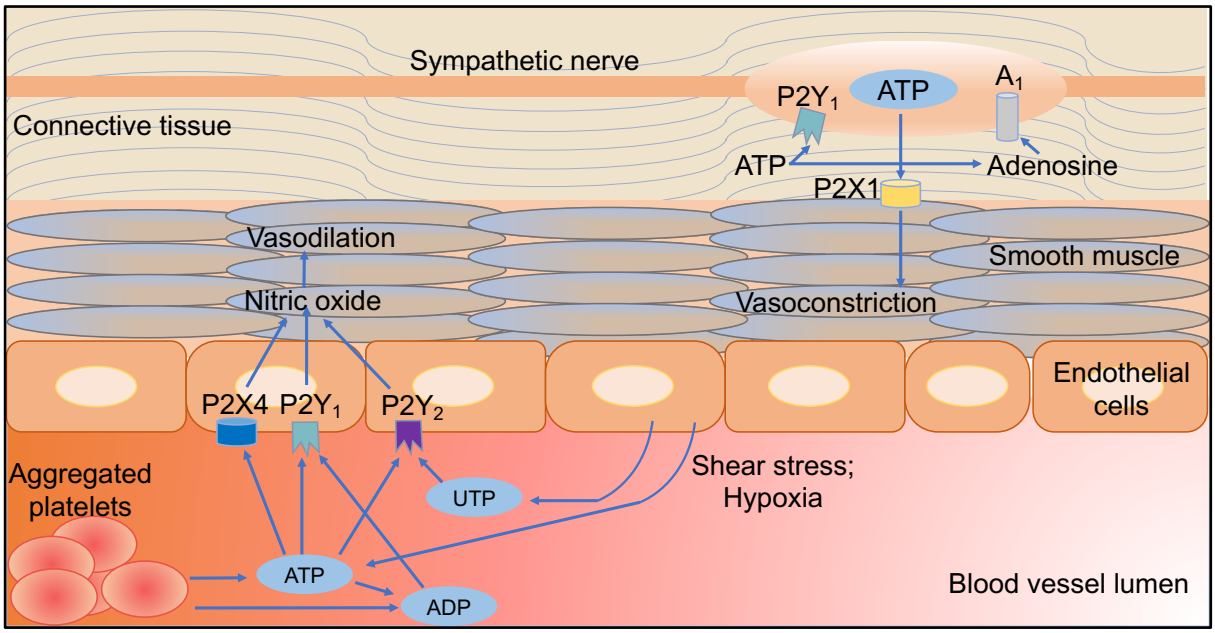


Figure 9. *This figure highlights the dual control of human vascular tone in a schematic fashion showing the purinergic signalling pathways involved in the initiation of vasodilation or vasoconstriction. This figure has been taken from Burnstock (2006) and slightly modified (hand drawn by Paul Fodor using Microsoft PowerPoint software version 16.53)* [173]*. The endothelial cells are the main contributors of vasorelaxation, along with the release of multiple endothelial cell vasodilator mediators for instance nitric oxide (NO), prostacyclin (PGI_2) or endothelium derived hyperpolarising factor (EDHF) which prevent platelets to adhere to the tunica intima layer. The A_{2A} and A_{2B} receptors are expressed on both endothelial and smooth muscle cells. Adenosine may become released from multiple sources including the endothelial cells as well as the red blood cells, with shear stress and low oxygen levels being well known activators of these cells. Purinergic P2Y and P2X1 receptors located at the level of the smooth muscle membrane play an important role in the initiation of vasoconstriction. Injured endothelial cells promote the adherence and accumulation of platelets at the site of damage and further promote the platelet release of adenosine 5'-triphosphate and adenosine 5'-diphosphate which cause vasoconstriction. Perivascular sympathetic nerves located at the level of tunica adventitia simultaneously release in the extracellular space ATP, noradrenaline (NA) and neuropeptide Y (NPY) which have the capacity to stimulate P2X1, α_1 and NPY receptors expressed on the smooth muscle to give rise to vasoconstriction.*

The feasibility that adenosine 5'-triphosphate (ATP) was released in tandem with noradrenaline from the sympathetic nerves located at the level of the portal vein in rabbits was proposed in the late 1970's by Che Su [174], followed by the recognition of two main classes of purine receptors [175]. Later on, in 1989, P2 receptors were found localised on vascular endothelial cells as well as smooth muscle cells [176]. Towards the early 1990's, the release of adenosine 5'-triphosphate from endothelial cells under

the exposure of multiple fluctuations of blood flow and decreased levels of oxygen has been shown by Bodin and colleagues [177]. Further conceptual advances were later proposed related to the process of ATP translocation from vascular endothelial cells via vesicular exocytosis [178–180] but also through connexin 43 hemichannels [181–183].

Ectonucleotidases are ectoenzymes present on the plasmalemma of cells and have an important function of detecting changes in the extracellular levels of nucleosides and nucleotides [184–186]. These enzymes consist of ectonucleotidase 5'-triphosphate diphosphohydrolases (E-NTPDases) for instance E-NTPDase1 or in other words CD39 which has a main function of hydrolysing nucleoside di- and tri-phosphates present at the level of plasma membrane of smooth muscle and endothelial cells [187]. Another important ectonucleotidase is E-NTPDase2 also called CD39L1 which is mainly located on the abluminal side of blood vessels with the main function of hydrolysing nucleoside triphosphates. Moreover, alkaline phosphatases and ecto-5'-nucleotidases for instance CD73 are involved in the conversion of AMP to adenosine in the extracellular space. Also, the concentration of nucleotides outside cells and their stimulation of purine receptors positioned on the membrane of cells is tightly regulated in terms of release towards the extracellular space and hydrolysis by ectonucleotidases [188]. Figure 10 highlights the extracellular metabolism of ATP to adenosine along with their corresponding vasoactive and inflammatory effects.

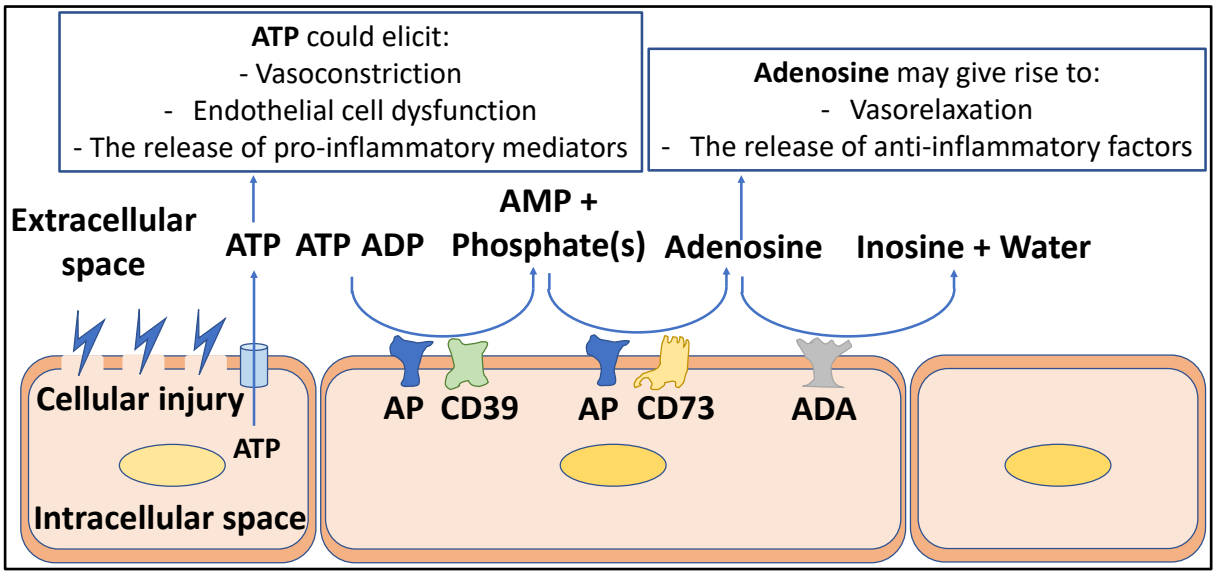


***Figure 10**. This scheme highlights the adenosine 5'-triphosphate and adenosine metabolism in vivo. Cellular injury causes the release of ATP outside of cells which in turn is hydrolysed giving rise to adenosine 5'-diphosphate, adenosine monophosphate as well as adenosine via ectonucleotidases CD39, CD73 and alkaline phosphatase (AP). Adenosine is then metabolised to inosine and water via adenosine deaminase (ADA). This figure has been hand drawn by Paul Fodor using Microsoft PowerPoint software version 16.53 and is taken from Spaans et al (2014)* [85].

1.3.1 Endothelial cells involvement in the management of vascular tone

Vascular endothelial cells possess purinergic P1 and P2 receptors. These cells are able to release purines which may further stimulate these receptors and could regulate the extracellular concentrations of liberated nucleotides via the activity of ectonucleotidases present on their membrane [189]. One of the most important roles of endothelial cells is the regulation of vasodilation by opposing the vasoconstrictor effects of ATP and noradrenaline secreted from perivascular sympathetic nerves [190]. Furthermore, beside the involvement of endothelial cells in autocrine stimulation by purines, these cells also interact with nucleosides and nucleotides secreted from blood cells or even myocytes under the stimulation of multiple factors, which may activate purinergic P2 receptors and ultimately giving rise to vasodilation [191].

Some important purinergic receptors present on the membrane of the human endothelial cells are A_{2A} and A_{2B} for adenosine and also $P2Y_1$, $P2Y_2$ and P2X4 [192]. The stimulation of endothelial cells via purines gives rise to the secretion of nitric oxide (NO), prostacyclin (PGI_2) and also endothelium-derived hyperpolarizing factor (EDHF) which in turn elicits a decrease in platelet accumulation and ultimately the relaxation of the vasculature [193–196].

Adenosine 5'-triphosphate is secreted from isolated primary endothelial cells under alterations of blood flow which also implicates shear stress [197–199] and also under activation via hypotonic test [200]. The adsorption by endothelial cells of adenosine and its metabolism leading to the synthesis of adenosine 5'-triphosphate was characterised in the late 1970's [176], accompanied by the secretion of ATP from neutrophil elastase [201]. The physiological importance of adenosine 5'-triphosphate secreted by endothelial cells under the influence of shear pressure is to stimulate purinergic P2 receptors, ultimately giving rise to a change in the territorial or potentially systemic contractility, especially in terms of vasorelaxation [202]. Secreted ATP into the extracellular space can also stimulate endothelial cells to further release adenosine 5'-triphosphate through local signalling by further managing an integrated endothelial cell feedback at the level of P2X4 and P2Y receptors [197,203]. The coordinated process of the secretion of adenosine 5'-triphosphate from endothelial cells has not been elucidated yet. In the early 2000's, a study revealed that the mechanism of ATP secretion from vascular endothelial cells was achieved via vesicles [178]. Approximately 10 years later, further research revealed that pannexin 1 and connexin channels also contribute to the secretion of adenosine 5'-triphosphate [204,205]. A further study published by Yamamoto and colleagues in 2011 has shown that caveolin-1 knockdown with siRNA prevented the confined secretion of adenosine 5'-triphosphate

from endothelial cells and that multiple Ca^{2+} pulsations at caveolae sites in vascular endothelial cells were initiated by the liberation of ATP from these cells [206]. Moreover, ATP is an exceptionally potent constrictor especially at the level of small diameter blood vessels and is mainly synthetized by the endothelium with the function to principally stimulate purinergic P2X1 receptors located on the surface of smooth muscle cells [207,208]. In another study, a further suggested endothelium synthetized vasoconstricting mediator released from isolated endothelial cells of human dermal microvessels was uridine adenosine tetraphosphate (Up_4A) [209]. The ectonucleotidase CD73 which is involved in the hydrolysis of adenosine monophosphate (AMP) giving rise to adenosine, is mainly localised on the membrane of endothelial cells with interferon-α promoting an increase in the expression of the enzyme, ultimately giving rise to adenosine synthesis especially in human umbilical vein endothelial cells [210,211].

1.3.1.1 P1 - Adenosine receptors

Two of the most important functions of adenosine are firstly to impede the release of sympathetic neurotransmitters through mechanisms involving receptors located in the prejunctional space [212] and secondly in vasorelaxation through interactions with smooth muscle and also endothelial cells [213,214]. These events result in an elevation in perfusion, especially towards tissue found in an ischaemic state or depleted of oxygen. Currently, all purinergic P1 receptors corresponding to adenosine such as A_1, A_{2A}, A_{2B} and A_3 have been localised at the level of the smooth muscle and endothelial cells with an elevated preponderance of A_{2A} and A_{2B} receptors [141]. Early studies in the 1990's have shown that the secretion of nitric oxide from endothelial cells gave rise to a potent vasorelaxation outcome which complemented the response of adenosine especially in humans at the site of the iliac artery [215,216]. Furthermore,

the purinergic A_{2A} and A_{2B} receptors have been comprehensively characterised in endothelial cells isolated from the human aorta [217].

Beside the fundamental function of adenosine in the vasorelaxation response under the influence of low levels of oxygen, a further study has suggested a potential involvement of the purine in the initiation of angiogenesis when a significant restriction of blood supply occurs to various tissues. In this case, the newly formed vasculature allows the delivery of elevated levels of oxygen to inadequately perfused blood vessels [218]. Another investigation by Feoktistov and colleagues in 2002 has also revealed that adenosine A_{2B} receptors present on the surface of isolated human microvascular endothelial cells were able to alter the presence of extracellular angiogenic mediators [219]. Moreover, the stimulation of A_{2B} receptors localised on primary retinal endothelial cells elevates the synthesis of vascular endothelial growth factor (VEGF) alone and also via exposure to low levels of oxygen and further promote cell growth [220,221]. Due to the fact that adenosine A_{2B} receptors play a crucial function in regulating the vascular tone, a further study has shown that decreased oxygen supply may influence the abundance of adenosine receptors in endothelial cells of human origin by encouraging a change in the presence of purinergic A_{2A} to A_{2B} receptors [222]. Another study has also highlighted dissimilarities among human small and large size blood vessel endothelium reactions to β adrenergic and adenosine receptors under the influence of decreased levels of oxygen [223].

Circulating adenosine has been proposed to possess properties against the formation of blood clots especially at the level of the vascular endothelium by stimulating A_{2A} and A_3 receptors and in turn supressing the endothelial cell tissue mediator levels notably via mechanisms involving hypoxia and the development of atherosclerotic plaques, which are strongly related to elevated concentrations of

purines [224,225]. Cytokines can also influence the presence of A_{2A} and A_{2B} receptors in endothelial cells of human blood vessels [226,227]. The importance of A_{2A} receptors expressed on endothelial cells has been extensively documented in a study by Thakur and colleagues in 2010 where the authors have suggested that the adenosine receptor plays a crucial role in the release of reactive oxygen species under the influence of angiotensin II, but also the involvement in regulating redox signalling pathways [228]. Additionally, the synthesis of adenosine is significantly restricted by white blood cells which can attach to the vascular endothelial cells and further impair the their permeability role via a CD73-reliant signalling pathway [229,230].

Adenosine has also been shown to mediate the function of endothelial progenitor cells [231,232]. This control is achieved by increasing the expression of CXCR4 receptor for cytokines involved in chemotaxis and also via activating their enrolment in the infarcted heart thereby supporting restoration [233]. A further study published in 2012 also revealed that A_{2A} and A_3 receptors play an important role in the movement of primary endothelial progenitor cells [232].

1.3.1.2 P2X receptors

A study published by Ray and colleagues in 2002 has highlighted that purinergic P2X1, P2X4, P2X7 and $P2Y_2$ receptors have been localised at a tissue level on human radial and internal mammary arteries, as well as on the saphenous vein particularly on the endothelium, with a high preponderance of P2X4 receptors present in the vein relative to the arteries [234]. A similar study investigated the preponderance of P2 receptors in human umbilical vein endothelial cells (HUVEC) and human mammary arteries and showed that P2X1 receptor was highly expressed on the smooth muscle and that P2X4, $P2Y_1$ and $P2Y_{11}$ receptors were present with an increased preponderance on the endothelial cells [235]. In this case, the group has also

presented evidence that the purinergic $P2Y_2$ and $P2Y_6$ receptors were also localised with a decreased preponderance in both endothelial and smooth muscle cells. Moreover, P2X4 and P2X5 receptors have been localised at the level of the human pulmonary and coronary arteries, aorta and also human umbilical vein endothelial cells [200,236,237]. P2X4 and P2X6 receptors have been shown to be locally expressed at the sites of paracellular overlapping regions of HUVEC cells and have been proposed to accompany CD144, which has been described as an important transmembrane adhesion mediator [238]. Currently, the role of endothelial purinergic P2X receptors has not been elucidated yet. The P2X4 receptor has been characterised in great detail compared to all other subtypes of P2X receptors as having an important role in the regulation of vasorelaxation from the perspective of functioning as mechanotransducers under the exposure of adenosine 5'-triphosphate originating from the endothelium [239,240]. Yamamoto and colleagues in 2006 have demonstrated that a knockout (KO) of the P2X4 receptor in mice gives rise to a significantly reduced vasorelaxation reaction of the endothelium to sheer stress, accompanied a considerable decrease in nitric oxide synthesis and an elevated blood pressure [239]. Moreover, P2X4 receptor knockout in isolated human umbilical vein endothelial cells has been shown to regulate adenosine 5'-triphosphate generated Ca^{2+} entry into the primary cells [241].

A minimum of 7 *P2rx7*$^{-/-}$ mouse models have been created and highlight deficiency in cytokine liberation towards the extracellular space, immune function and diminished neuropathic and inflammatory pain [146]. The removal of *P2rx7* is advantageous in multiple inflammatory disorders. Moreover, changes in bone composition (*P2rx7*^{tm1Gab}) and an anti-depressant-like characterisation (*P2rx7*^{tm1Lex}) have been described. A floxed humanised P2X7 receptor knock-in mouse

(*P2rx7*$^{tm1.1(P2RX7)Jde}$) highlighted an atypical sleep cycle following hP2X7R removal [146]. Although important information has emerged based on early studies involving knock-out models, a few limitations have to be taken into account: *P2rx7*^{tm1Ipch} and *P2rx7*^{tm1Gab} mice possess different splice variants and incomplete receptor transcripts. As an example, the P2X7k variant present in the *P2rx7*^{tm1Ipch} mouse is functional and particularly expressed in T cells [242]. There are no studies on P2rx7 KO mice that have characterised the pregnancy phenotype in these mice. However, P2rx7 knockout mice under various genetic background are affected by glucose intolerance, elevated glucose levels, defective beta cells activity under the exposure to a high-sucrose diet [243], but also exhibit pathophysiological adipose tissue distribution [244].

On the contrary, assessments of isolated HUVEC cells in terms of UTP- and ATP-generated Ca^{2+} movement, as well as nitric oxide synthesis and membrane hyperpolarisation did not establish any functional role of P2X receptors, concluding that the purinergic $P2Y_2$ isoform was responsible for the corresponding cellular actions mediating vasorelaxation [245]. Human umbilical vein endothelial cells exposed to changes in laminar flow highlighted a gradual decrease of mRNA expression starting after 60 minutes to the point of declining to 60% at 24 hours [246]. A study published by Wilson and colleagues in 2007 has shown that under the influence of an inflammatory microenvironment, the expression of purinergic P2X4 and P2X7 receptors by HUVEC cells significantly increased [247]. In this case, the stimulation of purinergic P2X7 receptors gave rise to an elevation of multiple subtypes of the potent interleukin type 1 cytokines, ultimately altering the equilibrium between anti- and pro-inflammatory mediators responsible in establishing the physiological function of the vasculature [247]. Also, interferon-γ mediated elevation in *P2RX4* gene expression has been described in HUVEC and microvascular endothelial cells by Tang and colleagues in 2008 [248].

Moreover, a study by Ray *et al* (2002) presented evidence that the expression of the purinergic P2X4 receptor was considerably elevated in the human saphenous vein relative to internal mammary and radial arteries [234]. The authors concluded that the for the purposes of coronary bypass operation, the potential vein grafts were highly vulnerable to generating a built-up of plaque inside the blood vessels [234].

1.3.1.3 P2Y receptors

The majority of blood vessels possess on the membrane of the endothelium cells two important purinergic receptors namely $P2Y_1$ stimulated by ATP and ADP and $P2Y_2$ stimulated by ATP and UTP, with a few vessels also expressing $P2Y_4$ receptors stimulated by UTP and $P2Y_6$ receptors stimulated by UDP [235,249]. The stimulation of P2Y receptors expressed on the surface of the endothelium gives rise to an elevation in intracellular Ca^{2+}, causing a secretion of PGI_2, NO and EDHF, with the last two generating a vasorelaxation effect via $P2Y_1$, $P2Y_2$ and $P2Y_4$ purinergic receptors [189,195,250]. In the case of PGI_2, the endothelium-reliant vasodilation consequences vary according to the purinergic receptor isoform and to the kind of blood vessel [251]. The nitric oxide and prostacyclin released from the endothelial cells prohibit platelet aggregation [252]. On the other side, adenosine 5'-diphosphate and adenosine 5'-triphosphate may activate the secretion of von Willebrand factor from endothelial cells *in vitro* potentially encouraging homeostasis [253–255]. Additionally, the stimulation of purinergic $P2Y_2$ receptors present on the surface of endothelial cells of the human coronary artery was demonstrated to elevate the synthesis of tissue factor (an important mediator of the physiological blood coagulation pathway) in the intracellular milieu [256,257]. As a result, beside the crucial straightforward actions of ATP and ADP in stimulating purinergic $P2Y_1$, $P2Y_{12}$ and P2X1 receptors to facilitate platelet aggregation, at the level of purinergic receptors expressed on the endothelium, the

activity of nucleotides and nucleosides may also give rise to anti- or pro-coagulant outcomes [258–260].

The process of nitric oxide secretion from the endothelium under the influence of adenosine 5'-triphosphate could implicate the Ca^{2+} stimulated Cl^- channels [250,261]. The greatly preserved sensor of decreased intracellular ATP concentrations namely adenosine monophosphate stimulated protein kinase (AMPK) could also participate in this mechanism by controlling the energy involved in maintaining a homeostatic equilibrium and is stimulated during particular challenging cellular demands for instance decreased oxygen levels or elevated concentrations of glucose [262]. This process leads to an accelerated secretion of adenosine 5'-triphosphate into the extracellular space especially from harmed tissues, platelets or even endothelial cells [263]. A study published by da Silva and colleagues (2006) has highlighted that UTP, ADP and ATP gives rise to phosphorylation and stimulation of AMPK in human umbilical vein endothelial cells through $P2Y_1$, $P2Y_2$ and potentially $P2Y_4$ [264]. Adenosine 5'-triphosphate stimulation of purinergic P2Y receptors especially in the aortic endothelial cells generates a continuous stimulation of phospholipase D which is closely associated with protein kinase C [265]. Da Silva and colleagues (2009) have presented evidence that extracellular nucleotide-dependent nitric oxide synthase activation via purinergic $P2Y_1$, $P2Y_2$ and potentially $P2Y_4$ receptors is protein kinase C-δ type and Ca^{2+} mediated, also further proposing that the signalling cascade could play a crucial role in the development of novel curative solutions for endothelial cell malfunction [266].

Furthermore, the activity of endothelial cells in maintaining physiological permeability levels has been shown to be mediated by adenosine 5'-triphosphate present in the extracellular space via stimulation of myosin light chain phosphatase

[267]. Also, β-nicotinamide adenine dinucleotide plays an important role in maintaining a healthy permeability activity of isolated primary pulmonary artery endothelial cells via $P2Y_1$, $P2Y_{11}$ purinoceptors, cyclic adenosine monophosphate (cAMP)- stimulated protein kinase A and also cAMP mediated signalling pathway EPAC1/Rap1/Rac1 involved in cytoskeleton readjustment [268].

Purinergic receptors namely $P2Y_2$, $P2Y_4$ and $P2Y_6$ expressed at the level of the smooth muscle cells possess a key role in vasoconstriction [154]. Furthermore, $P2Y_{12}$ receptors are expressed in the rat capillary endothelial cells [269]. However, other authors have presented evidence that the $P2Y_{12}$ receptor is expressed on the smooth muscle cells, potentially being involved in generating vasoconstriction as well as smooth muscle cell expansion in the course of atherosclerosis [270]. P2Y receptors are crucial in regulating vascular responses to injury in the case of restenosis [271] and atherosclerosis [272]. P2Y purinoceptors give rise to Ca^{2+} signals in vascular smooth muscle cells resulting in vasoconstriction, however the function of various P2Y subdivisions has not been fully elucidated yet [273].

1.4 The human P2X7 receptor

Abnormal placental development represents the principal pathophysiology in most disorders associated with the gestation period for instance preeclampsia (regarded as the most important cause of fetal and maternal mortality at a global level), recurrent miscarriage, fetal growth restriction and stillbirth [274,275]. From a cellular perspective, it has been indicated that preeclampsia and preterm birth [276] are caused by the stimulation of the P2X7 receptor [275]. The activation of this purinoceptor present on the surface of the placental cells [277] involves multiple signalling pathways which contribute to the pathogenesis of preeclampsia giving rise to necrosis, apoptosis [278] and inflammation via the assembly of the NLRP3 inflammasome and stimulation of

caspase-1 [279]. Since adenosine 5'-triphosphate is liberated into the extracellular space from endothelial cells under the influence of multiple stimuli such as inflammation, ischemia or hypoxia, it is anticipated that the nucleotide receptors especially P2X7 may be involved in adjusting the blood flow of the human placenta chorionic plate arteries through smooth muscle and endothelial cell mechanisms [280]. As the human placenta and umbilical vessels are unique in that they do not possess innervation [281], this process may take place in healthy and complicated pregnancies such as pre-eclamptic cases where the extracellular levels of ATP may increase up to 3-fold [282,283]. The NLRP3 inflammasome is assembled via the action of toxins such as lipopolysaccharide (LPS) activation of toll-like receptors (TLR's) [284]. A well-described mechanism connecting TLR's with the NLRP3 inflammasome involves the P2X7 receptor which was demonstrated to be localised and functional in cord blood mononuclear cells [285]. Although TLR4 gives rise to elevated synthesis of mRNA for pro-IL-1β, the processing of the pro-inflammatory cytokine to its mature and releasable form IL-1β is dependent on the K^+ exit from cells – a function which is undertaken by the P2X7 receptor [286]. Although multiple investigations have highlighted the connection between TLR4 and LPS resulting in pro-inflammatory cytokine liberation into the extracellular space, the activation with ATP further elevates IL-1β exit from cells via the P2X7 purinoceptor, a mechanism that could be the missing element of further understanding preterm birth.

1.4.1 Structure and function of the P2X7 receptor

The *P2RX7* gene encodes for the P2X7 receptor which is part of the P2X receptor sub-class of trimeric ligand-gated ion pores of which there are 7 separate channels (P2X1-7) [287,288]. From the entire family of purinergic P2X receptors, the human P2X7 monomeric subunit is composed of 595 amino acids [289]. The stimulation

with adenosine 5'-triphosphate of the P2X7 receptor enables the transmigration of Na^+, K^+ and Ca^{2+} through the membrane of cells [290–292]. On the other side, extended activation of P2X7 receptor with ATP gives rise to the establishment of a dilated pore through which organic ions may enter the cell [293–295]. The function of ectonucleotidases is to breakdown nucleotides for instance adenosine 5'-triphosphate and in turn to mediate the levels and the period of accessibility of extracellular agonists acting at the P2 purinoceptors [184,296]. As a result, the P2X7 receptor may solely become stimulated following cellular damage, infection, during elevation of extracellular adenosine 5'-triphosphate (eATP) in tumour environment or potentially when the expression of these enzymes becomes decreased [297,298].

1.4.2 Distribution of the P2X7 receptor

In the mammalian body, the purinergic P2X7 receptor is broadly expressed [132,299]. Initial studies highlighted that P2X7 was located on the surface of multiple cell types of hematopoietic lineage for instance macrophages, monocytes, dendritic cells, lymphocytes, mast cells, eosinophils, erythrocytes and osteoclasts [300,301]. Furthermore, emerging evidence suggests that the purinoceptor is also present on other variety of cells for instance fibroblasts, epithelial cells as well as osteoblasts [302]. Also, the P2X7 receptor is expressed by cells in the CNS and PNS such as astrocytes, oligodendrocytes, Schwann cells as well as microglia [303,304]. This receptor is also expressed in a few neuronal populations located in the hypothalamus, cerebellum, spinal cord and lastly substantia nigra [297,305,306].

The presence of the P2X7 receptor has been noted in both the smooth muscle and endothelium in the majority of the systemic venous and arterial vasculature in animal and human tissues [307–309]. The P2X7 distribution was reported as increased in the retinal microvasculature of a rat model of type 1 diabetes mellitus supporting an

elevated permeability of the microvasculature [310]. However, in human retinal endothelial cells, the P2X7 receptor stimulation gave rise to endothelial apoptosis [311].

Also, surgical elongation of saphenous veins of human origin used for coronary artery bypass grafts gave rise to P2X7 receptor stimulation, programmed cell death and ultimately abnormal vascular function [312]. The stimulation of this purinoceptor gives rise to vasoconstriction of the renal and retinal microvasculature and of increased internal diameter veins which in turn may cause elevated systemic vascular resistance [307,313–315]. Furthermore, the P2X7 receptor antagonism augmented endothelium-dependent vasodilation and in the aorta lowered vasoconstriction reactions to phenylephrine [316]. A further model evaluating the injury caused by vascular surgical elongation highlighted that the P2X7 receptor stimulation decreased endothelium-dependent vasodilation via lowered nitric oxide synthesis [317].

On the contrary, other studies have proposed that the P2X7 receptor stimulation could also be involved in vasorelaxation. P2X7 receptor stimulation of endothelial cells originating from murine mesenteric artery gave rise to elevated nitric oxide synthesis [318]. Furthermore, P2X7-dependent reaction to lipopolysaccharides has been shown to generate hyporeactivity of the thoracic aorta in mice resulting in P2X7-arbitrated low blood pressure in an IL-1β and nitric oxide dependent process [319,320].

Roberts and colleagues (2007) have highlighted that in first trimester (8-12 weeks' gestation) and term (38-41 weeks' gestation) human placental villous tissue, the P2X7 receptor expression at an mRNA level was particularly weak [321]. Also, the same study has shown that the P2X7 receptor expression at a protein level in the first trimester and term placental villous samples was often weak and not consistently detected [321]. The same study has also presented immunohistochemistry data

highlighting that the localisation of the P2X7 receptor in the first trimester and term villous placental tissue was predominantly intracellularly in association with the nuclei with minimal diffuse staining in the cytoplasm and a more intense staining in term tissue compared to the first trimester tissue especially at the level of the syncytiotrophoblast layer [321]. Another investigation has also highlighted that the P2X7 receptor was detected consistently in the protein extracted from isolated cytotrophoblast cells from term placental villous tissue using western blotting, with the P2X7 receptor products detected at approximately 145kDa [277].

Even if the P2X7 receptor is expressed in a variety of mammalian cells, its presence on various cells within whole tissues has not been elucidated yet.

1.4.3 The permeability of the P2X7 receptor

The purinergic P2X7 receptor was initially termed the P2Z receptor and is involved in regulating cellular permeability following the exposure to adenosine 5'-triphosphate [322]. This capability of the receptor following stimulation has been thoroughly investigated over the last few decades. This receptor is frequently capable of permeabilizing cells by allowing the passage of organic cations for instance YO-PRO-1^{2+}, ethidium^{+} as well as *N*-methyl-D-glucamine^{+} through the membrane of cells [323–325]. Furthermore, organic anions for instance carboxyfluorescein as well as lucifer yellow could penetrate through the plasmalemma potentially via a similar permeabilization route [326–328]. Ongoing studies have attempted to investigate if this P2X7 receptor property of allowing increased anion and cation entry is due to an intrinsic capability of the purinoceptor or potentially via association with a certain protein. Multiple investigations have revealed that the exclusive distinguishing carboxyl-group terminal of P2X7 receptor is vital in the establishment of the dilated channel [329]. Moreover, the truncation of this receptor supresses the entry of dyes

without compromising ion currents passing through the pore [290,291,329,330]. In this case, an important leap in comprehending this process came with the discovery of pannexin-1 (Panx1) as a potential hemichannel participating in dye entry into the cytosol [295,331]. However, subsequent investigations showed that Panx1 was unlikely to contribute to the establishment of a P2X7 macropore [332–334]. On the other side, patch clamp traces of biphasic P2X7 receptor currents indicate the possibility of a macropore formation, as the majority of current that enters the cell is facilitated through a complementary permeability signalling cascade [335,336].

1.4.4 Gating of the P2X7 receptor

The interaction between ligand-gated ion pores and their corresponding agonists gives rise to the initiation of a signal at the domain of the protein associated with closing and opening of the pore, ultimately enabling ion transfer to take place across the membrane of cells. The P2X7 receptor has a trimeric arrangement having three nucleotide binding pockets, with domains from two separate monomers forming the area which is responsible for compound interaction [143,337,338]. In total, the P2X7 receptor has six helical membrane spanning regions with the second one (TM2) belonging to an individual P2X7 monomer potentially assembling together giving rise to a channel that allows the transmembrane crossing of ions [322,338]. Following transmembrane domain 2 motion and the dilation of the pore, current can pass through with an inward and outward direction governed via the difference in electrical potential between inside and outside of the cells. Once the ligand interacts with the purinergic receptor and the rotation of the transmembrane domains occurs, mono- or bi-phasic currents may be determined via whole cell patch clamp technique [335,336,339]. Moreover, single channel traces of P2X7 pore were also determined using *Xenopus laevis* oocytes with pore conductance ranging from 9 up to 13 pS [340].

1.4.5 P2X7 receptor-dependent signalling pathways

1.4.5.1 The release of cytokines

Beside the release of two important cytokines under the stimulation of the P2X7 receptor namely IL-1β and IL-18, this purinoceptor has been shown to stimulate the secretion of other crucial mediators for instance IL-1 receptor antagonist, IL-1α as well as IL-36α [243,341–343] highlighting the crucial importance of this receptor in the release of IL-1 type of pro-inflammatory cytokines. A novel study addressed the signalling pathway supporting the NLR family pyrin domain containing 3 (NLRP3) inflammasome stimulation as well as IL-1β release via multiple initiators and highlighted that potassium efflux may strongly stimulate the multimeric aggregate [344].

1.4.5.2 Reactive oxygen species formation

The synthesis of reactive oxygen species (ROS) following adenosine 5'-triphosphate stimulation of purinergic P2X7 receptor has been thoroughly documented especially in microglia, macrophages, erythrocytes and submandibular gland cells [345–351]. Stimulation of nicotinamide adenine dinucleotide phosphate (NADPH) oxidase 2 via purinergic P2X7 receptors has been a frequent characteristic established in each of the cell classes investigated. Emerging studies suggest that a possible stimulation of P2X7 receptor via adenosine 5'-triphosphate may similarly elevate the levels of mitochondrial ROS [352,353]. A signalling pathway outcome due to elevated synthesis of reactive oxygen species originating from cells of myeloid origin is the stimulation of the NLR family pyrin domain containing 3 inflammasome complex and ultimately the release of IL-1β [243,354]. On the other side, emerging evidence also suggests that in macrophages which are bone marrow-derived, the reactive oxygen species do not influence NLRP3 assembly [344].

1.4.5.3 Protease stimulation and release

Stimulation of purinergic P2X7 receptor gives rise to multiple cell membrane-associated modifications for instance the release of small particles as well as exosomes, membrane swelling, the establishment of multinucleated cells, partial presentation to phosphatidylserine and lastly stimulation of metalloproteases present on the membrane of cells, ultimately giving rise to breakdown of membrane-bound mediators [305,355,356]. Novel studies have determined multiple mediators embedded on the membrane of cells that may be released into the extracellular space following the stimulation of the P2X7 receptor for instance the adhesion mediator CD44, CXCL16, IL-6 receptor, CD62L or in other words L-Selectin, soluble amyloid precursor protein, CD27 and lastly CD23 also known as the low-affinity IgE receptor [357–363].

1.4.5.4 Prostaglandin release

In murine macrophages, the stimulation of the P2X7 receptor gives rise to an elevation in the levels of multiple prostanoids for instance thromboxane B_2, prostaglandin E_2 (PGE_2) as well as leukotriene B_4 [364,365]. The function of phospholipases is to regulate the hydrolysis of phospholipids giving rise to arachidonic acid, a signalling cascade which has been shown to be tightly modulated by the activation of the P2X7 receptor via stimulating of the intracellular phospholipase A_2 [363,366], as well as phospholipase D and calcium independent phospholipase A_2 analogues [367]. Following this stimulation of the purinergic receptor, arachidonic acid is further converted by prostaglandin E synthases and cyclooxygenase to the mediator PGE_2 [364]. This prostaglandin which is one of the end products of this signalling cascade mediated by the P2X7 receptor has crucial functions in pain, elevated temperature as well as inflammation [364,368].

1.5 The role of P2X7 receptor in inflammation

The P2X7 receptor is considered as a crucial proinflammatory protein [288,356,369]. Following the stimulation of this receptor, multiple chemokines as well as cytokines are released from a variety of cells of which IL-1β has attracted the most attention [370]. The release process of IL-1β which is the active form of the proinflammatory cytokine is governed by a two-step mechanism starting with the stimulation of a Toll-like receptor (TLR) which facilitates the transcription of the *IL-1β* gene and encouraging the built-up of pro-IL-1β (inactive form) in the cytosol, followed by the second step which is the stimulation of the NLRP3 multimeric complex ultimately resulting in the conversion of pro-IL-1β to its active form IL-1β [371]. This maturation giving rise to the biologically active form of the pro-inflammatory cytokine is strongly associated to its release from cells as a follow up mechanism which has not been fully understood yet [372]. The activation of P2X7 receptor significantly encourages the aggregation and stimulation of the NLRP3 multimeric complex [373,374]. A further study by Munoz-Planillo and colleagues (2013) has proposed that a decline of the local intracellular potassium levels may constitute the connection between the P2X7 receptor stimulation and the activation of the NLRP3 inflammasome [344]. As a result, by convention, the stimulation of the P2X7 macropore might not be crucial in supporting the assembly of this multimeric aggregate as different ion species can cross the membrane of cells following the activation of the P2X7 receptor [329]. The stimulation of the P2X7 receptor at delimitated cellular membrane regions may potentially favour the initiation of an accentuated local potassium depletion without a prolonged and particularly alarming distress of the established intracellular homeostasis [375].

1.5.1 The inflammasome

All inflammasomes possess a common architecture comprised of an elemental domain namely the pattern recognition receptor (PRR) (usually a NOD-like receptor), procaspase-1 and the apoptosis-mediated speck-like protein including a CARD (ASC; or in other words PYCARD) that anchors at the N-tail a pyrin (PYD) block and at the C-terminal a CARD domain [376,377]. The current ASC arrangement promotes similar interactions with further CARD or PYD domains belonging to other proteins which are essential for the aggregation of the inflammasome via associations between procaspase 1 and NLRs [376,378].

1.5.1.1 Types of inflammasomes

The NLRP1 inflammasome or in other words NALP1 is one of the initial multimeric aggregates which was identified and comprises of NLRP1, caspase-1, ASC and likely caspase-5 [379,380]. This inflammasome is unique in the sense that it comprises of a FIIND (function to find) terminal that can be subjected to self-cleavage for the purposes of enhancing its role during inflammation [381].

The NLRC4 also termed IPAF inflammasome contains an elemental CARD terminal which can associate straightforwardly with procaspase-1 [382,383]. The bacterial flagellins belonging to gram-negative subcategory containing type IV or type III release mechanisms for instance *Shigella flexneri* and *Salmonella typhimurium* are the principal activators of this multimeric complex [382,384–386]. A study published by Suzuki and colleagues (2007) has highlighted that the stimulation of NLRC4 does not depend on flagellin, suggesting that multiple compounds of bacterial origin may participate in mechanisms that are less well understood in activating NLRC4 [387].

The NLRP3 (Cryopyrin, NALP3 or CIAS) inflammasome is a special multimeric complex due to its intrinsic capability to react to multiple stimuli which are not restricted

solely to microbial traces such as pathogen-associated molecular patterns (PAMPs) [284,388] but rather also being activated by glucose [389], monosodium urate [390] or even extracellular adenosine 5'-triphosphate [284,391]. In order to deliver its physiological role, this inflammasome promotes the formation of PYD-PYD interactions between its PYD terminal and the PYD domain of ASC [392].

The non-NLR AIM2 or in other words absent in melanoma 2 (AIM2) inflammasome contains a HIN 200 (hematopoietic interferon-stimulated nuclear proteins containing a 200 amino-acid terminal) domain positioned at the C-terminal of the multimeric complex [393–395]. This HIN aggregate binds to the PYD domain belonging to ASC in order to exert the physiological function of this inflammasome [393,396]. The AIM2 complex is also able to recognise double stranded deoxyribonucleic acid present in the intracellular space as it has been shown in a study published by Hornung and colleagues (2009) [397,398].

1.5.1.2 The assembly of inflammasomes

The typical stages involved in the aggregation of the majority of inflammasomes start with a suitable stimulus that encourages a modification which promotes adenosine 5'-triphosphate-mediated synthesis of the same nucleotide [399]. Following this stimulation, the PYD terminal belonging to inflammasomes such as AIM-2, NLRP3 or NLRP1 binds to ASC (which contains a CARD domain) for the purposes of accumulating cytoplasmic resident procaspase-1 monomers via CARD-CARD interactions [400,401]. This process results in a fully assembled inflammasome that is involved in the autoproteolysis of procaspase-1 into its active form (caspase-1) which further facilitates the conversion of pro-IL-1β into its biologically active form IL-1β [400,402]. A study by Lu and colleagues (2014) has highlighted a reciprocal signalling cascade with regards to the aggregation of both AIM2 and NLRP3 multimeric

complexes via a pathway implicating the relocation to the nucleus of PYD terminals of caspase-1, ASC and CARD [403]. In this case, the authors suggest that both PYD and CARD domains of inflammasomes give rise to filamentous structures [403]. Figure 11 highlights the process by which the NLRP3 inflammasome becomes primed and activated in a 2-step mechanism, which ultimately results in the release of the biologically active IL-1β and IL-18 in the extracellular space.

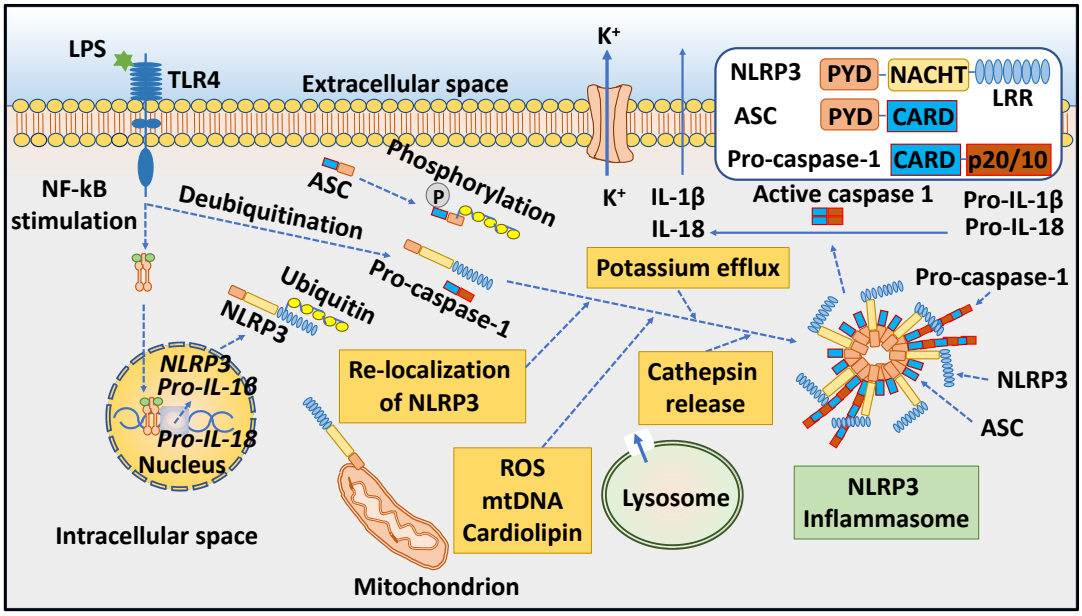


Figure 11. *This scheme highlights some of the mechanisms involved in the assembly of the NLRP3 inflammasome. The activation of this multimeric protein involves two main processes. This figure has been hand drawn by Paul Fodor using Microsoft PowerPoint software version 16.53 and is taken from from Guo et al (2015)* [404]*. The first step is marked by lipopolysaccharide activation of the TLR4 receptor which acts as a stimulator of the NF-kB, giving rise to increased expression of NLRP3 as well as IL-1β, ultimately resulting in elevated synthesis of the NLRP3 protein. The priming of NLRP3 also promotes its deubiquitination. Also, prior to inflammasome assembly, an adaptor mediator of the multiprotein signalling complex namely ASC (the adaptor molecule apoptosis-associated speck-like protein containing a CARD) is subjected to phosphorylation and ubiquitination. Following the priming of NLRP3 inflammasome, the second step, namely the activation of the canonical NLRP3 requires a recognizable signal in order to promote its intracellular assembly. Some of these signals include relocation of NLRP3 to the mitochondria, intracellular release of mitochondrial reactive oxygen species, mitochondrial DNA or cardiolipin, K^+ release into the extracellular space via ion pores or cathepsin release into the intracellular environment following lysosomal destabilisation. The assembled NLRP3 inflammasome promotes the autoproteolytic activation of pro-caspase-1 into its active form caspase-1, which in turn catalyses the conversion of pro-IL-1β and pro-IL-18 into their mature forms namely IL-1β and IL-18, resulting in their release into the extracellular space.*

1.5.1.3 Inflammasomes in early and term pregnancy

The isolation of human first trimester cytotrophoblasts, decidual endothelial and stromal cells and their stimulation with lipopolysaccharide (LPS) has revealed the presence of various inflammasomes during the early stages of the gestation period highlighted via the transcription of NLRP3, NLRC1, NLRP1, PYCARD, IL-1β and caspase-1 genes originating from these primary cells [405]. This study showed that LPS increased the mRNA levels especially of IL-1β and caspase-1 and also of the NLRP3 inflammasome out of the three NOD-like receptor family multimeric complexes tested, suggesting that lipopolysaccharide plays an important role in supporting the release of IL-1β originating from decidual stromal cells and cytotrophoblasts and not endothelial cells [405]. Furthermore, this investigation by Pontillo and colleagues (2013) highlights the importance of decidual stromal cells in supporting the function of innate immunity and the synthesis of pro-inflammatory cytokines, as well as the production of mature IL-1β originating from isolated cytotrophoblast cells, implying that the human placenta is strongly implicated in the regulation and release of pro-inflammatory cytokines [405].

In the case of inflammasomes in term pregnancy, a recent study has highlighted that isolated fetal membranes with undamaged amnion and chorion layers have been shown to possess substantial mRNA levels of all 10 human toll like receptors (TLR's) as well as NLRP3, NLRP1, ASC and lastly caspase-1 [406]. Moreover, this investigation has also presented data suggesting that in isolated fetal membranes, the concentration of biologically active IL-1β was particularly elevated following the activation with PAMPs such as peptidoglycan, lipopolysaccharide and flagellin [406].

A considerable number of studies investigating the potential involvement in inflammation of isolated fetal membranes acquired before or following the onset of

unplanned commencement of parturition have suggested a possible role of these tissues in the regulation of inflammasome assembly due to the presence of elevated mRNA levels of caspase-1 [407,408]. Moreover, similar findings have also been reported in the human myometrium [407]. In addition, the culture of myometrial explants or fetal membranes has highlighted that lipopolysaccharide activation gives rise to a release of IL-1β into the media which was significantly accentuated via the exposure to nigericin and adenosine 5'-triphosphate, with the released levels of the pro-inflammatory cytokine also being mediated via carbenoxolone which is an antagonist acting at the P2X7 and pannexin-1 hemichannel [407]. These results are further supported by a study published in 2008 highlighting that adenosine 5'-triphosphate encourages the release of IL-1β via the stimulation of the P2X7 receptor in human cord blood white blood cells originating from labouring and non-labouring patients [285]. The concentration of the natural agonist adenosine 5'-triphosphate considered as a "danger" mediator which acts at the purinergic P2X7 receptor *in vivo* is extremely well managed even if elevated eATP levels (in the region of mM) are required in order to stimulate the P2X7 receptor [409]. During pregnancy, especially in the uterus, an increased adenosine 5'-triphosphate concentration may originate from endothelial cells present in either human umbilical vein or arteries [180,410] or potentially from sheer stress caused by myometrial contractions [411]. In another study, the presence of the P2X7 receptor in the rat myometrium became significantly elevated before the onset of parturition and also in an animal model simulating preterm birth, the mRNA and protein levels of the P2X7 receptor became between 18 to 22 times higher at day 19 during pregnancy, suggesting a recognisable potential involvement of the receptor in stimulating multiple signalling pathways involved in inflammation [412].

1.5.2 The P2X7 receptor involvement in DAMPs and PAMPs associated switch for the initiation of immune responses

Atmospheric and self-derived microparticle hazards activate the innate immunity via the association of NLRP3 multimeric complex, ultimately triggering the conversion of the inactive pro-IL-1β to the biologically active form of the pro-inflammatory cytokine IL-1β [413]. There are a considerable number of studies which have shown that the P2X7-NLRP3-IL-1β signalling pathway consists of two parts, the first one mainly involved in the production of pro-IL-1β due to transcriptional stimulation and the second one being involved in NLRP3 multimeric complex oligomerisation, caspase-1 self-stimulation and caspase-1 mediated conversion of pro-IL-1β into its active form IL-1β [414,415]. The second part of this signalling cascade may also become activated via pathogen-associated molecular patterns or in other words PAMPs, toxins or danger-associated molecular patterns also known as DAMPs[416].

Danger-associated molecular patterns or in other words DAMPs or alarmins [417] are non-microbial “damage” mediators which are released from the cytosol following exposure to mechanical disturbance [417–419] and give rise to a sterile inflammatory response via the intracellular assembly of inflammasomes [420,421].

DAMPs can arise from toxic waste present in the atmosphere for instance asbestos or silica [422,423], but also from vaccines containing adjuvants for instance aluminum salt (Alum) [424] or from intrinsic homeostasis disturbances for instance elevated cholesterol [425], glucose [389], biglycan [426], adenosine 5’-triphosphate [284], *β*-amyloid protein [427] or even monosodium urate (MSU) [390,424] . Other important DAMPs include HMGB1 (a nuclear protein which interacts with nucleosomes and further facilitates DNA bending) [428,429], S100 proteins (functioning as intracellular Ca^{2+}

sensors) [430], hepatoma derived growth factor (HDGF) (involved in proliferation migration of multiple cell types including smooth muscle cells) [431,432] and heat shock proteins (HSP's) (which play a regulatory function in the folding of proteins) [433,434].

There are multiple suggested processes that can potentially activate the NLRP3 multimeric complex for instance membrane disturbance such as soluble adenosine 5'-triphosphate, as well as bacterial toxins or cytoplasmic engulfing of crystal fragments (e.g. MSU) via phagocytosis [435,436]. Moreover, bacterial toxins or extracellular adenosine 5'-triphosphate gives rise to an accentuated potassium exit from cells and the establishment of pannexin-1 hemichannels which are both necessary in the stimulation of this inflammasome [437,438]. The internalisation of particles for instance monosodium urate or silica has been shown to give rise to lysosomal rupture and in turn leakage of the protease cathepsin B towards the intracellular space which further regulates the stimulation of ROS [423,427,439].

Further research investigating the extracellular adenosine 5'-triphosphate release from activated cells and the initiation and follow-up of the purinergic cascade of events leading the stimulation of the NLRP3 multimeric complex could constitute a significant leap forward in terms of elucidating the cellular signalling pathways involved in the regulation of innate and potentially adaptive immunity [440]. Activation of cells gives rise to adenosine 5'-triphosphate release and in turn stimulation of multiple purinoceptors such as P2Y and P2X located on the membrane (autocrine stimulation) or present on the plasmalemma of nearby cells (paracrine stimulation), resulting in a tight coordination of cellular signalling pathways especially from an immunological point of view [441]. The majority of cells are capable of liberating in the extracellular space various nucleotides, although the signalling pathways involved in the accomplishment of this process are vaguely known especially in the case of non-

excitable cells such as endothelial cells [442–444]. In the case of cellular malfunction, an increased level of adenosine 5'-triphosphate originating from cells subjected to substantial injury is liberated towards the extracellular compartment and serves as a danger-associated molecular pattern stimulus, encouraging the onset of inflammation via binding to the P2X7 purinoceptor and in turn stimulating the intracellular assembly of NLRP3 multimeric complex [445,446].

A further study has demonstrated that microparticles for instance silica and aluminum or even endogenous microcrystals such as MSU are able to stimulate an effective liberation of adenosine 5'-triphosphate towards the extracellular space especially in the case of isolated human macrophages potentially via the stimulation of pannexin pores and the P2X7 receptor [447]. Additionally, this study has also shown that primed isolated murine macrophages which have been exposed to crystals strongly encourage the conversion of pro-IL-1β to its active form IL-1β via the participation of a purinergic receptor signalling cascade [447].

Generally, one of the principal dangers faced by resident defence mechanisms originates from organisms which possess exclusive motifs that are not expressed in eukaryotes also known as pathogen-associated molecular patterns or in other words PAMPs [448–450]. In order to cope with this permanent dynamic exposure to micro-pathogens, multiple types of PRR's are localised on the membrane of cells, in the intracellular compartment or even released into the extracellular space and have the capacity to identify PAMPs [451,452]. A good example in this case is the human TLR family which comprises of 10 receptors (Toll-like receptor 1-10) that are able to identify a variety of danger signals for instance LPS [453], peptidoglycan, lipoteichoic acid [454] bacterial flagellin [455], bacterial unmethylated CpG motifs [456] and many more. These exogenous PAMPs can be identified by cells belonging to both innate and adaptive

immune systems via various TLR's that in turn can stimulate multiple signalling cascades with the NF-kB pathway being a pivotal one [417,457]. In the case in which these signals gain entry into the intracellular space, the microorganisms are faced with another layer of protection being recognised by NOD-like receptors or in other words NLRs [458–460]. In total, there are 22 human NLR genes which have been classified [461]. From a structural point of view, these NLR's are composed of three main domains namely a principal nucleotide-binding and oligomerisation domain (NOD) which is also named NACHT, a zone composed of leucine-reach repeats (LRR) positioned at the C-terminal and lastly a N-terminal region specialised in protein-protein interactions [462,463]. Overall, both PAMPs and DAMPs give rise to the commencement of multiple inflammatory signalling pathways which ultimately result in the release of regulators that favour the onset of inflammation via the assembly of inflammasomes.

1.6 The role of nucleotides in human placental vascular tone regulation

The human placenta as well as the single umbilical vein and two umbilical arteries actively participate in the adjustment of blood flow and in the regulation of nutrient and fluid transfer between the mother and the fetus but also in the synthesis of steroid hormones [464]. A recent study has shown that an elevation in adenosine levels present in plasma of pregnant women could be due to not only to the stimulation of platelets, but also as a result of an elevation of 5'-nucleotidase action for the duration of the gestation period [465]. Long term exposure to theophylline or caffeine during the course of gestation supresses the adenosine A_1 receptor activity especially in the brain of the mother and the fetus [466,467]. Moreover, another study has revealed that the human placenta expresses binding domains with typical attributes corresponding to a type of adenosine receptor, most likely the A_2 purinoceptor [468]. A

potential mechanism of adenosine adsorption has been described in the context of the human placenta and also its conversion to other mediators taking place inside and outside of cells [469]. In this context, the transport of the nucleotide at the level of the syncytiotrophoblast on both apical and basal surfaces has been extensively described, with dipyridamole strongly supressing its bidirectional transport, denoting a crucial function of the placenta in mediating the physiological effects of adenosine during pregnancy [470]. Also, adenosine gave rise to vasorelaxation in ring preparations belonging to human chorionic arteries as well as veins which have been previously constricted using a high potassium physiological solution, with the pharmacological evaluation highlighting a potential participation of A_1 and possibly A_2 adenosine receptors [471]. A further study highlighted that in ovine fetal placental blood vessels, this nucleotide gives rise to a vasocontraction effect succeeded by a vasorelaxation response [472,473].

Adenosine 5'-triphosphate has been shown to give rise to vasocontraction of the human fetoplacental blood vessels potentially through stimulating purinergic P2X receptors and adenosine highlighted a decreased sensitivity especially in placental cotyledons, potentially due to a marked reduction of its corresponding receptors following a prolonged exposure to the nucleotide at the time of parturition [474,475].

A prolonged quantification of adenosine 5'-triphosphate using human perfused placenta samples which have been subjected to ischemia has been carried out *ex vivo* using ^{31}P-nuclear magnetic resonance spectroscopy, with results highlighting that following 4 hours of ischemic exposure, the levels of adenosine 5'-triphosphate declined by 85% from control values but following reperfusion, the nucleotide concentration significantly raised [476]. Moreover, adenosine 5'-triphsphate and uridine 5'-triphosphate possess the capacity to encourage the elevation of intracellular

calcium levels in primary cells isolated from placental samples, potentially via the participation of $P2Y_2$ and $P2Y_4$ purinoceptors [477].

A further study investigating the function of human purinergic P2 receptor subcategories in perfused placental cotyledons has highlighted that adenosine 5'-triphosphate and α,β-methylene adenosine 5'-triphosphate dependent vasoactive property (potentially mediated via vascular smooth muscle) did not favour the establishment of a desensitization effect and also was not susceptible to blocking via pyridoxalphosphate-6-azophenyl-2',4'-disulfonic acid, suggesting that the P2X1 purinoceptor might not be involved in the development of a contractile event [478]. This study has also showed that adenosine 5'-triphosphate and uridine 5'-triphosphate act via purinergic $P2Y_2$ and $P2Y_4$ receptors present on the smooth muscle in order to regulate a contractile effect of the placental blood vessels and that adenosine 5'triphosphate acts at $P2Y_1$ purinoceptors in order to give rise to the relaxation of blood vessels via the synthesis of nitric oxide [478].

Considerable levels of mRNA corresponding to multiple purinergic receptors such as P2X1, P2X4, P2X5, P2X6 and P2X7 have been found especially on the smooth muscle layer of the chorionic blood vessels of the human placenta, as well as the umbilical vein and arteries and, overall, the investigation concluded that the circulating nucleotides play an important function in mediating the blood flow between the mother and the fetus [479]. Another study has suggested that adenosine has the potential to constrict human chorionic blood vessels in the case of the perfused cotyledon, mainly through activating A_{2B} purinoceptors via the production of a stimulating agent acting at a thromboxane receptor or the synthesis of a prostanoid [473]. Also, the same study has suggested that human adenosine A_3 receptors may play an important role in the vasorelaxation of placental chorionic arteries via

regulating the function of smooth muscle [473]. Human purinergic P2 receptors especially P2X4, P2X7 and $P2Y_2$ subcategories have been identified at an mRNA as well as protein level in isolated placental villous tissue in both early (first trimester) and late pregnancy (term) [480]. This study also presented fluorescent calcium imaging data highlighting that uridine 5'-triphosphate, adenosine 5'-triphosphate, as well as 2'(3')-*O*-(4-benzoyl benzoyl) adenosine 5'-triphosphate have led to an accentuated increase in intracellular calcium especially in late pregnancy [480]. Furthermore, another study by Roberts and colleagues published (2006) has shown that cytotrophoblast cells express functionally active P2X4, P2X7, $P2Y_2$ and $P2Y_6$ purinoceptors which, under stimulation, may increase the intracellular calcium concentration, ultimately regulating the metabolism of the syncytiotrophoblast layer as well as the transfer of various ion species between the mother and the fetus [277]. Buvinic and colleagues (2006) have also shown that human purinergic $P2Y_1$ and $P2Y_2$ receptor expression varies in the vasculature of the placenta, with 6 to 8 times higher levels in placental chorionic and cotyledon vasculature compared to the umbilical cord [481]. In this case, the authors further suggested that $P2Y_1$ and $P2Y_2$ receptors were mainly expressed on the smooth muscle cells in the cord and the chorionic vasculature, accompanied by a comparable expression level on both smooth muscle and endothelial cells in the cotyledon region of the human placenta [481]. Moreover, further evidence suggests that P2X1, P2X4 and P2X7 receptors are also expressed in the human chorionic plate vasculature, especially on the surface of the smooth muscle cells [479].

1.7 Hypothesis and aims

The hypothesis of this study was that purinergic receptor agonists as well as DAMPs and PAMPs regulate the blood flow of the chorionic plate and stem villous vasculature of the human placenta given their known role in vasoconstriction and vasorelaxation. This process is mainly achieved by involving the P2X7 receptor in the autoregulation of blood flow and vessel tone, which is perturbed by DAMPs, PAMPs and inflammation especially in the case of healthy and pregnancies complicated by pre-eclampsia or gestational diabetes mellitus.

The principal objectives of this study were to:

- Investigate the mechanisms of pro-inflammatory cytokine release from isolated placental tissues under the influence of DAMPs, PAMPs and purinergic receptor agonists and antagonists
- Determine the expression levels of the P2X7 receptor using western blotting in placental chorionic plate arteries, stem villous arteries, trophoblast tissue and myometrium in healthy and pregnancies complicated by pre-eclampsia.
- Explore the P2X7 receptor expression in isolated vascular smooth muscle cells originating from the placental chorionic plate arteries of healthy human subjects
- Investigate the protein and mRNA levels of P2X7, Caspase-1 and NLRP3 inflammasome in stem villous arteries
- Evaluate the P2X7 receptor expression in isolated sections of human placental villous tissue at the level of the syncytiotrophoblast and fetal capillaries in healthy and diet managed gestational diabetes mellitus patients.
- Study the involvement of the P2X7 receptor playing a functional role in the regulation of vascular smooth muscle cell contractility of human placenta chorionic plate arteries using wire myography

- Fabricate an accurate and reproducible *in vitro* cell co-culture model using primary human umbilical vascular endothelial cells (HUVEC) and freshly isolated placental chorionic plate artery smooth muscle cells (CPA-SMC).
- To characterise the surface antigenic profiling of human placenta chorionic plate artery smooth muscle cells originating from healthy and gestational diabetes mellitus placental samples using cell surface markers characteristic of human multipotent mesenchymal stem cells.

CHAPTER 2

MATERIALS AND METHODS

2.1 Patient recruitment

Human placental samples, myometrial and blood samples were obtained from subjects attending the Department of Obstetrics and Gynaecology, Royal Derby Hospital, Derby, United Kingdom. Ethical approval for the investigation was received from the Derbyshire Research Ethics Committee (Ref: 09/H0401/90) [482].

Similarly, entire human placental samples have been acquired via the Department of Obstetrics and Gynaecology at The University Hospital, Queen's Medical Centre, Nottingham, United Kingdom and with the permission from the Nottingham University Hospitals, NHS Trust, U.K. Ethical authorization was granted via the NHS Health Research Authority UK (Ref. 14/SC/1194) [483]. This study had the approval of the East Midland Nottingham 2 – Health Research Authority (Ref: OG010101) [484].

All work described has been undertaken in accordance with The Code of Ethics of the World Medical Association (Declaration of Helsinki) [119,484] and all patients provided fully informed, written consent prior to the collection of placental, myometrial and blood samples before undergoing elective or emergency lower segment caesarean section. All volunteers included in the investigation delivered via caesarean section [482].

2.2 Inclusion and exclusion criteria

The inclusion criteria of the study established that following informed written consent, healthy patients undergoing elective caesarean section at term gestation (>37 weeks) were eligible to enter in the study. All mothers had to be between 17 and 49 years old. This inclusion criteria are based on previously published studies [485–487].

Patients eligible into the inclusion criteria had to be non-smokers and included healthy volunteers, gestational diabetic mellitus subjects (oral 75g glucose tolerance

test) managed with diet, metformin or insulin and type 1 diabetic volunteers who have become pregnant after the diagnosis. This eligibility criteria is based on two studies namely Razak *et al* (2018) [488] and Villota *et al* (2021) [484]. Also, placental samples originating from pregnancies complicated by preeclampsia (gestational age range 33-39 weeks), intrauterine growth restriction (gestational age range 34-36 weeks) and oligohydramnios were eligible to enter the study. The intrauterine growth restricted group consisted of clinically suggested cesarean section for childbirth of a small-for-gestational age new-born with a birth weight under the 10th centile with reference to regional hospital personalised resource tables [489]. Also, the preeclampsia group was comprised of clinically indicated cesarean section in women which have been diagnosed with hypertension (>140/90 mmHg) and proteinuria (>0.3g/24h) either of late (>34 weeks) or early (<34weeks) onset. The inclusion criteria for pre-eclamptic and intrauterine growth restriction pregnancy cases is based on a study published by Pearson *et al* (2010) [489].

The treatment administered for the duration of the pregnancy period was controlled in conformity with approved protocols. All subjects proceeded with their insulin management for appropriate glucose regulation. Also, in order to be eligible for the study, all patients had to be hemodynamically stable (systolic blood pressure of more than 100mm Hg with a pulse of less than 110 beats per minute). Further suitable subjects included those with previous elective caesarean section, breech presentation and also maternal request.

The exclusion criteria for the study contains patients with underlying pregnancy complications such as meconium staining, cases of microvascular complications (retinopathy, nephropathy), renal or cardiac disorders and other conditions that may compromise patient health [484]. Also, further exclusion criteria from the study are

karyotypic abnormalities including confined placental mosaicism, syndromic disorders or birth anomalies (i.e. Silver-Russell Syndrome), placental abnormalities (such as low-lying placentas and abnormally invasive placentas, with the exception of velamentous umbilical cord insertion and placenta previa), maternal chronic illnesses (acquired immune deficiency syndrome, endocrinological, hepatitis) and Rh disease. Exclusion criteria also comprises of patients unable to give informed consent, placenta accreta / percreta / increta and subjects that have taken alcohol in the last 24 hours.

2.3 Human tissue collection

After the patient provided informed consent and the follow up contact from the midwife that the consented subject has given birth and the placenta sample has been checked with the umbilical cord clamped being ready for collection, all placental specimens were transported to the laboratory within 20 minutes of delivery. Once the placenta sample has been weighed and the umbilical cord clamped next to the chorionic plate and placed in sterile 0.9% (w/v) NaCl (aq.) supplemented with 100 units/mL penicillin and 100µg/mL streptomycin up to 24 hours until further experiments, the placenta was further processed according to the experimental needs. The tissue collection is based studies published by Pearson *et al* (2009) [490] and Maneta *et al* (2015) [491] with the modification that the physiological salt solution in the current study contains 3.2mM $CaCl_2$ and 6.05mM D-Glucose.

After finishing collecting all placental biopsies and isolating the human umbilical vein endothelial cells, the leftover placental tissue and separated umbilical cord were both placed in a clinical waste bag with the patient information sicker on it and returned on the same day to the labour suite. The remaining returned samples were kept at 4^0C for a further 48 hours just in case the health of the new-born becomes unstable, and the pathologist requests a further placental or umbilical cord biopsy test.

In the case when the human umbilical vein endothelial cells were isolated 24 hours after the collection of the placenta sample, the cord was similarly placed in a clinical waste bag and kept at 4^0C until disposed of accordingly. Circa 10-20ml of cord blood was obtained from the umbilical vein right after placenta collection, added into sterile heparinized tubes (BD vacutainer LH PST™ II) and carefully shaken in order to avoid the formation of coagulation. Maternal peripheral blood samples (approximately 10mL) were obtained from the median cubital vein by a registered midwife from pregnant mothers during appointments at the antenatal clinic and added to sterile heparinized tubes (BD vacutainer LH PST™ II) after transport to the laboratory prior to commencement of peripheral blood mononuclear cells (PBMC) isolation [491]. Furthermore, myometrial biopsies of circa $2cm^3$ were obtained from the area superior to the transverse incision performed during the elective lower segment caesarean section. The myometrial specimens were placed in physiological salt solution (PSS; 119mM NaCl, 4.69mM KCl, 2.4mM $MgSO_4$, 25mM $NaHCO_3$, 1.17mM KH_2PO_4, 6.05mM D-Glucose, 3.2mM $CaCl_2$, pH 7.4), transported to the laboratory, thoroughly washed in PSS, immediately snap frozen in liquid nitrogen and stored at -80^0C until processed [53]. The number of placental samples used in each experiment is stated individually in each section.

2.4 Isolation of placental arteries

After transport of placental samples to the laboratory, the amnion was gently dethatched from the surface of the chorionic plate which resulted in the exposure of the vast chorionic plate blood vessel network. Following identification of the two umbilical arteries, the chorionic plate arteries were recognised by inspecting the point of umbilical cord insertion into the chorionic plate and tracing the branches of the smaller internal diameter resistance size arteries across the fetal surface of the

placenta. In this case, the first order CPA was considered the blood vessel which branched from the umbilical artery immediately after the point of umbilical cord insertion into the chorionic plate. At the level of the 2nd and 4th order branches of the chorionic plate artery, an incision into the tissue was undertaken and arteries were dissected with the adjacent connective tissue. CPA's were immediately depleted of the surrounding connective tissue via fine dissection prior to the start of the wire myography experiments. Three independent biopsies were collected from an individual placenta sample. The chorionic plate artery branching towards the maternal surface of the human placenta was used as a reference point for the purposes of recognising the emerging stem villous arteries (SVA). In this case, SVA's were isolated by gently scraping away the surrounding villous tissue via the rounded edge of a pair of forceps and using fine scissors [53]. The isolation of placental arteries is based on the following studies: Sander *et al* (2019) [482] and Tayyba *et al* (2014) [53].

2.5 Wire myography

Following the removal of all connective tissue, the chorionic plate arteries were transferred to PSS (119mM NaCl, 4.69mM KCl, 2.4mM $MgSO_4$, 25mM $NaHCO_3$, 1.17mM KH_2PO_4, 6.05mM D-Glucose, 3.2mM $CaCl_2$, pH 7.4). Each individual blood vessel segment (2mm) was mounted on the wire myograph (M610, DMT, Aarhus, Denmark) by passing a 49µm tungsten wire through the lumen and securing the blood vessel on the force transducer using two screws. A second wire was passed through the lumen of the CPA and connected to the opposite myograph jaw. The other adjacent isolated CPA segments were also mounted and left to equilibrate at 37^0C prior to normalisation. In this case, the effective pressure was calculated for all four CPA rings and normalised to an effective pressure of 5.1kPa and set at an internal circumference of $0.9*IC_{5.1kPa}$. The chosen 5.1kPa pressure was used to duplicate the

transmural pressure reported across the intervillous space of the human placenta. CPA's were preconstricted with the thromboxane A_2 mimetic U46619 (10^{-10}M to $3.3*10^{-6}$M) (Tocris, 1932) and responses to endothelium independent vasodilators namely riluzole (Sigma-Aldrich, R116) and sodium nitroprusside (SNP) (Sigma-Aldrich, 228710) were assessed. U46619 was reconstituted with physiological salt solution and the stock concentration was 10^{-2}M (solution A). Using PSS, U46619 solution A was further diluted to obtain the following concentrations: 10^{-4}M (solution B), 10^{-6}M (solution C) and 10^{-8}M (solution D). The stock U46619 solution A (aliquoted into 10µL) was frozen at -20^{0}C and solution B, C and D were prepared fresh each day. SNP was prepared fresh each day using distilled water to produce a stock concentration of 10^{-2}M (solution A). Using PSS, SNP solution A was further diluted to obtain the following concentrations: 10^{-4}M (solution B) and 10^{-6}M (solution C). Riluzole was prepared using dimethyl sulfoxide (DMSO) to obtain a stock concentration of 10^{-2}M (solution A). The riluzole stock solution A (aliquoted into 10µL) was frozen at -20^{0}C. Using PSS, riluzole stock solution A was further diluted to obtain the following concentrations: 10^{-4}M (solution B) and 10^{-6}M (solution C). Riluzole solution B and C were prepared fresh each day. Following preparation, PSS, 60mM KPSS and 123mM KPSS was stored at 4^{0}C for a period of up to 4 weeks.

Pharmacologically, the P2X7 receptor necessitates higher adenosine 5'-triphosphate concentrations for its stimulation, with an EC_{50} **≥** 100µM which is approximately 100-fold greater compared to other P2X receptors and 2,3-O-(4-benzoylbenzoyl)-ATP (BzATP) is circa 30-fold more potent than ATP at the P2X7 receptor [492] (with a low micromolar EC_{50}) [493] whereas at other P2X receptors it is less potent [494]. Another study has highlighted an ATP EC_{50} at the P2X7 receptor of approximately 0.3-1mM at physiological concentrations of calcium and magnesium

[242]. This elevated concentration of adenosine 5'-triphosphate is not frequently expressed in healthy tissues. Despite this, at sites of cellular injury, inflammation, phagocytic degranulation and necrosis, the circulating adenosine 5'-triphosphate concentration may rise to circa mM levels stimulating the P2X7 receptor. As a result, the purinoceptor is recognised to respond to "danger" signals [495]. The P2X7 receptor antagonist A740003 IC_{50} is 0.040μM at the human P2X7 receptor [493]. The U46619 EC_{50} has been reported at 28nM in human placenta chorionic plate arteries [54]. The SNP IC_{50} in human placenta stem villous arteries has been reported at $5.8*10^{-8}$M [482]. In chorionic plate arteries a log EC50 for SNP was determined at -5.5 in a study published by Ali *et al* (2014) [53]. Similarly, in human placenta chorionic plate arteries, the same study has highlighted a log EC50 for riluzole calculated at -6.6 [53].

The tissue baths were constantly perfused with 2% O_2, 5% CO_2 and 93% N_2 (BOC special gas, British Oxygen Company, UK) to mimic placental conditions at term and kept at 37^0C. Experiments were initiated with either a cumulative concentration response curve to U46619 (10^{-10}M - $3.3*10^{-6}$M) or with an initial contraction to the thromboxane A_2 mimetic ($3.3*10^{-6}$M) which served as a viability control. Furthermore, an initial contraction to 60mM KPSS was also used in a few wire myography experiments as a viability control. The vasoactive effects of the investigated compounds were expressed as a percentage of this contraction or as stated in individual figures presented in chapter 4.3. For the purposes of investigating the vasorelaxant effects, riluzole or SNP were added in increasing concentrations immediately after the initial U46619 contraction. The thromboxane A_2 agonist was selected due to its reproducible vasoconstrictor properties at the level of the placental arteries. In the case of investigating the contractile properties of a compound, the commencing cumulative U46619 concentration in the bath was washed out with PSS

and the CPA's were left to equilibrate to baseline tension prior to adding incremental concentrations of ATP or BzATP.

ATP was prepared using PSS to obtain a stock concentration of 10^{-1}M (solution A) at a pH of 7.4. The ATP stock solution A (aliquoted into 1mL) was frozen at -80^{0}C. Using PSS, ATP stock solution A was further diluted to obtain the following concentrations: 10^{-3}M (solution B) and 10^{-5}M (solution C). ATP solution B and C were prepared fresh every day. BzATP was prepared using PSS to obtain a stock concentration of 10^{-2}M (solution A). The BzATP stock solution A (aliquoted into 10µL) was frozen at -20^{0}C. Using PSS, BzATP stock solution A was further diluted to 10^{-4}M (solution B) and 10^{-6}M (solution C). BzATP solution B and C were prepared fresh each day.

All experiments were accomplished with a final contraction to either increasing cumulative concentrations of U46619 (10^{-10}M – $3.3*10^{-7}$M), a single U46619 concentration ($3.3*10^{-7}$M), 60mM KPSS or 123mM KPSS to validate blood vessel viability. The effects of purinergic receptor agonists (adenosine 5'-triphosphate; ATP, Benzoylbenzoyl-ATP; BzATP) were assessed by applying increasing cumulative or non-cumulative concentrations to the bath, in the presence and absence of the selective P2X7 receptor antagonist A740003 (10^{-6}M) (Tocris, 3701) as well as various concentrations (30, 40, 50 and 70mM) of high potassium physiological salt solution (KPSS). A740003 was prepared using DMSO to obtain a stock concentration of 10^{-3}M (aliquoted into 100µL) and frozen at -20^{0}C. Each vasoactive modulator was added directly to the bath and the CPA vessels were incubated with A740003 for either 15 or 30 minutes prior to the application of cumulative concentrations of ATP. The baseline tension of all four CPA preparations was assessed pre- and 5-30 minutes post-application of each compound. Some wire myography experiments contained one

CPA preparation to which no compounds were added and was used as a time control, or in other cases the vehicle control dimethyl sulfoxide (DMSO) was only added to distinguish specific compound-induced vasoactive effects. The concentration of compounds used in this study were based on previously published studies from our laboratories and from the wider literature [53,482]. The wire myography protocol used in the current study is based on Sander *et al* (2019) [482] and Tayyba *et al* (2014) [53] with the modification that the arteries were perfused with 2% O_2, 5%CO_2 and 93%N_2 compared to 5%O_2, 5%CO_2 and 90%N_2 as highlighted in Tayyba *et al* (2014) [53].

2.5.1 Data analysis

The acquired wire myography data (using LabChart Pro software, version 8.1.6) was transformed from tension to active effective pressure (AEP) for the purposes of taking into account the blood vessel size. AEP was determined using Laplace's equation by dividing the acquired active tension (mN/mm) measurements with the radius of the blood vessel (mm). The effects are presented in AEP as a percentage of the maximal AEP obtained with an initial contraction to $3.3*10^{-7}$M (unless otherwise stated) U46619 or to 60mM KPSS. A nonlinear curve fit was undertaken using GraphPad Prism software (version 8.2.1, La Jolla, USA) for the purposes of calculating EC_{50}, EC_{80}, EC_{90} and IC_{50} of a concentration response curve. A nonlinear regression fit (three-parameter logistic equation) was used in order to fit all concentration response curves. EC_{50} is the concentration of a compound that elicits half-maximal response. EC_{80} is defined as the concentration of a compound that produces a 80% response of the maximum possible response for that ligand. EC_{90} refers to the concentration of a compound which produces a 90% response of the maximum possible response for that ligand. IC_{50} is the concentration of an inhibitor where the response is diminished by half. R_{max} is maximal relaxation. The agonist

vasoactive responses were measured as increases above the established baseline. Data are expressed as mean±S.E.M. and analysed using the following statistical tests": Shapiro Wilk normality test, a two-way ANOVA test using Geisser-Greenhouse correction and Sidak's multiple comparison tests, Tukey's multiple comparison tests, unpaired two-tailed T-test with Welch's correction, two-tailed paired T-test and Brown-Forsythe ANOVA test with Dunnett's T3 multiple comparison tests. A value of $P<0.05$ was taken to suggest a statistically significant difference [53,482]. The data analysis of wire myography is based on Sander *et al* (2019) [482] and Tayyba *et al* (2014) [53].

2.6 Western blotting

Western blotting protocol is based on Maneta *et al* (2015) [491], Pearson *et al* (2009) [490] and Warren *et al* (2008) [285].

2.6.1 Collection of placental tissue and PBMC cells

Villous tissue (referred in the current investigation as trophoblast tissue), chorionic plate artery, stem villous artery and choriodecidua were collected from either healthy or preeclamptic placental samples, washed multiple times in physiological salt solution (PSS) to remove any traces of the remaining blood and immediately snap-frozen in liquid nitrogen, followed by storing the samples at -80^{0}C until processed. In this case, villous core tissue was gently separated by sterile dissection from different cotyledons excluding chorionic and basal plates. Choriodecidua was obtained about 2-3 cm from the placental disc by manually separating the amnion with forceps. The trophoblast tissue collected which was further subjected to D-glucose stimulation (chapter 3.3.5) was vigorously washed in D-glucose free PSS immediately after collection. However, on one occasion trophoblast tissue and stem villous artery were collected from a healthy placenta sample, washed thoroughly in PSS and directly homogenised without snap-freezing in liquid nitrogen and storing the tissue at -80^{0}C.

In this case, following homogenisation, the protein determination of the tissue homogenates (second supernatant fraction) was carried out during the same day of the placenta collection, while the second pellet fraction was left overnight at 4^0C in solubilization buffer prior to evaluating the protein content of the preparation on the following day (western blotting data highlighted in chapter 3.2.2). Following isolation of peripheral blood mononuclear cells (PBMC) from the maternal blood originating from two healthy patients, the primary cells were stored at -80^0C until the homogenisation process took place [491] .

2.6.2 Control tissue and cells

Patients undergoing elective caesarean section were also consented for myometrium biopsies as highlighted in chapter 2.3. In this case, myometrium tissue (second pellet fraction) was used as a positive control for the P2X7 receptor protein expression. Similarly, cord blood mononuclear cells isolated from the umbilical vein of a placenta sample originating from a gestational diabetic patient were stimulated with 10µg/mL LPS (3.5h) + 300µM BzATP (0.5h) and the second supernatant fraction used as a positive control for the NLRP3 inflammasome protein expression levels.

2.6.3 Tissue and primary cell homogenisation

All homogenisation and solubilization buffers were initially prepared and kept cold at all times. All tissue samples were taken from the -80^0C freezer and maintained chilled on ice at all times. The mechanical homogenisation was the most suitable method of homogenising stiff muscle tissue for instance myometrium which is generally challenging to homogenise via only cutting the tissue using a scalpel blade. During the fractionation of the isolated tissue, an increased amount of heat is generally produced which may denature the proteins of interest present in the tissue lysate.

Therefore, a particular attention was allocated to keep all buffers and tissue cold at all times during the homogenisation process [285,491].

2.6.3.1 Homogenisation of human tissue using the Ultra turrax method

The human tissue was removed from -80^{0}C tubes and deposited on a glass petri dish which was rested on ice in order to maintain the biopsies cold at all times. A 22-gauge scalpel blade (which was continuously maintained cold) was used to cut the biopsies into multiple reduced size fragments. 500mg of the freshly dissected small tissue pieces (wet weight) were transferred to a 14mL BD Falcon round bottom tube containing 2.5mL homogenisation buffer using a 3mL plastic Pasteur pipette. The composition of the homogenisation buffer (HB) consisted of sucrose (300mM), Tris base (25mM), ethylenediaminetetraacetic acid (EDTA) (1mM), monothioglycerol (10mM), tween 20 (0.1% v/v), 1/500 protease inhibitors and 1/100 phosphatase inhibitors (Sigma-Aldrich, Poole, UK) at a pH of 7.4. The HB was supplemented with protease and phosphatase inhibitors for the purposes of supporting protein integrity. The main benefit of working with a round bottom tube was that the tip of the homogeniser remained in direct proximity with the small tissue pieces at all stages of the fractionation process. The tube with tissue was placed on a polystyrene box containing ice. The tip of the Ultra Turrax T25 tissue homogeniser (Janke and Kunkel IKA-Labortechnik, Germany) (referred in the current investigation as Ultra turrax homogenisation method) was then placed into the tube and turned on and off at intervals of 30 seconds for the purposes of enabling the tissue sample to cool prior to further homogenisation of the biopsy. The process was repeated to the point where no visible tissue fragments were present in the suspension. The remaining tissue samples were individually homogenised using the same methodology. After all tissue

samples were adequately homogenised, all cold suspensions were split into 2 x 1.5mL Eppendorf tubes followed by spinning the samples at 1400g for 10 minutes at 4^0C in order to eliminate any small tissue fragments. The resulting supernatant (first supernatant) was transferred to a new 1.5mL tube and the emerging pellet (first pellet) was discarded since it contained tissue debris. The first supernatant was further centrifuged at 14000g (EBA 12R, Hettich) for 60 minutes at 4^0C. The resulting supernatant (second supernatant) contained the cytosolic fraction of cells and the emerging pellet (second pellet) comprised of the cell membranous fraction. The second supernatant was transferred to a clean 1.5mL Eppendorf tube and placed at -80^0C until further processed. 416μL of solubilisation buffer (SB) (20mM Tris base, 120mM NaCl, 10mM EDTA, 50mM KCl, 2.5% (v/v) Igepal, 2mM DTT, 1/500 protease inhibitors and 1/100 phosphatase inhibitors, pH 7.5) was added to the second pellet which was thoroughly vortexed and the tubes left overnight at 4^0C. On the following day, the second pellet was further vortexed and sonicated using an Ultra-Turrax sonicator (USC100T, VWR) for 15 minutes on ice. The resulting suspension was centrifuged at 1000g for 10 minutes at 4^0C which resulted in the second solubilised pellet (referred in the current study as second pellet) and in an insoluble pellet fraction which was discarded. The second pellet was placed at -80^0C until further processed. Figure 12 shows a visual scheme highlighting the steps of the tissue homogenisation process using the Ultra Turrax method [285,491].

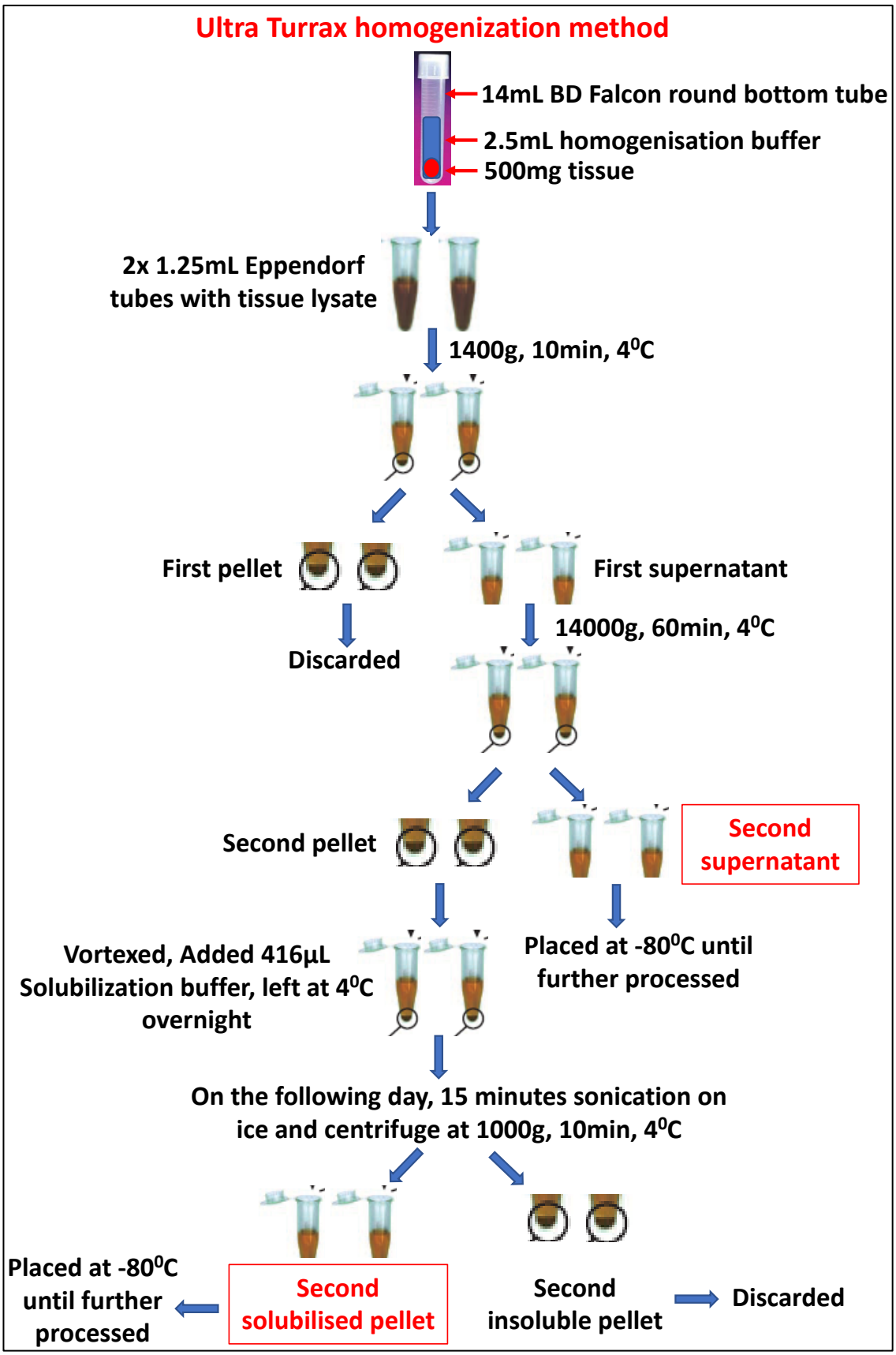


Figure 12. *This scheme shows the process of homogenising human tissue using the Ultra turrax homogenisation method. This figure has been created by Paul Fodor using Microsoft PowerPoint software version 16.53.*

2.6.3.2 Homogenisation of tissue using the Lysing matrix D ceramic spheres method

Tissue samples were also homogenised using a similar method as described in chapter 2.6.3.1. but with minor changes. 100mg of freshly dissected small tissue fragments (CPA, SVA, trophoblast, myometrium; wet weight) were transferred into a 2mL Eppendorf tube containing Lysing matrix D 1.4mm ceramic spheres (MP Biomedicals, 116913100) and 0.5mL HB. The tube with tissue was then placed in a polystyrene box containing ice and the procedure repeated with the remaining tissue biopsies. Following this, all tissue samples were placed inside the benchtop homogeniser (MP Biomedicals Fast Prep 24 Classic) and processed at 6m/s for 40 seconds. The biopsies were then removed from the homogeniser and placed on ice for 5 minutes to cool down. In total, the tissue samples were homogenised 3 times using the same benchtop homogeniser settings with all biopsies being placed on ice in between the processing cycles. From this point, a similar processing protocol was used for all tissue samples as presented in chapter 2.6.3.1 and in the case of solubilizing the second pellet fraction, only 166.6µL SB was used. A schematic representation of the homogenisation of tissue using the Lysing matrix D ceramic spheres is presented in figure 13. The advantage of this homogenisation method compared to the Ultra turrax method is that multiple (up to 24) tissue biopsies can be fractionated at the same time [285,491,496].

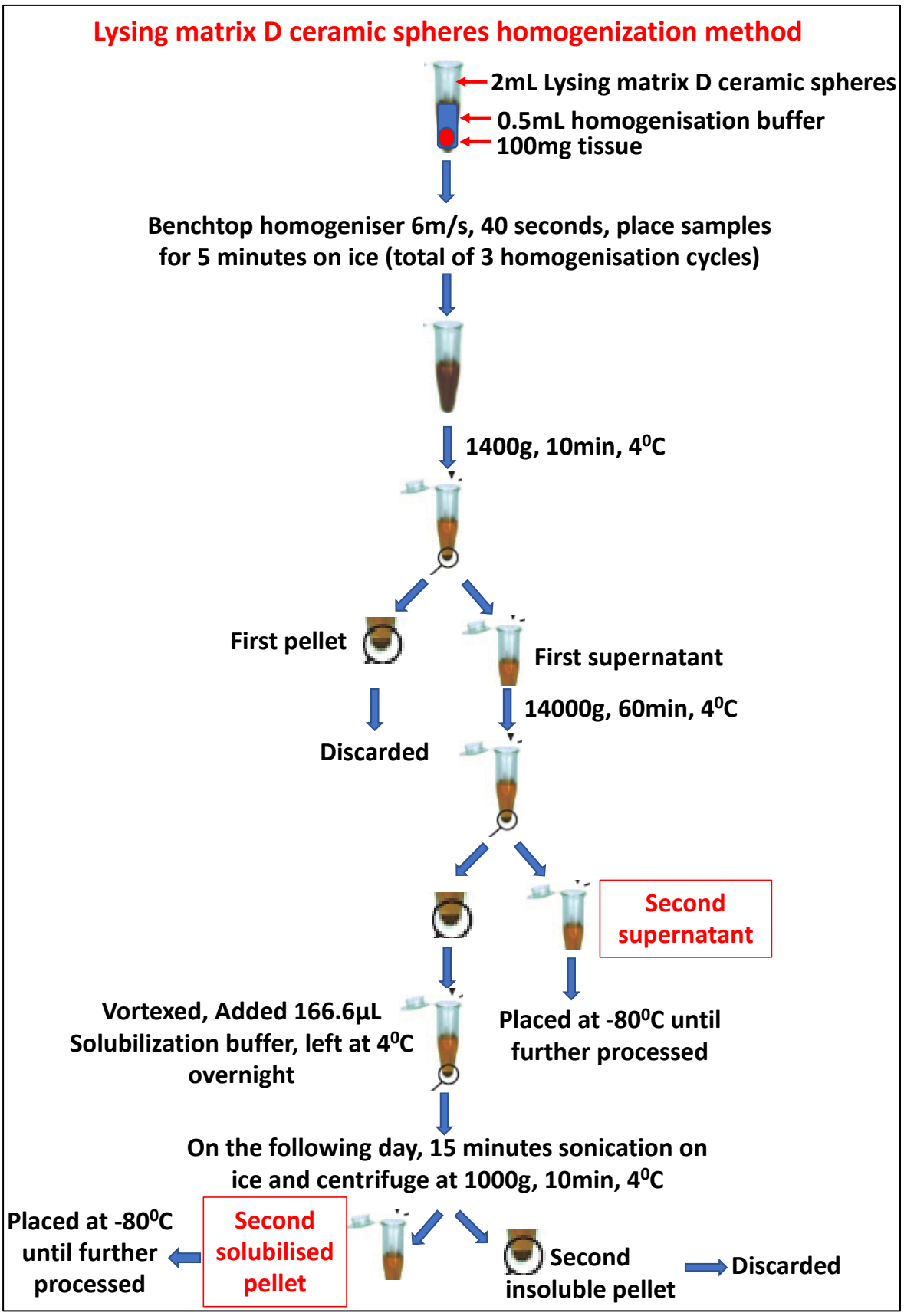


Figure 13. *This scheme shows the process of homogenising human tissue using the Lysing matrix D ceramic spheres homogenisation method. This figure has been created by Paul Fodor using Microsoft PowerPoint software version 16.53.*

2.6.3.3 Homogenisation of primary cells

A similar fractionation protocol as described in chapter 2.6.3.1 was applied in the case of isolated primary cells (peripheral blood mononuclear cells - PBMC) but with subtle modifications. Following isolation, the cells were taken out from the -80^{0}C freezer and 300µL of homogenisation buffer which consisted of sucrose (320mM), Tris base (10mM), KCl (50mM), EDTA (1mM), Igepal (0.5% v/v), 1/500 protease inhibitors and 1/100 phosphatase inhibitors, pH 7.8 was added to the cell pellet. Following this, the cells were thoroughly vortexed and disrupted by passing them through a 21 g needle for 25 times. The suspension was then vortexed and sonicated using an Ultra-Turrax sonicator (USC100T, VWR) for 15 minutes on ice. The primary cells were again disrupted by passing them through a 21 g needle for 25 times. The cell lysates were spun at 1300g for 5 minutes at 4^{0}C and the resulting first supernatant was again centrifuged at 14000g for 60 minutes at 4^{0}C. The emerging second supernatant was transferred into a clean 1.5mL Eppendorf tube and then stored at -80^{0}C until further processed. In this case, emerging second pellet was discarded. Figure 14 highlights the process involved in the homogenisation of primary cells [285,491].

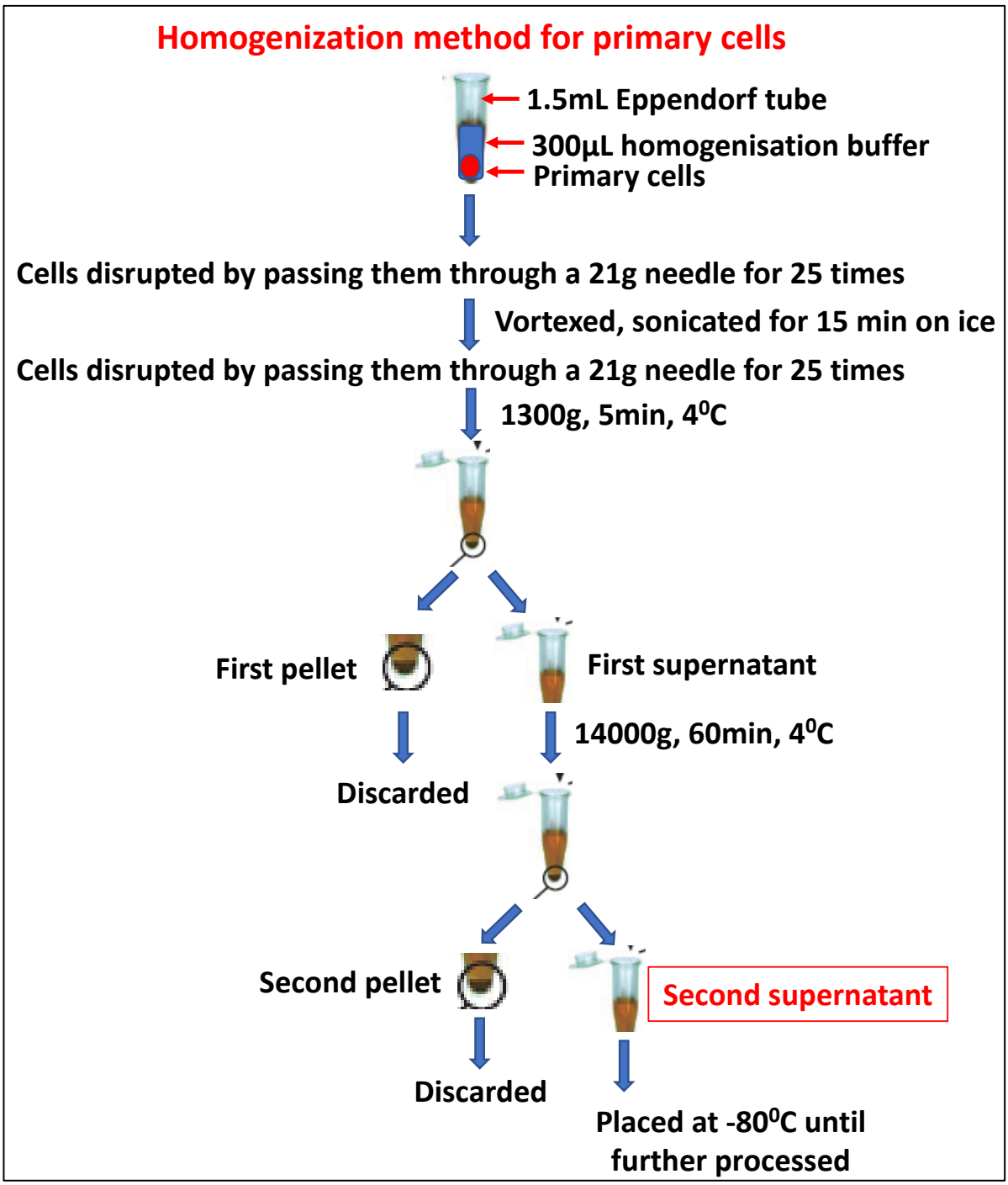


Figure 14. *This scheme shows the homogenisation method for isolated primary cells. This figure has been created by Paul Fodor using Microsoft PowerPoint software version 16.53.*

2.6.4 Protein determination

The protein content of second supernatant and second pellets originating from the human tissue and primary cell lysates was measured using the bicinchoninic acid (BCA) assay. Bovine serum albumin (BSA) protein standards were constructed at known concentrations of 0, 0.05, 0.1, 0.2, 0.4, 0.6, 0.8 and 1mg/mL using a BSA stock solution at a concentration of 10mg/mL diluted in 0.9% (w/v) NaCl (aq). Following this, 10µL of test samples (which have been diluted in 0.9% (w/v) NaCl (aq) accordingly) and protein standards were added to a 96 well plate in duplicate followed by the addition of 200µL of freshly prepared BCA working solution i.e. BCA with 2% (v/v) Copper sulphate ($CuSO_4$). The 96 well plate was incubated at 37^0C for 30 minutes with gentle shaking. The plate was read using a spectrophotometer at 562nm with a Thermo plate reader (MultiSkan Spectrum and SkanIt software v. 2.2). The protein concentration of unknown samples (mg/mL) was calculated based on a straight-line equation (y=mx+c) which was obtained by plotting the known concentration of BSA protein against the average absorbance values and by taking into account the test sample dilution factor. Following this, the western blotting samples were prepared by diluting the determined protein content of samples to the desired western blot concentration (e.g. 40µg/10µL) with Laemmli loading buffer (BioRad, Hemel Hempstead, UK, 161-0737) supplemented with 2% (v/v) β-mercaptoethanol (M6250, Sigma Aldrich) (50µL β-mercaptoethanol for every 950µL loading buffer). Western blotting sample aliquots were prepared (100µL) for each specimen in order to prevent freeze-thaw cycles and were stored at -80^0C until used [285,491].

2.6.5 IgG immunodepletion from trophoblast, SVA and myometrium tissue

Immunoprecipitation buffer (IP) was firstly prepared which consisted of Tris base (50mM), NaCl (150mM), EDTA (1mM), ethylene glycol tetraacetic acid (EGTA) (0.2mM) SDS (0.1%), Sodium Deoxycholate (0.3% w/v), 1/500 protease inhibitors and 1/100 phosphatase inhibitors, pH 7.5. 50µL of anti-human IgG (whole molecule)-agarose antibody developed in goat (Sigma, A3543) was added to a 0.5mL Eppendorf tube containing 200µL of ice-cold IP buffer. The tubes were thoroughly vortexed and spun at 1500RPM for 10 minutes at 4^0C (EBA 12R Hettich). The resulting supernatant was discarded and 200µL of fresh IP buffer was added to the agarose pellet. The tubes were again vortexed and centrifuged at the same parameters and the resulting supernatant discarded. In total there were three cycles of centrifugation and removal of supernatants. 150µL second supernatant or second pellet at a concentration of 13.3mg/mL (samples for IgG immunodepletion protocol were prepared following BCA assay protein measurement) was added to the emerging washed agarose pellet and the samples were left at 4^0C for 2 hours with gentle agitation. Following this, the tubes were spun again at 1500RPM for 10 min at 4^0C. The resulting supernatant (containing the protein samples which have been immunodepleted of IgG) was kept and subjected to a further BCA assay protein measurement prior to western blotting sample preparation and the emerging pellet discarded. Figure 15 highlights the process involved in the IgG immunodepletion of the placental and myometrium tissue lysates.

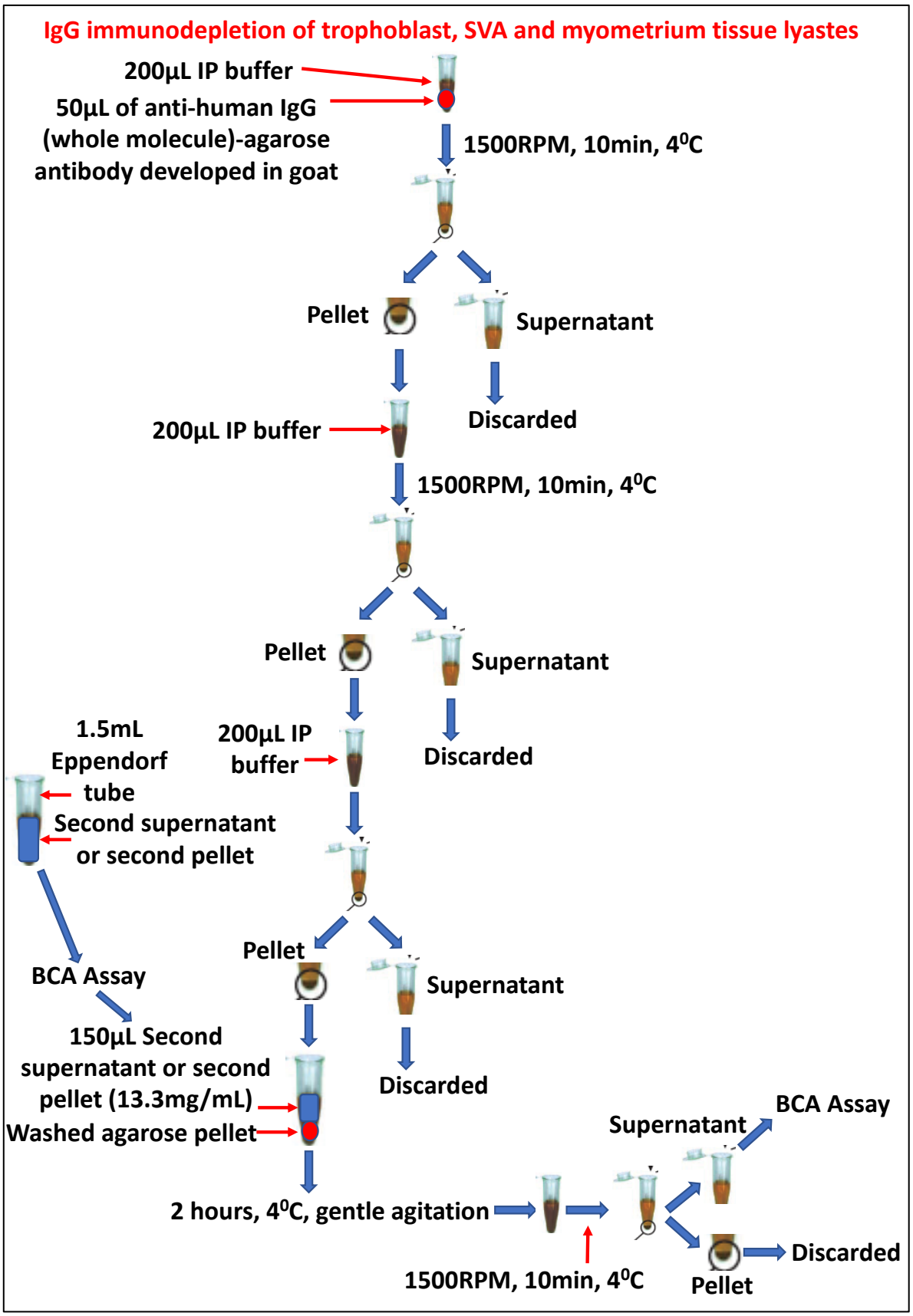


***Figure 15**. This scheme highlights the IgG immunodepletion method of trophoblast, SVA and myometrium tissue lysates. This figure has been created by Paul Fodor using Microsoft PowerPoint software version 16.53.*

2.6.6 SDS PAGE Electrophoresis and electroblotting

Sodium Dodecyl Sulphate Polyacrylamide Gel Electrophoresis (SDS-PAGE) was used as a method of separating the proteins according to their molecular weight and charge. In the present study, 7%, 10% and 15% (wt/vol) hand casted polyacrylamide gels were prepared (composition presented in appendix 7) and used for an adequate separation of small (Procaspase-1), medium (P2X7 receptor) and large size (NOD-like receptor protein 3 - NLRP3 inflammasome) proteins with a running buffer containing 0.025mM Tris base (pH 8.3), 0.192mM glycine, 0.1% (w/v) SDS. Similarly, 15 well 10% Mini-Protean TGX precast gels (Bio-Rad, catalogue number 4561036) were also used in the study. All tissue and cell western blotting samples were removed from -80^{0}C, denatured by boiling at 80^{0}C for 5 minutes (Techne, Dri-Block® Heater, DB-2D) and rested on ice. Each western blotting sample was then loaded into the polyacrylamide gel (15µL/15-well polyacrylamide gel or 30µL/10-well polyacrylamide gel). 5µL of precision plus protein Kaleidoscope Prestained protein standard (10-250kDa) was loaded into each gel to survey the migration of proteins (BioRad, 1610375). The same protein amount of tissue and cells was loaded into each gel as indicated in Chapter 3 unless otherwise stated (validation experiments to determine the optimal protein load into the gel or confirmation of no P2X7 receptor specific bands in the second supernatant of tissue and cells). The proteins were resolved for 50-60 minutes at 40mA (20mA for each polyacrylamide gel). Following this, the proteins were transferred on to the nitrocellulose membrane (0.45µm pore size, BioRad, 1620094) by electroblotting using a Bio-Rad Miniprotean 3 wet blot system (165-3301, Bio-Rad) for either 1 hour at 100V at 4^{0}C (for the purposes of further evaluating the P2X7 receptor and Procaspase-1 protein expression levels, unless otherwise stated) or for 1.5 hours at 100V at 4^{0}C (for further

investigating the NLRP3 inflammasome protein expression levels). The transfer buffer composition was 25mM Tris, 192mM Glycine, 20% (v/v) Methanol, pH 8.3. After this, all proteins were visualised using Ponceau S red solution (Sigma-Aldrich, Poole, UK, P7170) (0.1% w/v Ponceau, 5% v/v acetic acid) to evaluate the success of the transfer. The Ponceau S red solution was washed with Tris Buffered Saline (TBS) (pH 7.4) with 0.1% (v/v) Tween 20 (TBS-T) for 5 minutes. Also, in some cases, the polyacrylamide gels were stained with Coomassie G-250 stain (Simply Blue safe stain, Thermo Fisher, LC6065) for visualising the resolved proteins which have not transferred to the nitrocellulose membrane [285,491].

2.6.7 Blocking, control peptide blocking and antibody application

The nitrocellulose membrane was blocked with 5% (w/v) non-fat dry milk Marvel (Lincolnshire, UK) diluted in TBS-T for 1.5 hours at room temperature with gentle shaking. Following this, the blots were washed 6 times for 10 minutes each (gentle shaking) with TBS-T prior to adding the primary antibodies (see figure legend for dilutions) which were diluted in 3% w/v Marvel milk/TBS-T. Following addition of the primary antibody, the nitrocellulose membranes were left at 4^0C overnight with gentle agitation.

The corresponding blocking peptide of the rabbit polyclonal IgG anti P2X7 receptor antibody (Alomone Labs, BLP-PR004) was incubated at a concentration of 1µg peptide per 1µg of primary antibody (Alomone Labs, APR-004) at room temperature for 30 minutes with gentle shaking prior to addition to the nitrocellulose membrane [285,491].

2.6.8 β Actin measurement

Following the detection of each target protein, the same nitrocellulose paper was used for the purposes of evaluating the levels of the loading control protein β Actin. All immunoblots were stripped using a mild antibody stripping solution (ReBlot Plus Mild Antibody Stripping Solution 10X, Millipore, 2502) according to the manufacturer's instructions for 10 minutes. The solution was washed with TBS-T for 10 minutes and the nitrocellulose membrane blocked with 5% (w/v) Marvel milk dissolved in TBS-T for 90 minutes at room temperature. The immunoblots were washed 6 times for 10 minutes each with TBS-T, prior to the application of the primary β-Actin antibody (Abcam, Ab8227) diluted at either 1:2500 or 1:8000 in 3% (w/v) marvel milk/TBS-T and left overnight at 4^0C with gentle snaking to check for equal loading. This also facilitated quantitation of the protein density of all human tissue and cell types studied to recognise any variations in the density of expression [285,491].

2.6.9 Secondary antibody and data analysis

Following the removal of the unbound primary antibody from the nitrocellulose membranes using 6 washes (10 minutes each) of TBS-T, the immunoblots were incubated with the secondary antibodies (see figure legend for dilutions) which were conjugated to alkaline phosphatase (AP) and diluted in 3% (w/v) marvel milk/TBS-T for 90 minutes at room temperature. Following this, all western blots were washed 6 times (10 minutes each) using TBS-T, followed by 2 washes (10 minutes each) with TBS. The immunoblots were then developed using the enhanced chemiluminescent (ECL) detection system Immun-Star™ AP substrate Pack (BioRad, 170-5012). 2.5mL substrate was combined with 50μL enhancer and the mix added evenly to the nitrocellulose membrane which was protected from light. Following 10 minutes, the immunoblots were visualised using a ChemiDoc™ MP imaging system (version 4.2.1)

and all micrographs acquired analysed using Image Lab software (version 6.0.1). The control immunoblots corresponding to the P2X7 receptor and P2X7 receptor + Blocking peptide were examined alongside, and each nitrocellulose membrane was exposed for less than 10 minutes, with the exception of the NLRP3 inflammasome immunoblot presented in figure 12 which was exposed for 15 minutes. Using Image Lab software, the total band intensities were quantified via subtracting the levels of the background staining and the approximate molecular weight for each of the protein bands identified was evaluated. GraphPad Prism software (version 8.2.1) was used to analyse all western blotting data [285,491].

2.7 Stimulation of trophoblast tissue with D-glucose

Firstly, 500µL of glucose free media (RPMI 1640, Thermo Fisher, 11879020) supplemented with 100 units/mL penicillin and 100µg/mL streptomycin and varying concentrations of D-Glucose (0, 5.5, 10, 20 and 30mM) was added to a 24 well plate. Secondly, trophoblast tissue (100mg wet tissue) originating from healthy patients was added in individual wells of the 24 well plate which was incubated at 37^0C for 4 or 48 hours. Following this, the trophoblast tissue was collected in individual 1.5mL Eppendorf tubes corresponding to each of the experimental conditions and snap-frozen in liquid nitrogen prior to storage at -80^0C until further processed. Similarly, the tissue culture media was collected in individual 1.5mL Eppendorf tubes corresponding to each D-glucose treatment and placed in the -80^0C freezer until required. Also, trophoblast tissue biopsies (100mg) were snap frozen in liquid nitrogen immediately after placenta collection (t=0) and stored at -80^0C until processed i.e. not subjected to D-glucose stimulation and referred in the current studies as frozen control. The relative P2X7 receptor protein expression levels were assessed using the homogenised (Lysing matrix D ceramic spheres method) trophoblast tissue which was D-glucose

stimulated or not incubated with D-glucose (0mM). Also, myometrium tissue (second pellet) was used as a positive control for the P2X7 receptor protein expression levels. D-glucose was prepared using distilled water and 5 stock concentrations were prepared separately (0mM, 5.5mM, 10mM, 20mM and 30mM) comprising of a volume of 50mL. Each of the stock concentrations were sterilised using a 0.2μm pore size filter and stored at 4^0C for a period of up to 14 days.

The chosen concentration of D-glucose was based on two studies namely Koenen *et al* (2011) [497] and Zhou *et al* (2010) [389].

The same D-glucose stimulation of trophoblast tissue protocol was applied in a complementary study with a minor modification. Here, 500μL of glucose free media (RPMI 1640, Thermo Fisher, 11879020) supplemented with 100 units/mL penicillin, 100μg/mL streptomycin (Thermo Fisher, 15140122), 10% (v/v) fetal bovine serum (Sigma Aldrich, F9665) and varying concentrations of D-Glucose (0, 5.5 and 30mM) was used. In this case, 100mg of trophoblast (wet) tissue was incubated for 4 or 24 hours and the relative P2X7 receptor protein expression levels assessed using western blotting.

The tissue culture media was further used to assess the levels of released IL-1β and lactate dehydrogenase (LDH) at 4 or 48 hours. Moreover, interleukin-1β levels were measured in the second supernatant fraction of trophoblast tissue lysates originating from two healthy patients using a commercially available IL-1β DuoSet enzyme-linked immunosorbent assay (ELISA) kit (R&D Systems, DY201) for the purposes of assessing the cytosolic expression levels of the mature IL-1β prior to release into the extracellular space.

The same methodology was used in a similar experiment where the trophoblast (wet) tissue (100mg) was collected from 3 healthy patients and incubated for 4 or 48

hours with D-glucose (Sigma Aldrich, G7021) supplemented RPMI 1640 media (Thermo Fisher, 11879020) at concentrations of 0, 5.5, 10, 20 and 30mM in the presence and absence of cell lysis solution (LDH-Cytotoxicity Assay Kit II, Abcam, Ab65393) for the purposes of measuring the released lactate dehydrogenase (LDH) levels in the tissue culture media. In this case, 2 wells of the 24 well plate contained no trophoblast tissue but just 0mM D-glucose in the absence of the cell lysis solution which were used as background control for the purposes of analysing the released LDH levels.

2.7.1 Stimulation of CPA, SVA and trophoblast tissue with LPS, ATP and BzATP

Isolated trophoblast (wet) tissue (100mg) originating from 10 healthy patients was stimulated with RPMI 1640 media (Thermo Fisher, 11885084) supplemented with 100 units/mL penicillin and 100µg/mL streptomycin (control) (4h), ATP (10mM) for 4 hours, LPS (10µg/mL) (3.5 hours) +ATP (10mM) (0.5 hours) and LPS (10µg/mL) (3.5 hours) +BzATP (300µM) (0.5 hours). ATP was sourced from Sigma Aldrich (A6419), LPS was obtained from Sigma Aldrich (L2630) and BzATP was sourced from Sigma Aldrich (B6396). 500µL of the corresponding media was placed in 24 well plates and 100mg of trophoblast tissue was added to each well. The plate was initially incubated under humidified conditions at 37^0C in 5%CO_2/95%air for 3.5 hours. At this timepoint, ATP and BzATP were added to the corresponding wells and the plate further incubated at 37^0C (5%CO_2/95%air) for another 30 minutes. At the timepoint of 4 hours, the trophoblast tissue was collected and snap-frozen in liquid nitrogen followed by storing the tissue at -80^0C until further processed. Similarly, at the same timepoint, tissue culture media was collected placed in -80^0C until required. ATP was prepared using PSS at a stock concentration of 1M with the pH adjusted to 7.4 and stored in

aliquots of 10µL at -20^{0}C until required. Similarly, BzATP was prepared using PSS at a stock concentration of 30mM and stored in aliquots of 10µL at -20^{0}C until required. LPS was prepared using RPMI 1640 media (Thermo Fisher, 21875034) at a stock concentration of 1mg/mL and stored in aliquots of 5µL at -20^{0}C until required.

A similar stimulation protocol was used in the case of CPA and SVA tissue. Trophoblast tissue originating from 3 healthy patients was then removed from -80^{0}C and homogenised using the Lysing matrix D ceramic spheres for the purposes of evaluating the relative NLRP3 inflammasome protein expression levels in the second supernatant fraction of the tissue lysate. Furthermore, the tissue culture media of control and stimulated CPA, SVA and trophoblast tissue originating from 10 healthy patients was used to measure the levels of released IL-1β, IL-6 and IL-18 using commercially available ELISA kits (R&D Systems, USA, DY201, DY206 and DY119) [285,491]. In this case, the protocol used in the stimulation of CPA, SVA and trophoblast tissue with LPS, ATP and BzATP was based on two studies namely Maneta *et al* (2015) and Warren *et al* (2008), with few modifications in terms of the concentrations of compounds used LPS (10µg/mL) compared to 1µg/mL [491], ATP (10mM) compared to 5mM [285] and BzATP (300µM) compared to 200nM [491].

2.8 Isolation of PBMC

Mononuclear cells were isolated from peripheral blood (PBMC) using Histopaque® density gradient medium (Sigma Aldrich, 10771). Eight mL of heparinized cord blood were diluted with 8mL of RPMI 1640 medium (Thermo Fisher, 21875034) supplemented with 5mM L-glutamine (Invitrogen, Paisley, Scotland, 25030081), 100 units/mL penicillin and 100µg/mL streptomycin (Thermo Fisher, 15140122). Following this, 8mL of diluted blood was carefully added to 15mL of Histopaque® - 1077 medium and the tubes spun at 400g for 30 minutes at room temperature (acceleration 3,

deceleration 3) (Thermo Fisher, SL 16R Centrifuge). After this, the cloudy middle layer comprising of white blood cells was collected into a clean 15mL falcon tube, RPMI 1640 media was added up to 15mL and the tube spun at 300g for 10 min at room temperature (acceleration 9, deceleration 9). The supernatant was discarded and 15 mL of RPMI 1640 media was added to the white blood cell pellet followed by centrifugation at 300g for 10 minutes at room temperature (acceleration 9, deceleration 9). The supernatant was removed, and the resulting pellet was resuspended in 1mL RPMI 1640 media. The primary cells were counted using TC20 automatic cell counter (BioRad, 1450102) and the viability of the purified cell population was investigated using trypan blue (BioRad, 1450021). In total there were two maternal blood samples which have been used to isolate PBMC. The second supernatant of homogenised PBMC cells was used to evaluate the relative P2X7 receptor protein expression levels.

The protocol for the isolation of PBMC was based on Maneta *et al* (2015) [491] and Warren *et al* (2008) [285].

2.9 Enzyme linked immunosorbent assay (ELISA)

IL-1β, IL-6 and IL-18 concentration in the tissue culture media of unstimulated (control) and stimulated (ATP, LPS+ATP and LPS+BzATP) CPA, SVA and trophoblast tissue originating from 10 healthy placental samples was measured using commercially available enzyme-linked immunosorbent assay DuoSet (ELISA) kits (R&D Systems, USA, IL-1β – catalogue number DY201, IL-6 catalogue number DY206 and IL-18 catalogue number DY119). ELISAs were performed according to the manufacturer's instructions. The optical absorbance was read at 450nm and 570nm with a Thermo plate reader (MultiSkan Spectrum and SkanIt software, version 2.2). The concentration of all three interleukins was determined from standard curves and

analysed using Dunn's multiple comparison tests (GraphPad Prism, Version 8.2.1) [285,491].

2.10 Lactate dehydrogenase (LDH) assay

The levels of lactate dehydrogenase (LDH) which have been released into the tissue culture media from D-Glucose stimulated (0, 5.5, 10, 20 and 30mM) trophoblast tissue after 4 and 48 hours of challenge originating from 4 healthy placental samples were measured using two commercially available kits (Abcam, AB102526 and AB65393) according to the manufacturer's instructions. The optical absorbance was read at 450nm with a Thermo plate reader (MultiSkan Spectrum and SkanIt software v. 2.2). The released LDH levels measured using AB102526 kit were calculated from a standard curve. In the case of measuring the released LDH levels using AB65393 kit, since the quantification of plasma membrane damage took place after the tissue stimulation, there was no high and low control for determining the cytotoxicity (%) levels. Therefore, the experiment was repeated, and D-glucose stimulated (0, 5.5, 10, 20 and 30mM) trophoblast tissue (originating from 3 healthy placental samples) for 4 and 48 hours was incubated in the presence and absence of the cell lysis solution. The low control (minimal LDH release) was 5.5mM D-Glucose stimulated trophoblast tissue without cell lysis, the high control (maximal LDH release) was 5.5mM D-Glucose stimulated trophoblast tissue with cell lysis and the background control was 0mM D-glucose media with no tissue and no cell lysis. In the analysis of data, each timepoint (4 and 48 hours) possessed its own high and a low control. All data was analysed using GraphPad Prism (version 8.2.1) [498].

2.11 Confocal and wide field microscopy

Chorionic plate artery smooth muscle cells which have been isolated via the explant method were cultured on glass coverslips (placed in a 24 well plate) in Dulbecco's Modified Eagle Medium (DMEM) (Thermo Fisher, 11885084) supplemented with 10% (v/v) heat inactivated FBS, 100 units/mL penicillin and 100µg/mL streptomycin until approximately 70% confluent. Following removal of media, the cells were washed twice with 1mL phosphate buffered saline (PBS; Sigma Aldrich, SKU806522) at room temperature for 5 minutes with gentle shaking. The primary cells were fixed using 4% (w/v) paraformaldehyde (PFA; Sigma Aldrich, P6148) (pH 7.4) for 5 minutes at 4^0C. PFA was carefully aspirated, and the coverslips washed 3 times with 1mL PBS at room temperature for 5 minutes with gentle shaking. The cells were incubated for 5 minutes at room temperature with 500µL 0.5% (v/v) Igepal (Sigma Aldrich, I8896)/PBS, followed by three washes with 1mL PBS at room temperature for 5 minutes with gentle shaking. The primary cells were then incubated with 500µL 3% BSA (Sigma Aldrich, A6043)/1%Glycine (w/v) (Sigma Aldrich, SKU-G2879) in phosphate buffered saline (w/v) for 15 minutes at room temperature. Following this, the cells were washed three times with PBS at room temperature for 5 minutes with gentle shaking. Blocking was undertaken using 250µL of 20% goat serum (v/v) (Sigma Aldrich, G9023) in PBS for 30 minutes at room temperature with gentle shaking. The blocking solution was removed, and the cells incubated with primary antibodies against the P2X7 receptor, α-Actin, CD31, Vimentin and NLRP3 inflammasome (P2X7 Primary antibody, Alomone Labs, APR004, 1:600 dilution, primary antibody for α smooth muscle actin was rabbit monoclonal [E184] to α smooth muscle actin, 1:500, Abcam, AB32575, NLRP3 primary antibody, Novus, NBP2-12446, 1:20 dilution, Vimentin primary antibody, Dako, M0725, 1:20, CD31 primary

antibody, Abcam Ab28364, 1:20 dilution) and left overnight at 4^0C with subtle shaking. A secondary antibody control was also used where the primary antibody against the P2X7 receptor and vimentin were omitted. Following aspiration of the primary antibody, the primary cells were washed 3 times with 1mL PBS at room temperature for 5 minutes with gentle shaking. The cells were coated with the corresponding secondary antibodies (anti-rabbit IgG (whole molecule) FITC antibody produced in goat, 1:100 dilution, Sigma, F9887) for 30 minutes in a dark environment with subtle shaking. The secondary antibody was removed, and the cells were washed 3 times with 1mL PBS at room temperature for 5 minutes with the 24 well plate containing the coverslips covered with aluminium foil. The coverslip with cells was mounted on a microscope slide using Vectashield HardSet anti fade mounting medium with DAPI (H1500, Vector Laboratories). An exception to this was the cells stained for the P2X7 receptor, vimentin and NLRP3 inflammasome (Figure 78 and 79) where 500µL of 100µg/mL DAPI (Thermo Fisher, 62248) in PBS was added to the cells for 5 minutes with gentle shaking and the 24 well plate covered with aluminium foil. The cells were then washed 3 times with PBS at room temperature with gentle shaking with the primary cells protected from light. In this case, the cells were then mounted on a microscope slide using Vectashield antifade mounting medium (H1000, Vector Laboratories). Mounted slides were positioned face down on a slide stage and analysed using Zeiss LSM880 confocal laser scanning microscope (Carl Zeiss, Germany) and Zen 2009 software for multichannel acquisition and image processing. Micrographs were acquired using three laser lines in single scans for the purposes of diminishing any overlap across the fluorescein isothiocyanate (FITC), tetramethylrhodamine (TRITC) and 4',6-diamidino-2-phenylindole (DAPI) channels. In this case, the pinhole diameter used in all confocal imaging was 1 airy unit. An

ultraviolet laser was used to inspect DAPI immunofluorescence (372nm excitation, 385nm emission), an agon laser was used to visualise FITC (488nm excitation, 505-530nm emission) and a Helium laser was used to assess TRITC immunofluorescence (546nm excitation, 560nm emission). Furthermore, the immunofluorescence characteristics a few of the cell preparations were visualised using Zeiss LSM Exciter widefield microscope [53,499,500]. The immunofluorescence protocol was based on Maneta *et al* (2015) [491] and Warren *et al* (2008) [285].

2.12 mRNA analysis and RT-qPCR

Total RNA was extracted from stem villous arteries (50mg frozen tissue) originating from 2 healthy and 2 preeclamptic placental samples using mechanical disruption. The tissue was added to Lysing Matrix D ceramic spheres (MP Biomedicals, Santa Ana, CA, USA, 116913100) and homogenised in 2mL tubes containing 600µL Buffer RLT (RNeasy Mini kit, QIAGEN, UK, 74104) (10mL RLT Buffer + 100µL β-mercaptoethanol). The SVA's were homogenised using MP Fast-Prep-24 homogeniser (MP Biomedicals) at 6m/s for 40 seconds for 3 cycles with the tubes rested on ice in between each cycle. The samples were spun at 12000g for 3 min at 4^0C and RNA extraction was undertaken according to the manufacturer's protocol. The RNA was cleared from genomic DNA using an RNase-Free DNase set (QUIAGEN, 79254) according to the instructions provided from the manufacturer. The total RNA extracted was finally eluted in RNase-free water. The purity and quantity of extracted total RNA was evaluated using a Nanodrop ND-1000 spectrophotometer (Thermo Fisher Scientific, USA) via absorbance ratio measurements of A_{260}/A_{280}. The integrity of extracted RNA was assessed using 1% (w/v) agarose gel electrophoresis which highlighted clear 18S and 28S rRNA bands.

First strand complementary DNA (cDNA) was synthetised from RNA using a High-capacity cDNA RT kit (Thermo Fisher, USA) according to the instructions provided by the manufacturer. Every reverse transcription reaction was undertaken in a 20µL final volume which comprised of 10µL RNA at a concentration of 120ng/µL (1200 ng/µL totRNA) with the incubations undertaken in duplicate, one containing the reverse transcription enzyme (+RT) and one where the reverse transcriptase is substituted with water (-RT). Using the synthetised cDNA as template, quantitative polymerase chain reactions were undertaken in a total volume of 20µL for the purposes of evaluating the expression levels of 3 target and 3 reference genes. All assays were undertaken in triplicate and were accompanied by a no-template and negative control using the CFX Connect Real-Time PCR Detection system (BioRad). The evaluated genes were sequence-specific Taq-Man® probes consisting of an oligonucleotide labelled with a quencher and a fluorescent dye. A master mix was produced for each target and reference genes studied using TaqMan® listed Assays-on-Demand probes (Life Technologies, Thermo Fisher Scientific). The quantitative polymerase chain reactions were undertaken in 20µL final volume consisting of 2µL complementary DNA and 18µL master mix using a qPCR schedule comprising of 40 cycles of 95^0C (10 minutes), 95^0C (15 seconds) and 60^0C for 1 minute. The target genes were *P2RX7*, *NLRP3* and *Caspase-1*. The reference genes were *HPRT-1*, *CYC-1* and *TOP-1*. The TaqMan® probes were purchased from Thermo Fisher Scientific: *NLRP3* (Hs00918082_m1), *P2RX7* (Hs00175721_m1), *Caspase-1* (Hs00354836_m1), *HPRT-1* (Hs02800695_m1), *TOP-1* (Hs00243257_m1), *CYC-1* (Hs00357717_m1). The PCR efficiency of the P2X7 and NLRP3 assays was investigated using a five-point 5-fold dilution series of complementary DNA which was

run using the above-mentioned conventional qPCR methodology and calculated from the slopes of the standard curves using equation 1:

$$Efficiency = \left(10^{\frac{-1}{Slope}}\right) * 100 \quad (1)$$

Equation 1. *This equation highlights the method of calculating the qPCR efficiency of P2X7 and NLRP3 TaqMan® assays.*

Quantification of *P2X7*, *NLRP3* and *Caspase-1* gene expression levels was undertaken in accordance with Minimum Information for Publication of Quantitative Real-Time PCR Experiments (MIQE) guidelines relative to the geometric mean of the reference genes *HPRT-1*, *CYC-1* and *TOP-1* using GenEx software (Version 7, MultiD Analysis, Göteborg, Sweden) [496,498]. The RT-qPCR protocol is based on Ofinran *et al* (2016) [496].

2.13 Dissociation of human placental vascular smooth muscle cells originating from chorionic plate artery (CPA)

Segments of chorionic plate artery were dissected, placed in a 1.5mL Eppendorf tube and incubated for 20 minutes at 35^0C and 800RPM (Eppendorf Thermomixer Comfort) with papain (1mg/mL) (Sigma-Aldrich, P4762) and dithiothreitol (DTT) (0.2mg/mL) (Sigma-Aldrich, D0632). Papain was prepared fresh each day using PSS at a stock concentration of 1mg/mL. Also, DTT was prepared fresh each day using PSS at a stock concentration of 0.2mg/mL. The 1.5mL Eppendorf tube containing the tissue was centrifuged at 1200RPM for 2 minutes at room temperature (EBA 12R, Hettich). The supernatant was discarded, and the tissue was subjected to a second incubation of 7 minutes at 35^0C in collagenase type 1A (1mg/mL) (Sigma-Aldrich, C9891). Similarly, collagenase type 1A was prepared fresh each day using PSS at a stock concentration of 1mg/mL. The 1.5mL Eppendorf tube containing the tissue was

centrifuged at 1200RPM for 2 minutes and the supernatant was discarded. This step was repeated for a total of 3 times. The disrupted tissue was resuspended in 500µL of DMEM (Thermo Fisher, 11885084) supplemented with 100 units/mL penicillin, 100µg/mL streptomycin and 10% (v/v) FBS, triturated and the cell suspension was plated on glass coverslips. Papain, DTT and collagenase type 1A were prepared in physiological salt solution buffer with the following composition: 119mM NaCl, 4.69mM KCl, 2.4mM $MgSO_4$, 25mM $NaHCO_3$, 1.17mM KH_2PO_4, pH 7.4. The cells were cultured until approximately 70% confluent in fixed in acetone (Sigma Aldrich, 179124): methanol (Sigma Aldrich, 322415) (1:1 ratio). A similar immunocytochemistry protocol was used as described in chapter 2.11 with a minor change in that the cells were blocked immediately after fixation. The smooth muscle cells were stained for the P2X7 receptor, Vimentin, CD31 and α-Actin. A secondary antibody control was also used where the primary antibody against the P2X7 receptor was omitted (in this case the isolated SMC were cultured on a collagen type 1 coated coverslip). The protocol of isolation of CPA-SMC is based on Brereton *et al* (2013) [501] with the following modifications in the concentration of compounds used: DTT (0.2mg/mL) compared to 1mg/mL [501] and beside collagenase type 1A (used at the same concentration of 1mg/mL), the authors have also used collagenase type F (1mg/mL) [501]. Also, the concentration of some of the compounds of physiological salt solution was different as the authors have used (in mM): 120 NaCl, 25 NaHCO3, 4.2 KCl, 0.6 KH2PO4, 1.2 MgCl2, 11 Glucose; pH 7.4 [501].

2.14 Isolation and culture of chorionic plate artery smooth muscle cells (CPA-SMC) from term healthy, gestational and type 1 diabetes mellitus human placenta samples

The isolation process of chorionic plate artery explants was undertaken in a sterile Class II biosafety cabinet using appropriate aseptic techniques. The smooth muscle cells were cultured from human placental chorionic plate artery explants. Isolated chorionic plate tissue fragments were added to Hanks Balanced Salt Solution (HBSS) (Thermo Fisher, 14175046) supplemented with 100 units/mL penicillin, 100µg/mL streptomycin and 10mM HEPES (Sigma Aldrich, H3537-100mL) which was warmed prior to collection of the placenta sample. The newly dissected chorionic plate arteries were cut along the segment of the artery for the purposes of revealing the lumen and 1cm^3 fragments were gently positioned with the endothelial cells facing down on a 24 well plate. After placing 1 piece in each well of the plate, warm DMEM low glucose (Thermo Fisher Scientific, 11885084) supplemented with 100 units/mL penicillin, 100µg/mL streptomycin and 10% (v/v) FBS was added to all wells of the 24 well plate. The culture plate was placed in an incubator at 37^{0}C which was supplied with 5%CO_2/95%air. After 24 hours, the media was carefully changed with 1mL DMEM + 100 units/mL penicillin + 100µg/mL streptomycin and 10% (v/v) FBS. The media was replaced at every 2-3 days. After approximately 23-30 days, the primary cells were serum starved for 24 hours with DMEM + 100 units/mL penicillin + 100µg/mL streptomycin for the purposes of removing any proliferating endothelial and fibroblast cells. The isolated smooth muscle cells were then passaged into a T-25 tissue culture flask by aspirating the culture media, washing the cells once with HBSS (to adequately remove the remaining FBS in the flask) and incubating the cells with 0.125% (v/v)

Trypsin ethylenediaminetetraacetic acid (Trypsin-EDTA; Sigma Aldrich, T3924) for approximately 2 minutes at 37^0C. The 12 well plate was gently tapped to encourage primary cell detachment from plastic. Fetal bovine serum was added to each well and the cells were relocated in a 15mL universal tube which was spun at 130g for 5 minutes at room temperature. Following this, the supernatant was aspirated, and the cells washed for a second time in HBSS supplemented with 100 units/mL penicillin, 100µg/mL streptomycin and 10mM HEPES for the purposes of removing remaining Trypsin-EDTA. The primary cell pellet was lastly resuspended in 5mL DMEM supplemented with 100 units/mL penicillin, 100µg/mL streptomycin and 10% (v/v) FBS and added to the T-25 flask [502]. This SMC isolation protocol is taken from Leik *et al* (2004) with a slight modification in that the primary cells were washed in HBSS without Nystatin (50 U/mL) as indicated by Leik and colleagues [502].

In terms of isolating the smooth muscle cells from the chorionic plate arteries of the human term placental samples, an advantage of the tissue explant method is that it yields to a high number of isolated cells that may be either passaged further, frozen in liquid nitrogen or even used directly for immunocytochemistry, immunophenotyping or permeability experiments. A further benefit of this isolation technique is that it gives rise to a single population of cells as shown from the immunophenotypic data presented in chapter 5.3.1.6 that are positive for CD73, CD105, CD90 and negative for CD45, CD34, CD14, CD11b, CD19 and HLA-DR.

However, the disadvantage of this technique is that it takes approximately 3-4 weeks for the cells to grow and reach a full confluency in the 6,12, or 24 well tissue culture plates. Special care must be taken when changing the media not to disturb the attached explants (as less cells will grow in the case if the explant becomes

disconnected) which might give rise to a more time-consuming procedure, especially when having to replace it in multiple 24 well plates.

A graphical representation of the CPA-SMC isolation technique is presented in the figure 16:

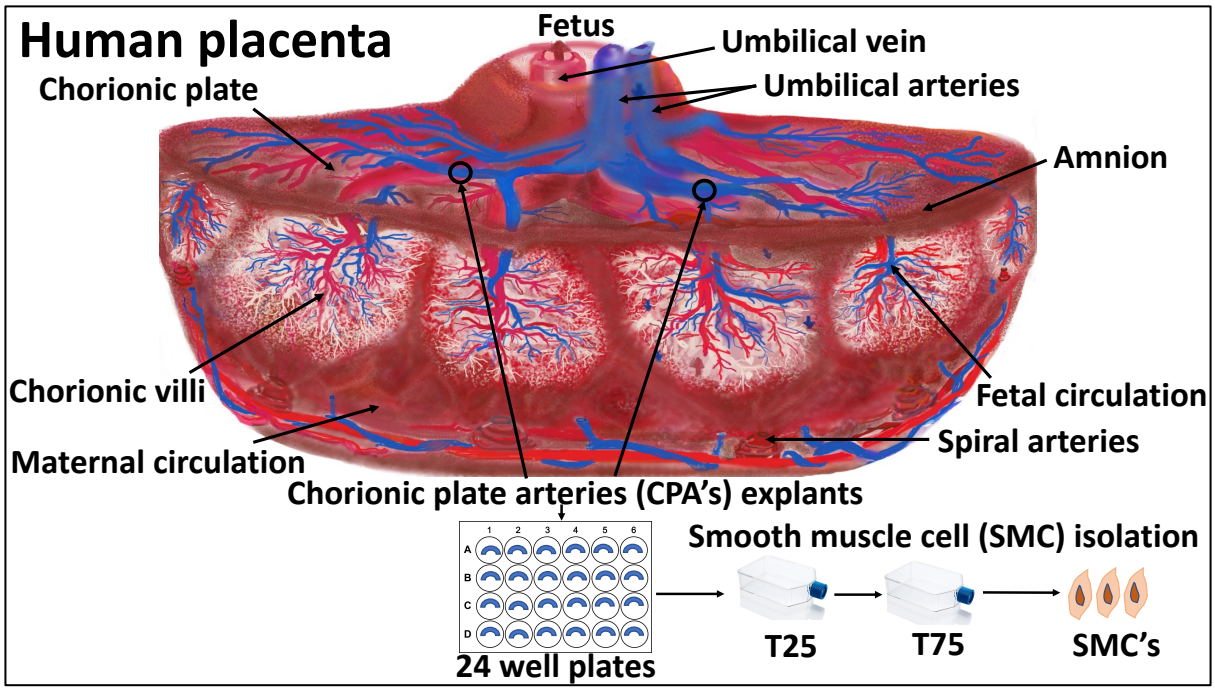


***Figure 16**. This scheme shows a generic summary of the isolation process of human placenta CPA-SMC cells. The chorionic plate explants are excised and placed with the endothelium facing down on a 24 well plate. Following several media changes and serum starvation for 24 hours the smooth muscle cells are further sub-cultured into T25 and T75 flasks before the start of further in vitro studies for instance immunocytochemistry, immunophenotyping or permeability studies. This figure has been hand drawn by Paul Fodor using Autodesk SketchBook software version 8.7.0.*

A further disadvantage of this smooth muscle cell isolation technique is the significant time spent at the beginning of the isolation in dissecting the arteries from the chorionic plate, preparing them into a flat surface and facing them with the endothelium touching the plastic of the tissue culture plates. This is due to the small explants that are approximately 1-2mm^3 in diameter involving a meticulous dexterity and taking into account 5 explants per well of a 6 well-plate. Also, all dissection instruments have to be autoclaved individually to avoid a potential contamination.

Another important advantage of this human smooth muscle cell isolation technique is that it does not involve special equipment or any digestion enzymes or reducing agents. This easy to follow and cost-effective isolation technique to retrieve the chorionic plate artery smooth muscle cells presents many advantages not only for the purposes of undertaking immuno-expression studies but also as a point of view of potentially using the cells for further *in vitro* functional investigations such as constructing a reliable chorionic blood vessel. This will contribute greatly to our understanding of placental vascular function and may be useful for further complementary studies.

2.15 Calculation of primary smooth muscle cells population doubling time

The doubling time of the human placenta chorionic plate artery smooth muscle cells is strongly linked with the advancement of the cell culture proliferation in terms of average time lapsed for a cell to get through all phases of the cell cycle and is usually approximated with counts of the cell population over a period of several days.

According to the American Type Culture Collection (ATCC), the cell population doubling time or in other words the period needed for cultured cells to double in number may be determined as follows:

$$DT = \frac{T * \ln(2)}{\ln\left(\frac{X_e}{X_b}\right)} \quad (2)$$

Equation 2. *This equation highlights the method of calculating the doubling time of the smooth muscle cells depending on the number of seeded and harvested cells and the time for the cells to grow to full confluency. DT represents the doubling time (days), T denotes the incubation time (days), X_b suggests the cell number at the start of the culture incubation time and X_e is the cell number at the end of culture incubation time.*

On the other side, this equation does not take into account the lag phase i.e. the period between seeding the cells and the start of cell growth, which may account from a few hours to potentially many days according to the cell classification. As a result, the estimation may highlight a declined growth trajectory, which may give rise to an abnormal elevated population doubling time.

As this cell proliferation parameter is characterised by the mean time of a cell population to double in number during the straight exponential growth stage, overall, the determination of the doubling time should account for the cell number measured for instance every day for a long enough period in order to observe lag, log and stationary proliferation phases of the cell-renewal curve. As a result, by plotting time versus the number of cells counted and determining the doubling time using data from the exponential growth phase of the cells, a more accurate and realistic representation of this parameter may be obtained.

Also, the equation used in calculating the doubling time of the chorionic plate artery smooth muscle cells does not take into account the plateau growth phase when the cells become confluent due to the fact that the sub-culturing period was subjectively determined when the confluency of the cells reached a percentage greater than 80%.

Moreover, when calculating the doubling time of primary cells, the viability of seeded and harvested cells should also be taken into account by using an exclusion dye for mammalian cells which have grown in monolayer culture conditions such as trypan blue.

2.16 Surveying the expression of human placenta smooth muscle cell myofilamentous protein α-smooth muscle actin

Isolated human placenta chorionic plate artery smooth muscle cells originating from a healthy volunteer (N15072019) were grown in a T75 flask until passage 2 followed by sub-culturing and seeding $1x10^4$ cells/$1.12cm^2$ directly on membrane inserts (12mm diameter, 0.4µm pore size polyethylene terephthalate membrane material; Corning, 3460). CPA-SMC's were left to grow on inserts for 13 days with media change (DMEM-low glucose+ 10% (v/v) FBS+100units/mL penicillin and 100µg/mL streptomycin) every 2 days in both apical and basal compartments of the transwell system. This experiment was primarily undertaken for the purposes of investigating the barrier integrity created by the smooth muscle cells using permeability studies. Following this preliminary experiment to initially establish a reliable chorionic vessel *in vitro*, the cells were further subjected to immunocytochemistry for α-smooth muscle actin using the methodology presented in figure 25. The primary antibody for α smooth muscle actin was rabbit monoclonal [E184] to α smooth muscle actin, 1:500 dilution, Abcam, AB32575. The secondary antibody was anti-rabbit IgG (whole molecule) FITC antibody produced in goat, 1:100 dilution, Sigma, F9887 [285,491]. The immunocytochemistry protocol is taken from Ebrahim and Leach (2015) [503] and Leach *et al* (2004) [97].

2.17 Stimulation of CPA-SMC with ATP, BzATP and A740003

CPA-SMC cells ($3*10^4$; passage 2) which have been isolated from a healthy placenta sample (T3027) using the tissue explant method were seeded on glass coverslips and cultured until 70% confluent. The primary cells were then stimulated with ATP, BzATP and A740003 as highlighted in table 4. ATP, BzATP and A740003 solvents and concentration of stock solutions are presented in chapter 2.5. The cells were then stained for the P2X7 receptor using the protocol highlighted in chapter 2.11. The coverslip with cells was mounted on a microscope slide using Vectashield HardSet anti fade mounting medium with DAPI (H1500, Vector Laboratories). Bright field micrographs were also acquired in this case. All images were acquired using Zeiss LSM Exciter widefield microscope. Following image acquisition, a pre-determined electronic grid was placed over each of the P2X7 receptor fluorescent micrographs (acquired using the FITC channel) and the mean fluorescence intensity (MFI) levels were quantified using systematic random sampling in every third consecutive square, resulting in 29 overall MFI levels obtained for each picture acquired using ImageJ software version 1.52q. The MFI data was analysed using GraphPad Prism software (version 8.2.1.).

CPA-SMC stimulations	
4 hours	
DMEM low glucose (control)	
Control + 0.1% DMSO	
Control + 1µM A740003	
1µM ATP	
10µM ATP	
100µM ATP	
1mM ATP	
5mM ATP	
10mM ATP	
3.5 hours +	**0.5 hours**
Control +	1µM ATP
Control +	10µM ATP
Control +	100µM ATP
Control +	1mM ATP
Control +	5mM ATP
Control +	10mM ATP
1µM A740003 +	1µM ATP
1µM A740003 +	10µM ATP
1µM A740003 +	100µM ATP
1µM A740003 +	1mM ATP
1µM A740003 +	5mM ATP
1µM A740003 +	10mM ATP
Control +	1µM BzATP
Control +	10µM BzATP
Control +	300µM BzATP
1µM A740003 +	1µM BzATP
1µM A740003 +	10µM BzATP
1µM A740003 +	300µM BzATP

Table 4. *This table highlights the concentration of compounds used to stimulate the CPA-SMC cells as well as the period of stimulation.*

2.18 Immunohistochemistry

The P2X7 receptor and CD31 immunolocalisation has been investigated in isolated human placental villous tissue samples originating from 12 healthy volunteers and 6 diet controlled gestational diabetic patients, as well as in isolated chorionic plate arteries originating from 2 placental samples of healthy patients. Placental villous biopsies and chorionic plate arteries were acquired from three quadrants, midway between the point of umbilical cord insertion into the chorionic plate and the placental rim. Fresh placental villous tissue was fixed in 4% (w/v) paraformaldehyde (Sigma Aldrich, P6148) (exception CPA which was fixed in 1% (w/v) paraformaldehyde), frozen in nitrogen-cooled isopentane (Sigma Aldrich, 78-78-4) and stored at -80^{0}C until required. One randomly chosen block (from a total of ten different blocks) per placenta sample was cryo-sectioned using Leica CM 3050S cryostat (Leica Biosystems) and two sections (10μm thick) were acquired at different depths. Cryo-sections were air dried and washed in 0.1M PBS (Thermo Fisher Scientific, BR0014G) / 0.1% (w/v) BSA (Sigma Aldrich, A9418) prior to permeabilization with 0.15% (v/v) Triton X-100 (Sigma Aldrich, X100) in 0.1% (w/v) BSA/PBS for 10 minutes. Following this, the cryosections were washed 3 times (10 minutes each) in 0.1% (w/v) BSA/PBS and blocked with 5% (v/v) normal human serum (Sigma Aldrich, S1) in 0.1% (w/v) BSA/PBS for 30 minutes at room temperature. Sections were incubated overnight at 4^{0}C with rabbit polyclonal IgG anti-human P2X7 receptor antibody (Alomone Labs, APR004, 1:50 dilution) and mouse monoclonal IgG_1 [JC/70A] anti-human CD31 antibody (Abcam, Ab9498, 1μg/mL) diluted in 5% (v/v) normal human serum in 0.1% (w/v) BSA/PBS. A secondary antibody control was also undertaken where the primary antibody against the P2X7 receptor and CD31 were omitted. After this, the cryo-sections were washed 3 times (10 minutes each) with 0.1% (w/v) BSA/PBS and the

sections incubated for 1 hour at 37^0C with anti-rabbit IgG (whole molecule) FITC antibody produced in goat (Sigma Aldrich, F9887, 1:100 dilution) and anti-mouse IgG (whole-molecule) TRITC antibody produced in goat (Sigma Aldrich, T5393, 1:50 dilution). The cryo-sections were washed 3 times (10 min each) with 0.1% (w/v) BSA/PBS in the dark, followed by 1 wash (10 minutes) with 0.1M PBS and lastly, 1 wash (5 minutes) with distilled water before to mounting with Vectashield® antifade mounting medium (Vector Laboratories, H1000). Seven images (obtained by systematic random sampling of entire sections) from both FITC and TRITC channels were acquired per block from random fields of view using a Nikon Coolpix 995 camera (Nikon, U.K.) ensuring all P2X7 receptor and CD31 positive placental villi microvessels were counted. The image files were renamed to ensure anonymity of the study group. Once counting has been finished, the files were unblinded to undertake the statistical analysis. Similarly, the P2X7 receptor positive syncytiotrophoblast profiles were also counted and the fluorescence intensity levels rated in a scale starting with 0 (least intense), 1, 2, 3 and 4 (most intense). All images were analysed using ImageJ (version 1.52q) and GraphPad Prism software (version 8.2.1.). A similar protocol was used in the case of isolated chorionic plate arteries originating from 2 healthy patients which were transversally cryosectioned and stained for the P2X7 receptor and CD31 [483,503]. The immunohistochemistry protocol is taken from Ebrahim and Leach (2015) [503] and Pang *et al* (2017) [119].

2.19 Human umbilical vein endothelial cells isolation

HUVEC cells were isolated from freshly collected term umbilical cords using the 0.1% (w/v) collagenase type II (Thermo Fisher Scientific, 17101015) flushing method. The cells were grown up to passage 5 in T25 or T75 flasks which were coated with 1% (w/v) gelatin (Sigma Aldrich, G9391-100g) in complete endothelial cell medium M199 (Thermo Fisher, 22340-020) supplemented with 20% (v/v) FBS (Sigma Aldrich, F9665) + heparin sodium salt (50µg/mL; Sigma Aldrich, H3149-100KU) + endothelial cell growth supplement (75µg/mL; Sigma Aldrich, E2759-15mg) + penicillin (100U/mL) + streptomycin (100µg/mL) (Thermo Fisher Scientific, 11536481) under humidified conditions at 37^0C and 5%CO_2/95%air . A schematic representation of the HUVEC isolation technique is presented in figure 17 which highlights the overall process after the freshly umbilical cords were received into the primary cell culture laboratory. The HUVEC isolation protocol is taken from Jaffe *et al* (1973) [504], Ebrahim and Leach (2015) [503] and Pang *et al* (2017) [119].

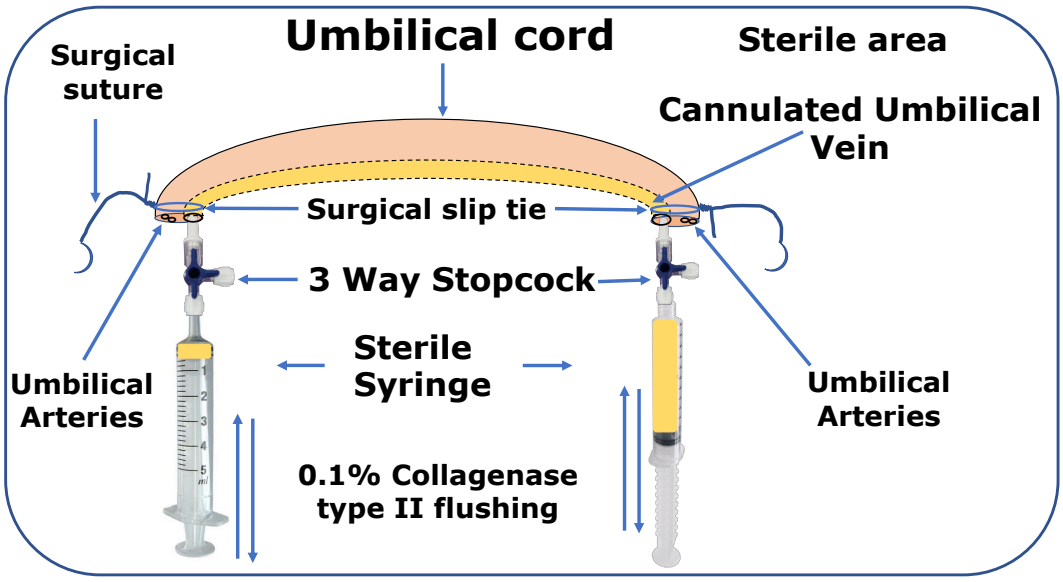


***Figure 17**. This scheme summarizes the isolation technique of HUVEC cells from the umbilical cord of healthy patients using the 0.1% (w/v) collagenase type II (dissolved in M199 medium supplemented with 100 U/mL penicillin and 100µg/mL streptomycin) flushing method. This figure has been hand drawn by Paul Fodor using Microsoft PowerPoint software version 16.53 and has been adapted from Marin et al (2001) [505].*

When it comes to isolation of HUVEC cells, one of the advantages of using the current technique is the rapidity of obtaining the cells and also the elevated number of endothelial cells isolated, which is in usually in the range between 1-2 million cells per umbilical cord. A further advantage of this technique is that the umbilical cord could be kept in 0.9% (w/v) NaCl (aq.) supplemented with 100units/mL penicillin and 100µg/mL streptomycin for up to 24 hours if the HUVEC isolation technique needs to be postponed. Also, even if the umbilical cord length is significantly reduced after the elective caesarean section surgery, the current method of HUVEC isolation may be used even with umbilical cords which are more than 10cm long. A further advantage of this cost-effective isolation protocol is that the endothelial cell population obtained resembles a similar cobblestone morphology characterised by the formation of large size dark nuclei across the entire monolayer formed which are present even in the following sub-cultures. Moreover, this method does not require any sophisticated equipment and, after obtaining a confluent cell culture flask at P0, the isolated high viability sub-cultured cells may be used straight away for further *in vitro* experiments. In terms of disadvantages of this isolation protocol, a high dexterity and focus is needed during the suturing process of the umbilical vein with the 3-way stopcock attached, as the umbilical cord is particularly slippery which makes the procedure sometimes lengthier and, if the cord is not clamped at the end before the collection of the placenta sample, the umbilical vein may collapse making it more difficult to insert the stopcock into the lumen of the vein. Moreover, particular attention must be paid when using the 2/0-gauge sterile surgical suture, firstly not to puncture the umbilical arteries as the surgical slip tie is undertaken around the stopcock and secondly, an increased focus must be allocated not to overtighten it around the umbilical vein to cut it, as the 0.1% (w/v) collagenase type II solution might leak during the flushing process.

Another disadvantage of this isolation protocol is that if the 3-way stopcock is not sutured tightly to the umbilical cord, there is the possibility of leakage of the 0.1% (w/v) collagenase type II with the isolated endothelial cells into the class 2 biological safety cabinet during the flushing of the enzyme into the umbilical vein.

2.20 Calculation of HUVEC cells population doubling time

According to the American Type Culture Collection (ATCC) formula for calculating the cell population doubling time (shown in equation 2), the human umbilical vein endothelial cells doubling period depends on three main variables: incubation time, number of cells seeded at the beginning and number of cells harvested at the end of culture incubation time. However, this equation does not take into account the lag and the stationary phases of the HUVEC growth curve in culture conditions, which might result in a less steep proliferation curve, giving rise to an abnormal elevated population doubling time. As a result, the cells should be counted on a daily basis for the purposes of determining the HUVEC cell doubling time only during the exponential growth phase.

2.21 Permeability studies

2.21.1 Initial transwell cell culture studies to investigate the adherence capability of CPA-SMC and HUVEC on polyester membrane inserts

In the initial phases of the construction of the *in vitro* co-culture model with the human placenta chorionic plate artery smooth muscle cells and the human umbilical vein endothelial cells, preliminary experiments involved the optimisation of the primary cell seeding density on two types of membrane inserts with characteristics presented in table 5.

	Product number	
	3460	3413
Brand	Corning	Corning
Plate format	12-well	24-well
Plate colour	Clear	Clear
Well Bottom	Flat	Flat
Well Bottom Colour	Clear	Clear
Well Shape	Round	Round
Cell Growth Area	1.12cm^2	0.33cm^2
Recommended Medium Well Volume	1.5mL	0.6mL
Recommended Medium Insert Volume	0.5mL	0.1mL
Surface Treatment	TC-Treated	TC-Treated
Sterile	Yes	Yes
Membrane Material	Polyethylene terephthalate (PET)	Polycarbonate
Membrane Pore Size	0.4µm	0.4µm
Membrane Thickness	10µm	10µm
Nominal Pore Density	4x10^6 pores per cm^2	1x10^8 pores per cm^2
Membrane Diameter	12mm	6.5 mm
Lids included	Yes	Yes

Table 5. *This table highlights the characteristics of the two main types of transwell membrane inserts used in all of the in vitro culture studies involving HUVEC and CPA-SMC cells for the purposes of establishing a reliable chorionic vessel system. The information regarding the transwell membrane inserts has been obtained from the Corning website available at: <<https://www.corning.com/emea/en.html>>*

2.21.2 Investigating the capability of $3x10^4$ chorionic plate artery smooth muscle cells to adhere to 6.5mm transwell with 0.4µm pore size polycarbonate membrane inserts

Following successful isolation and growth of CPA-SMC's, an optimised seeding density of these cells on polycarbonate membrane inserts had to be established.

$3x10^4$ viable CPA-SMC cells were seeded on 6.5mm membrane diameter 0.4µm pore size polycarbonate transwell inserts. Figure 18 shows the experimental design in which the smooth muscle cells were seeded on the transwell membrane insert.

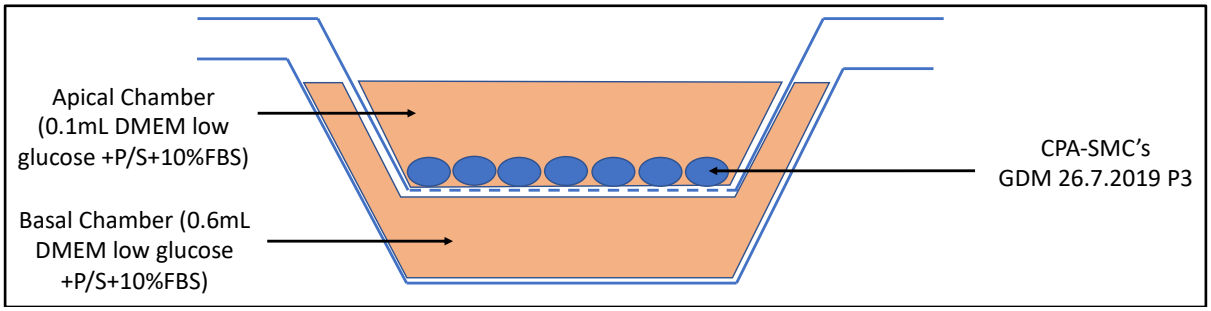


Figure 18. *This scheme highlights the structure of the transwell system with the chorionic plate artery smooth muscle cells originating from a gestational diabetic patient at passage 3 (GDM 26.07.2019) seeded on the 0.4µm membrane pore size insert. FBS denotes fetal bovine serum, P/S penicillin/streptomycin, DMEM Dulbecco's modified eagle medium. This figure has been hand drawn by Paul Fodor using Microsoft PowerPoint software version 16.53.*

The primary smooth muscle cells were monitored for a period of 24 hours to investigate the capability to adhere to the inserts and to observe the morphology of the cells by acquiring images using an inverted microscope.

2.21.3 Optimisation of CPA-SMC seeding density on 6.5mm diameter polycarbonate transwell polyester inserts

As the cell seeding density of $3x10^4$ CPA-SMC per $0.33cm^2$ of polycarbonate membrane insert was too high due to the formation of calcification nodules within 24 hours post seeding, further experiments aimed at determining the optimal seeding density of these cells on the same inserts. This was undertaken by choosing a range of primary cell seeding densities ($1x10^3$, $3x10^3$, $5x10^3$, $1x10^4$, $1.5x10^4$ and $2x10^4$ CPA-SMC's) and monitoring the cells (GDM26072019, P3) over a period of 120 hours post-seeding to investigate the growth pattern and monolayer forming capability of smooth muscle cells in a transwell system. Images with the human placenta chorionic plate artery smooth muscle cells were acquired at multiple timepoints specifically at seeding (0 hours), 24 hours, 48 hours and 120 hours to examine the morphology of all adhered cells to the polycarbonate inserts and to determine the optimal cell culture period until a monolayer was formed. This was undertaken for the purposes of further co-culturing the CPA-SMC with HUVEC cells on the same polycarbonate insert and to determine the timepoint at which the HUVEC cells could have been potentially seeded above the adhered CPA-SMC.

2.21.4 Optimisation of HUVEC seeding density on 6.5mm diameter transwell polyester inserts

In a similar way, the optimal seeding density of HUVEC cells (N21082019, P4) was investigated by placing $1x10^3$, $3x10^3$, $5x10^3$, $1x10^4$, $1.5x10^4$ and $2x10^4$ endothelial cells on 1% gelatin (Sigma Aldrich, G9391) coated 6.5mm diameter polycarbonate inserts (Figure 19). Images with the endothelial cell morphology and confluence were taken at the seeding point (0 hours), 24, 48 and 72 hours during the primary cell

proliferation phase. Also, at the timepoint of 48 hours after seeding the HUVEC with the cell densities of $1x10^4$, $1.5x10^4$ and $2x10^4$ per membrane insert, $1x10^4$ CPA-SMC's (N15072019, P3) were placed on top of the adhered endothelial cells. This was undertaken for the purposes of investigating the capability of primary smooth muscle cells to be co-cultured with HUVEC cells in an *in vitro* transwell system. HUVEC cells with densities of $1x10^3$, $3x10^3$, $5x10^3$ were not able to form a monolayer at 48 hours post seeding in the 6.5mm diameter insert, therefore CPA-SMC's were not seeded above these cultured endothelial cells at 48 hours.

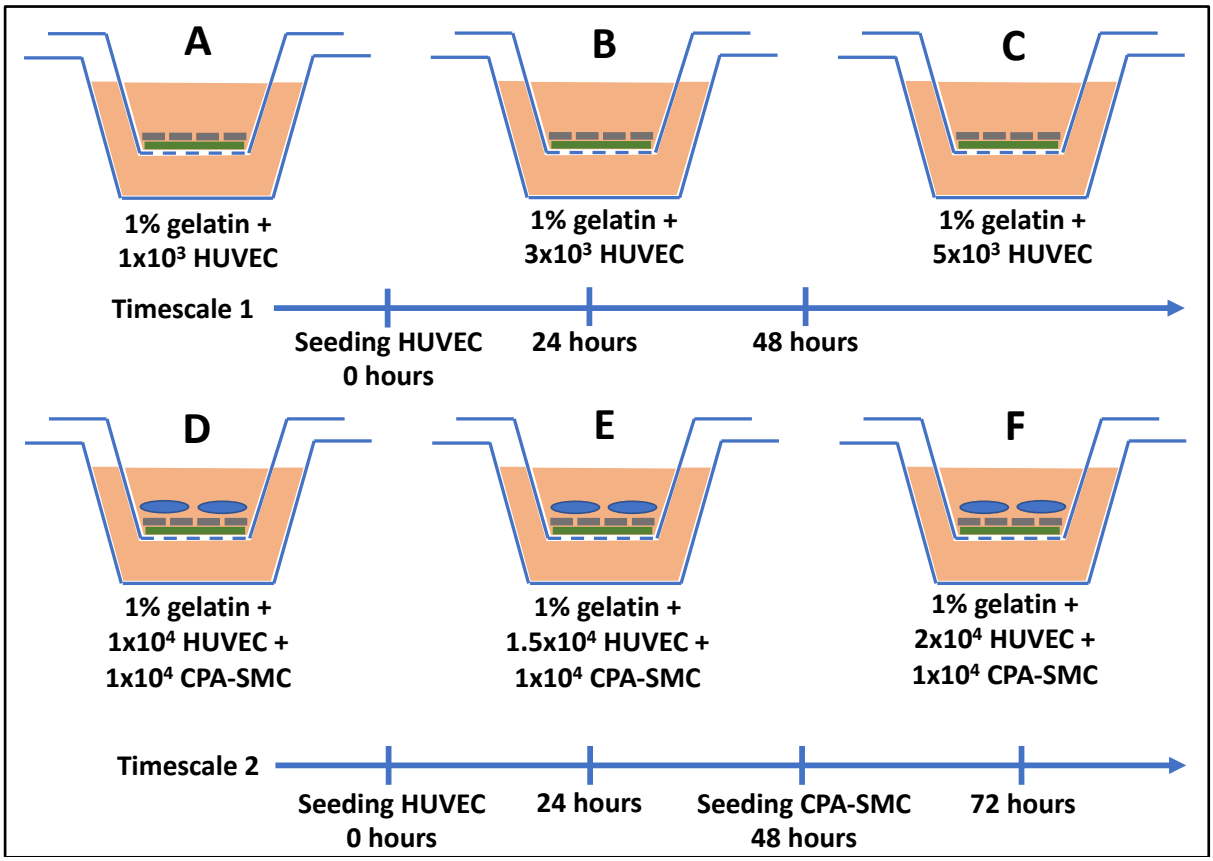


Figure 19. *This scheme shows the experimental design for optimising the cell seeding density of HUVEC and SMC in 6.5mm diameter transwell insert with 0.4µm pore size polycarbonate membrane inserts. Images were acquired at 0, 24 and 48 hours (**A-C**) as shown in the timescale 1 to investigate the morphology of HUVEC cells seeded at various cell densities (1%gelatin+$1x10^3$ HUVEC, 1%gelatin+$3x10^3$ HUVEC and 1%gelatin+$5x10^3$ HUVEC) on polycarbonate membrane inserts. Similarly, images were obtained at 0, 24, 48 and 72 hours (**D-F**) as highlighted in timescale 2 for the purposes of evaluating the appearance of HUVEC cells which were seeded at different cell densities (1%gelatin+$1x10^4$ HUVEC, 1%gelatin+$1.5x10^4$ HUVEC and 1%gelatin+$2x10^4$ HUVEC) on polycarbonate membrane inserts. In this case, the*

HUVEC cells were left to grow for 48 hours on the inserts and at this timepoint, 1x10^4 CPA-SMC's were seeded on top of the proliferating HUVEC cells. The co-culture was left to grow for another 24 hours and further images were taken to evaluate the morphology of both cell types. CPA-SMC cells are represented by a blue elipse, HUVEC cells are highlighted with a grey square and 1% gelatin layer is illustrated as a green box. This figure has been hand drawn by Paul Fodor using Microsoft PowerPoint software version 16.53.

2.21.5 Investigating the capacity of 1x10^5 HUVEC cells to adhere to 12mm membrane diameter 0.4µm pore size polyethylene terephthalate (PET) membrane inserts

1x10^5 viable HUVEC cells were seeded on 12mm membrane diameter 0.4µm pore size polyethylene terephthalate transwell inserts. Figure 20 highlights the experimental design in which the primary endothelial cells were seeded on the PET membrane insert with the characteristics presented in table 5.

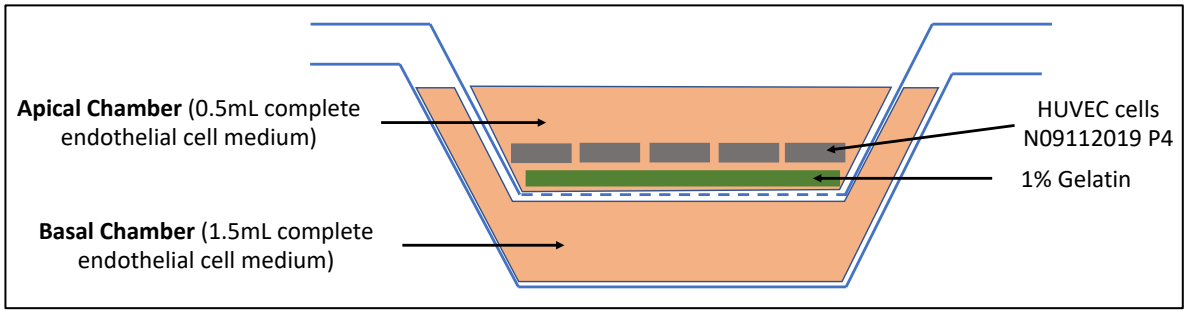


Figure 20. *This scheme highlights the structure of the transwell system with the human umbilical vein endothelial cells seeded on 1% (w/v) gelatinised 12mm membrane diameter 0.4µm pore size polyethylene terephthalate membrane inserts originating from a healthy patient at passage 4 (N09112019). This figure has been hand drawn by Paul Fodor using Microsoft PowerPoint software version 16.53.*

The complete media in which the endothelial cells were cultured was M199 (Thermo Fisher, 22340020) supplemented with 20% fetal bovine serum (Sigma Aldrich, F9665), heparin sodium salt (50µg/mL) (Sigma Aldrich, H3149), endothelial cell growth factor supplement (75µg/mL) (Sigma Aldrich, E2759), penicillin (100U/mL) and streptomycin (100µg/mL) (Sigma, P0781). When compared with the 6.5mm

diameter membrane inserts, in the current case, the volume of the culture media in the apical chamber was 0.5mL and in the basal chamber was 1.5mL.

The proliferation of HUVEC cells was monitored for a period of 48 hours by observing the morphology and adherence property of the cells to the polyethylene terephthalate membrane insert. Using an inverted microscope, images were acquired just after seeding the cells on the membrane inserts (0 hours) and also at 48 hours.

2.21.6 Characterisation of CPA-SMC phenotype cultured in HUVEC media

Further validation experiments aimed to determine if human placenta chorionic plate artery smooth muscle cells were able to proliferate in complete endothelial cell medium used for the growth of HUVEC cells, specifically M199 supplemented with 20% (v/v) fetal bovine serum, heparin sodium salt (50µg/mL), endothelial cell growth factor supplement (75µg/mL), penicillin (100units/mL) and streptomycin (100µg/mL). CPA explants originating from a healthy patient (N15072019) were placed in a 24 well plate and the SMC's were grown until confluency. Following detachment of the chorionic plate artery explants from the 24 well plate after 13 days of culture and serum starving the cells for 24 hours, the media of confluent CPA-SMC cells was replaced with complete endothelial cell medium. The morphology of the smooth muscle cells was surveyed for a further 120 hours by acquiring images using an inverted microscope. This was undertaken firstly for the purposes investigating if the primary cells were able to proliferate and survive in complete endothelial cell media and secondly to evaluate the potential of co-culturing the CPA-SMC's with HUVEC cells using a single type of media.

2.21.7 Preliminary permeability studies to investigate the barrier integrity of cultured human CPA-SMC and HUVEC on transwell polyester membrane inserts

Initial phases related to the establishment of experimental conditions suitable for the permeability experiments in terms of co-culturing the CPA-SMC's with HUVEC cells involved selecting a suitable cell seeding density for the primary cells, as well as characterising multiple transwell mono- or co-culture cellular arrangements. This was undertaken for the purposes of investigating the barrier integrity properties created by these human cells using macromolecular permeability assays involving fluorescein isothiocyanate dextran (70kDa) as a tracer (Sigma Aldrich, FD70-250mg).

In total there were 8 preliminary experimental conditions (figure 21) involving mono- or co-culture of the primary cells as highlighted in figure 21. $1x10^4$ CPA-SMC's (N15072019, P3) were grown on 12mm diameter transwell with 0.4µm pore size polyethylene terephthalate membrane inserts in DMEM low glucose (Thermo Fisher Scientific, 11885084) supplemented with 10% (v/v) FBS and penicillin (100U/mL) and streptomycin (100µg/mL) for 11 days with media change every 2 days. At this timepoint, 1% gelatin was added above empty or confluent CPA-SMC transwell inserts and left for 30 minutes. Following this, $1x10^4$ HUVEC cells (N21082019 P5) were seeded on empty or above 1%gelatin inserts with the apical and basal media being replaced with complete endothelial cell growth medium comprising of M199 supplemented with 20% (v/v) fetal bovine serum (FBS), heparin sodium salt (50µg/mL), endothelial cell growth factor supplement (75µg/mL), penicillin (100U/mL) and streptomycin (100µg/mL). The primary cells were left to grow for a further 48 hours. At day 13, the preliminary permeability experiment was undertaken followed by

the fixation of the primary cells in 4% (w/v) paraformaldehyde and further immunocytochemistry staining for α smooth muscle actin (Chapter 2.16 – antibody dilutions and chapter 2.21.10 – immunocytochemistry protocol).

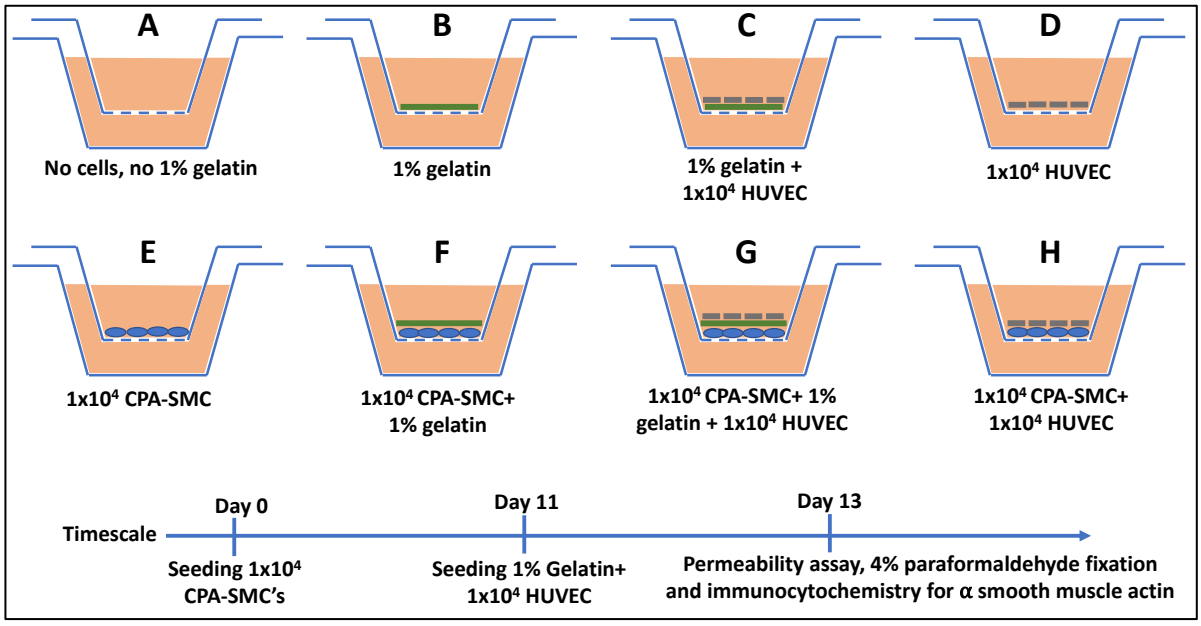


Figure 21. *This scheme (**A-H**) shows eight mono- and co-culture in vitro preliminary conditions involving CPA-SMC's and HUVEC cells grown on 12mm diameter 0.4µm pore size polyethylene terephthalate membrane inserts. The timescale in terms of seeding the cells on the inserts highlights that 1x10^4 CPA-SMC's were seeded first and left to grow for 264 hours as shown in transwells **E-H**. After 11 days following seeding of CPA-SMC's, 1% gelatin was added above empty (wells **B and C**) or CPA-SMC confluent transwells as represented in wells **F and G**. Also, at the same timepoint of 11 days, 1x10^4 HUVEC cells were also seeded on empty (well **D**), above 1% (w/v) gelatin as shown in well **C,** on top of 1% (w/v) gelatin + 1x10^4 CPA-SMC's as highlighted in well **G** and directly on confluent CPA-SMC cells as presented in well **H**. The cells were left to grow for a further 48 hours. At day 13, the permeability assay was run followed by fixation of cells in 4% (w/v) paraformaldehyde and further immunostaining for α smooth muscle actin. CPA-SMC are represented by a blue circle, HUVEC are illustrated as a grey box and 1%gelatin is highlighted by a green box. This figure has been hand drawn by Paul Fodor using Microsoft PowerPoint software version 16.53.*

2.21.8 Characterising the optimised cell culture conditions of HUVEC and CPA-SMC for undertaking permeability and endothelial junction formation studies

Following initial validation experiments investigating the properties of CPA-SMC and HUVEC cells to adhere, proliferate and to give rise to the monolayer formation on 0.4µm pore size PET membrane inserts, the experimental conditions for producing the optimised *in vitro* co-culture model contributing to the current knowledge of placental vascular function were established (figure 23). The efficacy of the model was further tested by evaluating the capacity of endothelial junction formation and barrier integrity, as illustrated in figure 23. Using a transwell system comprised of 12mm diameter, 0.4µm pore size polyethylene terephthalate membrane inserts, $6x10^4$ HUVEC cells were seeded on 1% gelatin coated inserts and left to grow in an incubator in humidified conditions for 48 hours at 37^0C in 5%CO_2/95% air. Once the endothelial cells became confluent, $1*10^4$ CPA-SMC's were seeded on top of the HUVEC monolayer and further monitored (Figure 22 and figure 24, panel D). After 26 hours of coculture, albumin-FITC (1mg/mL) (Sigma Aldrich, A9771) was introduced into the apical chamber followed by the collection of media from the basal chamber at every 30 minutes for up to 2 hours. Co-cultures were then immunostained for VE-Cadherin using the immunocytochemistry protocol described in chapter 2.21.10. The growth media chosen for the purposes of culturing the primary endothelial cells on transwell membrane inserts until the point of confluence was M199 low glucose supplemented with 20% FBS, endothelial cell growth factor supplement (75µg/mL), heparin sodium salt (50µg/mL), penicillin (100U/mL) and streptomycin (100µg/mL). After the primary smooth muscle cells were seeded above confluent HUVEC cells, the co-culture media

chosen was the same as complete endothelial cell media but without heparin sodium salt as it inhibits the proliferation of the smooth muscle cells (highlighted in figure 23, panels C and D) [119,484].

The protocol of permeability studies is adapted from Pang *et al* (2017) [119] and Villota *et al* (2021) [484] in that the current study used $6x10^4$ HUVEC cells compared to $5x10^3$ HUVEC [119] and the tracer was Albumin-FITC compared to FITC-conjugated dextran [484].

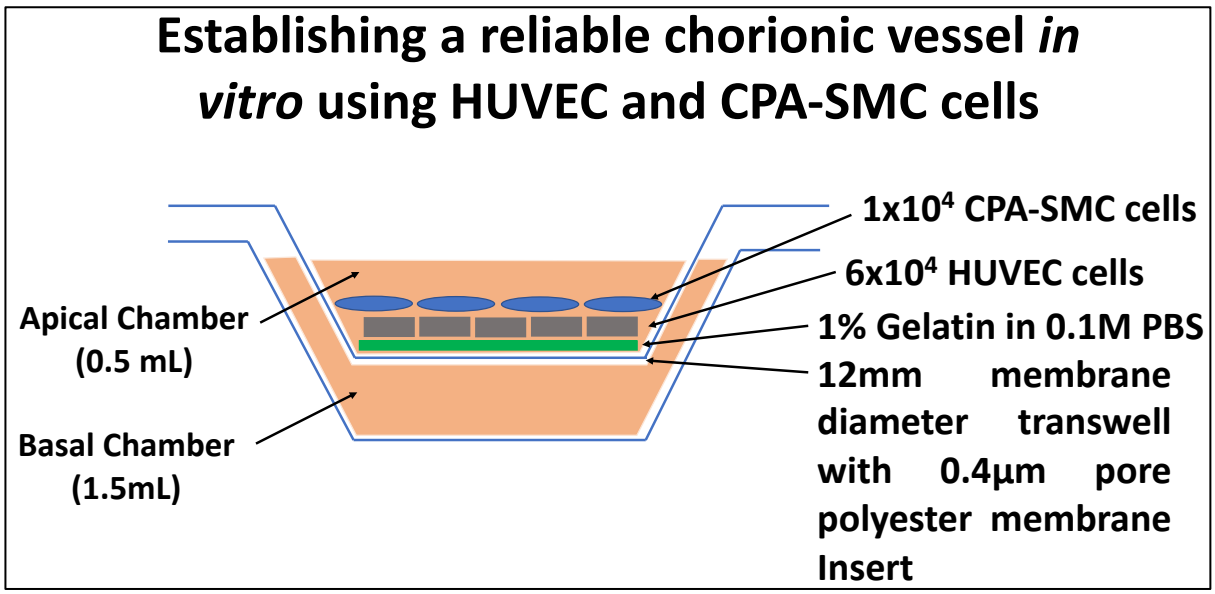


Figure 22. *This scheme shows the characteristics of the transwell system model used in assessing the capacity of endothelial junction formation and barrier integrity formed by the mono- or co-culture of $1x10^4$ CPA-SMC's and $6x10^4$ HUVEC cells. This figure has been hand drawn by Paul Fodor using Microsoft PowerPoint software version 16.53.*

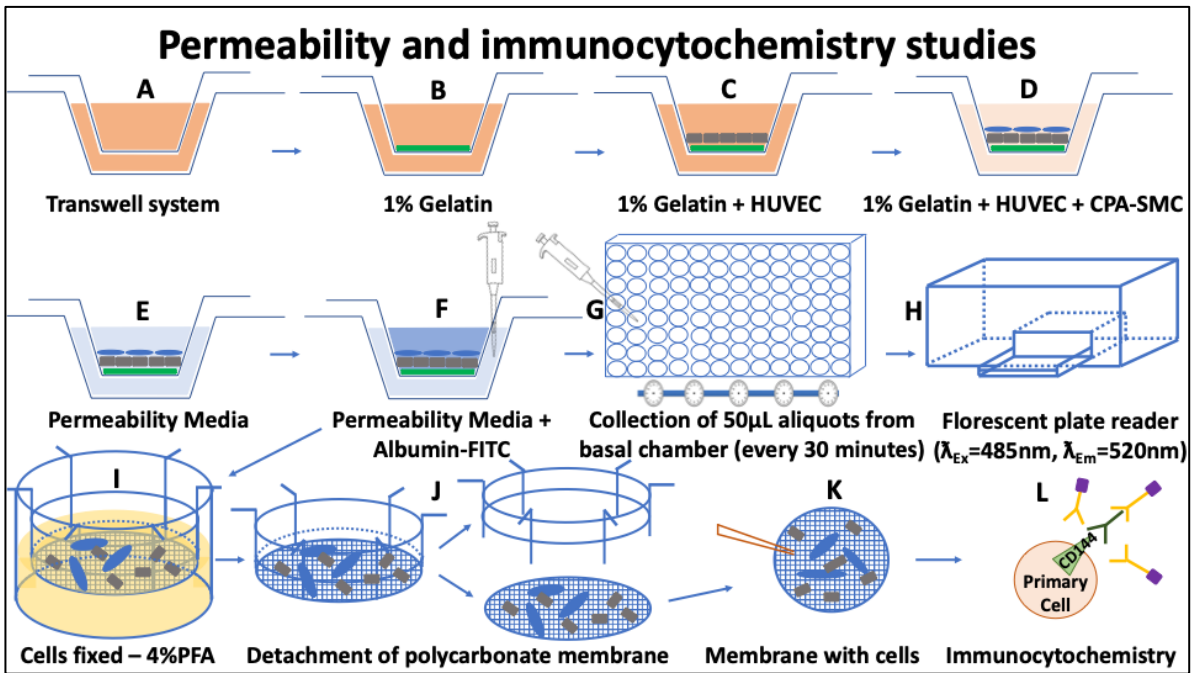


Figure 23. *This scheme (**A-L**) illustrates the process of constructing the in vitro co-culture model using human placental chorionic plate artery smooth muscle cells and human umbilical vein endothelial cells and the follow-up permeability and immunostaining studies for CD144. This figure has been hand drawn by Paul Fodor using Microsoft PowerPoint software version 16.53.*

2.21.9 Tracer leakage permeability studies of HUVEC and CPA-SMC

In total, there were N=4 permeability experiments performed using isolated primary cells originating from 7 different healthy patients as shown in table 6. There were three inbuilt experimental repeats (transwell assays) per experiment. After the permeability assays were run, all monolayers were immediately fixed in 4% paraformaldehyde and the primary cells immunostained for CD144 (figure 23, panels I-L and figure 25).

Permeability experiment	CPA-SMC sample	Passage of CPA-SMC cells	HUVEC sample	Passage of HUVEC cells
First	N17092019	P2	N10072019	P2
Second	N05122019	P1	N05122019	P3
Third	N18092019	P3	N21082019	P3
Fourth	N11112019	P3	N12082019	P3

Table 6. *This table shows the patient sample numbers and the passage of human placenta chorionic plate artery smooth muscle cells (CPA-SMC) and human umbilical vein endothelial cells (HUVEC) used in all four permeability and the follow-up immunocytochemistry experiments.*

In terms of analysing all data from the permeability results, standard curves were created in each of the four experiments in order to interpolate unknown albumin-FITC concentration values in the basal compartment of the transwell system based on their corresponding fluorescence intensities (arbitrary units) obtained from SpectraMax M2^e microplate reader (Molecular Devices). In order to achieve this, a 5-point standard curve was created using known concentrations of the albumin-FITC (0, 5, 15, 25 and 50µg/mL) tracer and measuring their corresponding fluorescence intensity values. A scatter plot was created using Graph Pad Prism (version 8.2.1) containing data from the standard curves with X-axis representing albumin-FITC concentration values measured in µg/mL and Y-axis denoting fluorescence arbitrary units (A.U.). In total, there were 3 standard curves created from all tracer leakage experiments as the third and fourth permeability assays were performed together in a 96-well plate which had a common standard curve (figure 24). A linear regression trendline was created for each of the standard curves with the corresponding equation used in determining the concentration of the unknown fluorescence intensities as shown in figure 24. In this case, the R^2 values for each linear regression trendlines are also presented. All unknown fluorescence values obtained from the four permeability experiments fell within the middle range of the standard curve with no fluorescence intensities falling below the minimum corresponding tracer concentration value of

0µg/mL or above the maximum matching tracer concentration value of 50µg/mL [119,484].

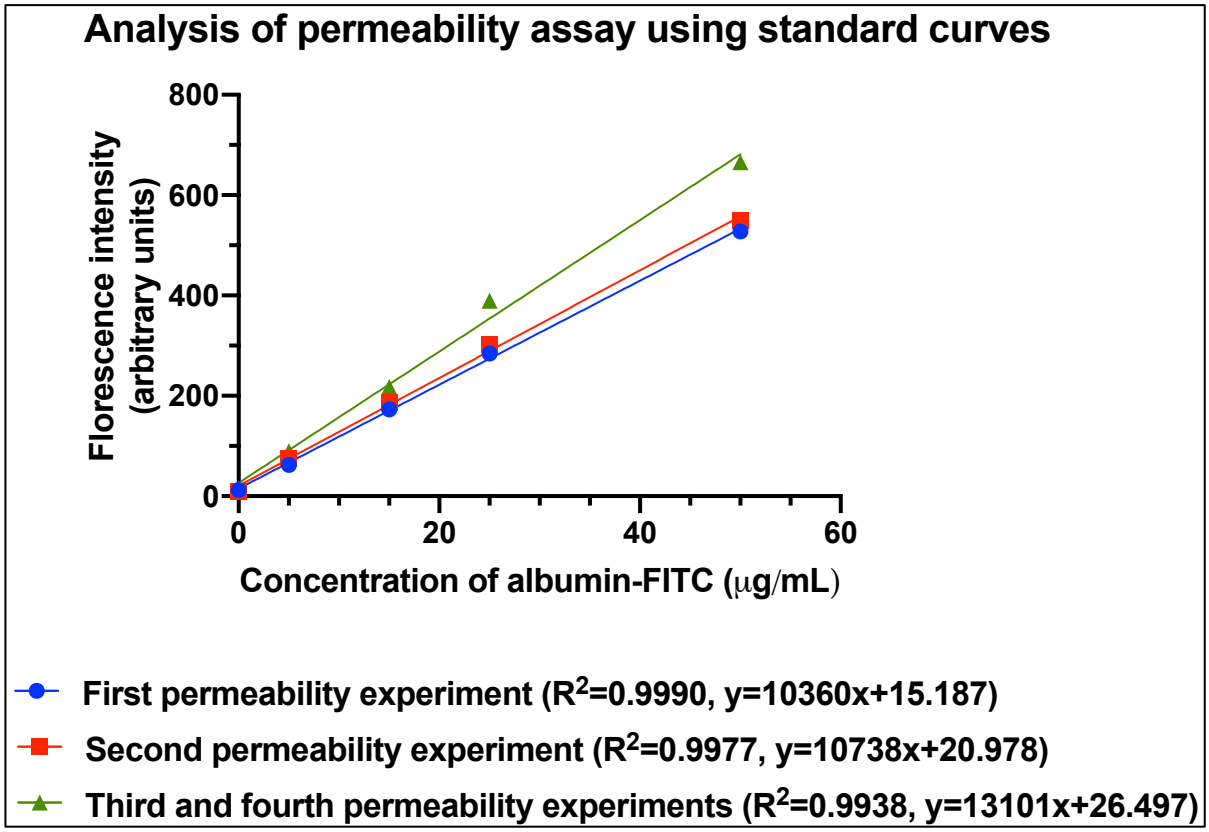


Figure 24. *This graph highlights the linear regression best fit plotted 5-point standard curves corresponding to all permeability experiments with their R^2 and first-order equations. X-axis shows the concentration of the tracer (µg/mL) and Y-axis denotes the fluorescence intensity values (arbitrary units).*

Permeability data of all four experiments highlights the tracer leakage in 3 main assay conditions i.e. 1%Gelatin (Control), 1% Gelatin + HUVEC and 1% Gelatin + HUVEC + CPA-SMC. From all 4 tracer leakage assays, in the first permeability experiment, a control condition (1% gelatin) was undertaken (triplicate) for the purposes of investigating the potential effects of the heterogenous mixture of high average molecular masses water-soluble proteins present in collagen on the fluorescein isothiocyanate-conjugated albumin leakage from the apical to the basal compartment of the transwell system, but also to serve as a reference point relative to

all other experimental conditions. Table 7 summarises the assay conditions used in all 4 permeability investigations and the length of each of the tracer leakage experiments.

Furthermore, on one occasion as highlighted in the second permeability experiment (Table 7), the length of the 120 minutes standard assay was further increased by one hour to explore the efficacy of the *in vitro* model of human chorionic vessel and to assess the potential of the co-culture barrier to reach a higher permeability when compared to the monoculture of primary endothelial cells.

		Experimental conditions		
Permeability experiment	**Length of permeability experiment (hours)**	**1% Gelatin**	**1% Gelatin + HUVEC**	**1%Gelatin + HUVEC+ CPA-SMC**
First	**2**	**Yes**	**Yes**	**Yes**
Second	**3**	**No**	**Yes**	**Yes**
Third	**2**	**No**	**Yes**	**Yes**
Fourth	**2**	**No**	**Yes**	**Yes**

Table 7. *This table highlights for each of the four permeability experiments the duration of the assay and the experimental conditions used in the generation of the mono- and co-culture of human placenta chorionic plate artery smooth muscle cells (CPA-SMC) and human umbilical vein endothelial cells (HUVEC).*

2.21.10 Post-permeability studies of endothelial junctional integrity

Following the completion of the permeability study, all membrane inserts of control, monoculture and coculture conditions were fixed in 4% (w/v) paraformaldehyde (Sigma Aldrich, P6148) and the cells immunostained for VE-cadherin. Figure 25 summarises the methodology used in the immunocytochemistry studies in terms of fixation, requisite washes, permeabilization, blocking, incubations with primary and secondary antibody and mounting of insert membranes on microscope slides (modified from [119,483]). All 0.4µm pore size polyethylene terephthalate membrane inserts with primary cells (triplicate) from the first permeability experiment (control, monoculture, coculture) were immunostained for VE-cadherin for

the purposes of investigating the efficacy of the co-culture model by evaluating the capacity of endothelial junction formation from the perspective of paracellular permeability. A no primary antibody control transwell insert staining for VE-Cadherin was undertaken by replacing it with 5% (v/v) normal human serum diluted in 0.1% (w/v) BSA/PBS. Transwell inserts were incubated at 4^0C overnight with primary antibody against VE-Cadherin (purified mouse IgG_1 anti human monoclonal antibody (BD Biosciences, 555661) used at a concentration of 5µg/mL. Secondary antibody (anti mouse IgG whole-molecule FITC antibody produced in goat, 10µg/mL, Sigma, F0257) was added the following day for 1 hour at 37^0C. Images were acquired using Nikon fluorescence microscope and NIS elements F3.0. The immunocytochemistry protocol is adapted from Ebrahim and Leach (2015) [503] in that the primary cells were fixed with 4% paraformaldehyde instead of 1% paraformaldehyde [503] and the secondary antibody was incubated with the primary cells for 1 hour compared to 2 hours [503].

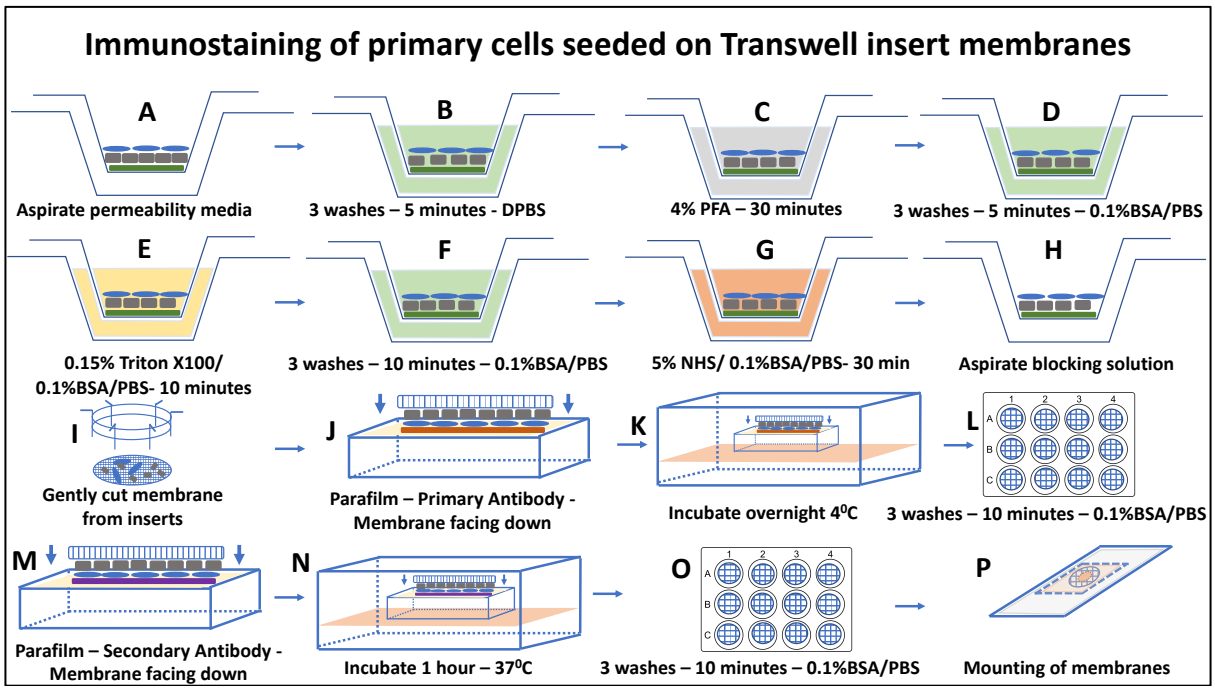


Figure 25. *This scheme (panels **A-P**) highlights the methodology used in immunostaining for VE-Cadherin of primary cells seeded on the polyethylene terephthalate (PET) transwell membrane inserts as a permeability follow-up study for the purposes of investigating the capacity of endothelial junction formation in the monolayer of human umbilical vein endothelial cells. The primary cells were washed 3 times with Dulbecco's phosphate buffered saline (DPBS; Sigma Aldrich, D8537) and fixed in 4% (w/v) paraformaldehyde (Sigma Aldrich, P6148) for 30 minutes. Three further washes with 0.1% (w/v) BSA/PBS were undertaken followed by permeabilizing the primary cells with 0.15% (v/v) triton X-100 diluted in 0.1% (w/v) BSA/PBS for 10 minutes. PET inserts were washed again in 0.1% (w/v) BSA/PBS followed by blocking with 5% (v/v) normal human serum in 0.1% (w/v) BSA/PBS for 30 minutes. The polyethylene terephthalate membranes were dethatched from the insert and were incubated overnight at 4^0C with VE-Cadherin primary antibody (mouse anti human CD144, 5µg/mL, BD Pharmingen, 555661). A no primary antibody control was also performed by replacing it with 5% (v/v) normal human serum in 0.1% (w/v) BSA/PBS. The following day, inserts were washed 3 times in 0.1% (w/v) BSA/PBS followed by incubation with secondary antibody for 1 hour at 37^0C (anti mouse IgG whole-molecule FITC antibody produced in goat, 10µg/mL, Sigma, F0257). Three last requisite washes were performed using 0.1% (w/v) BSA/PBS for 10 minutes each and the PET inserts were mounted on a microscope slide using vectashield antifade mounting medium (Vector Laboratories, H1000). This figure has been hand drawn by Paul Fodor using Microsoft PowerPoint software version 16.53.*

Due to the fact that in the majority of micrographs taken there was a considerable level of background staining possibly caused by the formation of albumin-FITC aggregates, all of the membrane inserts originating from the first permeability experiment were un-mounted and re-washed again. This procedure was

undertaken for the purposes of eliminating the non-specific background staining which was noticed in most fields of view when the inserts were examined microscopically for the presence of VE-Cadherin junction integrity. The membrane inserts were washed 3 times with 0.1% (w/v) BSA/PBS for 10 minutes and permeabilized again with 0.15% (v/v) Trition X-100 in 0.1% (w/v) BSA/PBS for 3 minutes. Inserts were washed with 0.1% (w/v) BSA/PBS for 10 minutes and re-mounted again on microscope slides using vectashield antifade mounting medium.

Following the second permeability experiment comprising of 1%gelatin+HUVEC and 1%gelatin+HUVEC+CPA-SMC culture conditions, a similar immunostaining protocol for VE-Cadherin junctions was performed with all transwell membrane inserts. Six fluorescence micrographs showing immunolocalization of VE-Cadherin were acquired for each of the triplicate permeability transwell assay membrane inserts of the monoculture or coculture conditions. In order to further investigate the origin of the non-specific background staining, one of the aims of the third and fourth permeability experiments was to replace the albumin-FITC tracer with unconjugated bovine serum albumin (Sigma Aldrich, A9771) in the apical chamber of the transwell system at the same concentration of 1mg/mL.

In this case, before the start of the permeability assay, BSA was added to the apical compartment and was left for 2 hours. The 1% (w/v) gelatin+HUVEC and 1% (w/v) gelatin+HUVEC+CPA-SMC primary cultures were then immunostained for VE-Cadherin and α smooth muscle actin using the protocol highlighted in figure 25. The primary antibody for VE-Cadherin was mouse anti human CD144, 1:100 dilution, BD Pharmingen, catalogue number 555661 and for α smooth muscle actin was rabbit monoclonal [E184] to α smooth muscle actin, 1:500 dilution, Abcam, AB32575. The secondary antibodies were anti-rabbit IgG (whole molecule) FITC antibody produced

in goat, 1:100 dilution, Sigma, F9887 and anti-mouse IgG (whole molecule) TRITC antibody produced in goat, 1:20 dilution, Sigma, T5393.

2.21.11 Investigating the potential membrane double labelling of isolated primary cells with PKH26 and PKH67 for studying the properties of trans-endothelial migration of CPA-SMC across HUVEC monolayers

Due to the fact that the human placenta chorionic plate artery smooth muscle cells co-express specific surface antigens that are characteristic to mesenchymal stem cells such as CD105, CD73 and CD90 and the absence of hematopoietic lineage markers for example CD45, CD34, CD14, CD11b, CD79α and HLA-DR, the potential transendothelial migration capacity of these primary cells was tested across established HUVEC monolayers on transwell polyethylene terephthalate membrane inserts.

Alongside the third and fourth permeability experiments, the same primary cells as highlighted in table 6 were seeded on separate 1% (w/v) gelatinised membrane inserts. $6x10^4$ HUVEC cells were labelled with a green fluorescent dye PKH67 according to the instructions provided by the manufacturer (Sigma-Aldrich, PKH67GL), seeded on 0.4μm pore size PET membrane inserts and left to grow for 48 hours. At this point, $1x10^4$ CPA-SMC cells were labelled with a red fluorescent dye PKH26 using the protocol suggested by the manufacturer (Sigma-Aldrich, PKH26GL), seeded above established HUVEC monolayers and left to grow for a further 24 hours. After this period, monocultures of HUVEC and cocultures of HUVEC with CPA-SMC were fixed in 4% (w/v) paraformaldehyde, washed 3 times with 0.1% (w/v) BSA/PBS and mounted on microscope slides using vectashield antifade mounting medium

(Vector Laboratories, H1000). The labelling with PKH26 fluorescent dye of CPA-SMC cells is adapted from Ebrahim and Leach (2015) in that the isolated smooth muscle cells were stained with PKH26 compared to Wharton's Jelly Mesenchymal Stem Cells (WJ-MSC) which were stained with the same fluorescent dye [503].

2.22 Immunophenotyping of isolated human primary smooth muscle cells originating from the chorionic plate artery

Human placental vascular smooth muscle cells represent an important cellular constituent which supports the functional and architectural stability of the vasculature. Over the last four decades, the description of smooth muscle cells both *in vitro* and *in vivo* has been considered particularly demanding because of the property of these cells to differentiate or potentially de-differentiate under the activation of various factors. In the case of the current isolated chorionic plate artery smooth muscle cells, the principle of de-differentiating is further supported by the presence of specific stem cell markers on the surface of the isolated human placental cells. The International Society for Cellular Therapy (ISCT) has suggested that the phenotype of multipotent mesenchymal stem cells to possess as a minimum the cell surface co-expression of the proteins CD73, CD105 and CD90 (≥95% positive) and not expressing the hematopoietic lineage markers CD34, CD14, CD45, CD11b, CD19, CD79-α and HLA-DR (≤2% positive). Following successful isolation, the primary smooth muscle cells were passaged at 80% confluency and phenotypically characterised using flow cytometry. The surface antigenic profiling of isolated human placenta chorionic plate artery smooth muscle cells was performed using BD FACSCanto™ II cell analyser (BD Biosciences). $1x10^4$ CPA-SMC's were stained with saturating concentrations of

fluorochrome conjugated antibodies (table 8) according to the manufacturer instructions (BD Stemflow hMSC Analysis Kit, BD Biosciences, 562245). Data analysis was performed using Kaluza Software Version 2.1 and GraphPad Prism version 8.2.1. The isolated human placenta chorionic plate artery smooth muscle cells that were immunophenotyped originated from 4 healthy and 4 gestational diabetic placental samples. Overall, three immunophenotyping experiments were undertaken. Figure 26-28 highlight the controls used to set up the flow cytometer (i.e. compensation) in the first, second and third immunophenotyping experiments using FITC mouse anti human CD90, PE mouse anti human CD44, Per-CP-Cy-5.5 mouse anti human CD105 and APC mouse anti human CD73 antibodies.

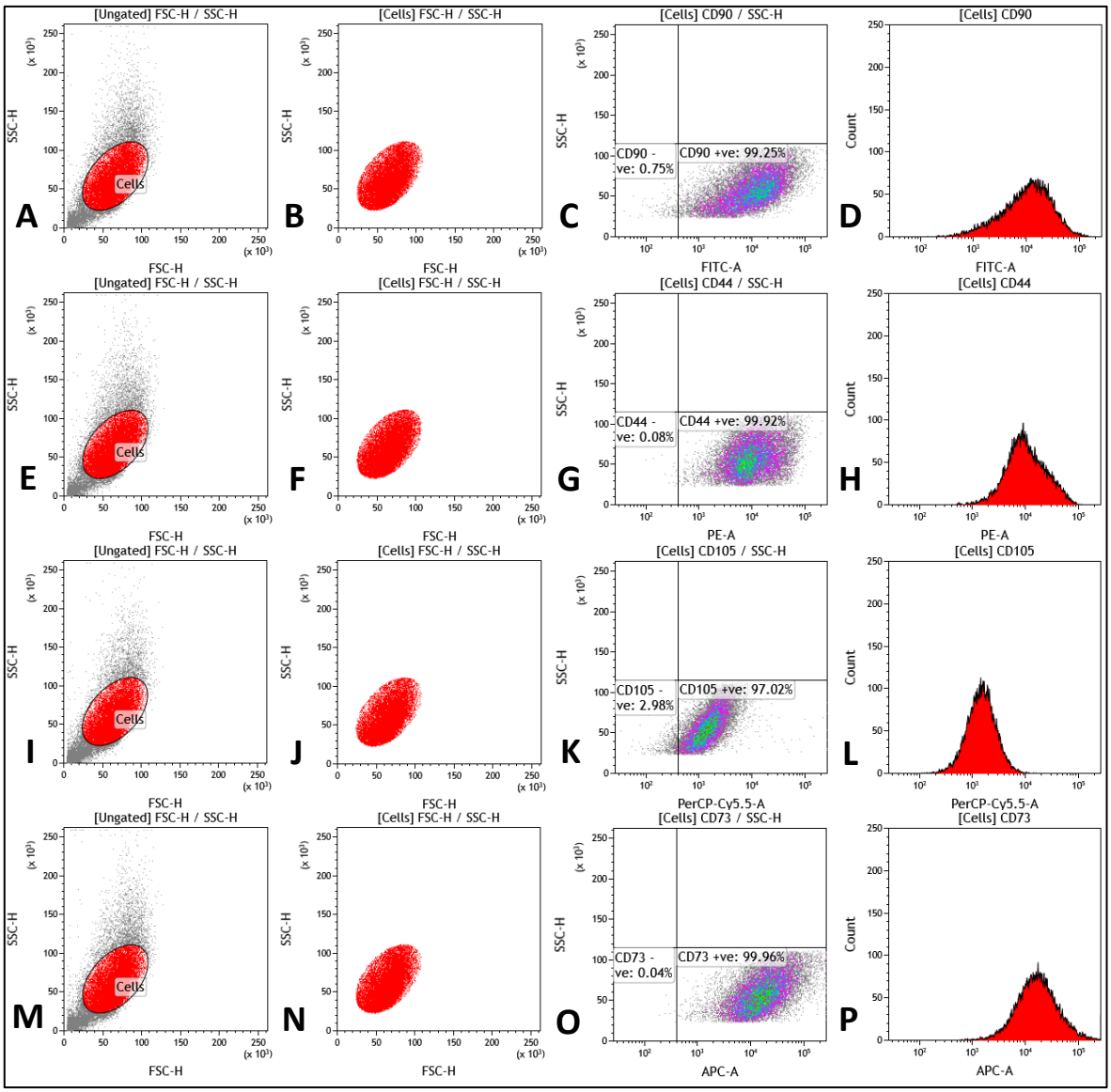


Figure 26. *This figure* ***(panels A-P)*** *highlights the compensation control from the first immunophenotyping experiment for the purposes of setting up the flow cytometer.* ***A,E,I,M*** *show ungated cells,* ***B,F,J,N*** *denote gated cells,* ***C,G,K,O*** *highlight scatter plots of CD90, CD44, CD105 and CD73 with their corresponding cell counts presented in* ***D,H,L,P****.*

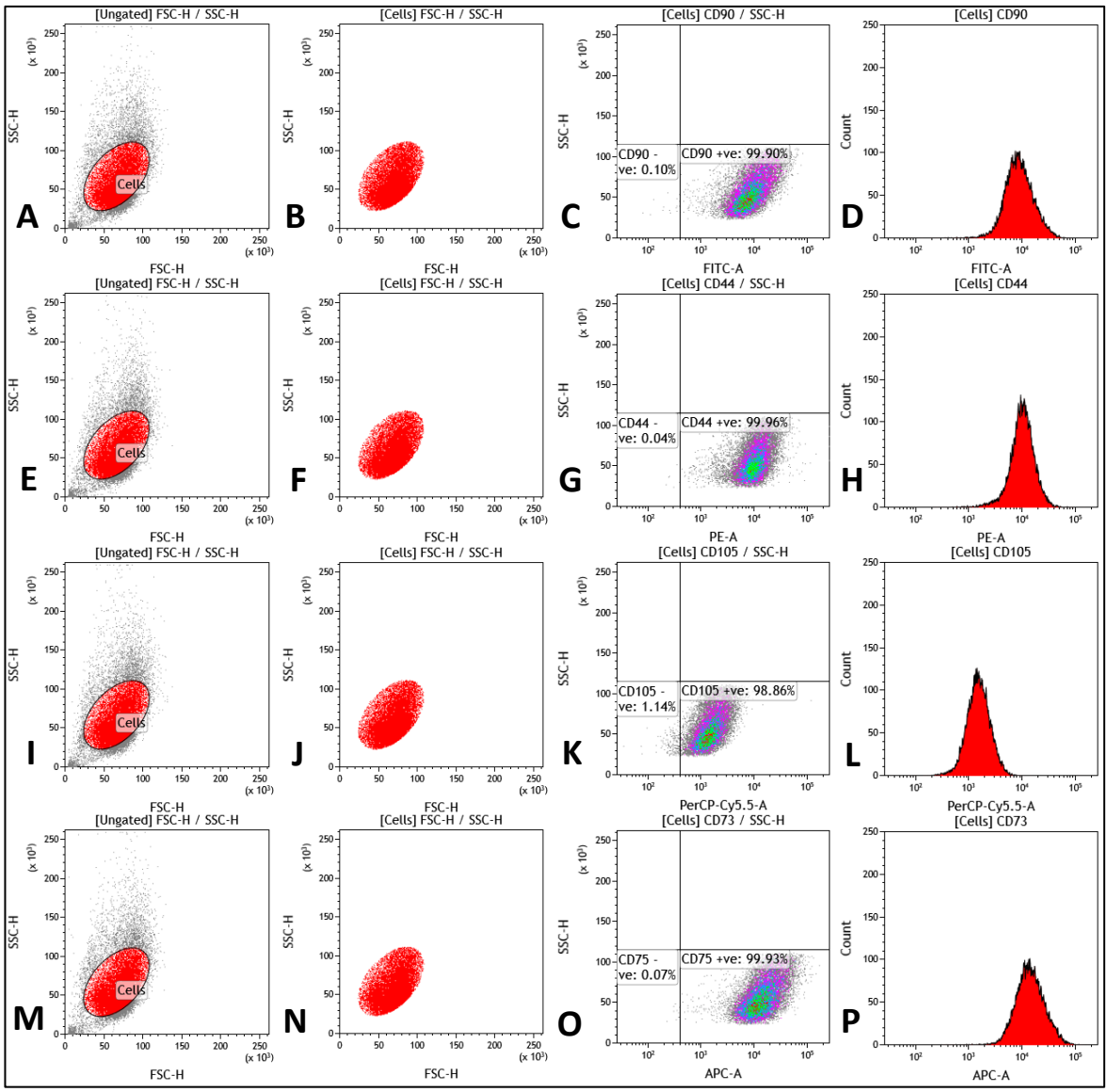


Figure 27. *This figure (panels **A-P**) highlights the compensation control from the second immunophenotyping experiment for the purposes of setting up the flow cytometer. **A,E,I,M** show ungated cells, **B,F,J,N** denote gated cells, **C,G,K,O** highlight scatter plots of CD90, CD44, CD105 and CD73 with their corresponding cell counts presented in **D,H,L,P**.*

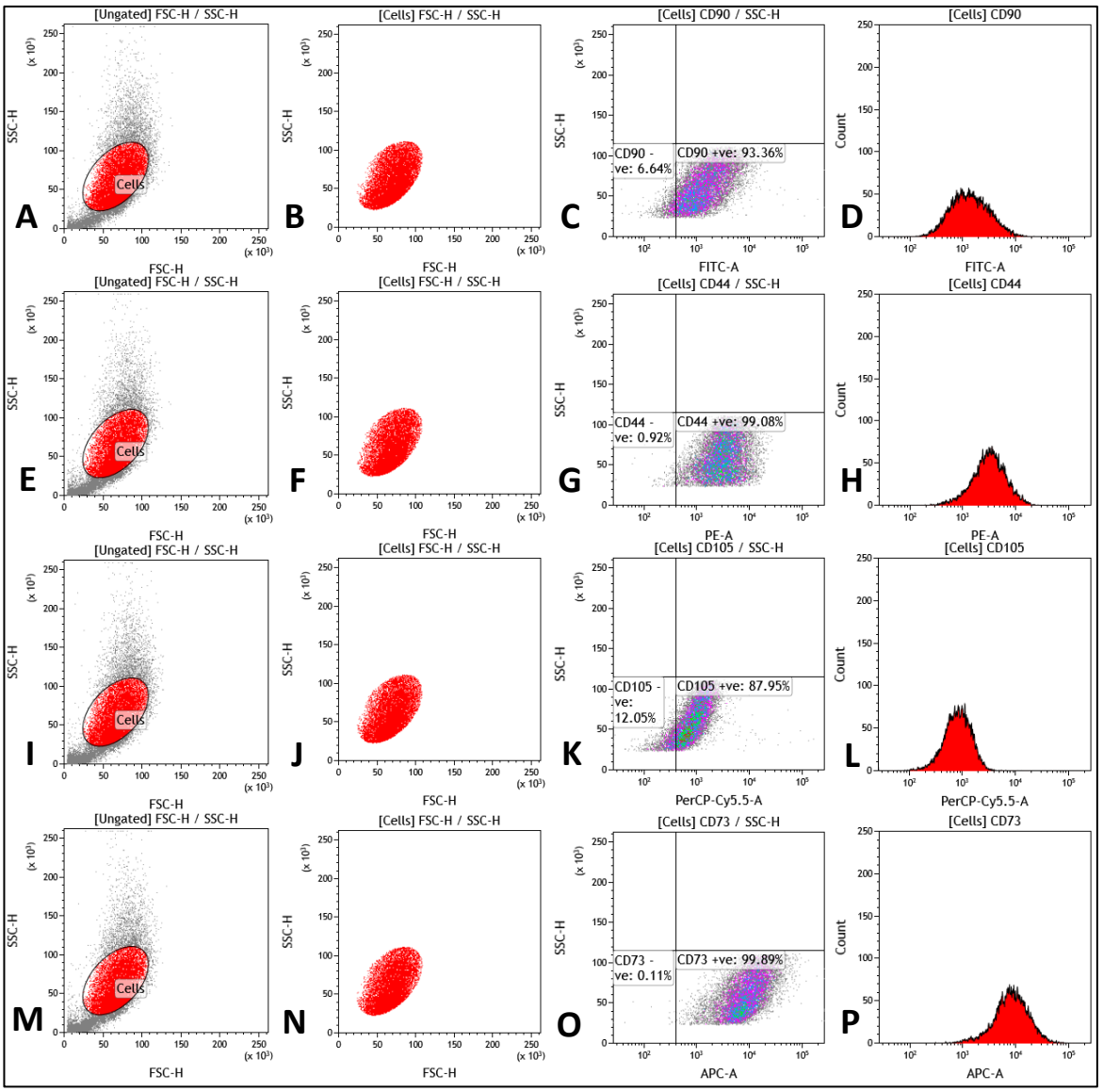


Figure 28. *This figure (panels **A-P**) highlights the compensation control from the third immunophenotyping experiment for the purposes of setting up the flow cytometer. **A,E,I,M** show ungated cells, **B,F,J,N** denote gated cells, **C,G,K,O** highlight scatter plots of CD90, CD44, CD105 and CD73 with their corresponding cell counts presented in **D,H,L,P**.*

Vial	Contents	Purpose
hMSC Positive Cocktail	CD90 FITC (Clone: 5E10)	Cocktail to positively identify hMSCs
	CD105 PerCP-Cy5.5 (Clone: 266)	
	CD73 APC (Clone: AD2)	
hMSC Positive Isotype Control Cocktail	mIgG1, κ FITC (Clone: X40)	Corresponding Isotype Control for hMSC Positive Cocktail
	mIgG1, κ PerCP-Cy5.5 (Clone: X40)	
	mIgG1, κ APC (Clone: X40)	
PE hMSC Negative Cocktail	CD34 PE (Clone:581)	Cocktail to identify potential contaminants
	CD11b PE (Clone: ICRF44)	
	CD19 PE (Clone: HIB19)	
	CD45 PE (Clone: HI30)	
	HLA-DR PE (Clone: G46-6)	
PE hMSC Negative Isotype Control Cocktail	mIgG1, κ PE (Clone: X40)	Corresponding isotype control for PE hMSC Negative Cocktail
	mIgG2a, κ PE (Clone:G155-178)	
FITC Mouse Anti-human CD90	CD90 FITC (Clone: 5E10)	Compensation control
PE Mouse Anti-Human CD44	CD44 PE (Clone: G44-26)	Compensation control/MSC positive drop-in
PerCP-Cy™5.5 Mouse Anti-Human CD105	CD105 PerCP-Cy™5.5 (Clone: 266)	Compensation control
APC Mouse Anti-Human CD73	CD73 APC (Clone:AD2)	Compensation control
PE Mouse IgG2b, κ Isotype Control	mIgG2b, κ (Clone: 27-35)	Corresponding Isotype Control for PE Mouse Anti-Human CD44, when used as a drop in

Table 8. *This table shows the description of the components of BD Stemflow hMSC Analysis Kit in terms of antibodies used in the immunophenotypic characterisation of stem cells and their corresponding experimental purpose. The information regarding the human MSC Analysis Kit has been obtained from the BD Biosciences website available at: <<https://www.bdbiosciences.com/en-eu/products/reagents/flow-cytometry-reagents/research-reagents/panels-multicolor-cocktails-ruo/human-msc-analysis-kit.562245>>*

CHAPTER 3

INVESTIGATING THE EXPRESSION OF THE P2X7 RECEPTOR IN THE VASCULATURE OF THE HUMAN PLACENTA

3.1 Introduction

3.1.1 P2X7 receptor involvement in the pathogenesis of type 2 diabetes from a microvascular complication point of view

Adenosine 5'-triphosphate may be liberated towards the extracellular milieu not only from apoptotic or wounded cells, but also from healthy cells under low oxygen levels, mechanical injury, vesicular release or through the activation of membrane transport receptors. This important extracellular signalling molecule may connect with two important subfamilies of the P2 purinoceptors: ligand-gated ion channels (P2X) and G-protein-coupled (P2Y). The activation of the P2X7 receptor gives rise to a trans-membrane flux of K^+, Na^+ and Ca^{2+} ions with sustained stimulation by dilating a pore permitting the flow of large molecules (>900Da) [506].

The P2X7 receptor is particularly prone to polymorphisms, is vastly spread and is implicated in many cellular roles. Some of these include involvement in certain immune reactions, as well as in specific inflammatory mechanisms (potentially being in charge with the assembly of the NLRP3 inflammasome and IL-1β release) and also in neoplastic changes [507–509]. Type 2 diabetes is a syndrome caused by numerous components and has a complicated pathogenesis that takes into account many organs as well as tissues which involves a complicated interaction of genetic susceptibility and many environmental factors [510]. Some of the characteristics of the disorder are hyperglycemia accompanied by abnormal clearance of free fatty acids and platelet over-reactivity, endothelial cell malfunction, low grade inflammation and oxidative stress, with many affecting the vasculature barrier. Novel studies have shown that the

P2X7 receptor participates in β cell activity, insulin release [511,512] and also in diabetes-related macro- or even microvascular aggravations [513,514].

As a result, the P2X7 purinoceptor could be a key modulator in the initiation of pathogenesis as well as possibly treatment of type 2 diabetes with an elevated clinical importance as a result of its dangerous widespread developing prevalence. On the other hand, the involvement of the P2X7 receptor in type 2 diabetes has not been fully elucidated yet. A study undertaken by Giacovazzo and colleagues (2018) has highlighted the fact that the P2X7 receptor null mice (P2X7 knockout) express to some extent a glucose intolerance profile with storage of triglycerides in other locations around the body other than adipose tissues and also possess an elevated body weight highlighting that the absence of the P2X7 receptor elevates the susceptibility of mice to insulin resistance [515]. However, other studies have shown that the absence of the P2X7 may protect the liver and also kidney from elevated fat diet-supported damage, resulting in decreased inflammation, fibrosis and ultimately lipid build-up [516,517].

A further study carried out by Vieira and colleagues (2016) has highlighted that using an inhibitor of the P2X7 receptor termed bright blue G as well as knockout of the same receptor may inhibit streptozocin-generated diabetes [518]. On the other side, the P2X7 receptor overexpression gives rise to unfavourable consequences when it comes to diabetic neuropathy, retinopathy and nephropathy [493,514,519]. Similarly, prevented stimulation of the same purinergic receptor signalling cascade especially in type 1 diabetes mellitus can influence the function of osteoblasts and in turn may affect bone metabolism [520,521]. In the case in which the metabolism of glucose is perturbed, elevated levels of extracellular adenosine 5'-triphosphate may activate the adipose tissue and pancreatic macrophages, enabling the P2X7 receptor to stimulate the NLRP3 inflammasome resulting in β-cell apoptosis and insulin resistance [391].

3.1.2 P2X and P2Y receptor expression in the human placenta

A study by Roberts and colleagues (2006) has highlighted that isolated cytotrophoblast cells possess at an mRNA level P2X1, P2X2, P2X4, P2X7, $P2Y_1$, $P2Y_2$, $P2Y_4$, $P2Y_6$ and $P2Y_{11}$ receptors at two stages of differentiation namely 18 hours where the majority of cytotrophoblast cells are mononuclear and 66 hours where the primary placental cells are multinucleate and resemble the syncytiotrophoblast *in situ* [277]. The same study has also shown using western blotting that the P2X4 receptor is expressed at a protein level in cytotrophoblast cells at both 18 and 66 hours during the differentiation process which has resulted in a strong band at approximately 65kDa [277]. Similarly, the P2X7 receptor was shown to be expressed at a protein level in cytotrophoblast cells via the detection of a product of circa 145kDa at both stages of differentiation. The $P2Y_2$ receptor was also expressed at a protein level in cytotrophoblast cells via the detection of a specific band at circa 65kDa in four of the six mononucleated and four of the six polynucleated cytotrophoblast cell preparations [277]. The $P2Y_4$ receptor was not present at a protein level in cytotrophoblast cells at either 18 or 66 hours of culture. Lastly, the same study has shown that the $P2Y_6$ receptor was weakly expressed at a protein level in cytotrophoblast cells which have been cultured for 18 or 66 hours via the detection of a band at approximately 110kDa [277].

Another study by Roberts *et al* (2007) has highlighted that the P2X4, P2X7 and $P2Y_2$ receptors were weakly expressed at an mRNA level in isolated villous tissue from first trimester (9-11 weeks of gestation) or term (38-41 weeks of gestation) placental specimens [321]. However, the same study has also provided evidence that a strong signal corresponding to the $P2Y_4$ receptor was present at an mRNA level in

the same tissue type [321]. Also, the investigation by Roberts and colleagues (2007) has illustrated that the P2X4 receptor expression at a protein level was detected in immunoblots at approximately 69kDa in both first trimester and term placental samples investigated [321]. The same study highlighted a particularly weak and not consistently detected P2X7 receptor expression at a protein level in villous tissue originating from both first trimester and term placental specimens [321]. Furthermore, $P2Y_2$ protein product band was identified at approximately 65kDa in the same specimens and $P2Y_4$ receptor products were not identified in any of the placenta samples investigated from both first trimester and term groups [321]. This investigation by Roberts and colleagues (2007) also presented data on localisation of the purinergic P2X4, P2X7, $P2Y_2$ and $P2Y_4$ receptors in villous tissue originating from first trimester and term placenta samples using immunohistochemistry and revealed that the P2X4 receptor was localised at the level of the syncytiotrophoblast layer in first trimester tissue and on the microvillus membrane and basal membrane in term placenta samples [321]. In this study, the P2X7 receptor was generally expressed at an intracellular level in conjunction with the nuclei with decreased levels of staining in the cytoplasm. The P2X7 receptor staining was also present at the level of the syncytiotrophoblast, particularly in term tissue compared to the first trimester specimens. The $P2Y_2$ receptor was immunolocalised on both syncytiotrophoblast membranes with a more prominent staining in term placental samples compared to first trimester. $P2Y_4$ receptor protein staining was not identified in any of the placental tissues studied [321].

Perfused human placental cotyledon has been shown to vasoconstrict under the exposure of α,β-meATP, βγ-methylene ATP and adenosine 5'-triphosphate and vasorelaxation through P2Y receptor-dependent nitric oxide liberation into the extracellular space from endothelial cells has also been demonstrated [475,522]. The

purinergic P2X1, P2X4, P2X5, P2X6 and P2X7 receptors have been found at an mRNA level in in the smooth muscle of chorionic and umbilical arteries and veins along with mRNA for $P2Y_1$, $P2Y_2$ and $P2Y_6$ purinoceptors expressed particularly on the endothelium of these blood vessels, emphasizing the function of the circulating nucleotides in the mediation of the blood flow at the level of the fetal circulation [522,523]. A study by Buvinic and colleagues (2006) has presented evidence that the $P2Y_1$ and $P2Y_2$ receptors are differentially expressed in the human placental vascular tree in terms of an increase between 6- to 8- fold from the umbilical cord to the chorionic or cotyledon blood vessels [481]. These two purinergic receptors are localised at the level of the smooth muscle in the chorionic and umbilical cord blood vessels and are expressed on both smooth muscle and endothelial cells in the cotyledon blood vessels. A study by Valdecantos *et al* (2003) has presented evidence that the P2X1, P2X4 and P2X7 receptors are expressed in human chorionic blood vessels particularly in the smooth muscle layer [479].

Pre-eclampsia is described by disturbed fetal development, proteinuria and increased maternal blood pressure. The start of the pathophysiology of pre-eclampsia has been proposed to involve abnormal trophoblast invasion giving rise to decreased circulating oxygen levels in the placenta, which in turn promote the liberation into the extracellular space of adenosine 5'-triphosphate that is eventually metabolised by ectonucleotidases to adenosine [524]. In the human placenta, this condition has been shown to cause post-translational modifications of the P2X4 receptor where elevated liberation of adenosine 5'-triphosphate into the extracellular space takes place. This process is due to low circulating oxygen levels accompanied by oxidative stress which in turn lead to the activation of the P2X4 purinoceptor therefore regulating the placental cell homeostasis [525].

This chapter presents novel data on the P2X7 receptor protein expression levels in the human placenta chorionic plate artery, stem villous artery, villous tissue and myometrium. The presence of the P2X7 receptor at a protein level in stem villous arteries has not been studied yet, hence this chapter helps to fill in this gap into the literature. Also, the P2X7 receptor has only been shown to be expressed at an mRNA level in chorionic plate arteries by Valdecantos *et al* (2003) [479], but not at a protein level using western blotting, hence this chapter addresses this gap by presenting western blotting data of the purinergic receptor expression in these human placenta blood vessels. The protein expression of the P2X7 receptor in human myometrium has been demonstrated before in a study by Maneta *et al* (2015) [491] and was used in the current investigation as a positive control for the purinergic receptor in P2X7 receptor western blots. Furthermore, villous tissue has been shown to express the P2X7 receptor at a tissue level using immunohistochemistry from term placental samples in a study by Roberts *et al* (2007) [480], with the authors also presenting data on the relatively weak expression of the purinergic receptor at an mRNA and protein level in the same tissue type. However, the purinoceptor has never been shown to be consistently expressed at a protein level in villous tissue using western blotting via the detection of expected protein product bands, hence this chapter has addressed this gap in the current knowledge. Although the study by Roberts *et al* (2007) [480] has found that the P2X7 receptor was expressed in villous tissue in association with syncytiotrophoblast nuclei, the authors did not rate the fluorescence intensity levels of the P2X7 receptor positive syncytiotrophoblast profiles using systematic random sampling and did not investigate the expression of the purinoceptor at the level of the fetal vessels. Since no other studies have assessed these objectives, the current investigation has addressed these gaps into the literature by providing

immunohistochemistry data on the expression of the P2X7 receptor in human placental villous tissue originating from both healthy and diet managed gestational diabetic pregnancies.

Although at the choriodecidua level, the NLRP3 inflammasome has been shown to be expressed at an mRNA level in a study by Bryant *et al* (2017) [526] which have also described the expression of the multimeric protein at an tissue level using immunohistochemistry, the protein expression level assessed using western blotting of the NLRP3 inflammasome in 4th order chorionic plate arteries, stem villous arteries and choriodecidua tissue has not been elucidated yet, hence this chapter helps to fill in the gap into the literature.

The NLRP3 inflammasome has been shown to be expressed at a protein level in isolated primary trophoblast cells which have been cultured in normoxia conditions for 3 days using western blotting [527]. Another study by Stødle *et al* (2018) has presented data on released IL-1β from LPS-primed cultured chorionic villi explants under the stimulation of cholesterol crystals and uric acid crystals [528]. Also, a study by Yang *et al* (2020) has highlighted that the NLRP3 inflammasome is expressed at a protein level in human placental villous tissue originating from healthy and pregnancies complicated by pre-eclampsia [529]. However, no studies have assessed the NLRP3 inflammasome protein expression levels in isolated placental villous tissue using western blotting under the priming with LPS and stimulation with ATP (acting as a danger associated molecular pattern) or BzATP (compound used for activation of the P2X7 receptor), hence the current investigation helps to fill in the gap into the literature.

The current study also provides novel data on the protein expression levels of the P2X7 receptor in D-glucose (acting as a danger associated molecular pattern)

stimulated human placental villous tissue for a period of 4, 24 or 48 hours using western blotting. Furthermore, this study provides further novel data on the protein expression levels of the P2X7 receptor, NLRP3 inflammasome and pro-caspase-1 in stem villous arteries of healthy compared to pregnancies complicated by pre-eclampsia.

Although a study by Maneta *et al* (2015) [491] has shown that the cord blood mononuclear cells and placental blood mononuclear cells originating from labouring and non-labouring women incubated with LPS and BzATP gave rise to elevated levels of IL-1β liberation into the extracellular space, no studies have investigated the pro-inflammatory cytokine (IL-1β, IL-6 and IL-18) release from villous tissue originating from healthy placental samples under the stimulation of LPS, ATP or BzATP, hence the current study fills in this gap in the literature. The current investigation also provides novel data on the expression of the P2X7 receptor in isolated human placenta chorionic plate artery smooth muscle cells which have been isolated using either the tissue explant or enzymatic digestion methods. Lastly, the current investigation has identified a novel optimised method for the immunodelpletion of IgG from villous tissue, SVA and myometrium.

3.2 Hypothesis and aims

The hypothesis of this study was that the P2X7 receptor, NLRP3 inflammasome and pro-caspase-1 protein expression levels in the human placenta stem villous arteries is higher in pregnancies complicated by pre-eclampsia compared to healthy patients.

Aims:

- To investigate the protein expression levels of the NLRP3 inflammasome in the second supernatant fraction of human placenta 4th order chorionic plate artery, stem villous artery and choriodecidua tissue lysates using western blotting
- To assess the protein expression levels of the P2X7 receptor in the second pellet and second supernatant fraction of human placenta chorionic plate artery, stem villous artery, villous tissue and myometrium tissue in lysates which have been immunodepleted of IgG or not immunodepleted of IgG using western blotting
- To investigate the protein expression levels of the NLRP3 inflammasome in the second supernatant fraction of control, ATP, LPS+ATP and LPS+BzATP stimulated human placenta villous tissue lysates using western blotting
- To determine the protein expression levels of the P2X7 receptor in the second pellet fraction of D-glucose stimulated human placenta villous tissue lysates using western blotting and to assess the released lactate dehydrogenase and IL-1β levels in the culture media following 4 or 48 hours of D-glucose stimulation along with the IL-1β levels in the second

supernatant of the villous tissue lysates at the same timepoints using western blotting

- To compare the protein expression levels of the P2X7 receptor, NLRP3 inflammasome and pro-caspase-1 originating from human placenta stem villous arteries in healthy and pre-eclamptic placental samples using western blotting
- To investigate the mRNA expression level of the P2X7 receptor, NLRP3 inflammasome and caspase-1 in stem villous arteries originating from healthy and pre-eclamptic placental samples using RT-qPCR
- To assess the released levels of IL-1β, IL-6 and IL-18 in villous tissue which has been stimulated with control, ATP, LPS+ATP and LPS+BzATP originating from healthy placental samples using ELISA
- To evaluate the immunolocalization of the P2X7 receptor in isolated human placenta chorionic plate artery smooth muscle cells which have been isolated either via the tissue explant or enzymatic digestion method using immunocytochemistry
- To characterise the distribution of the P2X7 receptor in isolated human placenta chorionic plate artery smooth muscle cells which have been stimulated with ATP, BzATP and A740003 using immunocytochemistry
- To describe the immunohistochemical expression of the P2X7 receptor in isolated sections of human placental villous tissue originating from healthy and diet managed gestational diabetic samples at the level of the syncytiotrophoblast and fetal capillaries

- To investigate the immunohistochemical expression of the P2X7 receptor in isolated sections of human placental chorionic plate arteries from healthy patients at the level of the smooth muscle and the endothelium

3.3 Results

The methods used in this results chapter have been described in chapter 2.6-2.14 and chapter 2.17. The expected band size for the P2X7 receptor is approximately 70kDa.

3.3.1 Two P2X7 receptor bands were identified at approximately 74kDa and circa 97kDa in the second pellet of CPA, SVA and trophoblast tissue lysates

Two bands were detected at approximately 74kDa and circa 97kDa in the second pellet (membrane protein fraction) of CPA, SVA and trophoblast tissue lysates originating from a healthy placenta sample as highlighted in figure 29, panel A (green boxes). No P2X7 receptor specific bands were detected in the second supernatant fraction of the same CPA, SVA and trophoblast tissue lysates. Less intense bands were observed in the same immunoblot at circa 152kDa, approximately 62kDa and about 52kDa particularly in the second pellet fraction (figure 29, panel A, red boxes) which were due to the non-specific binding of the P2X7 receptor primary antibody as suggested from the P2X7 receptor secondary antibody control immunoblot presented in figure 31, panel A where no bands were detected. The P2X7 receptor protein specificity was confirmed using the P2X7 receptor specific blocking peptide on a separate blot using the same tissue lysates as highlighted in figure 30, panel A (green boxes). Here, all bands disappeared after the preincubation with the antigenic peptide.

The Ponceau S staining of all three immunoblots presented in figures 29-31 highlighted equal protein loading.

As a result, two P2X7 receptor specific protein products were identified at approximately 74kDa and 97kDa in the second pellet fraction (membrane protein fraction) of human placenta chorionic plate arteries, stem villous arteries and villous tissue lysates using western blotting.

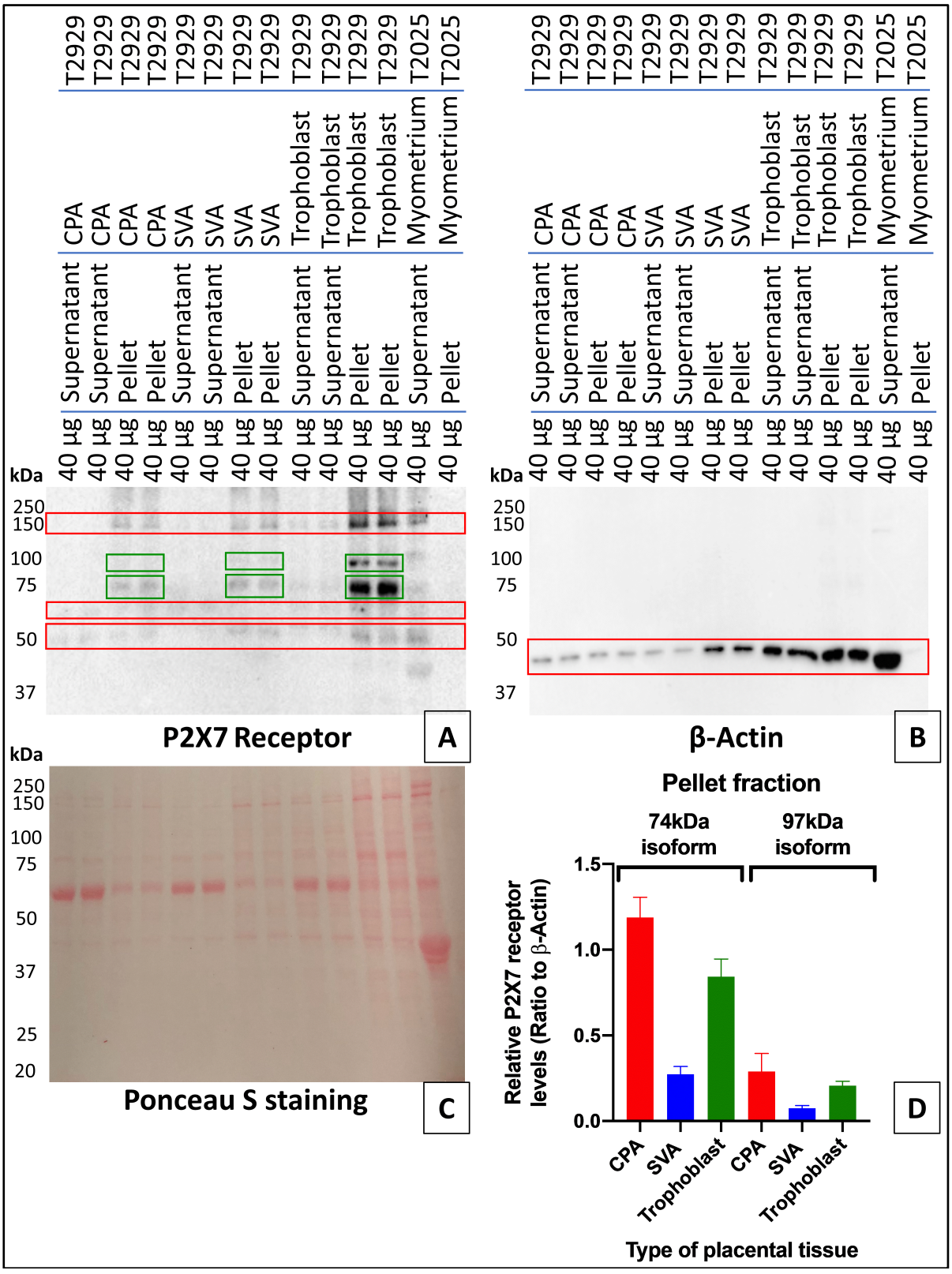


Figure 29. *This figure shows the P2X7 receptor expression (panel **A**, green boxes, 73kDa and 97kDa isoforms) in the second supernatant and the second pellet fractions of CPA, SVA and trophoblast tissue lysates originating from a placenta sample of a healthy patient (T2929) and in myometrium (healthy patient, T2025). The protein bands highlighted with red boxes (152kDa, 62kDa and 52kDa) denote non-specific binding of the P2X7 receptor primary antibody. Myometrium was used as a positive*

*control for the P2X7 receptor **B**. The immunoblot was stripped and then reblotted with β actin for loading control (red box). The β actin protein expression level in the second pellet (membrane) fraction of myometrium tissue lysate sample originating from patient T2025 shown in the last western blot lane has degraded, hence no band was detected **C**. Ponceau S staining of the nitrocellulose membrane prior to immunoblotting for the P2X7 receptor **D**. Relative P2X7 receptor protein expression levels (74kDa and 97kDa isoforms) normalised to β actin. Data are expressed as mean ± SEM. Each well was loaded with 40μg of total protein. Antibodies used: P2X7 primary antibody (Rabbit polyclonal IgG, Alomone Labs, APR-004) at a dilution of 1:600, P2X7 secondary antibody (Polyclonal goat anti rabbit immunoglobulins alkaline phosphatase, Dako, D0487) at a dilution of 1:1000, β actin primary antibody (rabbit polyclonal IgG, Abcam, Ab8227) at a dilution of 1:8000 and β actin secondary antibody (Polyclonal goat anti rabbit immunoglobulins alkaline phosphatase, Dako, D0487) at a dilution of 1:1000. In this case, all tissue samples were homogenised using lysing matrix D ceramic spheres and IgG was immunodepleted from protein lysates using a well-established immunoprecipitation protocol involving anti-human IgG (whole molecule)-agarose antibody developed in goat (Sigma, A3543).*

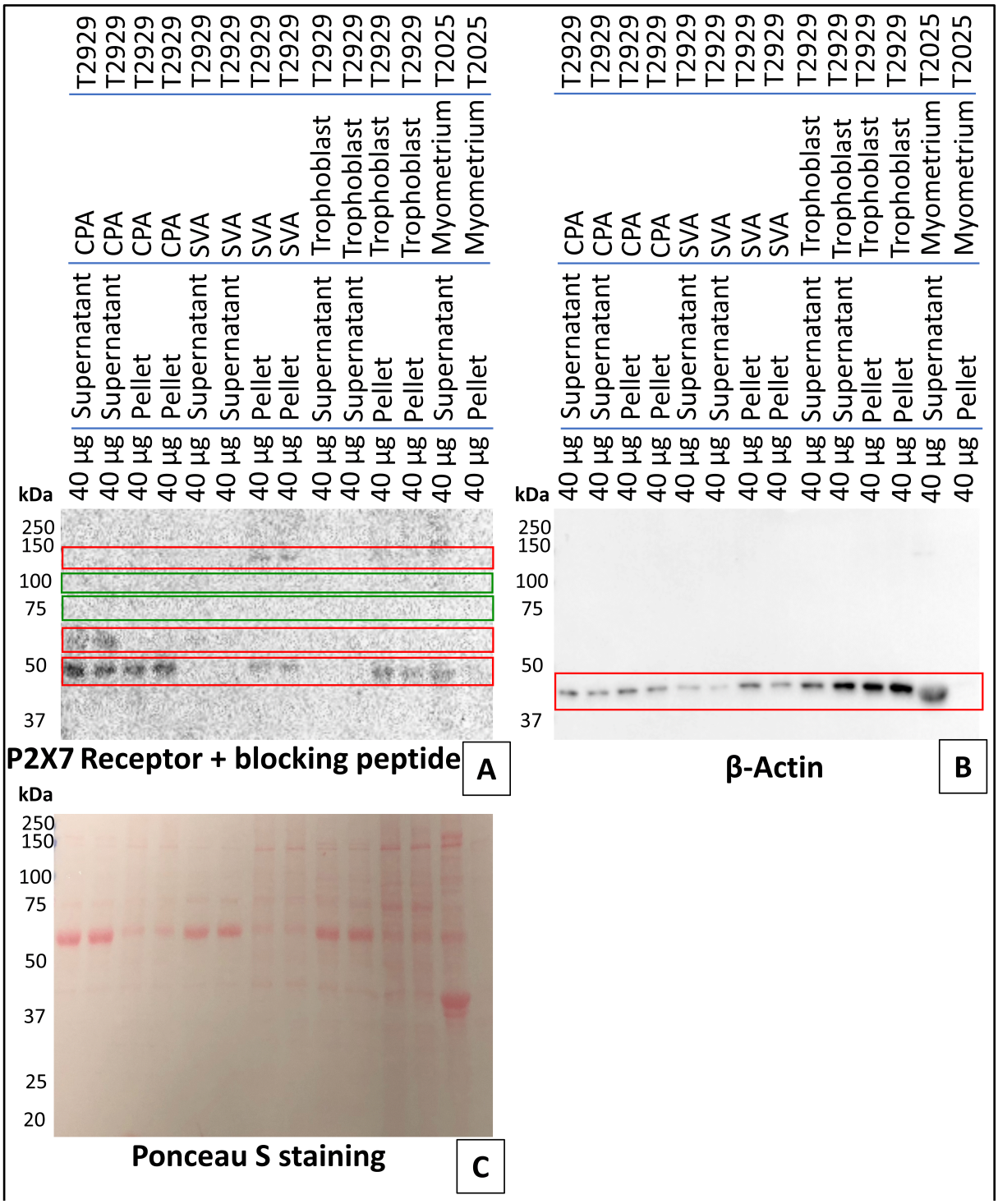


Figure 30. *Immunoblot highlighting that the bands corresponding to the molecular weight of the native P2X7 receptor (highlighted with green boxes) disappeared after pre-adsorption of the P2X7 receptor primary antibody with a control peptide antigen equivalent to the amino acid residues 576-595 of the intracellular C-terminus of the P2X7 receptor (negative control). In this study, the second supernatant and second pellet fractions of fourth order CPA, SVA and choriodecidua tissue lysates was used originating from a placenta sample of a healthy patient (T2929) as well as myometrium tissue originating from a healthy patient (T2025). The protein bands highlighted with red boxes (137kDa, 59kDa and 48kDa) denote non-specific binding of the primary*

antibody. ***B****. The immunoblot was stripped and then reblotted with β actin for loading control (red box). The β actin protein expression level in the second pellet (membrane) fraction of myometrium tissue lysate originating from patient T2025 shown in the last western blot lane has degraded, hence no band was detected* ***C****. Ponceau S staining of the nitrocellulose membrane prior to immunoblotting for the P2X7 receptor. Each well was loaded with 40μg of total protein. Antibodies used: P2X7 primary antibody (Rabbit polyclonal IgG, Alomone Labs, APR-004) at a dilution of 1:600, P2X7 secondary antibody (Polyclonal goat anti rabbit immunoglobulins alkaline phosphatase, Dako, D0487) at a dilution of 1:1000, β actin primary antibody (rabbit polyclonal IgG, Abcam, Ab8227) at a dilution of 1:8000 and β actin secondary antibody (Polyclonal goat anti rabbit immunoglobulins alkaline phosphatase, Dako, D0487) at a dilution of 1:1000. In this case, all tissue samples were homogenised using lysing matrix D ceramic spheres and IgG was immunodepleted from protein lysates using a well-established immunoprecipitation protocol involving anti-human IgG (whole molecule)-agarose antibody developed in goat (Sigma, A3543). In this case, the transfer of the resolved proteins from the polyacrylamide gel to the nitrocellulose membrane did not work very well, therefore fewer proteins have transferred to the nitrocellulose membrane which gave rise to a less intense β-actin staining.*

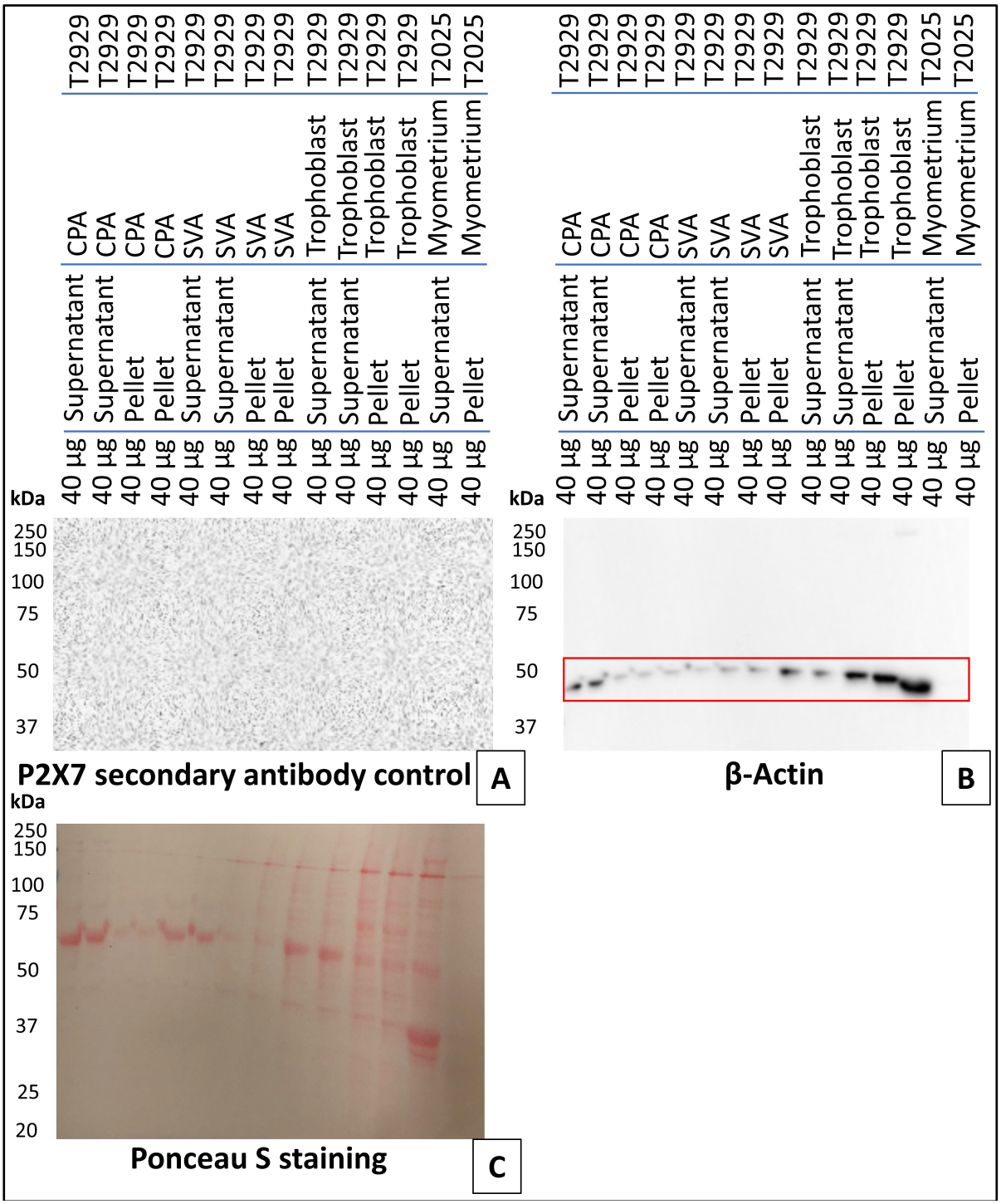


Figure 31. *Immunoblot highlighting the P2X7 receptor secondary antibody control where the primary antibody corresponding to the purinergic receptor has been replaced with 3% marvel milk/TBST as presented in panel **A**. In this study, the second supernatant and second pellet fractions of fourth order CPA, SVA and choriodecidua tissue lysates was used originating from a placenta sample of a healthy patient (T2929) as well as myometrium tissue originating from a healthy patient (T2025) **B**. The immunoblot was stripped and then reblotted with β actin for loading control (red box) **C**. Ponceau S staining of the nitrocellulose membrane corresponding to the P2X7 receptor secondary antibody control. Each well was loaded with 40µg of total protein. Antibodies used: P2X7 receptor secondary antibody (Polyclonal goat anti rabbit*

immunoglobulins alkaline phosphatase, Dako, D0487) at a dilution of 1:1000, β actin primary antibody (rabbit polyclonal IgG, Abcam, Ab8227) at a dilution of 1:8000 and β actin secondary antibody (Polyclonal goat anti rabbit immunoglobulins alkaline phosphatase, Dako, D0487) at a dilution of 1:1000. In this case, all tissue samples were homogenised using lysing matrix D ceramic spheres and IgG was immunodepleted from protein lysates using a well-established immunoprecipitation protocol involving anti-human IgG (whole molecule)-agarose antibody developed in goat (Sigma, A3543).

3.3.2 P2X7 receptor specific bands were identified in the second pellet fraction of SVA, trophoblast tissue and myometrium tissue lysates which have been successfully immunodepleted of IgG originating from 3 healthy placental samples

A strong signal corresponding to the P2X7 receptor was identified in the second pellet fraction of trophoblast tissue (approximately 79kDa), SVA (circa 80kDa) and myometrium tissue (about 78kDa) lysates originating from N=3 healthy placental samples as highlighted by the red box in figure 33 (panel A), figure 36 (panel A) and figure 39 (panel A). All P2X7 receptor protein specificity was confirmed using the P2X7 specific blocking peptide which caused the disappearance of the 78-80kDa bands in the second pellet fraction of all placental tissue types studied as illustrated by the red box in figure 33 (panel D), figure 36 (panel D) and figure 39 (panel D). Immunodepletion of IgG successfully removed the intense band at approximately 48-49kDa in the P2X7 receptor immunoblots (in the absence and presence of the blocking peptide) using the second pellet fraction of trophoblast tissue, SVA and myometrium tissue lysates as highlighted by the green box presented in figure 33 (panels A and D), figure 36 (panels A and D) and figure 39 (panels A and D). The P2X7 receptor western blots (with and without the blocking peptide) showed the presence of a strong

band at approximately 48-49kDa using the second pellet fraction of the same tissue lysates which have not been immunodepleted of IgG as indicated by the violet boxes in figures 33, 36 and 39. Similarly, a strong signal was observed at approximately 60kDa in the P2X7 receptor immunoblots using the second pellet fraction of the trophoblast tissue, SVA and myometrium tissue lysates, which was due to the non-specific binding of the P2X7 receptor primary antibody as suggested from the P2X7 receptor secondary antibody control immunoblot presented in figure 43 (panel A). No statistically significant differences were found between the relative P2X7 receptor protein expression levels of non-immunodepleted and IgG immunodepleted second pellet fraction of SVA (Dunnett T3 multiple comparison tests) and myometrium tissue (Dunn's multiple comparison tests) lysates which have been homogenised using either the ultra turrax method or lysing matrix D ceramic spheres as presented in figure 37 (panel A) and figure 40 (panel A). However, a statistically significant difference was found in the relative P2X7 receptor protein expression levels between non-immunodepleted and IgG immunodepleted second pellet fraction of trophoblast tissue lysates obtained via the ultra turrax method using an unpaired T-test (*P=0.0398) as illustrated in figure 34 (panel A). No statistically significant differences were found between the relative IgG (heavy chain) protein expression levels of non-immunodepleted and IgG immunodepleted second pellet fraction of SVA (Dunnett's T3 multiple comparisons test) and myometrium tissue (Dunn's multiple comparisons test) lysates which have been homogenised using either the ultra turrax method or lysing matrix D ceramic spheres as illustrated in figure 37 (panel B) and figure 40 (panel B). However, there was a statistically significant difference (*P=0.0184; Dunnett's T3 multiple comparisons test) in the relative IgG heavy chain protein expression levels between non-immunodepleted (Lysing matrix D homogenised) and

IgG immunodepleted (ultra turrax homogenised) second pellet fraction of trophoblast tissue lysates as presented in figure 34 (panel B).

No P2X7 receptor specific bands were observed in the second supernatant fraction of trophoblast tissue, SVA and myometrium tissue lysates originating from N=3 healthy placental samples as highlighted by the red box in figure 32 (panel A), figure 35 (panel A) and figure 38 (panel A). Immunodepletion of IgG successfully removed a strong signal at approximately 46-49kDa in the P2X7 receptor immunoblots using the second supernatant fraction of trophoblast tissue, SVA and myometrium tissue lysates as illustrated by the green boxes in figures 32, 35 and 38. An intense band was observed at 46-49kDa in the P2X7 receptor western blots using the second supernatant fraction of the same tissue lysates which have not been immunodepleted of IgG as indicated by the violet boxes in figures 32, 35 and 38. Furthermore, an intense band was also observed at approximately 58kDa in the same P2X7 receptor immunoblots which was due to the non-specific binding of the P2X7 receptor primary antibody as suggested from the P2X7 receptor secondary antibody control immunoblot presented in figure 43 (panel A). No statistically significant differences in the relative IgG (heavy chain, approximately 46-49kDa) protein expression levels were found between non-immunodepleted and IgG immunodepleted second supernatant fraction of trophoblast tissue (Dunnett's T3 multiple comparisons test), SVA (Dunn's multiple comparisons test) and myometrium tissue (Dunnett's T3 multiple comparisons test) lysates which have been homogenised using either the ultra turrax method or lysing matrix D ceramic spheres as illustrated in figure 32 (panel D), figure 35 (panel D) and figure 38 (panel D).

No P2X7 receptor specific bands were observed in immunoblots using the second supernatant fraction of trophoblast tissue and SVA lysates which have been

either stored at -80^{0}C prior to homogenisation or homogenised using the lysing matrix D ceramic spheres immediately after the collection of the placental samples as highlighted by the red box in figure 41 (panel A) and figure 42 (panel B). In this case, immunodepletion of IgG resulted in the absence of a strong signal at approximately 47-50kDa in the P2X7 receptor immunoblots using the second supernatant fraction of trophoblast tissue and SVA lysates as illustrated by the green box in figure 41 (panel A) and figure 42 (panel A). However, the P2X7 receptor western blots showed the presence of an intense signal at circa 47-50kDa using the second supernatant fraction of the same tissue lysates which have not been immunodepleted of IgG as indicated by the violet box in figure 41 (panel A) and figure 42 (panel A). An intense band was observed in the P2X7 receptor immunoblots using the same second supernatant of SVA (58kDa) and trophoblast tissue (59kDa) lysates which was due to the non-specific binding of the P2X7 receptor primary antibody as suggested from the P2X7 receptor secondary antibody control immunoblot presented in figure 43 (panel A). Figure 41 (panel D) and figure 42 (panel D) highlight the relative IgG (heavy chain) expression levels in the second supernatant of trophoblast tissue and SVA lysates which have been either stored at -80^{0}C prior to homogenisation or homogenised using lysing matrix D ceramic spheres immediately after the collection of the placenta sample.

No bands were detected in the immunoblot corresponding to the P2X7 receptor secondary antibody control using the second pellet fraction of trophoblast tissue, SVA and myometrium tissue lysates originating from 3 healthy placental samples which have been either non-immunodepleted or IgG immunodepleted as highlighted in figure 43 (panel A). The ponceau S staining of all immunoblots presented in figures 32-33, 35-36, 38-39 and 41-43 highlighted equal protein loading.

As a result, protein products corresponding to the P2X7 receptor were identified in the second pellet fraction (membrane protein fraction) of human placenta villous tissue (approximately 79kDa), SVA (circa 80kDa) and myometrium (approximately 78kDa) tissue lysates which were successfully immunodepleted of IgG (resulting in the removal of an intense band at circa 48-49kDa in all immunoblots) or not immunodepleted of IgG. Furthermore, no P2X7 receptor specific bands were detected in the second supernatant fraction (containing the cytoplasmic fraction) of the same tissue lysates.

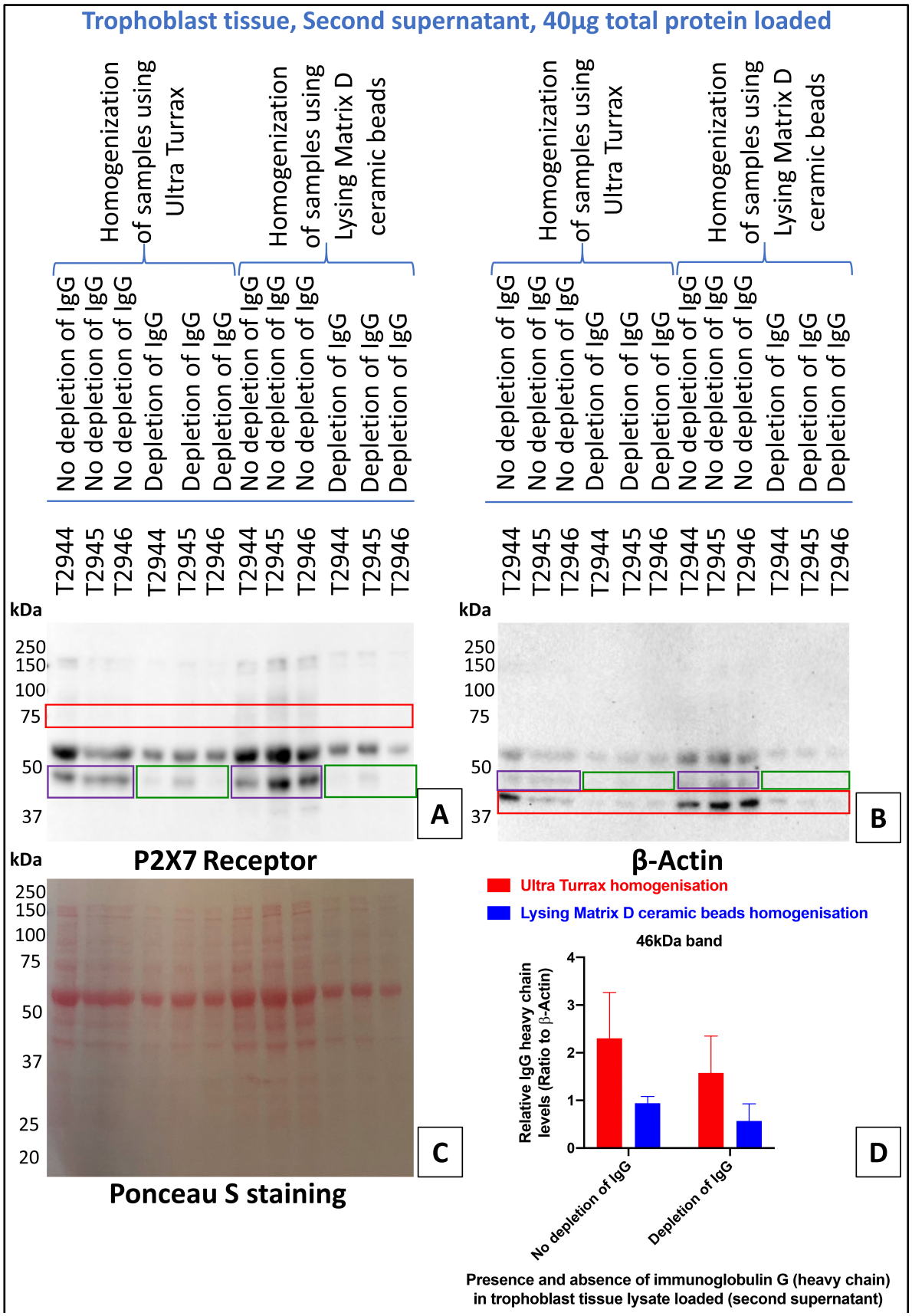


Figure 32. *This figure shows the P2X7 receptor protein expression levels (panel **A**, red box) in the second supernatant of trophoblast tissue lysate originating from three placental samples of healthy patients (T2944, T2945, T2946). In this case, the tissue*

samples were homogenised using either the ultra turrax method (as highlighted in panel D, red bars) or using lysing matrix D ceramic spheres (as presented in panel D, blue bars). The tissue lysates were either IgG immunodepleted using a well-established immunoprecipitation protocol involving anti-human IgG (whole molecule)-agarose antibody developed in goat (Sigma, A3543) as illustrated in panel A (green boxes) or not IgG immunodepleted (panel A, violet boxes). Each well was loaded with 40µg of total protein. ***B****. The immunoblot was stripped and then reblotted with β actin for loading control (red box). The green boxes highlight the absence of IgG and the violet boxes denote the presence of IgG in the trophoblast tissue lysates.* ***C****. Ponceau S staining of the nitrocellulose membrane prior to immunoblotting for the P2X7 receptor* ***D****. Graph highlighting the relative IgG heavy chain levels normalised to β actin in trophoblast tissue lysates which have been either depleted or non-depleted of immunoglobulin G. Data are expressed as mean ± SEM. Antibodies used: P2X7 primary antibody (Rabbit polyclonal IgG, Alomone Labs, APR-004) at a dilution of 1:600, P2X7 secondary antibody (Polyclonal goat anti rabbit immunoglobulins alkaline phosphatase, Dako, D0487) at a dilution of 1:1000, β actin primary antibody (rabbit polyclonal IgG, Abcam, Ab8227) at a dilution of 1:8000 and β actin secondary antibody (Polyclonal goat anti rabbit immunoglobulins alkaline phosphatase, Dako, D0487) at a dilution of 1:1000.*

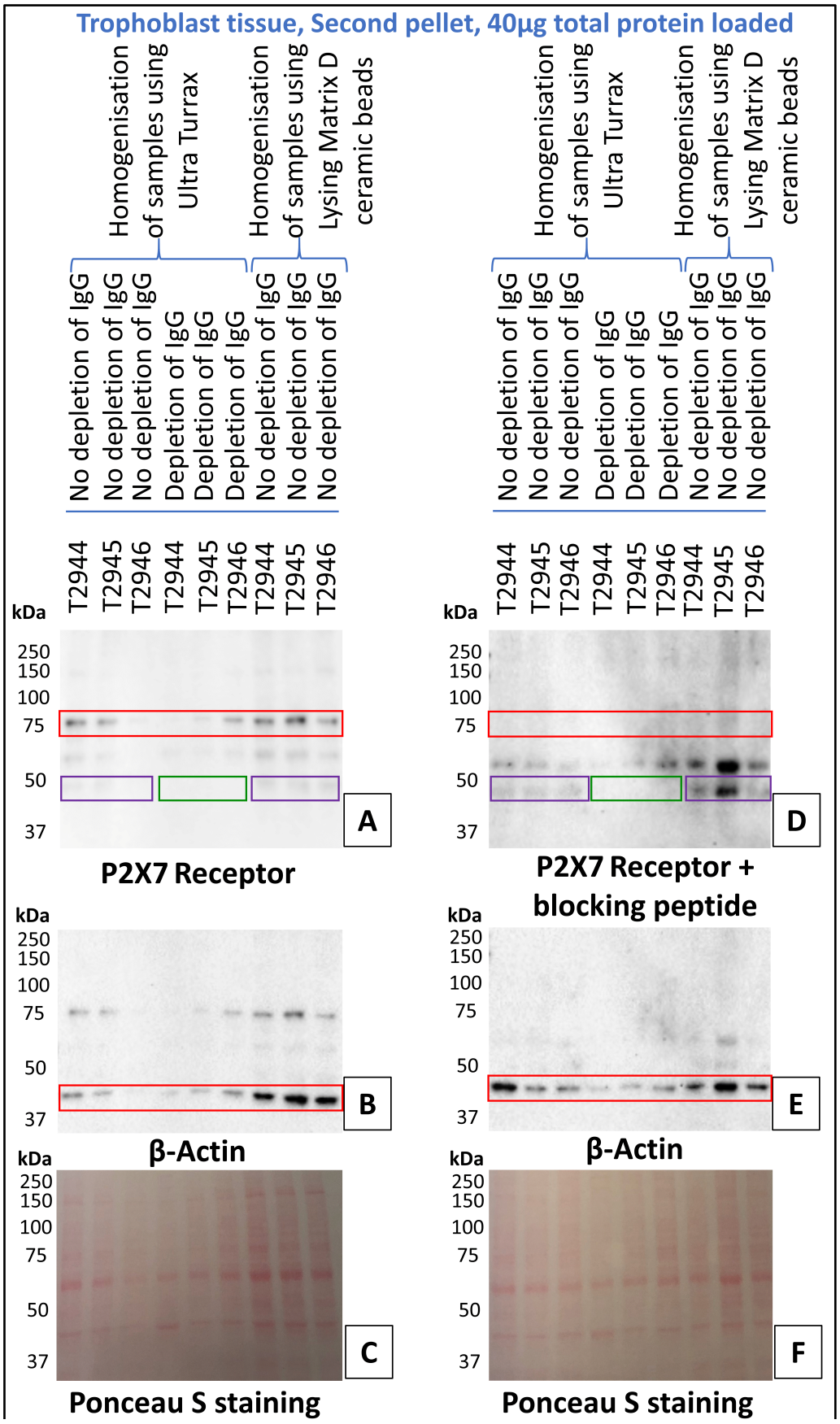


Figure 33. *This figure shows the P2X7 receptor protein expression levels (panel **A**, red box) in the second pellet fraction of trophoblast tissue lysates originating from three*

placental samples of healthy patients (T2944, T2945, T2946). The tissue samples were homogenised using either the ultra turrax method or using lysing matrix D ceramic spheres. The tissue lysates were either IgG immunodepleted using a well-established immunoprecipitation protocol involving anti-human IgG (whole molecule)-agarose antibody developed in goat (Sigma, A3543) as illustrated in panel A (green box) or not IgG immunodepleted (panel A, violet boxes). Each well was loaded with 40μg of total protein ***B****. The immunoblot was stripped and then reblotted with β actin for loading control (red box)* ***C****. Ponceau S staining of the nitrocellulose membrane prior to immunoblotting for the P2X7 receptor* ***D****. Immunoblot highlighting that the bands corresponding to the molecular weight of native P2X7 receptor (red box) disappeared after pre-adsorption of the P2X7 primary antibody with a blocking peptide equivalent to the amino acid residues 576-595 of the intracellular C-terminus of the P2X7 receptor (negative control). The green box highlights the absence of the 48kDa band in tissue lysates which have been immunodepleted of IgG and the violet boxes denote the presence of the 48kDa band in tissue lysates which have not been immunodepleted of IgG* ***E****. The immunoblot presented in panel D was stripped and then reblotted with β actin for loading control (red box)* ***F****. Ponceau S staining of nitrocellulose membrane prior to immunoblotting for the P2X7 receptor with blocking peptide. Antibodies used: P2X7 primary antibody (Rabbit polyclonal IgG, Alomone Labs, APR-004) at a dilution of 1:600, P2X7 secondary antibody (Polyclonal goat anti rabbit immunoglobulins alkaline phosphatase, Dako, D0487) at a dilution of 1:1000, β actin primary antibody (rabbit polyclonal IgG, Abcam, Ab8227) at a dilution of 1:8000 and β actin secondary antibody (Polyclonal goat anti rabbit immunoglobulins alkaline phosphatase, Dako, D0487) at a dilution of 1:1000.*

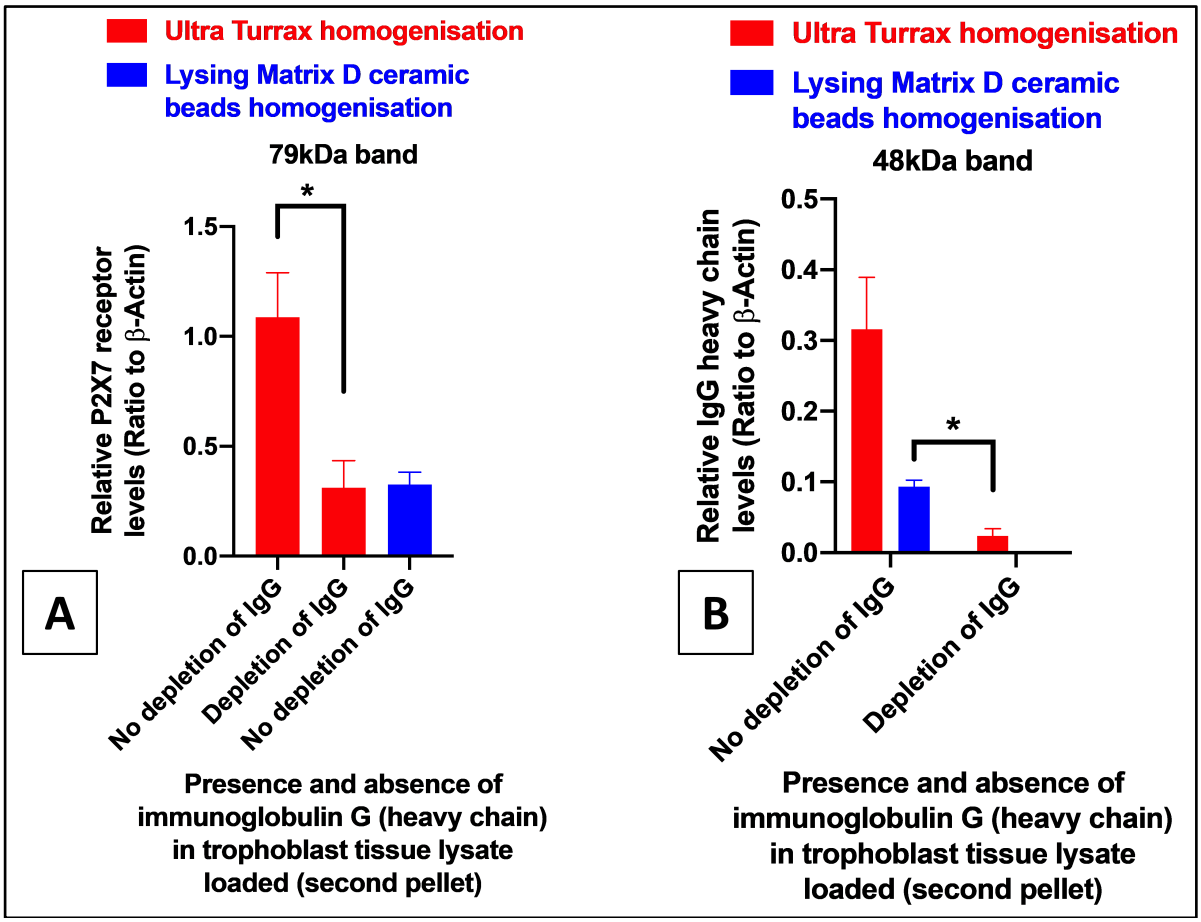


Figure 34. *These graphs highlight the relative P2X7 receptor protein expression levels (panel **A**) and IgG heavy chain levels (panel **B**) normalised to β actin in trophoblast tissue lysates (second pellet) which have been either depleted or non-depleted of immunoglobulin G. The tissue was homogenised using either the ultra turrax method (red bars) or using lysing matrix D ceramic spheres (blue bars). Data are expressed as mean ± SEM. *P≤0.05, **P≤0.01, ***P≤0.001, ****P≤0.0001.*

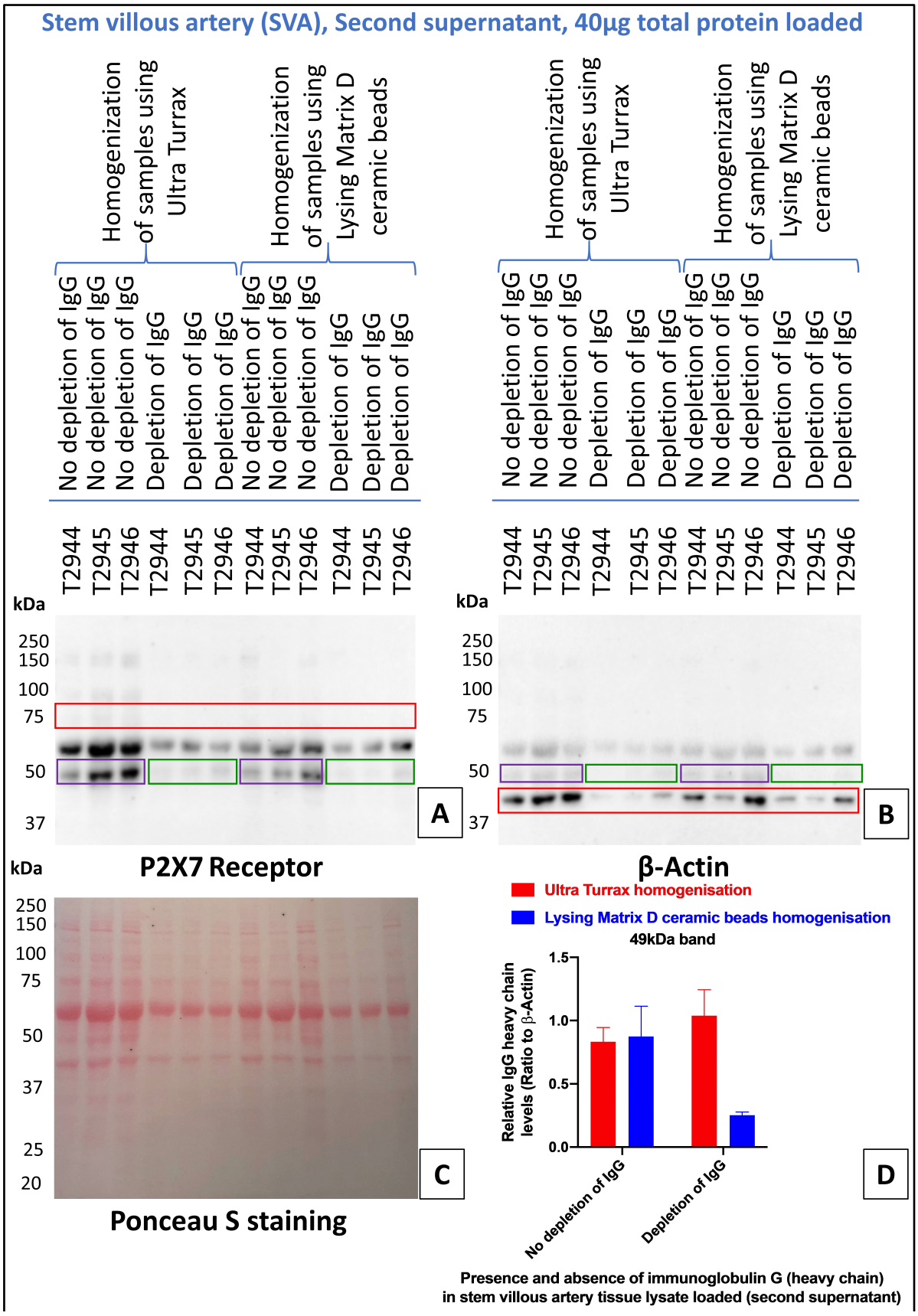


Figure 35. *This figure shows the relative P2X7 receptor protein expression levels (panel **A**, red box) in the second supernatant fraction of stem villous artery (SVA) originating from three placental samples of healthy patients (T2944, T2945, T2946).*

In this case, the tissue samples were homogenised using either the ultra turrax method (as highlighted in panel D, red bars) or using lysing matrix D ceramic spheres (as presented in panel D, blue bars). The tissue lysates were either IgG immunodepleted using a well-established immunoprecipitation protocol involving anti-human IgG (whole molecule)-agarose antibody developed in goat (Sigma, A3543) as illustrated in panel A (green boxes) or not IgG immunodepleted (panel A, violet boxes). Each well was loaded with 40µg of total protein. ***B****. The immunoblot was stripped and then reblotted with β actin for loading control (red box). The green boxes highlight the absence of IgG and the violet boxes denote the presence of IgG in the stem villous artery lysates.* ***C****. Ponceau S staining of nitrocellulose membrane prior to immunoblotting for the P2X7 receptor* ***D****. Graph highlighting the relative IgG heavy chain protein expression levels normalised to β actin in stem villous artery lysates which have been either depleted or non-depleted of immunoglobulin G. Data are expressed as mean ± SEM. Antibodies used: P2X7 primary antibody (Rabbit polyclonal IgG, Alomone Labs, APR-004) at a dilution of 1:600, P2X7 secondary antibody (Polyclonal goat anti rabbit immunoglobulins alkaline phosphatase, Dako, D0487) at a dilution of 1:1000, β actin primary antibody (rabbit polyclonal IgG, Abcam, Ab8227) at a dilution of 1:8000 and β actin secondary antibody (Polyclonal goat anti rabbit immunoglobulins alkaline phosphatase, Dako, D0487) at a dilution of 1:1000.*

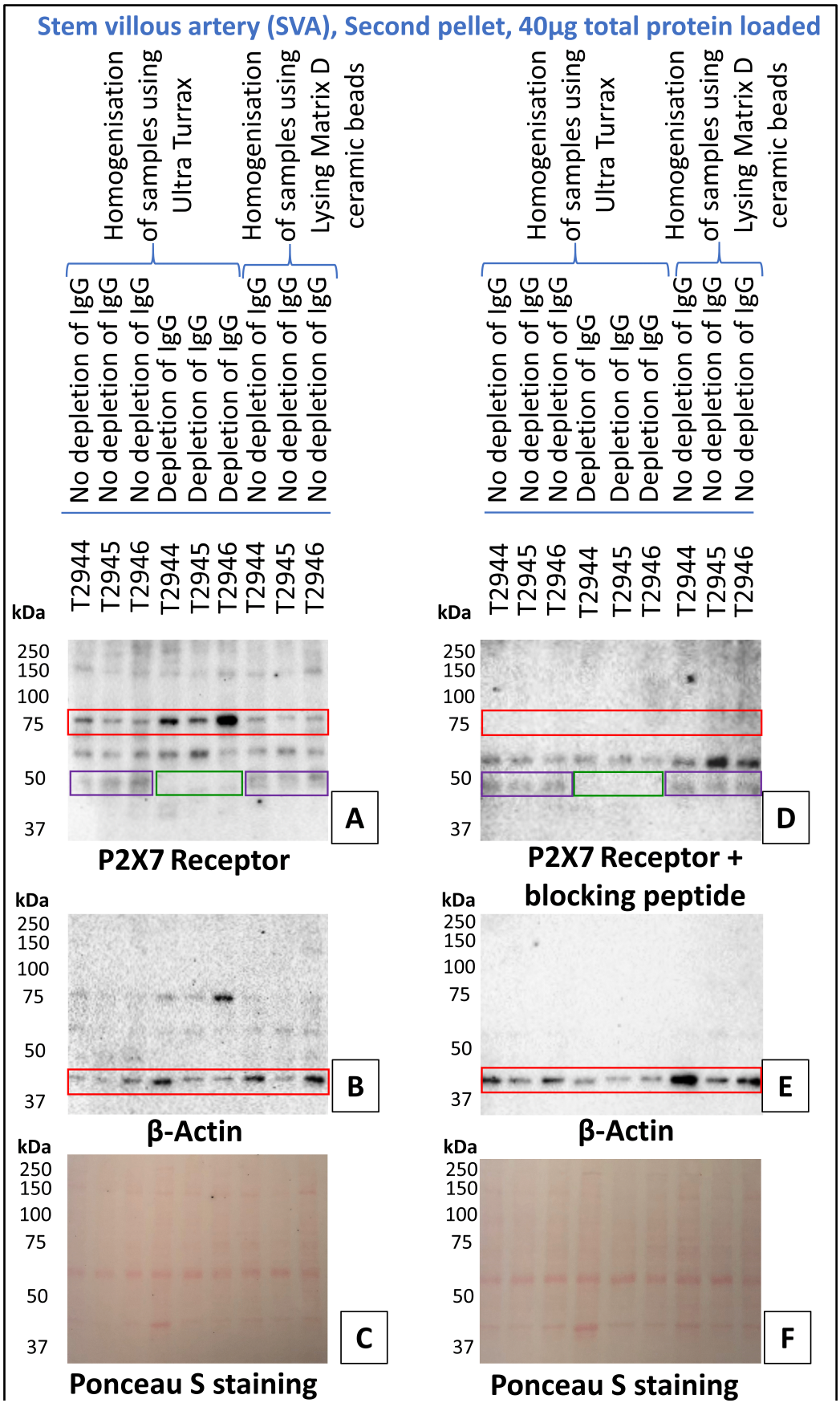


Figure 36. *This figure shows the P2X7 receptor protein expression levels (panel **A**, red box) in the second pellet fraction of stem villous artery (SVA) lysates originating*

from three placental samples of healthy patients (T2944, T2945, T2946). The tissue samples were homogenised using either the ultra turrax method or using lysing matrix D ceramic spheres. The tissue lysates were either IgG immunodepleted using a well-established immunoprecipitation protocol involving anti-human IgG (whole molecule)-agarose antibody developed in goat (Sigma, A3543) as illustrated in panel A (green box) or not IgG immunodepleted (panel A, violet boxes). Each well was loaded with 40µg of total protein ***B****. The immunoblot was stripped and then reblotted with β actin for loading control (red box)* ***C****. Ponceau S staining of nitrocellulose membrane prior to immunoblotting for the P2X7 receptor* ***D****. Immunoblot highlighting that the bands corresponding to the molecular weight of native P2X7 receptor (red box) disappeared after pre-adsorption of the P2X7 primary antibody with a blocking peptide equivalent to the amino acid residues 576-595 of the intracellular C-terminus of the P2X7 receptor (negative control). The green box highlights the absence of the 48kDa band in tissue lysates which have been immunodepleted of IgG and the violet boxes denote the presence of the 48kDa band in tissue lysates which have not been immunodepleted of IgG* ***E****. The immunoblot presented in panel D was stripped and then reblotted with β actin for loading control (red box)* ***F****. Ponceau S staining of the nitrocellulose membrane prior to immunoblotting for the P2X7 receptor with blocking peptide. Antibodies used: P2X7 primary antibody (Rabbit polyclonal IgG, Alomone Labs, APR-004) at a dilution of 1:600, P2X7 secondary antibody (Polyclonal goat anti rabbit immunoglobulins alkaline phosphatase, Dako, D0487) at a dilution of 1:1000, β actin primary antibody (rabbit polyclonal IgG, Abcam, Ab8227) at a dilution of 1:8000 and β actin secondary antibody (Polyclonal goat anti rabbit immunoglobulins alkaline phosphatase, Dako, D0487) at a dilution of 1:1000.*

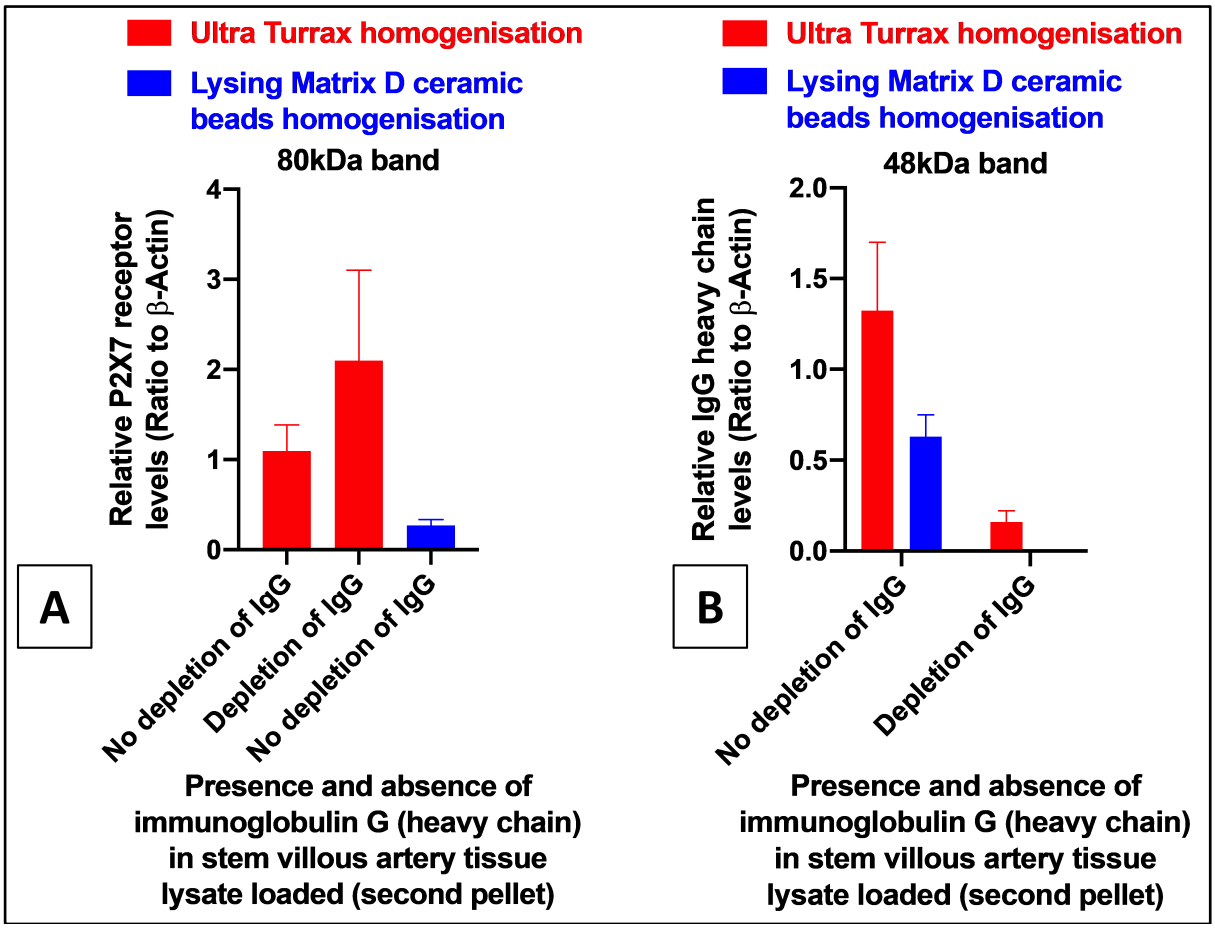


Figure 37. *These graphs highlight the P2X7 receptor protein expression levels (panel **A**) and IgG heavy chain levels (panel **B**) normalised to β actin in stem villous artery lysates (second pellet fraction) which have been either depleted or non-depleted of immunoglobulin G. The tissue was homogenised using either the ultra turrax method (red bars) or using lysing matrix D ceramic spheres (blue bars). Data are expressed as mean ± SEM.*

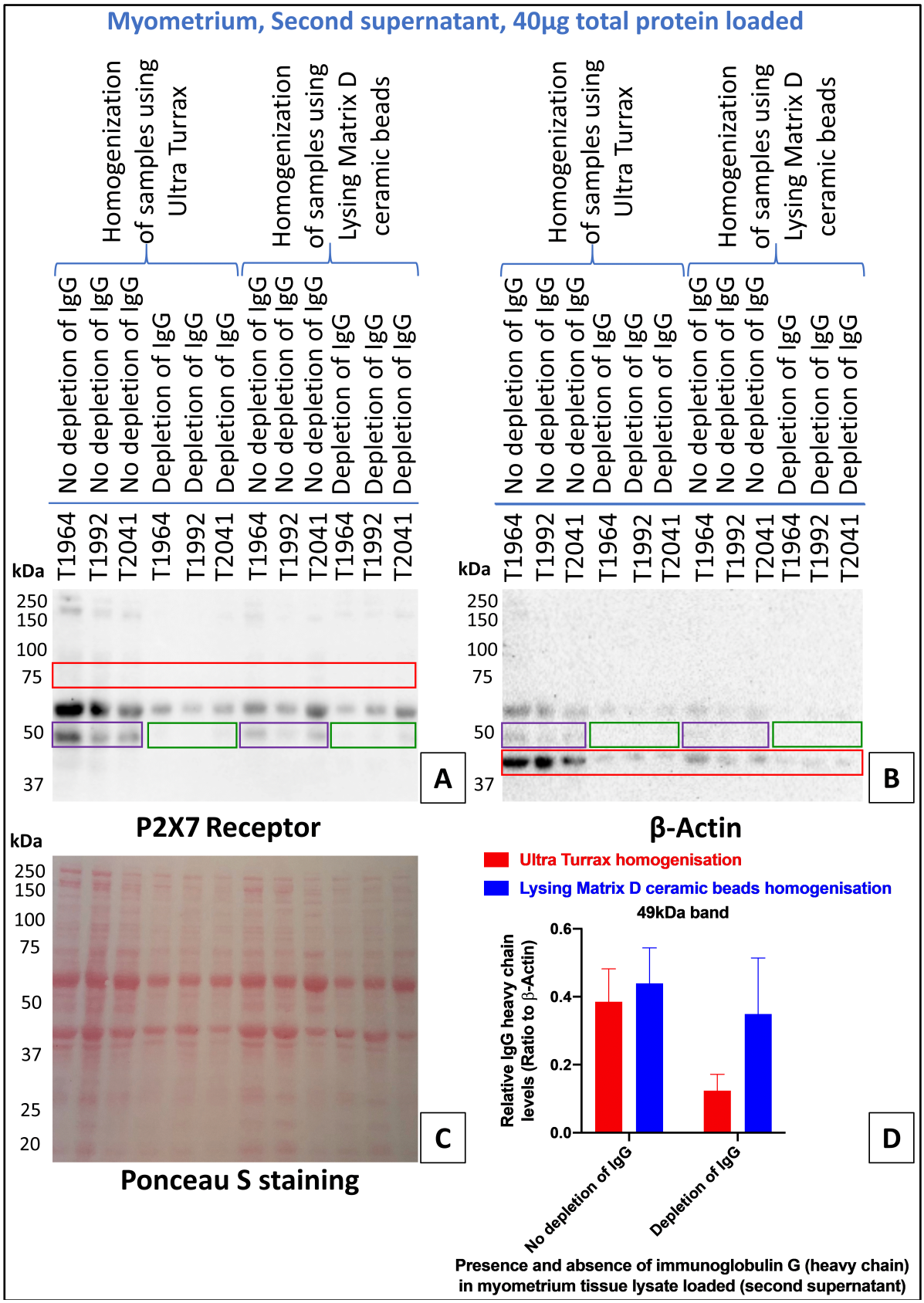


Figure 38. *This figure shows the P2X7 receptor protein expression levels (panel **A**, red box) in the second supernatant fraction of myometrium tissue lysates originating from three placental samples of healthy patients (T1964, T1992 and T2041). In this*

case, the tissue samples were homogenised using either the ultra turrax method (as highlighted in panel D, red bars) or using lysing matrix D ceramic spheres (as presented in panel D, blue bars). The tissue lysates were either IgG immunodepleted using a well-established immunoprecipitation protocol involving anti-human IgG (whole molecule)-agarose antibody developed in goat (Sigma, A3543) as illustrated in panel A (green boxes) or not IgG immunodepleted (panel A, violet boxes). Each well was loaded with 40µg of total protein. Myometrium was used as a positive control for the P2X7 receptor ***B****. The immunoblot was stripped and then reblotted with β actin for loading control (red box). The green boxes highlight the absence of IgG and the violet boxes denote the presence of IgG in the myometrium tissue lysates.* ***C****. Ponceau S staining of nitrocellulose membrane prior to immunoblotting for the P2X7 receptor* ***D****. Graph highlighting the relative IgG heavy chain levels normalised to β actin in myometrium tissue lysates which have been either depleted or non-depleted of immunoglobulin G. Data are expressed as mean ± SEM. Antibodies used: P2X7 primary antibody (Rabbit polyclonal IgG, Alomone Labs, APR-004) at a dilution of 1:600, P2X7 secondary antibody (Polyclonal goat anti rabbit immunoglobulins alkaline phosphatase, Dako, D0487) at a dilution of 1:1000, β actin primary antibody (rabbit polyclonal IgG, Abcam, Ab8227) at a dilution of 1:8000 and β actin secondary antibody (Polyclonal goat anti rabbit immunoglobulins alkaline phosphatase, Dako, D0487) at a dilution of 1:1000.*

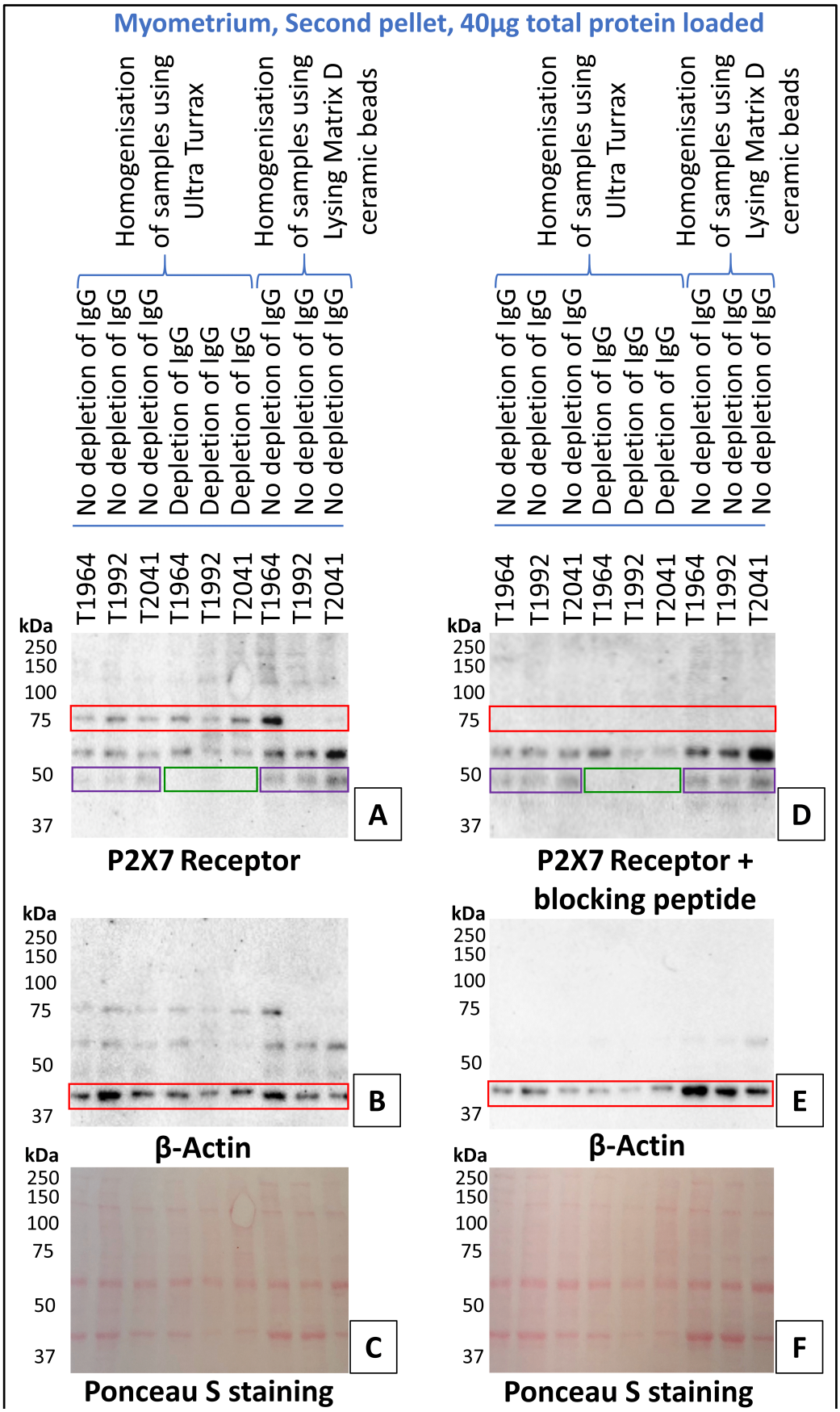


Figure 39. *This figure shows the P2X7 receptor protein expression levels (panel **A**, red box) in the second pellet fraction of myometrium tissue lysates originating from*

three placental samples of healthy patients (T1964, T1992 and T2041). The tissue samples were homogenised using either the ultra turrax method or using lysing matrix D ceramic spheres. The tissue lysates were either IgG immunodepleted using a well-established immunoprecipitation protocol involving anti-human IgG (whole molecule)-agarose antibody developed in goat (Sigma, A3543) as illustrated in panel A (green box) or not IgG immunodepleted (panel A, violet boxes). Each well was loaded with 40µg of total protein. Myometrium was used as a positive control for the P2X7 receptor ***B****. The immunoblot was stripped and then reblotted with β actin for loading control (red box)* ***C****. Ponceau S staining of the nitrocellulose membrane prior to immunoblotting for the P2X7 receptor* ***D****. Immunoblot highlighting that the bands corresponding to the molecular weight of native P2X7 receptor (red box) disappeared after pre-adsorption of the P2X7 primary antibody with a blocking peptide equivalent to the amino acid residues 576-595 of the intracellular C-terminus of the P2X7 receptor (negative control). The green box highlights the absence of the 49kDa band in tissue lysates which have been immunodepleted of IgG and the violet boxes denote the presence of the 49kDa band in tissue lysates which have not been immunodepleted of IgG* ***E****. The immunoblot presented in panel D was stripped and then reblotted with β actin for loading control (red box)* ***F****. Ponceau S staining of nitrocellulose membrane prior to immunoblotting for the P2X7 receptor with blocking peptide. Antibodies used: P2X7 primary antibody (Rabbit polyclonal IgG, Alomone Labs, APR-004) at a dilution of 1:600, P2X7 secondary antibody (Polyclonal goat anti rabbit immunoglobulins alkaline phosphatase, Dako, D0487) at a dilution of 1:1000, β actin primary antibody (rabbit polyclonal IgG, Abcam, Ab8227) at a dilution of 1:8000 and β actin secondary antibody (Polyclonal goat anti rabbit immunoglobulins alkaline phosphatase, Dako, D0487) at a dilution of 1:1000.*

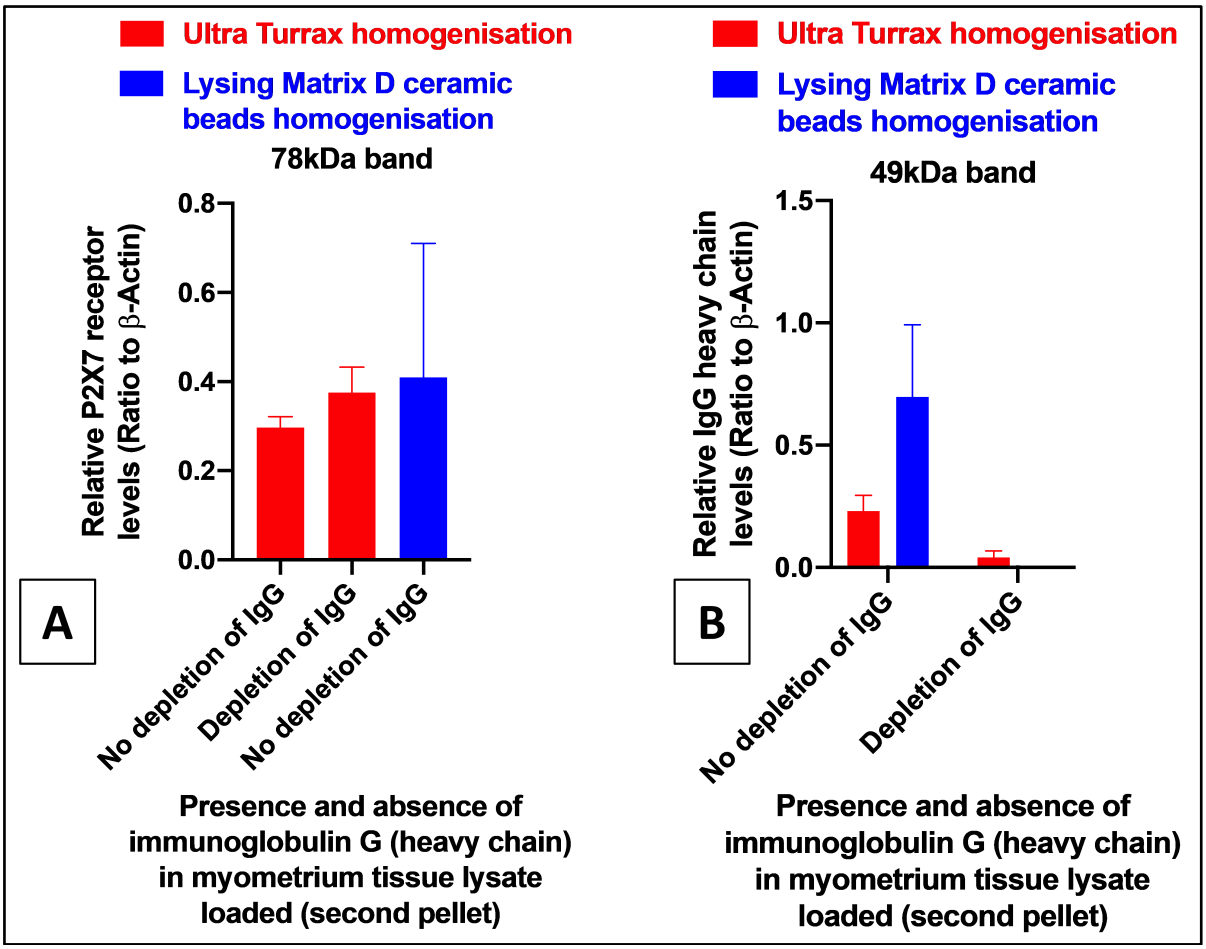


Figure 40. *These graphs highlight the P2X7 receptor protein expression levels (panel **A**) and IgG heavy chain levels (panel **B**) normalised to β actin in myometrium tissue lysates (second pellet fraction) which have been either depleted or non-depleted of immunoglobulin G. The tissue was homogenised using either the ultra turrax method (red bars) or using lysing matrix D ceramic spheres (blue bars). Data are expressed as mean ± SEM.*

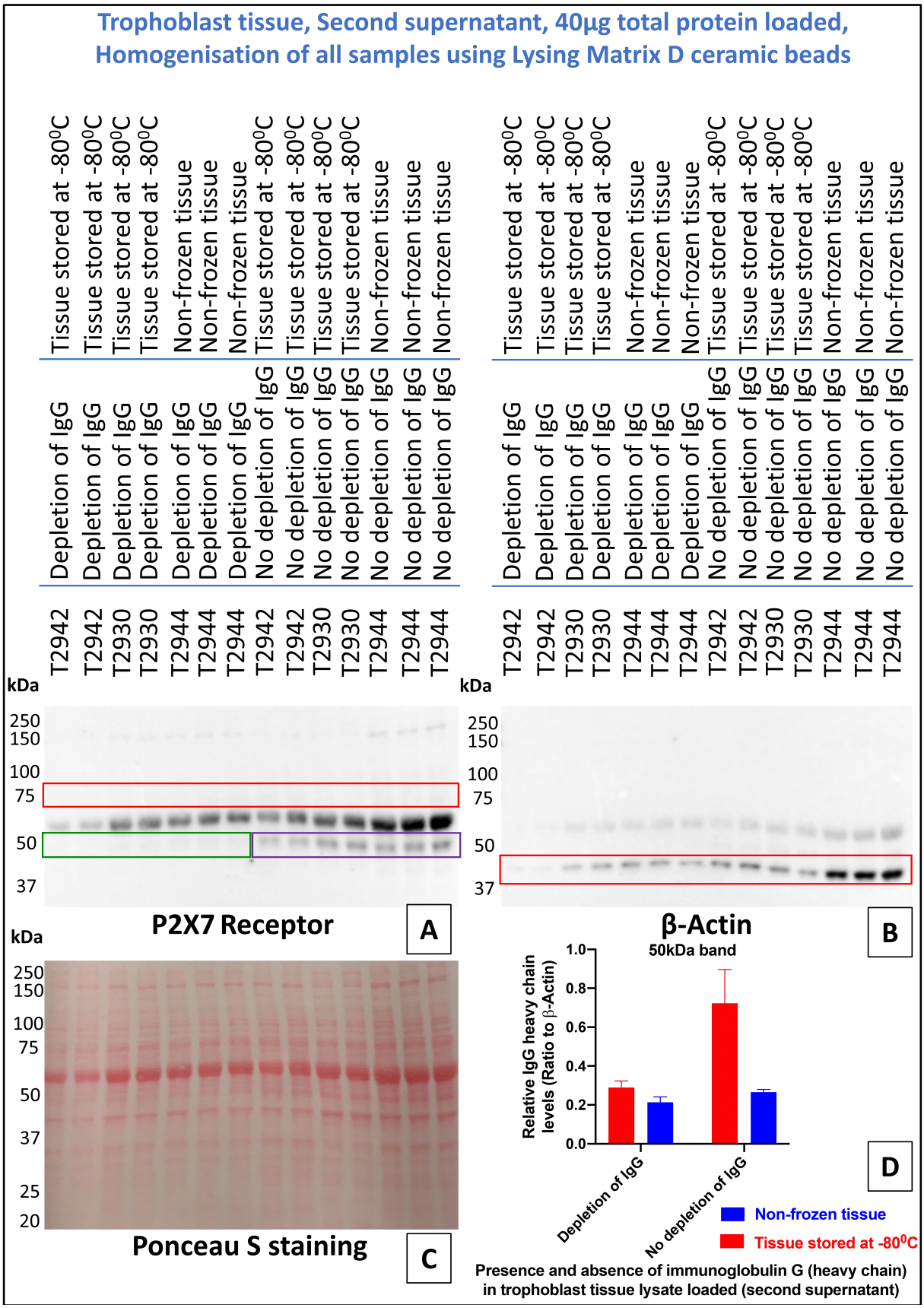


Figure 41. *This figure shows the P2X7 receptor protein expression levels (panel **A**, red box) in the second supernatant of trophoblast tissue lysates originating from three placental samples of healthy patients (T2942, T2930, T2944). In this case, all tissue*

samples were homogenised using lysing matrix D ceramic spheres. The tissue lysates were either IgG immunodepleted using a well-established immunoprecipitation protocol involving anti-human IgG (whole molecule)-agarose antibody developed in goat (Sigma, A3543) as illustrated in panel A (green box) or not IgG immunodepleted (panel A, violet box). Each well was loaded with 40µg of total protein. ***B****. The immunoblot was stripped and then reblotted with β actin for loading control (red box).* ***C****. Ponceau S staining of the nitrocellulose membrane prior to immunoblotting for the P2X7 receptor* ***D****. Graph highlighting the relative IgG heavy chain levels normalised to β actin in trophoblast tissue lysates which have been either depleted or non-depleted of immunoglobulin G. The homogenised trophoblast tissue used in these studies was either non-frozen (blue bars) or snap frozen in liquid nitrogen immediately after collection and stored at -80^{0}C until processed (red bars). Data are expressed as mean ± SEM. Antibodies used: P2X7 primary antibody (Rabbit polyclonal IgG, Alomone Labs, APR-004) at a dilution of 1:600, P2X7 secondary antibody (Polyclonal goat anti rabbit immunoglobulins alkaline phosphatase, Dako, D0487) at a dilution of 1:1000, β actin primary antibody (rabbit polyclonal IgG, Abcam, Ab8227) at a dilution of 1:8000 and β actin secondary antibody (Polyclonal goat anti rabbit immunoglobulins alkaline phosphatase, Dako, D0487) at a dilution of 1:1000.*

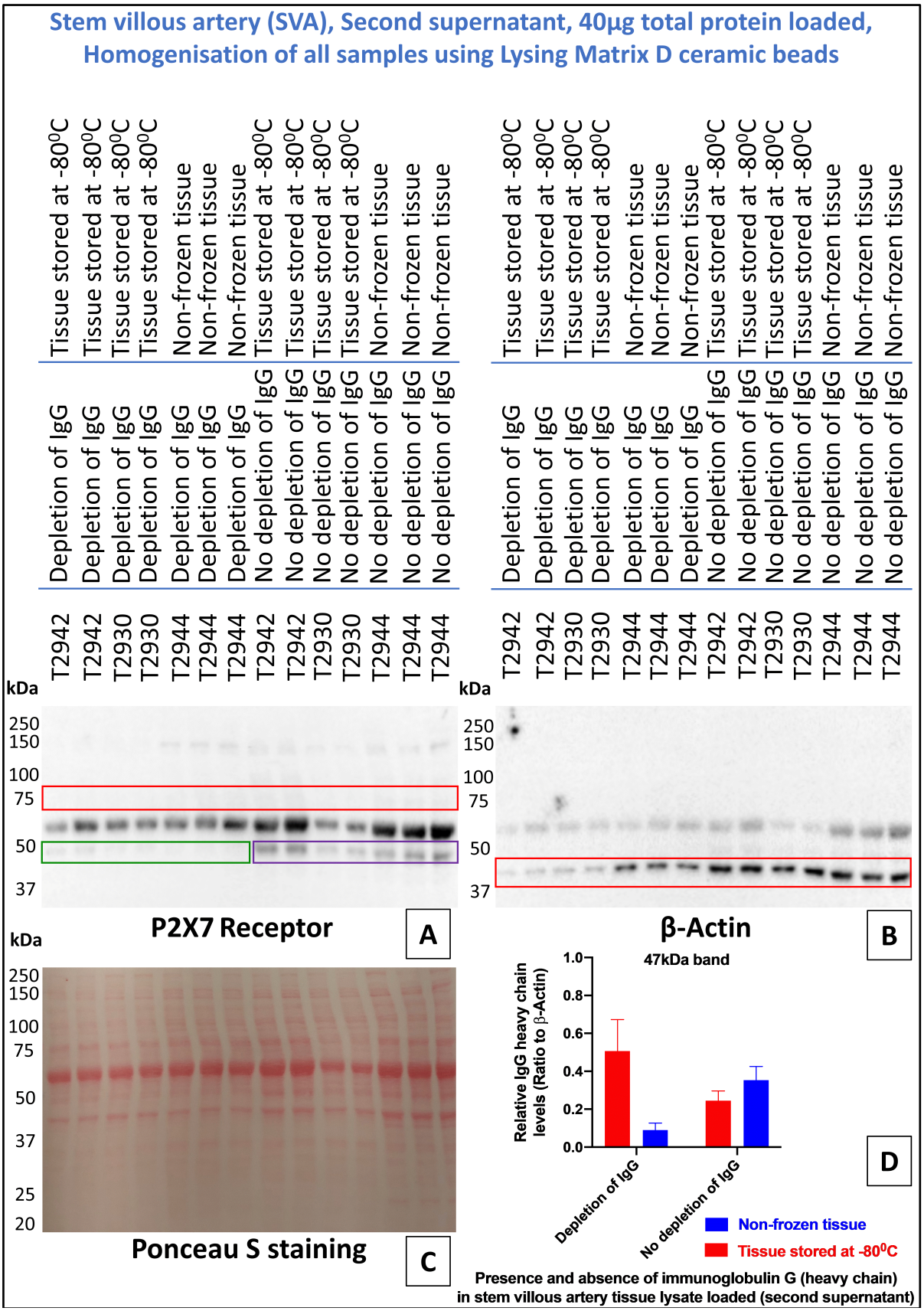


Figure 42. *This figure shows the P2X7 receptor protein expression levels (panel **A**, red box) in the second supernatant fraction of stem villous artery tissue lysates originating from three placental samples of healthy patients (T2942, T2930, T2944).*

In this case, all tissue samples were homogenised using lysing matrix D ceramic spheres. The tissue lysates were either IgG immunodepleted using a well-established immunoprecipitation protocol involving anti-human IgG (whole molecule)-agarose antibody developed in goat (Sigma, A3543) as illustrated in panel A (green box) or not IgG immunodepleted (panel A, violet box). Each well was loaded with 40µg of total protein. ***B****. The immunoblot was stripped and then reblotted with β actin for loading control (red box).* ***C****. Ponceau S staining of the nitrocellulose membrane prior to immunoblotting for the P2X7 receptor* ***D****. Graph highlighting the relative IgG heavy chain levels normalised to β actin in stem villous artery tissue lysates which have been either depleted or non-depleted of immunoglobulin G. The homogenised trophoblast tissue used in these studies was either non-frozen (blue bars) or snap frozen in liquid nitrogen immediately after collection and stored at -80^{0}C until processed (red bars). Data are expressed as mean ± SEM. Antibodies used: P2X7 primary antibody (Rabbit polyclonal IgG, Alomone Labs, APR-004) at a dilution of 1:600, P2X7 secondary antibody (Polyclonal goat anti rabbit immunoglobulins alkaline phosphatase, Dako, D0487) at a dilution of 1:1000, β actin primary antibody (rabbit polyclonal IgG, Abcam, Ab8227) at a dilution of 1:8000 and β actin secondary antibody (Polyclonal goat anti rabbit immunoglobulins alkaline phosphatase, Dako, D0487) at a dilution of 1:1000.*

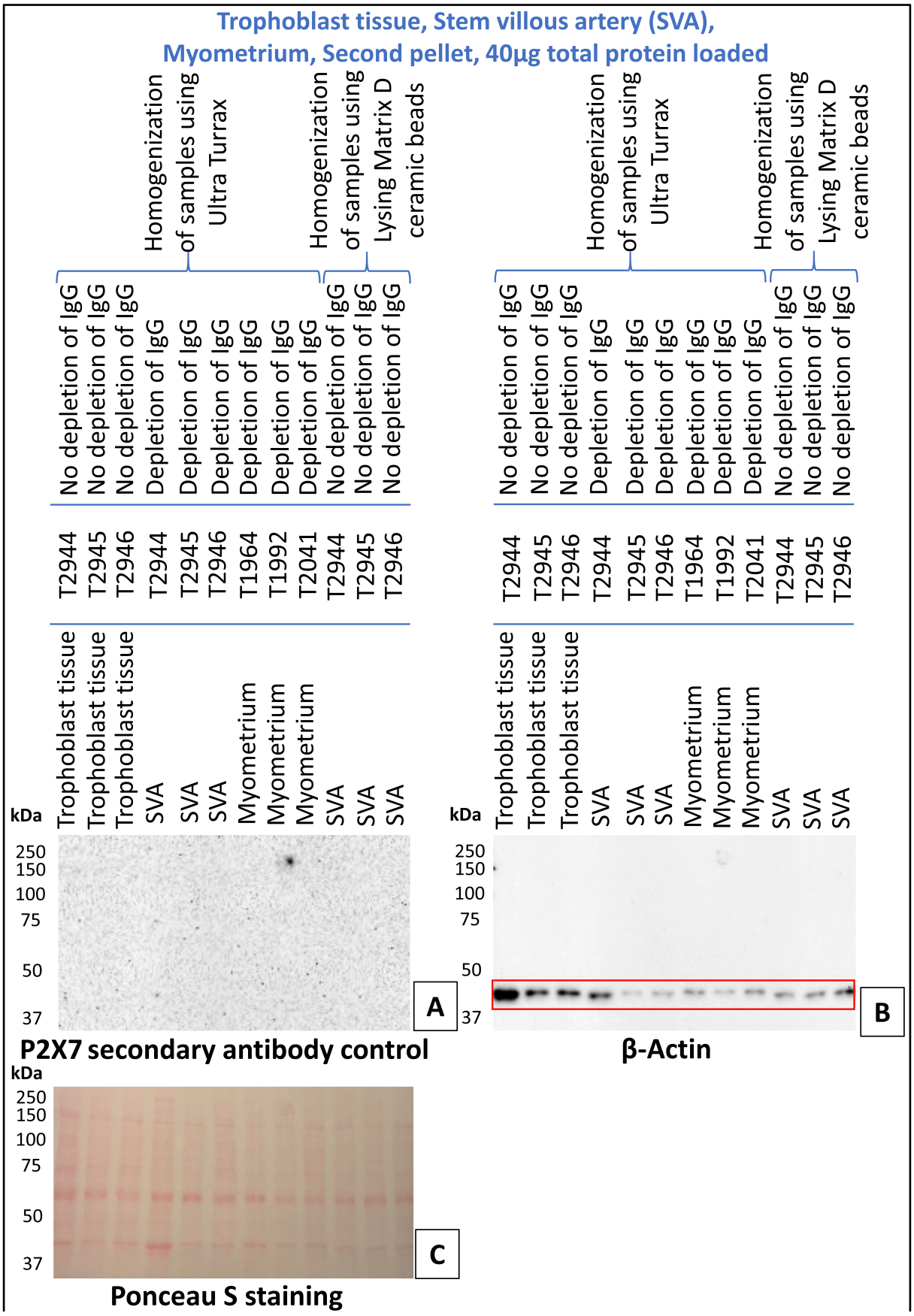


Figure 43. *Immunoblot highlighting the P2X7 receptor secondary antibody control where the primary antibody corresponding to the purinergic receptor has been*

*replaced with 3% (w/v) marvel milk/TBS-T as presented in panel **A**. In this study, the second pellet of trophoblast tissue and SVA was used originating from three placental samples of healthy patients (T2944, T2945, T2946) as well as myometrium tissue originating from three healthy patients (T1964, T1992 and T2041). The tissue samples were homogenised using either the ultra turrax method or using lysing matrix D ceramic spheres. The tissue lysates were either IgG immunodepleted using a well-established immunoprecipitation protocol involving anti-human IgG (whole molecule)-agarose antibody developed in goat (Sigma, A3543) or not IgG immunodepleted **B**. The immunoblot was stripped and then reblotted with β actin for loading control (red box) **C**. Ponceau S staining of the nitrocellulose membrane corresponding to the secondary antibody control. Each well was loaded with 40μg of total protein. Antibodies used: P2X7 secondary antibody (Polyclonal goat anti rabbit immunoglobulins alkaline phosphatase, Dako, D0487) at a dilution of 1:1000, β actin primary antibody (rabbit polyclonal IgG, Abcam, Ab8227) at a dilution of 1:8000 and β actin secondary antibody (Polyclonal goat anti rabbit immunoglobulins alkaline phosphatase, Dako, D0487) at a dilution of 1:1000.*

3.3.3 The NLRP3 inflammasome expression in the second supernatant of fourth order CPA, SVA and choriodecidua tissue lysates highlighted the presence of 4 isoforms at approximately 79kDa, 107kDa, 171kDa and 222kDa

NLRP3 inflammasome products were detected in two western blots at a molecular weight of approximately 118kDa (figure 44, panel A) and circa 107kDa (figure 45, panel A) in the second supernatant of fourth order CPA, SVA and choriodecidua tissue lysates originating from three placental samples of healthy patients. In both western blots, the fourth order CPA possessed the highest relative protein expression levels of the NLRP3 inflammasome compared to SVA and choriodecidua as highlighted in figure 44, panel D and figure 45, panel D. A Shapiro-Wilk test of the relative NLRP3 inflammasome levels presented in figure 44 and figure 45 highlighted that all data was normally distributed. No statistically significant differences of the relative NLRP3 inflammasome protein expression levels (figure 44) were found across all tissue types using a Brown-Forsythe ANOVA test (P=0.4928) and Dunnett's T3 multiple comparisons test. Similarly, the same tests highlighted no statistically significant differences in NLRP3 inflammasome expression levels between all placental tissues studied in the western blot presented in figure 45. In both NLRP3 inflammasome western blots presented in figure 44 and 45, a strong signal was detected at approximately 52kDa (figure 44) and circa 49kDa (figure 45) which was due to the non-specific binding of the NLRP3 inflammasome secondary antibody (anti-rabbit IgG (whole molecule), $F(ab')_2$ fragment - alkaline phosphatase antibody produced in goat, Sigma, A3937) as suggested from the immunoblot presented in figure 46, panel D. Furthermore, a faint band was also detected in the NLRP3

immunoblot illustrated in figure 45 at a molecular weight of circa 58kDa which was also due to the non-specific binding of the same NLRP3 secondary antibody. The ponceau S staining presented in figure 44 (panel C) and figure 45 (panel C) highlight equal protein loading.

A further investigation of the NLRP3 western blot illustrated in figure 45 which involved cutting of the nitrocellulose membrane in two parts (figure 46, panel A) and subjecting again the 75-250kDa strip to chemiluminescent western blot detection for the NLRP3 inflammasome (figure 46, panel B) revealed the presence of 3 isoforms of approximately 79kDa, 107kDa and 222kDa. In this case, the protein expression levels of all three NLRP3 inflammasome isoforms in fourth order CPA, SVA and choriodecidua originating from N=3 placental samples of healthy patients (figure 46, panel C) were subjected to a Shapiro-Wilk test which highlighted that all data was normally distributed with the exception of the 79kDa isoform in the choriodecidua subgroup (*P=0.0307). A Kruskal-Wallis test (*P=0.0162) with Dunn's multiple comparison tests highlighted no statistically significant differences between the fourth order CPA, SVA and choriodecidua tissue types in each of NLRP3 inflammasome isoform subgroups. Here, the 107kDa NLRP3 inflammasome isoform possessed the highest protein expression level in all three placental tissue types studied compared to the 79kDa and 222kDa inflammasome isoforms (figure 46, panel C).

The immunoblot of NLRP3 inflammasome secondary antibody control illustrated in figure 46 (panel D) highlighted the presence of one intense band of an approximate size of 49kDa and a faint band of circa 57kDa in all second supernatants of fourth order CPA, SVA and choriodecidua tissue lysates originating from three placental samples of healthy patients. In this case, the ponceau S staining of the nitrocellulose membrane showed equal protein loading (figure 46, panel E).

The NLRP3 inflammasome protein expression levels in 10-60μg of total protein per well (second supernatant) of fourth order CPA lysate originating from a placenta sample of a healthy patient is presented in two western blots (figure 47 and figure 48). In this case, no protein bands corresponding to the NLRP3 inflammasome were detected in one of the western blots (figure 47). However, a faint signal was identified at approximately 104kDa in the remaining NLRP3 western blot as shown in figure 48 (panel A). An additional analysis of the NLRP3 immunoblot presented in figure 48 which implicated the cutting of nitrocellulose membrane in two segments (figure 48, panel E) and subjecting again the 100-250kDa part to chemiluminescent detection for the relative NLRP3 inflammasome protein expression levels showed the presence of two isoforms of approximately 104kDa and 171kDa (figure 48, panel F). The relative NLRP3 inflammasome protein expression levels in 10-60μg of total protein per well of fourth order CPA lysate are illustrated in figure 48, panels D and G. A faint signal was observed in the NLRP3 inflammasome western blot presented in figure 47 (panel A) possessing a molecular weight of approximately 50kDa which was due to the non-specific binding of the NLRP3 inflammasome secondary antibody (anti-rabbit IgG (whole molecule), $F(ab')_2$ fragment - alkaline phosphatase antibody produced in goat, Sigma, A3937) as indicated from the immunoblot presented in figure 46, panel D. Similarly, a strong signal was detected in the NLRP3 immunoblot presented in figure 48 (panel A) at approximately 49kDa, accompanied by a smaller, less intense band observed at circa 45kDa which was also due to the non-specific binding of another NLRP3 inflammasome secondary antibody (Polyclonal goat anti rabbit immunoglobulins alkaline phosphatase, Dako, D0487) as shown from the western blot illustrated in figure 50, panel A. Furthermore, the densitometric analyses of β-Actin protein expression levels illustrated in figure 47 (panel E) and figure 49 (panel A) show

the linear range of sample loading corresponding to the standard curve elicited using the fourth order CPA tissue lysates. In this case, the optimal amount of total protein load for the purposes of semi-quantifying β-Actin (loading control) levels falling within the linear range was between 20-40μg per well (figure 47, panel E and figure 49, panel A). Similarly, the densitometric analyses of the NLRP3 inflammasome protein expression levels are also presented in figure 49 (panel B) for both 104kDa and 171kDa isoforms. In this case, the optimal amount of total protein load for the purposes of NLRP3 inflammasome semi-quantification was determined at 20-40μg per well (figure 49, panel B). In this case, the ponceau S staining presented in figure 47 (panel C and D) and figure 48 (panel C) showed a successful transfer of the resolved proteins from the 10% polyacrylamide gels to the nitrocellulose membranes.

The immunoblot highlighting the NLRP3 inflammasome secondary antibody control presented in figure 50 showed the presence of 2 faint bands of an approximate size of 43kDa and 51kDa in all second supernatants of fourth order CPA, SVA and choriodecidua tissue lysates originating from two placental samples of healthy patients. The ponceau S staining of the nitrocellulose membrane showed equal protein loading (figure 50, panel C).

As a result, in the second supernatant (containing the cytoplasmic fraction) of fourth order CPA, SVA and choriodecidua tissue lysates, four NLRP3 inflammasome isoforms have been detected at the molecular weight of approximately 79kDa, 107kDa, 171kDa and 222kDa.

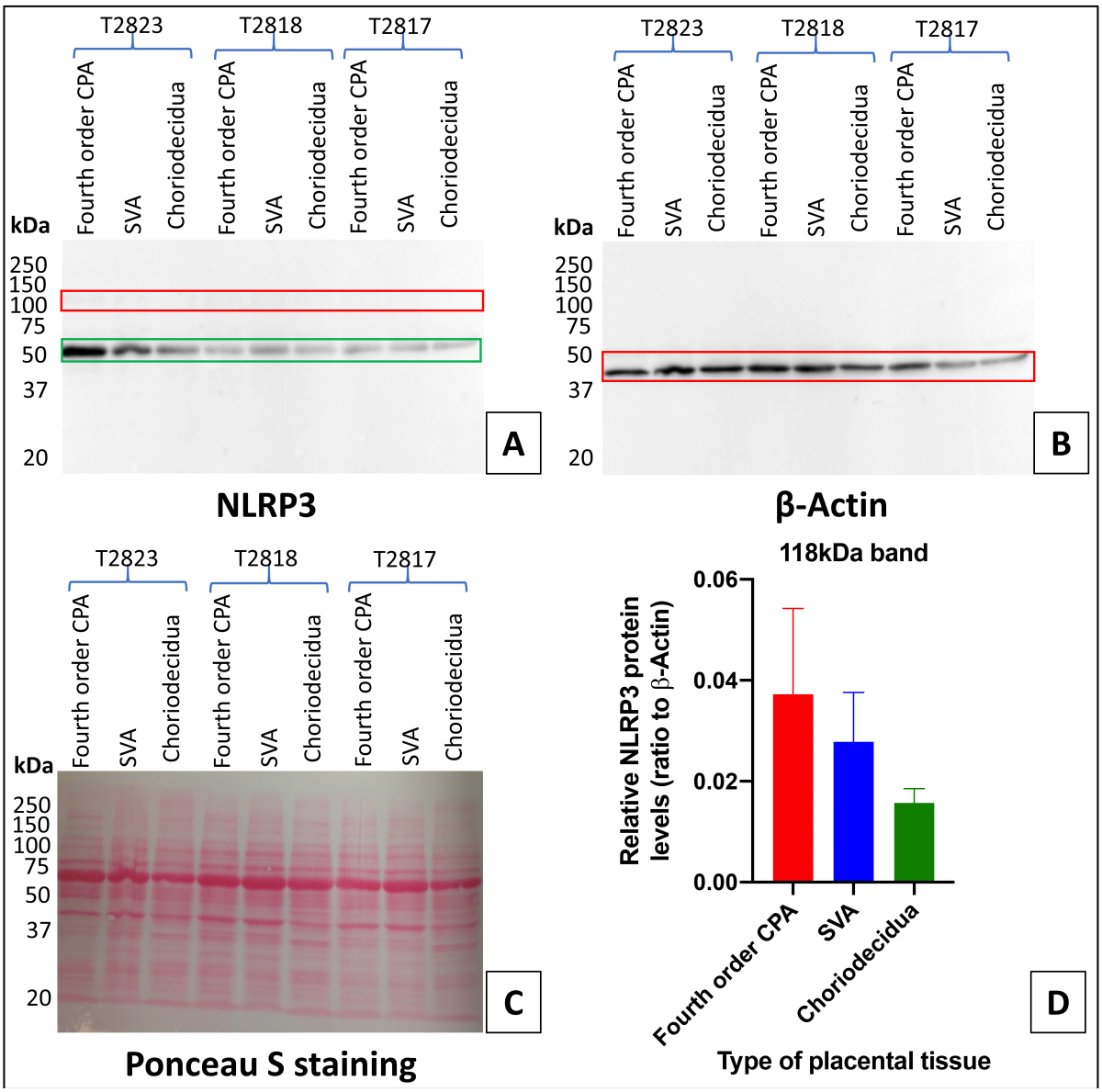


Figure 44. *This figure shows the NLRP3 inflammasome protein expression levels (panel **A**, red box) in the second supernatant of fourth order CPA, SVA and choriodecidua tissue lysates originating from three placental samples of healthy patients (T2823, T2818 and T2817). The protein bands highlighted with the green (52kDa) box correspond to non-specific binding of the NLRP3 inflammasome secondary antibody **B**. The immunoblot was stripped and then reblotted with β actin for loading control (red box) **C**. Ponceau S staining of the nitrocellulose membrane prior to the commencement of immunoblotting for the NLRP3 inflammasome **D**. Relative NLRP3 inflammasome protein expression levels (118kDa isoform) normalised to β actin. Data are expressed as mean ± SEM. Each well was loaded with 40μg of total protein. Antibodies used: NLRP3 primary antibody (rabbit polyclonal IgG, Abcam, Ab91413) at a dilution of 1:300, NLRP3 secondary antibody (anti-rabbit IgG (whole molecule), F(ab')$_2$ fragment - alkaline phosphatase antibody produced in goat, Sigma, A3937) at a dilution of 1:30000, β actin primary antibody (rabbit polyclonal IgG, Abcam, Ab8227) at a dilution of 1:2500 and β actin secondary antibody (Anti-rabbit IgG (whole molecule), F(ab')$_2$, fragment – alkaline phosphatase antibody produced in goat – Sigma, A3937) at a dilution of 1:30000.*

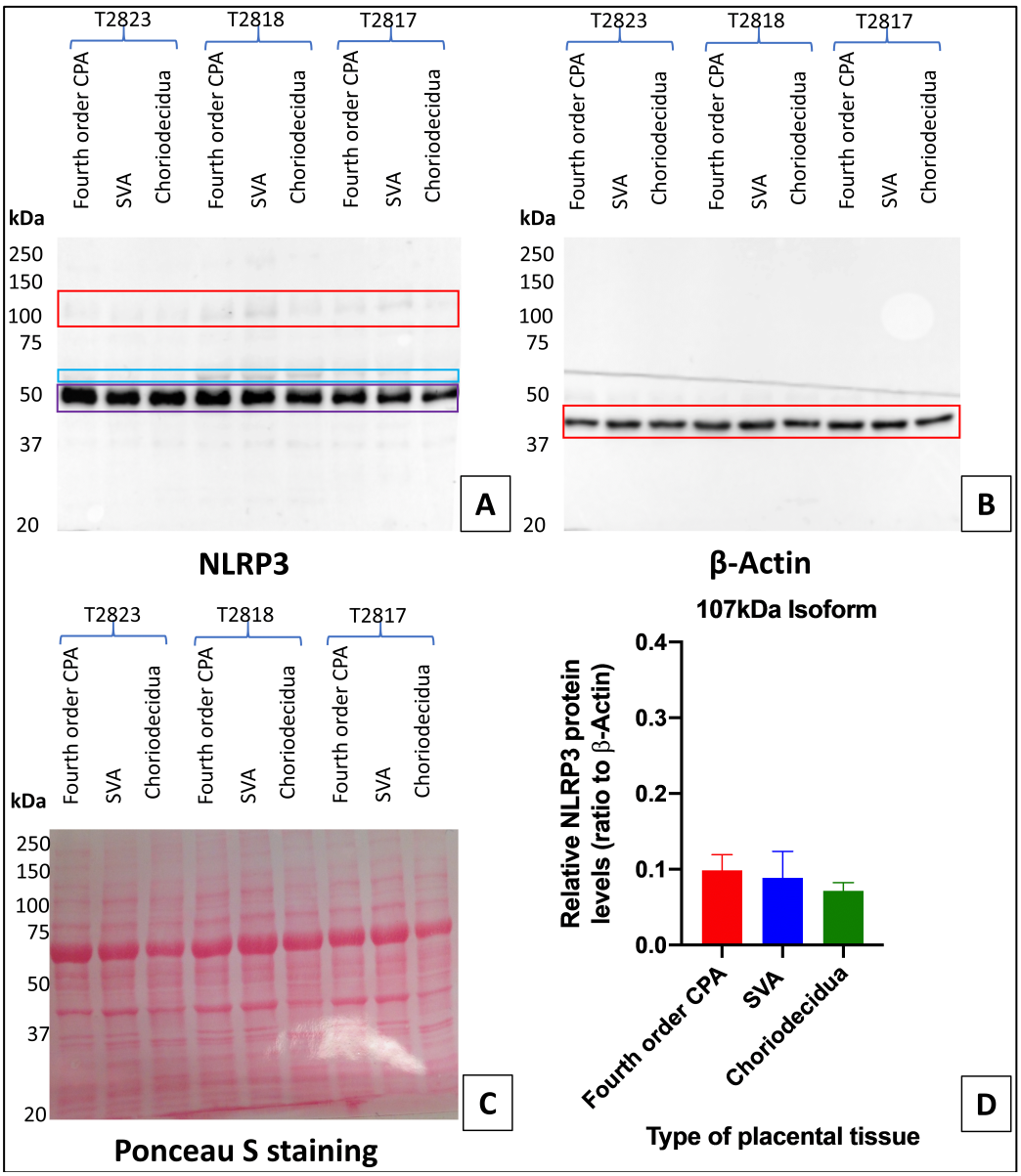


Figure 45. *This figure shows the NLRP3 inflammasome protein expression levels (panel **A**, red box) from a repeated western blotting experiment using the second supernatant of fourth order CPA, SVA and choriodecidua tissue lysates originating from three placental samples of healthy patients (T2823, T2818 and T2817). The protein bands highlighted with blue (58kDa) and violet (49kDa) boxes denote non-specific binding of the NLRP3 secondary antibody **B**. The immunoblot was stripped and then reblotted with β actin for loading control (red box) **C**. Ponceau S staining of the nitrocellulose membrane prior to immunoblotting for the NLRP3 inflammasome **D**. Relative NLRP3 inflammasome protein expression levels (107kDa isoform) normalised to β actin. Data are expressed as mean ± SEM. Each well was loaded with 40μg of total protein. Antibodies used: NLRP3 primary antibody (rabbit polyclonal IgG, Abcam, Ab91413) at a dilution of 1:300, NLRP3 secondary antibody (anti-rabbit IgG (whole molecule), F(ab')$_2$ fragment - alkaline phosphatase antibody produced in goat, Sigma, A3937) at a dilution of 1:30000, β actin primary antibody (rabbit polyclonal IgG, Abcam, Ab8227) at a dilution of 1:2500 and β actin secondary antibody (Anti-rabbit IgG (whole molecule), F(ab')$_2$, fragment – alkaline phosphatase antibody produced in goat – Sigma, A3937) at a dilution of 1:30000.*

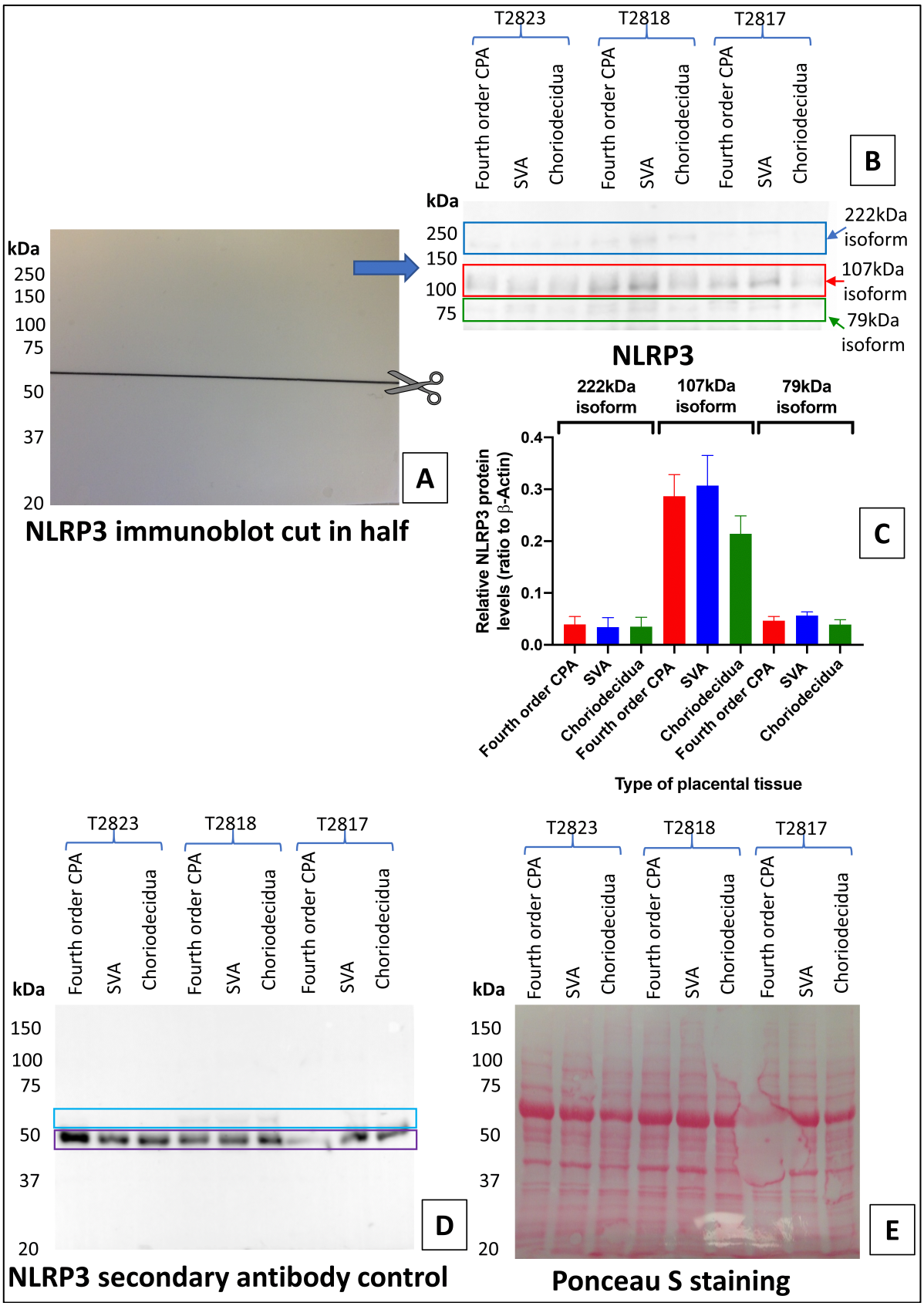


***Figure 46**. This figure shows the NLRP3 inflammasome protein expression levels in the second supernatant of fourth order CPA, SVA and choriodecidua tissue lysates originating from three placental samples of healthy patients (T2823, T2818 and*

*T2817) where the NLRP3 inflammasome immunoblot presented in figure 45 was cut in half (panel **A**) and the 75-250kDa strip was further subjected to chemiluminescent western blot detection of other NLRP3 inflammasome isoforms as presented in panel **B**. The proteins highlighted with blue (approximately 222kDa), red (circa 107kDa) and green (about 79kDa) boxes suggest three NLRP3 inflammasome isoforms that have been detected **C**. Relative NLRP3 inflammasome protein expression levels (222kDa, 107kDa and 79kDa isoforms) normalised to β actin. Data are expressed as mean ± SEM **D**. Immunoblot highlighting the NLRP3 inflammasome secondary antibody control where the primary antibody corresponding to the multimeric protein has been replaced with 3% marvel milk/TBS-T. The protein bands highlighted with blue (approximately 57kDa) and violet (circa 49kDa) boxes denote non-specific binding of the secondary antibody **E**. Ponceau S staining of the nitrocellulose membrane corresponding to the NLRP3 inflammasome secondary antibody control. Each well was loaded with 40µg of total protein. The artifacts present on the Ponceau S staining of the nitrocellulose membrane and on the immunoblot corresponding to the NLRP3 inflammasome secondary antibody control are due to air bubbles present between the polyacrylamide gel and the nitrocellulose membrane. Antibodies used: NLRP3 primary antibody (rabbit polyclonal IgG, Abcam, Ab91413) at a dilution of 1:300, NLRP3 secondary antibody (anti-rabbit IgG (whole molecule), F(ab')$_2$ fragment - alkaline phosphatase antibody produced in goat, Sigma, A3937) at a dilution of 1:30000, β actin primary antibody (rabbit polyclonal IgG, Abcam, Ab8227) at a dilution of 1:2500 and β actin secondary antibody (Anti-rabbit IgG (whole molecule), F(ab')$_2$, fragment – alkaline phosphatase antibody produced in goat – Sigma, A3937) at a dilution of 1:30000.*

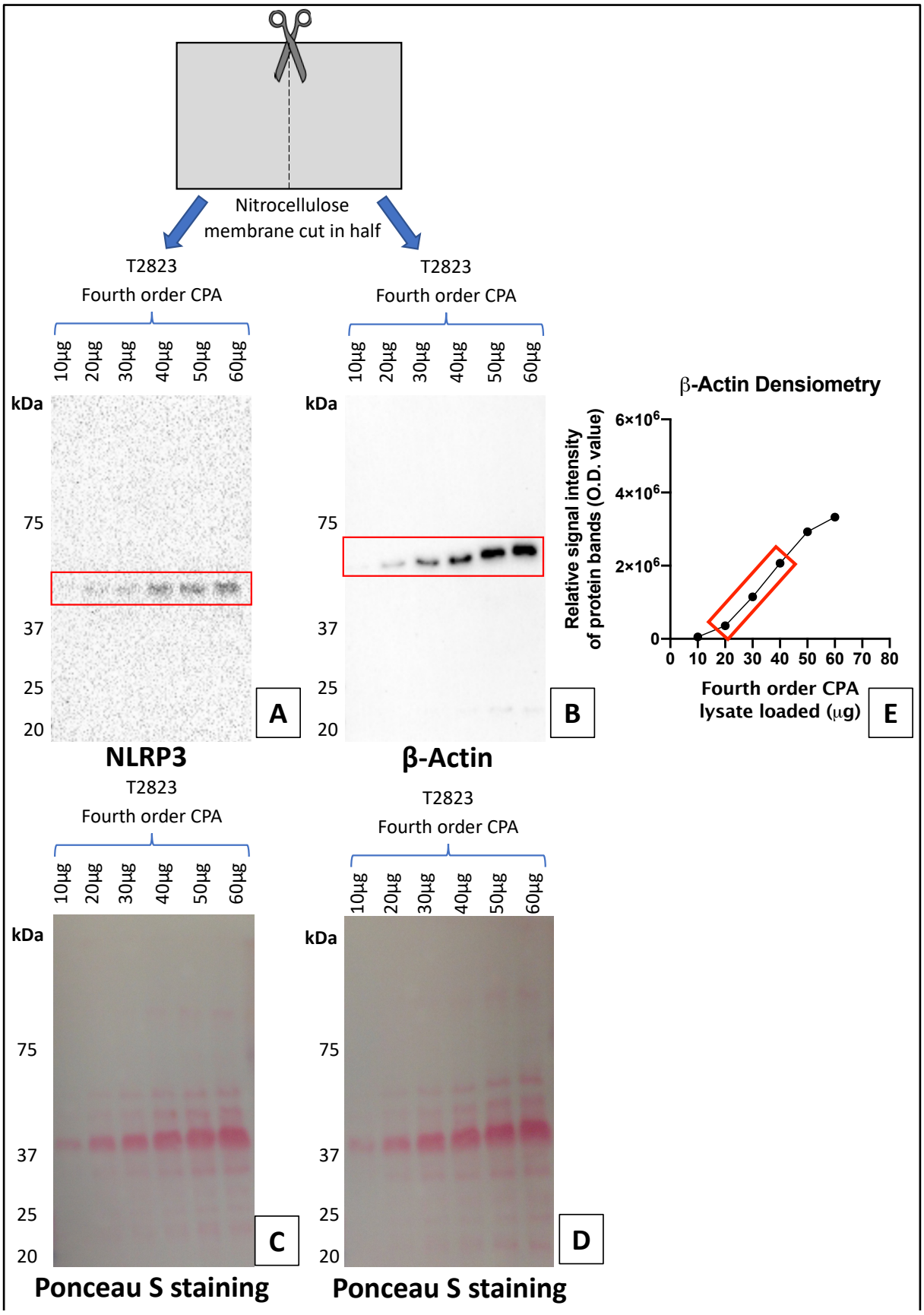


Figure 47. *This figure shows the NLRP3 inflammasome protein expression levels in second supernatant of fourth order CPA lysate originating from a placenta sample of*

a healthy patient (T2823) ***A****. Western blot of chorionic plate artery homogenate with 10-60µg of total protein loaded per well probing for the NLRP3 inflammasome protein expression levels. The protein bands highlighted with the red box (50kDa) denote non-specific binding of the NLRP3 inflammasome secondary antibody* ***B****. Adjacent western blot of CPA homogenate with 10-60µg of total protein loaded per well probing for β actin (red box)* ***C****. Ponceau S staining of the nitrocellulose membrane prior to immunoblotting for the NLRP3 inflammasome* ***D****. Ponceau S staining of adjacent nitrocellulose membrane prior to immunoblotting for β actin* ***E****. Graph highlighting the relative signal intensity of β actin protein bands using total protein (10-60µg per well) originating from the second supernatant of the CPA lysate. Red box highlights the optimal load (20-40µg total protein per well) for loading control protein detection. Antibodies used: NLRP3 primary antibody (rabbit polyclonal IgG, Abcam, Ab91413) at a dilution of 1:300, NLRP3 secondary antibody (anti-rabbit IgG (whole molecule), F(ab')$_2$ fragment - alkaline phosphatase antibody produced in goat, Sigma, A3937) at a dilution of 1:30000, β actin primary antibody (rabbit polyclonal IgG, Abcam, Ab8227) at a dilution of 1:2500 and β actin secondary antibody (Anti-rabbit IgG (whole molecule), F(ab')$_2$, fragment – alkaline phosphatase antibody produced in goat – Sigma, A3937) at a dilution of 1:30000. O.D. denotes optical density. In this case, the resolved proteins were transferred to the nitrocellulose membrane for a period of 90 minutes.*

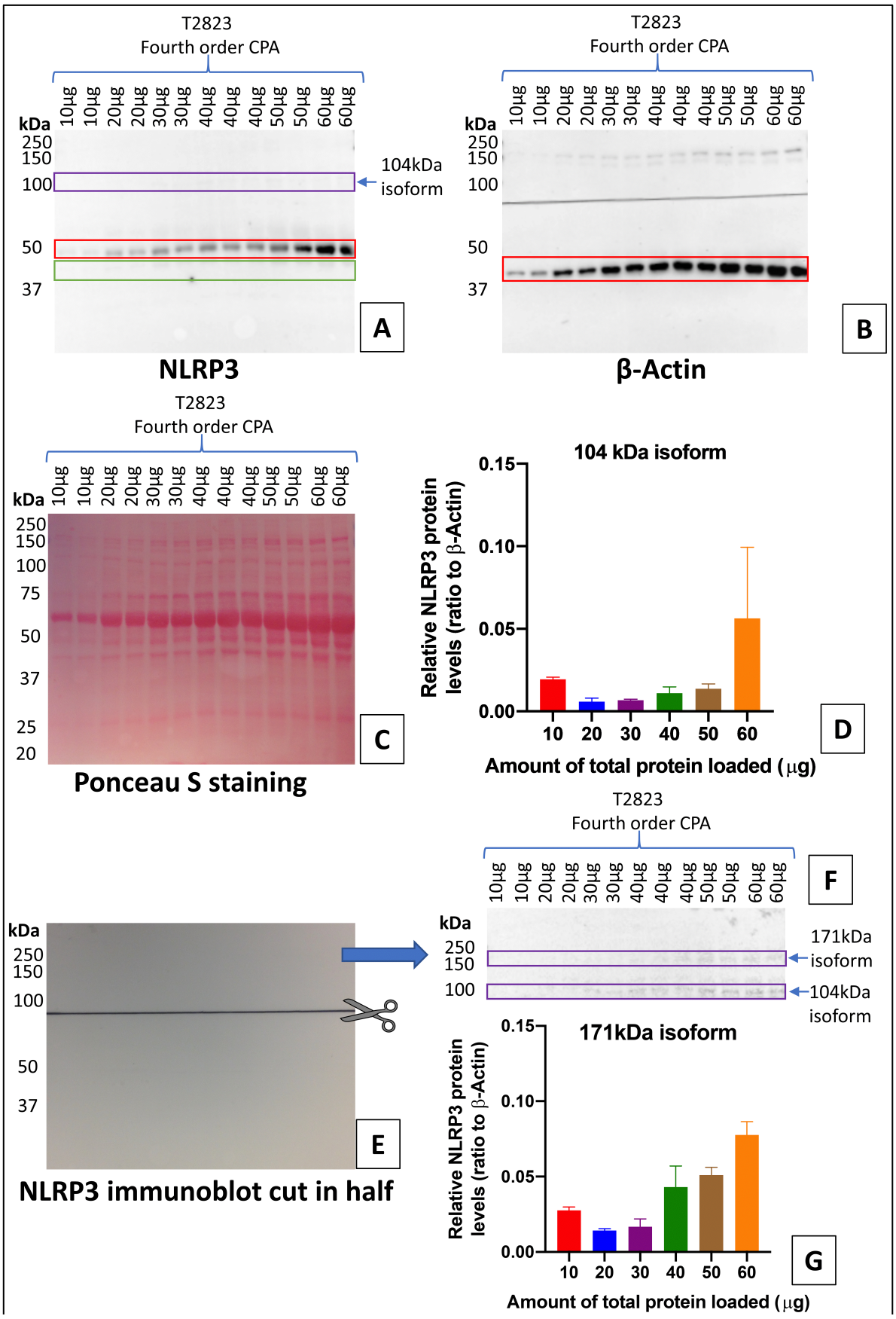


Figure 48. *This figure highlights the NLRP3 inflammasome protein expression levels (panel **A**, violet box, approximately 104kDa isoform) in the second supernatant of*

fourth order CPA originating from a placenta sample of a healthy patient (T2823). The protein bands highlighted with the red (approximately 49kDa) and green (circa 45kDa) boxes denote the non-specific binding of the NLRP3 inflammasome secondary antibody. In this case, the total protein loaded ranged from 10-60µg per well ***B****. The immunoblot was stripped and then reblotted with β actin for loading control (red box)* ***C****. Ponceau S staining of the nitrocellulose membrane prior to immunoblotting for the NLRP3 inflammasome* ***D****. Relative NLRP3 inflammasome protein expression levels (approximately 104kDa isoform) normalised to β actin. Data are expressed as mean ± SEM* ***E****. The NLRP3 inflammasome immunoblot presented in panel A was then cut in half and the 100-250kDa strip was further subjected to chemiluminescent western blot detection for the NLRP3 inflammasome isoforms as presented in panel* ***F.*** *The proteins highlighted with violet boxes (approximately 171kDa and circa 104kDa) suggest two NLRP3 inflammasome isoforms have been detected* ***G****. Relative NLRP3 inflammasome levels (approximately 171kDa isoform) normalised to β actin. Data are expressed as mean ± SEM. Antibodies used: NLRP3 primary antibody (rabbit polyclonal IgG, Abcam, Ab91413) at a dilution of 1:200, NLRP3 secondary antibody (Polyclonal goat anti rabbit immunoglobulins alkaline phosphatase, Dako, D0487) at a dilution of 1:1000, β actin primary antibody (rabbit polyclonal IgG, Abcam, Ab8227) at a dilution of 1:2500 and β actin secondary antibody (Polyclonal goat anti rabbit immunoglobulins alkaline phosphatase, Dako, D0487) at a dilution of 1:1000. In this case, the resolved proteins were transferred to the nitrocellulose membrane for a period of 90 minutes.*

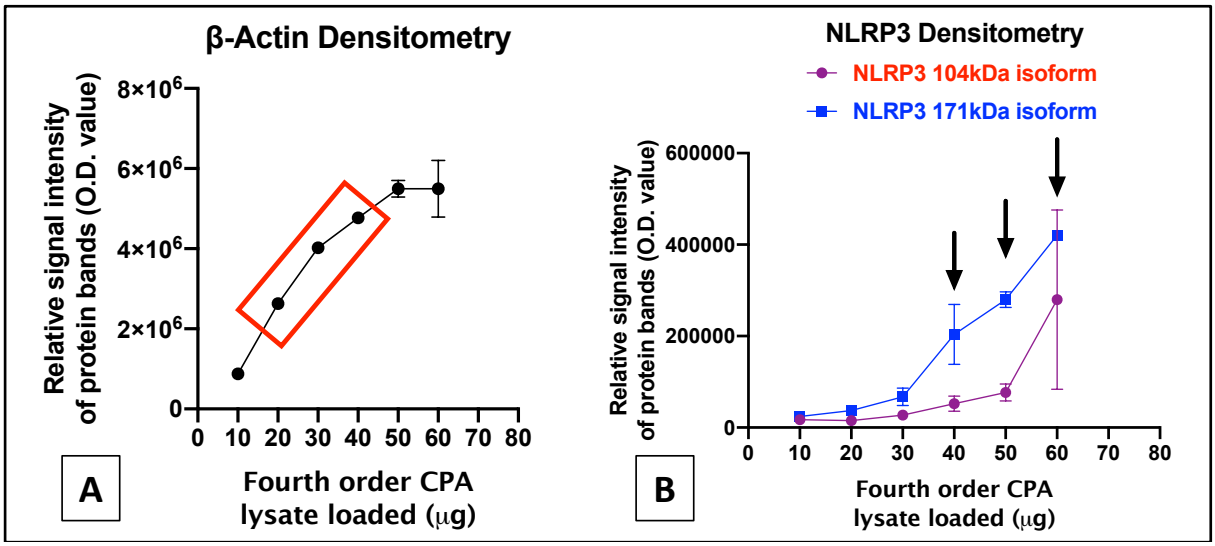


Figure 49. *Densitometry analyses of β actin and NLRP3 inflammasome optical density values corresponding to the nitrocellulose membrane presented in figure 48* ***A****. Graph highlighting the relative signal intensity of β actin protein bands using total protein (10-60µg per well) originating from the second supernatant of the CPA lysate. Red box highlights the optimal load (20-40µg total protein per well) for loading control protein detection* ***B****. Graph showing the relative signal intensity of NLRP3 inflammasome protein bands (approximately 104kDa and circa 171kDa isoforms) using a total protein amount between 10-60µg. Black arrows show the optimal load (40-60µg total protein per well) for NLRP3 inflammasome detection. Data are expressed as mean ± SEM. O.D. denotes optical density.*

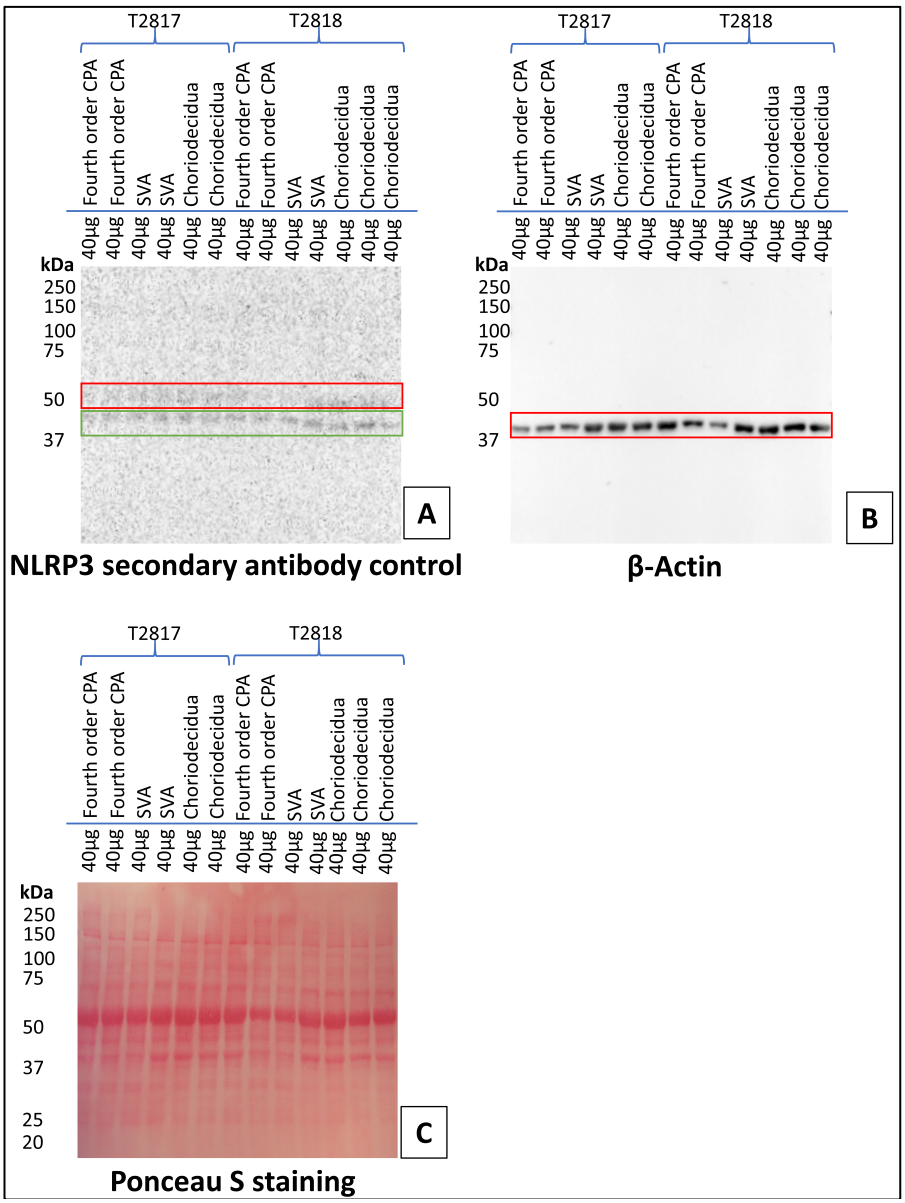


Figure 50. *This figure highlights the western blot of NLRP3 inflammasome secondary antibody control where the primary antibody corresponding to the NLRP3 inflammasome has been replaced with 3% (w/v) marvel milk/TBS-T (panel **A**). In this study, the second supernatant of fourth order CPA, SVA and choriodecidua was used originating from two placental samples of healthy patients (T2817 and T2818). Each well was loaded with 40µg of total protein. The protein bands highlighted with red (approximately 51kDa) and green (circa 43kDa) boxes denote non-specific binding of the NLRP3 inflammasome secondary antibody **B**. The immunoblot was stripped and then reblotted with β actin for loading control (red box) **C**. Ponceau S staining of the nitrocellulose membrane corresponding to the NLRP3 inflammasome secondary antibody control. Each well was loaded with 40µg of total protein. Antibodies used: NLRP3 secondary antibody (Polyclonal goat anti rabbit immunoglobulins alkaline phosphatase, Dako, D0487) at a dilution of 1:1000, β actin primary antibody (rabbit polyclonal IgG, Abcam, Ab8227) at a dilution of 1:2500 and β actin secondary antibody (Polyclonal goat anti rabbit immunoglobulins alkaline phosphatase, Dako, D0487) at a dilution of 1:1000. In this case, the resolved proteins were transferred to the nitrocellulose membrane for a period of 90 minutes.*

3.3.4 Stimulated human trophoblast tissue with ATP, LPS+ATP and LPS+BzATP does not significantly alter the relative protein expression levels of three NLRP3 inflammasome isoforms

The relative protein expression levels of three (approximately 78kDa, circa 92kDa and about 131kDa) NLRP3 inflammasome isoforms in stimulated trophoblast tissue with 10mM ATP, 10μg/mL LPS+10mM ATP and 10μg/mL LPS+300μM BzATP originating from 3 healthy placental samples are presented in figure 51. The trophoblast tissue stimulation with ATP, LPS+ATP and LPS+BzATP did not significantly alter the relative protein expression levels of each of the approximately circa 78kDa (blue box), about 92kDa (green box) and approximately 131kDa (brown box) NLRP3 inflammasome isoforms (Dunnett's T3 multiple comparison tests) relative to control (RPMI 1640 media low glucose supplemented with antibiotics) as highlighted in figure 51 (panels D and E). In this case, the NLRP3 inflammasome immunoblot showed the presence of intense bands at approximately 78kDa in each of the stimulated and unstimulated trophoblast tissue lysates (second supernatant fraction) as highlighted by the blue box in figure 51 (panel A). The ponceau S staining of all immunoblots presented in figure 51 showed equal protein loading.

As a result, the stimulation of human placental villous tissue with ATP, LPS+ATP or LPS+BzATP does not significantly alter the NLRP3 inflammasome protein expression levels of the identified 78kDa, 92kDa or 131kDa isoforms found in the second supernatant fraction (containing the cytoplasmic fraction) of the placental tissue lysates.

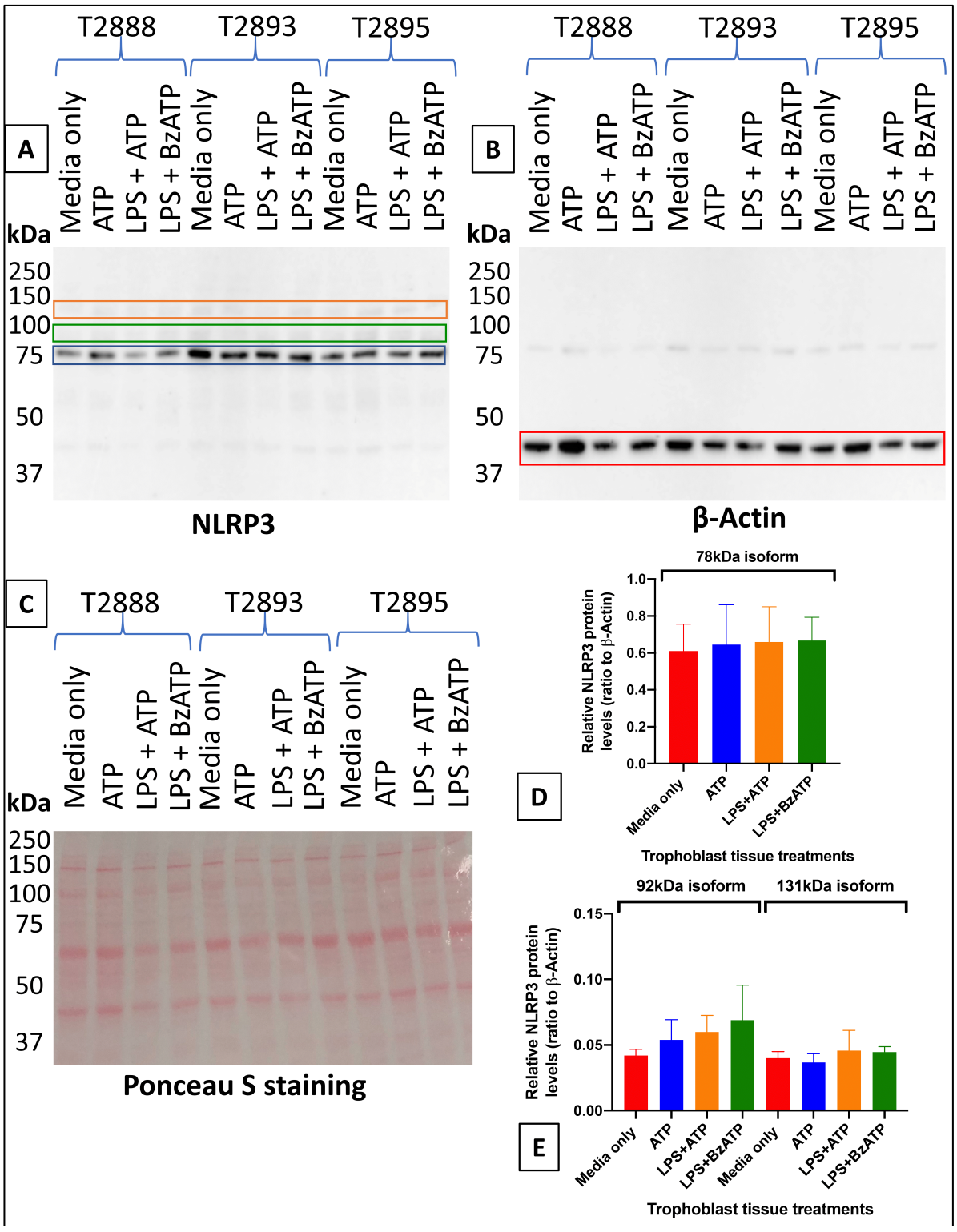


Figure 51. *This figure shows the NLRP3 inflammasome protein expression levels (panel **A**, approximately 131kDa isoform- brown box, circa 92kDa isoform- green box and about 78kDa isoform- blue box) in the second supernatant fraction of trophoblast tissue lysates originating from three placental samples of healthy patients (T2888, T2893 and T2895). The trophoblast tissue was stimulated as follows: RPMI 1640 media+100 units/mL penicillin and 100µg/mL streptomycin for 4 hours, ATP (10mM) for 4 hours, LPS (10µg/mL) (3.5 hours) +ATP (10mM) (0.5 hours) and LPS (10µg/mL) (3.5 hours) +BzATP (300µM) (0.5 hours). Following stimulation, the trophoblast tissue*

was immediately snap frozen in liquid nitrogen and stored at -80^{0}C until processed. In this case, all tissue samples were homogenised using lysing matrix D ceramic spheres and all tissue lysates were IgG immunodepleted using a well-established immunoprecipitation protocol involving anti-human IgG (whole molecule)-agarose antibody developed in goat (Sigma, A3543). The proteins were resolved using a 10% hand casted polyacrylamide gel. The resolved proteins were transferred to the nitrocellulose membrane for a period of 90 minutes. Each well was loaded with 60µg of total protein ***B****. The immunoblot was stripped and then reblotted with β actin for loading control (red box)* ***C****. Ponceau S staining of the nitrocellulose membrane prior to immunoblotting for the NLRP3 inflammasome* ***D****. Graph highlighting the relative NLRP3 inflammasome protein expression levels normalised to β actin (approximately 78kDa isoform) in trophoblast tissue lysates which have been stimulated with PAMP's (LPS), DAMP's (ATP) and the selective P2X receptor agonist (BzATP)* ***E****. Graph showing the relative NLRP3 inflammasome protein expression levels normalised to β actin (circa 92kDa and about 131kDa isoforms) in stimulated trophoblast tissue lysates. Data are expressed as mean ± SEM. Antibodies used: NLRP3 primary antibody (rabbit polyclonal IgG, Abcam, Ab91413) at a dilution of 1:200, NLRP3 secondary antibody (Polyclonal goat anti rabbit immunoglobulins alkaline phosphatase, Dako, D0487) at a dilution of 1:1000, β actin primary antibody (rabbit polyclonal IgG, Abcam, Ab8227) at a dilution of 1:8000 and β actin secondary antibody (Polyclonal goat anti rabbit immunoglobulins alkaline phosphatase, Dako, D0487) at a dilution of 1:1000. LPS denotes lipopolysaccharide, ATP indicates adenosine 5'-triphosphate and BzATP stands for* 2′(3′)-O-(4-Benzoylbenzoyl) adenosine 5′-triphosphate.

3.3.5 D-glucose stimulation of trophoblast tissue for 4, 24 and 48 hours does not significantly alter the relative P2X7 receptor protein expression levels

The relative P2X7 receptor protein expression levels in the second pellet fraction of trophoblast tissue (N=3 healthy placental samples) which was stimulated with RPMI 1640 media supplemented with antibiotics and either 0, 5.5, 10, 20 or 30mM D-glucose for 4 or 48 hours are presented in figures 52-54. A strong signal was observed at approximately 78kDa in all three P2X7 receptor immunoblots as illustrated by the blue box in figures 52-54. An intense band was also detected at circa 78kDa in the second pellet fraction of myometrium tissue lysate which was used as a positive control for the P2X7 receptor. All D-glucose stimulations (0, 5.5, 10, 20 or 30mM) of trophoblast tissue for 4 or 48 hours did not significantly change the relative P2X7

receptor protein expression levels compared to control (0 hours) as highlighted in figure 55. Similarly, the relative P2X7 receptor protein expression levels in trophoblast tissue (second pellet fraction) stimulated with RPMI 1640 media supplemented with 100U/mL penicillin, 100µg/mL streptomycin, 10% (v/v) FBS and either 0, 5.5 or 30mM D-glucose for 4 or 24 hours originating from three healthy placental samples are presented in figures 58-60. An intense band was detected at circa 76kDa in all three P2X7 receptor western blots as indicated by the blue box in figures 58-60. Positive control (myometrium) also gave a single band at approximately 76kDa. There were no statistically significant differences (Dunn's multiple comparisons test) in the relative P2X7 receptor protein expression levels between 0, 5.5 or 30mM D-glucose treated trophoblast tissue at both 4 or 24 hours relative to control (0 hours) (Figure 61). Ponceau S staining highlighted equal protein loading (figures 52-54 and 58-60).

Released IL-1β levels measured in the culture media of trophoblast tissue which was stimulated with D-glucose (0, 5.5, 10, 20 or 30mM) for 4 hours or 48 hours originating from four healthy placental samples (T2959, T2956, T2957 and T2960) are presented in figure 56 (panel A). Dunn's multiple comparison tests revealed no statistically significant differences in released IL-1β levels between all D-glucose stimulated trophoblast tissue at both 4 or 48 hours. Released IL-1β levels were also measured in the culture media and in the second supernatant fraction of D-glucose stimulated (0, 5.5, 10, 20 or 30mM) trophoblast tissue lysate for 4 or 48 hours originating from two healthy placental samples as highlighted in figure 56 (panel B).

The lactate dehydrogenase (LDH) levels which have been released in the culture media from D-glucose stimulated (0, 5.5, 10, 20 or 30mM) trophoblast tissue for 4 or 48 hours originating from 4 healthy placental samples (T2959, T2956, T2957 and T2960) measured using LDH assay kit (Abcam, AB102526) are presented in

figure 56 (panel C). Multiple statistically significant differences in released LDH levels at 48 hours were found using Dunn's multiple comparison tests between 0mM vs. 20mM D-glucose (*P=0.0395), 5.5mM vs. 20mM D-glucose (*P=0.0101) and 5.5mM vs. 30mM D-glucose (*P=0.0254) as highlighted in figure 56 (panel C). Furthermore, the released LDH levels in the same culture media measured using a different kit (LDH cytotoxicity assay kit II; Abcam, AB65393) are presented in figure 56 (panel D). Dunn's multiple comparison test highlighted the presence of multiple statistically significant differences in released LDH levels in the culture media at 48 hours between 0mM vs. 20mM D-glucose (*P=0.0101), 0mM vs. 30mM D-glucose (**P=0.0080), 5.5mM vs. 20mM D-glucose (*P=0.0203) and 5.5mM vs. 30mM D-glucose (*P=0.0161) as illustrated in figure 56 (panel D).

Figure 57 shows the levels of LDH which have been released in the culture media from D-glucose stimulated (0, 5.5, 10, 20 or 30mM) trophoblast tissue for 4 hours (panel A) or 48 hours (panel B) in the presence and absence of cell lysis solution originating from 3 healthy placental samples. Two statistically significant differences were found at 48 hours between 5.5mM vs. 20mM D-glucose (*P=0.0448) and 10mM vs. 20mM D-glucose (*P=0.0136) treated trophoblast tissue in the absence of cell lysis solution using an unpaired t-test (figure 57).

As a result, the P2X7 receptor protein expression levels identified in the second pellet fraction (membrane protein fraction) of human placental villous tissue lysates were not significantly altered compared to control in D-glucose stimulated (0, 5.5, 10, 20 and 30mM) villous tissue for 4 or 48 hours assessed using western blotting. Also, the P2X7 receptor protein expression levels assessed in the second pellet fraction of villous tissue were not significantly altered compared to control in D-glucose stimulated (0, 5,5 and 30mM) villous tissue for 4 or 24 hours assessed using western

blotting. Furthermore, no statistically significant differences were found in released IL-1β levels between D-glucose stimulated villous tissue at both 4 hours and 48 hours. However, there was multiple statistically significant differences were found in released LDH levels between 0mM vs. 20mM D-glucose (*P=0.0395), 5.5mM vs. 20mM D-glucose (*P=0.0101) and 5.5mM vs. 30mM D-glucose (*P=0.0254) at 48 hours using Dunn's multiple comparison tests.

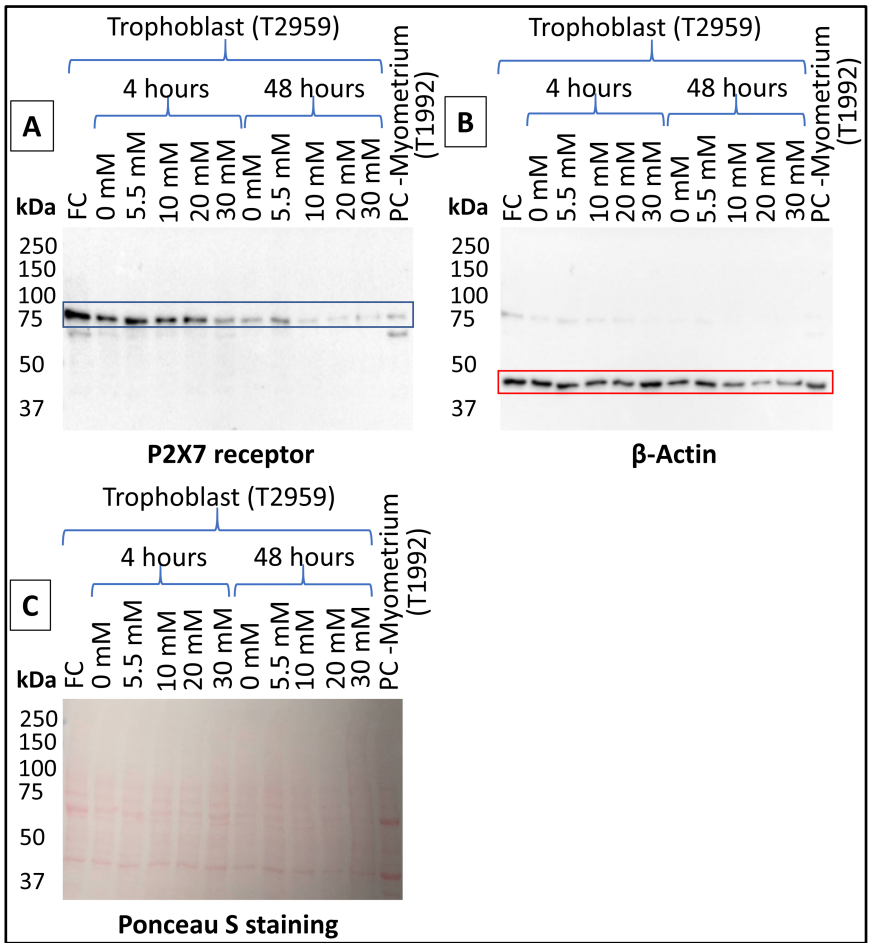


Figure 52. *This figure shows the P2X7 receptor protein expression levels (panel **A**, blue box) in the second pellet fraction of trophoblast tissue lysate originating from a placenta sample of a healthy patient (T2959) and myometrium tissue lysate originating from a healthy volunteer (T1992). In this case, the isolated trophoblast tissue was stimulated with D-glucose at a concentration of 0mM, 5.5mM, 10mM, 20mM or 30mM for either 4 hours or 48 hours in the presence of RPMI 1640 media supplemented with 100U/mL penicillin, 100µg/mL streptomycin without fetal bovine serum (FBS). FC (frozen control) denotes that the trophoblast tissue biopsies were snap frozen in liquid nitrogen immediately after collection and stored at -80^{0}C until processed i.e. not subjected to D-glucose stimulation. All tissue samples were homogenised using lysing matrix D ceramic spheres with the exception of myometrium tissue which has been homogenised using the ultra turrax method. Each well was loaded with 40µg of total protein. Myometrium was used as a positive control (PC) for the P2X7 receptor and was the only tissue type to have been subjected to IgG immunodepletion using a well-established immunoprecipitation protocol involving anti-human IgG (whole molecule)-agarose antibody developed in goat (Sigma, A3543) **B**. The immunoblot was stripped and then reblotted with β actin for loading control (red box) **C**. Ponceau S staining of the nitrocellulose membrane prior to immunoblotting for the P2X7 receptor. Antibodies used: P2X7 primary antibody (Rabbit polyclonal IgG, Alomone Labs, APR-004) at a dilution of 1:600, P2X7 secondary antibody (Polyclonal goat anti rabbit immunoglobulins alkaline phosphatase, Dako, D0487) at a dilution of 1:1000, β actin primary antibody (rabbit polyclonal IgG, Abcam, Ab8227) at a dilution of 1:8000 and β actin secondary antibody (Polyclonal goat anti rabbit immunoglobulins alkaline phosphatase, Dako, D0487) at a dilution of 1:1000.*

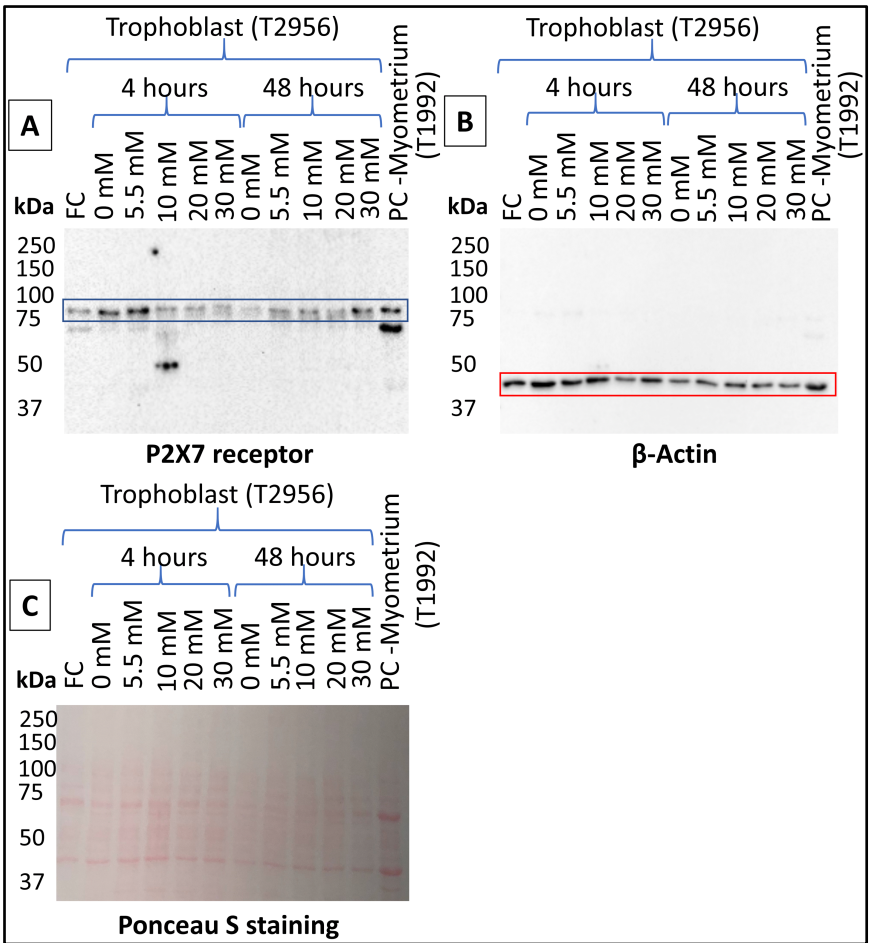


Figure 53. *This figure shows the P2X7 receptor protein expression levels (panel **A**, blue box) in the second pellet fraction of trophoblast tissue lysate originating from a placenta sample of a healthy patient (T2956) and myometrium tissue lysate originating from a healthy volunteer (T1992). In this case, the isolated trophoblast tissue was stimulated with D-glucose at a concentration of 0mM, 5.5mM, 10mM, 20mM or 30mM for either 4 hours or 48 hours in the presence of RPMI 1640 media supplemented with 100U/mL penicillin, 100µg/mL streptomycin without fetal bovine serum (FBS). FC (frozen control) denotes that the trophoblast tissue biopsies were snap frozen in liquid nitrogen immediately after collection and stored at -80^{0}C until processed i.e. not subjected to D-glucose stimulation. All tissue samples were homogenised using lysing matrix D ceramic spheres with the exception of myometrium tissue which has been homogenised using the ultra turrax method. Each well was loaded with 40µg of total protein. Myometrium was used as a positive control (PC) for the P2X7 receptor and was the only tissue type to have been subjected to IgG immunodepletion using a well-established immunoprecipitation protocol involving anti-human IgG (whole molecule)-agarose antibody developed in goat (Sigma, A3543) **B**. The immunoblot was stripped and then reblotted with β actin for loading control (red box) **C**. Ponceau S staining of the nitrocellulose membrane prior to immunoblotting for the P2X7 receptor. Antibodies used: P2X7 primary antibody (Rabbit polyclonal IgG, Alomone Labs, APR-004) at a dilution of 1:600, P2X7 secondary antibody (Polyclonal goat anti rabbit immunoglobulins alkaline phosphatase, Dako, D0487) at a dilution of 1:1000, β actin primary antibody (rabbit polyclonal IgG, Abcam, Ab8227) at a dilution of 1:8000 and β actin secondary antibody (Polyclonal goat anti rabbit immunoglobulins alkaline phosphatase, Dako, D0487) at a dilution of 1:1000.*

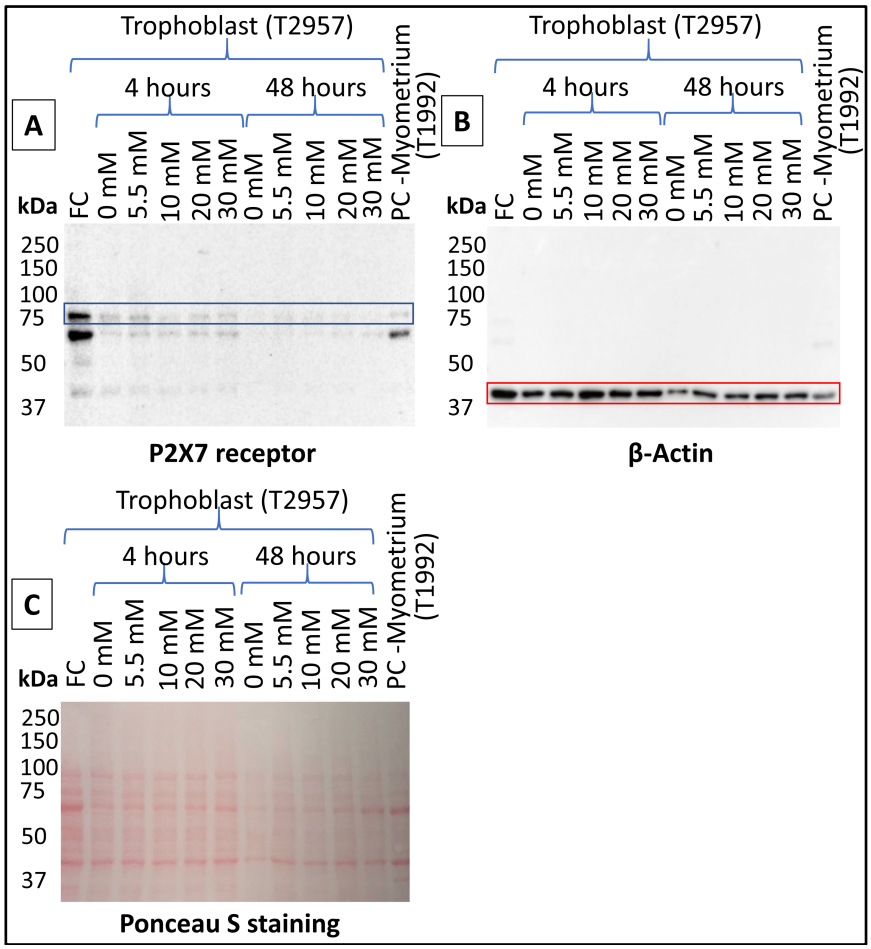


Figure 54. *This figure shows the P2X7 receptor protein expression levels (panel **A**, blue box) in the second pellet fraction of trophoblast tissue lysate originating from a placenta sample of a healthy patient (T2957) and myometrium tissue lysate originating from a healthy volunteer (T1992). In this case, the isolated trophoblast tissue was stimulated with D-glucose at a concentration of 0mM, 5.5mM, 10mM, 20mM or 30mM for either 4 hours or 48 hours in the presence of RPMI 1640 media supplemented with 100U/mL penicillin, 100µg/mL streptomycin without fetal bovine serum (FBS). FC (frozen control) denotes that the trophoblast tissue biopsies were snap frozen in liquid nitrogen immediately after collection and stored at -80^{0}C until processed i.e. not subjected to D-glucose stimulation. All tissue samples were homogenised using lysing matrix D ceramic spheres with the exception of myometrium tissue which has been homogenised using the ultra turrax method. Each well was loaded with 40µg of total protein. Myometrium was used as a positive control (PC) for the P2X7 receptor and was the only tissue type to have been subjected to IgG immunodepletion using a well-established immunoprecipitation protocol involving anti-human IgG (whole molecule)-agarose antibody developed in goat (Sigma, A3543) **B**. The immunoblot was stripped and then reblotted with β actin for loading control (red box) **C**. Ponceau S staining of the nitrocellulose membrane prior to immunoblotting for the P2X7 receptor. Antibodies used: P2X7 primary antibody (Rabbit polyclonal IgG, Alomone Labs, APR-004) at a dilution of 1:600, P2X7 secondary antibody (Polyclonal goat anti rabbit immunoglobulins alkaline phosphatase, Dako, D0487) at a dilution of 1:1000, β actin primary antibody (rabbit polyclonal IgG, Abcam, Ab8227) at a dilution of 1:8000 and β actin secondary antibody (Polyclonal goat anti rabbit immunoglobulins alkaline phosphatase, Dako, D0487) at a dilution of 1:1000.*

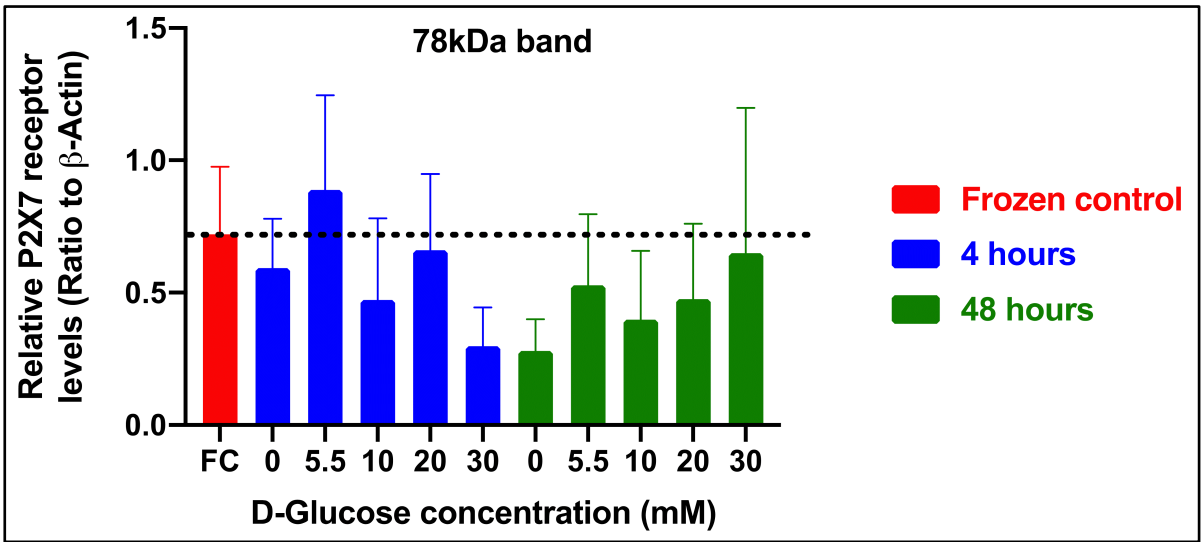


Figure 55. *Graph highlighting the relative P2X7 receptor (78kDa band) protein expression levels normalised to β actin in trophoblast tissue lysates originating from N=3 placental samples of healthy patients (T2959, T2956 and T2957) which have been stimulated with D-glucose at a concentration of 0mM, 5.5mM, 10mM, 20mM or 30mM for either 4 hours or 48 hours in the presence of RPMI 1640 media without FBS. FC (frozen control) denotes that the trophoblast tissue biopsies were snap frozen in liquid nitrogen immediately after collection and stored at -80^{0}C until processed i.e. not subjected to D-glucose stimulation. Data are expressed as mean ± SEM.*

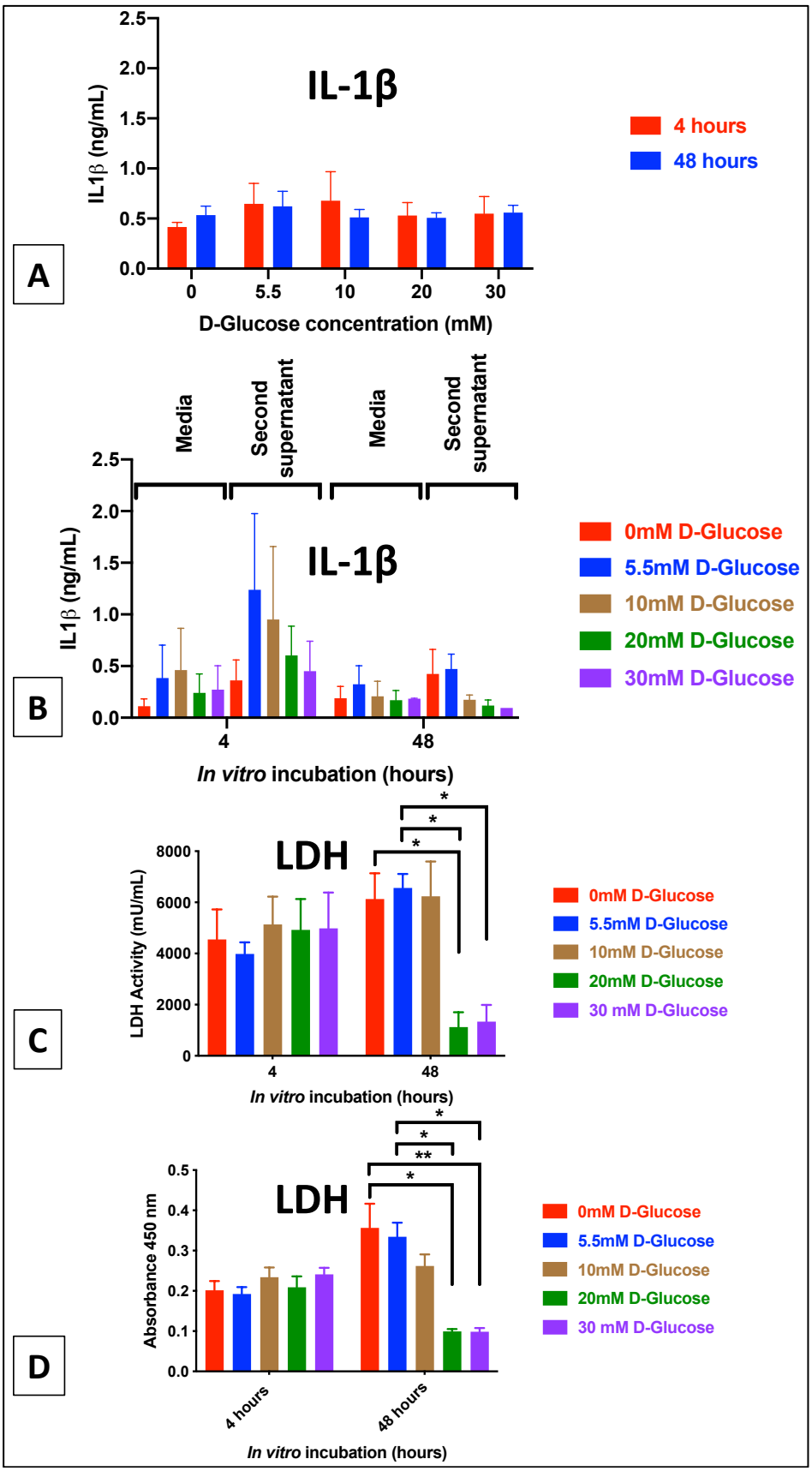


Figure 56. *This figure shows the levels of IL-1β and lactate dehydrogenase (LDH) which have been released in the culture media from D-glucose stimulated (0, 5.5, 10, 20 or 30mM) trophoblast tissue for 4- or 48-hours* ***A****. Released IL-1β levels measured*

in the culture media of trophoblast tissue which has been stimulated with D-glucose (0, 5.5, 10, 20 or 30mM) for 4 hours (red bars) or 48 hours (blue bars) originating from four healthy placental samples (T2959, T2956, T2957 and T2960) ***B****. IL-1β levels measured in the culture media and in the second supernatant of D-glucose stimulated (0, 5.5, 10, 20 or 30mM) trophoblast tissue lysate for 4 or 48 hours originating from two healthy placental samples (T2959 and T2956)* ***C****. Released LDH levels measured in the culture media of D-glucose stimulated (0, 5.5, 10, 20 or 30mM) trophoblast tissue for 4 or 48 hours originating from 4 healthy placental samples (T2959, T2956, T2957 and T2960) using LDH assay kit (Abcam, AB102526)* ***D****. Released LDH levels measured in the culture media of D-glucose stimulated (0, 5.5, 10, 20 or 30mM) trophoblast tissue for 4 or 48 hours originating from 4 healthy placental samples (T2959, T2956, T2957 and T2960) using LDH cytotoxicity assay kit II (Abcam, AB65393). Data are expressed as mean ± SEM. * P*≤0.05, ** P≤0.01, *** P≤0.001, **** P≤0.0001.

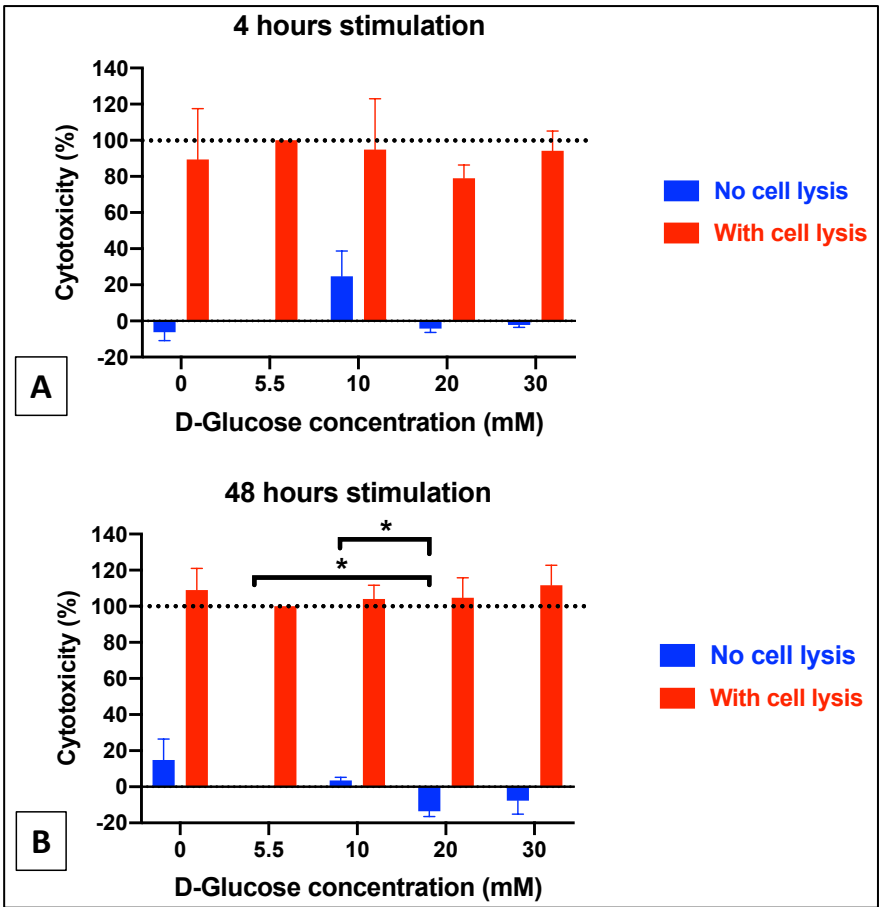


Figure 57. *This figure shows the levels of lactate dehydrogenase (LDH) which have been released in the culture media from D-glucose stimulated (0, 5.5, 10, 20 or 30mM) trophoblast tissue for 4 hours (panel* ***A****) or 48 hours (panel* ***B****) in the presence (red bars) or absence (blue bars) of cell lysis solution originating from 3 healthy placental samples (T3025, T3026, T3027). The lactate dehydrogenase levels were measured using LDH cytotoxicity assay kit II (Abcam, AB65393). Data are expressed as mean ± SEM. * P*≤0.05, ** P≤0.01, *** P≤0.001, **** P≤0.0001. Cytotoxicity (%) was calculated using the low control (5.5mM D-glucose with no cell lysis) and the high control (5.5mM D-glucose with cell lysis; discontinued line).

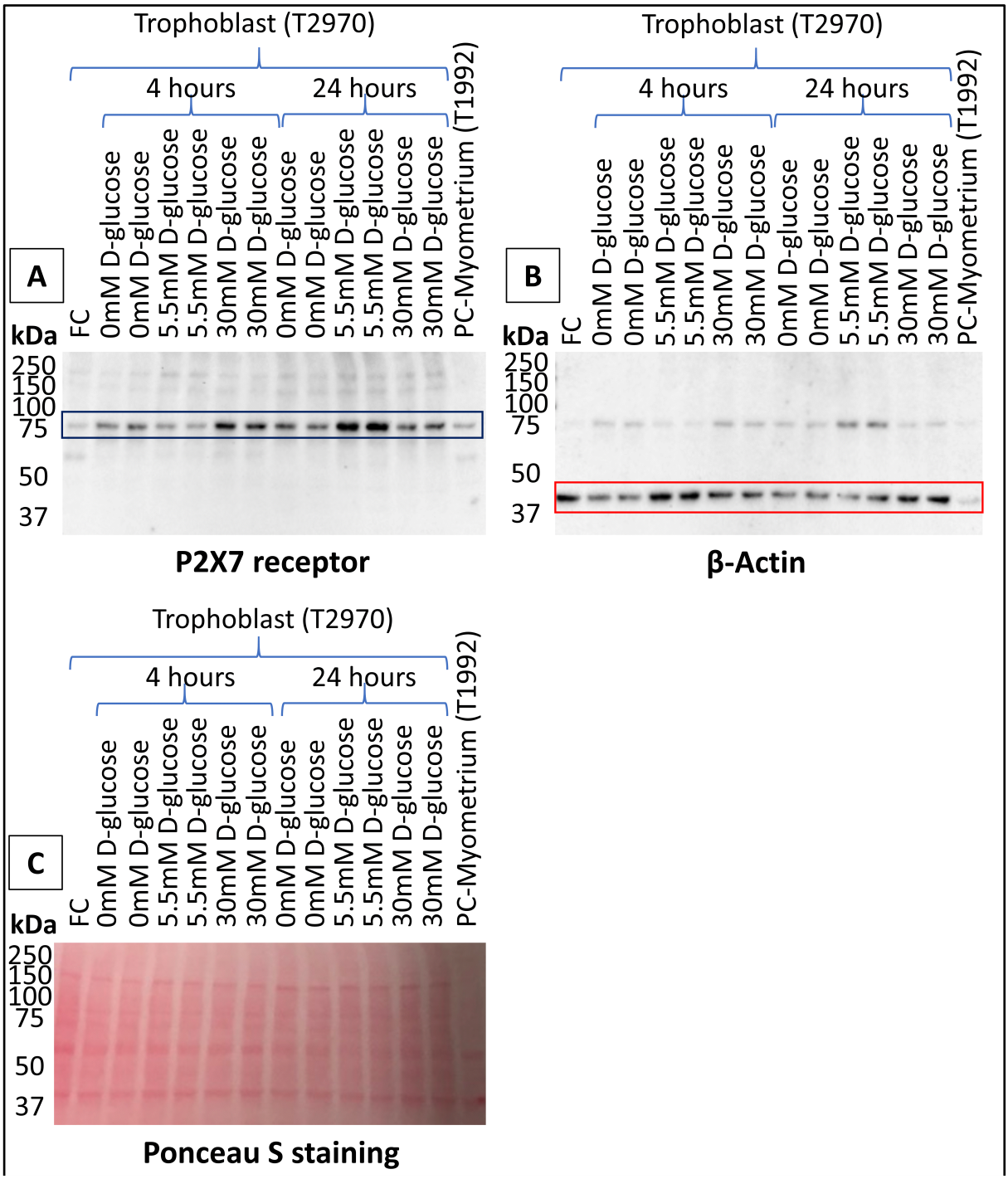


Figure 58. *This figure shows the P2X7 receptor protein expression levels (panel **A**, blue box) in the second pellet fraction of trophoblast tissue lysate originating from a placenta sample of a healthy patient (T2970) and myometrium tissue lysate originating from a healthy volunteer (T1992). In this case, the isolated trophoblast tissue was stimulated with D-glucose at a concentration of 0mM, 5.5mM or 30mM for either 4 hours or 24 hours in the presence of RPMI 1640 media supplemented with 100U/mL penicillin, 100µg/mL streptomycin and 10% (v/v) fetal bovine serum (FBS). FC (frozen control) denotes that the trophoblast tissue biopsies were snap frozen in liquid nitrogen immediately after collection and stored at -80^{0}C until processed i.e. not subjected to D-glucose stimulation. All tissue samples were homogenised using lysing matrix D ceramic spheres with the exception of myometrium tissue which has been*

homogenised using the ultra turrax method. Each well was loaded with 40µg of total protein. Myometrium was used as a positive control (PC) for the P2X7 receptor and was the only tissue type to have been subjected to IgG immunodepletion using a well-established immunoprecipitation protocol involving anti-human IgG (whole molecule)-agarose antibody developed in goat (Sigma, A3543) ***B****. The immunoblot was stripped and then reblotted with β actin for loading control (red box)* ***C****. Ponceau S staining of the nitrocellulose membrane prior to immunoblotting for the P2X7 receptor. Antibodies used: P2X7 primary antibody (Rabbit polyclonal IgG, Alomone Labs, APR-004) at a dilution of 1:600, P2X7 secondary antibody (Polyclonal goat anti rabbit immunoglobulins alkaline phosphatase, Dako, D0487) at a dilution of 1:1000, β actin primary antibody (rabbit polyclonal IgG, Abcam, Ab8227) at a dilution of 1:8000 and β actin secondary antibody (Polyclonal goat anti rabbit immunoglobulins alkaline phosphatase, Dako, D0487) at a dilution of 1:1000.*

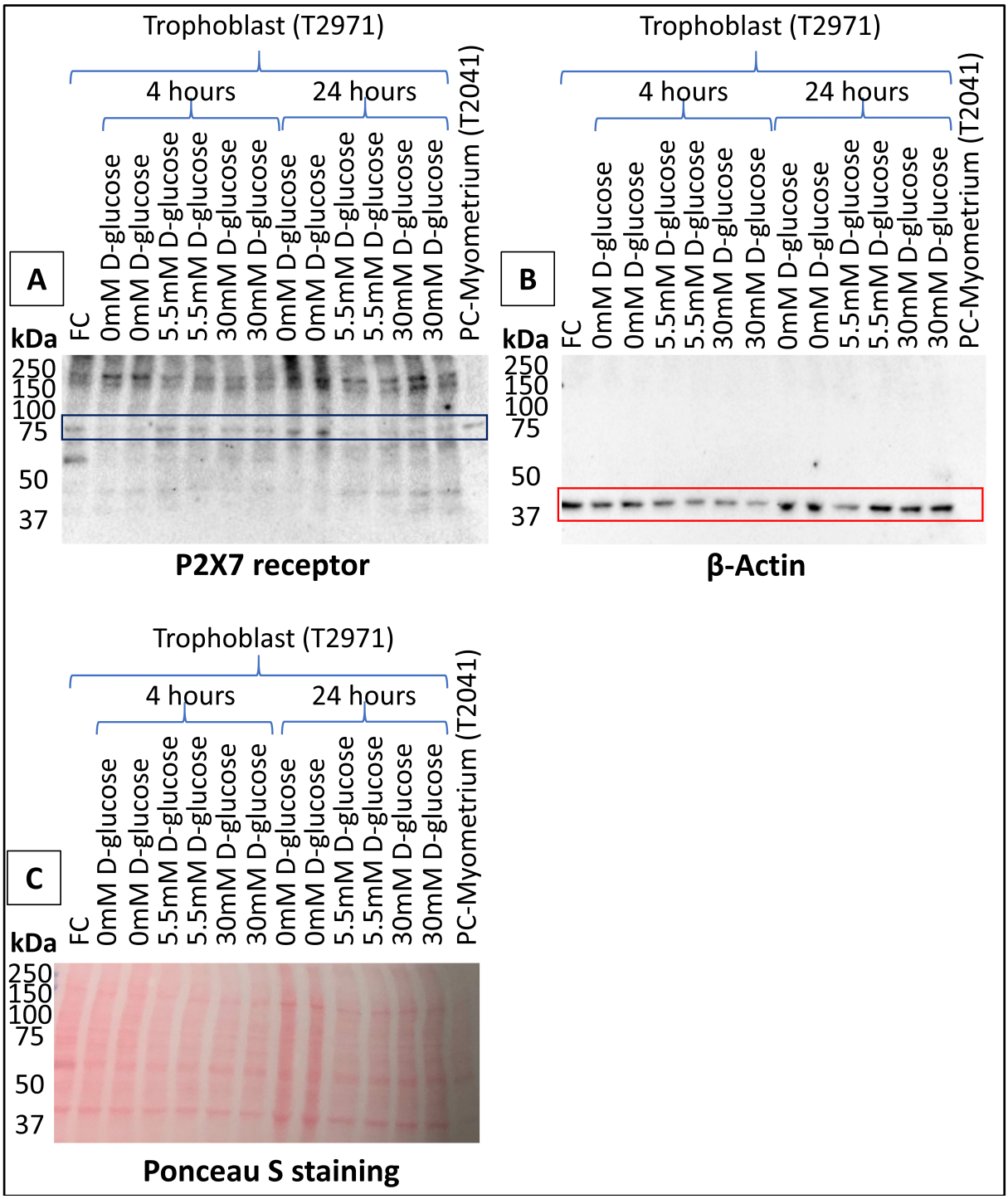


Figure 59. *This figure shows the P2X7 receptor protein expression levels (panel **A**, blue box) in the second pellet fraction of trophoblast tissue lysate originating from a placenta sample of a healthy patient (T2971) and myometrium tissue lysate originating from a healthy volunteer (T2041). In this case, the isolated trophoblast tissue was stimulated with D-glucose at a concentration of 0mM, 5.5mM or 30mM for either 4 hours or 24 hours in the presence of RPMI 1640 media supplemented with 100U/mL penicillin, 100µg/mL streptomycin and 10% (v/v) fetal bovine serum. FC (frozen control) denotes that the trophoblast tissue biopsies were snap frozen in liquid nitrogen immediately after collection and stored at -80^{0}C until processed i.e. not subjected to D-glucose stimulation. All tissue samples were homogenised using lysing matrix D*

ceramic spheres with the exception of myometrium tissue which has been homogenised using the ultra turrax method. Each well was loaded with 40µg of total protein. Myometrium was used as a positive control (PC) for the P2X7 receptor and was the only tissue type to have been subjected to IgG immunodepletion using a well-established immunoprecipitation protocol involving anti-human IgG (whole molecule)-agarose antibody developed in goat (Sigma, A3543) ***B****. The immunoblot was stripped and then reblotted with β actin for loading control (red box)* ***C****. Ponceau S staining of the nitrocellulose membrane prior to immunoblotting for the P2X7 receptor. Antibodies used: P2X7 primary antibody (Rabbit polyclonal IgG, Alomone Labs, APR-004) at a dilution of 1:600, P2X7 secondary antibody (Polyclonal goat anti rabbit immunoglobulins alkaline phosphatase, Dako, D0487) at a dilution of 1:1000, β actin primary antibody (rabbit polyclonal IgG, Abcam, Ab8227) at a dilution of 1:8000 and β actin secondary antibody (Polyclonal goat anti rabbit immunoglobulins alkaline phosphatase, Dako, D0487) at a dilution of 1:1000.*

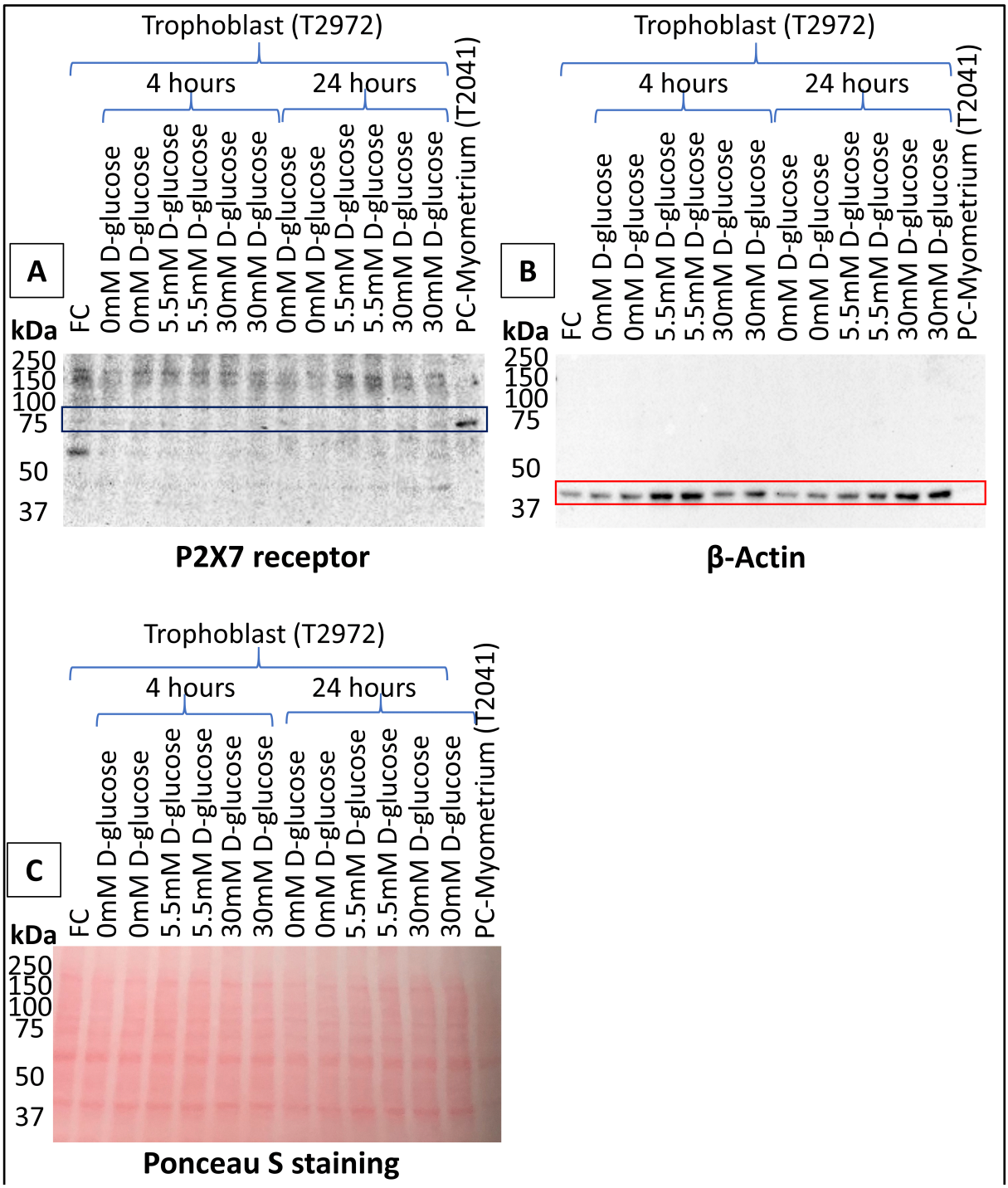


Figure 60. *This figure shows the P2X7 receptor protein expression levels (panel **A**, blue box) in the second pellet fraction of trophoblast tissue lysate originating from a placenta sample of a healthy patient (T2972) and myometrium tissue lysate originating from a healthy volunteer (T2041). In this case, the isolated trophoblast tissue was stimulated with D-glucose at a concentration of 0mM, 5.5mM or 30mM for either 4 hours or 24 hours in the presence of RPMI 1640 media supplemented with 100U/mL penicillin, 100µg/mL streptomycin and 10% (v/v) fetal bovine serum. FC (frozen control) denotes that the trophoblast tissue biopsies were snap frozen in liquid nitrogen immediately after collection and stored at -80^{0}C until processed i.e. not subjected to D-glucose stimulation. All tissue samples were homogenised using lysing matrix D*

ceramic spheres with the exception of myometrium tissue which has been homogenised using the ultra turrax method. Each well was loaded with 40µg of total protein. Myometrium was used as a positive control (PC) for the P2X7 receptor and was the only tissue type to have been subjected to IgG immunodepletion using a well-established immunoprecipitation protocol involving anti-human IgG (whole molecule)-agarose antibody developed in goat (Sigma, A3543) ***B****. The immunoblot was stripped and then reblotted with β actin for loading control (red box). The β actin protein expression level in the second pellet (membrane) fraction of myometrium tissue lysate sample originating from patient T2041 shown in the last western blot lane has degraded, hence no band was detected* ***C****. Ponceau S staining of the nitrocellulose membrane prior to immunoblotting for the P2X7 receptor. Antibodies used: P2X7 primary antibody (Rabbit polyclonal IgG, Alomone Labs, APR-004) at a dilution of 1:600, P2X7 secondary antibody (Polyclonal goat anti rabbit immunoglobulins alkaline phosphatase, Dako, D0487) at a dilution of 1:1000, β actin primary antibody (rabbit polyclonal IgG, Abcam, Ab8227) at a dilution of 1:8000 and β actin secondary antibody (Polyclonal goat anti rabbit immunoglobulins alkaline phosphatase, Dako, D0487) at a dilution of 1:1000.*

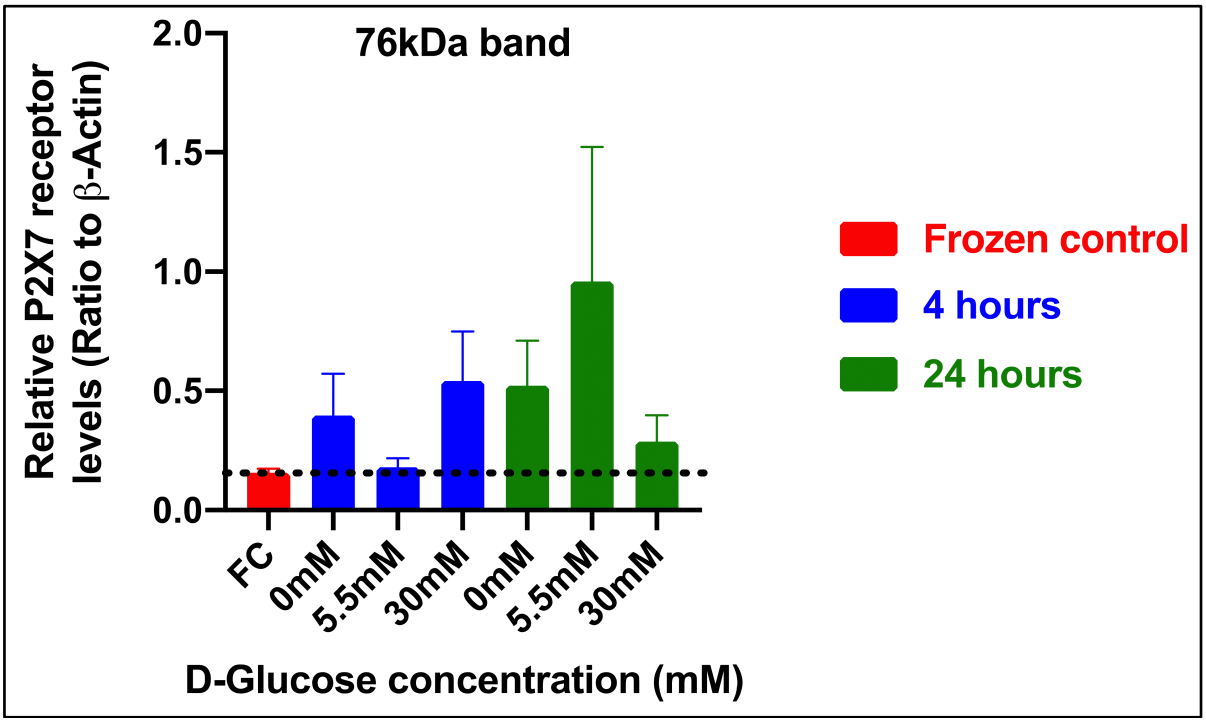


Figure 61. *Graph highlighting the relative P2X7 receptor protein expression levels normalised to β actin (approximately 76kDa band) in trophoblast tissue lysates originating from N=3 placental samples of healthy patients (T2970, T2971, T2972) which have been stimulated with D-glucose at a concentration of 0mM, 5.5mM or 30mM for either 4 hours or 24 hours in the presence of RPMI 1640 media supplemented with 100U/mL penicillin, 100µg/mL streptomycin and 10% (v/v) FBS. FC (frozen control) denotes that the trophoblast tissue biopsies were snap frozen in liquid nitrogen immediately after collection and stored at -80^{0}C until processed i.e. not subjected to D-glucose stimulation. Data are expressed as mean ± SEM.*

3.3.6 The relative P2X7 receptor, NLRP3 inflammasome and procaspase-1 protein expression levels in stem villous artery do not significantly alter between healthy (N=8) and preeclamptic (N=8) placental samples

The relative protein expression levels of two (approximately 74kDa and 92kDa) NLRP3 inflammasome isoforms in stem villous arteries originating from 8 healthy and 8 preeclamptic placental samples are presented in figures 62-63. Two bands were detected at circa 74kDa (green box) and approximately 92kDa (blue box) in the second supernatant fraction of SVA lysates of both healthy and preeclamptic placental samples. A strong signal at approximately 49kDa was detected in the NLRP3 inflammasome immunoblots which was due to the non-specific binding of the NLRP3 inflammasome secondary antibody as suggested from figure 50 (panel A). There were no statistically significant differences (P=0.4521; Unpaired T-test) in the relative NLRP3 inflammasome protein expression levels of the approximately 74kDa isoform between stem villous artery lysates of healthy and preeclamptic placental samples as highlighted in figure 66 (panel A). Similarly, in the case of the approximately 92kDa NLRP3 inflammasome isoform, no statistically significant differences were observed (P=0.8785; Mann-Whitney test) between the stem villous artery lysates of healthy and preeclamptic placental samples (figure 66, panel A).

The relative P2X7 receptor protein expression levels in the second pellet fraction of SVA lysates originating from 8 healthy and 8 preeclamptic placental samples are presented in figures 64-65. A strong signal was detected at approximately 79kDa in both P2X7 receptor immunoblots as illustrated by the blue box in figures 64-65. An intense band was also detected at circa 79kDa in the second pellet fraction of

myometrium tissue lysate which was used as a positive control for the P2X7 receptor. All P2X7 receptor protein specificity was confirmed using the P2X7 receptor specific blocking peptide which caused the disappearance of the approximately 79kDa band in the same SVA lysates (second pellet fraction) originating from N=8 healthy and N=8 preeclamptic placental samples as illustrated by the blue box in figures 67-68. There were no statistically significant differences (P=0.3823; Mann Whitney test) in the relative P2X7 receptor protein expression levels between stem villous artery lysates of healthy and preeclamptic placental samples as highlighted in figure 66 (panel B).

The relative procaspase-1 protein expression levels in the second supernatant fraction of the stem villous artery lysates originating from N=8 healthy and N=8 preeclamptic placental samples are illustrated in figure 69-70. A strong signal was detected at approximately 47kDa in both procaspase-1 immunoblots as illustrated by the green box in figure 69 (panel A) and figure 70 (panel A). There were no statistically significant differences (P=0.8785, Mann-Whitney test) in the relative procaspase-1 expression levels between SVA lysates (second supernatant fraction) originating from healthy and preeclamptic placental samples as presented in figure 71.

Coomassie-Brilliant blue staining of the 10% and 15% hand casted polyacrylamide gels following the transfer of the resolved proteins from the gels to the nitrocellulose membranes showed the presence of multiple bands particularly between 50kDa-250kDa as highlighted in figures 62-65 (panel D) and figures 67-70 (panel D). Ponceau S staining of the nitrocellulose membranes showed equal protein loading as illustrated in figures 62-65 (panel C) and figures 67-70 (panel C). As a result, no statistically significant differences were found in P2X7 receptor, NLRP3 inflammasome and pro-caspase-1 protein expression levels in SVA's between healthy and pre-eclamptic patients assessed using western blotting.

Table 9 highlights the clinical characteristics of the N=8 normotensive and N=8 pre-eclamptic patients that had placental stem villous arteries samples used for investigating the relative P2X7 receptor, NLRP3 inflammasome and pro-caspase-1 protein expression levels using western blotting.

			Maternal age	Gestational Age	Gravida	Parity	BMI	Notes
Normotensive	Patient number	T910	28 years	39 weeks	2	1	35	N.A.
		T952	29 years	39 weeks	4	3	24	Breech
		T928	36 years	N.A.	2	1	N.A.	Breech
		T962	29 years	39 weeks+1day	2	1	N.A	Breech
		T927	22 years	N.A.	2	1	N.A.	N.A.
		T829	31 years	39 weeks+3days	2	1	N.A.	Sex of offspring female
		T840	29 years	N.A.	N.A.	N.A.	N.A.	N.A.
		T1469	39 years	39 weeks	4	1	N.A.	N.A.
Pre-eclampsia		T997	29 years	34 weeks+4days	1	0	N.A.	Blood pressure 141/91, dipstick proteinuria 2+, leg edema, occasional headache, no epigastric pain, no visual disturbance, uncomplicated blood test
		T860	36 years	38 weeks+4 days	N.A.	N.A.	N.A.	Blood pressure 140/100, dipstick proteinuria 1+, uncomplicated blood test, taking labetolol and nifedipine
		T853	30 years	33 weeks+1 day	3	1	37	Blood pressure 186/91, previous pre-eclamptic elective caesarean section, blurry vision, swollen face, dipstick proteinuria 3+
		T738	24 years	34 weeks+6 days	N.A.	1	N.A.	Breech
		T994	25 years	34 weeks +6 days	N.A.	N.A.	N.A.	Intrauterine growth restriction, blood pressure 141/90, dipstick proteinuria 2+, Elevated alanine transaminase, decreased platelets
		T1269	34 years	34 weeks + 6 days	N.A.	2	N.A.	Intrauterine growth restriction, Mild edema, dipstick proteinuria 3+, Decreased platelets, blood pressure 136/84
		T1609	24 years	N.A.	N.A.	N.A.	N.A.	Dipstick proteinuria 2+
		T1145	33 years	36 weeks	1	0	41	Labetolol, nifedipine, blood pressure 142/88, Dipstick proteinuria 2+, visual disturbance, epigastric pain

Table 9. *This table shows the clinical characteristics of N=8 normotensive and N=8 pre-eclamptic patients that had the placental samples used for P2X7, NLRP3 and pro-caspase-1 protein expression studies in isolated stem villous arteries. N.A denotes not available. BMI suggests body mass index.*

The maternal age (years) of normotensive patients was 30.38±5.181 and of pre-eclamptic patients was 29.38±4.719 expressed as mean±SD. Also, the gestational age (weeks) of the normotensive patients was 39.11±0.182 and of pre-eclamptic patients was 35.26±1.682 expressed as mean±SD. A Shapiro-Wilk test highlighted that all maternal age data was normally distributed. Furthermore, the same statistical test also showed that all gestational age data was normally distributed with the exception of the healthy patients (*P=0.0214). An unpaired two-tailed T-test with Welch's correction was undertaken between the maternal age of normotensive and pre-eclamptic patients which highlighted no statistically significant differences between the two groups (P=0.6926). However, a two-tailed Mann Whitney test between the gestational age normotensive and pre-eclamptic patients highlighted a statistically significant difference between the two groups (**P=0.0025).

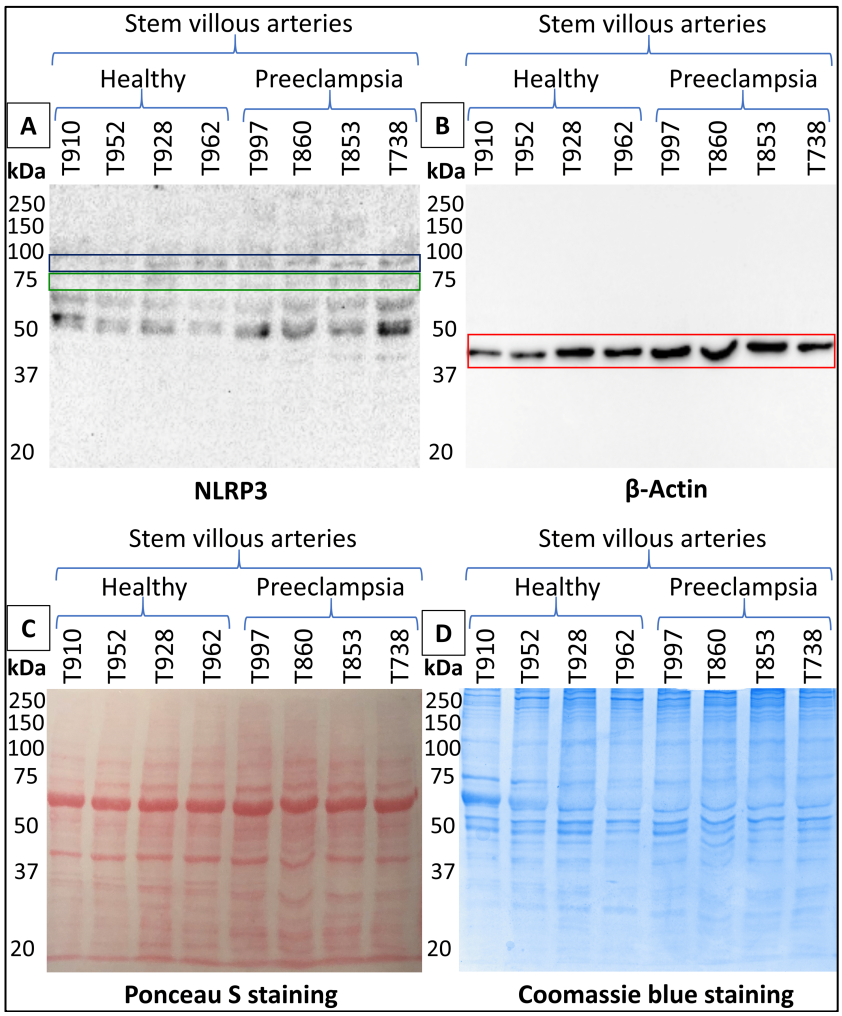


Figure 62. *This figure shows the NLRP3 inflammasome protein expression levels (panel **A**, approximately 92kDa isoform- blue box and circa 74kDa isoform- green box) in the second supernatant fraction of stem villous artery lysates originating from four placental samples of healthy patients (T910, T952, T928 and T962) and four placental samples of preeclamptic patients (T997, T860, T853 and T738). Following collection, the stem villous artery tissue was immediately snap frozen in liquid nitrogen and stored at -80^{0}C until processed. All tissue samples were homogenised using the ultra turrax method and all tissue lysates were IgG immunodepleted using a well-established immunoprecipitation protocol involving anti-human IgG (whole molecule)-agarose antibody developed in goat (Sigma, A3543). The proteins were resolved using a 10% hand casted polyacrylamide gel. The resolved proteins were transferred to the nitrocellulose membrane for a period of 90 minutes. Each well was loaded with 40µg of total protein **B**. The immunoblot was stripped and then reblotted with β actin for loading control (red box) **C**. Ponceau S staining of the nitrocellulose membrane prior to immunoblotting for the NLRP3 inflammasome **D**. Coomassie blue staining of the 10% gel following the transfer of proteins to the nitrocellulose membrane. Antibodies used: NLRP3 primary antibody (rabbit polyclonal IgG, Abcam, Ab91413) at a dilution of 1:200, NLRP3 secondary antibody (Polyclonal goat anti rabbit immunoglobulins alkaline phosphatase, Dako, D0487) at a dilution of 1:1000, β actin primary antibody (rabbit polyclonal IgG, Abcam, Ab8227) at a dilution of 1:8000 and β actin secondary antibody (Polyclonal goat anti rabbit immunoglobulins alkaline phosphatase, Dako, D0487) at a dilution of 1:1000.*

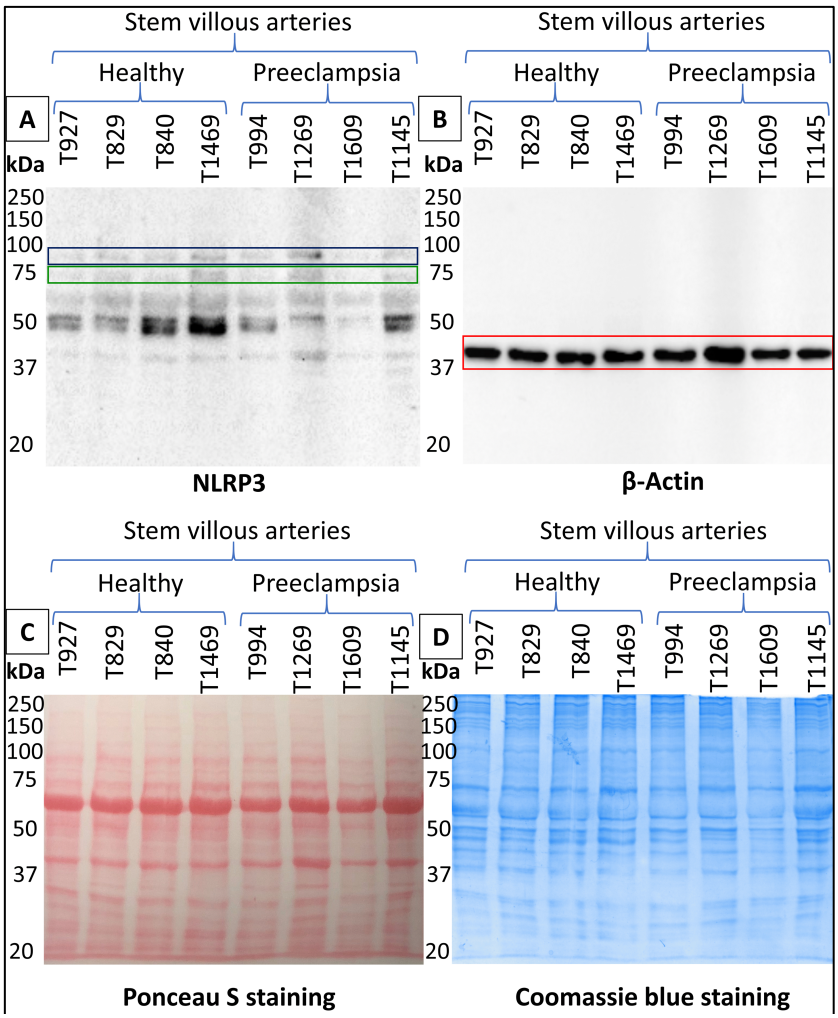


Figure 63. *This figure shows the NLRP3 inflammasome protein expression levels (panel **A**, approximately 92kDa isoform- blue box and circa 74kDa isoform- green box) in the second supernatant fraction of stem villous artery lysates originating from four placental samples of healthy patients (T927, T829, T840 and T1469) and four placental samples of preeclamptic patients (T994, T1269, T1609 and T1145). Following collection, the stem villous artery tissue was immediately snap frozen in liquid nitrogen and stored at -80^{0}C until processed. All tissue samples were homogenised using the ultra turrax method and all tissue lysates were IgG immunodepleted using a well-established immunoprecipitation protocol involving anti-human IgG (whole molecule)-agarose antibody developed in goat (Sigma, A3543). The proteins were resolved using a 10% hand casted polyacrylamide gel. The resolved proteins were transferred to the nitrocellulose membrane for a period of 90 minutes. Each well was loaded with 40µg of total protein **B**. The immunoblot was stripped and then reblotted with β actin for loading control (red box) **C**. Ponceau S staining of the nitrocellulose membrane prior to immunoblotting for the NLRP3 inflammasome **D**. Coomassie blue staining of the 10% gel following the transfer of proteins to the nitrocellulose membrane. Antibodies used: NLRP3 primary antibody (rabbit polyclonal IgG, Abcam, Ab91413) at a dilution of 1:200, NLRP3 secondary antibody (Polyclonal goat anti rabbit immunoglobulins alkaline phosphatase, Dako, D0487) at a dilution of 1:1000, β actin primary antibody (rabbit polyclonal IgG, Abcam, Ab8227) at a dilution of 1:8000 and β actin secondary antibody (Polyclonal goat anti rabbit immunoglobulins alkaline phosphatase, Dako, D0487) at a dilution of 1:1000.*

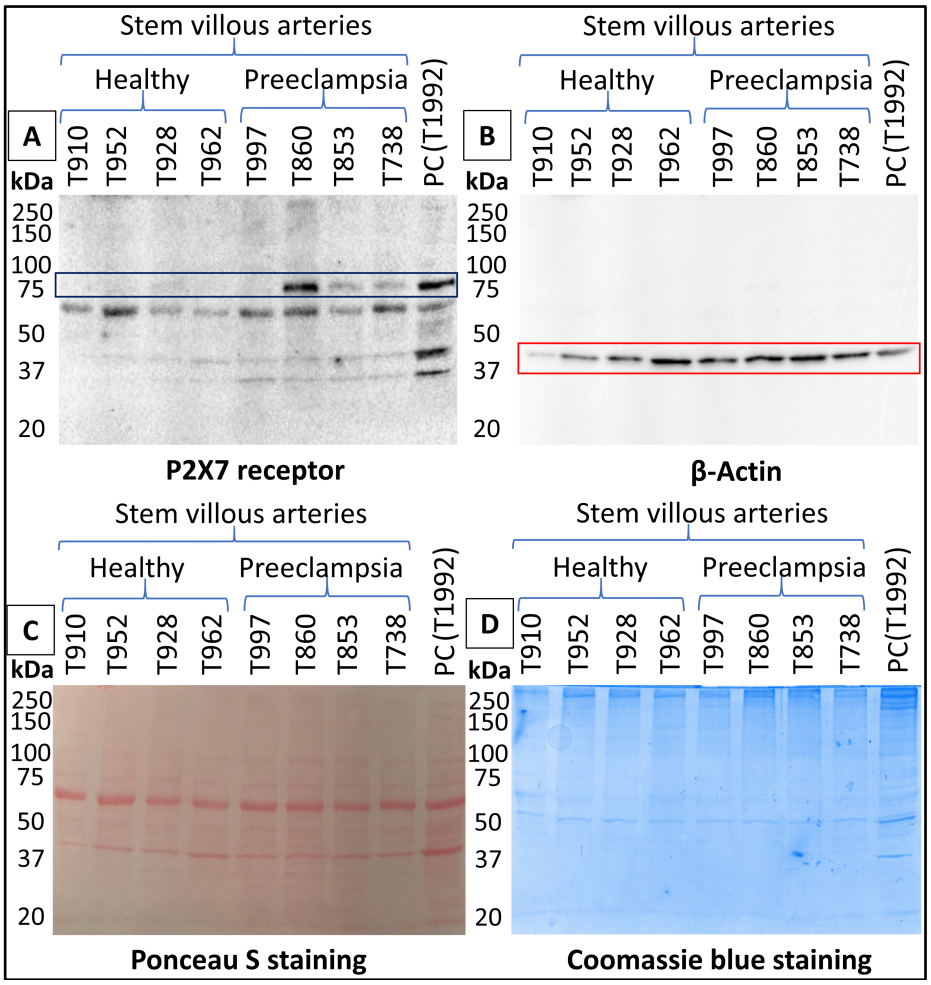


Figure 64. *This figure shows the P2X7 receptor protein expression levels (panel **A**, approximately 79kDa band -blue box) in the second pellet fraction of stem villous artery lysates originating from four placental samples of healthy patients (T910, T952, T928 and T962) and four placental samples of preeclamptic patients (T997, T860, T853 and T738) as well as myometrium tissue lysate originating from a healthy volunteer (T1992). PC (positive control) for the P2X7 receptor used in these studies was myometrium. Following collection, the stem villous artery tissue was immediately snap frozen in liquid nitrogen and stored at -80^{0}C until processed. All tissue samples were homogenised using the ultra turrax method and all tissue lysates were IgG immunodepleted using a well-established immunoprecipitation protocol involving anti-human IgG (whole molecule)-agarose antibody developed in goat (Sigma, A3543). The proteins were resolved using a 10% hand casted polyacrylamide gel. The resolved proteins were transferred to the nitrocellulose membrane for a period of 60 minutes. Each well was loaded with 20µg of total protein **B**. The immunoblot was stripped and then reblotted with β actin for loading control (red box) **C**. Ponceau S staining of the nitrocellulose membrane prior to immunoblotting for the P2X7 receptor **D**. Coomassie blue staining of the 10% gel following the transfer of proteins to the nitrocellulose membrane. Antibodies used: P2X7 primary antibody (Rabbit polyclonal IgG, Alomone Labs, APR-004) at a dilution of 1:600, P2X7 secondary antibody (Polyclonal goat anti rabbit immunoglobulins alkaline phosphatase, Dako, D0487) at a dilution of 1:1000, β actin primary antibody (rabbit polyclonal IgG, Abcam, Ab8227) at a dilution of 1:8000 and β actin secondary antibody (Polyclonal goat anti rabbit immunoglobulins alkaline phosphatase, Dako, D0487) at a dilution of 1:1000.*

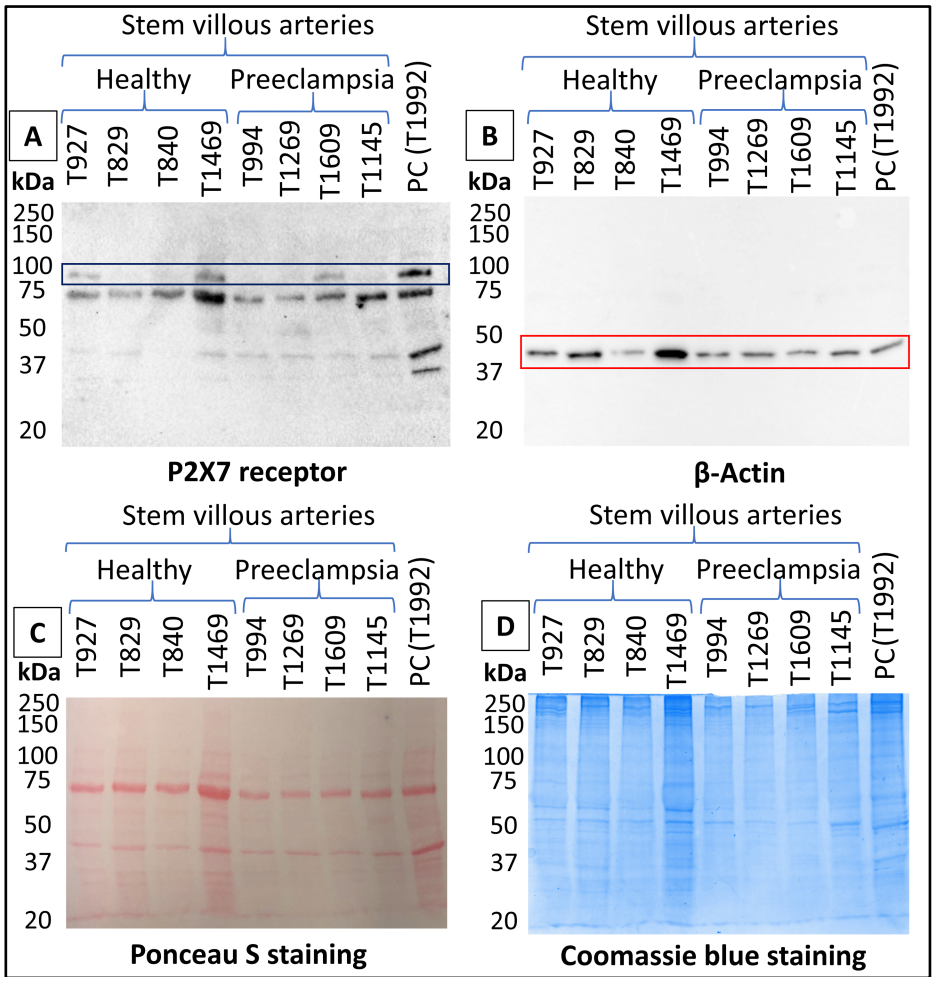


Figure 65. *This figure shows the P2X7 receptor protein expression levels (panel **A**, approximately 79kDa band -blue box) in the second pellet fraction of stem villous artery lysates originating from four placental samples of healthy patients (T927, T829, T840 and T1469) and four placental samples of preeclamptic patients (T994, T1269, T1609 and T1145) as well as myometrium tissue lysate originating from a healthy volunteer (T1992). PC (positive control) for the P2X7 receptor used in these studies was myometrium. Following collection, the stem villous artery tissue was immediately snap frozen in liquid nitrogen and stored at -80^{0}C until processed. All tissue samples were homogenised using the ultra turrax method and all tissue lysates were IgG immunodepleted using a well-established immunoprecipitation protocol involving anti-human IgG (whole molecule)-agarose antibody developed in goat (Sigma, A3543). The proteins were resolved using a 10% hand casted polyacrylamide gel. The resolved proteins were transferred to the nitrocellulose membrane for a period of 60 minutes. Each well was loaded with 20µg of total protein **B**. The immunoblot was stripped and then reblotted with β actin for loading control (red box) **C**. Ponceau S staining of the nitrocellulose membrane prior to immunoblotting for the P2X7 receptor **D**. Coomassie blue staining of the 10% gel following the transfer of proteins to the nitrocellulose membrane. Antibodies used: P2X7 primary antibody (Rabbit polyclonal IgG, Alomone Labs, APR-004) at a dilution of 1:600, P2X7 secondary antibody (Polyclonal goat anti rabbit immunoglobulins alkaline phosphatase, Dako, D0487) at a dilution of 1:1000, β actin primary antibody (rabbit polyclonal IgG, Abcam, Ab8227) at a dilution of 1:8000 and β actin secondary antibody (Polyclonal goat anti rabbit immunoglobulins alkaline phosphatase, Dako, D0487) at a dilution of 1:1000.*

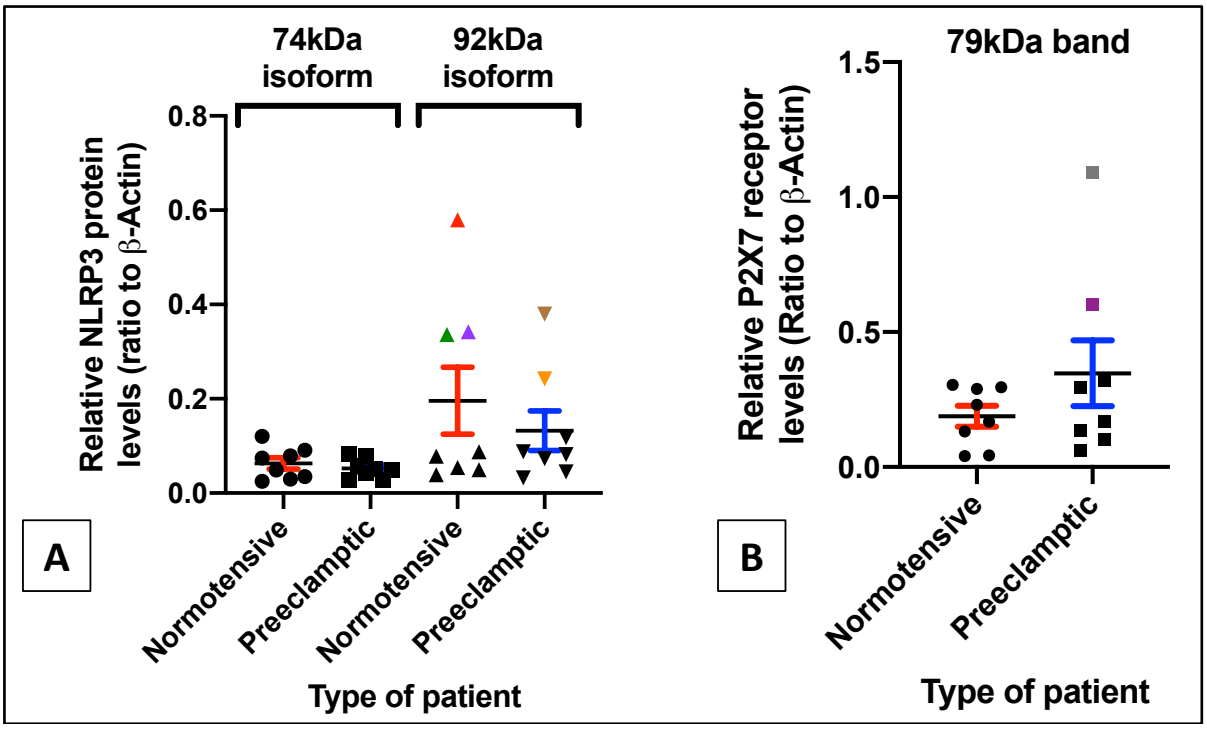


Figure 66. *Graphs highlighting the relative NLRP3 inflammasome protein expresson expression (panel **A**, approximately 74kDa and circa 92kDa isoforms) and P2X7 receptor levels (panel **B**, circa 79kDa band) normalised to β actin in stem villous artery tissue lysates originating from N=8 placental samples of healthy patients (T910, T952, T928, T962, T927, T829, T840 and T1469) and N=8 placental samples of preeclamptic patients (T997, T860, T853, T738, T994, T1269, T1609 and T1145). Three of the healthy and two of the preeclamptic patients which expressed particularly high relative NLRP3 inflammasome levels (approximately 92kDa isoform) in the second supernatant fraction of SVA lysate are as follows: T910 (red triangle), T952 (green triangle), T962 (violet triangle), T738 (brown triangle) and T997 (orange triangle). Similarly, two of the preeclamptic patients which expressed notably elevated relative P2X7 receptor protein expression levels in the second pellet fraction of SVA lysate are as follows: T860 (grey square), T1609 (purple square). Data are expressed as mean ± SEM.*

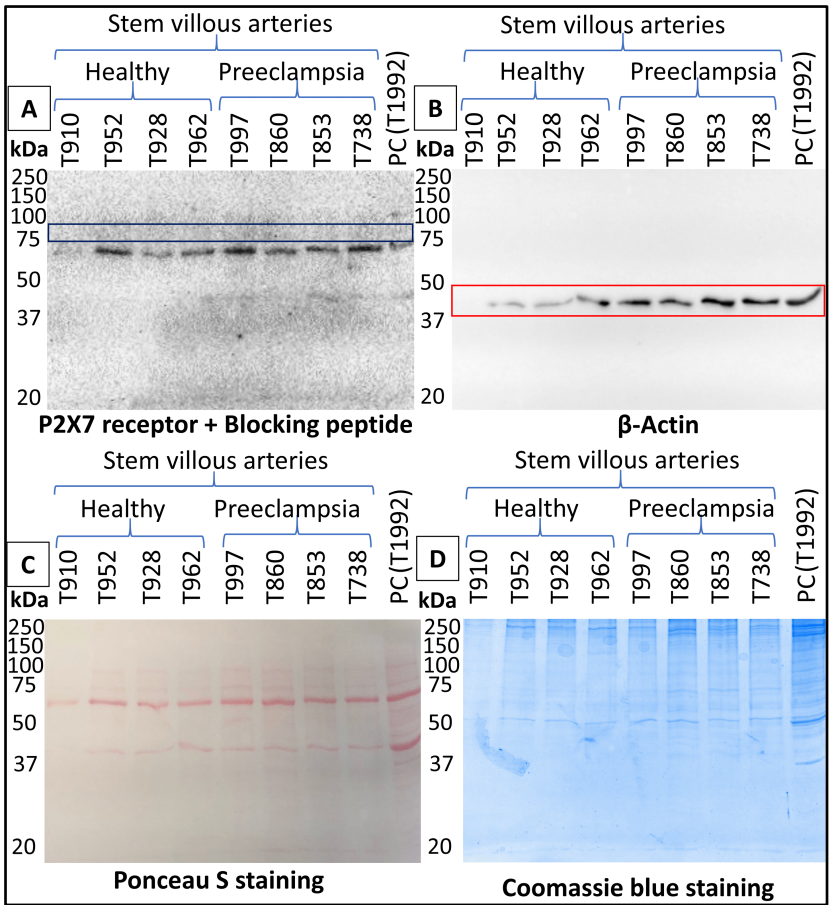


Figure 67. *This figure shows the P2X7 receptor protein expression levels (panel **A**, approximately 79kDa band -blue box) in the second pellet fraction of stem villous artery lysates originating from four placental samples of healthy patients (T910, T952, T928 and T962) and four placental samples of preeclamptic patients (T997, T860, T853 and T738) as well as myometrium tissue lysate originating from a healthy volunteer (T1992). In this case, the P2X7 receptor primary antibody was pre-absorbed with a blocking peptide (negative control). PC (positive control) for the P2X7 receptor used in these studies was myometrium. Following collection, the stem villous artery tissue was immediately snap frozen in liquid nitrogen and stored at -80^{0}C until processed. All tissue samples were homogenised using the ultra turrax method and all tissue lysates were IgG immunodepleted using a well-established immunoprecipitation protocol involving anti-human IgG (whole molecule)-agarose antibody developed in goat (Sigma, A3543). The proteins were resolved using a 10% hand casted polyacrylamide gel. The resolved proteins were transferred to the nitrocellulose membrane for a period of 60 minutes. Each well was loaded with 20µg of total protein **B**. The immunoblot was stripped and then reblotted with β actin for loading control (red box) **C**. Ponceau S staining of the nitrocellulose membrane prior to immunoblotting for the P2X7 receptor with blocking peptide **D**. Coomassie blue staining of the 10% gel following the transfer of proteins to the nitrocellulose membrane. Antibodies used: P2X7 primary antibody (Rabbit polyclonal IgG, Alomone Labs, APR-004) at a dilution of 1:600, P2X7 secondary antibody (Polyclonal goat anti rabbit immunoglobulins alkaline phosphatase, Dako, D0487) at a dilution of 1:1000, β actin primary antibody (rabbit polyclonal IgG, Abcam, Ab8227) at a dilution of 1:8000 and β actin secondary antibody (Polyclonal goat anti rabbit immunoglobulins alkaline phosphatase, Dako, D0487) at a dilution of 1:1000.*

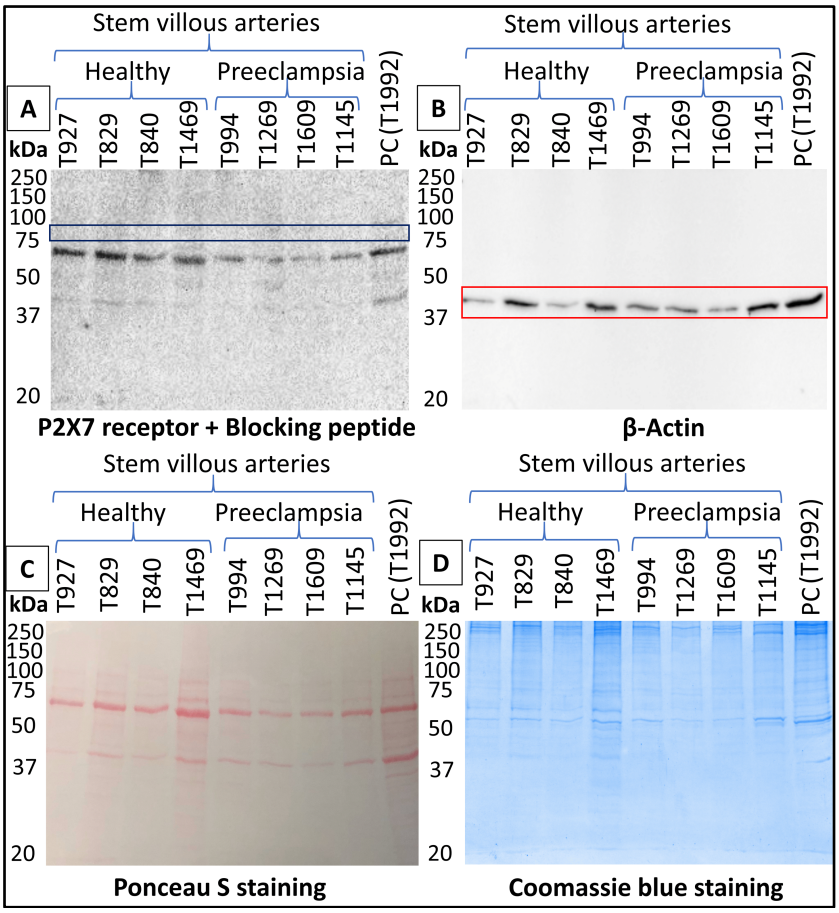


Figure 68. *This figure shows the P2X7 receptor protein expression levels (panel **A**, approximately 79kDa band -blue box) in the second pellet fraction of stem villous artery lysates originating from four placental samples of healthy patients (T927, T829, T840 and T1469) and four placental samples of preeclamptic patients (T994, T1269, T1609 and T1145) as well as myometrium tissue lysate originating from a healthy volunteer (T1992). In this case, the P2X7 receptor primary antibody was pre-absorbed with a blocking peptide (negative control). PC (positive control) for the P2X7 receptor used in these studies was myometrium. Following collection, the stem villous artery tissue was immediately snap frozen in liquid nitrogen and stored at -80^{0}C until processed. All tissue samples were homogenised using the ultra turrax method and all tissue lysates were IgG immunodepleted using a well-established immunoprecipitation protocol involving anti-human IgG (whole molecule)-agarose antibody developed in goat (Sigma, A3543). The proteins were resolved using a 10% hand casted polyacrylamide gel. The resolved proteins were transferred to the nitrocellulose membrane for a period of 60 minutes. Each well was loaded with 20µg of total protein **B**. The immunoblot was stripped and then reblotted with β actin for loading control (red box) **C**. Ponceau S staining of the nitrocellulose membrane prior to immunoblotting for the P2X7 receptor **D**. Coomassie blue staining of the 10% gel following the transfer of proteins to the nitrocellulose membrane. Antibodies used: P2X7 primary antibody (Rabbit polyclonal IgG, Alomone Labs, APR-004) at a dilution of 1:600, P2X7 secondary antibody (Polyclonal goat anti rabbit immunoglobulins alkaline phosphatase, Dako, D0487) at a dilution of 1:1000, β actin primary antibody (rabbit polyclonal IgG, Abcam, Ab8227) at a dilution of 1:8000 and β actin secondary antibody (Polyclonal goat anti rabbit immunoglobulins alkaline phosphatase, Dako, D0487) at a dilution of 1:1000.*

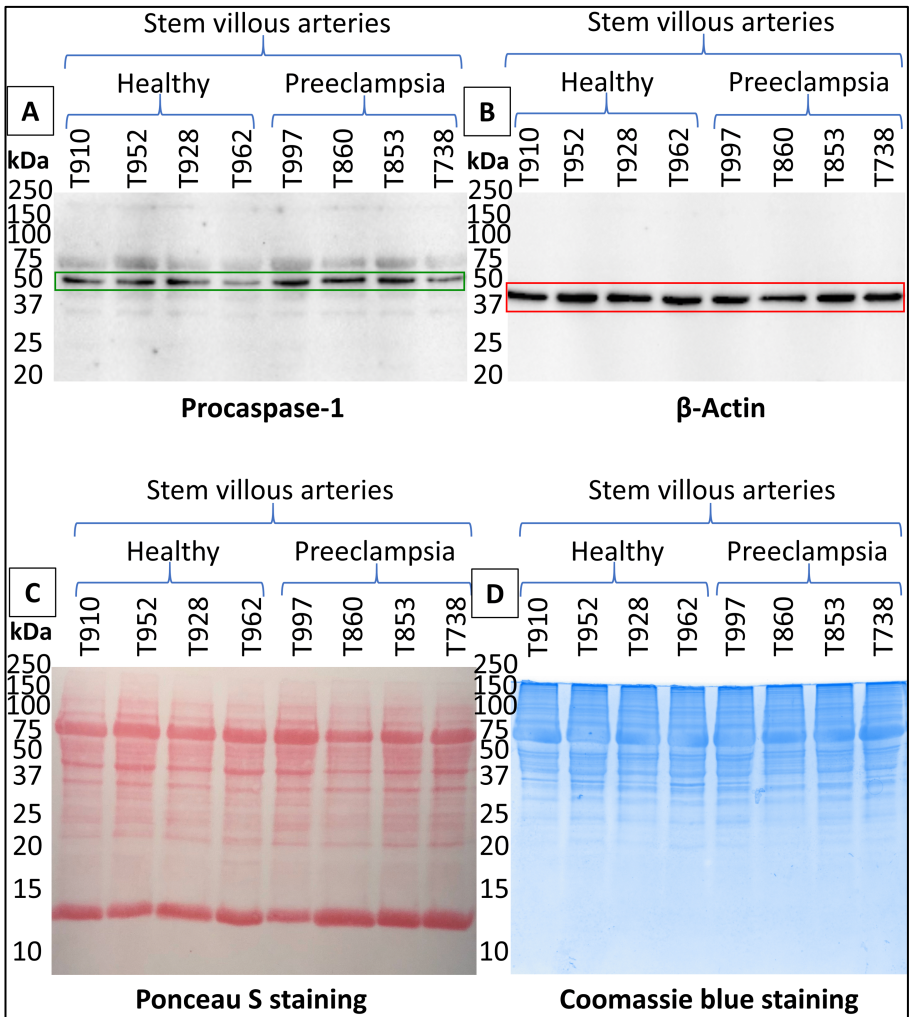


Figure 69. *This figure shows procaspase-1 protein expression levels (panel **A**, approximately 47kDa band -green box) in the second supernatant fraction of stem villous artery lysates originating from four placental samples of healthy patients (T910, T952, T928 and T962) and four placental samples of preeclamptic patients (T997, T860, T853 and T738). Following collection, the stem villous artery tissue was immediately snap frozen in liquid nitrogen and stored at -80^{0}C until processed. All tissue samples were homogenised using the ultra turrax method and all tissue lysates were IgG immunodepleted using a well-established immunoprecipitation protocol involving anti-human IgG (whole molecule)-agarose antibody developed in goat (Sigma, A3543). The proteins were resolved using a 15% hand casted polyacrylamide gel. The resolved proteins were transferred to the nitrocellulose membrane for a period of 60 minutes. Each well was loaded with 40µg of total protein **B**. The immunoblot was stripped and then reblotted with β actin for loading control (red box) **C**. Ponceau S staining of the nitrocellulose membrane prior to immunoblotting for procaspase-1 **D**. Coomassie blue staining of the 15% gel following the transfer of proteins to the nitrocellulose membrane. Antibodies used: procaspase-1 primary antibody (Rabbit polyclonal IgG, Bio Vision, 3019-100) at a concentration of 2µg/mL, procaspase-1 secondary antibody (Polyclonal goat anti rabbit immunoglobulins alkaline phosphatase, Dako, D0487) at a dilution of 1:1000, β actin primary antibody (rabbit polyclonal IgG, Abcam, Ab8227) at a dilution of 1:8000 and β actin secondary antibody (Polyclonal goat anti rabbit immunoglobulins alkaline phosphatase, Dako, D0487) at a dilution of 1:1000.*

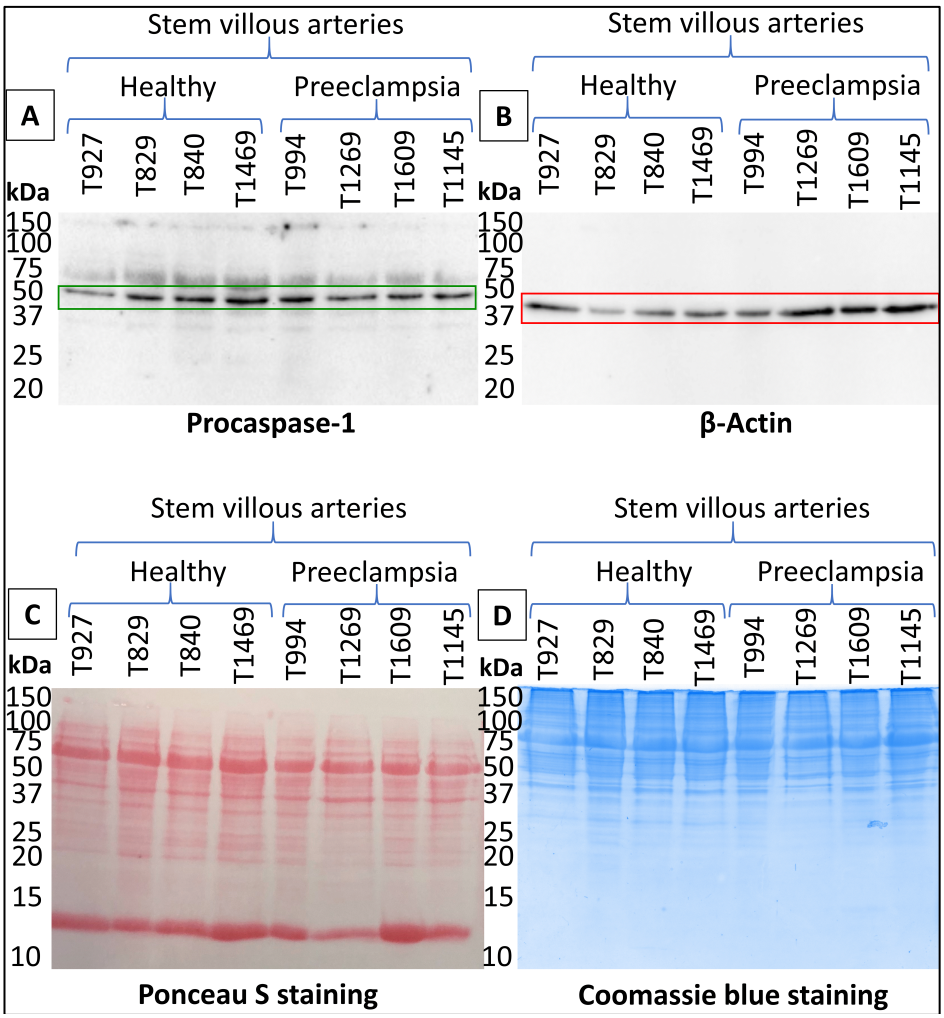


Figure 70. *This figure shows procaspase-1 protein expression levels (panel **A**, approximately 47kDa band -green box) in the second supernatant fraction of stem villous artery lysates originating from four placental samples of healthy patients (T927, T829, T840 and T1469) and four placental samples of preeclamptic patients (T994, T1269, T1609 and T1145). Following collection, the stem villous artery tissue was immediately snap frozen in liquid nitrogen and stored at -80^{0}C until processed. All tissue samples were homogenised using the ultra turrax method and all tissue lysates were IgG immunodepleted using a well-established immunoprecipitation protocol involving anti-human IgG (whole molecule)-agarose antibody developed in goat (Sigma, A3543). The proteins were resolved using a 15% hand casted polyacrylamide gel. The resolved proteins were transferred to the nitrocellulose membrane for a period of 60 minutes. Each well was loaded with 40µg of total protein **B**. The immunoblot was stripped and then reblotted with β actin for loading control (red box) **C**. Ponceau S staining of the nitrocellulose membrane prior to immunoblotting for procaspase-1 **D**. Coomassie blue staining of the 15% gel following the transfer of proteins to the nitrocellulose membrane. Antibodies used: procaspase-1 primary antibody (Rabbit polyclonal IgG, Bio Vision, 3019-100) at a concentration of 2µg/mL, procaspase-1 secondary antibody (Polyclonal goat anti rabbit immunoglobulins alkaline phosphatase, Dako, D0487) at a dilution of 1:1000, β actin primary antibody (rabbit polyclonal IgG, Abcam, Ab8227) at a dilution of 1:8000 and β actin secondary antibody (Polyclonal goat anti rabbit immunoglobulins alkaline phosphatase, Dako, D0487) at a dilution of 1:1000.*

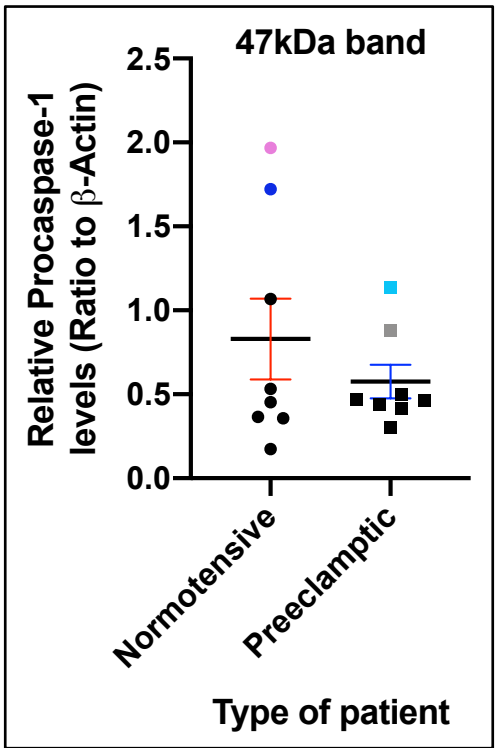


Figure 71. *Graph highlighting the relative procaspase-1 protein expression levels (approximately 47kDa band) normalised to β actin in stem villous artery tissue lysates originating from N=8 placental samples of healthy patients (T910, T952, T928, T962, T927, T829, T840 and T1469) and N=8 placental samples of preeclamptic patients (T997, T860, T853, T738, T994, T1269, T1609 and T1145). Two of the healthy and two of the preeclamptic patients which expressed particularly high relative procaspase-1 levels in the second supernatant of SVA lysate are as follows: T829 (pink circle), T1469 (dark blue circle), T994 (light blue square) and T860 (grey square). Data are expressed as mean ± SEM.*

3.3.7 Investigating the relative mRNA expression levels of the P2X7 receptor, NLRP3 inflammasome and caspase-1 in stem villous arteries originating from 2 healthy and 2 preeclamptic placental samples

The relative mRNA expression levels of the P2X7 receptor, NLRP3 inflammasome and caspase-1 which have been normalised to the reference genes HPRT1, CYC1 and TOP1 originating from 2 healthy and 2 preeclamptic placental samples are presented in figure 72 (panel A). The P2X7 receptor mRNA levels were lower in preeclamptic compared to healthy placental samples, whereas the NLRP3 inflammasome and caspase-1 mRNA expression level showed a marked upregulation in preeclamptic placental samples. The totRNA yield from the stem villous artery tissue samples was as follows: healthy patients (T910 was 242.84 ng/μL, T952 was 130.46ng/μL) and preeclamptic patients (T853 was 195.86ng/μL, T738 was 262.47ng/μL). The spectrophotometric experiments showed RNA with the following absorbance ratios (A_{260}/A_{280}) as follows: healthy patients (T910 was 2.03, T952 was 1.95) and preeclamptic patients (T853 was 2.15 and T738 was 2.11). These results showed that the totRNAs possessed an excellent quality and were largely free of DNA contamination. Typical 1% (w/v) agarose gel electrophoresis of the heathy SVA samples did not show any RNA degradation prior to use for reverse transcription as highlighted in figure 72 (panel B). In this case, the integrity of extracted RNA highlighted clear 28S and 18S rRNA bands. Furthermore, the PCR efficiency of the P2X7 receptor and NLRP3 inflammasome assays determined from the slope of the standard curves of the serial dilutions highlighted a similar performance of the polymerase chain reaction assays (table 10). All three chosen reference genes

showed ubiquitous expression and were moderately expressed in all SVA tissue samples studied with C_q values varying from 23-29 (representative amplification plots presented in appendix 8). As a result, the P2X7 receptor, NLRP3 inflammasome and caspase-1 were found to be expressed at an mRNA level in stem villous arteries originating from 2 healthy and 2 pre-eclamptic patients assessed using RT-qPCR.

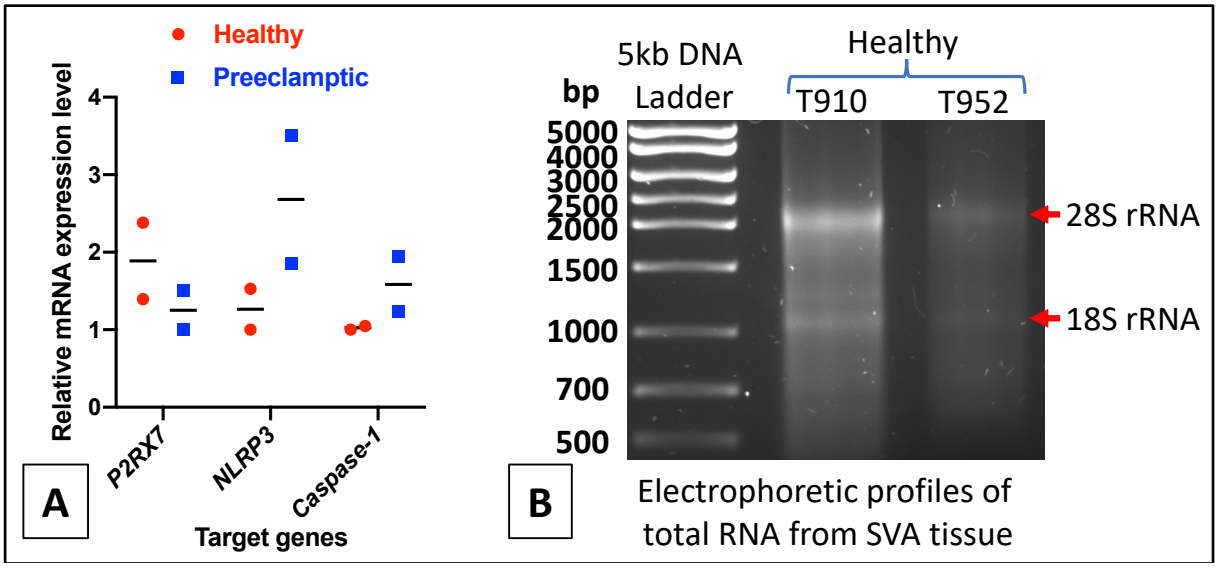


Figure 72. *This figure shows the relative mRNA expression levels of the P2X7 receptor, NLRP3 inflammasome and caspase-1 in stem villous artery originating from 2 healthy and 2 preeclamptic placental samples (**A**) and the RNA integrity assessment of SVA (healthy patients) using 1% (w/v) agarose gel electrophoresis (**B**). The respective ribosomal RNA's appeared as sharp bands. Data are expressed as mean ± S.E.M. bp denotes base pairs.*

Gene	Slope	Assay efficiency (%)	Correlation coefficient (r^2)
P2RX7	-3.885	80.88	0.9993
NLRP3	-3.305	100.69	0.9669

Table 10. *This table highlights the PCR efficiency of P2RX7 and NLRP3 target genes by presenting their corresponding slope and r^2 correlation coefficients. Both P2X7 and NLRP3 gene assays possessed efficiencies within the desired spectrum of 80-115%.*

3.3.8 LPS+ATP stimulation elicited the highest IL-1β release from CPA, SVA and trophoblast tissue originating from 10 healthy placental samples

The levels of released IL-1β, IL-6 and IL-18 in the culture media of CPA, SVA and trophoblast tissue which have been stimulated with RPMI 1640 media supplemented with 100U/mL penicillin, 100μg/mL streptomycin and either ATP, LPS+ATP or LPS+BzATP originating from 10 healthy placental samples are presented in figure 73. IL-1β release was the highest in CPA, SVA and trophoblast tissue stimulated with LPS+ATP compared to control, ATP or LPS+BzATP. ATP did not elicit a statistically significant difference in IL-1β, IL-6 and IL-18 release levels relative to their corresponding control in CPA, SVA and trophoblast tissue. LPS+ATP stimulation induced a statistically significant difference in IL-1β release levels relative to the corresponding control in CPA, SVA and trophoblast tissue (table 11). LPS+ATP and LPS+BzATP stimulations did not induce a statistically significant difference in IL-6 release levels relative to their corresponding control in CPA, SVA and trophoblast tissue. However, there was a statistically significant difference in IL-6 release levels between ATP vs. LPS+ATP (**P=0.0062) in the case of SVA and ATP vs. LPS+BzATP (*P=0.0115) in the case of trophoblast tissue as illustrated in table 12. ATP, LPS+ATP and LPS+BzATP stimulations did not elicit a statistically significant difference in IL-18 release levels relative to their corresponding control in all placental tissue types studied. Multiple statistically significant differences (Dunn's and Dunnett's T3 multiple comparison tests) were found in released IL-1β (table 11), IL-6 (table 12) and IL-18 (table13) levels in the culture media accross CPA, SVA and trophoblast tissue which

have been stimulated with RPMI 1640 media supplemented with 100U/mL penicillin, 100μg/mL streptomycin and either ATP, LPS+ATP or LPS+BzATP.

As a result, the stimulation of CPA, SVA and villous tissue with LPS+ATP elicited the highest IL-1β release compared to stimulation of LPS+BzATP, ATP or control in all three human placental tissue types studied.

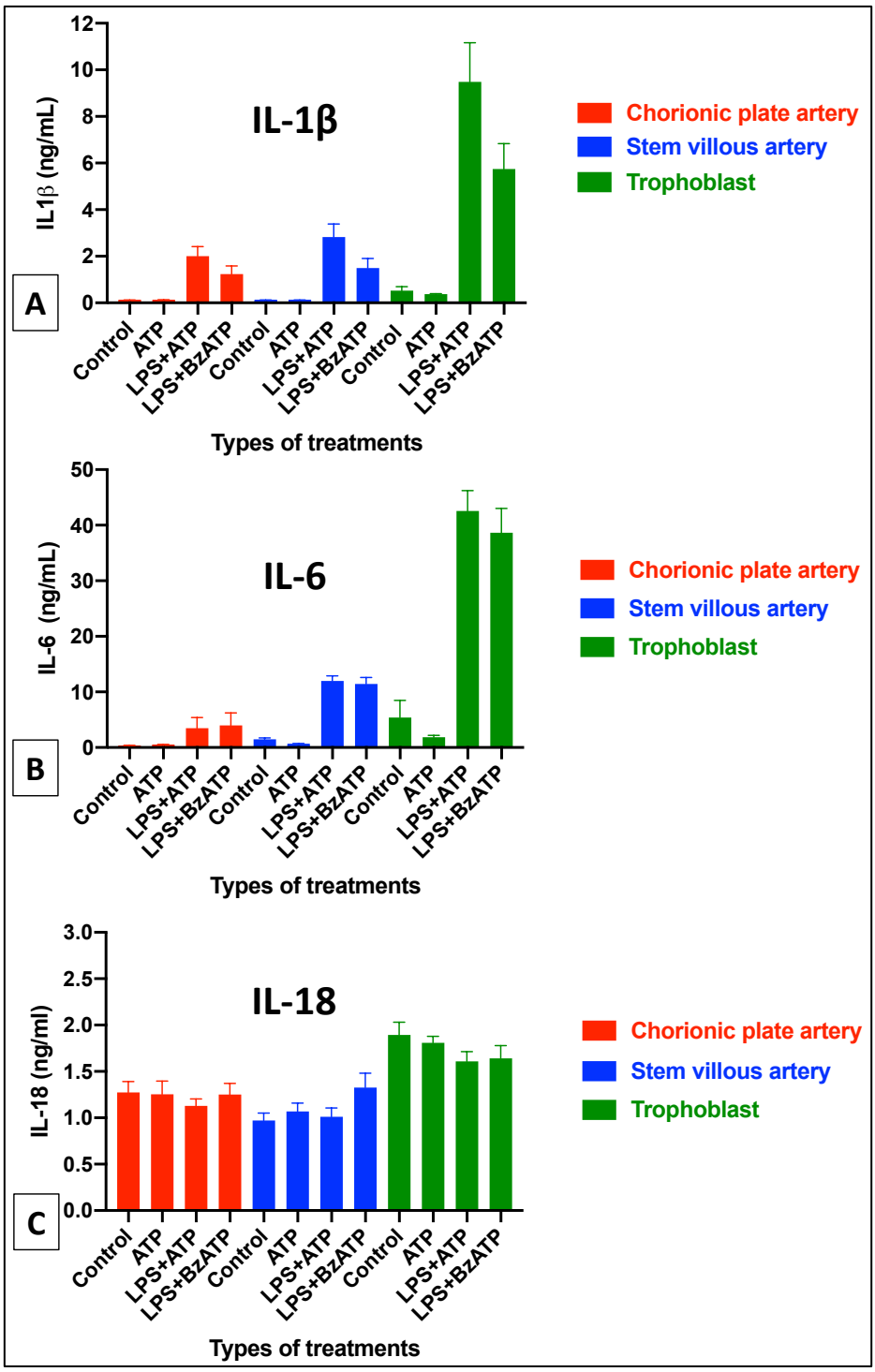


Figure 73. *This figure shows the levels of released IL-1β (panel **A**), IL-6 (panel **B**) and IL-18 (panel **C**) in the culture media from chorionic plate artery, stem villous artery and trophoblast tissue which have been stimulated with RPMI 1640 media+100 units/mL penicillin and 100μg/mL streptomycin for 4 hours (control), ATP (10mM) for 4 hours, LPS (10μg/mL) (3.5 hours) +ATP (10mM) (0.5 hours) or LPS (10μg/mL) (3.5 hours) +BzATP (300μM) (0.5 hours) originating from 10 healthy patients. Data are expressed as mean ± SEM. CPA and SVA originated from the following healthy patients: T2878, T2879, T2880, T2881, T2884, T2885, T2886, T2887, T2888, T2889. Trophoblast tissue originated from the following healthy patients: T2884, T2885, T2886, T2887, T2888, T2889, T2890, T2891, T2892 and T2893.*

	P Value
Control (CPA) vs. LPS+ATP (CPA)	*P=0.0139
Control (CPA) vs. LPS+ATP (SVA)	**P=0.0020
Control (CPA) vs. LPS+ATP (Trophoblast tissue)	****P<0.0001
Control (CPA) vs. LPS+BzATP (Trophoblast tissue)	****P<0.0001
ATP (CPA) vs. LPS+ATP (CPA)	*P=0.0174
ATP (CPA) vs. LPS+ATP (SVA)	**P=0.0026
ATP (CPA) vs. LPS+ATP (Trophoblast tissue)	****P<0.0001
ATP (CPA) vs. LPS+BzATP (Trophoblast tissue)	****P<0.0001
LPS+ATP (CPA) vs. Control (SVA)	***P=0.0006
LPS+ATP (CPA) vs. ATP (SVA)	**P=0.0020
LPS+BzATP (CPA) vs. Control (SVA)	**P=0.0087
LPS+BzATP (CPA) vs ATP (SVA)	*P=0.0265
Control (SVA) vs. LPS+ATP (SVA)	****P<0.0001
Control (SVA) vs. LPS+BzATP (SVA)	**P=0.0052
Control (SVA) vs. LPS+ATP (Trophoblast tissue)	****P<0.0001
Control (SVA) vs. LPS+BzATP (Trophoblast tissue)	****P<0.0001
ATP (SVA) vs. LPS+ATP (SVA)	***P=0.0002
ATP (SVA) vs. LPS+BzATP (SVA)	*P=0.0164
ATP (SVA) vs. LPS+ATP (Trophoblast tissue)	****P<0.0001
ATP (SVA) vs. LPS+BzATP (Trophoblast tissue)	****P<0.0001
Control (Trophoblast tissue) vs. LPS+ATP (Trophoblast tissue)	*P=0.0168
ATP (Trophoblast tissue) vs. LPS+ATP (Trophoblast tissue)	**P=0.0098

Table 11. *This table shows the statistically significant results of Dunn's multiple comparison tests between the levels of released IL-1β in the culture media from chorionic plate artery (CPA), stem villous artery (SVA) and trophoblast tissue which have been stimulated with RPMI 1640 media* supplemented with 100U/mL penicillin, 100µg/mL streptomycin *(control), ATP, LPS+ATP or LPS+BzATP originating from 10 healthy patients. A Shapiro Wilk test highlighted that the data was not normally distributed (LPS+BzATP stimulation of CPA **P=0.0086, control stimulation of SVA ***P=0.0002, ATP stimulation of SVA **P=0.0046, LPS+BzATP stimulation of SVA *P=0.0499, control stimulation of villous tissue ****P<0.0001 and LPS+BzATP stimulation of villous tissue *P=0.0488), hence a non-parametric Dunn's multiple comparison test was conducted by comparing the mean rank of each column with the mean rank of every other column. *P*≤0.05, ** P≤0.01, *** P≤0.001, **** P≤0.0001.

	P Value
Control (CPA) vs. LPS+ATP (SVA)	***P=0.0001
Control (CPA) vs. LPS+BzATP (SVA)	***P=0.0002
Control (CPA) vs. LPS+ATP (Trophoblast tissue)	****P<0.0001
Control (CPA) vs. LPS+BzATP (Trophoblast tissue)	****P<0.0001
ATP (CPA) vs. LPS+ATP (SVA)	***P=0.0002
ATP (CPA) vs. LPS+BzATP (SVA)	***P=0.0002
ATP (CPA) vs. LPS+ATP (Trophoblast tissue)	****P<0.0001
ATP (CPA) vs. LPS+BzATP (Trophoblast tissue)	****P<0.0001
LPS+ATP (CPA) vs. LPS+ATP (Trophoblast tissue)	*P=0.0269
LPS+BzATP (CPA) vs. LPS+ATP (Trophoblast tissue)	*P=0.0181
LPS+BzATP (CPA) vs. LPS+BzATP (Trophoblast tissue)	*P=0.0385
Control (SVA) vs. LPS+ATP (Trophoblast tissue)	**P=0.0035
Control (SVA) vs. LPS+BzATP (Trophoblast tissue)	**P=0.0080
ATP (SVA) vs. LPS+ATP (SVA)	**P=0.0062
ATP (SVA) vs. LPS+BzATP (SVA)	**P=0.0069
ATP (SVA) vs. LPS+ATP (Trophoblast tissue)	****P<0.0001
ATP (SVA) vs. LPS+BzATP (Trophoblast tissue)	****P<0.0001
ATP (Trophoblast tissue) vs. LPS+ATP (Trophoblast tissue)	*P=0.0115
ATP (Trophoblast tissue) vs. LPS+BzATP (Trophoblast tissue)	*P=0.0250

Table 12*. This table shows the statistically significant results of Dunn's multiple comparison tests between the levels of released IL-6 in the culture media from chorionic plate artery (CPA), stem villous artery (SVA) and trophoblast tissue which have been stimulated with RPMI 1640 media* supplemented with 100U/mL penicillin, 100µg/mL streptomycin *(control), ATP, LPS+ATP or LPS+BzATP originating from 10 healthy patients. A Shapiro Wilk test highlighted that the data was not normally distributed (ATP stimulation of CPA ***P=0.0004, LPS+ATP stimulation of CPA ****P<0.0001, LPS+BzATP stimulation of CPA ****P<0.0001, control stimulation of villous tissue ****P<0.0001), hence a non-parametric Dunn's multiple comparison test was conducted by comparing the mean rank of each column with the mean rank of every other column. * P*≤0.05, ** P≤0.01, *** P≤0.001, **** P≤0.0001.

	P Value
LPS+ATP (CPA) vs. Control (Trophoblast tissue)	*P=0.0121
LPS+ATP (CPA) vs. ATP (Trophoblast tissue)	***P=0.0002
Control (SVA) vs. Control (Trophoblast tissue)	**P=0.0021
Control (SVA) vs. ATP (Trophoblast tissue)	****P<0.0001
Control (SVA) vs. LPS+ATP (Trophoblast tissue)	**P=0.0083
Control (SVA) vs. LPS+BzATP (Trophoblast tissue)	*P=0.0389
ATP (SVA) vs. Control (Trophoblast tissue)	**P=0.0073
ATP (SVA) vs. ATP (Trophoblast tissue)	***P=0.0004
LPS+ATP (SVA) vs. Control (Trophoblast tissue)	**P=0.0040
LPS+ATP (SVA) vs. ATP (Trophoblast tissue)	***P=0.0002
LPS+ATP (SVA) vs. LPS+ATP (Trophoblast tissue)	*P=0.0230

Table 13*. This table shows the statistically significant results of Dunnett's T3 multiple comparison tests between the levels of released IL-18 in the culture media from chorionic plate artery (CPA), stem villous artery (SVA) and trophoblast tissue which have been stimulated with RPMI 1640 media* supplemented with 100U/mL penicillin, 100µg/mL streptomycin *(control), ATP, LPS+ATP or LPS+BzATP originating from 10 healthy patients. A Shapiro Wilk test highlighted that all data was normally distributed, hence a parametric Dunnett's T3 multiple comparison test was conducted by comparing the mean rank of each column with the mean rank of every other column.** *P*≤0.05, ** P≤0.01, *** P≤0.001, **** P≤0.0001.

3.3.9 Human chorionic plate artery smooth muscle cells isolated using an enzymatic digestion method are positive for α-actin, P2X7 receptor and vimentin but not CD31

Immunocytochemistry revealed that isolated chorionic plate artery smooth muscle cells (CPA-SMC) originating from a healthy placenta sample (T3012) using an enzymatic digestion method were positive for α smooth muscle actin, P2X7 receptor and vimentin and negative for CD31 as highlighted in figures 74-77. In this case, CPA-SMC showed an uniform immunostaining for α smooth muscle actin localised at the level of the microfilament bundles which were evenly distributed along the cytoplasmic compartment of the primary cells (figure 74). The P2X7 receptor was immunolocalised at the level of the CPA-SMC plasma membrane as a punctate staining which was particularly clustered inside the nucleus (figure 75). No signal was detected in the absence of the P2X7 receptor primary antibody as highlighted in figure 77 (panels D-F). CPA-SMC stained positive for vimentin which was clearly immunolocalised at the level of the plasma membrane (figure 76). The isolated primary placental chorionic plate artery smooth muscle cells stained negative for CD31 as illustrated in figure 77 (panels A-C). In this case, all fluorescent micrographs of α smooth muscle actin, P2X7 receptor, vimentin and CD31 presented in figures 74-77 were acquired using a Zeiss LSM880 confocal laser scanning microscope.

As a result, the P2X7 receptor has been shown to be expressed on human placental chorionic plate arteries smooth muscle cells which have been isolated using an enzymatic digestion method assessed using immunocytochemistry.

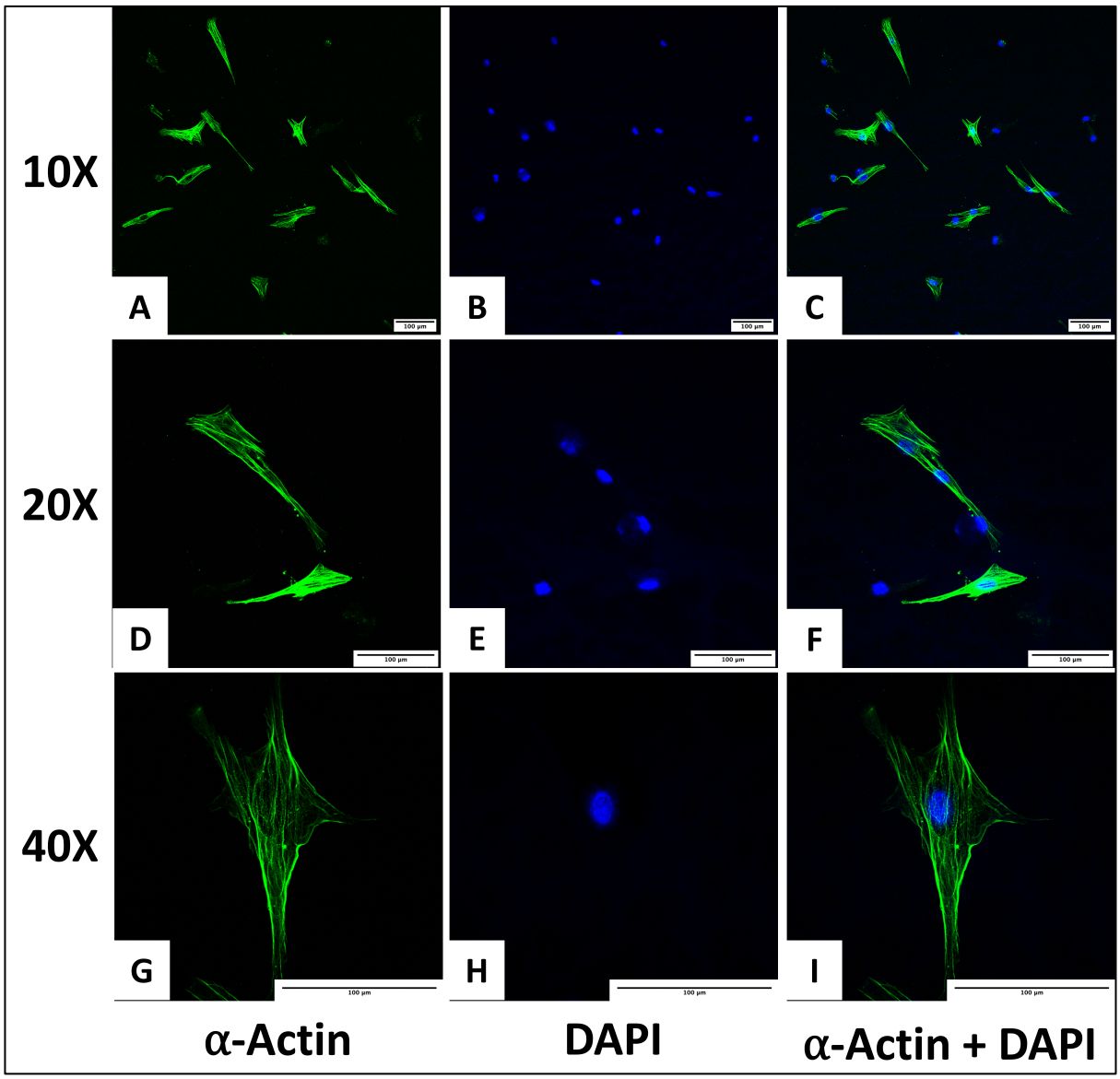


Figure 74. *Confocal microscopy of immunofluorescent staining of α smooth muscle actin (green) in chorionic plate artery smooth muscle cells (isolated using an enzymatic digestion method) grown on coverslips. The primary placental cells showed an uniform filamentous expression of α smooth muscle actin. Scalebar 100μm. Nuclear DAPI staining is blue.* ***A-C*** *10X magnification,* ***D-F*** *20X magnification,* ***G-I*** *40X magnification. All fluorescent micrographs were acquired using Zeiss LSM880 confocal laser scanning microscope.*

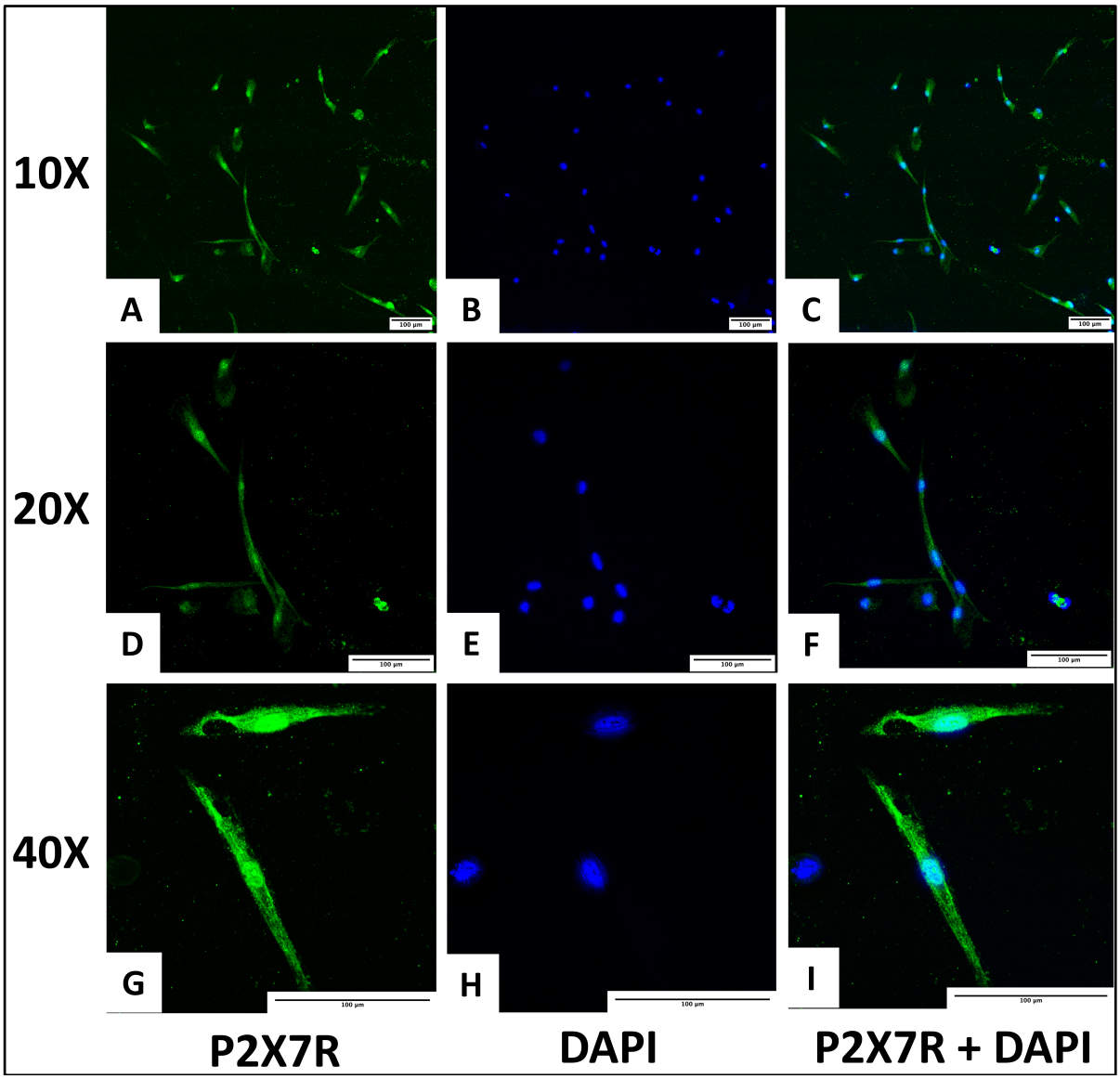


Figure 75. *Confocal microscopy of immunofluorescent staining of the P2X7 receptor (green) in chorionic plate artery smooth muscle cells (isolated using an enzymatic digestion method) grown on coverslips. Immunofluorescence data highlighted that the P2X7 receptor was localised on the cell body but more intense at the level of the nucleus. Scalebar 100μm. Nuclear DAPI staining is blue.* ***A-C*** *10X magnification,* ***D-F*** *20X magnification,* ***G-I*** *40X magnification. All fluorescent micrographs were acquired using Zeiss LSM880 confocal laser scanning microscope.*

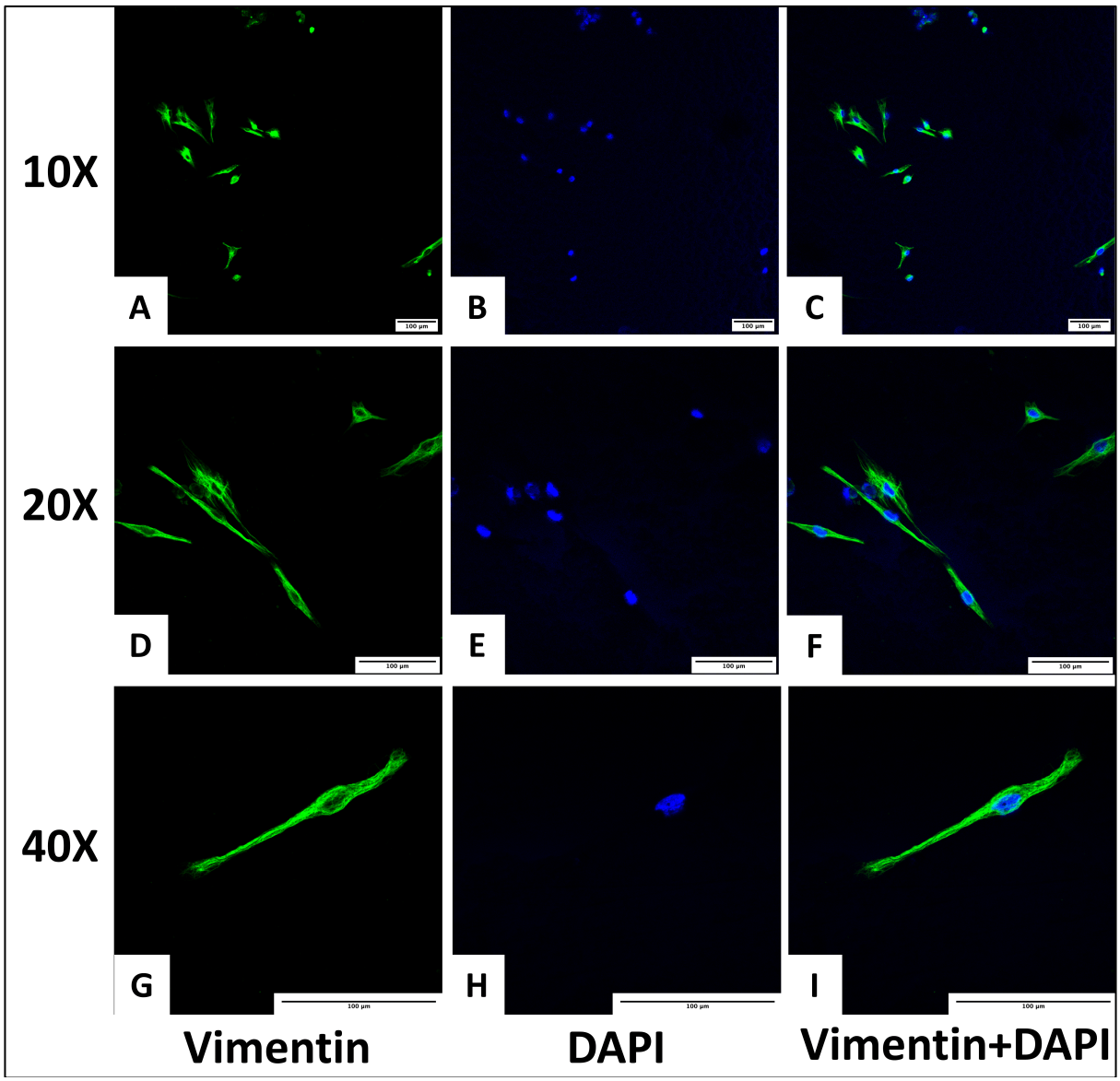


Figure 76. *Confocal microscopy of immunofluorescent staining of vimentin (green) in chorionic plate artery smooth muscle cells (isolated using an enzymatic digestion method) grown on coverslips. Vimentin was confined to the body of the primary cell. Scalebar 100μm. Nuclear DAPI staining is blue.* ***A-C*** *10X magnification,* ***D-F*** *20X magnification,* ***G-I*** *40X magnification. All fluorescent micrographs were acquired using Zeiss LSM880 confocal laser scanning microscope.*

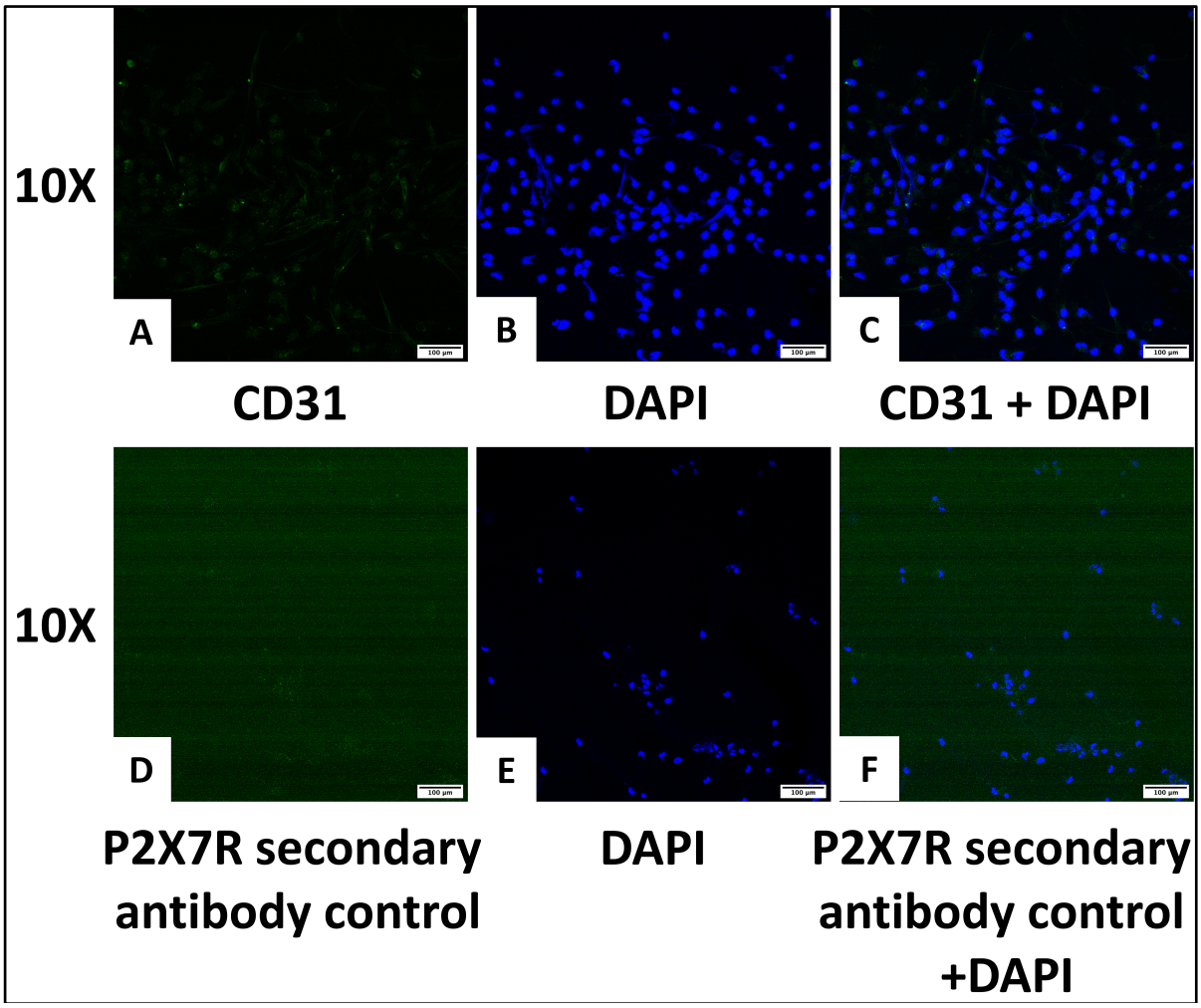


Figure 77. *Confocal microscopy of immunofluorescent staining of CD31 (**A-C**) and P2X7 receptor secondary antibody control **(D-F)** in chorionic plate artery smooth muscle cells (isolated using an enzymatic digestion method) grown on coverslips. The primary placental cells did not stain positive for the endothelial cell marker CD31. No green-fluorescent staining was observed in the P2X7 receptor secondary antibody control (panels D-F). Scalebar 100μm. Nuclear DAPI staining is blue. All fluorescent micrographs were acquired at 10X magnification using Zeiss LSM880 confocal laser scanning microscope.*

3.3.10 Chorionic plate artery smooth muscle cells isolated using the tissue explant method are positive for the P2X7 receptor and vimentin and negative for the NLRP3 inflammasome

Immunocytochemistry showed that the chorionic plate artery smooth muscle cells isolated using the tissue explant method originating from a healthy placenta sample (T3023) were positive for the P2X7 receptor and vimentin and negative for the NLRP3 inflammasome as highlighted in figure 78. The distribution of the P2X7 receptor highlighted a diffuse staining across the primary cell body with a particularly intense stain at the level of the nucleus (figure 78, panel A). In this case, the nucleus was also labelled with DAPI (blue) and the merged micrographs do show co-localisation with the P2X7 receptor (figure 78, panel C). The CPA-SMC cells also stained positive for vimentin which was immunolocalised at the level of the cell body (figure 78, panel E). The primary placental cells did not stain positive for the NLRP3 inflammasome as illustrated in figure 78 (panel E). No signal was detected in the absence of the primary antibody against the P2X7 receptor (P2X7 receptor secondary antibody control) as presented in figure 79 (panel A). Similarly, no signal was observed in the absence of the primary antibody against vimentin (vimentin secondary antibody control) as shown in figure 79 (panel E). Here, all micrographs were acquired using Zeiss LSM Exciter widefield microscope.

As a result, the P2X7 receptor has been shown to be expressed in human placenta chorionic plate arteries smooth muscle cells which have been isolated via a tissue explant method assessed using immunocytochemistry.

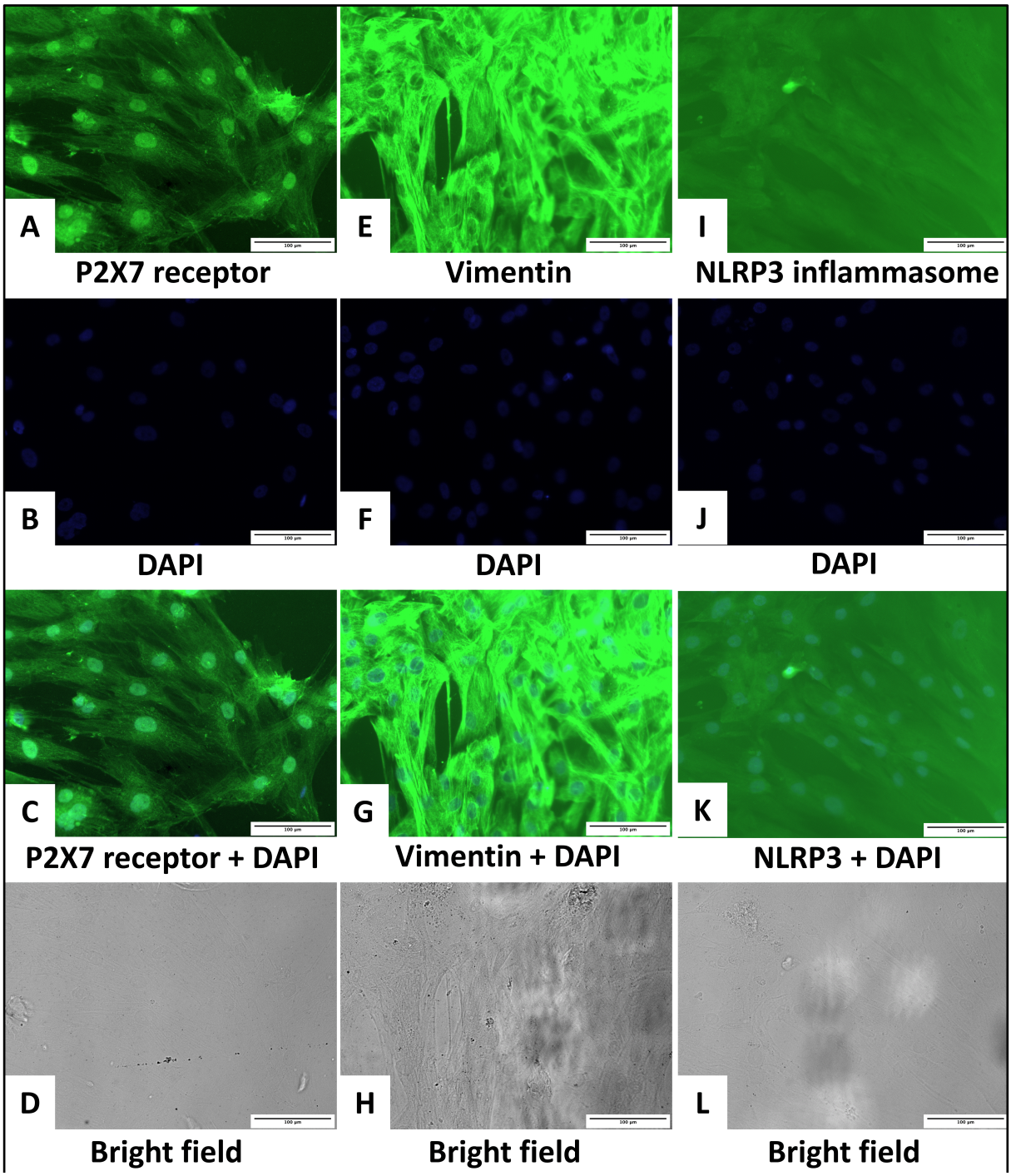


Figure 78. *Immunocytochemistry showing expression of the P2X7 receptor (**A-D**), vimentin (**E-H**) and NLRP3 inflammasome (**I-L**) in cultured CPA-SMC cells originating from a healthy patient (T3023) which have been isolated using the tissue explant method. The P2X7 receptor did overlap with DAPI stain denoting some nuclear expression. CPA-SMC's stained positive for vimentin which was localised across the cell body. The primary placental cells did not stain positive for the NLRP3 inflammasome. Scalebar 100µm. Nuclear DAPI staining is blue. All micrographs were acquired at 20X magnification using Zeiss LSM Exciter widefield microscope.*

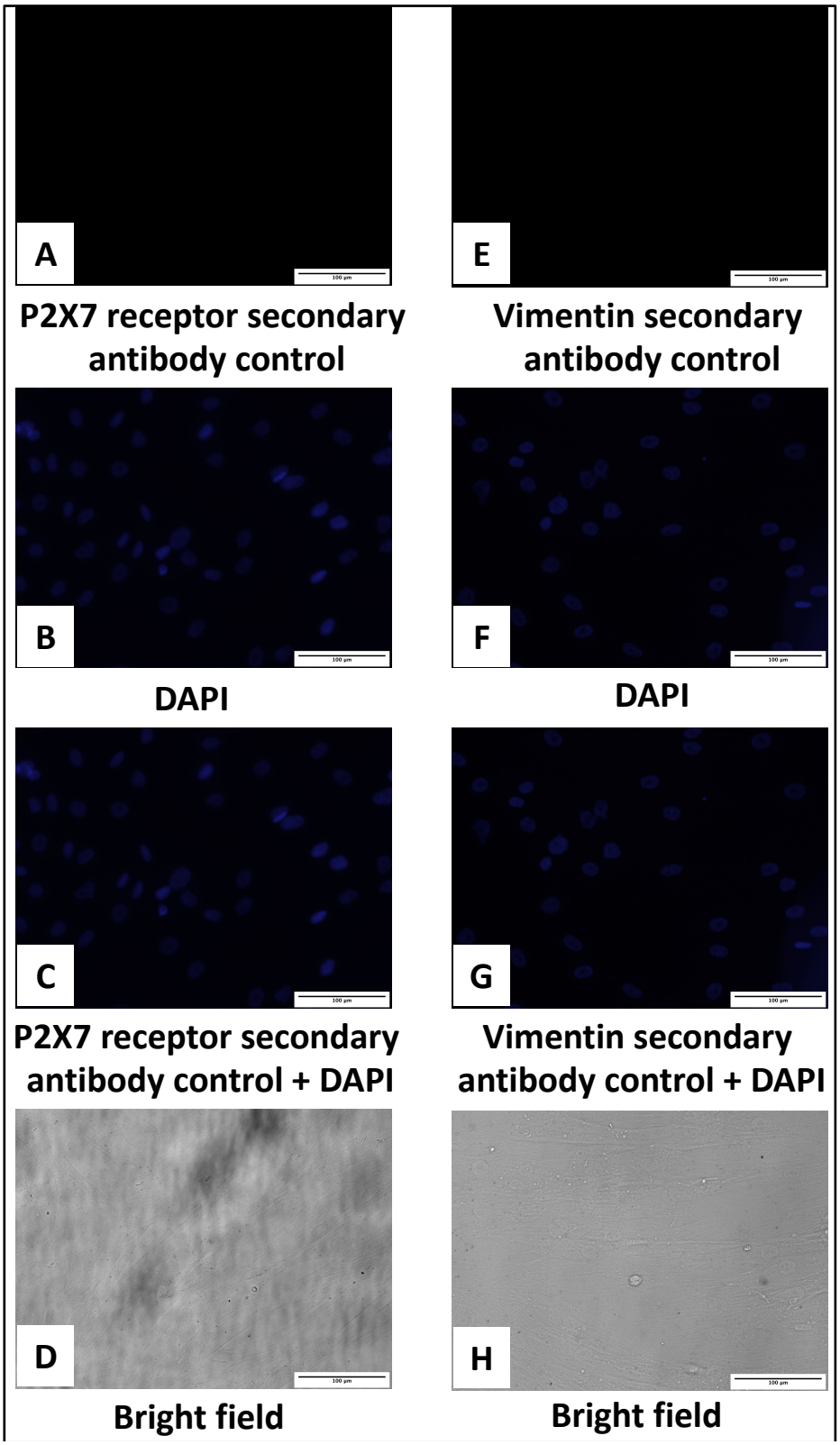


Figure 79. *Immunocytochemistry showing expression of the P2X7 receptor and vimentin in cultured CPA-SMC cells originating from a healthy patient (T3023) which have been isolated using the tissue explant method. Here, the primary antibody against the P2X7 receptor and vimentin were absent, therefore no signal was detected. Scalebar 100µm. Nuclear DAPI staining is blue. All micrographs were acquired at 20X magnification using Zeiss LSM Exciter widefield microscope.*

3.3.11 Stimulation of chorionic plate artery smooth muscle cells with 100μM ATP for 4 hours gives rise to a localised increase in the P2X7 receptor density (punctuate staining) that is clustered around the nuclear membrane

Stimulated chorionic plate artery smooth muscle cells with ATP at concentrations of 1μM, 10μM or 100μM for 4 hours resulted in the formation of numerous P2X7 receptor distinct clusters relative to control (DMEM low glucose media) as highlighted by the fluorescent micrographs presented in figure 80 and figure 85 (panels A-D). The distribution of the P2X7 receptor clustering was characterised as a dense punctuate staining which was present across the primary cell body particularly around the nucleus (figure 80). A notable decrease in the abundance of the P2X7 receptor cluster formation was observed in stimulated CPA-SMC cells with the same 100μM ATP concentration for 0.5 hours compared to 4 hours (P=0.2270; two-tailed Mann Whitney test) as suggested by the fluorescent micrographs presented in figure 81. However, a statistically significant increase (two-tailed Mann Whitney test) in P2X7 receptor MFI levels took place between 0.5 hours and 4 hours of ATP stimulations with 1μM (****P<0.0001) or 10μM (****P<0.0001). The incubation of CPA-SMC cells with 1μM A740003 (highly selective P2X7 receptor antagonist) for 3.5 hours followed by the stimulation of the primary placental cells with ATP (100μM) for 0.5 hours did not fundamentally alter the presence (P=8169; two-tailed Mann Whitney test) of P2X7 receptor cluster formation or distribution on the primary placental cell body compared to ATP stimulation (100μM) of 4 hours as illustrated by figure 82.

The stimulation of CPA-SMC cells with 10μM or 300μM BzATP for 0.5 hours gave rise to the formation of P2X7 receptor clusters relative to control (DMEM low

glucose media) in areas adjacent to the nucleus as highlighted by the fluorescent micrographs illustrated in figure 83 (panels E-L). CPA-SMC cells stimulated with 1μM BzATP for 0.5 hours did not induce the formation of the P2X7 receptor clusters characterised by a dense punctuate staining on the primary placental cell body as illustrated in figure 83 (panels A-D). The incubation of CPA-SMC with 1μM A740003 for 3.5 hours followed by the stimulation of the primary placental cells with BzATP (1μM, 10μM and 300μM) for 0.5 hours did not fundamentally alter the immunolocalization of the P2X7 receptor on the smooth muscle cell body compared to BzATP (1μM, 10μM or 300μM) of 0.5 hours as presented in figure 84. The stimulation of CPA-SMC cells with either DMEM low glucose media + 0.1% (v/v) DMSO or DMEM low glucose media + 1μM A740003 for 4 hours gave rise to a reduced P2X7 receptor cluster formation which was immunolocalised in areas close to the nuclear membrane as illustrated in figure 85 (panels E-L).

As a result, isolated human placenta chorionic plate artery smooth muscle cells which have been stimulated with ATP at concentrations of 1μM, 10μM or 100μM gave rise to a clustered distribution of the P2X7 receptor characterised by a punctuate staining present on the cell body in association with the nucleus.

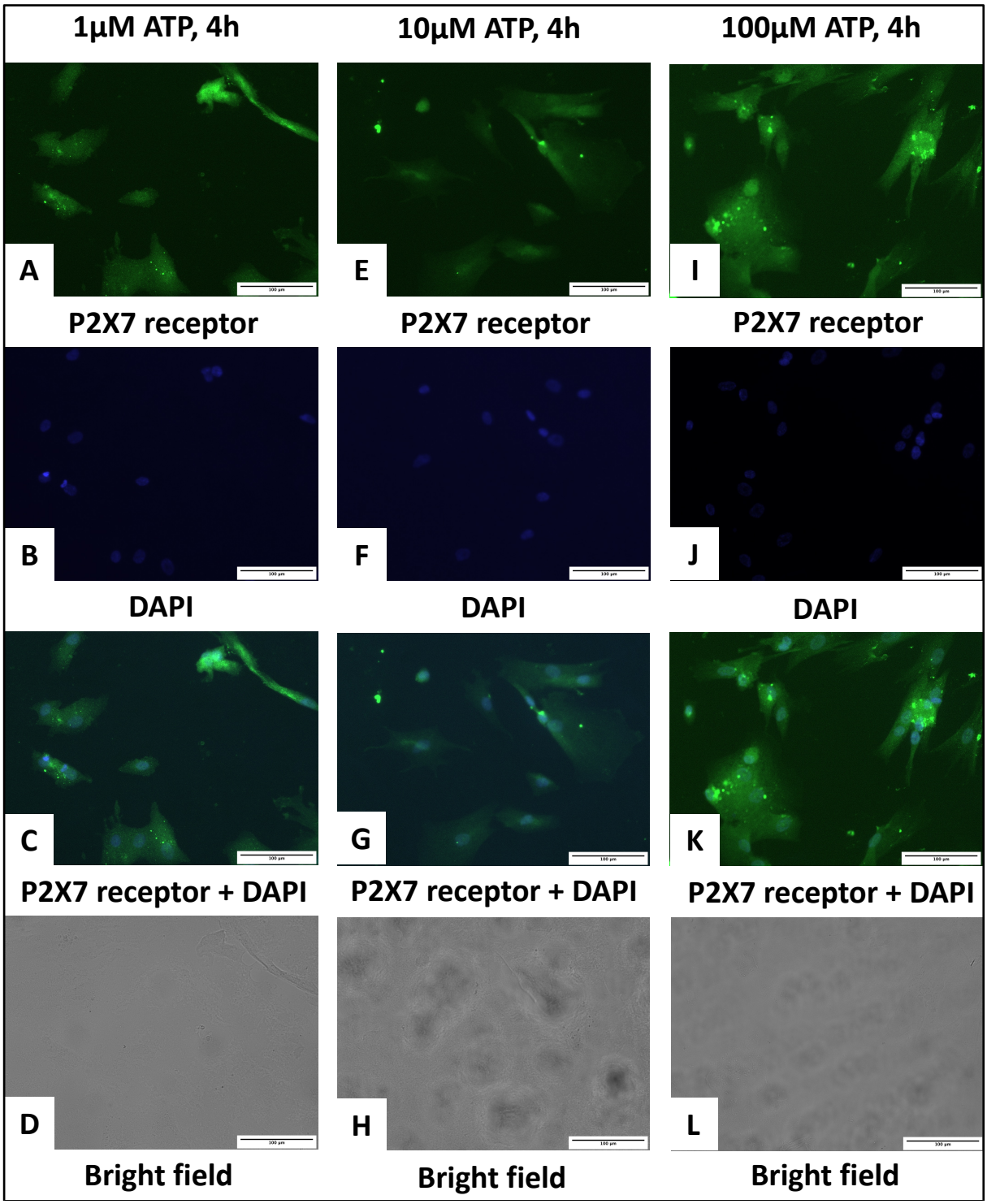


Figure 80. *Fluorescent micrographs showing the P2X7 receptor (green) immunolocalization in CPA-SMC cells originating from a healthy patient (T3024) which have been stimulated with 1µM ATP (panel **A-D**), 10µM ATP (panel **E-H**) and 100µM ATP (panel **I-L**) for 4 hours. The primary placental cells were isolated using the tissue explant method. Scalebar 100µm. Nuclear DAPI staining is blue. All micrographs were acquired at 20X magnification using Zeiss LSM Exciter widefield microscope.*

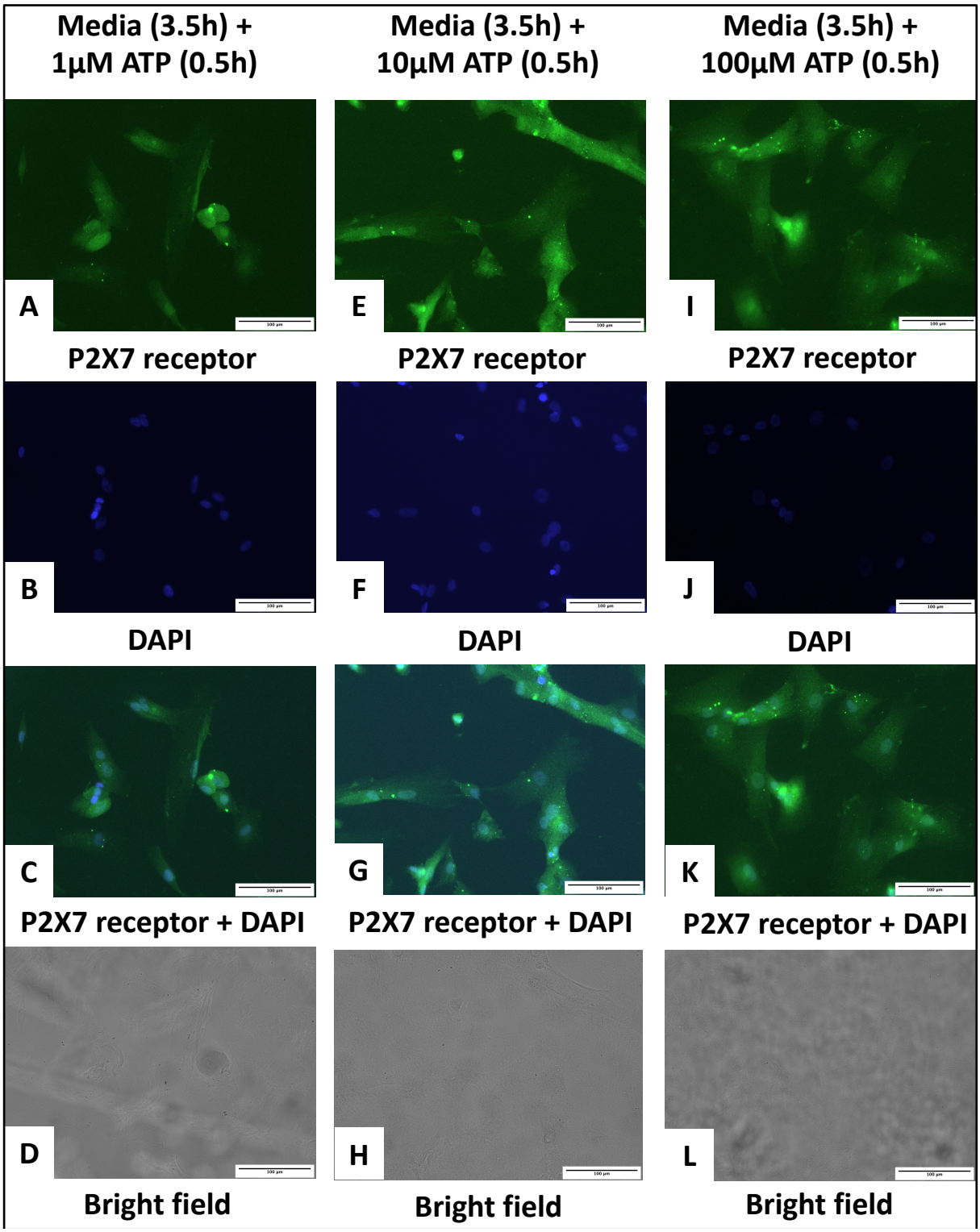


Figure 81. *Fluorescent micrographs showing the P2X7 receptor (green) immunolocalization in CPA-SMC cells originating from a healthy placenta (T3024). The primary cells were stimulated with DMEM low glucose media (3.5h) + 1µM ATP (0.5h) (panel **A-D**), DMEM low glucose media (3.5h) + 10µM ATP (0.5h) (panel **E-H**) and DMEM Low glucose media (3.5h) + 100µM ATP (0.5h) (panel **I-L**). The primary placental cells were isolated using the tissue explant method. Scalebar 100µm. Nuclear DAPI staining is blue. All micrographs were acquired at 20X magnification using Zeiss LSM Exciter widefield microscope.*

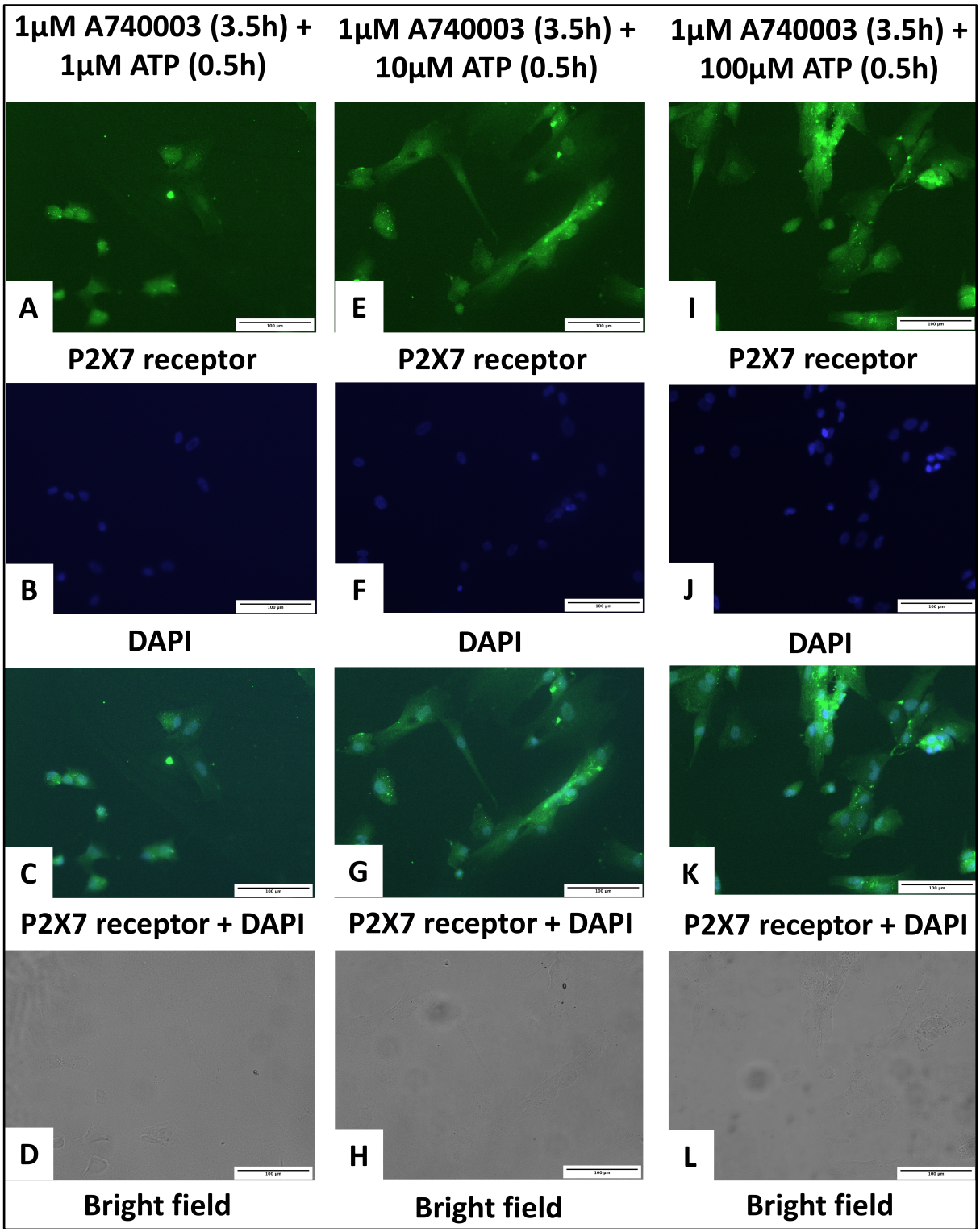


Figure 82. *Fluorescent micrographs showing the P2X7 receptor (green) immunolocalization in CPA-SMC cells originating from a healthy placenta (T3024). The primary cells were stimulated with 1µM A740003 (3.5h) + 1µM ATP (0.5h) (panel **A-D**), 1µM A740003 (3.5h) + 10µM ATP (0.5h) (panel **E-H**) and 1µM A740003 (3.5h) + 100µM ATP (0.5h) (panel **I-L**). The primary placental cells were isolated using the tissue explant method. Scalebar 100µm. Nuclear DAPI staining is blue. All micrographs were acquired at 20X magnification using Zeiss LSM Exciter widefield microscope.*

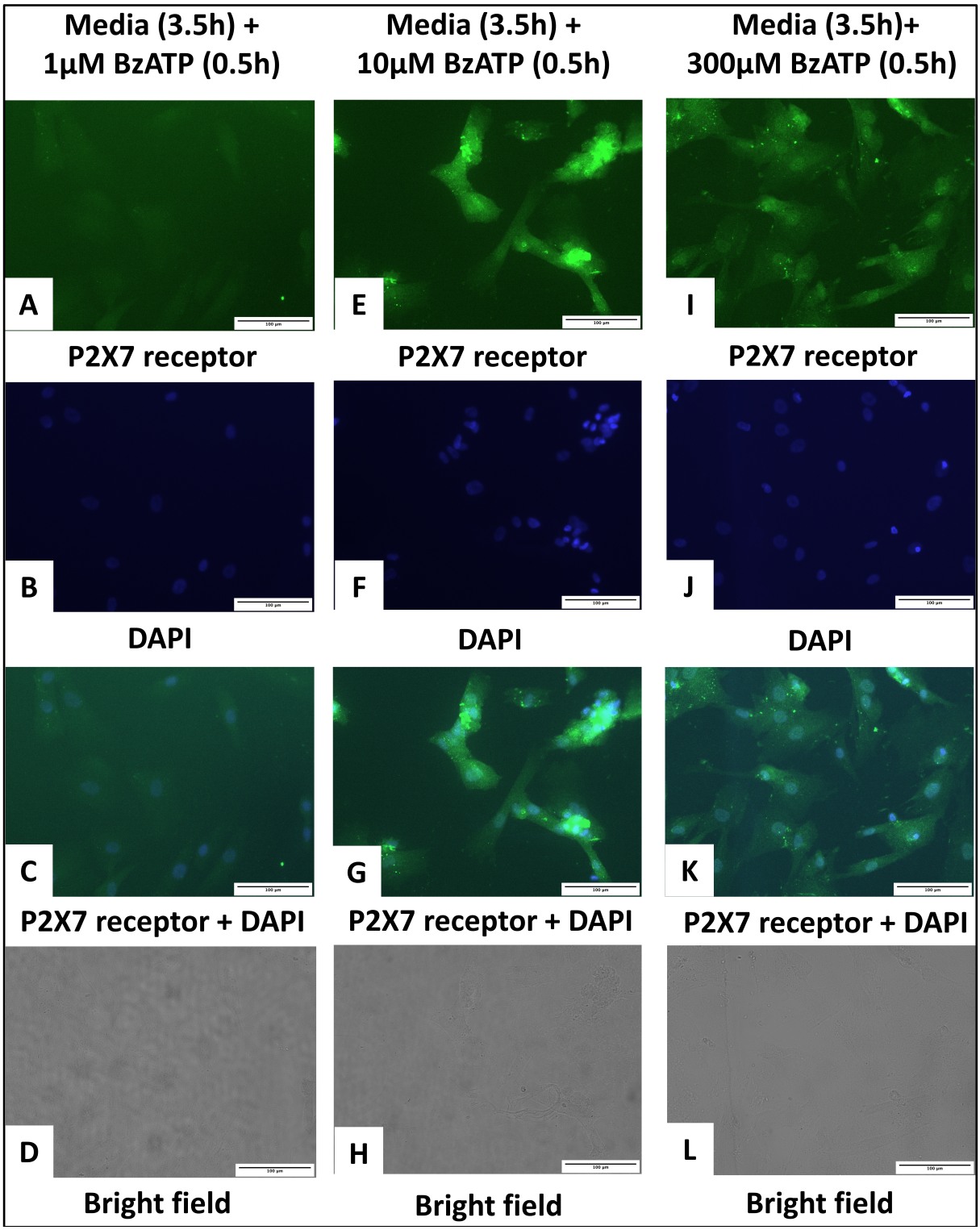


Figure 83. *Fluorescent micrographs showing the P2X7 receptor (green) immunolocalization in CPA-SMC cells originating from a healthy placenta (T3024). The primary cells were stimulated with DMEM low glucose media (3.5h) + 1µM BzATP (0.5h) (panel **A-D**), DMEM low glucose media (3.5h) + 10µM BzATP (0.5h) (panel **E-H**) and DMEM low glucose media (3.5h) + 300µM BzATP (0.5h) (panel **I-L**). The primary placental cells were isolated using the tissue explant method. Scalebar 100µm. Nuclear DAPI staining is blue. All micrographs were acquired at 20X magnification using Zeiss LSM Exciter widefield microscope.*

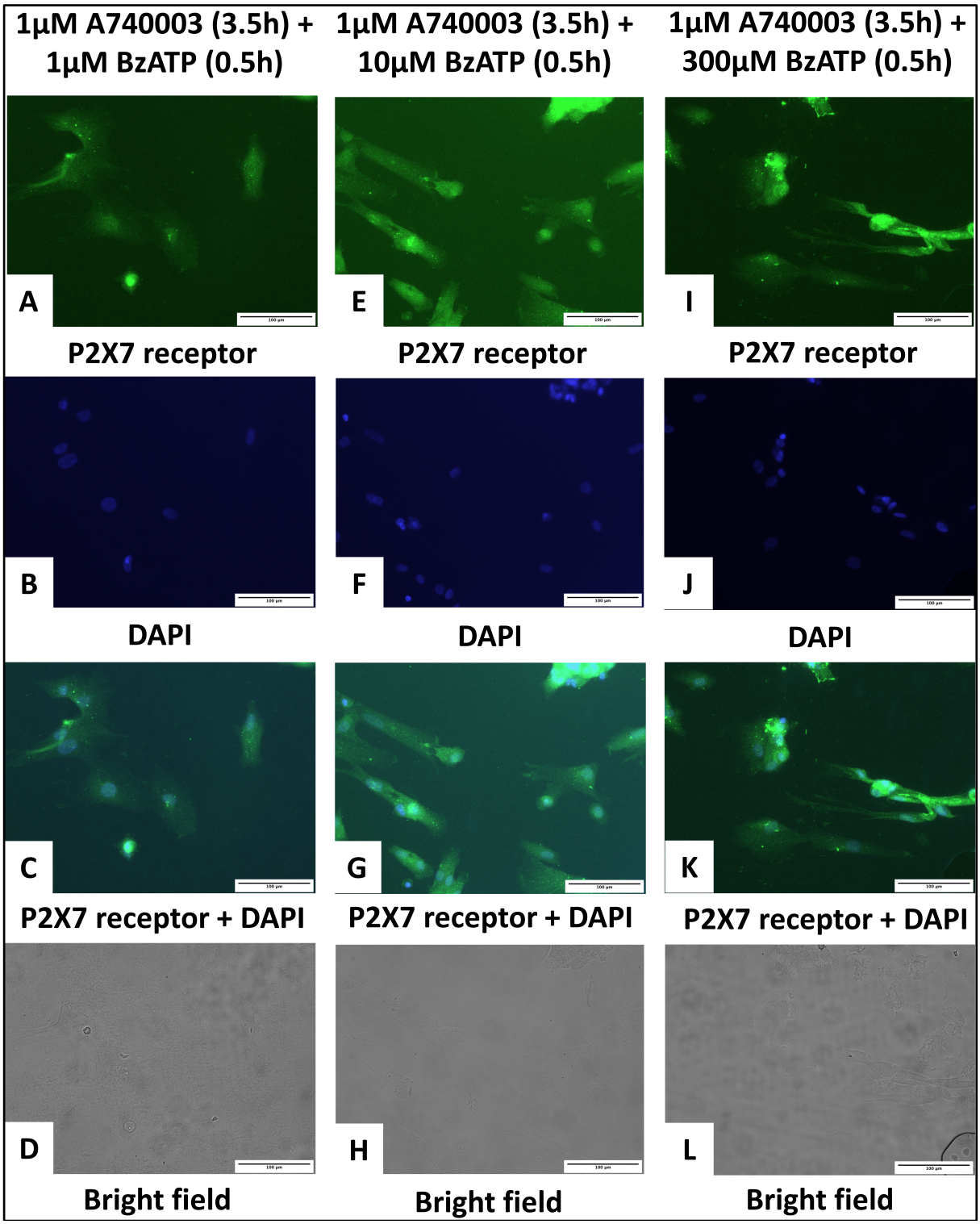


Figure 84. *Fluorescent micrographs showing the P2X7 receptor (green) immunolocalization in CPA-SMC cells originating from a healthy placenta (T3024). The primary cells were stimulated with 1µM A740003 (3.5h) + 1µM BzATP (0.5h) (panel **A-D**), 1µM A740003 (3.5h) + 10µM BzATP (0.5h) (panel **E-H**) and 1µM A740003 (3.5h) + 300µM BzATP (0.5h) (panel **I-L**). The primary placental cells were isolated using the tissue explant method. Scalebar 100µm. Nuclear DAPI staining is blue. All micrographs were acquired at 20X magnification using Zeiss LSM Exciter widefield microscope.*

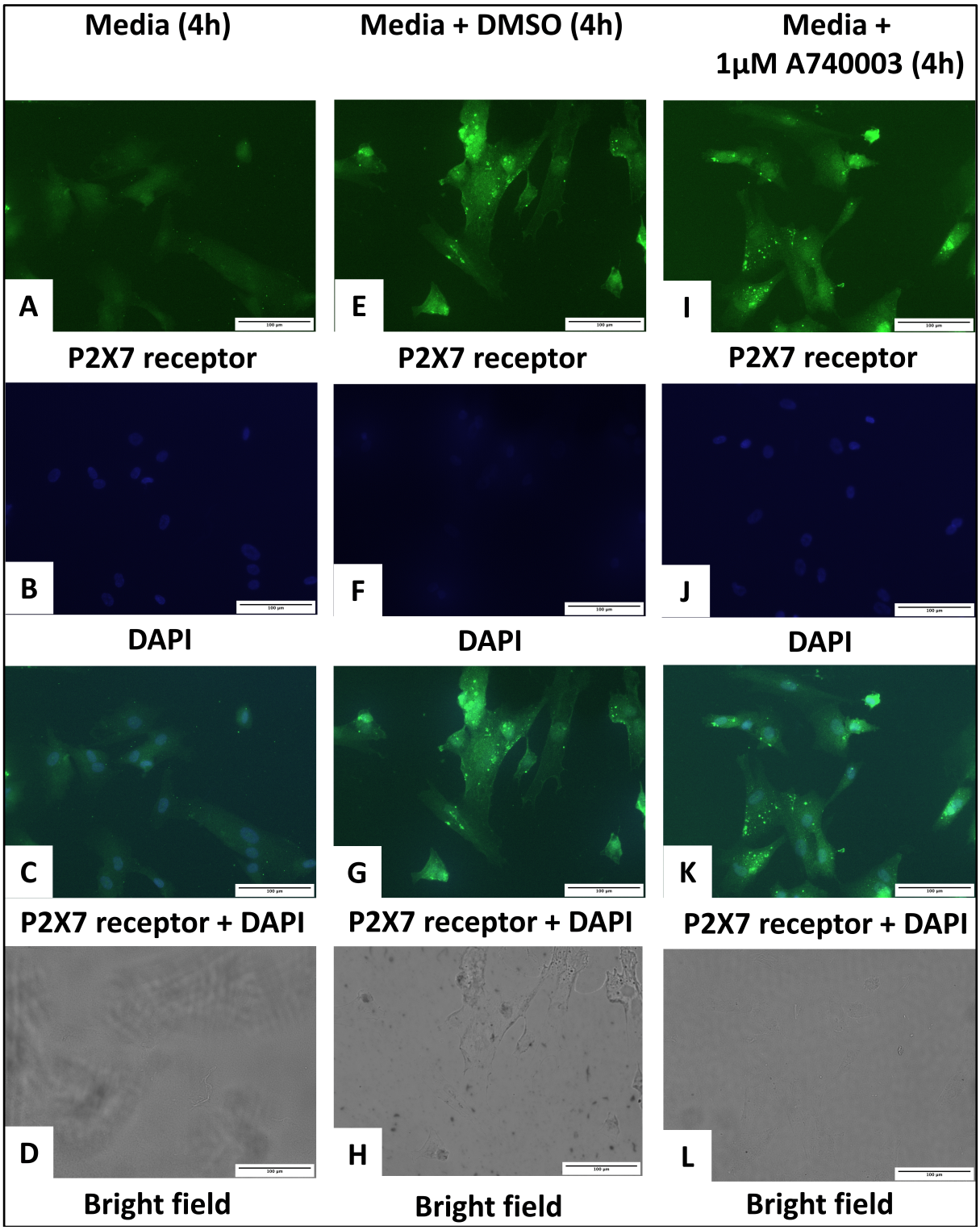


Figure 85. *Fluorescent micrographs showing the P2X7 receptor (green) immunolocalization in CPA-SMC cells originating from a healthy placenta (T3024). The primary cells were stimulated with DMEM low glucose media (4h) (panel **A-D**), DMEM low glucose media + 0.1% (v/v) DMSO (4h) (panel **E-H**) and DMEM low glucose media + 1µM A740003 (4 h) (panel **I-L**). The primary placental cells were isolated using the tissue explant method. Scalebar 100µm. Nuclear DAPI staining is blue. All micrographs were acquired at 20X magnification using Zeiss LSM Exciter widefield microscope.*

3.3.12 Stimulation of human chorionic plate artery smooth muscle cells with 1mM, 5mM or 10mM ATP for 4 hours gave rise to the formation of numerous P2X7 receptor clusters evenly distributed on the primary placental cell body

Stimulation of CPA-SMC cells originating from a healthy placenta sample (T3027) with ATP at a concentration of either 1mM, 5mM or 10mM for 4 hours elicited the establishment of numerous P2X7 receptor distinct clusters relative to control (DMEM low glucose media) as highlighted by the fluorescent micrographs presented in figure 86. The distribution of the P2X7 receptor uniform punctuate staining was evenly expressed on the primary placental cell body and also with a high preponderance at the level of the nucleus (figure 86). The merged micrographs of the P2X7 receptor with DAPI staining further confirmed the presence of the purinergic receptor inside the nucleus. The stimulation of CPA-SMC cells with the same concentrations of ATP for 30 minutes did not fundamentally alter the distribution of the P2X7 receptor compared to the challenge of 4 hours (figure 87). Similarly, the incubation of CPA-SMC cells with 1μM A740003 for 3.5 hours followed by the stimulation of the primary placental cells with either 1mM, 5mM or 10mM ATP for 30 minutes did not give rise to a change in the P2X7 receptor immunolocalization compared to the same nucleotide challenge for 30 minutes in the absence of the P2X7 receptor antagonist (figure 88). The stimulation of CPA-SMC cells with either DMEM low glucose media + 0.1% (v/v) DMSO or DMEM low glucose media + 1μM A740003 for 4 hours showed the presence of an intense P2X7 receptor staining at the level of the nucleus (figure 89, panels A-D and I-L). No signal was detected in the absence of the P2X7 receptor primary antibody (figure 89, panel E-H). As a result, CPA-SMC cells

stimulated with ATP at concentrations of 1mM, 5mM or 10mM gives rise to a localised P2X7 receptor distribution particularly in association with the nucleus.

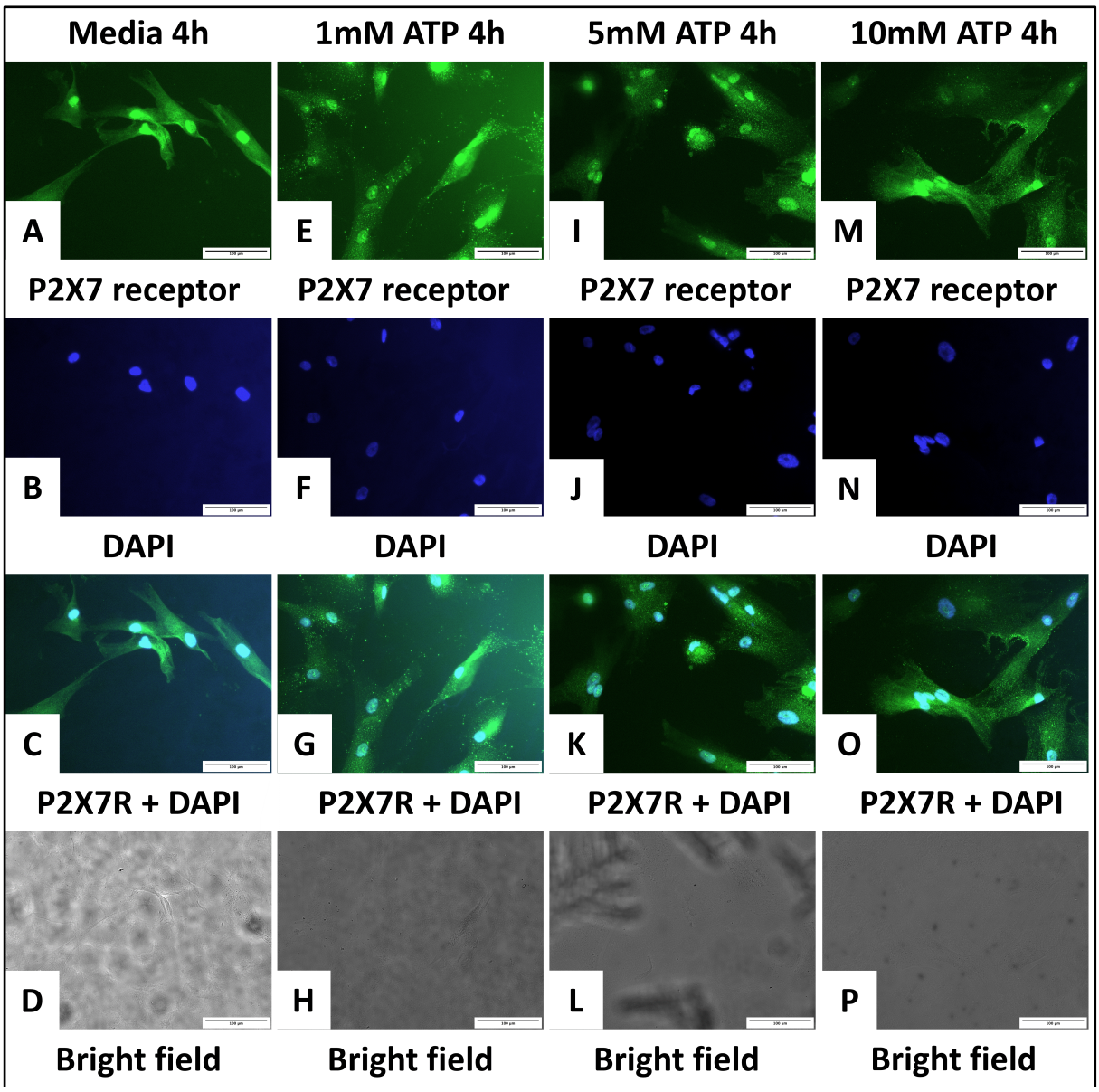


Figure 86. *Fluorescent micrographs showing the P2X7 receptor (green) immunolocalization in CPA-SMC cells originating from a healthy patient (T3027) which were not stimulated i.e. DMEM low glucose media for 4 hours (panel **A-D**) or stimulated with 1mM ATP (panel **E-H**), 5mM ATP (panel **I-L**) and 10mM ATP (panel **M-P**) for 4 hours. The primary placental cells were isolated using the tissue explant method. Scalebar 100μm. Nuclear DAPI staining is blue. All micrographs were acquired at 20X magnification using Zeiss LSM Exciter widefield microscope.*

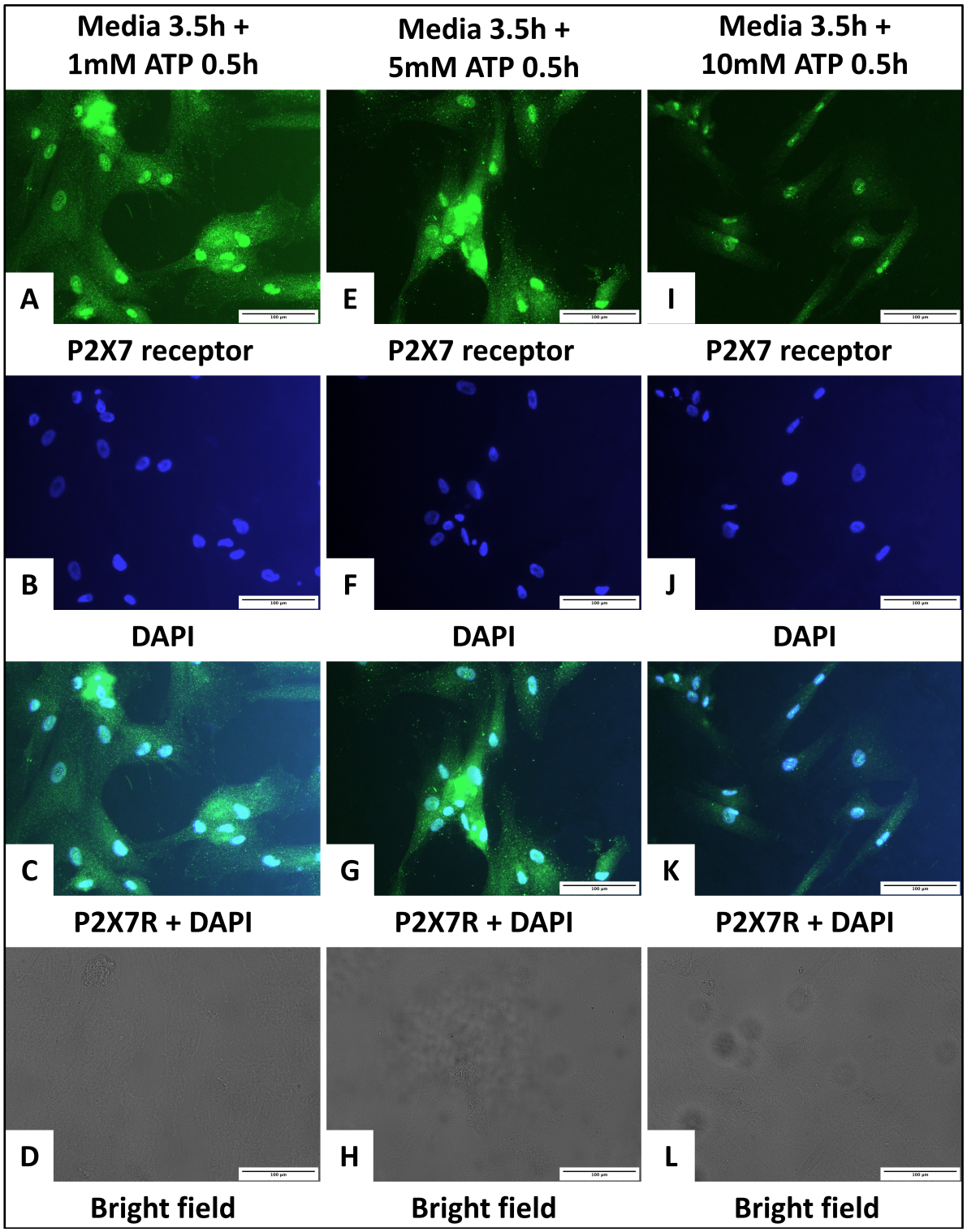


Figure 87. *Fluorescent micrographs showing the P2X7 receptor (green) immunolocalization in CPA-SMC cells originating from a healthy placenta (T3027). The primary cells were stimulated with DMEM low glucose media (3.5h) + 1mM ATP (0.5h) (panel **A-D**), DMEM low glucose media (3.5h) + 5mM ATP (0.5h) (panel **E-H**) and DMEM Low glucose media (3.5h) + 10mM ATP (0.5h) (panel **I-L**). The primary placental cells were isolated using the tissue explant method. Scalebar 100μm. Nuclear DAPI staining is blue. All micrographs were acquired at 20X magnification using Zeiss LSM Exciter widefield microscope.*

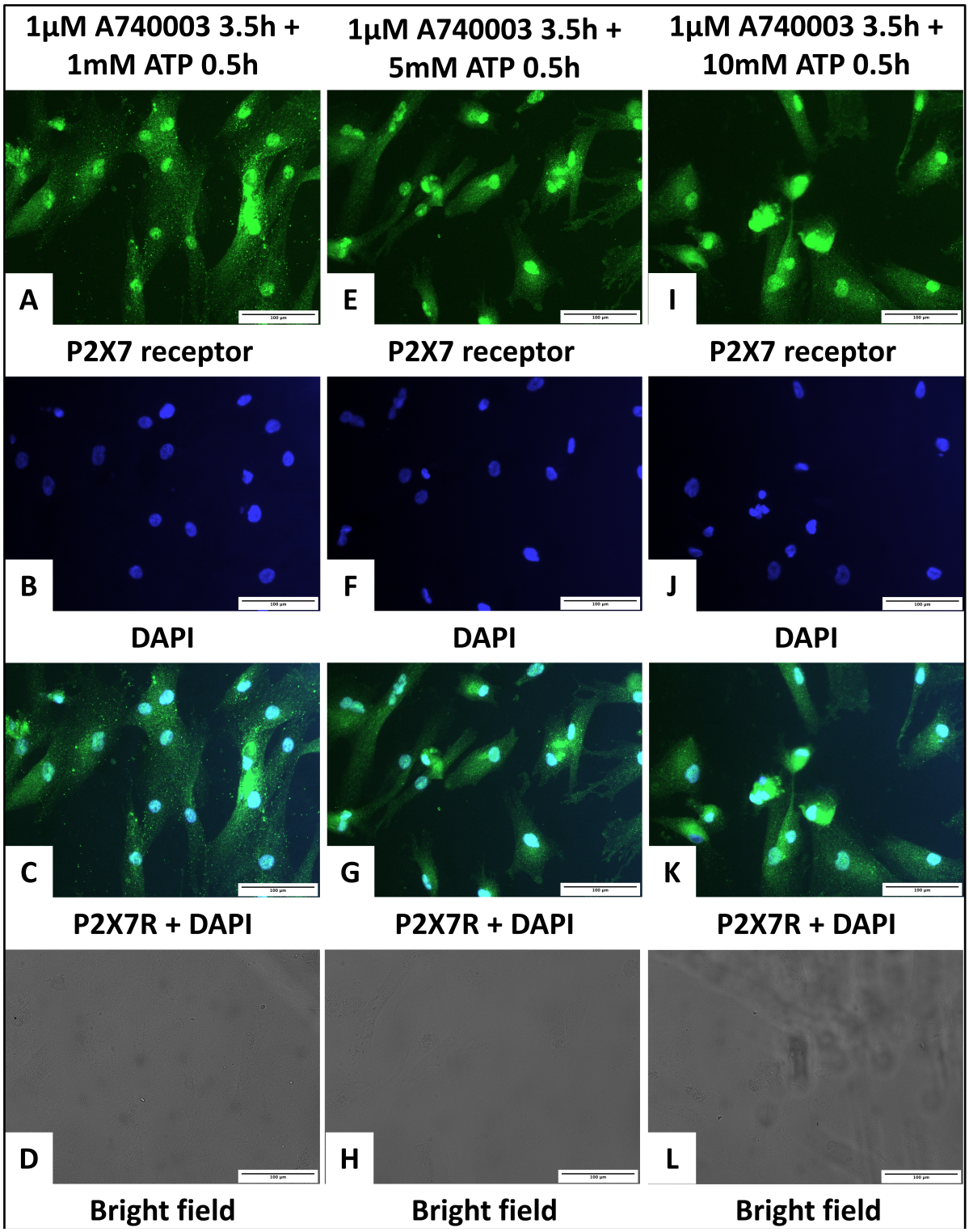


Figure 88. *Fluorescent micrographs showing the P2X7 receptor (green) immunolocalization in CPA-SMC cells originating from a healthy placenta (T3027). The primary cells were stimulated with 1µM A740003 (3.5h) + 1mM ATP (0.5h) (panel **A-D**), 1µM A740003 (3.5h) + 5mM ATP (0.5h) (panel **E-H**) and 1µM A740003 (3.5h) + 10mM ATP (0.5h) (panel **I-L**). The primary placental cells were isolated using the tissue explant method. Scalebar 100µm. Nuclear DAPI staining is blue. All micrographs were acquired at 20X magnification using Zeiss LSM Exciter widefield microscope.*

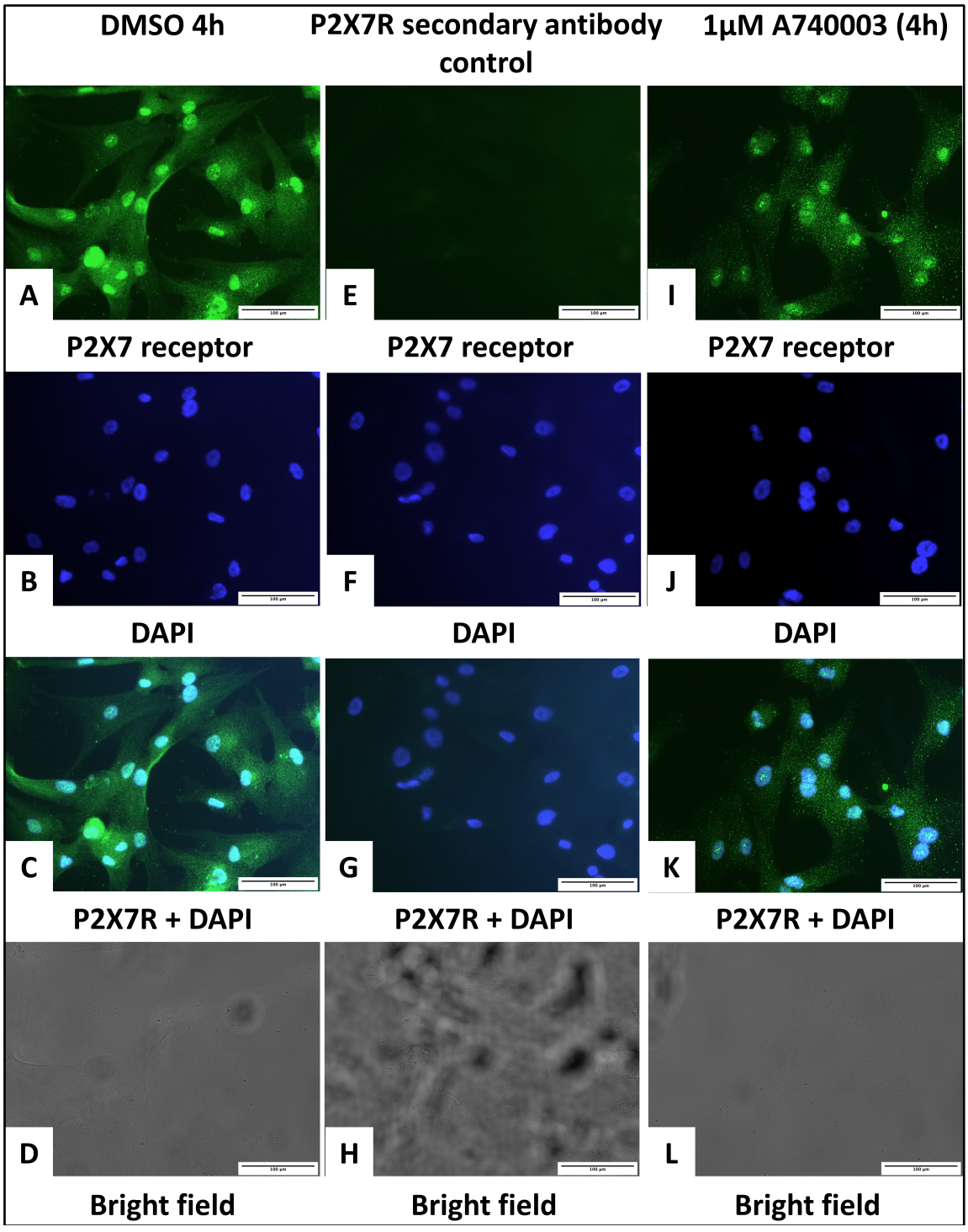


Figure 89. *Fluorescent micrographs showing the P2X7 receptor (green) immunolocalization in CPA-SMC cells originating from a healthy placenta (T3027). The primary cells were stimulated with DMEM low glucose media + 0.1% (v/v) DMSO (4h) (panel **A-D**) and DMEM low glucose media + 1µM A740003 (4 h) (panel **I-L**). Panels **E-H** highlight the P2X7 receptor secondary antibody control in unstimulated CPA-SMC cells (i.e. DMEM low glucose media; 4 hours) where the primary antibody against the purinergic receptor was omitted. The primary placental cells were isolated using the tissue explant method. Scalebar 100µm. Nuclear DAPI staining is blue. All micrographs were acquired at 20X magnification using Zeiss LSM Exciter widefield microscope.*

3.3.13 Immunohistochemical expression of the P2X7 receptor in isolated sections of human placental villous tissue showed that the syncytiotrophoblast layer and fetal capillaries stained positive for the purinergic receptor

The immunostaining for the P2X7 receptor and CD31 of the human placental villous tissue was carried out using two patient groups namely healthy volunteers (N=12) and diet managed gestational diabetic mellitus subjects (N=6). The human placental villous tissue is composed of tree-like arranged placental villi which branch from the chorionic plate and protrude into the intervillous space. The trophoblastic surface of the villous is in direct contact with the maternal blood and is composed of the villous syncytiotrophoblast which is the outer continuous layer and villous cytotrophoblast which is the inner discontinuous layer. All P2X7 receptor (positive and negative), CD31 positive and P2X7 receptor + CD31 double positive placental villi microvessels (referred in the current investigation as vascular profiles) were counted using systematic random sampling in all images acquired from both study groups. As highlighted in figure 90, each bar of the graphs presented in panels A, B and C highlights the percentage of placental vascular profiles from the total of all (100%) vascular profiles counted in each of the healthy and diet managed GDM groups that are P2X7 receptor positive and P2X7 receptor negative (illustrated in panel A), CD31 positive (shown in panel B) or P2X7 receptor + CD31 double positive (presented in panel C).

Figures 92 and 93 highlight representative fluorescence images of the P2X7 receptor (green) and CD31 (red) immunolocalization in human placental villous tissue originating from healthy and gestational diabetes mellitus -diet managed (GDM-Diet)

placental samples. In all fluorescent images acquired, the P2X7 receptor expression on the syncytiotrophoblast layer was highlighted with red arrows, and the immunolocalization of the purinergic receptor on cytotrophoblasts was signposted with yellow arrows. Similarly, CD31 positive vascular profiles were labelled with white asterisks. The vascular profiles which were double positive for the P2X7 receptor and CD31 were indicated via white arrows. Figure 94 highlights representative no primary antibody control fluorescence images of the P2X7 receptor and CD31 in placental villous tissue originating from a healthy placenta sample. A Shapiro-Wilk test highlighted that all placental vascular profile data was normally distributed with the exception of CD31 positive blood vessels corresponding to healthy patients (*P=0.0116). A Kruskal-Wallis test (****P<0.0001) with Dunn's multiple comparison tests were undertaken between all vascular profiles of healthy and GDM-Diet patient subgroups and highlighted multiple statistically significant differences as presented in table 14 and figure 90. Moreover, Mann-Whitney tests were conducted between healthy and GDM-Diet patient groups in each of the placental vascular profiles that were positive for the P2X7 receptor, negative for the P2X7 receptor, positive for CD31 and double positive for the P2X7 receptor+CD31 which highlighted a single statistically significant difference in the P2X7 receptor+CD31 positive group between healthy and GDM-Diet (**P=0.0063) as illustrated in figure 90 (panel C). These data highlight that in the human placental samples from the two different study groups, the vascular profiles showed no difference in immunopositivity for the P2X7 receptor. Similarly, the same vascular profiles showed no statistically significant difference between healthy and GDM-Diet in terms of immunopositivity to CD31. However, a significant change of double positive P2X7+CD31 vascular profiles took place between healthy (84.92±4.011% - mean±SEM) and GDM-Diet (61.67±5.415% - mean±SEM). These

data also show that 84.92% of placental vascular profiles corresponding to healthy patients were P2X7+CD31 positive which implies that the ATP receptor is expressed at the level of the fetal vascular system. Similarly, 61.67% of placental vascular profiles of GDM-Diet patients were P2X7+CD31 positive which implies that the P2X7 receptor is expressed in the majority of the feto-placental vasculature in diet managed gestational diabetic pregnancies.

The representative fluorescent micrographs of placental villous biopsies highlighted that the P2X7 receptor was expressed on the membrane of cytotrophoblast cells and also on the plasmalemma of villous stromal cells. Placental villous immunohistochemistry micrographs of secondary antibody control (figure 94) showed no green or red background staining which implies that both primary antibodies possess a high specificity for the P2X7 receptor and CD31. Similar P2X7 receptor and CD31 immunolocalization and fluorescence intensities of the ATP receptor staining were observed in the remainder of the placental vascular and syncytiotrophoblast profiles investigated in healthy and GDM-Diet study groups.

As a result, a significant difference in P2X7+CD31 vascular profiles (**P=0.0063) was found in human placental villous tissue in healthy compared to diet managed gestational diabetic mellitus patients using a Mann-Whitney test.

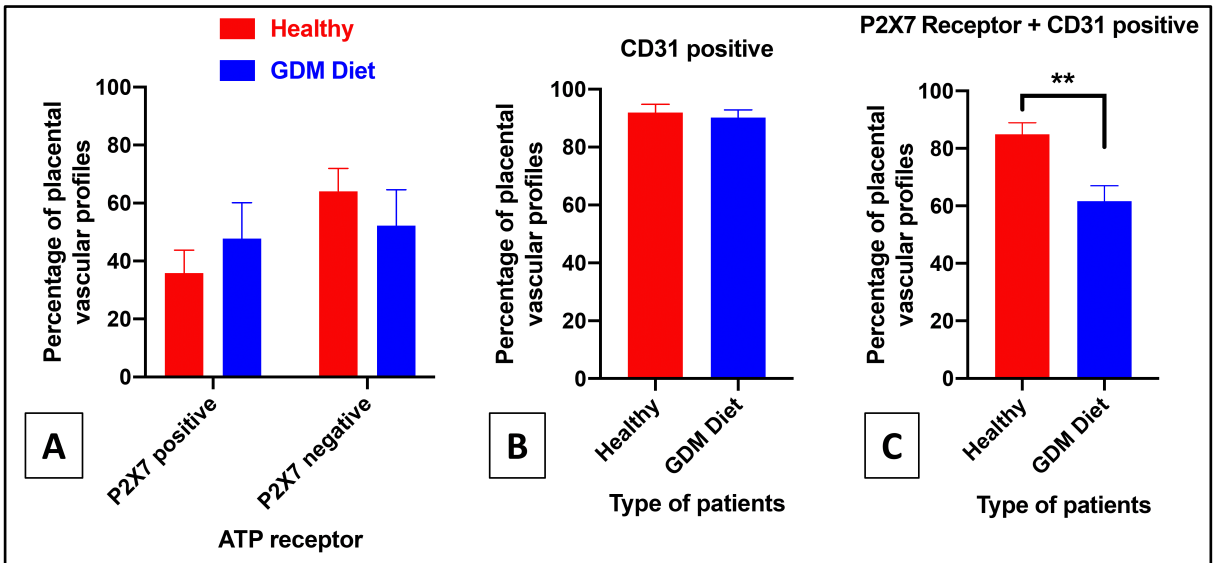


Figure 90. *These graphs show the percentage of placental vascular profiles that are positive or negative for the P2X7 receptor (**A**), positive for CD31 (**B**) or double positive for the P2X7 receptor+CD31 (**C**) originating from placental samples of healthy patients (N=12; N04022020, N05032020, N05122019, N06022020, N11112019B, N12072019B, N16012020, N19022020, N20022020, N23012020, N27012020A, N27012020B) and GDM-Diet volunteers (N=6; GDM20022020D, GDM14022020D, GDM12082019D, GDM10122019D, GDM02122019D, GDM09012020D). Data are presented as mean±SEM.*

	Adjusted P Value
P2X7 positive (healthy patients) vs. CD31 positive (healthy patients)	****P<0.0001
P2X7 positive (healthy patients) vs. CD31 positive (GDM-Diet patients)	**P=0.0055
P2X7 positive (healthy patients) vs. P2X7+CD31 positive (healthy patients)	**P=0.0036
CD31 positive (healthy patients) vs. P2X7 positive (GDM-Diet patients)	*P=0.0235

Table 14. *This table shows the statistically significant results of Dunn's multiple comparison tests across all vascular profiles that were positive or negative for the P2X7 receptor, positive for CD31 or double positive for the P2X7 receptor+CD31 originating from placental samples of N=12 healthy and N=6 GDM-Diet patients.* * P≤0.05, ** P≤0.01, *** P≤0.001, **** P≤0.0001.

A Shapiro-Wilk test highlighted that some of the data corresponding to the P2X7 receptor positive syncytiotrophoblast profiles was not normally distributed as presented in table 15. A Kruskal-Wallis test (****P<0.0001) with Dunn's multiple comparison tests were undertaken between all florescence intensity levels of the P2X7 receptor staining in the human placental samples originating from two different study groups and highlighted multiple statistically significant differences as illustrated in table 16. Concentrating on the syncytiotrophoblast layer of the placental villi, there were no statistically significant differences between healthy and GDM-Diet at the same fluorescence intensity levels of P2X7 receptor staining. In the case of healthy patients, 49.77% of syncytiotrophoblast profiles did not stain positive for the P2X7 receptor (0+ intensity level) as highlighted in figure 91. The remainder of the syncytiotrophoblast profiles did stain positive for the ATP receptor, with the highest percentage corresponding to a fluorescence intensity level of 1+ (29.97%). Similarly, in GDM-Diet group, the highest percentage of syncytiotrophoblast profiles stained negative (0+ intensity level) for the P2X7 receptor with values of 51.27% as illustrated in figure 91. In terms of syncytiotrophoblast profiles corresponding to GDM-Diet that stained positive for the P2X7 receptor, the highest percentage were assigned to a fluorescence intensity level of 1+ with values of 29.72%. These data show that GDM-Diet did not significantly alter the fluorescence intensity levels the P2X7 receptor staining at the level of the syncytiotrophoblast compared to healthy patients.

As a result, no statistically significant differences in P2X7 receptor fluorescence intensity levels of human placenta villous tissue syncytiotrophoblast profiles were found between healthy and diet managed gestational diabetic mellitus patients using Dunn's multiple comparison tests.

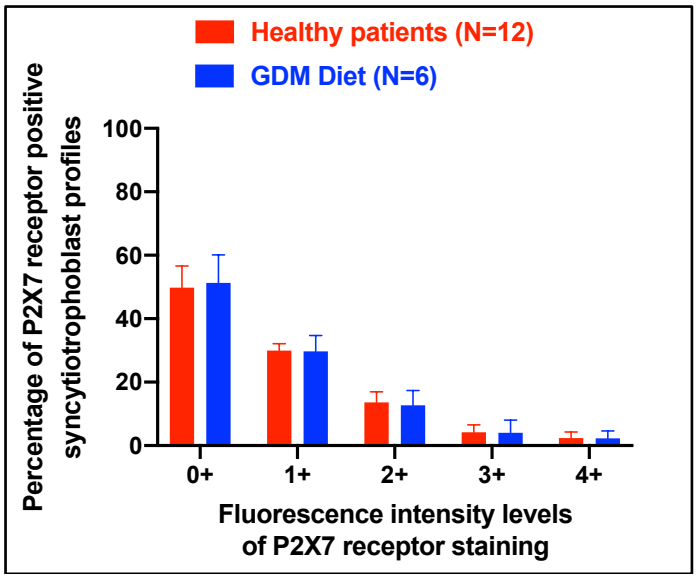


Figure 91. *This graph shows the percentage of the P2X7 receptor positive syncytiotrophoblast profiles according to the fluorescence intensity levels of the ATP receptor staining in placental villous tissue originating from healthy patients (N=12) and GDM-Diet volunteers (N=6). Data are illustrated as mean±SEM.*

	Fluorescence intensity levels of P2X7 receptor staining	P Value	Passed normality test
Healthy	0+	P=0.0794	Yes
	1+	P=0.9192	Yes
	2+	*P=0.0286	No
	3+	****P<0.0001	No
	4+	****P<0.0001	No
GDM-Diet	0+	P=0.7817	Yes
	1+	P=0.6311	Yes
	2+	P=0.4830	Yes
	3+	****P<0.0001	No
	4+	****P<0.0001	No

Table 15. *This table highlights the results of a Shapiro-Wilk test using the P2X7 receptor positive syncytiotrophoblast profile data. * P*≤0.05, ** P≤0.01, *** P≤0.001, **** P≤0.0001.

Fluorescence intensity levels of P2X7 receptor staining	Adjusted P Value
0+ (Healthy) vs. 3+ (Healthy)	***P=0.0002
0+ (Healthy) vs. 4+ (Healthy)	****P<0.0001
0+ (Healthy) vs. 3+ (GDM-Diet)	**P=0.0018
0+ (Healthy) vs. 4+ (GDM-Diet)	**P=0.0011
1+ (Healthy) vs. 3+ (Healthy)	*P=0.0116
1+ (Healthy) vs. 4+ (Healthy)	**P=0.0017
1+ (Healthy) vs. 3+ (GDM-Diet)	*P=0.0396
1+ (Healthy) vs. 4+ (GDM-Diet)	*P=0.0265
3+ (Healthy) vs. 0+ (GDM-Diet)	**P=0.0037
4+ (Healthy) vs. 0+ (GDM-Diet)	***P=0.0007
4+ (Healthy) vs. 1+ (GDM-Diet)	*P=0.0328
0+ (GDM-Diet) vs. 3+ (GDM-Diet)	**P=0.0094
0+ (GDM-Diet) vs. 4+ (GDM-Diet)	**P=0.0064

Table 16. *This table shows all of the statistically significant results of Dunn's multiple comparison tests across all fluorescence intensity levels of the P2X7 receptor staining of syncytiotrophoblast profiles of the human placental samples originating from healthy and GDM-Diet patients. * P*≤0.05, ** P≤0.01, *** P≤0.001, **** P≤0.0001.

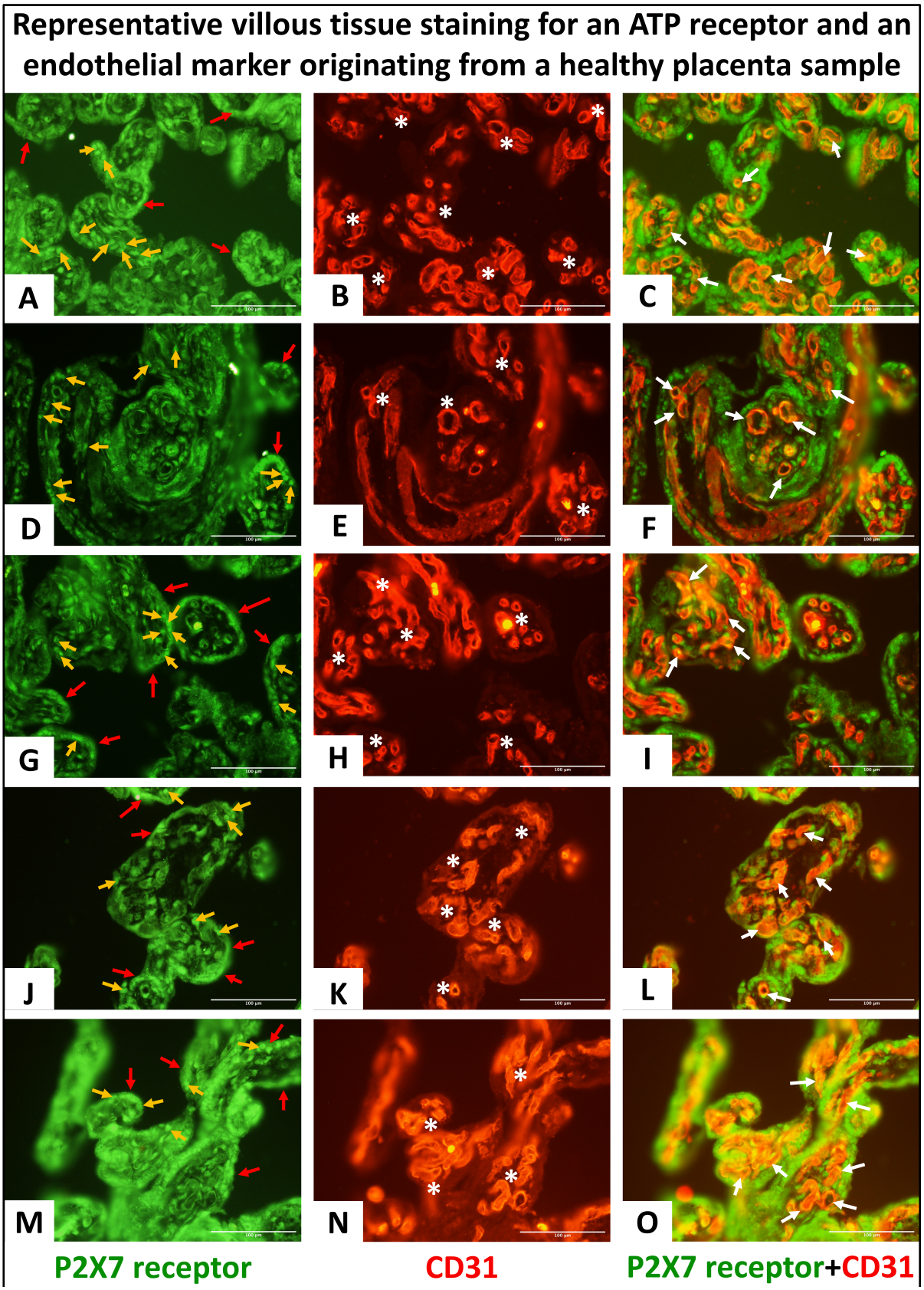


Figure 92. *This figure* ***(A-O)*** *shows representative fluorescent micrographs highlighting the P2X7 (green), CD31 (red) and the P2X7 receptor+CD31 (merged) immunolocalization in placental villous tissue originating from a healthy patient (N27012020A). Scalebar 100μm.*

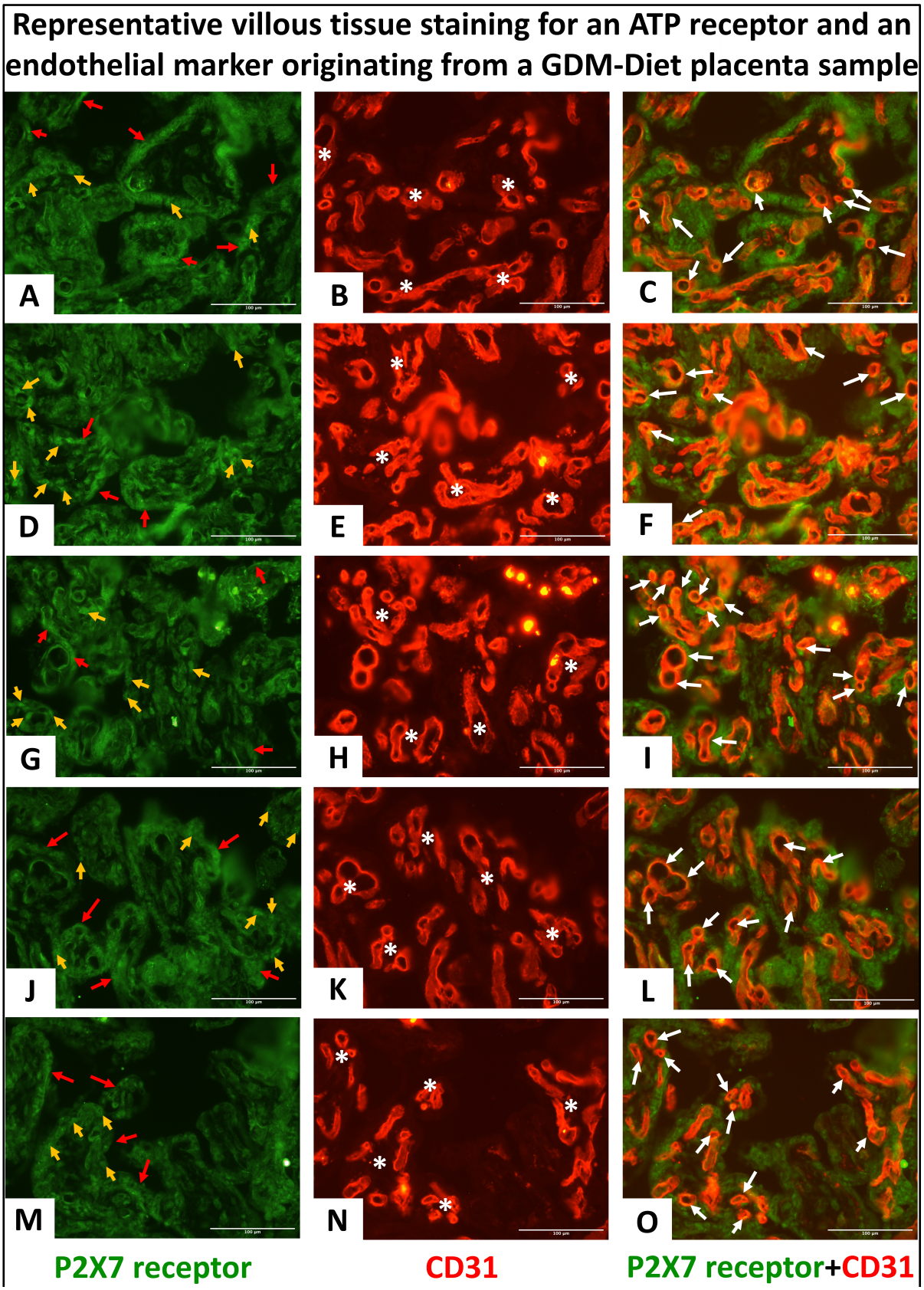


Figure 93. *This figure* ***(A-O)*** *shows representative fluorescent micrographs highlighting the P2X7 (green), CD31 (red) and the P2X7 receptor +CD31 (merged) immunolocalization in placental villous tissue originating from a placenta sample of a diet managed gestational diabetic patient (GDM Diet 12082019). Scalebar 100μm.*

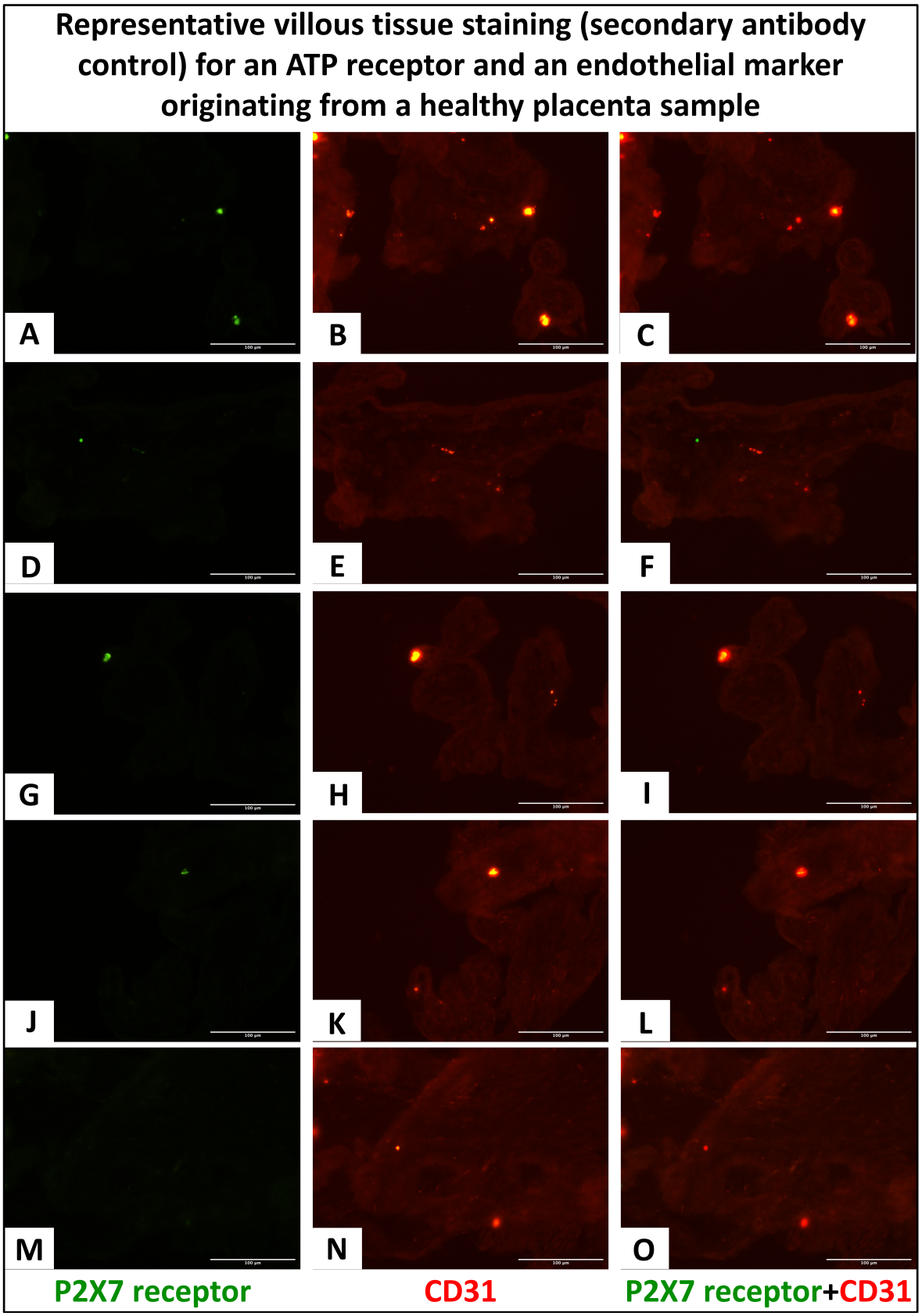


Figure 94. *This figure* ***(A-O)*** *shows representative secondary antibody control fluorescent micrographs highlighting the P2X7 (green), CD31 (red) and the P2X7 receptor+CD31 (merged) immunolocalization in placental villous tissue originating from a placenta sample of a healthy patient (N05032020). Scalebar 100μm.*

3.3.14 Immunohistochemical expression of the P2X7 receptor in isolated sections of human placenta chorionic plate artery showed that the endothelial cells stained positive for the purinergic receptor

The representative distribution of the P2X7 receptor and CD31 on chorionic plate arteries in transverse section isolated from a healthy patient is presented in figure 95. The CD31 marker was only immunolocalised at the level of the endothelial lining of the placental blood vessels which is highlighted with a white star in figure 95, panel B. Similarly, the P2X7 receptor was also immunolocalised at the level of the endothelium as highlighted by red arrows in figure 95, panel A. The ATP receptor immunohistochemical expression at the level of the smooth muscle layer (tunica media) was particularly decreased as illustrated in figure 95, panel D, G, J and M. A similar decreased purinergic receptor expression level was found in tunica adventitia layer of the chorionic plate arteries as presented in figure 95, panel D, G, J and M. These data provide novel evidence that the P2X7 receptor is primarily expressed on the endothelial cells of the chorionic plate arteries originating from a healthy patient. A similar P2X7 receptor immunohistochemical expression in CPA artery was found in biopsies originating from a different healthy patient. Figure 96 highlights the florescent micrographs corresponding to the secondary antibody control of P2X7 and CD31 in chorionic plate arteries originating from a healthy patient, which imply that both primary antibodies possess a high specificity for the P2X7 receptor and CD31, as no red or green background staining was observed. As a result, the P2X7 receptor was found to be expressed at the level of the endothelial cells in isolated human placenta chorionic plate artery assessed using immunohistochemistry.

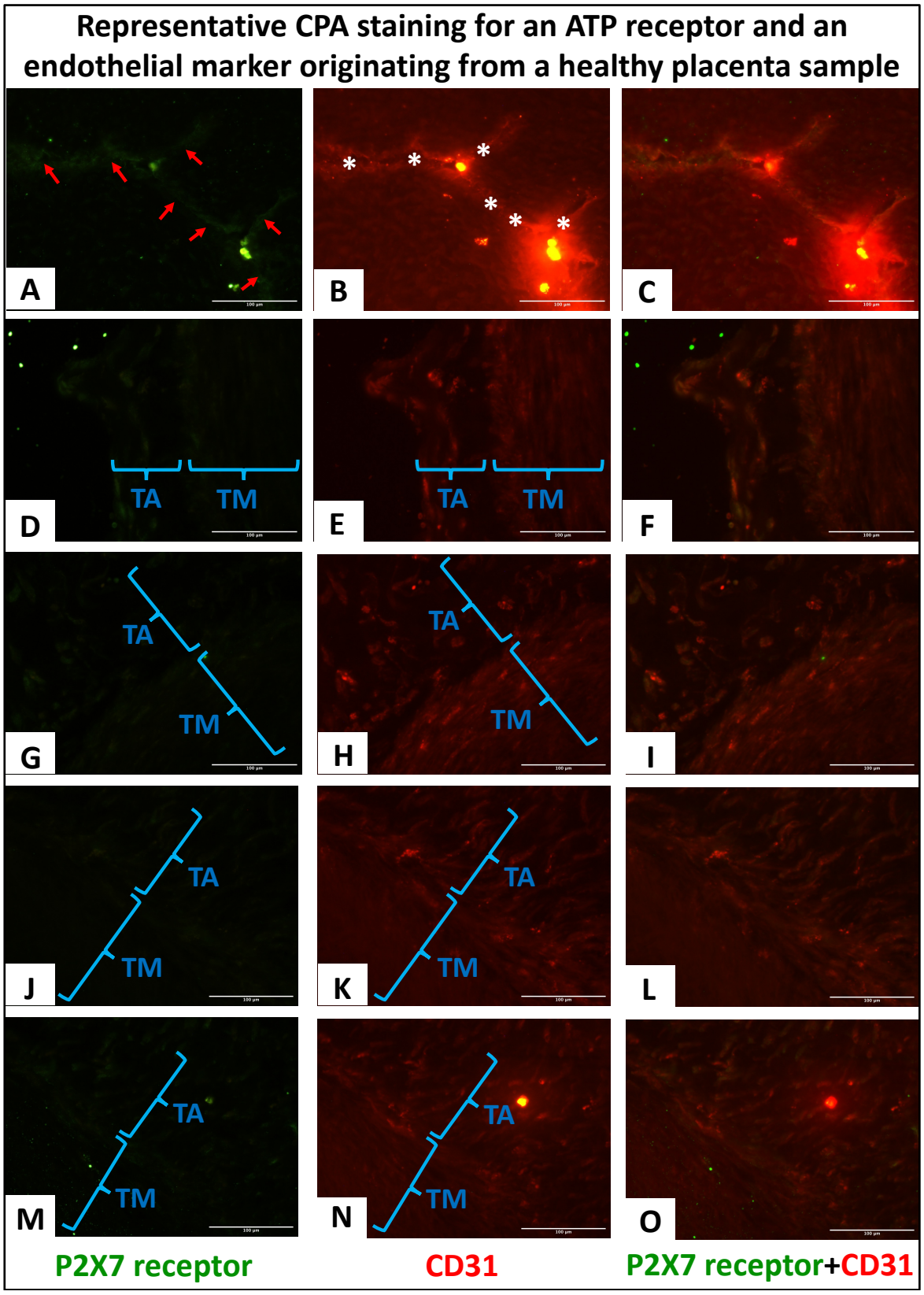


***Figure 95**. This figure (**A-O**) highlights representative fluorescent micrographs of the P2X7 (green), CD31 (red) and the P2X7 receptor+CD31 (merged) immunolocalization in transverse chorionic plate artery sections originating from a healthy patient (N19022020). TM denotes tunica media; TA suggests tunica adventitia. Scalebar 100μm.*

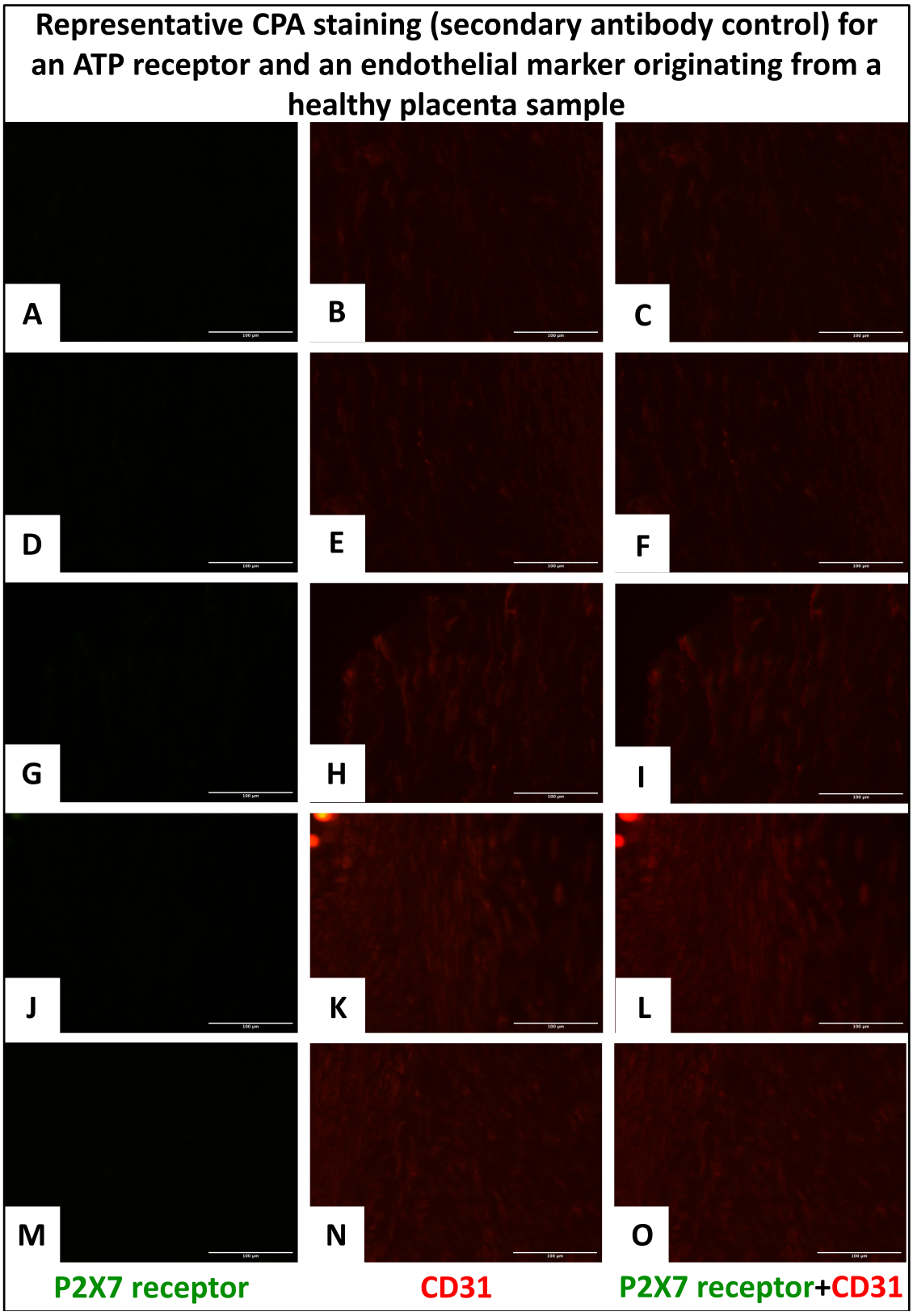


Figure 96. *This figure (**A-O**) highlights representative fluorescent micrographs of secondary antibody control of the P2X7 receptor (green), CD31 (red) and the P2X7 receptor+CD31 (merged) immunolocalization in transverse chorionic plate artery sections originating from a healthy patient (N20022020). TM denotes tunica media; TA suggests tunica adventitia. Scalebar 100μm.*

3.4 Discussion

Western blotting data highlighted that no P2X7 receptor specific bands were identified in the second supernatant (i.e. cytosolic fraction) of fourth order CPA, SVA, choriodecidua and trophoblast tissue lysates originating from healthy placental samples, which is in accordance with previously published peer-reviewed literature since the purinergic receptor is a ligand gated ion channel [493]. Continuous activation of the P2X7 receptor with millimolar concentrations of extracellular ATP gives rise to the assembly of a non-selective pore that allows the flow of mediators of less than 900 Da through the plasma membrane, giving rise to fundamental alterations in the cellular ionic homeostasis [530]. The results of the current study have confirmed the presence of the P2X7 receptor in the membranous fraction (i.e. second pellet) of the CPA, SVA, trophoblast and myometrium tissue lysates.

The protein expression levels of the NLRP3 inflammasome in the second supernatant fraction of fourth order CPA, SVA and choriodecidua tissue lysates revealed the detection of 4 isoforms at approximately 79kDa, circa 107kDa, about 171kDa and ~222kDa. These data further complement a study published by Kummer and colleagues (2007) where the authors have found 2 isoforms of the NLRP3 inflammasome in western blots at circa 75kDa and 130kDa in Jurkat and THP-1 cell lines [531]. The same study has also highlighted the presence of a predominant band corresponding to the NLRP3 inflammasome at approximately 75kDa in primary immune cells (PBMC, monocytes, B cells, T cells and dendritic cells) and also detected both NLRP3 isoforms in human neutrophils stimulated with LPS for 2 and 4 hours [531]. NLRP3 has been categorised as a 115kDa cytosolic protein by Zahid *et al* (2019) [532] and Groslambert and Py (2018) [533] which is relatively close in molecular weight to the results presented in the current study, with a difference of circa 8kDa compared to the

107kDa isoform. Furthermore, a study by Cheng *et al* (2019) has highlighted that higher protein levels of the NLRP3 inflammasome were detected in hypoxia treated primary trophoblast cells compared to normoxia treated cells using western blotting, with a detected protein product size of approximately 100kDa [527]. Also, a study by Yang *et al* (2020) has highlighted that the NLRP3 inflammasome is expressed at a protein level in human placental villous tissue originating from healthy and pre-eclamptic patients, possessing a molecular weight of approximately 110kDa which is circa 3kDa above the 107kDa isoform that was found in the current study.

The current study provides novel evidence of the establishment of a rapid, reproducible and scalable IgG immunodepletion method from the second supernatant and second pellet fractions of trophoblast, SVA and myometrium tissue lysates for the purposes of removing interfering immunoglobulin G from detecting less ubiquitous protein targets at approximately 50kDa using western blotting technique. The removal of immunoglobulin G was carried out since the heavy chain (approximately 50kDa) and the light chain (circa 25kDa) are highly abundant proteins in the plasma and serum which tend to obscure the identification of potential biomarkers that are generally found in lower concentrations using western blotting [534]. This process is further complicated by the intricacy and compelling range of the plasma proteome in which the abundance of the least ubiquitous and the most ubiquitous proteins may alter by as much as ten orders of magnitude [535]. As an example, albumin is the protein that is found at the highest concentration in serum which is circa 55% of the total protein amount. Albumin alongside IgA, IgG, transferrin, α-1-antitrypsin and haptoglobin account for circa 85% of the total proteome [535]. Currently, no investigations have presented data on an optimised protocol for the removal of IgG from the second pellet (membrane) or second supernatant (cytoplasmic) fractions of human placental CPA, SVA, villous

tissue or myometrium tissue lysates, hence the current study has addressed this gap into the literature. Also, since the expected P2X7 receptor molecular weight is approximately 70kDa and the IgG heavy chain molecular weight is approximately 50kDa, the P2X7 receptor visualisation may become affected due to the high preponderance of IgG protein expression level into the maternal blood. Moreover, the predicted molecular weight for the NLRP3 inflammasome is isoform 1 approximately 106kDa and isoform 2 circa 118kDa. The molecular weight of one of the detected NLRP3 inflammasome isoforms in western blots (highlighted in chapter 3.3.6) was approximately 74kDa and compared to IgG heavy chain molecular weight of approximately 50kDa, the multimeric protein visualisation could become obscured, since IgG is highly abundant in the maternal blood. Lastly, from the perspective of visualising pro-caspase-1 which was found in western blots at approximately 47kDa (chapter 3.3.6), the detection of the protein would have not been possible without the immunodepletion of IgG from the second supernatant (cytosolic) fraction of the stem villous artery tissue lysates, since the heavy chain of IgG was circa 50kDa and would have partially obscured the identification of the biomarker which is less ubiquitously expressed in this human placental tissue type.

Stimulation of trophoblast tissue with ATP, LPS+ATP or LPS+BzATP did not significantly change the NLRP3 inflammasome protein expression levels relative to unstimulated tissue. The results of this western blotting investigation further complement a study published by Maneta *et al* (2015) which highlighted that mononuclear cells isolated from cord blood, maternal blood and placental blood stimulated with LPS+BzATP induced a significant upregulation in IL-1β release relative to control [491]. The same study also highlighted that stimulation of cord blood

mononuclear cells with LPS+BzATP caused an upregulation in the expression of the NLRP3 inflammasome compared to unstimulated primary cells [491].

A recent study by Green *et al* (2018) has highlighted that fluctuating flow or elevated glucose or palmitate levels in the extracellular space such as in diabetes favour the P2X7 receptor surface expression [536], increased extracellular adenosine 5'-triphosphate [198,537] and downregulation of CD39 expression [538] at the level of the endothelium via generating an extracellular milieu suitable for elevated P2X7 receptor stimulation. In addition, exposure of human fibroblasts to increased levels of glucose triggers extracellular ATP liberation into the extracellular space and the establishment of P2X7 receptor aggregates close to the plasma membrane [539–541]. Furthermore, these P2X7 aggregates regulate endothelial cell dysfunction via increased reactive oxygen species synthesis, elevated cell permeability and expression of vascular cell adhesion molecule-1 and intracellular adhesion molecule-1 [539,540,542]. As a result, since extracellular glucose might play a key role in modulating the protein expression level of the P2X7 receptor in human fibroblasts and endothelial cells and no studies have investigated the exogenous influence of D-glucose on human placental villous tissue originating from healthy patients, the current investigation provides western blotting data to fill in this gap into the literature. The likely pathological mechanism of diabetes mellitus induced by the P2X7-NLRP3-IL-1β signalling pathway involves 4 important steps namely long-term elevated glucose levels promote the P2X7 receptor stimulation and in turn NLRP3 inflammasome stimulation, ultimately resulting in IL-1β release into the extracellular space [543]. This mechanism is achieved via induced pancreatic β cell malfunction and apoptosis due to elevated extracellular IL-1β levels, which also give rise to diminished insulin release and abnormal insulin signalling pathway that ultimately cause an exacerbation in elevated glucose levels [543].

Furthermore, IL-1β promotes the establishment of insulin resistance via impaired insulin sensitivity, diminished cellular uptake and metabolism of glucose [543].

The 5.5mM D-glucose concentration used in to stimulate the human placental villous tissue was chosen to mimic the physiological glucose plasma concentration of the pregnant mother. Also, the 10mM D-glucose concentration was used to mimic the gestational diabetes condition, as the disorder is diagnosed if one or more values equals or exceeds thresholds as fasting plasma glucose level (5.1mmol/l), one hour plasma glucose (10mmol/l) and 2 hour plasma glucose (8.5mmol/l) [544]. The 20mM and 30mM D-glucose concentrations were used to mimic type 1 diabetes mellitus since patients are diagnosed with the disorder when a plasma glucose level is more than 11.1mM measured 2 hours after a glucose load of 1.75g per kg (maximum dose of 75g) via an oral glucose tolerance test [545]. The 0mM D-glucose stimulation of villous tissue was used as a background control for the purposes of analysing released LDH levels from the human placental tissue.

A potential limitation of performing physiological studies on isolated human placental villous tissue in the current case by stimulating the explants with D-glucose for 4, 24 and 48 hours is that the syncytiotrophoblast undergoes continuous renewal, shedding aged nuclei in the form of syncytial knots and incorporating fresh CTBs by fusion as it has been shown by Zhou *et al* (2013) using isolated cytotrophoblast cells during the first 24-48 hours [546]. In this case, the authors demonstrated that the primary cytotrophoblast cells stained positive for CK7 and presented western blotting data showing that β-hCG expression gradually increased at 24 and 48 hours [546]. As a result, the first 48 hours following isolation of placental villous tissue could be sub-optimal to perform physiological studies on this tissue.

An elevated glucose level is a distinct danger mediator in diabetes. Long term physiological elevation of glucose levels gives rise to progressive suppression of insulin production and β-cell apoptosis in an autocrine process giving rise to insulin resistance [389,547]. Glucose has been shown to promote IL-1β release from monocytes, β-cells, endothelial cells and other islet cells. Following liberation into the extracellular space, IL-1β regulates the damaging effects of elevated glucose by promoting Fas-triggered programmed cell death via NF-kB and c-Jun N-terminal kinase (JNK) or by suppressing insulin metabolism in type 1 or type 2 diabetes mellitus [547,548]. Furthermore, the NLRP3 inflammasome is stimulated by thioredoxin-interacting protein (TXNIP) which has been shown to be closely related to insulin resistance along with diabetes and participates in glucose-induced interleukin-1β synthesis [389]. Moreover, TXNIP expression is activated by glucose and the protein expression levels of the biomarker are particularly elevated in subjects with diabetes mellitus [549]. The NLRP3 inflammasome has been shown to be stimulated by TXNIP in a reactive oxygen species-dependent manner. Furthermore, under the stimulation of elevated glucose concentration, thioredoxin-interacting protein is synthetised from thioredoxin to interact with the NLRP3 inflammasome and to activate the multimeric protein, ultimately giving rise to the synthesis of the pro-inflammatory cytokine IL-1β [389,497]. As a result, the released levels of IL-1β from placental villous tissue were measured in the tissue culture supernatant under the exposure of D-glucose acting as a danger associated molecular pattern since hyperglycemia has been categorised as a principal inducer of the NLRP3 inflammasome stimulation and IL-1β liberation into the extracellular space particularly in patients with type 2 diabetes mellitus [550].

The released lactate dehydrogenase levels measured in the culture media of placental villous tissue which has been stimulated with D-glucose at a concentration

of 20mM and 30mM were found particularly low following 48 hours of treatment especially compared to 5.5mM D-glucose concentration which suggests that an elevated D-glucose stimulation might have a protective function in human placental villous tissue since lower levels of the enzyme were liberated into the extracellular space. The enzyme LDH is a crucial component of glucose turnover since it catalyses the breakdown of pyruvate (end compound of glycolysis) to lactate and vice versa. In an aerobic environment, primary cells translocate pyruvate into their mitochondria to metabolise it via the tricarboxylic acid (TCA) cycle into carbon dioxide and water [551]. During the TCA cycle, nicotinamide adenine dinucleotide is synthetised and is reoxidized in the oxidative phosphorylation, ultimately giving rise to energy in the form of adenosine 5'-triphosphate. The turnover of a single molecule of glucose elicits the production of up to 36 molecules of ATP [551]. However, in an environment with low oxygen levels, pyruvate is metabolised into lactate via lactate dehydrogenase enzyme in a signalling cascade known as the anaerobic glycolysis where only two molecules of adenosine 5'-triphosphate are synthetised [551]. A possible explanation of a high extracellular glucose concentration downregulating the release of LDH into the extracellular space from villous tissue is that the syncytiotrophoblast, cytotrophoblast and endothelial cells may under aerobic conditions upregulate the glycolysis process resulting in the synthesis of elevated concentrations of pyruvate at an intracellular level which is further transported to the mitochondria, ultimately giving rise to the synthesis of elevated intracellular ATP levels. Since pyruvate might not be primarily metabolised to lactate by LDH in aerobic conditions, a downregulation of the LDH enzyme in primary placental cells might take place in an environment characterised by a high glucose concentration in the extracellular space.

A limitation of the western blotting data highlighting the relative P2X7 receptor protein expression levels in isolated human placental villous tissue which has been stimulated with D-glucose at concentrations of 0mM, 5.5mM, 10mM, 20mM or 30mM for 4, 24 or 48 hours is a noticeable variability in the corresponding relative β-actin protein expression levels across samples of the same placental tissue type. In this case, no optimisation in choosing a suitable loading control used to normalize the signals from the proteins of interest took place, therefore the selection of a different housekeeping protein which remains constant (relative to the total protein content) under the test conditions might be advantageous in the analysis of the results from the western blotting experiment.

The current study highlighted no statistically significant differences in the P2X7 receptor, NLRP3 inflammasome and procaspase-1 protein expression levels in stem villous artery between healthy and preeclamptic placental samples. These novel results further complement a study published by Valdecantos and colleagues (2003) where the authors have suggested that the P2X7 receptor was expressed on the smooth muscle of human chorionic blood vessels at an mRNA level [479].

A potential limitation of the western blotting data highlighting the relative protein expression levels of the P2X7 receptor, NLRP3 inflammasome and pro-caspase-1 in isolated human placental stem villous arteries is that two of the eight pre-eclamptic patients were also co-diagnosed with intrauterine growth restriction which is a confounder in the analysis of the western blotting data in terms of the association between patients solely diagnosed with pre-eclampsia and subjects diagnosed with both pre-eclampsia and IUGR. Furthermore, another limitation of this western blotting data using placental samples of normotensive and pre-eclamptic patients is that no optimisation in selecting a suitable loading control took place, more importantly in the

case of tissue originating from pre-eclamptic subjects where the disorder might affect constitutively expressed proteins depending on the selected treatment of patients which may result in a variation as in the current case of β-actin levels across the same tissue type (stem villous arteries) originating from different hypertensive volunteers.

Also, a limitation of multiple comparison tests undertaken between released IL-1β, IL-6 and IL-18 pro-inflammatory cytokines from human placental chorionic plate arteries, stem villous arteries and villous tissue which have been stimulated with control, ATP, LPS+ATP or LPS+BzATP is an increased statistical risk that a proportion of associations are false positives. Therefore, during the process of simultaneously evaluating multiple hypotheses, drawing valid conclusions may necessitate to consider correction approaches in the number of undertaken statistical tests and adjusting the statistical confidence measures using one of the several published strategies such as the Benferroni, the Holm or the Hochberg corrections which allow to determine false discovery rates and q-values [552].

The P2X7 receptor antagonist A740003 and agonists ATP and BzATP were used to determine whether the P2X7 receptor inhibition or activation in human placenta chorionic plate artery smooth muscle cells influence its intrinsic ability to form clusters via large scale changes in purinergic receptor density which have been shown to regulate pore formation in cells that endogenously express the P2X7 receptor [553].

Immunocytochemistry data of the P2X7 receptor expression in human placental chorionic plate artery smooth muscle cells which have been unstimulated or stimulated with ATP, BzATP or A740003 highlighted that the purinergic receptor was localised in the nuclear region of the primary cells and primarily located intracellularly, which is particularly unexpected for a membrane receptor. A possible explanation for this P2X7 receptor immunolocalization could be that the internalization of the receptor may act

as a protective mechanism for primary cells to avoid programmed cell death by preventing the recruitment of the purinergic receptor to the membrane of cells. However, during cellular stress the P2X7 receptor might become translocated to the membrane of cells when the extracellular adenosine 5'-triphosphate levels become particularly high and the primary cell is incapable of undertaking its physiological function. This intracellular immunolocalization of the P2X7 receptor in association with the nuclei of syncytiotrophoblast (particularly in term villous tissue) and cytotrophoblasts (especially in first trimester villous tissue) has also been observed by Roberts *et al* (2007) [321].

The P2X7 receptor has been shown to be expressed in multiple cell types including immune cells especially macrophages, mast cells, T-cells and microglia but also in Schwann cells of the peripheral nervous system, oligodendrocytes of the central nervous system and in epithelial cells [306,328]. The same purinergic receptor has also been shown to be expressed at a protein level on primary cytotrophoblast cells using western blotting and also at a tissue level in first trimester and term placental villous tissue especially in association with syncytiotrophoblast nuclei using immunohistochemistry [321]. Since no other investigations have assessed the fluorescence intensity levels of the P2X7 receptor positive syncytiotrophoblast profiles via systematic random sampling and have not investigated the expression of the purinoceptor at the level of the fetal vessels using immunohistochemistry, little is known about its distribution in human placental villous tissue originating from healthy and diet managed gestational diabetic subjects, hence the current study helps to fill in this gap into the literature.

P2X7 receptor was visualised as a thin circular staining present on the endothelial cells forming the fetal capillaries (25-40μm diameter) located in the vicinity

of the syncytiotrophoblast and the cytotrophoblast cells. Also, the purinergic receptor was located on the apical surface of the uniform syncitiotrophoblastic layer (10-15μm thick) and also on cytotrophoblast cells. The current P2X7 receptor immunolocalization results at a placental villous tissue level further complement a published study by Roberts and colleagues (2006) where the authors have demonstrated that the purinergic receptor was expressed at a cellular level in isolated cytotrophoblast cells from 3 placental preparations using the western blotting technique [277]. Also, the same systematic pharmacological study demonstrated that the P2X7 receptor was functionally active in the isolated human placental cytotrophoblast cells and suggested that the activation of this purinergic receptor gives rise to a consequent increase in intracellular Ca^{2+} concentration, therefore regulating the syncytiotrophoblast metabolism and the feto-maternal ion translocation [277].

Another study published by Roberts and colleagues (2007) revealed that the P2X7 receptor was expressed at an mRNA level in isolated placental villous tissue and that immunohistochemical localisation of the purinergic receptor in both first trimester (n=3) and term villous tissue (n=3) was visualised intracellularly in conjunction with multiple nuclei accompanied by a dispersed staining present in the cytosol [480]. In this case, the authors have also shown that the P2X7 receptor staining was also present at the level of syncytiotrophoblast with a higher intensity in term tissue samples compared with the first trimester [480].

This chapter presents novel western blotting data on the P2X7 receptor protein expression levels in the human placenta, particularly in the chorionic plate artery, stem villous artery, villous tissue and myometrium. In this case, no studies have yet investigated the P2X7 receptor expression at a protein level in SVA's and CPA's originating from placental samples of healthy or complicated pregnancies, even if the

P2X7 receptor has been shown to be expressed at an mRNA level in CPA's by Valdecantos *et al* (2003) [479]. Although the P2X7 receptor has been demonstrated to be localised in human placental villous tissue using immunohistochemistry, especially at the level of the syncytiotrophoblast tissue [321] and to be expressed at an mRNA level in the same tissue type [321], no studies have yet assessed the protein expression levels of the P2X7 receptor in villous tissue using western blotting. However, the P2X7 receptor protein expression levels in the human myometrium have been investigated before in a study published by Maneta *et al* (2015) [554]. The current study has also confirmed that the P2X7 receptor is expressed at a protein level in myometrium tissue using western blotting.

This study has identified a novel method for the immunodepletion of IgG from human placental villous tissue, SVA and myometrium originating from healthy patients. Although the study by Roberts *et al* (2007) [321] has found that the P2X7 receptor was expressed in villous tissue in association with syncytiotrophoblast nuclei, the immunolocalization of the P2X7 receptor in human placental villous tissue originating from healthy and diet managed gestational diabetes mellitus pregnancies, which has been comprehensively described in the current investigation and rated according to the fluorescence intensity levels of the positive syncytiotrophoblast profiles using systematic random sampling as well as characterised at the level of the fetal vessels constitutes novel data.

Furthermore, the current study presents novel western blotting data in terms of characterising the protein expression level of the NLRP3 inflammaosme at the level of the 4th order chorionic plate arteries, stem villous arteries and choriodecidua. Moreover, the findings that the protein expression levels of the NLRP3 inflammasome did not significantly change under the stimulation of isolated human placental villous

tissue with ATP, LPS+ATP or LPS+BzATP originating from healthy patients assessed using western blotting are also novel.

The protein expression studies which have assessed the relative P2X7 receptor levels in D-glucose stimulated placental villous tissue using western blotting are novel. These studies are also complemented by further novel data which has showed that the P2X7 receptor, NLRP3 inflammasome and pro-caspase-1 protein expression levels in human placental villous tissue are not significantly different between normotensive and pre-eclamptic subjects assessed using western blotting.

The current study presents novel data about the pro-inflammatory cytokine (IL-1β, IL-6 and IL-18) release from human placental villous tissue, CPA and SVA originating from healthy subjects which have been stimulated with control, ATP, LPS+ATP or LPS+BzATP. Moreover, the current study shows novel data about the P2X7 receptor immunolocalization in human placental chorionic plate artery smooth muscle cells which were isolated using either the tissue explant or enzymatic digestion method.

In terms of limitations of the current study, multiple western blots of the P2X7 receptor have shown the presence of non-specific binding in the region of approximately 46kDa to 152kDa which was due to the primary antibody chosen as indicated from both the P2X7 receptor with blocking peptide immunoblots and P2X7 receptor secondary antibody control immunoblots. Also, in the case of the NLRP3 inflammasome, multiple western blots highlighted the presence of non-specific binding in the region of circa 49kDa to 58kDa which was due to the secondary antibody chosen as suggested from the NLRP3 inflammasome secondary antibody control immunoblots. A further limitation of the current western blotting studies is the absence

of blocking peptide controls for the NLRP3 inflammasome and pro-caspase-1 since no blocking peptide could not be sourced from the corresponding manufacturers.

Another limitation of the current investigation is that a limited proportion of the western blotting, RT-qPCR, immunocytochemistry, pro-inflammatory cytokine and LDH measurement studies contained relatively few numbers of participants included, which may prevent the findings from being extrapolated.

The results from this investigation have showed that the P2X7 receptor is expressed at a protein level (membrane fraction of tissue lysates) in isolated human placental chorionic plate arteries, stem villous arteries, villous tissue and myometrium using western botting and at an mRNA level in stem villous arteries using RT-qPCR. The P2X7 receptor has been shown to be expressed at a cellular level in human placental chorionic plate artery smooth muscle cells which have been isolated via enzymatic digestion or explant method using immunocytochemistry. These primary placental cells which have been isolated using the tissue explant method and stimulated with ATP at concentrations of 1μM or 10μM showed a statistically significant difference in P2X7 receptor mean fluorescence intensity levels between 0.5 hours and 4 hours of stimulation with the nucleotide. Also, the purinergic receptor has been shown to be expressed in isolated sections of human placental villous tissue especially at the level of the syncytiotrophoblast layer, fetal capillaries and on cytotrophoblast cells. In this case, a statistically significant difference in the P2X7 receptor+CD31 double positive placental vascular profiles was found between healthy and diet managed gestational diabetes mellitus patients. This result complements two studies by Rodrigues *et al* (2014) [555] and Menzies *et al* (2017) [556] which have highlighted that in renal biopsy sections from diabetic patients, the P2X7 receptor expression was upregulated.

The P2X7 receptor has also been shown to be expressed at a tissue level in isolated sections of human placenta chorionic plate arteries at the level of the endothelial cells. Also, the protein expression levels of the P2X7 receptor in villous tissue stimulated with D-glucose for 4, 24 or 48 hours did not significantly change relative to control (0 hours). In this case, no statistically significant differences were found between 4 and 48 hours in the released IL-1β levels measured in the culture media for each of the D-glucose concentrations used. However, a statistically significant decrease in the released LDH levels measured in the culture media were found at 48 hours from villous tissue which has been stimulated with 20mM and 30mM D-glucose compared to control (5.5mM D-glucose). Also, no statistically significant change in the P2X7 receptor protein expression levels was identified between normotensive and pre-eclamptic patients assessed using western blotting. A study by Tozzi *et al* (2017) have demonstrated that an increase in glucose stimulation from 5.5mM to 16.7mM of INS-1E cells (rat pancreatic β cell line) induced a fast and large increase in the extracellular ATP concentration [512]. The same study has also shown that a high glucose stimulation (16.7mM) of the same cells for 48 hours caused an elevation in P2X7 receptor protein expression levels compared to the same cells grown in low glucose (2.8mM) by the identification of a P2X7 receptor protein product at approximately 75kDa in the western blot [512]. Although P2X7 receptor-mediated apoptosis is elevated in human fibroblasts exposed to an elevated glucose concentration [540] and in fibroblasts from type 2 diabetes [557] patients, in the current study, D-glucose stimulation of human placental villous tissue for 4, 24 or 48 hours did not significantly alter the P2X7 receptor protein expression levels and at 48 hours caused a significant decrease in the released LDH levels in the culture media from

20mM and 30mM D-glucose stimulated villous tissue compared to control (5.5mM D-glucose).

The novel results that the P2X7 receptor is expressed at the level of the syncytiotrophoblast layer, cytotrophoblast cells and fetal capillaries are of particular interest especially in the case of pre-eclamptic patients where elevated maternal extracellular ATP concentrations (circa 2.5 times higher compared to healthy patients [558]) present at the level of the intervillous space might activate the purinergic receptor which in turn could cause the assembly of the NLRP3 inflammasome and ultimately resulting in an exacerbated release of IL-1β into the extracellular space. Although the current study has found no statistically significant differences in the P2X7 receptor protein expression level between normotensive and pre-eclamptic patients, the purinergic receptor activation by elevated circulating extracellular ATP levels may cause further P2X7-mediated ATP release which is exacerbated in pre-eclampsia by abnormal placental oxygenation, fetal hypoxia and platelet aggregation [277].

The finding that the P2X7 receptor is expressed at a protein level in CPA, SVA, villous tissue and myometrium and at an mRNA level in stem villous arteries hints at a function for extracellular nucleotides in this vascular territory which is novel since the placental blood vessels are not innervated. Also, since the P2X7 receptor has been found at a cellular level in isolated chorionic plate artery smooth muscle cells, the function of adenosine 5'-triphosphate in these blood vessels is even more crucial as α_1-adrenoreceptors for instance norepinephrine and phenylephrine do not modulate the vasoconstriction or vasorelaxation of these blood vessels [479].

The results from this investigation have also showed that the NLRP3 inflammasome is expressed at a protein level in the fourth order CPA, SVA and choriodecidua isolated from human placental tissues originating from healthy patients

using western blotting. In these tissue types, four NLRP3 inflammasome isoforms have been identified at approximately 79kDa, 107kDa, 171kDa and 222kDa. No statistically significant changes in the relative protein expression levels of the NLRP3 inflammasome have been identified between villous tissue originating from healthy patients which has been stimulated with control, ATP, LPS+ATP or LPS+BzATP in the case of all three protein products detected at circa 78kDa, approximately 92kDa and circa 131kDa using western blotting. Similarly, the current study has found no statistically significant differences in the relative protein expression levels of the NLRP3 inflammasome in stem villous arteries between normotensive and pre-eclamptic patients in the case of both protein products detected at approximately 74kDa and 92kDa using western blotting. The current results have also shown that the NLRP3 inflammasome is expressed at an mRNA level in stem villous arteries originating from healthy and pre-eclamptic patients using RT-qPCR. The current study has presented immunocytochemistry data which showed that the NLRP3 inflammasome is not expressed in human placental chorionic plate artery smooth muscle cells which have been isolated using the tissue explant method.

This study found no statistically significant differences in the relative pro-caspase-1 protein expression levels between in stem villous arteries of normotensive and pre-eclamptic patients using western blotting. This study has also presented evidence that caspase-1 is expressed at an mRNA level in stem villous arteries originating from healthy volunteers using RT-qPCR.

The current investigation has also demonstrated that the IL-1β release measured in the tissue culture media using ELISA from villous tissue, chorionic plate artery and stem villous artery which have been stimulated with control, ATP, LPS+ATP and LPS+BzATP was the highest in the LPS+ATP group followed by the LPS+BzATP

group compared to control. However, LPS+ATP and LPS+BzATP stimulations of the villous tissue, CPA and SVA did not induce a statistically significant difference in the released IL-6 levels compared to control. A limitation of this study is that no LPS control experimental condition was undertaken, which limits the interpretation of these results. Since no statistically significant differences in the release of IL-1β, IL-6 and IL-18 were found between control and ATP stimulations of CPA, SVA and villous tissue, and no LPS control experimental condition was undertaken, the cytokine release effect of LPS+ATP stimulation was due to LPS with an unknown contribution of ATP. The activation of the P2X7-NLRP3-IL-1β signalling pathway involves a two-step mechanism firstly the activation of TLR-4 by LPS which facilitates the transcription of the *IL-1β* gene and encouraging the built-up of pro-IL-1β (inactive form) in the cytosol, followed by the second step which is the stimulation of the P2X7 receptor by ATP, ultimately causing the assembly of the NLRP3 multimeric complex, which results in the conversion of pro-IL-1β to its active form IL-1β. Since no priming of the isolated placental tissue with LPS control took place (which is required for pro-IL-1β synthesis), the ATP stimulation of CPA, SVA and villous tissue did not induce the release of the active form of the cytokine (IL-1β) towards the extracellular space, hence the current study has shown that the mature form of the cytokine measured in the culture media was particularly decreased in all three placental tissue types studied.

The compound BzATP is occasionally characterised as a selective P2X7 receptor agonist but in fact it has the highest potency at P2X1 receptors followed by P2X3 receptors [146]. Since the compound is approximately 10 times more potent than ATP, it has been regularly used for the stimulation of the P2X7 receptor to avoid elevated cytotoxic levels of the nucleotide [146]. The BzATP EC_{50} values (μM) at P2X receptors is the following: 0.002 at P2X1, 0.75 at P2X2, 0.08 at P2X3, 0.5 at P2X4, 6-

40 at P2X5, 25 at P2X6 and 5 at P2X7 [146]. BzATP was originally reported to be selective for the P2X7 receptor [291] however, emerging studies have found that it also stimulated $P2Y_1$ and $P2Y_{11}$ purinoceptors [559]. At particularly elevated concentrations (100 μM or higher) BzATP caused a rise in intracellular Ca^{2+} concentration and stimulated K^+ liberation towards the extracellular space from cytotrophoblast cells [277]. This could indicate stimulation of receptors other than the P2X7 since the purinoceptor is generally stimulated at decreased levels of BzATP for instance 15μM [560].

In the case of A740003, a study by Honore *et al* (2006) have highlighted that the compound potently blocks the human P2X7 receptor, with a determined IC_{50} value of 40nM [561]. In the current study, the chosen concentration of A740003 which was used to block the P2X7 receptor was 1μM.

Although the P2X7 receptor has been found to be expressed in isolated human placental chorionic plate artery smooth muscle cells using both enzymatic digestion and tissue explant method, the current study has also found the purinergic receptor to be expressed on endothelial cells but not smooth muscle cells in isolated sections of the chorionic plate artery. In this case, a limitation of the immunohistochemistry study is that the P2X7 receptor expression was only investigated in isolated sections of chorionic plate artery tissue originating from two healthy patients which limits the interpretation of these results.

Another limitation of the current study is that no positive (for instance HEK293 cells stably transfected with the P2X7 receptor [562]) or negative controls (for example an isotype-specific immunoglobulin, in this case rabbit IgG) for the P2X7 receptor staining were undertaken alongside immunocytochemistry experiments investigating the immunolocalization of the purinergic receptor in isolated human chorionic plate artery smooth muscle cells.

CHAPTER 4

INVESTIGATING THE EFFECTS OF PURINERGIC AGONISTS AND ANTAGONISTS ON ISOLATED HUMAN PLACENTAL BLOOD VESSELS USING WIRE MYOGRAPHY

4.1 Introduction

The function of circulating extracellular nucleotides in particular ATP has drawn a significant amount of physiological attention as, over the last few decades, multiple clones of nucleotide purinoceptors were comprehensively described [563,564]. Multiple reviews have meticulously and elegantly highlighted the expression of nucleotide receptors [130,565] located at the level of skeletal and non-vascular smooth muscle [566–568], human thrombocytes [569–571] as well as neurons [572,573]. The distribution of the nucleotide receptors in blood vessels highlights a localisation at the level of the smooth muscle and endothelial cells, as well as the adjacent nerves [130]. In the case of blood vessels, the purinergic P2Y receptors are particularly expressed on the endothelial cells, while the P2X receptors are found predominantly on the surface of the smooth muscle cells. Decreased diameter arteries and arterioles located at the level of the systemic vasculature have been widely recognised as being regulated via the sympathetic nervous system [574].

Due to the fact that the endothelial cells release adenosine 5'-triphosphate into the extracellular space under the stimulation of multiple factors especially decreased oxygen levels [130,575], a potential involvement of nucleotide receptors in modulating the vascular contractility through interactions involving both smooth muscle and endothelial cells has attracted much interest over the last few decades. The fetoplacental vasculature comprises of the umbilical arteries, umbilical vein, the chorionic plate and lastly the stem villous blood vessels. The umbilical arteries extensively divide following the point of umbilical cord insertion into the chorionic plate, giving rise to a vast network of chorionic plate arteries which possess important attributes typical of the resistance circulation (<300μm internal diameter), overall suggesting a significant contribution in regulating the vascular tone of the fetoplacental

blood vessels [576]. Despite a crucial role in supporting the development of a healthy pregnancy, the molecular processes involved in managing the blood flow as well as vasomotor tone at the level of the fetoplacental vasculature have not been fully elucidated yet. Taking into account that the human placenta accompanied by the umbilical cord blood vessels possess the exclusive property of not being innervated [281,577], the current study allocated a particular interest into evaluating the involvement of purinergic receptor agonists and antagonists in the regulation of the human placenta chorionic plate arteries. Since Buvinic *et al* (2006) have shown that contractions to purines in human chorionic plate arteries involved both the endothelium and smooth muscle [481], using classical pharmacology protocols, the present research functionally describes canonical purinergic receptors, with a particular focus on the potential involvement of the P2X7 receptor localised at the level of the smooth muscle and endothelial layer of the chorionic plate arteries in regulating the feto-placental circulation.

The absence of autonomic innervation at the level of the fetoplacental vasculature denotes the presence of a different physiological mechanism regulating the resistance of the placental blood vessels which could include circulating mediators, endothelial cell involvement, regional paracrine signalling or even the involvement of regional physical mediators [576]. The fetoplacental arteries have been suggested to possess a significantly decreased sensitivity to mediators which elicit a dominant vasoactive response in alternative blood vessels [61,578]. Endothelial cells synthetise multiple factors involved in mediating the contractility property of blood vessels. Placental and umbilical blood vessels originating from human subjects have shown to release various vasocontractile agents for instance endothelin-1 [579] and endothelium-derived vasorelaxation mediators such as nitric oxide (NO) [580,581]. The current

knowledge regarding the regulation of the fetoplacental blood vessels originates from research based on excised *in vitro* perfused cotyledon preparations where the suppression of nitric oxide synthesis has been shown to elevate the perfusion pressure, indicating the crucial function of NO in mediating vascular contractility [582,583], or from small vessel myography studies [49,576]. Furthermore, a study by Parisi and Walsh (1989) has highlighted that endothelial-derived eicosanoids can similarly coordinate the feto-placental vasculature, especially changes in the levels of prostacyclin and thromboxane A_2, which have been strongly correlated to an elevated resistance of blood vessels characteristic of pre-eclamptic patients [584].

A limited body of literature has directly investigated the physiological reactions of narrow fetoplacental blood vessels which may potentially be involved in the general management of blood flow across the human placenta. Some of these investigations include measurements of isometric tension using the wire myography technique under the exposure of various mediators [585–587]. The blood vessels studied in this case were chorionic plate arteries (CPA's) and veins, as well as stem villous arteries, with a wide body of the literature focusing on assessing the CPA contribution towards the establishment of a physiological fetoplacental blood flow. In this case, a vasoconstriction effect has been described under the exposure of thromboxane A_2 [588,589] and vasopressin [576,590]. On the other side, endothelium-dependent vasodilation has been challenging to achieve, particularly with mediators for instance histamine, acetylcholine or bradykinin [576,585], even if stem villous arteries were able to significantly vasodilate under the exogenous application of prostacyclin I_2 [591] or histamine [586].

Prior studies investigating the vasoactive effects of extracellular nucleotides including adenosine in isolated human placental chorionic blood vessels and perfused

cotyledons have highlighted a reproducible and effective vasoconstriction response [475,478,523]. Despite of this, the vasoactive function of extracellular ATP in placental blood vessels has not been fully elucidated yet. A further investigation has highlighted that adenosine 5'-triphosphate elicits a vasoconstriction effect in superficial chorionic plate vessels originating from the human placenta [479]. By taking into account that extracellular ATP is quickly metabolised by releasable ectonucleotidases [592], a potential mechanism regulating the placental vasculature could involve the release of ATP into the feto-placental circulation, resulting in the synthesis of adenosine, which has been shown to possess a potent vasomotor property in isolated human chorionic vessel ring preparations and intact perfused cotyledons [473].

4.2 Hypothesis and aims

The hypothesis of this study is that purinergic receptor agonists regulate the blood flow of the chorionic plate and stem villous vasculature of the human placenta given their known function in vasoconstriction and vasorelaxation via involving the P2X7 receptor in the humoral regulation of this placental vascular territory.

The aims of this study were to:

- Assess the vasoactive effects of sodium nitroprusside dihydrate in isolated human placenta chorionic plate artery originating from healthy patients
- Investigate the vasoactive effects of riluzole in isolated human placenta chorionic plate artery originating from healthy and pre-eclamptic subjects
- Evaluate the influence of the P2X7 receptor antagonist A740003 in U46619-induced vasoactive effects of isolated chorionic plate artery preparations originating from healthy volunteers

- Assess the influence of the P2X7 receptor antagonist A740003 in ATP-induced vasoconstriction effects in the second and fourth order chorionic plate artery originating from healthy patients
- Describe the vasoactive effects of ATP in the second order and resistance (<520μm internal diameter) chorionic plate artery by undertaking three consecutive ATP cumulative concentration curves (10^{-5}M, $3.3*10^{-5}$M, 10^{-4}M, $3.3*10^{-4}$M, 10^{-3}M, $3.3*10^{-3}$M, 10^{-2}M) in the presence and absence of A740003
- Characterise the vasoactive effects of ATP in isolated resistance CPA's by undertaking three consecutive ATP cumulative concentration curves (10^{-3}M, $3.3*10^{-3}$M and 10^{-2}M) in the presence and absence of A740003
- Investigate the vasoactive effects initiated by ATP in isolated resistance CPA's using sequential applications of the nucleotide at concentrations of $3.3*10^{-4}$M, 10^{-3}M, $3.3*10^{-3}$M and 10^{-2}M
- Assess the vasoactive effects of ATP on isolated resistance CPA's in the presence and absence of a 30mM and 40mM KPSS-induced elevation in the resting basal tone
- Determine the vasoactive effects of the P2X7 receptor agonist BzATP in isolated resistance CPA's
- Characterise the vasoactive effects of BzATP on isolated resistance CPA's in the presence and absence of a 30mM, 50mM and 70mM KPSS-induced elevation in the resting basal tone
- To characterise the vasoactive effects of ATP in isolated stem villous arteries originating from a metformin managed gestational diabetic patient

4.3 Results

The methods used in this results chapter have been described in chapter 2.3-2.5.

4.3.1 Sodium nitroprusside dihydrate caused an effective vasorelaxation response in preconstricted chorionic plate arteries whereas riluzole elicited a limited vasoactive modulator capacity in adjacent human placental artery preparations of a healthy patient

The CPA's isolated from a healthy placenta sample showed an effective vasodilation effect under the exogenous application of SNP, as highlighted in figure 97, but also in the SNP log concentration-effect curve presented in figure 98. A significant vasodilation response under the exposure of SNP was recorded in this investigation highlighting a maximal vasorelaxation (R_{max}) of 69.98% of the topmost U46619-induced vasoconstriction detected at the nitric oxide donor concentration of $3.3*10^{-6}$M. Riluzole showed a limited capacity to induce a considerable vasorelaxation response which showed a maximal riluzole-induced vasodilation (R_{max}) effect of 13.06% of the topmost U46619-preconstriction at a concentration of $3.3*10^{-6}$M, as shown in figure 97 and figure 98. In this investigation, one CPA preparation was used as a time control which highlighted that an insubstantial vasorelaxation response (R_{max}) was observed (maximal vasodilation of 17.26% relative to maximal U46619 vasoconstriction) as shown in figures 97 and 98. Similarly, a separate CPA preparation was subjected to a vehicle control dimethyl sulfoxide (DMSO) which highlighted a maximal CPA vasorelaxation (R_{max}) effect of 34.48% of topmost preconstriction to

U46619 at a concentration of 0.033% (v/v) of the total chamber volume as shown in figure 97 and figure 98. The maximal vasoconstriction elicited by KPSS (α) was 186.04% of the topmost U46619-induced vasoconstriction as highlighted in figure 98, CPA 1. This preliminary wire myography study provides evidence that pre-constricting the isolated CPA's with U46619 to a maximal cumulative concentration of $3.3*10^{-7}$M results in an effective vasorelaxation response to sodium nitroprusside dihydrate.

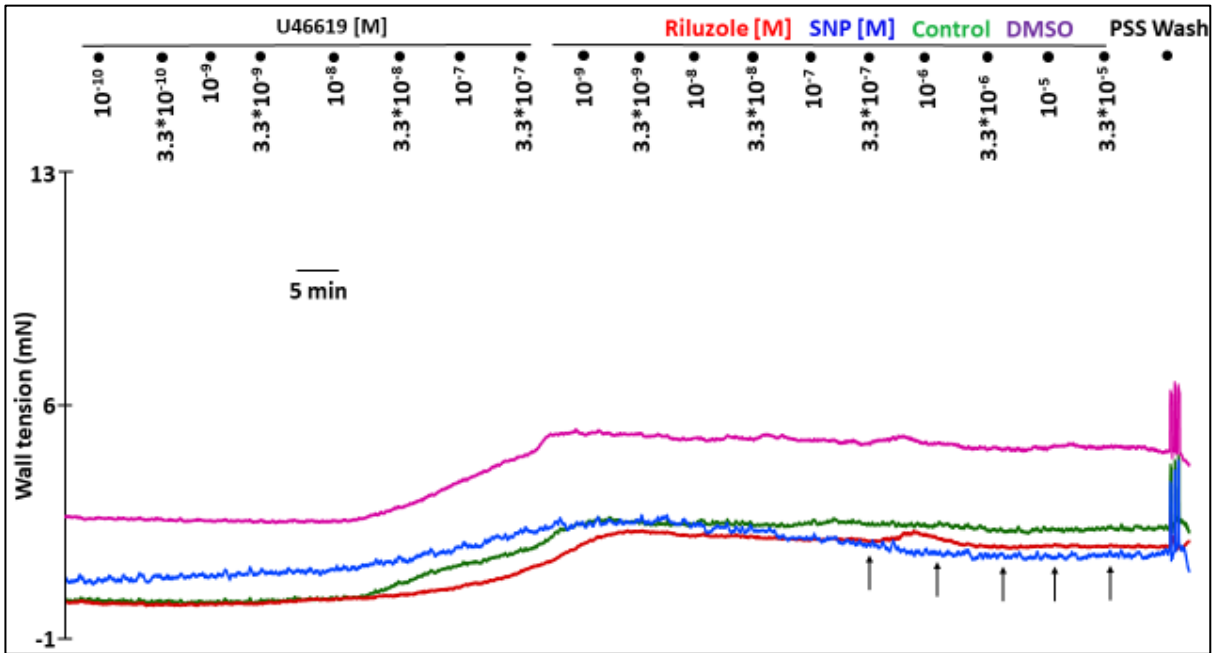


Figure 97. *Preliminary wire myography trace highlighting the vasoactive properties of riluzole (red trace), sodium nitroprusside (blue trace), time control (no drugs added) (green trace) and vehicle control (DMSO) (purple trace) evoked by isolated chorionic plate arteries originating from a healthy patient (T2665). In this case, the CPA's were initially preconstricted using cumulative concentrations of the thromboxane A_2 mimetic U46619 (10^{-10}M to $3.3*10^{-7}$M) at approximately 3 to 10 minutes intervals. Black arrows highlight a considerable vasorelaxation response generated by SNP at concentrations ranging from $3.3*10^{-7}$M to $3.3*10^{-5}$M. Internal diameters of CPA's were as follows: red trace 0.217mm, blue trace 0.219mm, green trace 0.248mm and purple trace 0.240mm Black dots denote drug additions to give indicated bath concentrations. Bar indicates the presence of the mentioned compound to the corresponding matching colour force myograph trace (with the exception of black colour which applies to all traces i.e. U46619) or physiological salt solution wash-out.*

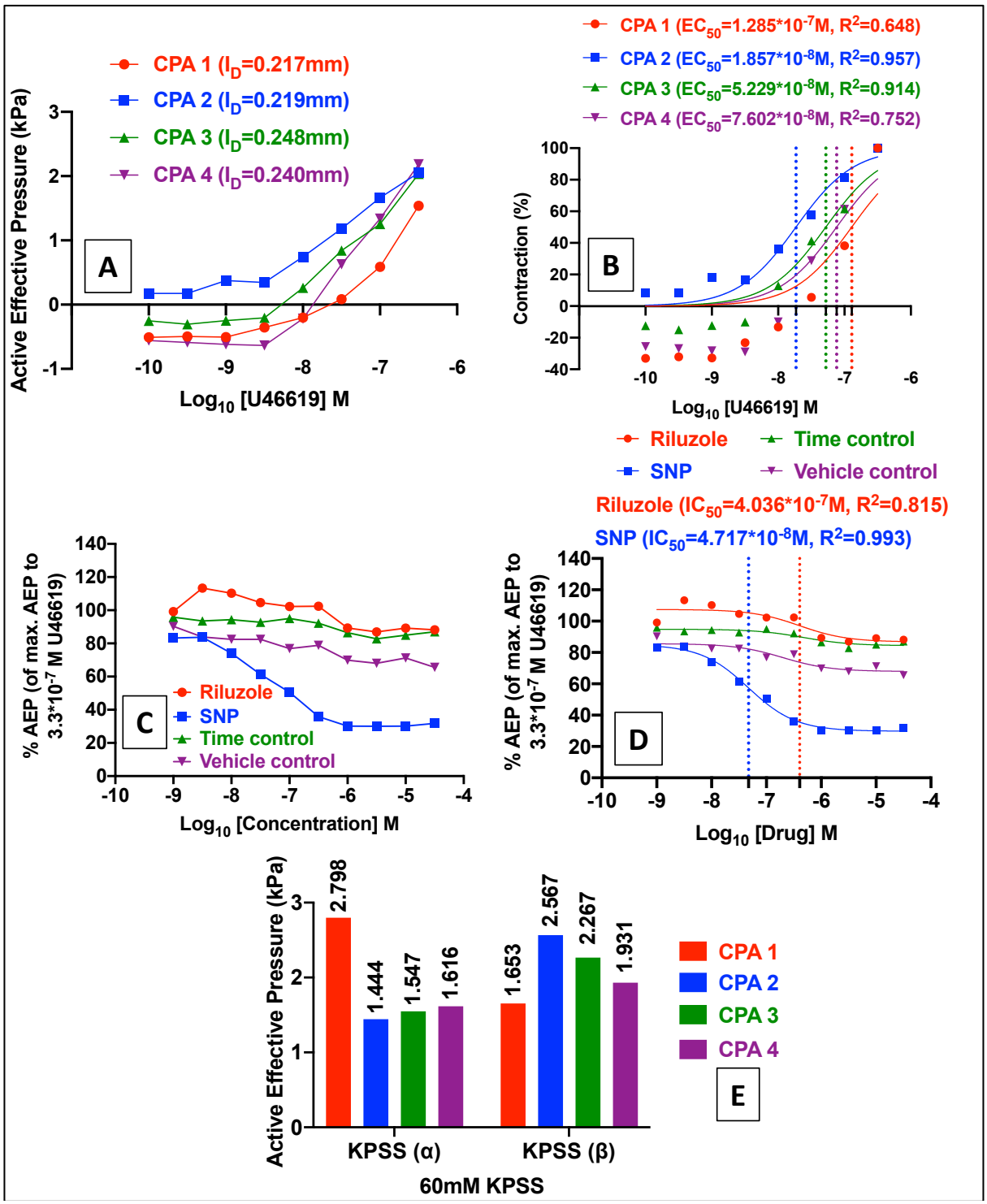


Figure 98. *Vasoactive effects of U46619, riluzole, SNP, time control (no drugs added), vehicle control (DMSO) and 60mM KPSS initiated by isolated CPA's originating from a healthy volunteer (T2665)* ***A***. *Log concentration-effect curve elicited by U46619 expressed as active effective pressure (AEP) (kPa), I_D denotes internal diameter* ***B***. *Nonlinear regression fit of log concentration-effect curve elicited by U46619 in CPA's highlighting the determined U46619 EC_{50} values of all four CPA's studied (illustrated by vertical discontinued lines)* ***C***. *Log concentration-effect curve of riluzole, SNP, time control and vehicle control expressed as percentage AEP of maximal AEP to 3.3*10-7M U46619* ***D***. *Nonlinear regression fit (three parameter logistic equation) of log*

concentration-effect curve initiated by riluzole, SNP, time control and vehicle control highlighting a calculated SNP IC_{50} value of $4.717*10^{-8}$M (illustrated by a blue vertical discontinued line) and a determined riluzole IC_{50} value of $4.036*10^{-7}$M (highlighted by a red vertical discontinued line) ***E****. Vasoconstriction induced by 60mM KPSS at the beginning KPSS (α) and completion KPSS (β) of the wire myography investigation presented as active effective pressure (kPa).*

4.3.2 The endothelium-independent dilator riluzole caused a limited vasorelaxation effect in preconstricted chorionic plate arteries of a healthy pregnancy case

All CPA vessels were preconstricted with U46619 (10^{-7}M; approximate EC_{80}) and relaxation measured in response to incremental concentrations of riluzole (10^{-9}M to $3.3*10^{-5}$M). The initial U46619 concentration response curve used to evaluate the CPA contractile function and to determine an approximate U46619 EC_{80} concentration. In this case, riluzole did not induce a notable vasorelaxation effect compared to time matched controls at the same timepoints (figure 99).

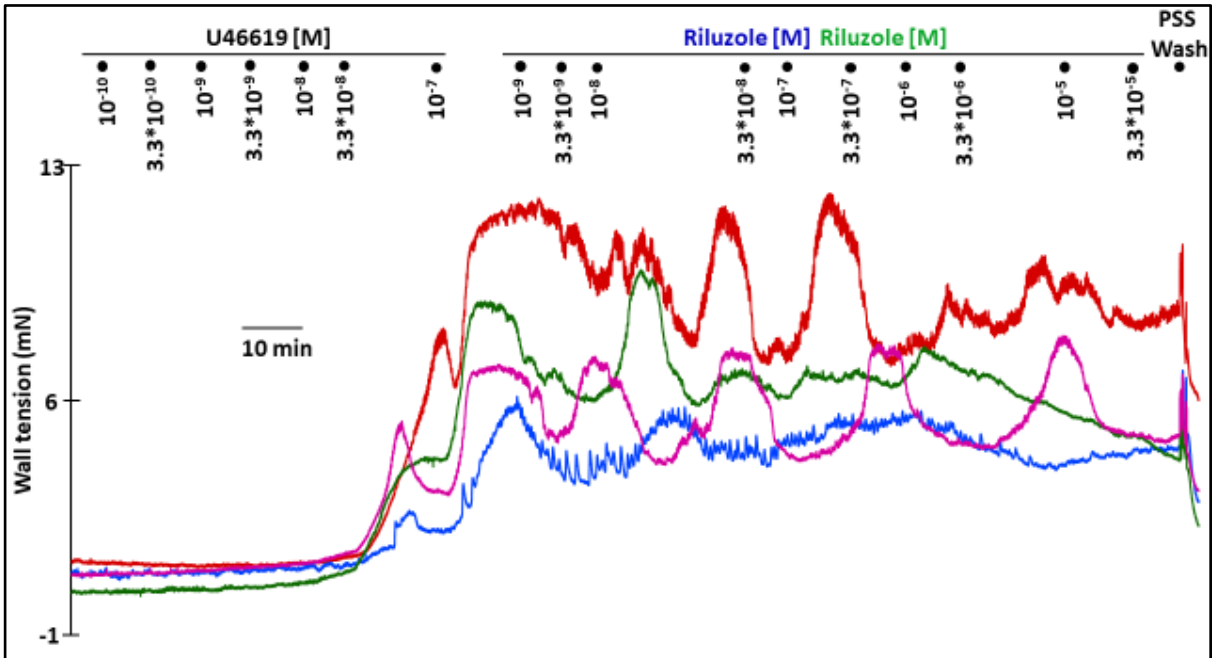


Figure 99*. Wire myography trace highlighting the vasoactive properties of riluzole in isolated chorionic plate arteries originating from a healthy patient (T2716). Following preconstruction with U46619, the red and violet recordings correspond to the time matched control (no drugs added). In this case, CPA's were preconstricted with*

U46619 (10^{-7}M; approximate EC_{80}). Internal diameters of CPA's were as follows: red trace 0.216mm, blue trace 0.273mm, green trace 0.259mm and purple trace 0.281mm. Black dots indicate drug additions to give indicated bath concentrations. Bar indicates the presence of the mentioned compound to the corresponding matching colour force myograph trace (with the exception of black colour which applies to all traces i.e. U46619) or physiological salt solution wash-out.

4.3.3 The potent and selective P2X7 receptor antagonist A740003 may elicit a significant reduction of U46619-induced vasoactive effects in isolated chorionic plate arteries of healthy placental samples

The modulation of U46619-induced vasoconstriction effects in the absence and presence of the P2X7 receptor antagonist A740003 was further investigated by acutely exposing n=4 second order and n=4 fourth order isolated CPA's originating from N=4 healthy patients with the potent and selective P2X7 receptor antagonist and constructing three concentration-response curves for U46619 (one before and two after the A740003 incubation) as highlighted by figures 100-102. In this case, the first U46619 stimulation prior to A740003 incubation comprised of cumulative thromboxane A_2 mimetic concentrations starting with $3.3*10^{-10}$M to 10^{-6}M, which resulted in a concentration-dependent vasoconstriction effect in both second and fourth order CPA preparations. The U46619-induced vasoactive effects were used in determining an approximate U46619 EC_{80} and EC_{90} concentration, as highlighted in figure 103, panels A, B, C and D. The determined second order CPA U46619 EC_{50} value was $4.182*10^{-8}$M and in the case of fourth order CPA, the calculated U46619 EC_{50} value was $1.231*10^{-7}$M. The calculated second order CPA U46619 EC_{80} value was $1.672*10^{-7}$M and EC_{90} value was $3.763*10^{-7}$M (figure 103, panel C). However, the determined fourth order CPA U46619 EC_{80} value was $4.924*10^{-7}$M and EC_{90} value

was $1.107*10^{-6}$M (figure 103, panel D). Following the incubation of the isolated placental vessels with the P2X7 receptor antagonist, a second subsequent U46619 stimulation with an approximate thromboxane A_2 mimetic EC_{80} cumulative concentration was undertaken as presented in figures 133-135. The calculated second U46619 stimulation EC_{50} values were $7.615*10^{-8}$M in the case of second order CPA's and $1.161*10^{-7}$M corresponding to fourth order CPA's as highlighted in figure 103, panels C and D. After a thorough washout of compounds in the bath, a third U46619 stimulation of all isolated placental vessels was performed using an approximate U46619 EC_{90} sequential cumulative concentration as shown in figure 103. The calculated third U46619 stimulation EC_{50} value was $1.100*10^{-7}$M in the case of second order CPA's and $1.843*10^{-7}$M corresponding to the fourth order CPA's (figure 103).

All of the U46619 cumulative concentration response curves were subjected to a Shapiro-Wilk normality test which highlighted that some of the data was not normally distributed. In the case of the first U46619 stimulation, the active effective pressure values corresponding to the second order CPA's were normally distributed, with the exception of 10^{-8}M (*P=0.0284). Considering the fourth order CPA's, the data was normally distributed, with the exception of thromboxane A_2 mimetic concentration of 10^{-8}M (*P=0.0286). Taking into account the second U46619 stimulation, the second order CPA data was normally distributed with the exception of $3.3*10^{-8}$M (*P=0.0175) and the fourth order CPA data was also normally distributed without the U46619 concentrations corresponding to $3.3*10^{-10}$M (**P=0.0046), 10^{-9}M (**P=0.0057), $3.3*10^{-9}$M (**P=0.0058) and 10^{-8}M (*P=0.0414). Furthermore, the active effective pressure data related to the third U46619 stimulation was normally distributed in the case of both second and fourth order CPA's. In the case of the second order CPA's, a two-way ANOVA test (****P<0.0001) with Geisser-Greenhouse correction (epsilon

0.9721) and Tukey's multiple comparisons test was carried out at the same U46619 concentration (ranging from 10^{-9}M to 10^{-7}M) between the first, second and third thromboxane A_2 mimetic cumulative concentration-response curves which highlighted multiple statistically significant differences as presented in table 17. The statistical test showed that between the second and the third U46619 stimulations, there were no statistically significant differences. The same statistical test was undertaken again in the case of fourth order CPA's between equivalent U46619 concentrations across all of the thromboxane A_2 mimetic concentration response curves which revealed no statistically significant differences between all datasets as highlighted in table 18.

The acute A740003 treatment of isolated second order CPA's may potentially cause a change in the potency of U46619, as both concentration response curves corresponding to the second and third thromboxane A_2 stimulations (after the incubation with the P2X7 antagonist) were notably rightward shifted. U46619 was circa 1.82-fold less potent in the case of the second stimulation compared to the first challenge and approximately 1.44-fold less potent when comparing the third with the second stimulation. Considering the exposure of isolated fourth order CPA's with A740003, the potency of U46619 following the incubation with the P2X7 receptor antagonist increased by approximately 1.06-fold between the second and first U46619 stimulations. However, a substantial decrease in the potency of U46619 by circa 1.58-fold was found when comparing the third with the second U46619 challenge.

Following the completion of all U46619 concentration response curves, all placental vessels were thoroughly washed with PSS and challenged with 60mM KPSS to assess any significant vasoconstriction differences elicited between the second and the fourth order CPA preparations originating from the same placenta samples as highlighted in figure 104, panel A. A Shapiro-Wilk test highlighted that data was

normally distributed. A paired two-tailed T-test revealed no statistically significant differences between the two groups (P=0.9071).

The calculated internal diameters of the second order CPA's were 0.623±0.041 and fourth order CPA's were 0.183±0.015 (expressed as mean±SEM). A Shapiro-Wilk test highlighted that data was normally distributed, with an unpaired two-tailed T-test revealing that there was a statistically significant difference between the two groups (**P=0.0020) as shown in figure 104, panel B.

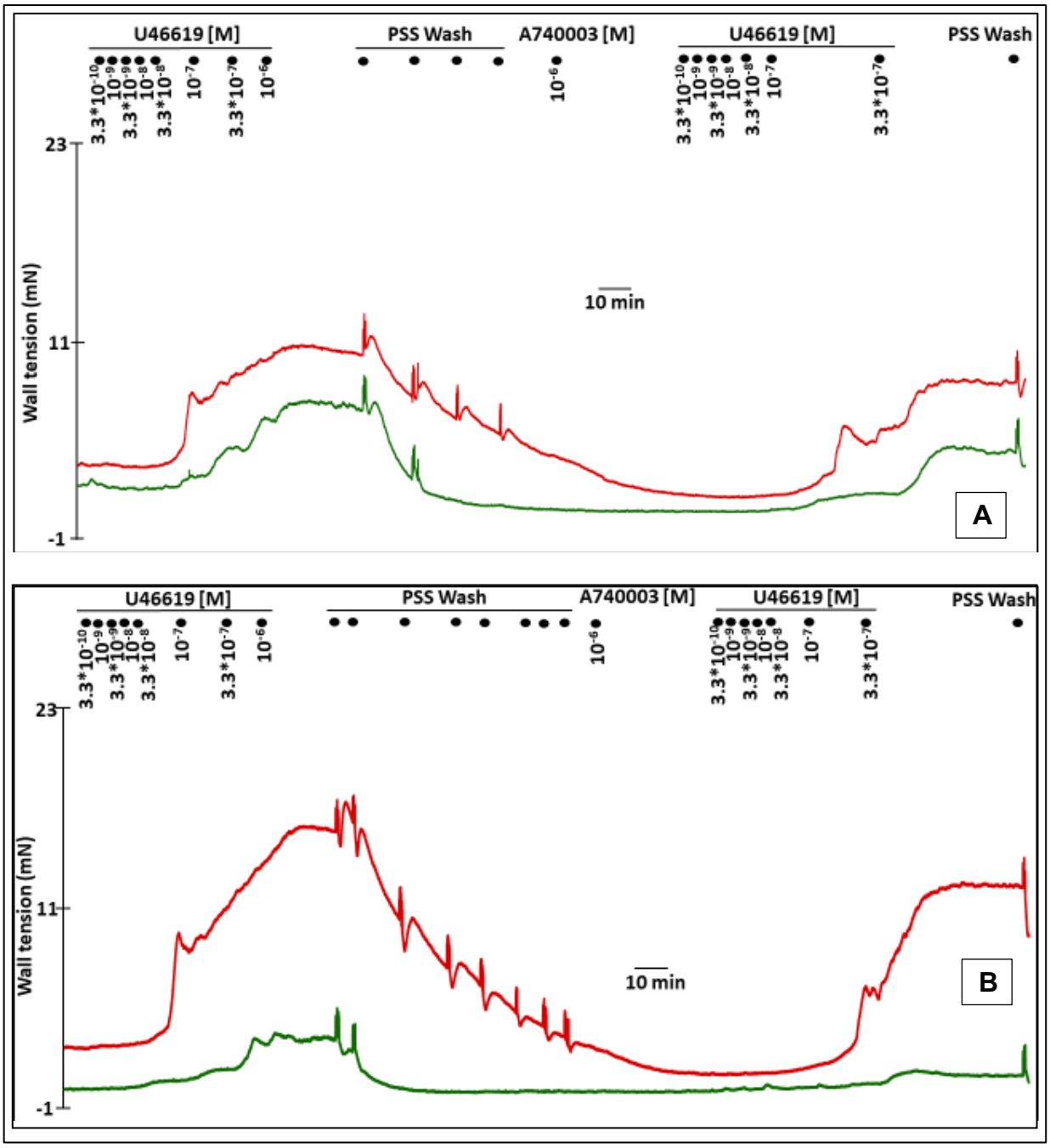


Figure 100. *Wire myography traces highlighting the vascular action of the specific P2X7 receptor antagonist A740003 in isolated second and fourth order CPA's originating from two healthy patients (T2775, T2776), which could result in a significant reduction of the vasoconstriction effect elicited by U46619 following an incubation of 15-minutes with the antagonist* ***A****. Typical responses of chorionic plate artery preparations to cumulative additions of U46619 before and immediately after the incubation with A740003. Internal diameter of second order CPA was 0.602mm (red trace) and fourth order CPA was 0.218mm (green trace)* ***B****. Conventional U46619-induced vasoconstriction effects prior and following the acute A740003 exposure of chorionic plate arteries. Internal diameter of second order CPA was 0.553mm (red trace) and fourth order CPA was 0.184mm (green trace). Black dots indicate drug additions to give indicated bath concentrations. Bar denotes the presence of the mentioned compound or physiological salt solution wash-out.*

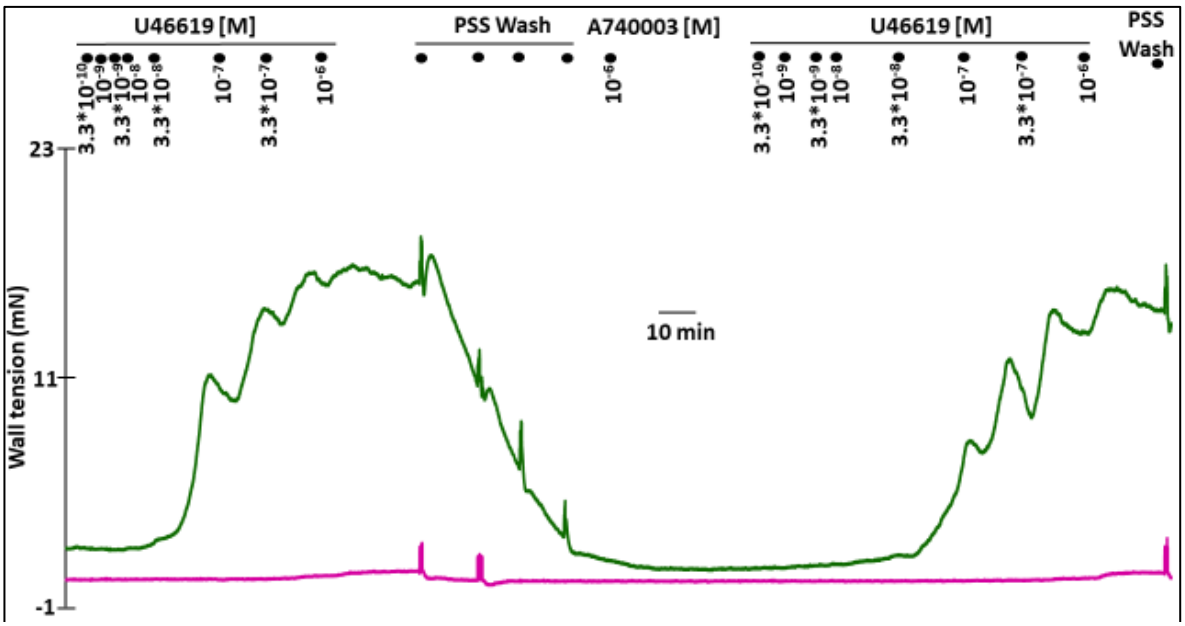


Figure 101. *Wire myography trace showing the U46619-induced vasoconstriction effects in the absence and presence of the P2X7 receptor antagonist A740003 elicited from second and fourth order isolated CPA's originating from a healthy patient (T2788). Internal diameter of second order CPA was 0.745mm (green trace) and fourth order CPA was 0.187mm (violet trace). Black dots indicate drug additions to give indicated bath concentrations. Bar suggests the presence of the mentioned compound or physiological salt solution wash-out.*

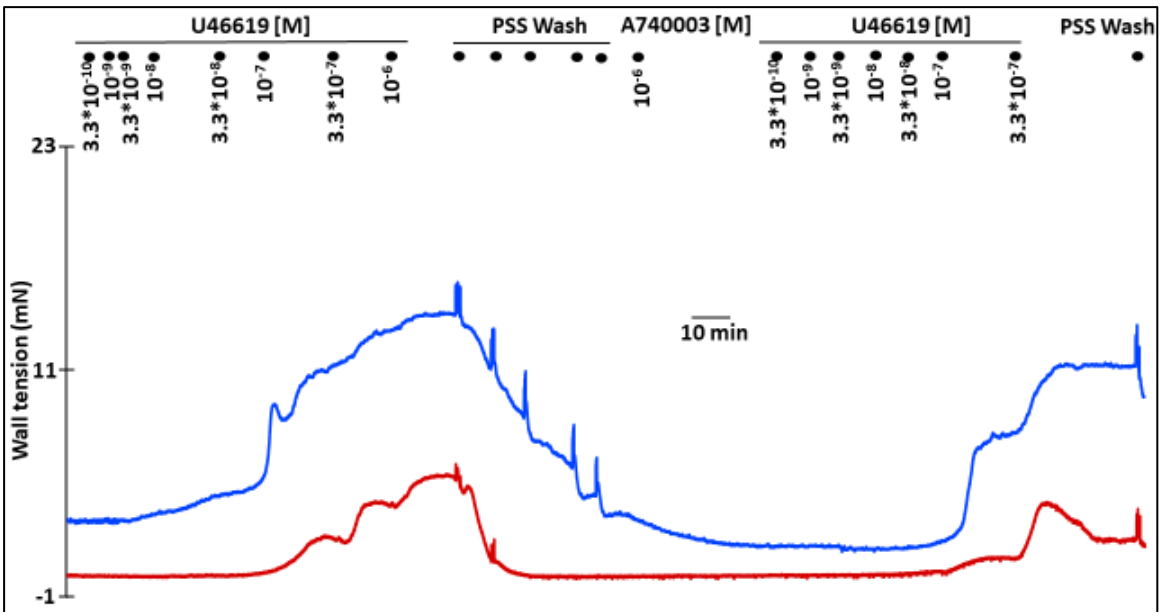


Figure 102*. Wire myography trace showing the U46619-induced vasoconstriction effects in the absence and presence of the P2X7 receptor antagonist A740003 elicited from second and fourth order isolated CPA's originating from a healthy volunteer (T2789). Internal diameter of second order CPA was 0.595mm (blue trace) and fourth order CPA was 0.144mm (red trace). Black dots indicate drug additions to give indicated bath concentrations. Bar suggests the presence of the mentioned compound or physiological salt solution wash-out.*

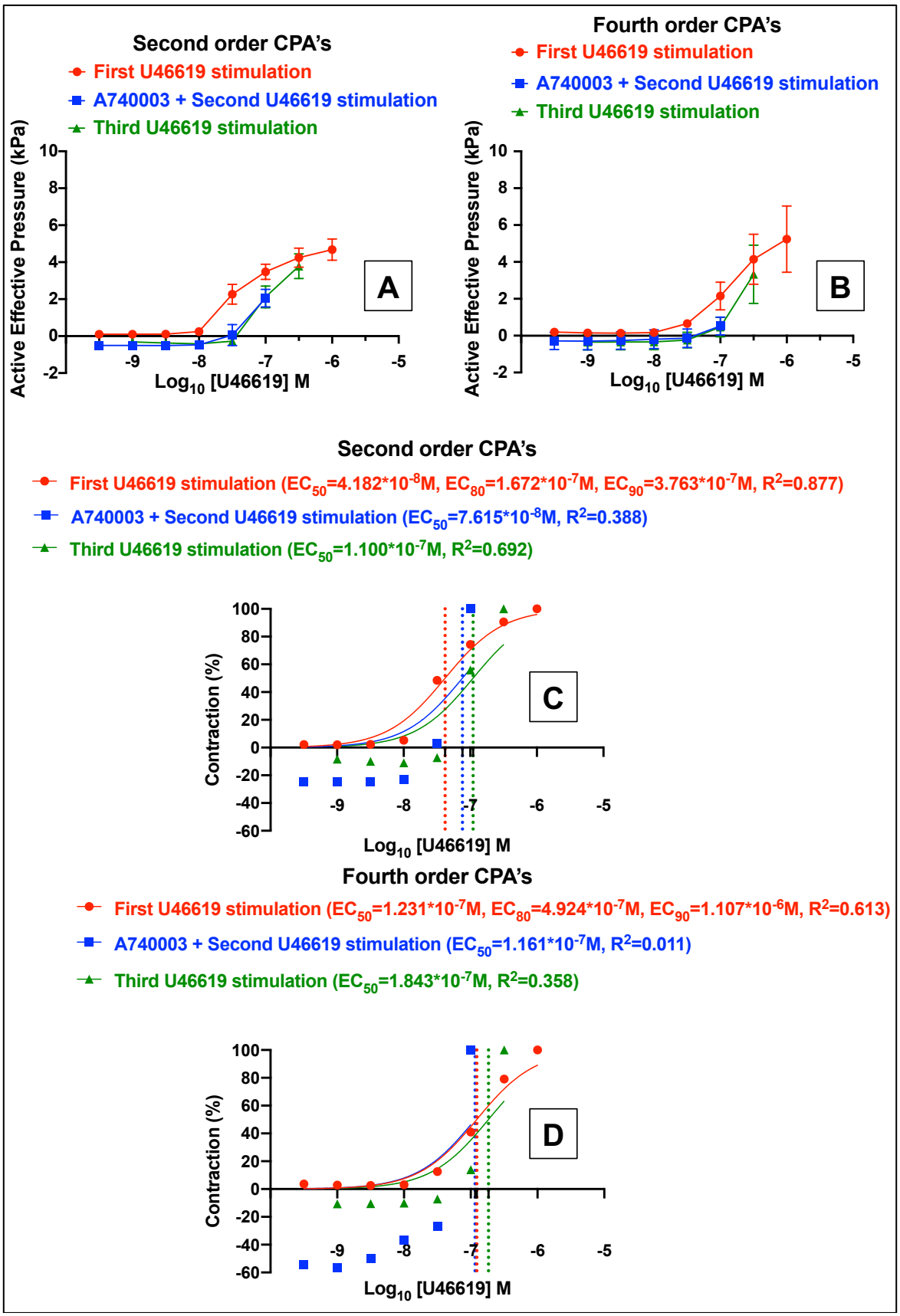


Figure 103. *Vasoactive effects of U46619 before and after the incubation with A740003 initiated by isolated second and fourth order CPA's originating from four healthy volunteers (T2775, T2776, T2788 and T2789)* ***A****. Log concentration-effect*

curve elicited by U46619 in second order CPA's expressed as active effective pressure (kPa) ***B****. Log concentration-effect curve elicited by U46619 in fourth order CPA's expressed as active effective pressure (kPa)* ***C****. Nonlinear regression fit of log concentration-effect curve elicited by U46619 in second order CPA's highlighting the determined first U46619 stimulation EC_{50} value (illustrated by a red vertical discontinued line), second U46619 stimulation EC_{50} value (presented as a blue vertical discontinued line) and third U46619 stimulation EC_{50} value (shown as a green vertical discontinued line). The first U46619 stimulation EC_{80} and EC_{90} values are also presented* ***D.*** *Nonlinear regression fit of log concentration-effect curve elicited by U46619 in fourth order CPA's highlighting the determined first U46619 stimulation EC_{50} value (illustrated by a red vertical discontinued line), second U46619 stimulation EC_{50} value (presented as a blue vertical discontinued line) and third U46619 stimulation EC_{50} value (shown as a green vertical discontinued line). The first U46619 stimulation EC_{80} and EC_{90} values are also shown. Data are expressed as mean±SEM.*

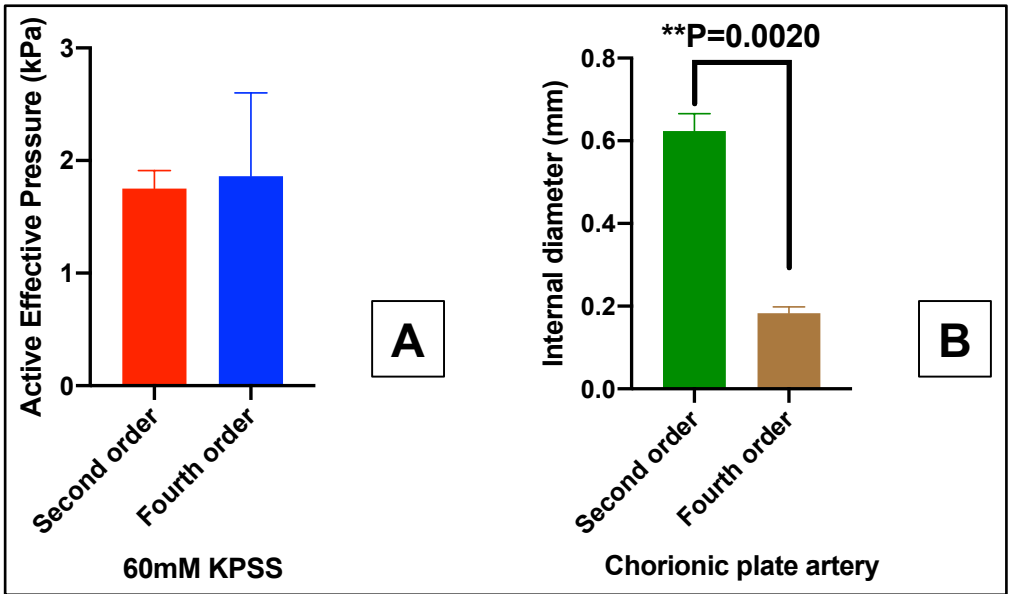


Figure 104. *Vasoactive response of 60mM potassium physiological salt solution (KPSS) in isolated second and fourth order CPA's originating from four healthy patients (T2775, T2776, T2788 and T2789) accompanied by the internal diameter of the placental vessel preparations* ***A.*** *The vasoconstriction effects elicited by 60mM KPSS in second and fourth order CPA's expressed as active effective pressure (kPa)* ***B****. Internal diameter (mm) corresponding to the second and fourth order CPA's. ***P≤0.001; Data are expressed as mean±SEM.*

	10^{-9}M	$3.3*10^{-9}$M	10^{-8}M	$3.3*10^{-8}$M	10^{-7}M
First U46619 Stimulation vs. A740003 + Second U46619 Stimulation	*P=0.0269	*P=0.0309	ns P=0.0751	ns P=0.0584	*P=0.0252
First U46619 Stimulation vs. Third U46619 Stimulation	*P=0.0323	**P=0.0036	*P=0.0249	*P=0.0312	ss P=0.0858
A740003 + Second U46619 stimulation vs. Third Stimulation	ns P=0.2321	ns P=0.3914	ns P=0.8761	ns P=0.7988	ns P=0.9945

Table 17. *This table shows the results of Tukey's multiple comparison test with regards to the correlation between the first, second and third U46619 stimulation of isolated second order CPA's across the same concentration of the thromboxane A_2 mimetic highlighting the adjusted P values. Ns denotes not significant. *P≤0.05, **P≤0.01, ***P≤0.001, ****P≤0.0001.*

	10^{-9}M	$3.3*10^{-9}$M	10^{-8}M	$3.3*10^{-8}$M	10^{-7}M
First U46619 Stimulation vs. A740003 + Second U46619 Stimulation	ns P=0.5961	ns P=0.6426	ns P=0.7146	ns P=0.5302	ns P=0.1693
First U46619 Stimulation vs. Third U46619 Stimulation	ns P=0.4692	ns P=0.4778	ns P=0.4329	ns P=0.4210	ns P=0.1957
A740003 + Second U46619 stimulation vs. Third Stimulation	ns P=0.9207	ns P=0.8405	ns P=0.7670	ns P=0.7756	ns P=0.7621

Table 18. *This table shows the results of Tukey's multiple comparison test with regards to the correlation between the first, second and third U46619 stimulation of isolated fourth order CPA's across the same concentration of the thromboxane A_2 mimetic highlighting the adjusted P values. Ns denotes not significant. *P≤0.05, **P≤0.01, ***P≤0.001, ****P≤0.0001.*

4.3.4 The P2X7 receptor antagonist A740003 elicited a desensitization effect of ATP-induced vasoconstriction in the second and fourth order chorionic plate arteries of healthy placental samples

A preliminary wire myography experiment has also assessed the vasoactive effects of adenosine 5'-triphosphate on two isolated segments of fourth order chorionic plate arteries originating from a healthy patient as highlighted by the trace presented in figure 105. The first ATP stimulation of CPA's with cumulative concentrations of the nucleotide ranging from 10^{-5}M to 10^{-3}M gave rise to spontaneous contractions of the fourth order CPA's in a concentration-dependent manner. Following the incubation with A740003, the second ATP stimulation of the same placental blood vessel preparations was undertaken with cumulative concentrations of the nucleotide ranging between 10^{-5}M to 10^{-3}M which has resulted in a notably attenuated vasomotor response of both CPA's as highlighted in figure 106, panel A. In this case, the maximal vasoconstriction effects elicited by ATP concentrations of 10^{-5}M, $3.3*10^{-5}$M and 10^{-4}M were below the baseline corresponding to the first ATP stimulation. Furthermore, the cumulative ATP concentrations of $3.3*10^{-4}$M and 10^{-3}M gave rise to vasoconstriction responses which were reduced by more than 50% compared to the first ATP stimulation of the same placental vessels. The calculated ATP EC_{50} value was $3.360*10^{-4}$M which corresponds to the first nucleotide stimulation of CPA's and $1.650*10^{-3}$M which correlates to the second ATP stimulation as highlighted in figure 106, panel B. The potency of ATP following the incubation with the P2X7 receptor antagonist notably decreased by approximately 4.91-fold when comparing the second with the first nucleotide stimulations of CPA's, denoting that A740003 may give rise to

a considerable reduction in ATP-induced vasoactive effects in the isolated placental blood vessels. In this case, the internal diameter of the two CPA's was 0.120mm and 0.217mm.

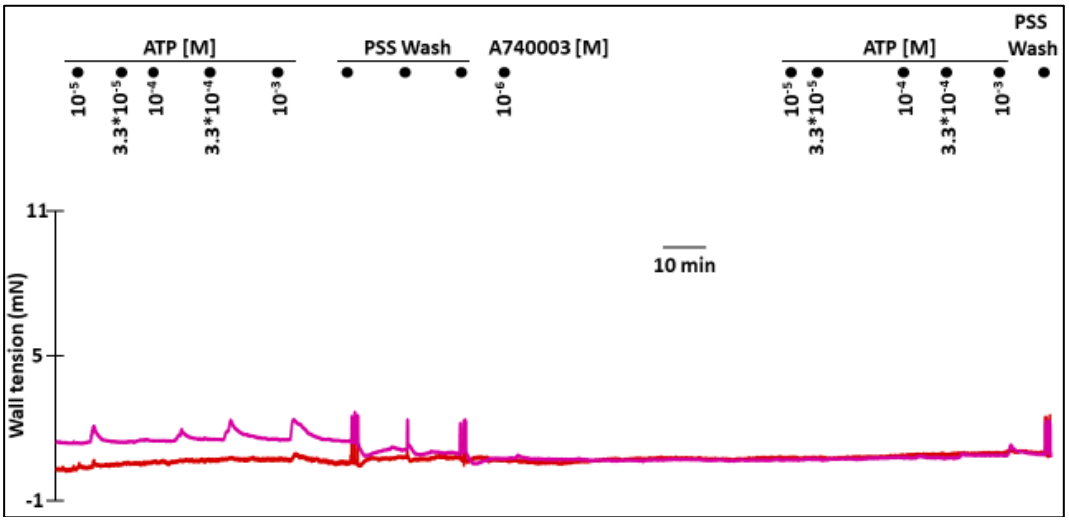


Figure 105. *Wire myography trace showing the ATP-induced vasoconstriction effects in the absence and presence of the P2X7 receptor antagonist A740003 elicited from isolated fourth order CPA's originating from a healthy volunteer (T2768). The internal diameter of the fourth order CPA's was 0.120mm (red trace) and 0.217mm (violet trace). Black dots indicate drug additions to give indicated bath concentrations. Bar suggests the presence of the mentioned compound or physiological salt solution wash-out.*

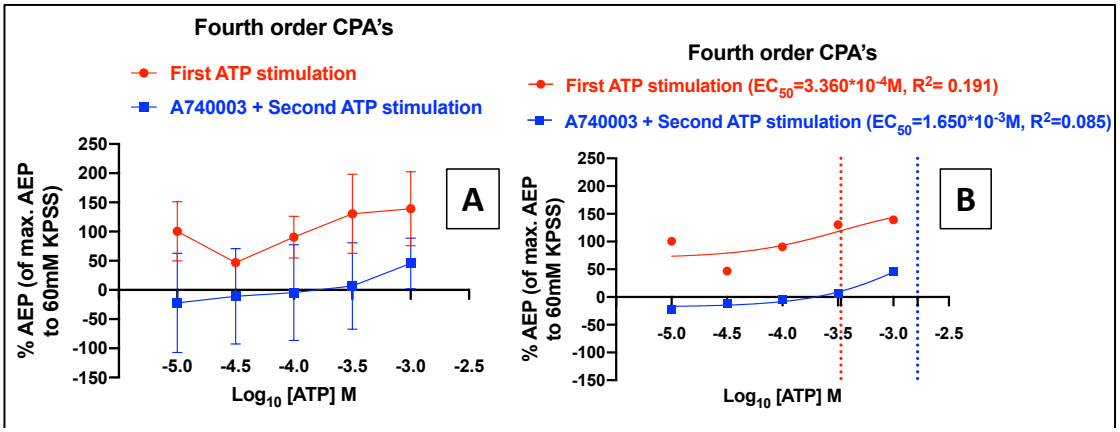


Figure 106*. Vasoactive effects of ATP before and after the incubation with A740003 initiated by isolated fourth order CPA's originating from a healthy volunteer (T2768)* ***A****. Log concentration-effect curve elicited by ATP in fourth order CPA's expressed as percentage active effective pressure (AEP) of maximal AEP to 60mM KPSS* ***B****. Nonlinear regression fit (three parameter logistic equation) of log concentration-effect curve initiated by ATP in fourth order CPA's highlighting the determined first ATP stimulation EC_{50} value (presented as a red vertical discontinued line) and second ATP stimulation EC_{50} value (illustrated as a blue vertical discontinued line). Data are expressed as mean±SEM.*

The ATP-induced vasoconstriction effects in the absence and presence of the P2X7 receptor antagonist A740003 elicited by second (n=4) and fourth order (n=4) isolated CPA's originating from healthy patients (N=4) are further presented in the wire myography traces shown in figures 107-108. Adenosine 5'-triphosphate contracts isolated CPA's in a concentration-dependent manner, especially in the absence of A740003 as highlighted in figure 109, panel C. The nucleotide gave rise to spontaneous maximal contractions that were close to 60% of the U46619 standard at cumulative concentrations ranging from 10^{-5}M to $3.3*10^{-4}$M in the case of second order CPA's without the presence of the P2X7 receptor antagonist. However, fourth order CPA's gave rise to progressively increased vasoconstriction responses starting with a cumulative concentration of 10^{-5}M until 10^{-3}M in the absence of A740003. Following the incubation of second order CPA's with A740003, the ATP-induced maximal vasoconstriction effects decreased by approximately 40%, with the concentration response curve becoming flat which may denote a loss of efficacy of the nucleotide. Similarly, after the acute exposure of isolated fourth order CPA's with the P2X7 receptor antagonist, the maximal ATP-induced vasoconstriction effects were below the first ATP stimulation baseline, particularly at the concentrations of 10^{-5}M, $3.3*10^{-5}$M and 10^{-4}M as highlighted by figure 109, panel C. In this case, further cumulative ATP concentrations of $3.3*10^{-4}$M and 10^{-3}M elicited maximal vasoconstriction effects of approximately 1% and 10% respectively. In both cases of second and fourth order CPA's, the ATP concentration response curves were notably displaced downwards following the incubation of the placental vessel preparations with the P2X7 receptor antagonist A740003.

All of the ATP cumulative concentration response curves were subjected to a Shapiro-Wilk normality test which highlighted that some of the data was not normally distributed as highlighted in table 19. A two-way ANOVA test (P=0.0873) with Geisser-Greenhouse correction (epsilon 0.3533) and Tukey's multiple comparisons test were undertaken between all of the ATP concentrations between all concentration response curves and highlighted no statistically significant differences. The same test was repeated again between all of the cumulative concentrations of ATP corresponding to each of the concentration-response curves separately. The test highlighted multiple statistically significant differences between 10^{-5}M vs. 10^{-3}M (*P=0.0217), 10^{-4}M vs. 10^{-3}M (*P=0.0314) and $3.3*10^{-4}$M vs. 10^{-3}M (*P=0.0275) in the case of the first ATP stimulation of fourth order CPA's as highlighted in figure 109, panel C. All of the U46619 cumulative concentration response curves were also subjected to a Shapiro-Wilk normality test which highlighted that all of the data was normally distributed with the exception of $3.3*10^{-10}$M U46619 (*P=0.0264) corresponding to the fourth order CPA's. A two-way ANOVA test (*P=0.0163) with Geisser-Greenhouse correction (epsilon 0.1623) and Sidak's multiple comparisons test were undertaken at the same U46619 concentration (ranging from $3.3*10^{-10}$M to 10^{-6}M) between the cumulative concentration-response curves of the second and fourth order CPA's which highlighted no statistically significant differences between the two groups. Furthermore, the same statistical test was undertaken again with Tukey's multiple comparison tests separately between all of the U46619 cumulative concentrations in the case of both second and fourth order CPA's, which highlighted no statistically significant differences (figure 109, panel A). The determined U46619 EC_{50} value in the case of the second order CPA's was $5.134*10^{-8}$M and fourth order CPA's was $1.585*10^{-7}$M as highlighted in figure 109, panel B. The calculated active effective

pressures (kPa) corresponding to 60mM KPSS vasoconstriction effects elicited by second and fourth order CPA's were subjected to a Shapiro-Wilk test which highlighted that the data was normally distributed. A two-tailed paired T-test was undertaken between the 60mM KPSS vasoactive responses corresponding to the second and fourth order CPA's which highlighted no statistically significant differences (P=0.6832) as presented in figure 109, panel D. The calculated internal diameter distances (mm) corresponding to the second and fourth order CPA's were also subjected to a Shapiro-Wilk test which highlighted that the data was normally distributed. A two-tailed unpaired T-test was undertaken between the internal diameter of the second and fourth order CPA's which highlighted no statistically significant differences (P=0.0561) between the two groups as illustrated in figure 109, panel E. In this case, the internal diameter of the isolated second order CPA's was 0.540±0.110 mm and fourth order CPA's was 0.210±0.022 mm (expressed as mean ± SEM).

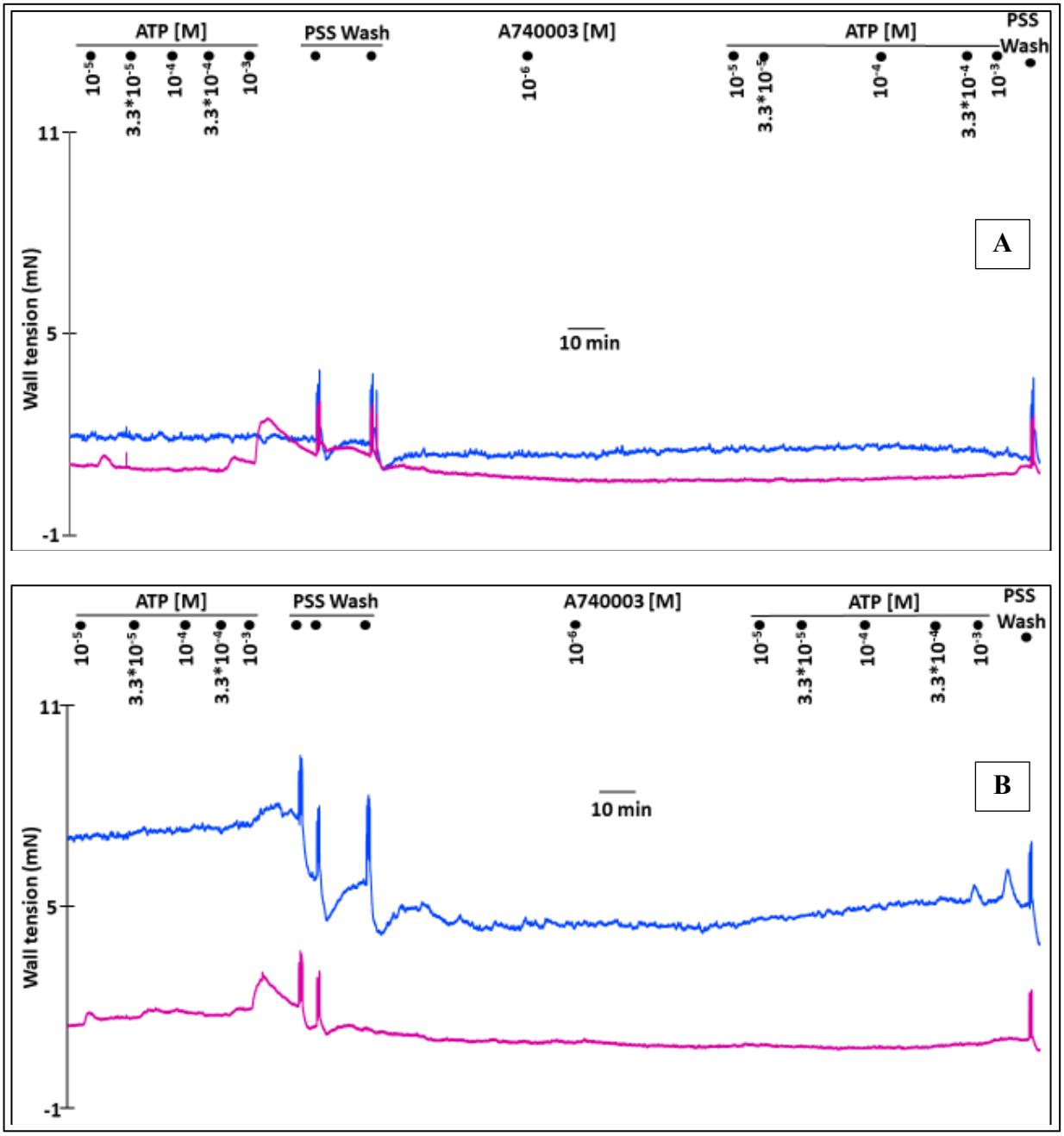


***Figure 107**. Wire myography traces showing adenosine 5'-triphosphate-induced vasoconstriction responses in the absence and presence of A740003 using isolated second (blue trace) and fourth (purple trace) order CPA's originating from two healthy patients (T2775 and T2776) **A**. Typical vasoactive effects of ATP generated before and after the incubation with A740003 by isolated chorionic plate artery preparations of a healthy patient. Internal diameter of the second order CPA was 0.268mm (blue trace) and fourth order CPA was 0.240mm (purple trace) **B**. Conventional ATP-induced vasoconstriction effects elicited prior and immediately following the acute incubation with the P2X7 receptor antagonist A740003 originating from CPA's of a healthy patient. Internal diameter of the second order CPA was 0.741mm (blue trace) and fourth order CPA was 0.255mm (purple trace). Black dots indicate drug additions to give indicated bath concentrations. Bar suggests the presence of the mentioned compound or physiological salt solution wash-out.*

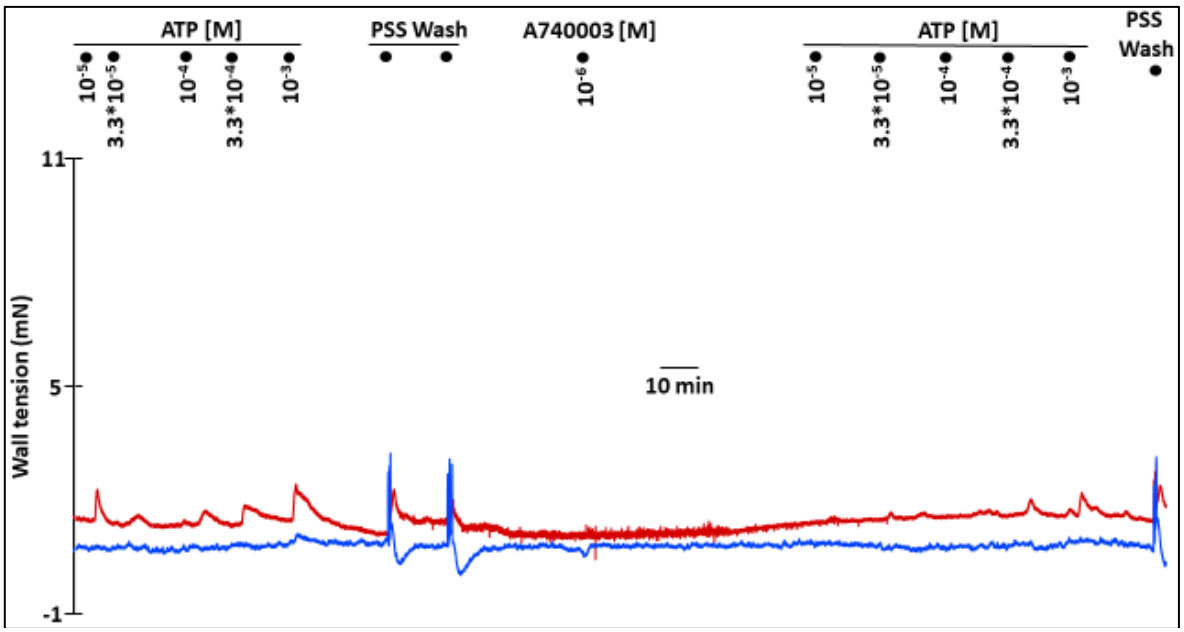


Figure 108. *Wire myography trace highlighting ATP-induced vasoconstriction responses in the absence and presence of A740003 using isolated second and fourth order CPA's originating from a healthy patient (T2788). Internal diameter of the second order CPA was 0.699mm (red trace) and fourth order CPA was 0.162mm (blue trace). Black dots indicate drug additions to give indicated bath concentrations. Bar suggests the presence of the mentioned compound or physiological salt solution wash-out.*

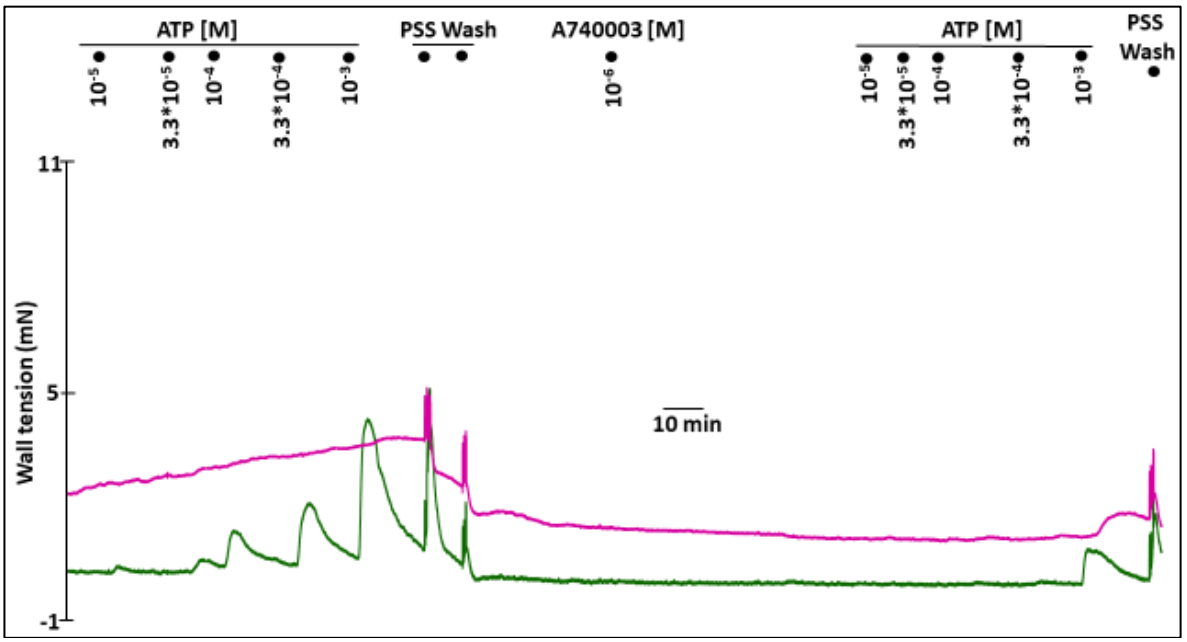


Figure 109*. Wire myography trace highlighting ATP-induced vasoconstriction responses in the absence and presence of A740003 using isolated second and fourth order CPA's originating from a healthy patient (T2789). Internal diameter of the second order CPA was 0.450mm (purple trace) and fourth order CPA was 0.183mm (green trace). Black dots indicate drug additions to give indicated bath concentrations. Bar suggests the presence of the mentioned compound or physiological salt solution wash-out.*

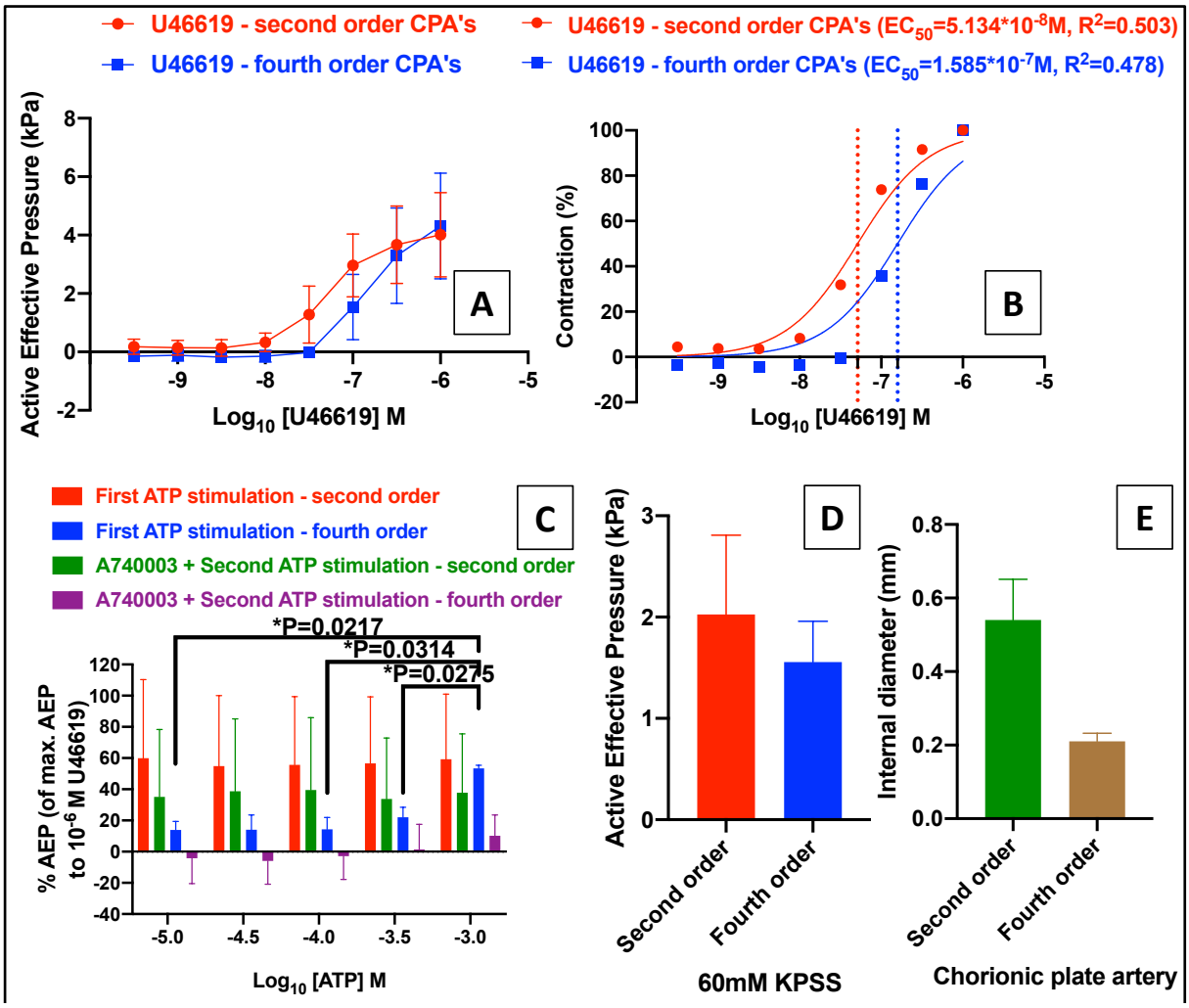


Figure 110. *Vasoactive effects of ATP before and after the incubation with A740003 initiated by isolated second and fourth order CPA's originating from four healthy volunteers* ***A****. Log concentration-effect curve elicited by U46619 in second and fourth order CPA's expressed as active effective pressure (kPa)* ***B****. Nonlinear regression fit of log concentration-effect curve elicited by U46619 in second and fourth order CPA's highlighting the determined U46619 EC_{50} values (presented as a red vertical discontinued line – second order CPA's and illustrated as a blue vertical discontinued line – fourth order CPA's)* ***C****. Vasoconstriction effects elicited by ATP in second and fourth order CPA's prior and following the incubation with A740003* ***D****. Vasoconstriction responses initiated by 60mM KPSS in second and fourth order CPA's expressed as active effective pressure* ***E****. Internal diameter (mm) of second and fourth order CPA's. Data are expressed as mean±SEM. *P≤0.05, **P≤0.01, ***P≤0.001, ****P≤0.0001.*

			First ATP stimulation		A740003 + Second ATP stimulation	
			Second order CPA's	Fourth order CPA's	Second order CPA's	Fourth order CPA's
ATP concentration	10^{-5}M	Passed normality test	No	Yes	No	Yes
		P value	**P=0.0061	P=0.7267	*P=0.0150	P=0.7482
	$3.3*10^{-5}$M	Passed normality test	No	Yes	No	Yes
		P value	*P=0.0158	P=0.8226	*P=0.0151	P=0.8061
	10^{-4}M	Passed normality test	No	Yes	No	Yes
		P value	*P=0.0263	P=0.7301	*P=0.0144	P=0.5159
	$3.3*10^{-4}$M	Passed normality test	No	Yes	No	Yes
		P value	*P=0.0377	P=0.9934	*P=0.0228	P=0.2638
	10^{-3}M	Passed normality test	No	Yes	No	Yes
		P value	*P=0.0493	P=0.0845	**P=0.0050	P=0.1958

Table 19. *This table shows the results of Shapiro-Wilk test corresponding to all of the ATP cumulative concentration response curves. *P≤0.05, **P≤0.01, ***P≤0.001, ****P≤0.0001.*

4.3.5 Adenosine 5'-triphosphate concentration response curves were notably displaced downwards in subsequent nucleotide challenges of second order CPA's in the presence and absence of A740003

The vasoactive action of ATP was further investigated in n=2 second order CPA's originating from a healthy patient by undertaking three consecutive ATP cumulative concentration response curves and incubating the placental vessel preparations with A740003 either before the second or third ATP stimulation as highlighted in the wire myography trace shown in figure 111. The first ATP stimulation of CPA's gave rise to an almost plateaued vasoconstriction effect that barely reached

10% of the maximal U46619 standard. Following the incubation of CPA's with A740003, the subsequent second and third ATP concentration response curves were notably attenuated and displaced downwards, with the vasoactive effects elicited by the nucleotide taking place below the baseline corresponding to the first ATP stimulation as presented in figure 112, panel A. Similar ATP vasoactive effects were elicited by placental blood vessel preparations following a second ATP stimulation in the absence of A740003, with the efficacy of ATP becoming very noticeably decreased as highlighted by figure 112, panel B. In this case, the third ATP stimulation in the presence of A740003 gave rise to an almost superimposed ATP concentration response curve with reference to the second ATP stimulation (absence of A740003), with both second and third ATP stimulations induced vasoactive responses taking place below the baseline corresponding to the first ATP stimulation as presented in figure 112, panel B.

The calculated U46619 EC_{50} value was $3.602*10^{-8}$M. The internal diameter of the n=2 CPA's studied was 0.543 and 0.326 mm. All CPA preparations were exposed to a 123mM KPSS challenge at the end of the wire myography experiment which elicited an active effective pressure of 4.340 and 6.190 kPa.

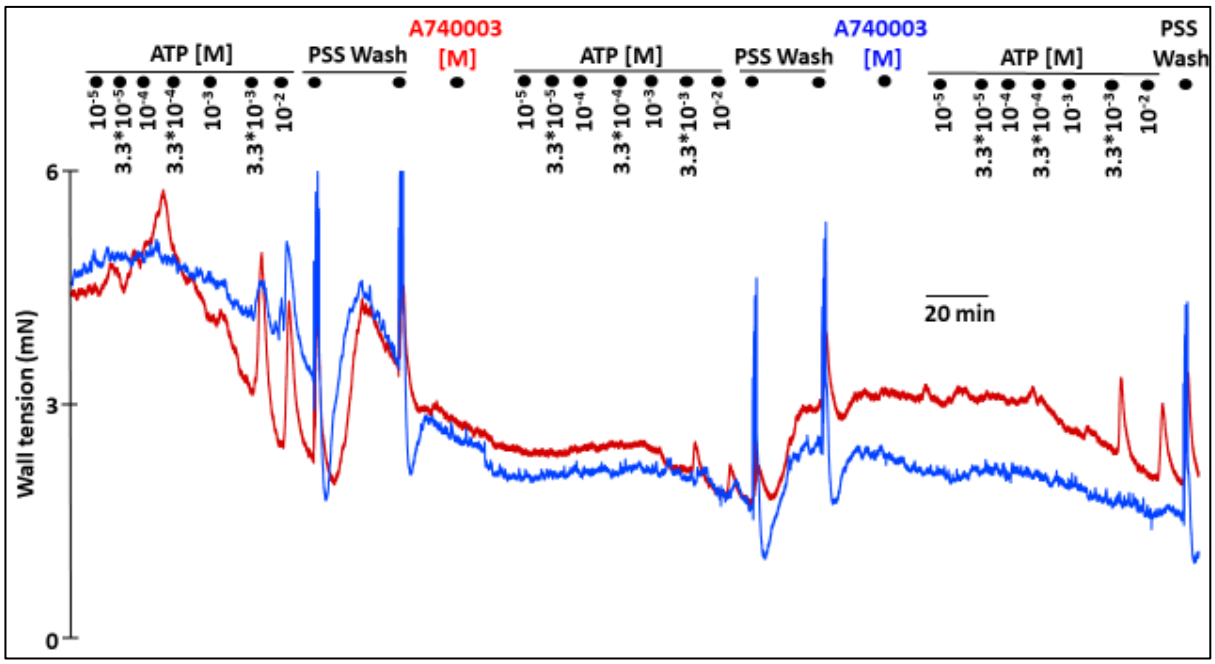


Figure 111. *Wire myography traces highlighting ATP-induced vasoconstriction responses in the absence and presence of A740003 using isolated second order CPA's originating from a healthy patient (T2806). Internal diameter of second order CPA's was 0.543mm (red trace) and 0.326mm (blue trace). Black dots indicate drug additions to give indicated bath concentrations. Bar suggests the presence of the mentioned compound to the corresponding matching colour force myograph trace (with the exception of black colour which applies to all traces) or physiological salt solution wash-out.*

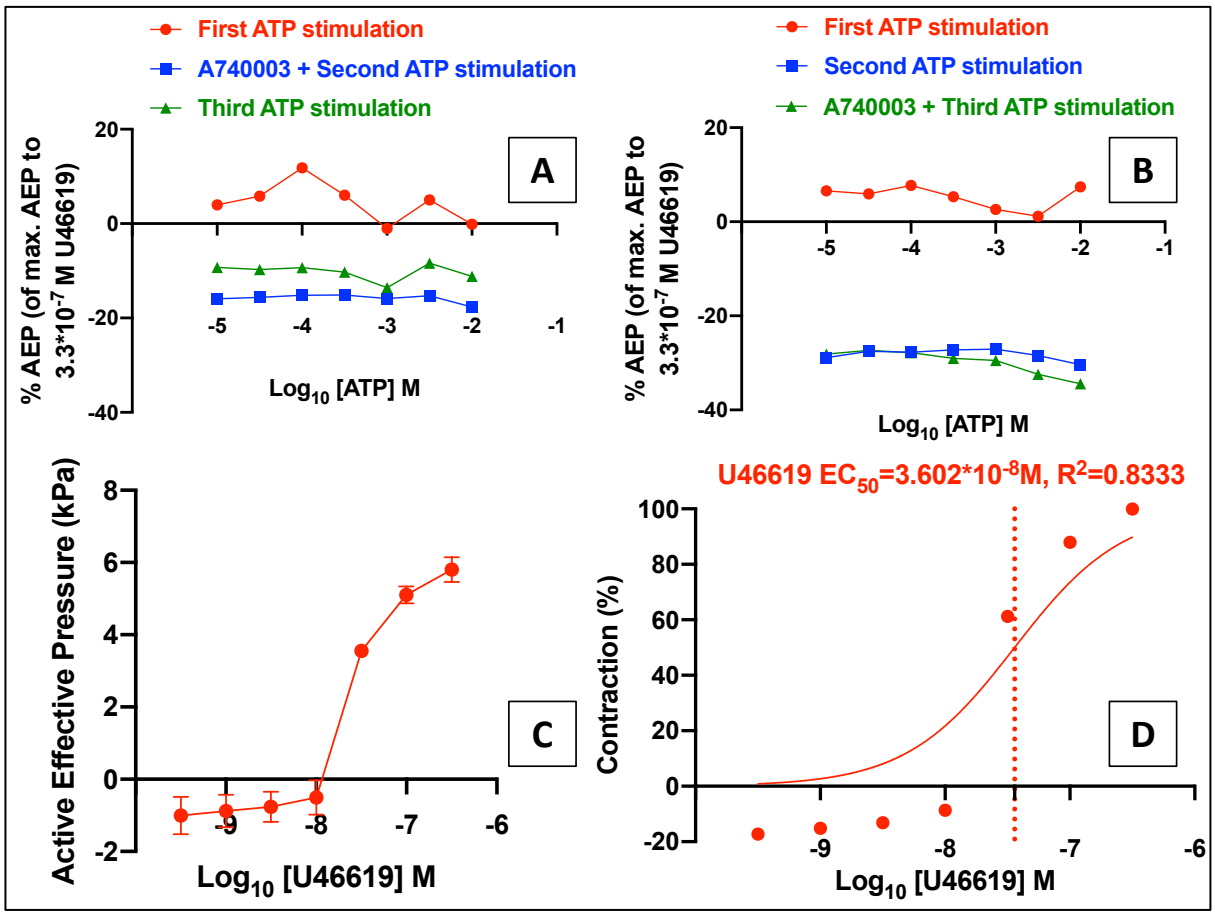


***Figure 112**. Vasoactive effects of ATP before and after the incubation with A740003 initiated by isolated second order CPA's originating from a healthy volunteer (T2806) **A**. Log concentration-effect curves elicited by ATP prior and following the incubation with A740003. In this case, the CPA's were incubated with the P2X7 receptor antagonist before the second ATP stimulation **B**. Log concentration-effect curves elicited by ATP prior and following the incubation with A740003. Here, the CPA's were incubated with the P2X7 receptor antagonist before the third ATP stimulation **C**. Log concentration-effect curve elicited by U46619 in second order CPA's expressed as active effective pressure (kPa) **D**. Nonlinear regression fit of log concentration-effect curve elicited by U46619 in second order CPA's highlighting the determined U46619 EC_{50} value (illustrated as a red vertical discontinued line). Data are expressed as mean±SEM.*

4.3.6 Repeated cumulative additions of ATP gave rise to a progressively reduced vasomotor response in the presence and absence of the P2X7 receptor antagonist A740003

The same wire myography protocol was used in assessing the vasoactive effects of ATP in the presence and absence of A740003 using isolated resistance CPA's (internal diameter of less than 520μm) originating from 5 healthy patients as presented in figures 113-115. In this case, n=10 CPA's originating from N=5 volunteers were exposed to the exogenic application of the nucleotide which evoked concentration-dependent contractions, particularly in the case of the first ATP stimulation of the placental blood vessel preparations as highlighted by figure 116, panels A and C. The second ATP stimulation (without A740003 incubation) of CPA's gave rise to a notably attenuated concentration response curve with maximal vasoconstriction responses which plateaued at approximately less than 20% of the U46619 standard, implying a major loss in the efficacy of the nucleotide, as illustrated in figure 116, panel A. The third ATP stimulation (in the presence of A740003) gave rise to a plateaued ATP concentration response curve that was notably displaced downwards demonstrating again a further reduction in contractions evoked by adenosine 5'-triphosphate when the P2X7 receptor antagonist was present. The determined ATP EC_{50} values were $7.624*10^{-5}$M (corresponding to the first ATP stimulation), $2.059*10^{-4}$M (corresponding to the second ATP stimulation) and $1.436*10^{-4}$M (corresponding to A740003 + Third ATP stimulation) as presented in figure 116, panel B.

However, following the incubation of CPA's with A740003, the second ATP stimulation of the placental blood vessel preparations gave rise to a concentration-

dependent vasoconstriction effect particularly between 10^{-5}M to $3.3*10^{-3}$M, giving rise to a notably downward shifted concentration response curve as highlighted in figure 116, panel C. In this case, the ATP cumulative concentration of 10^{-2}M gave rise to a particularly decreased maximal vasoconstriction response compared to $3.3*10^{-3}$M concentration, implying a marked loss of ATP efficacy. A third ATP stimulation of the same CPA preparations gave rise to a slightly downward shifted, almost superimposed concentration response curve compared to the second ATP stimulation as highlighted in figure 116, panel C. In this case, the determined ATP EC_{50} values were $3.068*10^{-5}$M (corresponding to the first ATP stimulation), $1.956*10^{-4}$M (initiated by A740003 + second ATP stimulation) and $1.361*10^{-4}$M (corresponding to the third ATP stimulation) as presented in figure 116, panel D.

All of the ATP cumulative concentration response curves were subjected to a Shapiro-Wilk normality test which highlighted that some of the data was not normally distributed as highlighted in table 20 and table 21. A two-way ANOVA test (***P=0.0001) with Geisser-Greenhouse correction (epsilon 0.5586) and Tukey's multiple comparison tests were undertaken at the same ATP concentration between all of the concentration response curves where A740003 was incubated with the isolated CPA's immediately before the third ATP stimulation and highlighted no statistically significant differences. In this case, the same test was repeated again separately between all of ATP concentrations of each of the concentration response curves and highlighted a single statistically significant difference (*P=0.0388) between the nucleotide concentrations of 10^{-3}M and 10^{-2}M corresponding to the second ATP stimulation (without A740003 incubation) as highlighted in figure 116, panel A.

A two-way ANOVA test (****P<0.0001) with Geisser-Greenhouse correction (epsilon 0.5315) and Tukey's multiple comparison tests were carried out at the same

ATP concentration across all of the concentration response curves where the P2X7 receptor antagonist was incubated with the chorionic plate arteries immediately before the second ATP stimulation which revealed a single statistically significant difference at 10^{-2}M ATP concentration between the first ATP stimulation vs. A740003 + second ATP stimulation (**P=0.0067) as highlighted in table 22 and figure 116, panel C. In this case, the same statistical test was undertaken again between all of the concentrations of each of the ATP cumulative concentration response curves which revealed no statistically significant differences across all groups. The active effective pressure data corresponding to a single application of U46619 at a concentration of $3.3*10^{-7}$M elicited by n=10 CPA's originating from N=5 healthy patients was also subjected to a Shapiro-Wilk normality test which highlighted that all of the data was normally distributed (P=0.6718). In this case U46619 gave rise to an active effective pressure of 4.980±1.017 kPa (mean±SEM) as highlighted in figure 116, panel E. Similarly, the active effective pressure data corresponding to a single application of 123mM KPSS elicited by n=10 CPA's originating from N=5 healthy volunteers was also subjected to a Shapiro-Wilk normality test which highlighted that all of the data was normally distributed (P=0.3223). Furthermore, 123mM KPSS elicited an active effective pressure of 4.143±0.963 kPa (mean±SEM) as presented in figure 116, panel E.

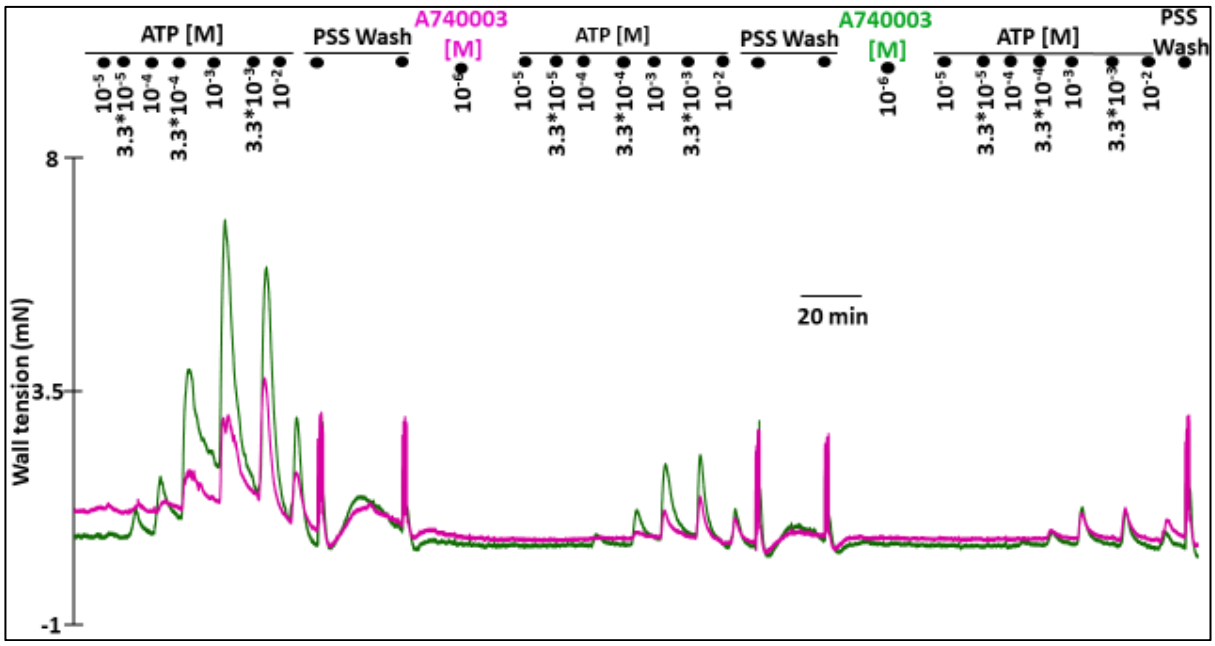


Figure 113. *Wire myography trace highlighting ATP-induced vasoconstriction responses in the absence and presence of A740003 using isolated resistance CPA's originating from a healthy patient (T2806). Internal diameter of CPA's was 0.219mm (green trace) and 0.185mm (purple trace). Black dots indicate drug additions to give indicated bath concentrations. Bar denotes the presence of the mentioned compound to the corresponding matching colour force myograph trace (with the exception of black colour which applies to all traces) or physiological salt solution wash-out.*

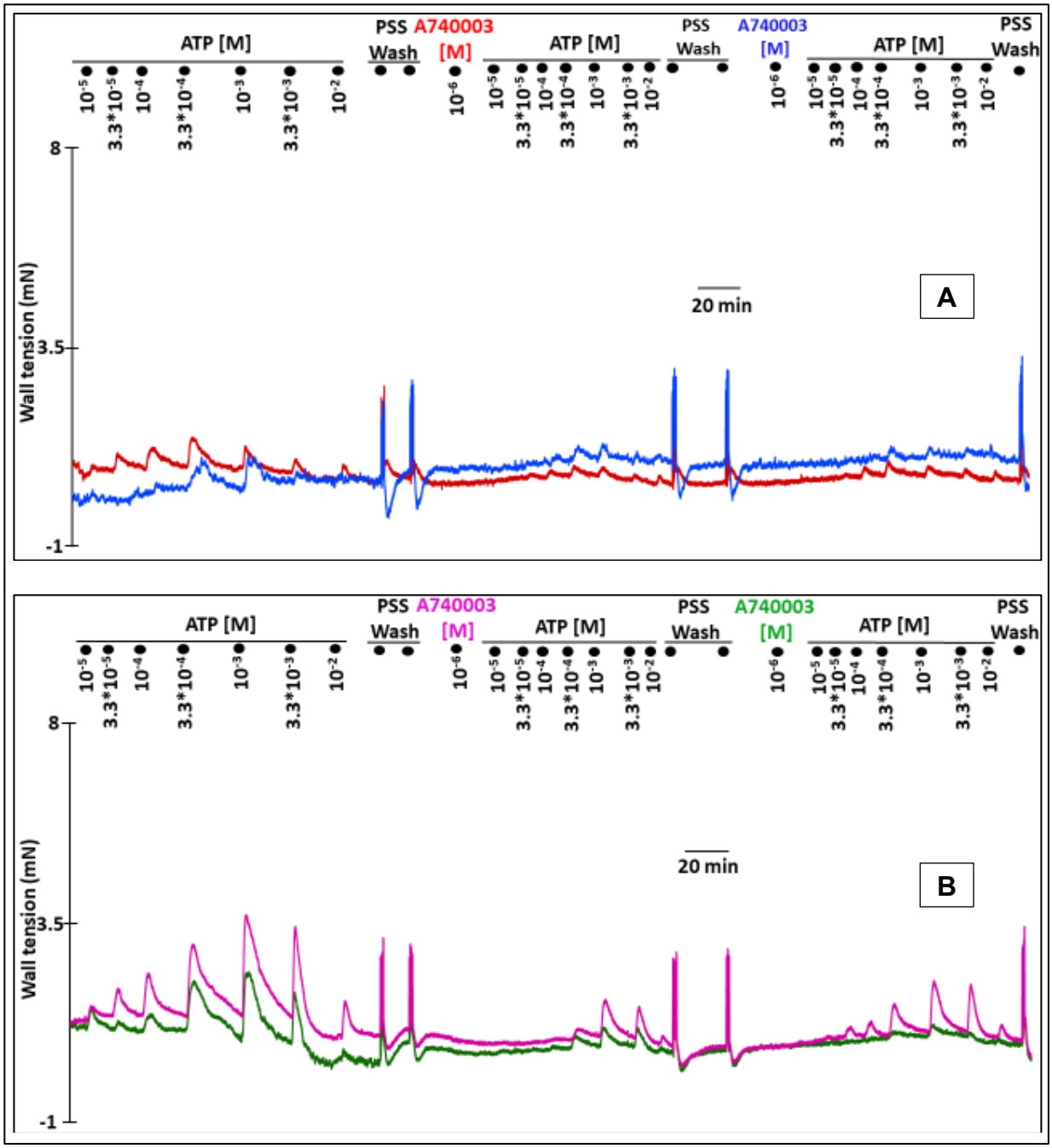


Figure 114. *Wire myography traces highlighting ATP-induced vasoconstriction responses in the absence and presence of A740003 using isolated resistance CPA's originating from two healthy patients (T2809 and T2810)* ***A***. *Typical vasoactive effects of ATP generated before and after the incubation with A740003 by isolated chorionic plate artery preparations of a healthy patient (T2809). Internal diameter of CPA's was 0.170mm (red trace) and 0.145mm (blue trace)* ***B***. *Conventional ATP-induced vasoconstriction effects elicited prior and immediately following the acute incubation with the P2X7 receptor antagonist A740003 originating from CPA's of a healthy patient (T2810). Internal diameter CPA's was 0.207mm (green trace) and 0.204mm (purple trace). Black dots indicate drug additions to give indicated bath concentrations. Bar suggests the presence of the mentioned compound to the corresponding matching colour force myograph trace (with the exception of black colour which applies to all traces) or physiological salt solution wash-out.*

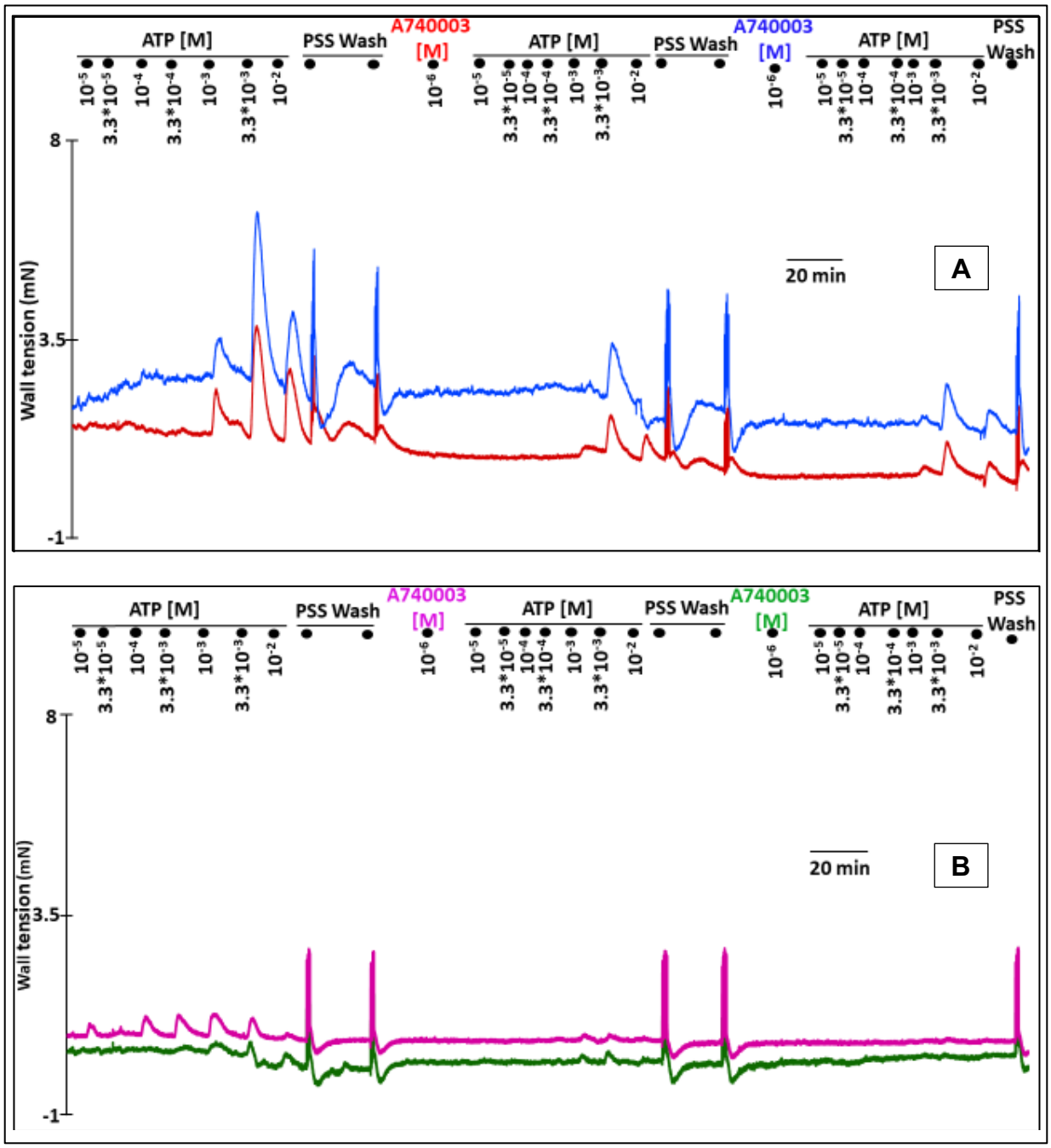


Figure 115*. Wire myography traces highlighting ATP-induced vasoconstriction responses in the absence and presence of A740003 using isolated resistance CPA's originating from two healthy patients (T2812 and T2813)* ***A****. Typical vasoactive effects of ATP generated before and after the incubation with A740003 by isolated chorionic plate artery preparations of a healthy patient (T2812). Internal diameter of CPA's was 0.149mm (red trace) and 0.242mm (blue trace)* ***B****. Conventional ATP-induced vasoconstriction effects elicited prior and immediately following the acute incubation with the P2X7 receptor antagonist A740003 originating from CPA's of a healthy patient (T2813). Internal diameter CPA's was 0.143mm (green trace) and 0.128mm (purple trace). Black dots indicate drug additions to give indicated bath concentrations. Bar suggests the presence of the mentioned compound to the corresponding matching colour force myograph trace (with the exception of black colour which applies to all traces) or physiological salt solution wash-out.*

			First ATP stimulation	Second ATP stimulation	A740003+Third ATP stimulation
ATP concentration	10^{-5}M	Passed normality test	Yes	Yes	Yes
		P value	P=0.2947	P=0.5664	P=0.2118
	$3.3*10^{-5}$M	Passed normality test	No	Yes	Yes
		P value	**P=0.0017	P=0.8934	P=0.5181
	10^{-4}M	Passed normality test	No	Yes	No
		P value	***P=0.0006	P=0.9518	**P=0.0035
	$3.3*10^{-4}$M	Passed normality test	Yes	Yes	No
		P value	P=0.8412	P=0.7869	**P=0.0021
	10^{-3}M	Passed normality test	Yes	Yes	No
		P value	P=0.7360	P=0.1149	*P=0.0401
	$3.3*10^{-3}$M	Passed normality test	Yes	Yes	Yes
		P value	P=0.4611	P=0.6401	P=0.1015
	10^{-2}M	Passed normality test	Yes	Yes	Yes
		P value	P=0.1972	P=0.3244	P=0.1682

Table 20. *This table shows the results of a Shapiro-Wilk test corresponding to all of the ATP cumulative concentration response curves where the P2X7 receptor antagonist was incubated with the CPA's just before the third ATP stimulation. *P≤0.05, **P≤0.01, ***P≤0.001, ****P≤0.0001.*

			First ATP stimulation	A740003 + Second ATP stimulation	Third ATP stimulation
ATP concentration	10^{-5}M	Passed normality test	No	Yes	Yes
		P value	**P=0.0027	P=0.2887	P=0.7820
	$3.3*10^{-5}$M	Passed normality test	Yes	Yes	Yes
		P value	P=0.0855	P=0.4062	P=0.7143
	10^{-4}M	Passed normality test	No	Yes	Yes
		P value	*P=0.0287	P=0.1779	P=0.5827
	$3.3*10^{-4}$M	Passed normality test	Yes	Yes	Yes
		P value	P=0.1417	P=0.4681	P=0.1651
	10^{-3}M	Passed normality test	Yes	Yes	Yes
		P value	P=0.1235	P=0.8317	P=0.7112
	$3.3*10^{-3}$M	Passed normality test	Yes	Yes	Yes
		P value	P=0.3358	P=0.0597	P=0.4223
	10^{-2}M	Passed normality test	Yes	Yes	Yes
		P value	P=0.1981	P=0.4897	P=0.7773

Table 21. *This table shows the results of a Shapiro-Wilk test corresponding to all of the ATP cumulative concentration response curves where the P2X7 receptor antagonist was incubated with the CPA's just before the second ATP stimulation. *P≤0.05, **P≤0.01, ***P≤0.001, ****P≤0.0001.*

	10^{-5}M	$3.3*10^{-5}$M	10^{-4}M	$3.3*10^{-4}$M	10^{-3}M	$3.3*10^{-3}$M	10^{-2}M
First ATP stimulation vs A740003 + Second ATP stimulation	P=0.3146	P=0.1659	P=0.3020	P=0.2453	P=0.1585	P=0.0748	**P=0.0067
First ATP stimulation vs Third ATP stimulation	P=0.3013	P=0.1819	P=0.3214	P=0.2838	P=0.2096	P=0.1342	P=0.0501
A740003 + Second ATP stimulation vs Third ATP stimulation	P=0.6421	P=0.8303	P=0.9486	P=0.9820	P=0.7351	P=0.8545	P=0.7545

***Table 22**. This table shows the results of a two-way ANOVA test with Geisser-Greenhouse correction and Tukey's multiple comparison tests which was carried out at the same ATP concentration across all of the concentration response curves where the P2X7 receptor antagonist was incubated with the chorionic plate arteries immediately before the second ATP stimulation. *P≤0.05, **P≤0.01, ***P≤0.001, ****P≤0.0001.*

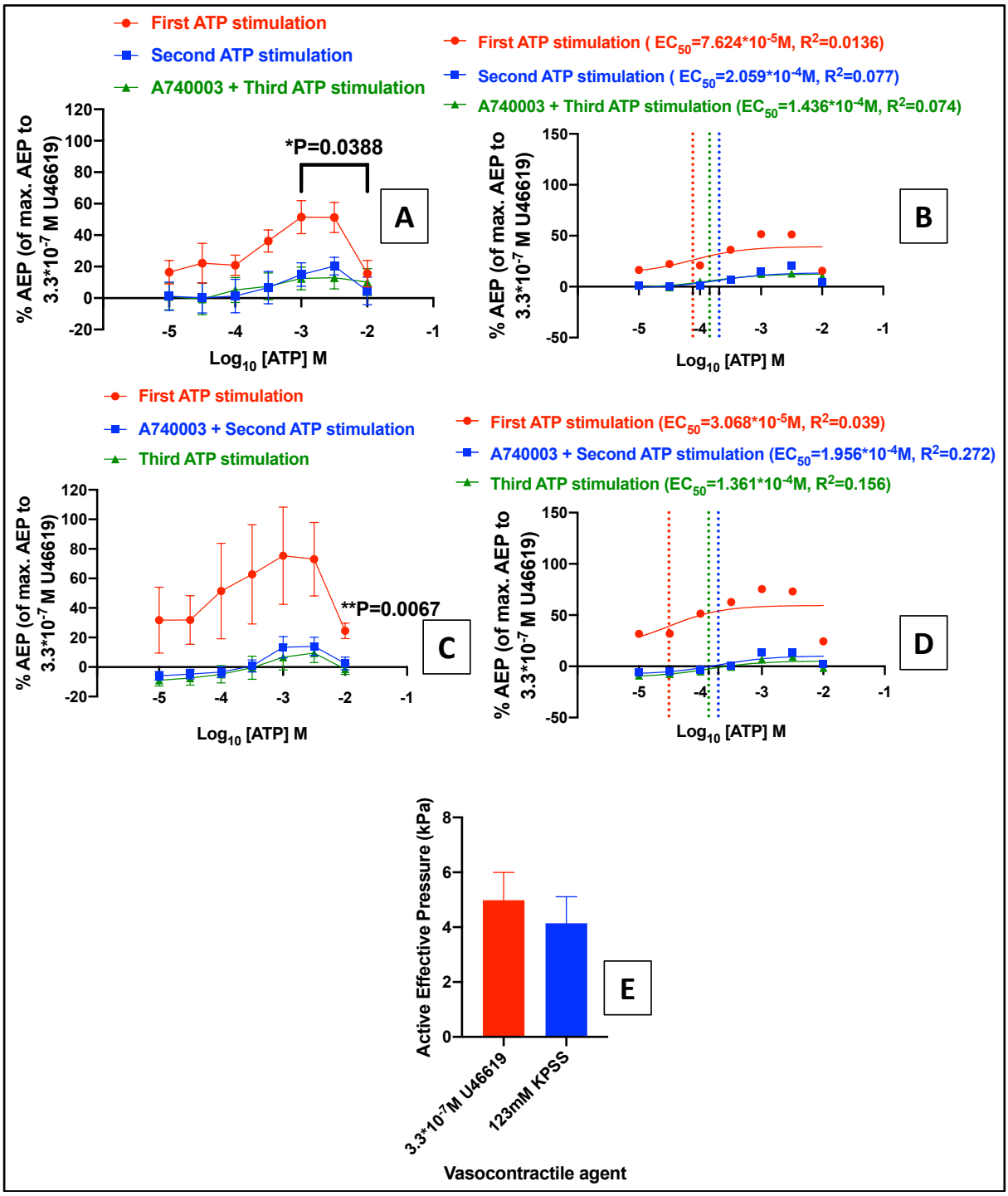


Figure 116. *Vasoactive effects of ATP before and after the incubation with A740003 initiated by isolated resistance CPA's originating from 5 healthy volunteers* ***A****. Log concentration-effect curves elicited by ATP prior and following the incubation with A740003. In this case, the CPA's were incubated with the P2X7 receptor antagonist before the third ATP stimulation* ***B****. Nonlinear regression fit (three parameter logistic equation) of log concentration-effect curve initiated by ATP highlighting the calculated ATP EC_{50} values (first ATP stimulation – illustrated as a red vertical discontinued line , second ATP stimulation – presented as a blue vertical discontinued line and A740003 + Third ATP stimulation – shown as a green vertical discontinued line). In this case, the CPA's were incubated with the P2X7 receptor antagonist before the third ATP*

*stimulation **C**. Log concentration-effect curves elicited by ATP prior and following the incubation with A740003. Here, the CPA's were incubated with the P2X7 receptor antagonist before the second ATP stimulation **D**. Nonlinear regression fit (three parameter logistic equation) of log concentration-effect curve initiated by ATP highlighting the calculated ATP EC_{50} values (first ATP stimulation – illustrated as a red vertical discontinued line, A740003 + Second ATP stimulation – presented as a blue vertical discontinued line and third ATP stimulation – shown as a green green vertical discontinued line). In this case, the CPA's were incubated with the P2X7 receptor antagonist before the second ATP stimulation. **E**. Vasoconstriction effects initiated by the exogenous application of U46619 ($3.3*10^{-7}$M) and 123mM KPSS by resistance CPA's expressed as active effective pressure (kPa). *P≤0.05, **P≤0.01, ***P≤0.001, ****P≤0.0001; Data are expressed as mean±SEM.*

4.3.7 Adenosine 5'-triphosphate gives rise to spontaneous progressively attenuated contractions of human placental chorionic plate artery preparations with increasing nucleotide cumulative concentrations in the presence and absence of the P2X7 receptor antagonist A740003

The vascular action of adenosine 5'-triphosphate on isolated resistance CPA's originating from N=3 healthy patients in the presence (n=6 CPA's) and absence (n=6 CPA's) of an acute incubation with the P2X7 receptor antagonist A740003 was further investigated using three cumulative ATP concentrations (10^{-3}M, $3.3*10^{-3}$M and 10^{-2}M) as highlighted in the wire myography traces illustrated in figures 117-119. The nucleotide elicited spontaneous vasoconstrictions of the placental blood vessel preparations that became progressively attenuated with increasing ATP cumulative concentrations as presented in figure 120, panels A and B. The first ATP stimulation without the presence of A740003 gave rise to a maximal vasoconstriction effect which was higher compared to the ATP-induced vasoconstriction responses in the presence of the P2X7 receptor antagonist at all cumulative concentrations of the nucleotide as shown in figure 120, panels A and B. The second ATP stimulation of the CPA's which

have either been incubated or not incubated with A740003 gave rise to a similar vasoconstriction effect that was notably attenuated, resulting in almost flat concentration response curves, denoting a loss in the efficacy of the nucleotide and a potential desensitization effect taking place as highlighted by figure 120, panels A and B. In this case, the maximal ATP-induced vasoconstriction response elicited was less than 10% of the U46619 standard at a concentration of 10^{-3}M. A Shapiro Wilk test highlighted that the active effective pressure data corresponding to the first and second ATP stimulations without the A740003 incubation of CPA's was normally distributed. A two-way ANOVA test (*P=0.0455) with Geisser-Greenhouse correction (epsilon 0.7366) and Sidak's multiple comparison tests between the first and second ATP stimulations at the same concentrations of the nucleotide highlighted no statistically significant differences between the two groups. The same test was undertaken again with Tukey's multiple comparison tests between all of the ATP concentrations of each of the nucleotide cumulative concentration curves and highlighted no statistically significant differences. In the case in which CPA's were initially incubated with A740003, a Shapiro-Wilk test highlighted that the active effective pressure data corresponding to the ATP-induced vasoconstriction effects was normally distributed with the exception of 10^{-3}M corresponding to the first ATP stimulation (**P=0.0019). A Sidak's multiple comparisons test between the first and second ATP stimulations at the same nucleotide concentration revealed a single statistically significant difference of *P=0.0333 corresponding to $3.3*10^{-3}$M as highlighted in figure 120, panel B. Furthermore, Tukey's multiple comparison tests revealed no statistically significant differences between all of the concentrations of each of the first and second ATP stimulations, in the case of CPA preparations which have initially been incubated with the P2X7 receptor antagonist. All CPA preparations

were also exposed to an initial U46619 challenge at the start of the wire myography experiment (first U46619 stimulation) and a final U46619 challenge at the end of the functional assessment (second U46619 stimulation) which were further subdivided into two categories of placental arteries that have been exposed or have not been exposed to A740003 as highlighted in figure 120, panel C. A Shapiro-Wilk test highlighted in this case that data was normally distributed. A two-way ANOVA test (***P=0.0002) and Sidak's multiple comparisons test was undertaken between the first and second U46619 stimulations which revealed multiple statistically significant differences as follows: **P=0.0035 (corresponding to CPA's which have been exposed to A740003) and **P=0.0042 (corresponding to placental blood vessel preparations which have not been exposed to A740003) as presented in figure 120, panel C. The internal diameter of all isolated chorionic plate artery preparations was 0.1661±0.014mm (mean±SEM).

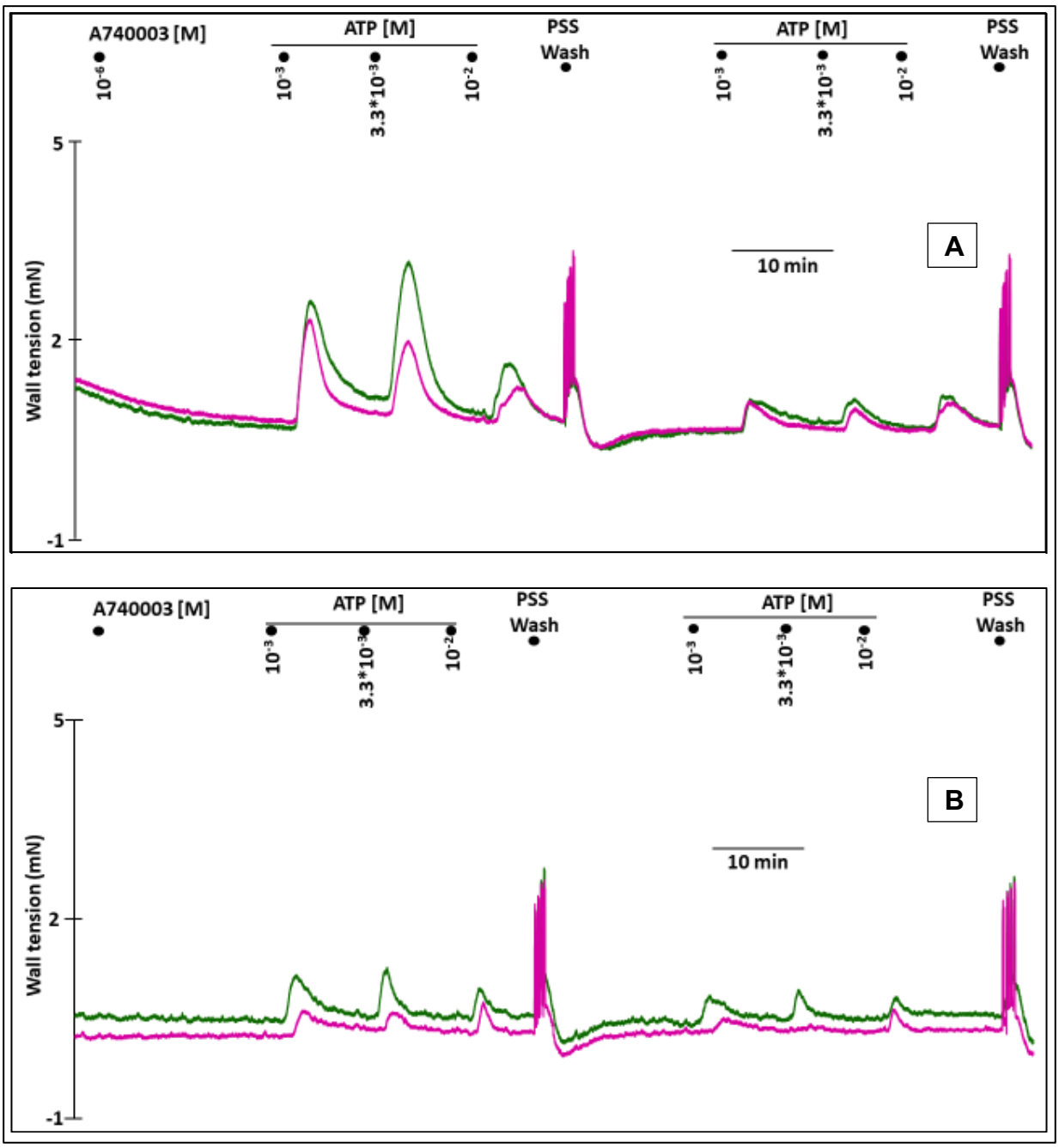


Figure 117. *Wire myography traces highlighting ATP-induced vasoconstriction responses in the absence and presence of A740003 using isolated resistance CPA's originating from two healthy patients (T2825 and T2826)* ***A****. Typical vasoactive effects of ATP generated after the incubation with A740003 by isolated chorionic plate artery preparations of a healthy patient (T2825). Internal diameter of CPA's was 0.212mm (green trace) and 0.205mm (purple trace)* ***B****. Conventional ATP-induced vasoconstriction effects originating from CPA's of a healthy patient (T2826) following the incubation with A740003. Internal diameter CPA's was 0.178mm (green trace) and 0.112mm (purple trace). Black dots indicate drug additions to give indicated bath concentrations. Bar suggests the presence of the mentioned compound or physiological salt solution wash-out.*

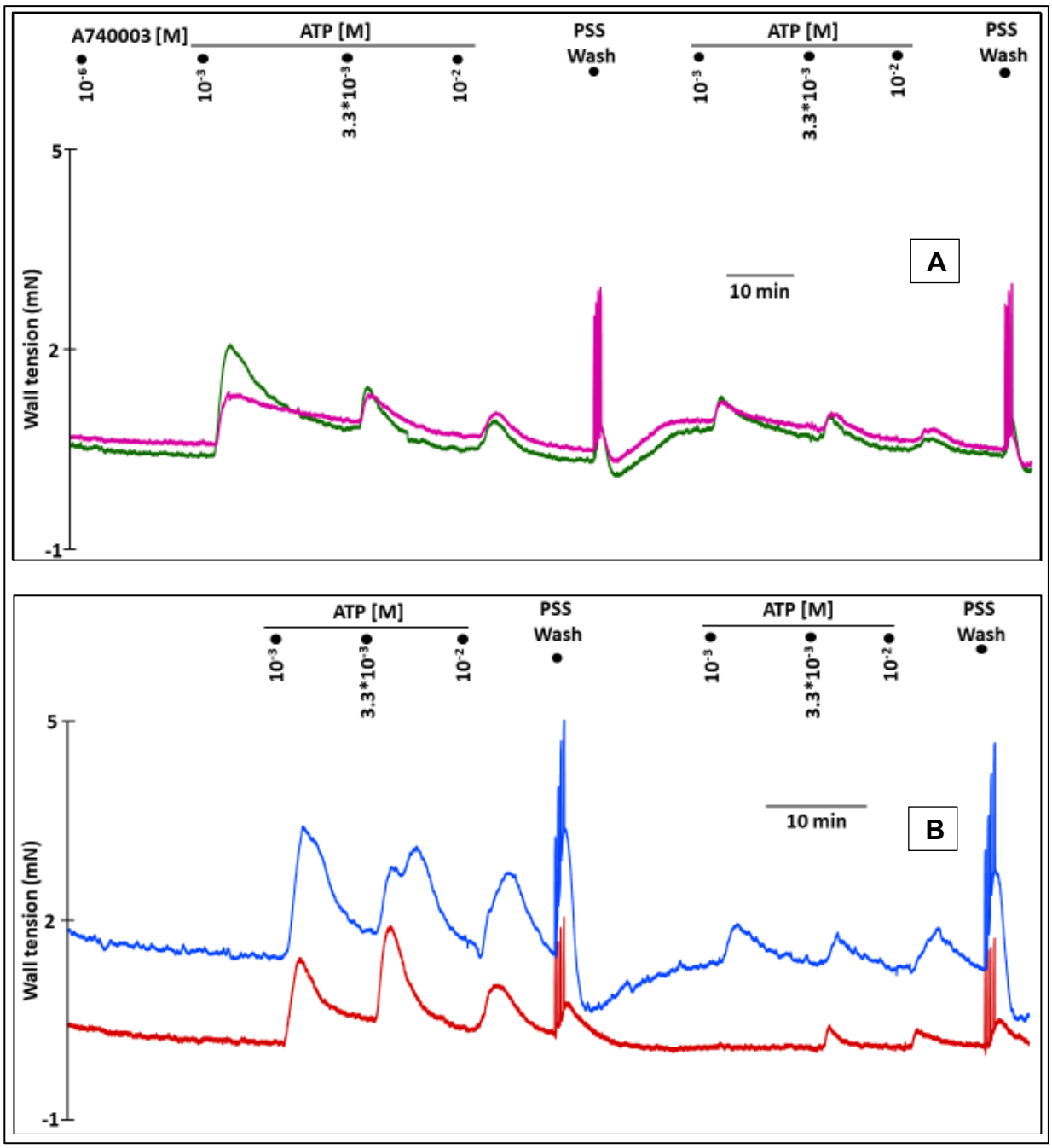


***Figure 118**. Wire myography traces highlighting ATP-induced vasoconstriction responses in the absence and presence of A740003 using isolated resistance CPA's originating from two healthy patients (T2828 and T2825) **A**. Typical vasoactive effects of ATP generated after the incubation with A740003 by isolated chorionic plate artery preparations of a healthy patient (T2828). Internal diameter of CPA's was 0.144mm (green trace) and 0.150mm (purple trace) **B**. Conventional ATP-induced vasoconstriction effects originating from CPA's of a healthy patient (T2825). Internal diameter CPA's was 0.102mm (red trace) and 0.256mm (blue trace). Black dots indicate drug additions to give indicated bath concentrations. Bar suggests the presence of the mentioned compound or physiological salt solution wash-out.*

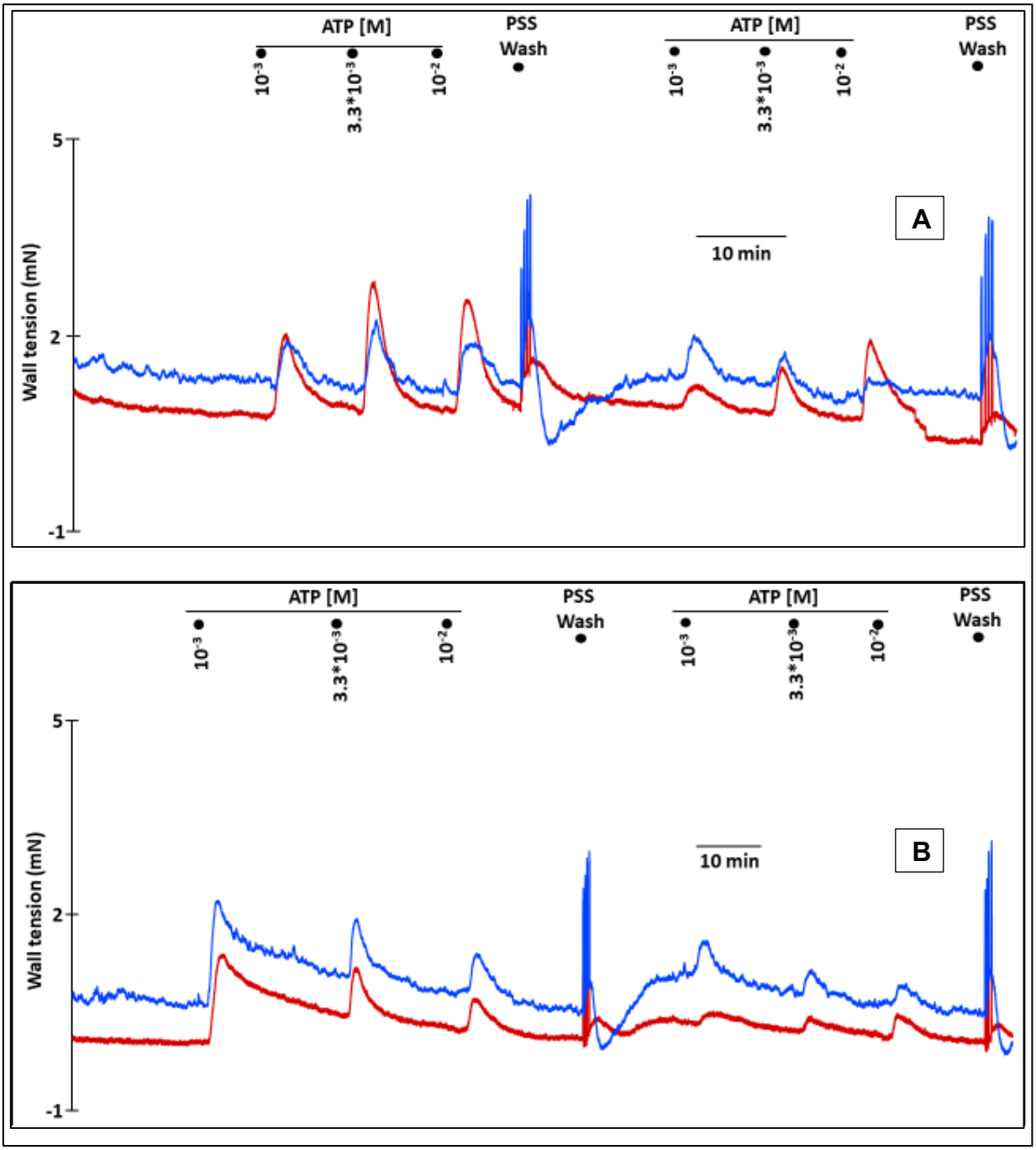


Figure 119. *Wire myography traces highlighting ATP-induced vasoconstriction responses in the absence of A740003 using isolated resistance CPA's originating from two healthy patients (T2826 and T2828)* ***A***. *Typical vasoactive effects of ATP generated by isolated chorionic plate artery preparations of a healthy patient (T2826). Internal diameter of CPA's was 0.179mm (red trace) and 0.201mm (blue trace)* ***B***. *Conventional ATP-induced vasoconstriction effects originating from CPA's of a healthy patient (T2828). Internal diameter CPA's was 0.095mm (red trace) and 0.154mm (blue trace). Black dots indicate drug additions to give indicated bath concentrations. Bar suggests the presence of the mentioned compound or physiological salt solution wash-out.*

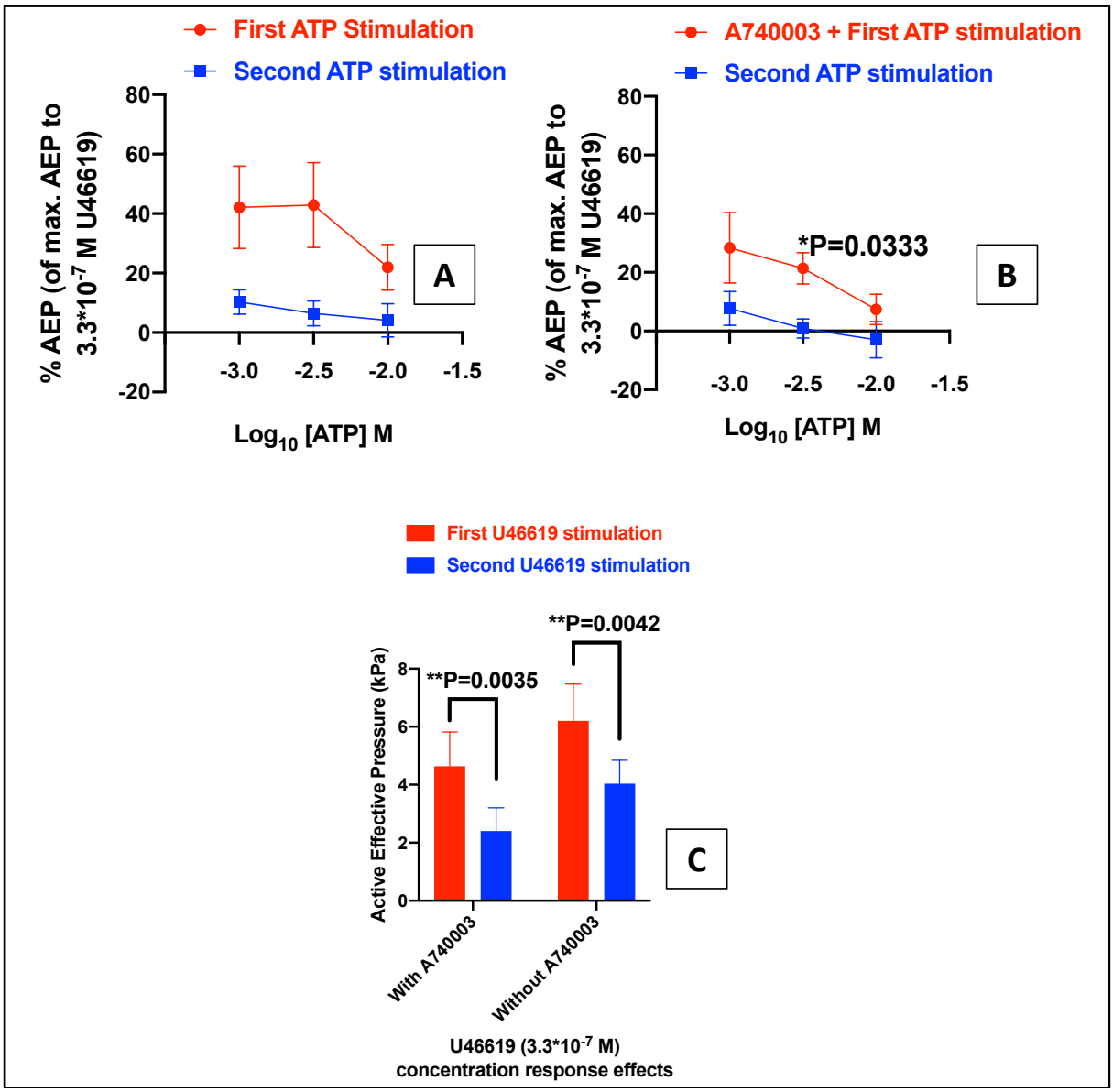


Figure 120. *Vasoactive effects of ATP in the presence and absence of A740003 initiated by isolated resistance CPA's originating from placental samples of N=3 healthy patients. The statistics were carried out using data obtained from n=6 CPA preparations* ***A****. Log concentration-effect curves elicited by ATP* ***B****. Log concentration-effect curves elicited by ATP following the incubation with A740003. In this case, the CPA's were incubated with the P2X7 receptor antagonist before the first ATP stimulation* ***C****. Vasoconstriction effects initiated via the exogenous application of U46619 (3.3*10^{-7}M) by resistance CPA's (that have been exposed or not exposed to A740003) at the start (first stimulation) and end (second stimulation) of the wire myography experiment expressed as active effective pressure (kPa). *P≤0.05, **P≤0.01, ***P≤0.001, ****P≤0.0001; Data are expressed as mean±SEM.*

4.3.8 Three consecutive additions of ATP gave rise to a progressively reduced vasomotor response which ultimately resulted in a maximal vasoconstriction effect that reached below 3% of the U46619 standard

In order to further describe the kind of contractile effects initiated by ATP in isolated resistance CPA's originating from 3 healthy patients, the P2X receptors were selectively desensitized using sequential applications of adenosine 5'-triphosphate at concentrations of $3.3*10^{-4}$M, 10^{-3}M, $3.3*10^{-3}$M and 10^{-2}M in a period of approximately 20 minutes as illustrated in the wire myography traces presented in figure 121 and figure 122. The three consecutive additions of the same ATP concentration gave rise to progressively decreased vasomotor contractions in all cases corresponding to the first ATP stimulation as highlighted in figure 123, panel A. Similar progressively reduced vasoconstriction effects took place in the case of the second ATP stimulation with the exception of $3.3*10^{-4}$M, where the three consecutive additions of the nucleotide gave rise to a maximal constriction response that plateaued below 3% of the maximal U46619 standard as presented in figure 123, panel A. Furthermore, the second and third consecutive additions of 10^{-2}M adenosine 5'-triphosphate in the case of the second nucleotide stimulation gave rise to a total desensitization effect with vasoactive responses taking place below the baseline corresponding to the first U46619 stimulation as presented in figure 123, panel A. A Shapiro-Wilk test revealed that all of the active effective pressure data corresponding to all ATP stimulations was normally distributed with one exception of the third consecutive nucleotide addition ($3.3*10^{-4}$M) in the case of the first ATP stimulation (*P=0.0161). A two-way ANOVA test (**P=0.0012) with Geisser-Greenhouse correction (epsilon 0.2865) and Tukey's

multiple comparison tests were undertaken between all nucleotide concentrations corresponding to each of the first, second or third consecutive ATP additions and highlighted multiple statistically significant differences as shown in figure 123, panel A and table 23. Furthermore, the same test was repeated again between the first, second and third consecutive additions of ATP, at the same nucleotide concentration which highlighted multiple statistically significant differences as presented in figure 123, panel A and table 24. A Shapiro-Wilk test was conducted using all active effective pressure data elicited by the first (at the beginning of the wire myography experiment) and second (at the end of the functional assessment) U46619 stimulations in CPA's which have been exposed to sequential applications of $3.3*10^{-4}$M, 10^{-3}M, $3.3*10^{-3}$M and 10^{-2}M ATP and highlighted that all data was normally distributed. Moreover, a two-way ANOVA test (***P=0.0001) and Tukey's multiple comparison tests were undertaken between the first and second U46619 stimulations in the case of CPA's which have been exposed to three consecutive identical additions of ATP which highlighted multiple statistically significant differences at nucleotide concentrations of 10^{-2}M (**P=0.0037) and $3.3*10^{-4}$M (*P=0.0392). The internal diameter of all resistance CPA's (n=12) originating from N=3 healthy patients was 0.197±0.012 mm presented as mean±SEM.

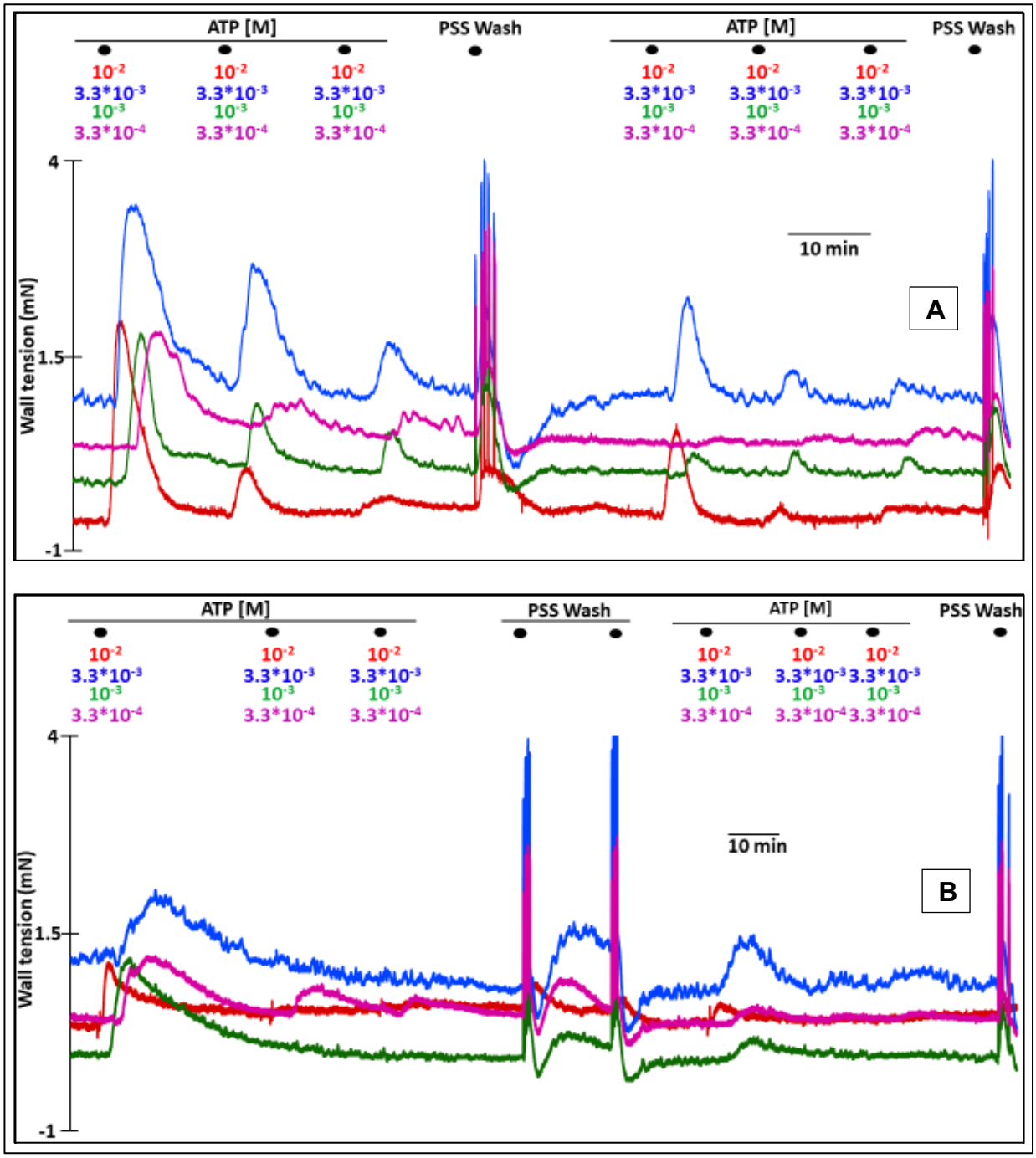


Figure 121*. Wire myography traces highlighting ATP-induced vasoconstriction responses using isolated resistance CPA's originating from two healthy patients (T2841 and T2831)* ***A****. Typical vasoactive effects of ATP generated from CPA's of a healthy patient (T2841) after three consecutive additions of the nucleotide. Internal diameter of CPA's was 0.141mm (red trace), 0.243mm (blue trace), 0.148mm (green trace) and 0.200mm (purple trace)* ***B****. Conventional ATP-induced vasoconstriction effects originating from CPA's of a healthy patient (T2831) following three sequential applications of the nucleotide. Internal diameter CPA's was 0.126mm (red trace), 0.217mm (blue trace), 0.144mm (green trace) and 0.215mm (purple trace). Black dots indicate drug additions to give indicated bath concentrations. Bar suggests the presence of the mentioned compound concentration to the corresponding matching colour force myograph trace or physiological salt solution wash-out.*

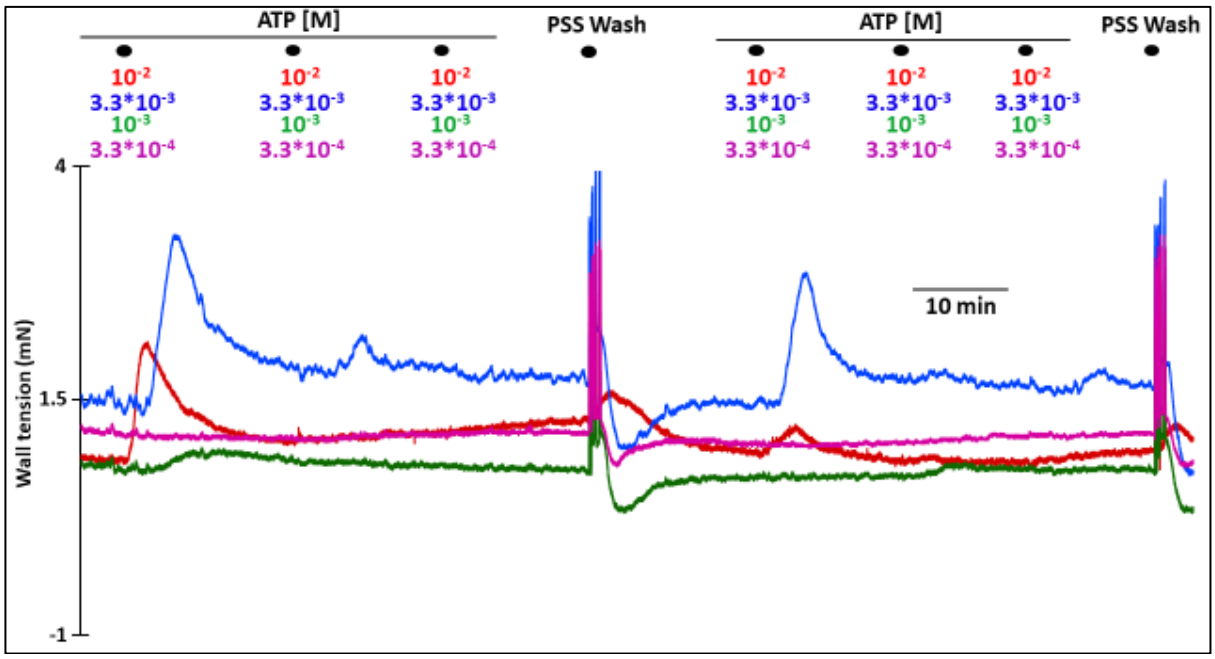


***Figure 122**. Wire myography trace highlighting ATP-induced vasoconstriction responses using isolated resistance CPA's originating from a healthy patient (T2837). Internal diameter of CPA's was 0.244mm (red trace), 0.225mm (blue trace), 0.222mm (green trace) and 0.236mm (purple trace). Black dots indicate drug additions to give indicated bath concentrations. Bar suggests the presence of the mentioned compound concentration to the corresponding matching colour force myograph trace or physiological salt solution wash-out.*

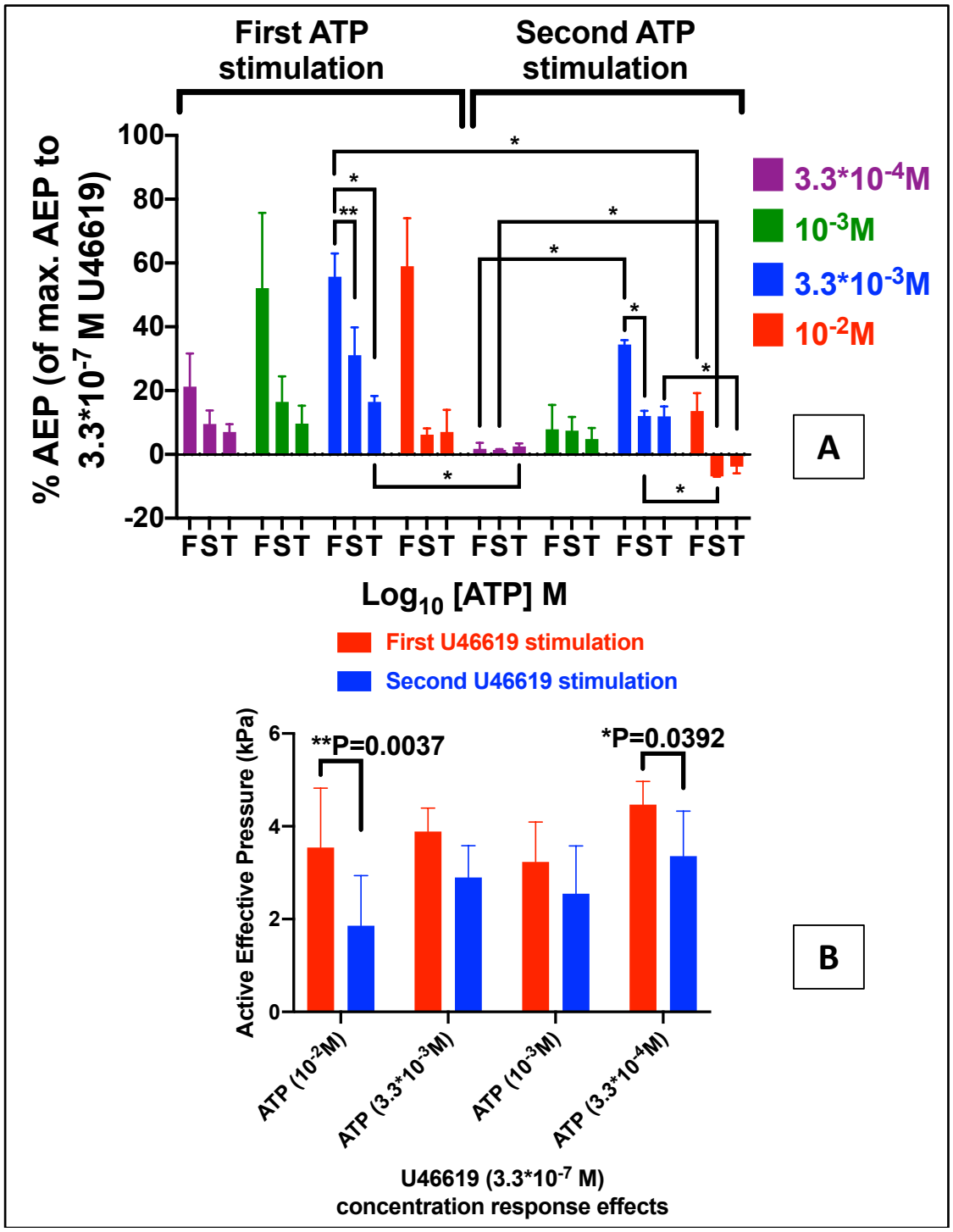


Figure 123. *Vasoactive effects of ATP and U46619 initiated by isolated resistance CPA's originating from human placental samples of N=3 healthy patients (T2841, T2831 and T2837)* ***A***. *Log concentration-effect responses elicited by three sequential applications of ATP. "F" denotes first application, "S" suggests second consecutive addition and "T" means third consecutive addition* ***B***. *Vasoconstriction effects initiated via the exogenous application of U46619 ($3.3*10^{-7}$M) at the start (first stimulation) and end (second stimulation) of the wire myography experiment using resistance CPA's which have been challenged with three sequential applications of ATP expressed as active effective pressure (kPa). *P≤0.05, **P≤0.01, ***P≤0.001, ****P≤0.0001; Data are expressed as mean±SEM.*

		Adjusted P value
First addition	First ATP stimulation ($3.3*10^{-3}$M) vs second ATP stimulation (10^{-2}M)	*P=0.0152
	Second ATP stimulation ($3.3*10^{-4}$M) vs second ATP stimulation ($3.3*10^{-3}$M)	*P=0.0416
Second consecutive addition	Second ATP stimulation ($3.3*10^{-4}$M) vs second ATP stimulation (10^{-2}M)	*P=0.0200
	Second ATP stimulation ($3.3*10^{-3}$M) vs second ATP stimulation (10^{-2}M)	*P=0.0286
Third consecutive addition	First ATP stimulation ($3.3*10^{-3}$M) vs second ATP stimulation ($3.3*10^{-4}$M)	*P=0.0220
	Second ATP stimulation (3.3*10-3M) vs second ATP stimulation (10^{-2}M)	*P=0.0208

Table 23. *This table shows the results of a two-way ANOVA test with Geisser-Greenhouse correction and Tukey's multiple comparison tests which were carried out between all nucleotide concentrations corresponding to each of the first, second or third consecutive ATP additions. *P≤0.05, **P≤0.01, ***P≤0.001, ****P≤0.0001.*

		Adjusted P value
First ATP stimulation	First addition ($3.3*10^{-3}$M) vs second consecutive addition ($3.3*10^{-3}$M)	**P=0.0099
	First addition ($3.3*10^{-3}$M) vs third consecutive addition ($3.3*10^{-3}$M)	*P=0.0351
Second ATP stimulation	First addition ($3.3*10^{-3}$M) vs second consecutive addition ($3.3*10^{-3}$M)	*P=0.0301

Table 24. *This table shows the results of a two-way ANOVA test with Geisser-Greenhouse correction and Tukey's multiple comparison tests which were carried out between the first, second and third consecutive additions of ATP, at the same nucleotide concentration. *P≤0.05, **P≤0.01, ***P≤0.001, ****P≤0.0001.*

4.3.9 The 30mM KPSS-induced elevation in the human placental chorionic plate artery resting basal tone increased the efficacy of the first ATP stimulation by more than 38% at a nucleotide concentration of 10^{-3}M and by more than 27% at an ATP concentration of $3.3*10^{-3}$M

The vasoactive effects of ATP on isolated resistance CPA's originating from N=3 healthy patients were investigated in the presence (n=3 CPA's) and absence (n=3 CPA's) of a 30mM KPSS-induced elevation in the resting basal tone as highlighted in the wire myography trace illustrated in the representative figure 124. Since both cumulative concentrations or three sequential applications of ATP gave rise to a progressively diminished vasomotor response from isolated chorionic plate arteries, the acute CPA challenge with 30mM KPSS served to assess if the ATP-induced desensitization effect could have been partially or totally reversed. In this case, the placental arteries were challenged twice with ATP cumulative concentrations of 10^{-3}M, $3.3*10^{-3}$M and 10^{-2}M as illustrated in the representative figure 124. In this case the first and second ATP stimulations of CPA's elicited progressively reduced spontaneous vasoconstriction effects in the absence and presence of 30mM KPSS as highlighted in figure 125, panel A. The preconstriction of placental arteries with 30mM KPSS gave rise to ATP-induced spontaneous maximal vasoconstriction effects which were higher at all cumulative concentrations of the nucleotide compared to CPA's which have not been initially preconstricted, with the exception of 10^{-2}M ATP corresponding to the first nucleotide stimulation. Furthermore, the second ATP stimulation of the isolated placental arteries in the absence of a 30mM KPSS-induced elevation in the resting basal tone elicited a maximal contraction which was notably attenuated, ultimately

resulting in a total desensitization effect taking place, particularly at ATP cumulative concentrations of $3.3*10^{-3}$M and 10^{-2}M as illustrated in figure 125, panel A. A Shapiro-Wilk test was undertaken across the active effective pressure values of all ATP cumulative concentrations of the first and second nucleotide stimulations of isolated CPA's which highlighted that all data was normally distributed with the exception of 10^{-2}M ATP concentration corresponding to the second ATP stimulation of CPA's which have initially been preconstricted with 30mM KPSS (*P=0.0183). A two-way ANOVA test (****P<0.0001) with Sidak's multiple comparison tests were undertaken at the same ATP concentrations between the first and second ATP stimulations which highlighted multiple statistically significant differences as presented in table 25, table 26 and figure 125, panel A. Also, the same test was undertaken again with Tukey's multiple comparison tests separately using the first and second ATP stimulations across all ATP concentrations which highlighted no statistically significant differences. The vasoconstriction effects initiated via the exogenous application of U46619 ($3.3*10^{-7}$M) by resistance CPA's (that have been exposed or not exposed to 30mM KPSS) at the start (first stimulation) and end (second stimulation) of the wire myography experiments are illustrated in figure 125, panel B. Also, the 30mM KPSS-induced vasoconstriction responses expressed as active effective pressure are presented in figure 125, panel C. A Shapiro-Wilk test was undertaken using all active effective pressure values of first and second U46619 stimulations which highlighted that all data was normally distributed. A two-way ANOVA test (*P=0.0129) with Sidak's multiple comparison tests have highlighted no statistically significant differences between the first and second U46619 stimulations of CPA's which have either been preconstricted or not preconstricted with 30mM KPSS as presented in figure 125, panel B. A Shapiro-Wilk test was performed using the active effective pressure values of the first and

second 30mM KPSS challenges which highlighted that all data was normally distributed. An unpaired two-tailed T-test with Welch's correction between the first and second 30mM KPSS challenges has highlighted no statistically significant differences between the two groups (P=0.3924). The internal diameter of n=6 CPA's used in this study was 0.217±0.052mm (mean±SEM).

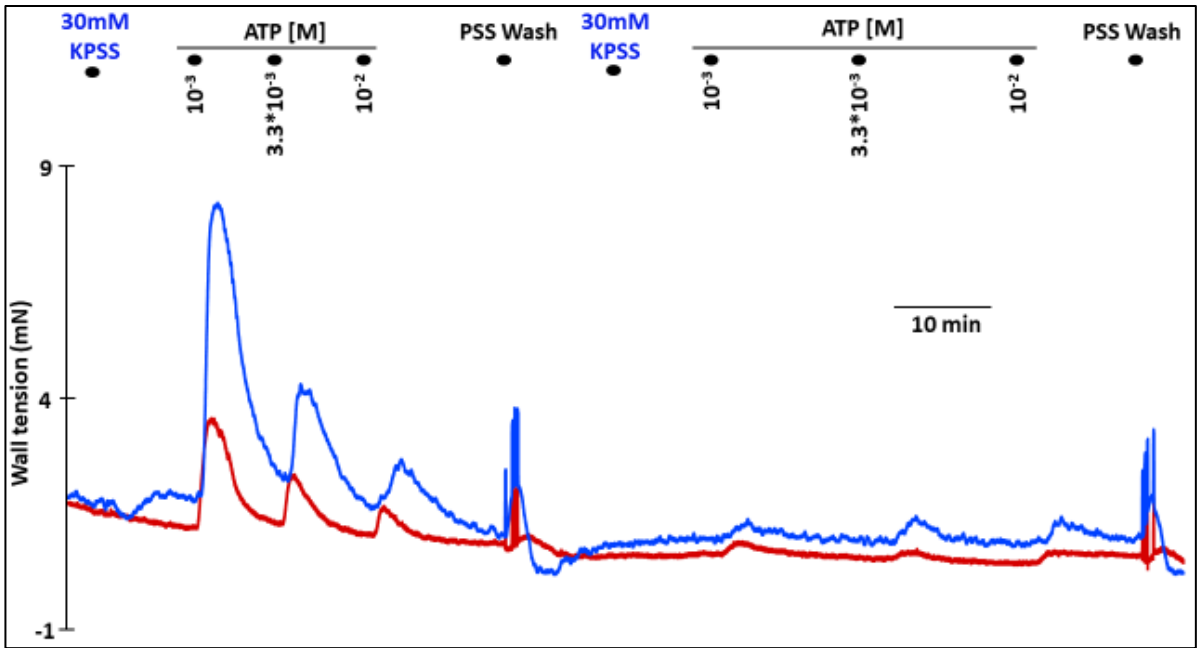


Figure 124. *Wire myography trace highlighting ATP-induced vasoconstriction responses in the presence (blue trace) and absence (red trace) of 30mM KPSS originating from isolated resistance CPA's of a healthy patient (T2857). Internal diameter of CPA's was 0.391mm (red trace) and 0.369mm (blue trace). Black dots suggest drug additions to give indicated bath concentrations. Bar denotes the presence of the mentioned compound concentration to the corresponding matching colour force myograph trace (with the exception of black colour which applies to all traces) or physiological salt solution wash-out.*

		First ATP stimulation vs second ATP stimulation
10^{-3}M ATP	**Without 30mM KPSS preconstriction**	****P<0.0001
3.3*10^{-3}M ATP		****P<0.0001
10^{-2}M ATP		*P=0.0264

Table 25. *This table shows the results of a two-way ANOVA test with Sidak's multiple comparison tests which were undertaken at the same ATP concentrations between the first and second ATP stimulations. In this case, the CPA's have not been preconstricted with 30mM KPSS. *P≤0.05, **P≤0.01, ***P≤0.001, ****P≤0.0001.*

		First ATP stimulation vs second ATP stimulation
10^{-3}M ATP	With 30mM KPSS preconstriction	****P<0.0001
3.3*10^{-3}M ATP		***P=0.0002
10^{-2}M ATP		P=0.6213

Table 26. *This table shows the results of a two-way ANOVA test with Sidak's multiple comparison tests which were undertaken at the same ATP concentrations between the first and second ATP stimulations. In this case, the CPA's were preconstricted with 30mM KPSS. *P≤0.05, **P≤0.01, ***P≤0.001, ****P≤0.0001.*

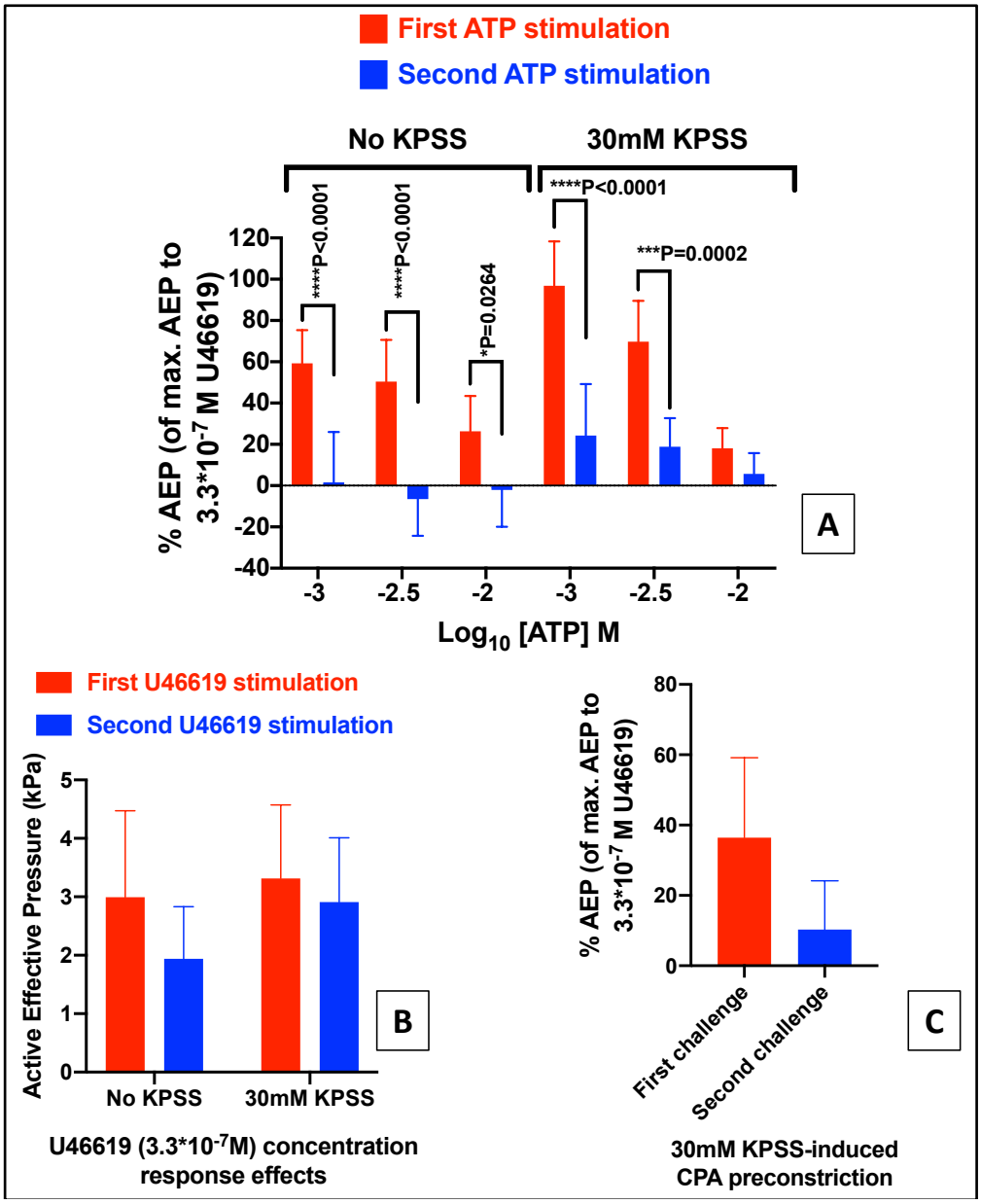


Figure 125. *Vasoactive effects of ATP, U46619 and 30mM KPSS initiated by isolated resistance CPA's originating from placental samples of N=3 healthy patients **A**. Log concentration-effect curves elicited by ATP in the absence and presence of 30mM*

KPSS. In this case, the preconstriction of CPA's with 30mM KPSS took place before the first and second ATP stimulation. The active effective pressure elicited by 30mM KPSS has been subtracted from the maximal ATP-induced vasoconstriction effects ***B****. Vasoconstriction effects initiated via the exogenous application of U46619 (3.3*10^{-7}M) at the start (first stimulation) and end (second stimulation) of the wire myography experiment using resistance CPA's which have been subjected to preconstriction with 30mM KPSS or not subjected to 30mM KPSS challenges expressed as active effective pressure (kPa)* ***C****. 30mM KPSS-induced vasoconstriction responses elicited by resistance CPA's before the first ATP stimulation (first challenge) and ahead of the second ATP stimulation (second challenge). *P≤0.05, **P≤0.01, ***P≤0.001, ****P≤0.0001; Data are expressed as mean±SEM.*

4.3.10 The 30mM KPSS preimposed tone did not increase the efficacy of three consecutive additions of 10^{-2}M ATP in isolated resistance human chorionic plate artery preparations originating from two healthy patients

A similar vasoactive effect of ATP was also elicited from isolated resistance CPA's originating from N=2 healthy patients using sequential applications of the nucleotide at a concentration of 10^{-2}M in the presence (n=2 CPA's) and absence (n=2 CPA's) of 30mM KPSS-induced elevation in the resting basal tone of the placental blood vessels as illustrated by the representative wire myography trace presented in figure 126. The second ATP stimulation gave rise to a notably attenuated maximal vasoconstriction response, with contractions substantially reduced by more than 63% compared to the first ATP stimulation of the resistance CPA's as highlighted in figure 126. Moreover, the second and third consecutive additions of 10^{-2}M ATP gave rise to a maximal contraction which was notably attenuated, ultimately resulting in a total desensitization effect taking place in the case of both first and second ATP stimulations. The internal diameter of all resistance CPA's (n=4) originating from N=2 healthy patients was 0.2205±0.05 mm presented as mean±SEM.

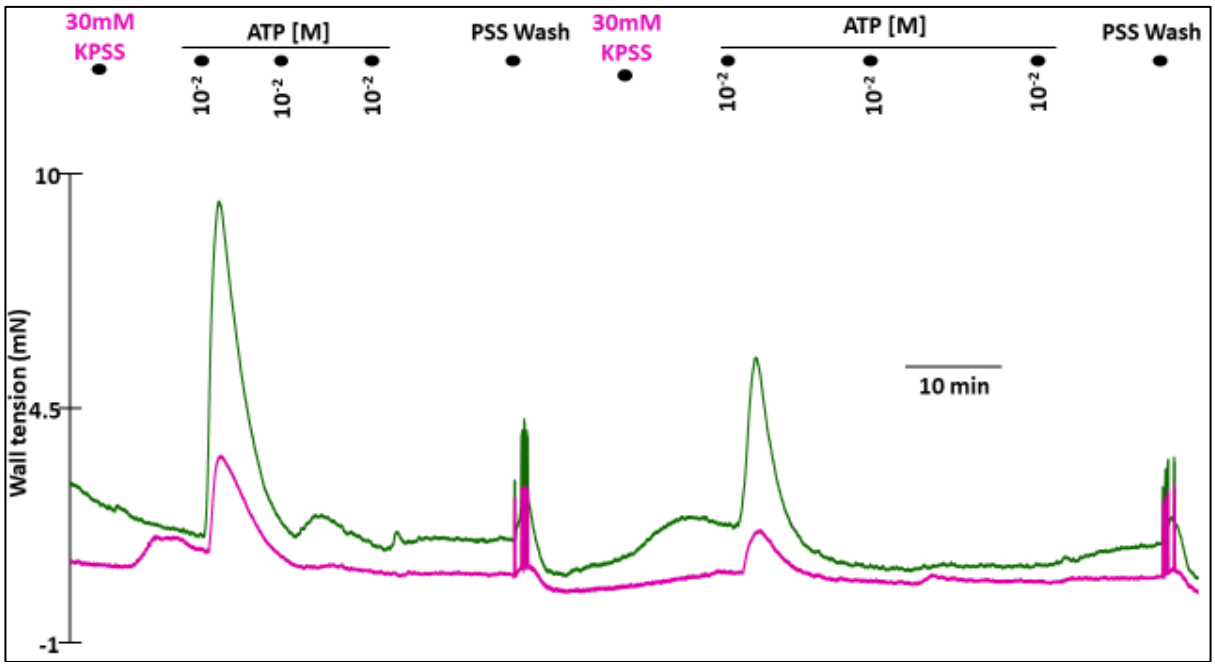


***Figure 126**. Wire myography trace highlighting ATP-induced vasoconstriction responses generated after three 10^{-2}M consecutive additions of the nucleotide using resistance CPA's originating from a healthy patient (T2857) in the presence and absence of 30mM KPSS. Internal diameter of CPA's was 0.358mm (green trace), 0.233mm (purple trace). Black dots indicate drug additions to give indicated bath concentrations. Bar indicates the presence of the mentioned compound concentration to the corresponding matching colour force myograph trace (with the exception of black colour which applies to all traces) or physiological salt solution wash-out.*

4.3.11 The 40mM KPSS-induced elevation in the resting basal tone did not significantly alter the efficacy of the first and second ATP stimulations in isolated chorionic plate arteries originating from three healthy patients

The vasoactive effects of ATP in isolated resistance CPA's originating from N=3 healthy patients were further investigated using cumulative concentrations of the nucleotide (10^{-3}M, $3.3*10^{-3}$M and 10^{-2}M) in the absence (n=3 CPA's) and presence (n=3 CPA's) of 40mM KPSS-induced elevation in the resting basal tone as highlighted in the representative wire myography trace illustrated in figure 127. The second ATP stimulation gave rise to progressively reduced vasomotor responses compared to the

first ATP stimulation, particularly in isolated CPA's that were initially preconstricted with 40mM KPSS as highlighted in figure 128, panel A. In this case, the nucleotide cumulative concentration of 10^{-2}M corresponding to the second ATP stimulation elicited a vasoactive effect that reached a total desensitization. On the other hand, the first ATP stimulation gave rise to a concentration response curve that was almost flat, characterised by maximal vasoconstriction effects which plateaued at approximately 55% of the U46619 standard in the case of CPA's which have not been initially preconstricted with 40mM KPSS as highlighted in figure 128, panel A. Furthermore, the second ATP stimulation elicited a notably attenuated concentration response curve, with the nucleotide induced contractions becoming reduced by more than 30% compared to the first ATP stimulation as illustrated in figure 128, panel A. The U46619-induced vasoconstriction effects at the beginning (first stimulation) and end (second stimulation) of the wire myography experiment elicited by CPA's which were initially preconstricted with 40mM KPSS prior to ATP stimulations or not preconstricted with 40mM KPSS are highlighted in figure 128, panel B. Also, the vasoconstriction effects initiated by the exposure of CPA's to 40mM KPSS prior to the first and second ATP stimulations are presented in figure 128, panel C. All ATP cumulative concentration response curves (presented in figure 128, panel A) were subjected to a Shapiro-Wilk normality test which highlighted that all data was normally distributed with the exception of $3.3*10^{-3}$M ATP concentration corresponding to the first nucleotide stimulation of CPA's which were not initially preconstricted with 40mM KPSS (*P=0.0156). A two-way ANOVA test (*P=0.0241) with Sidak's multiple comparison tests were carried out between the first and second ATP stimulations at the same nucleotide cumulative concentrations which highlighted no statistically significant differences across all subgroups. Furthermore, the same test with Tukey's multiple

comparison tests were carried out separately using the first and second ATP stimulations between all ATP cumulative concentrations which also highlighted no statistically significant differences between all subgroups. All active effective pressure data corresponding to U46619-induced maximal vasoconstriction effects was subjected to a Shapiro-Wilk test which highlighted that all data was normally distributed, with the exception of the first U46619 stimulation corresponding to CPA's which were subsequently preconstricted with 40mM KPSS (*P=0.0220). In this case, a two-way ANOVA test (P=0.2934) with Sidak's multiple comparison tests were carried out between the first and second U46619 stimulations and revealed no statistically significant differences across the two groups. A Shapiro-Wilk test was performed using the active effective pressure values of the first and second 40mM KPSS challenges which highlighted that all data was normally distributed. An unpaired two-tailed T-test with Welch's correction between the first and second 40mM KPSS challenges highlighted no statistically significant differences between the two groups (P=0.8721). The internal diameter of n=6 CPA's used in this study was 0.185±0.037mm (mean±SEM).

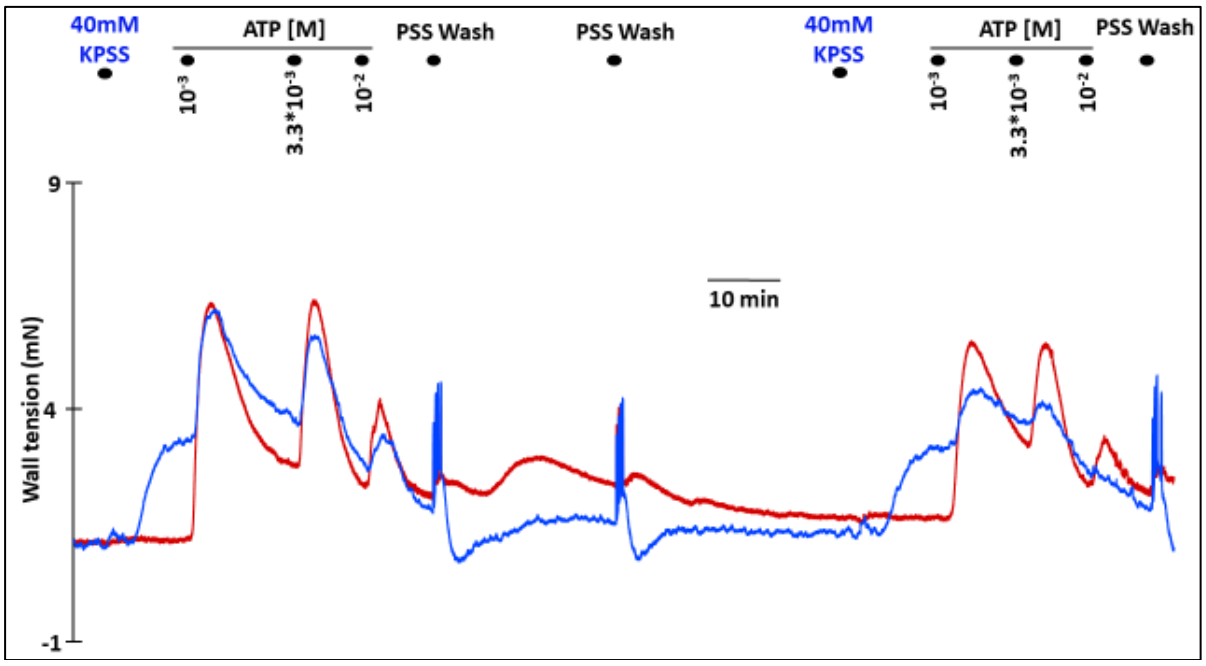


Figure 127. *Wire myography traces highlighting ATP-induced vasoconstriction responses in the presence and absence of 40mM KPSS originating from isolated resistance CPA's of two healthy patients (T2874 and T2875)* ***A***. *Vasoactive effects of ATP generated by isolated chorionic plate artery preparations of a healthy patient (T2874) which have been either preconstricted or not preconstricted with 40mM KPSS. Internal diameter of CPA's was 0.295mm (red trace) and 0.292mm (blue trace)* ***B***. *Conventional ATP-induced vasoconstriction effects originating from CPA's of a healthy patient (T2875) in the presence and absence of 40mM KPSS. Internal diameter CPA's was 0.091mm (green trace) and 0.090mm (purple trace). Black dots indicate drug additions to give indicated bath concentrations. Bar denotes the presence of the mentioned compound concentration to the corresponding matching colour force myograph trace (with the exception of black colour which applies to all traces) or physiological salt solution wash-out.*

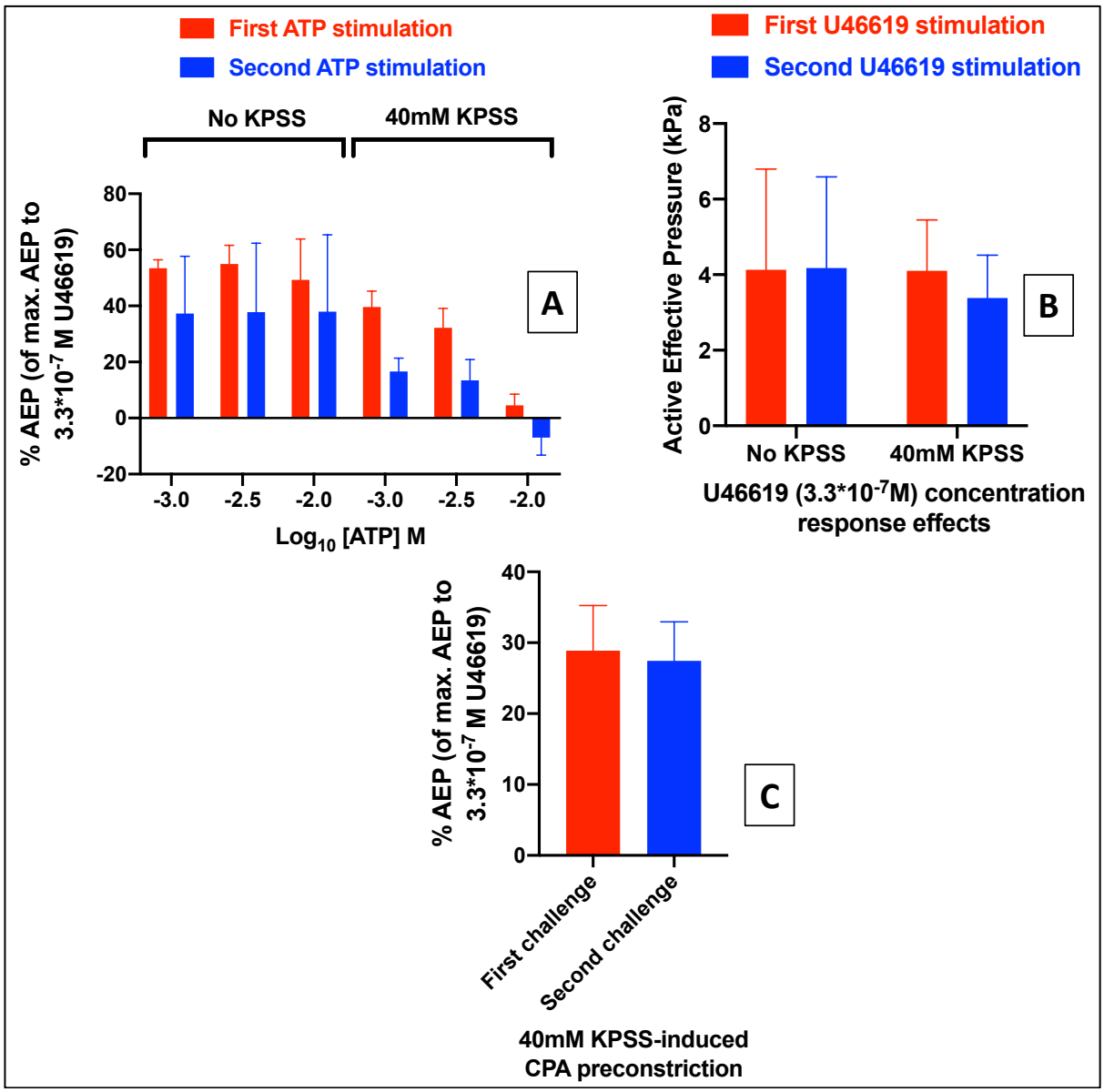


Figure 128. *Vasoactive effects of ATP, U46619 and 40mM KPSS initiated by isolated resistance CPA's originating from placental samples of N=3 healthy patients* ***A****. Log concentration-effect curves elicited by ATP in the absence and presence of 40mM KPSS. In this case, the preconstriction of CPA's with 40mM KPSS took place before the first and second ATP stimulation. The active effective pressure elicited by 40mM KPSS has been subtracted from the maximal ATP-induced vasoconstriction effects* ***B****. Vasoconstriction effects initiated via the exogenous application of U46619 (3.3*10^{-7}M) at the start (first stimulation) and end (second stimulation) of the wire myography experiment using resistance CPA's which have been subjected to preconstriction with 40mM KPSS or not subjected to 40mM KPSS challenge expressed as active effective pressure (kPa)* ***C****. 40mM KPSS-induced vasoconstriction responses elicited by resistance CPA's before the first ATP stimulation (first challenge) and ahead of the second ATP stimulation (second challenge). *P≤0.05, **P≤0.01, ***P≤0.001, ****P≤0.0001; Data are expressed as mean±SEM.*

4.3.12 The P2X7 receptor agonist BzATP gave rise to a substantially reduced vasoconstriction effect of less than 25% of the U46619 standard characterised by an almost flat concentration response curve

The vasoactive effects of the P2X7 receptor agonist BzATP were investigated using n=4 isolated resistance CPA's originating from N=2 healthy patients at cumulative concentrations starting with $3.3*10^{-6}$M to $3.3*10^{-4}$M as highlighted in the wire myography traces presented in figure 129 and figure 130. In this case, BzATP was almost inactive and gave rise to a maximal vasoconstriction effect that barely reached 24% of the U46619 standard which resulted in an almost flat concentration response curve as highlighted in figure 131, panel A. A progressive increase in BzATP-induced maximal vasoconstriction responses took place between the P2X7 receptor agonist cumulative concentrations of $3.3*10^{-6}$M to $3.3*10^{-5}$M followed by a progressively decreased vasomotor response particularly at BzATP cumulative concentrations of 10^{-4}M and $3.3*10^{-4}$M as presented in figure 131, panel A. All BzATP cumulative concentration response curves (presented in figure 131, panel A) were subjected to a Shapiro-Wilk normality test which highlighted that all data was normally distributed. A Brown-Forsythe Anova test (P=0.9995) with Dunnett T3 multiple comparison tests were undertaken between all BzATP cumulative concentrations which highlighted no statistically significant differences between all subgroups. Moreover, the vasoconstriction effects initiated via the exogenous application of U46619 ($3.3*10^{-7}$M) by resistance CPA's at the start (first stimulation) and end (second stimulation) of the wire myography experiments are illustrated in figure 131, panel B. In this case, U46619-induced maximal vasoconstriction effects were subjected to a

Shapiro-Wilk test which highlighted that all data was normally distributed. An unpaired two-tailed T-test with Welch's correction between the first and second U46619 stimulations highlighted no statistically significant differences between the two groups (P=0.7678). The internal diameter of n=4 CPA's used in this study was 0.160±0.017mm (mean±SEM).

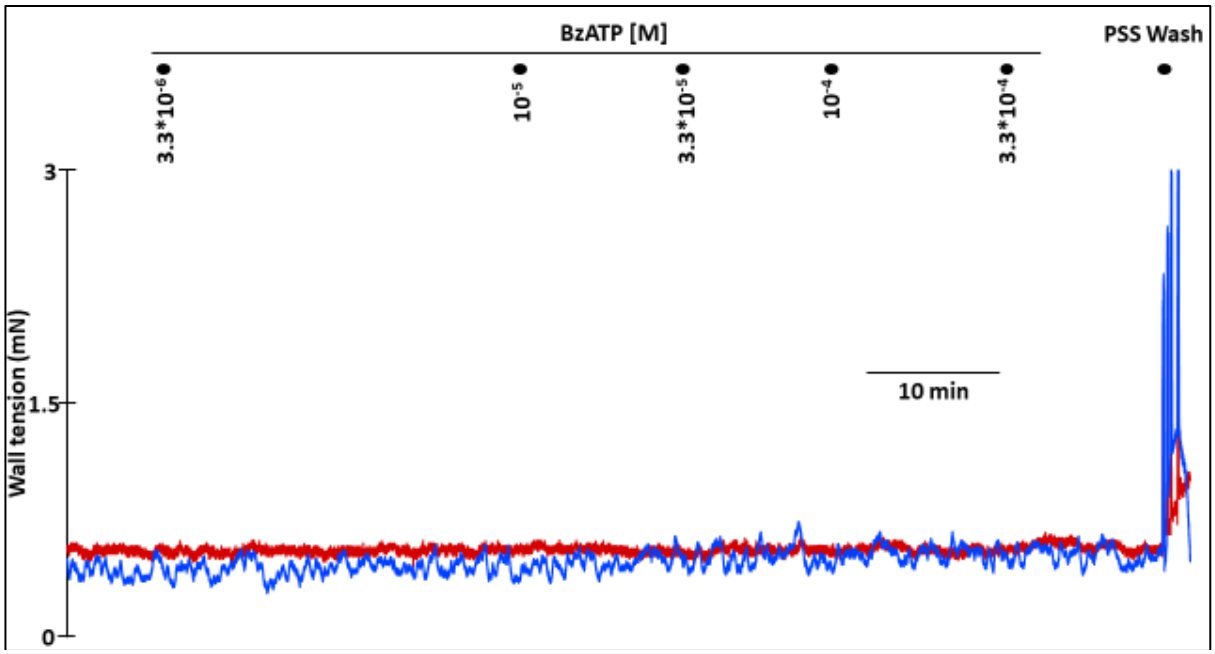


***Figure 129**. Vasoactive effects of BzATP initiated by isolated resistance CPA's with internal diameters of 0.144mm (red trace) and 0.122mm (blue trace) originating from a placenta sample of a healthy patient (T2858). Black dots indicate drug additions to give indicated bath concentrations. Bar suggests the presence of the mentioned compound or physiological salt solution wash-out.*

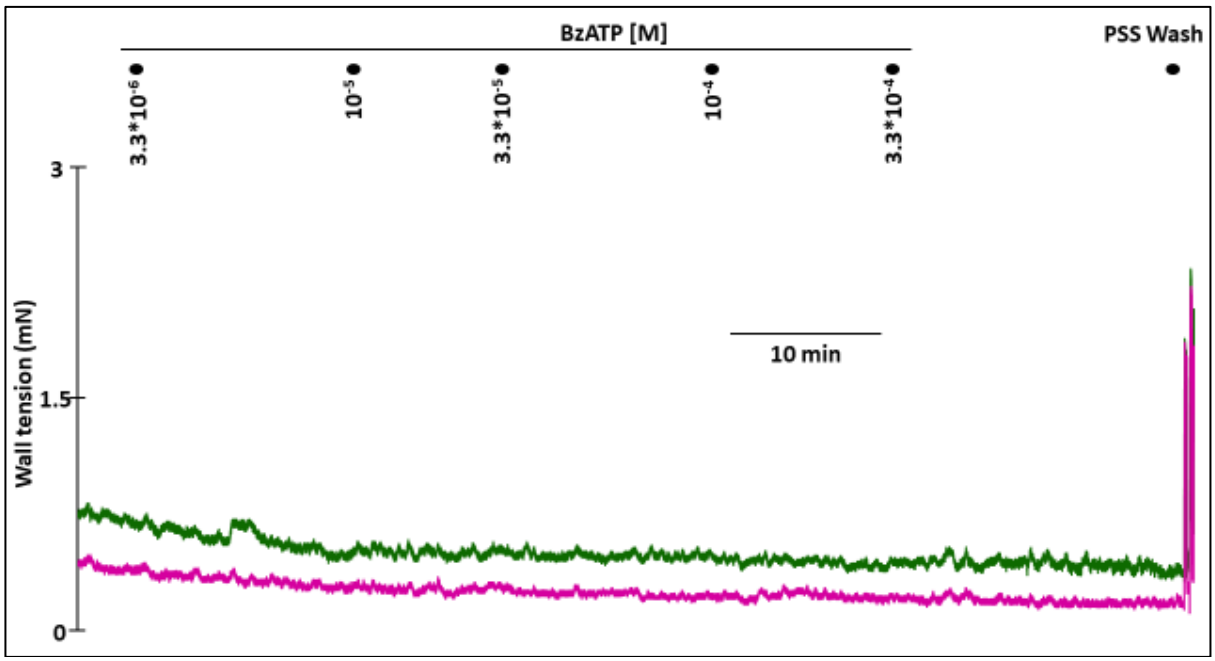


Figure 130. *Vasoactive effects of BzATP initiated by isolated resistance CPA's with internal diameters of 0.201mm (green trace) and 0.173mm (purple trace) originating from a placenta sample of a healthy patient (T2863). Black dots indicate drug additions to give indicated bath concentrations. Bar suggests the presence of the mentioned compound or physiological salt solution wash-out.*

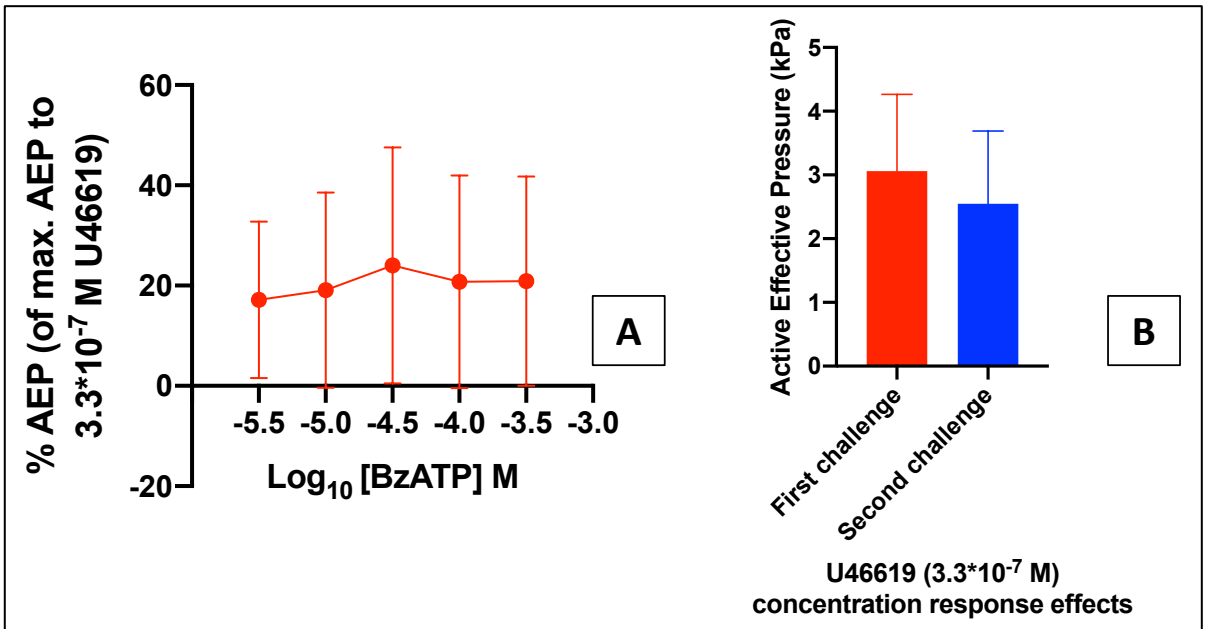


Figure 131. *Vasoactive effects of BzATP and U46619 initiated by isolated resistance CPA's originating from two placental samples of healthy patients (T2858 and T2863)* ***A***. *Log concentration-effect curve elicited by BzATP* ***B***. *Vasoconstriction effects initiated via the exogenous application of U46619 (3.3*10^{-7}M) at the start (first stimulation) and end (second stimulation) of the wire myography experiment expressed as active effective pressure (kPa). Data are expressed as mean±SEM.*

4.3.13 A 30mM KPSS-induced elevation in the resting basal tone caused a substantially reduced spontaneous BzATP maximal vasoconstriction effect of less than 6% of the U46619 standard

The vasoactive effects of BzATP on isolated resistance CPA's originating from N=2 healthy patients were investigated in the presence (n=4 CPA's) of a 30mM KPSS-induced elevation in the resting basal tone as highlighted in the wire myography traces illustrated in figure 132. The P2X7 receptor agonist gave rise to spontaneous vasoconstriction effects particularly at cumulative concentrations of 10^{-4}M and $3.3*10^{-4}$M that barely reached 5% of the U46619 standard as presented in figure 133, panel A. Also, BzATP elicited a progressively reduced vasomotor response that reached a total desensitization especially at cumulative concentrations of 10^{-5}M and $3.3*10^{-5}$M as illustrated in figure 133, panel A. All BzATP cumulative concentration response curves (presented in figure 133, panel A) were subjected to a Shapiro-Wilk normality test which highlighted that all data was normally distributed. A Brown-Forsythe ANOVA test (P=0.4431) with Dunnett's T3 multiple comparison tests were undertaken between all cumulative concentrations of BzATP which highlighted no statistically significant differences between all groups. The vasoconstriction effects initiated via the exogenous application of U46619 ($3.3*10^{-7}$M) by resistance CPA's at the start (first stimulation) and end (second stimulation) of the wire myography experiments are illustrated in figure 133, panel B. The U46619-induced maximal vasoconstriction effects were subjected to a Shapiro-Wilk test which highlighted that all data was normally distributed. An unpaired two-tailed T-test with Welch's correction between the first and second U46619 stimulations highlighted no statistically significant

differences between the two groups (P=0.5679). The 30mM KPSS-induced vasoconstriction effects elicited by n=4 CPA's expressed as percentage active effective pressure of maximal active effective pressure induced by $3.3*10^{-7}$M U46619 were 23.06±5.474%. The internal diameter of n=4 CPA's used in this study was 0.257±0.012mm (mean±SEM).

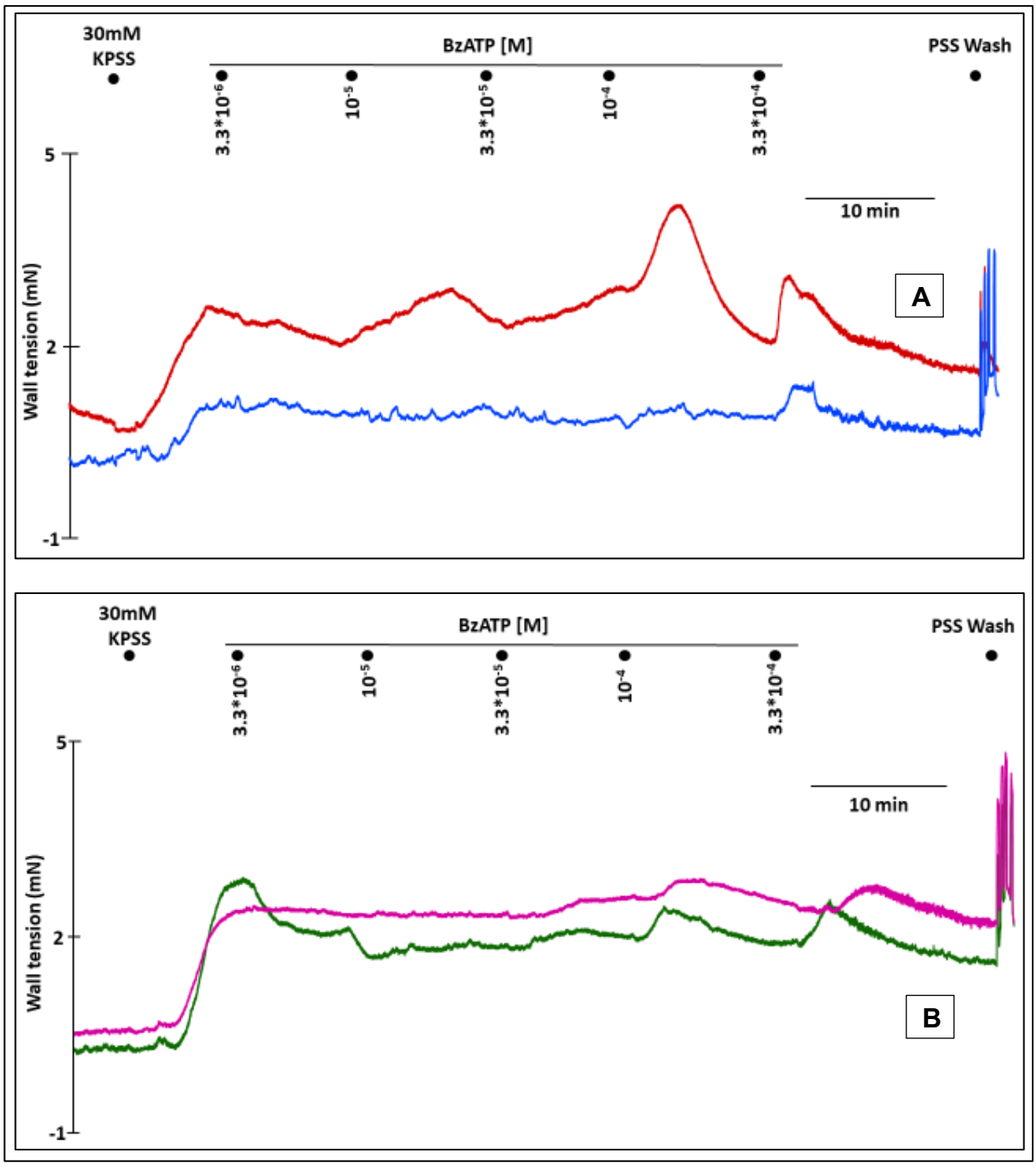


***Figure 132**. Vasoactive effects of BzATP initiated by isolated resistance CPA's in the presence of 30mM KPSS originating from placental samples of two healthy patients (T2865 and T2866) **A**. Vasoactive effects of BzATP generated by isolated chorionic plate artery preparations (T2865) with internal diameters of 0.286mm (red trace) and 0.246mm (blue trace) **B**. BzATP-induced vasoconstriction effects originating from CPA's (T2866) with internal diameters of 0.230mm (green trace) and 0.266mm (purple trace). Black dots indicate drug additions to give indicated bath concentrations. Bar suggests the presence of the mentioned compound or physiological salt solution wash-out.*

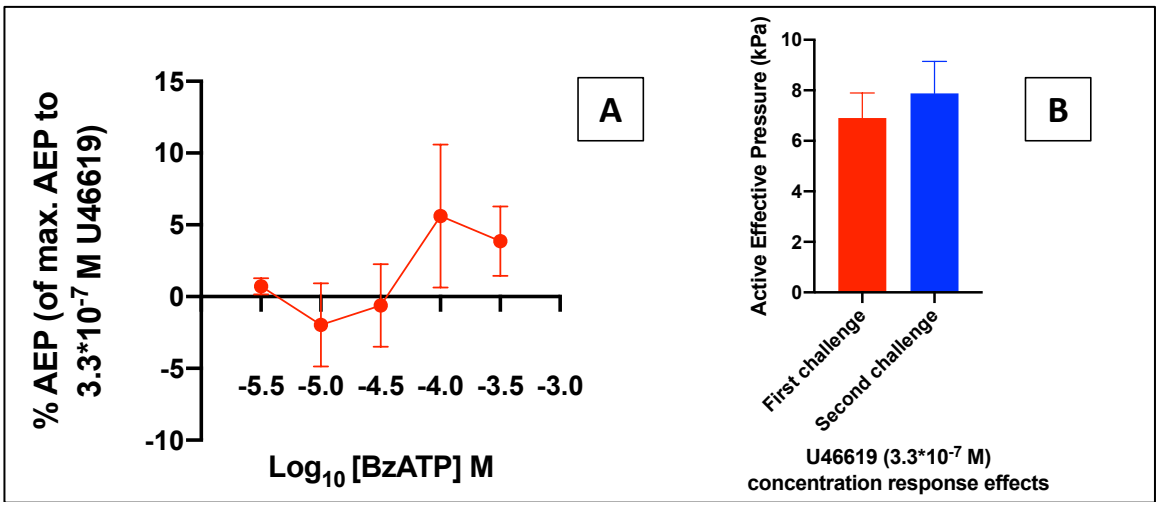


***Figure 133**. Vasoactive effects of BzATP and U46619 initiated by isolated resistance CPA's originating from placental samples of two healthy patients (T2865 and T2866) **A**. Log concentration-effect curve elicited by BzATP in the presence of 30mM KPSS. In this case, the preconstriction of CPA's with 30mM KPSS took place prior to BzATP stimulation. The active effective pressure elicited by 30mM KPSS has been subtracted from the maximal BzATP-induced vasoconstriction effects **B**. Vasoconstriction effects initiated via the exogenous application of U46619 ($3.3*10^{-7}$M) at the start (first challenge) and end (second challenge) of the wire myography experiment expressed as active effective pressure (kPa). Data are expressed as mean±SEM.*

4.3.14 A 50mM KPSS-induced rise in the chorionic plate artery resting basal tone caused a progressively reduced vasomotor response initiated by the exogenous application of BzATP

The vasoactive effects of BzATP were further investigated using resistance CPA's isolated from N=3 healthy patients in the presence (n=3 CPA's) and absence (n=3 CPA's) of 50mM KPSS-induced elevation in the resting basal tone as illustrated in the wire myography traces presented in figure 134 and figure 135. In the absence of 50mM KPSS, cumulative concentrations of BzATP gave rise to progressively increased vasoconstriction effects starting with $3.3*10^{-6}$M to $3.3*10^{-4}$M, characterised by a maximal vasomotor response that barely reached 12% of the U46619 standard at the cumulative BzATP concentration of $3.3*10^{-4}$M, as shown in figure 136, panel A.

In this case the calculated BzATP EC_{50} concentration was $1.354*10^{-4}$M as highlighted in figure 136, panel B. On the other hand, following the preconstriction of CPA's with 50mM KPSS, the P2X7 receptor agonist initiated a vasomotor response that was progressively reduced and did not elicit any spontaneous vasoconstriction effects as presented in figure 136, panel A. All BzATP cumulative concentration response curves (presented in figure 136, panel A) were subjected to a Shapiro-Wilk normality test which highlighted that all data was normally distributed as presented in table 27. A Brown-Forsythe ANOVA test (P=0.2078) with Dunnett's T3 multiple comparison tests were undertaken between all BzATP concentrations and highlighted a single statistically significant difference (**P=0.0042) between $3.3*10^{-6}$M vs 10^{-5}M BzATP in the case of arteries which have been preconstricted with 50mM KPSS. The vasoconstriction effects initiated via the exogenous application of U46619 ($3.3*10^{-7}$M) by resistance CPA's at the start (first stimulation) and end (second stimulation) of the wire myography experiments are illustrated in figure 136, panel C. The U46619-induced maximal vasoconstriction effects were subjected to a Shapiro-Wilk test which highlighted that all data was normally distributed with the exception of the second U46619 stimulation of CPA's which were not preconstricted with 50mM KPSS (*P=0.0376). A Brown-Forsythe ANOVA test (P=0.4914) with Dunnett's T3 multiple comparison tests were undertaken between all U46619 stimulations of resistance CPA's at the start (first stimulation) and end (second stimulation) of the wire myography experiments which highlighted no statistically significant differences between all groups. The 50mM KPSS-induced vasoconstriction effects elicited by n=3 CPA's expressed as percentage active effective pressure of maximal active effective pressure induced by $3.3*10^{-7}$M U46619 were 31.42±8.473%. The internal diameter of n=6 CPA's used in this study was 0.232±0.061mm (mean±SEM).

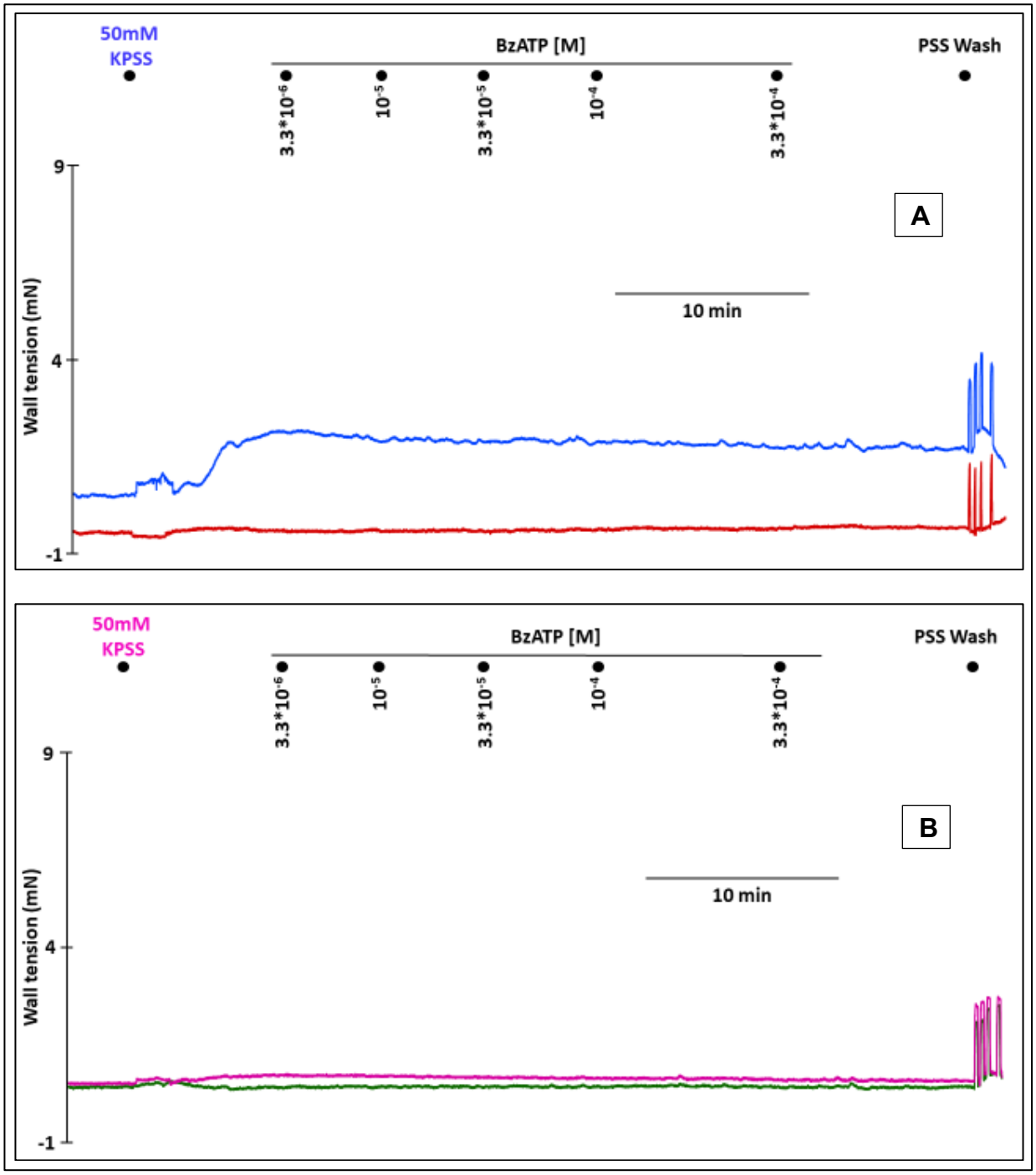


***Figure 134**. Vasoactive effects of BzATP initiated by isolated resistance CPA's in the absence and presence of 50mM KPSS originating from placental samples of two healthy patients (T2890 and T2891) **A**. Vasoactive effects of BzATP generated by isolated chorionic plate artery preparations (T2890) with internal diameters of 0.116mm (red trace) and 0.201mm (blue trace) **B**. BzATP-induced vasoconstriction effects originating from CPA's (T2891) with internal diameters of 0.126mm (green trace) and 0.147mm (purple trace). Black dots indicate drug additions to give indicated bath concentrations. Bar denotes the presence of the mentioned compound concentration to the corresponding matching colour force myograph trace (with the exception of black colour which applies to all traces) or physiological salt solution wash-out.*

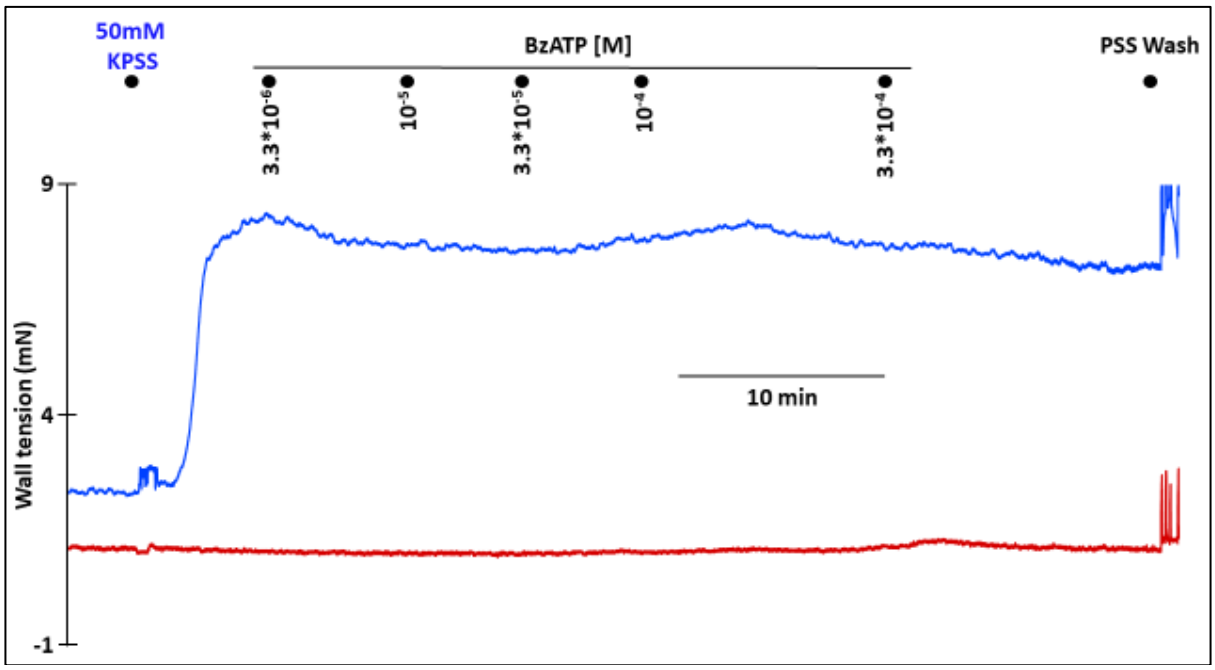


***Figure 135**. Vasoactive effects of BzATP initiated by isolated resistance CPA's with internal diameters of 0.293mm (red trace) and 0.512mm (blue trace) in the absence and presence of 50mM KPSS originating from a placenta sample of a healthy patient (T2893). Black dots indicate drug additions to give indicated bath concentrations. Bar suggests the presence of the mentioned compound concentration to the corresponding matching colour force myograph trace (with the exception of black colour which applies to all traces) or physiological salt solution wash-out.*

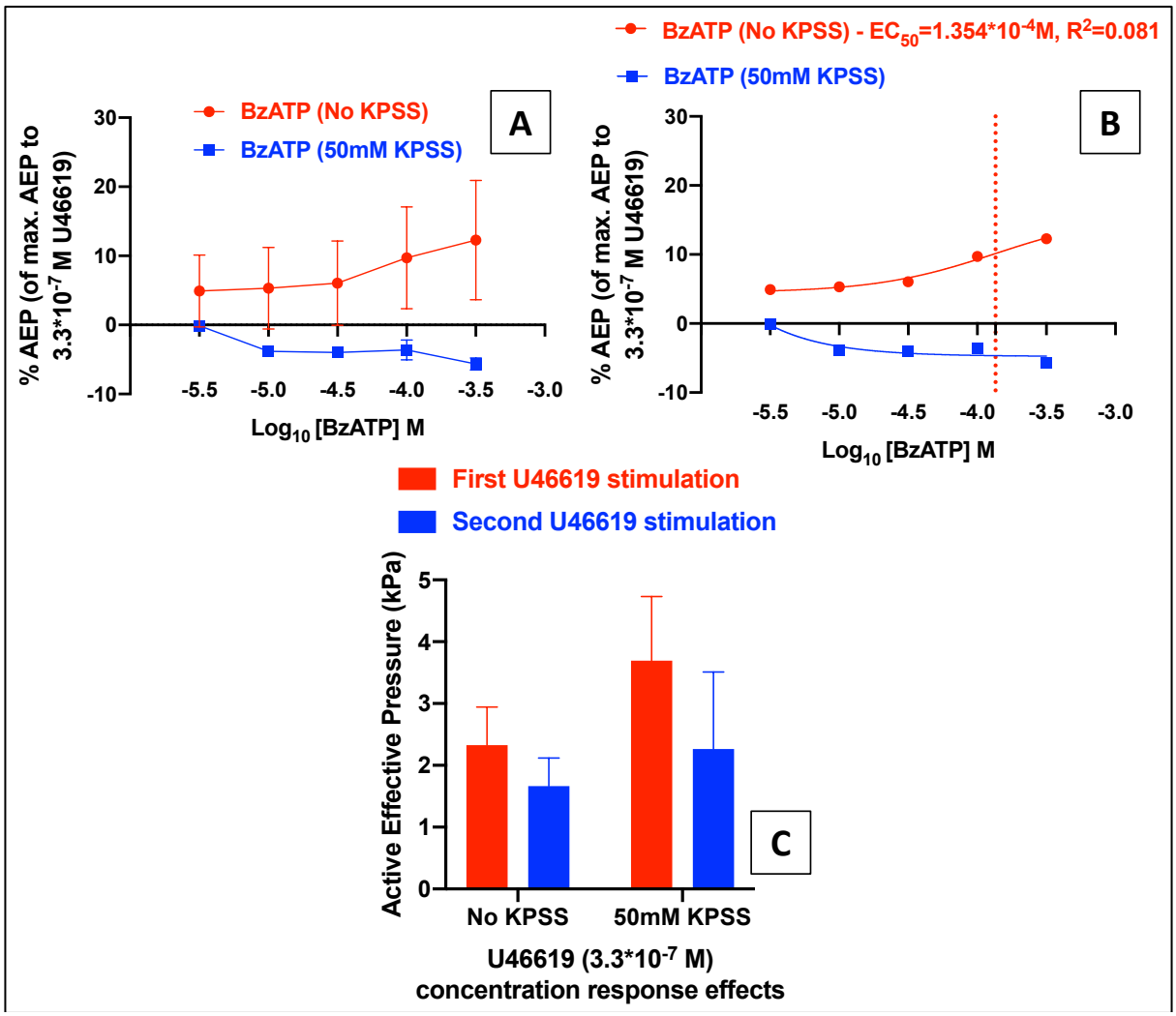


Figure 136. *Vasoactive effects of BzATP, U46619 and 50mM KPSS initiated by isolated resistance CPA's originating from placental samples of N=3 healthy patients (T2890, T2891 and T2893)* ***A****. Log concentration-effect curves elicited by BzATP in the absence and presence of 50mM KPSS. In this case, the preconstriction of CPA's with 50mM KPSS took place prior to BzATP stimulation. The active effective pressure elicited by 50mM KPSS has been subtracted from the maximal BzATP-induced vasoconstriction effects* ***B****. Nonlinear regression fit (three parameter logistic equation) of log concentration-effect curve initiated by BzATP highlighting the calculated BzATP EC_{50} value (in the absence of 50mM KPSS – illustrated as a red vertical discontinued line)* ***C****. Vasoconstriction effects initiated via the exogenous application of U46619 ($3.3*10^{-7}$M) at the start (first challenge) and end (second challenge) of the wire myography experiment expressed as active effective pressure (kPa). Data are expressed as mean±SEM.*

		No KPSS	50mM KPSS
BzATP concentration	$3.3*10^{-6}$M	P=0.9364	P=0.5845
	10^{-5}M	P=0.9926	P=0.6183
	$3.3*10^{-5}$M	P=0.8744	P=0.1102
	10^{-4}M	P=0.9722	P=0.9682
	$3.3*10^{-4}$M	P=0.8644	P=0.5166

***Table 27**. This table shows the results of a Shapiro-Wilk test corresponding to all of the BzATP cumulative concentration response curves elicited by resistance CPA's in the absence and presence of 50mM KPSS. *P≤0.05, **P≤0.01, ***P≤0.001, ****P≤0.0001.*

4.3.15 Elevated chorionic plate artery resting basal tone using 70mM KPSS notably decreases the BzATP-induced vasoconstriction responses below 6% of the U46619 standard

The vasoactive properties of BzATP on isolated resistance chorionic plate arteries originating from N=2 healthy patients were further investigated in the absence (n=2 CPA's) and presence (n=2 CPA's) of 70mM KPSS-induced elevation in the resting basal tone as shown in the wire myography trace presented in figure 137. The P2X7 receptor agonist gave rise to progressively increased vasoconstriction effects starting with $3.3*10^{-6}$M until $3.3*10^{-4}$M as highlighted in figure 138, panel A. In the absence of 70mM KPSS, the maximal vasoconstriction effect took place at a BzATP cumulative concentration of $3.3*10^{-4}$M characterised by a maximal vasomotor response that almost reached 20% of the U46619 standard. The calculated BzATP EC_{50} concentration in this case was $4.655*10^{-5}$M (figure 138, panel B). On the other side, CPA's which were initially preconstricted with 70mM KPSS gave rise to a maximal BzATP-induced vasoconstriction effect which barely reached 5% of the U46619 standard at a concentration of $3.3*10^{-4}$M. In this case, the BzATP cumulative

concentration response curve was almost flat and notably displaced downwards, with vasoactive responses significantly attenuated compared to CPA's which were not initially preconstricted prior to BzATP stimulation as highlighted in figure 138, panel A. The calculated BzATP EC_{50} value in the presence of 70mM KPSS was $2.649*10^{-5}$M suggesting that the P2X7 receptor agonist was approximately 0.5-fold more potent compared to no elevation in CPA resting tone prior to BzATP stimulation. A Brown-Forsythe ANOVA test (P=0.9991) with Dunnett's T3 multiple comparison tests across all BzATP cumulative concentrations highlighted no statistically significant differences between all groups. Furthermore, the same test was undertaken between all U46619 stimulations of resistance CPA's at the start (first stimulation) and end (second stimulation) of the wire myography experiments which highlighted no statistically significant differences between all groups (figure 138, panel C). The internal diameter of n=4 CPA's used in this study was 0.154±0.011mm (mean±SEM).

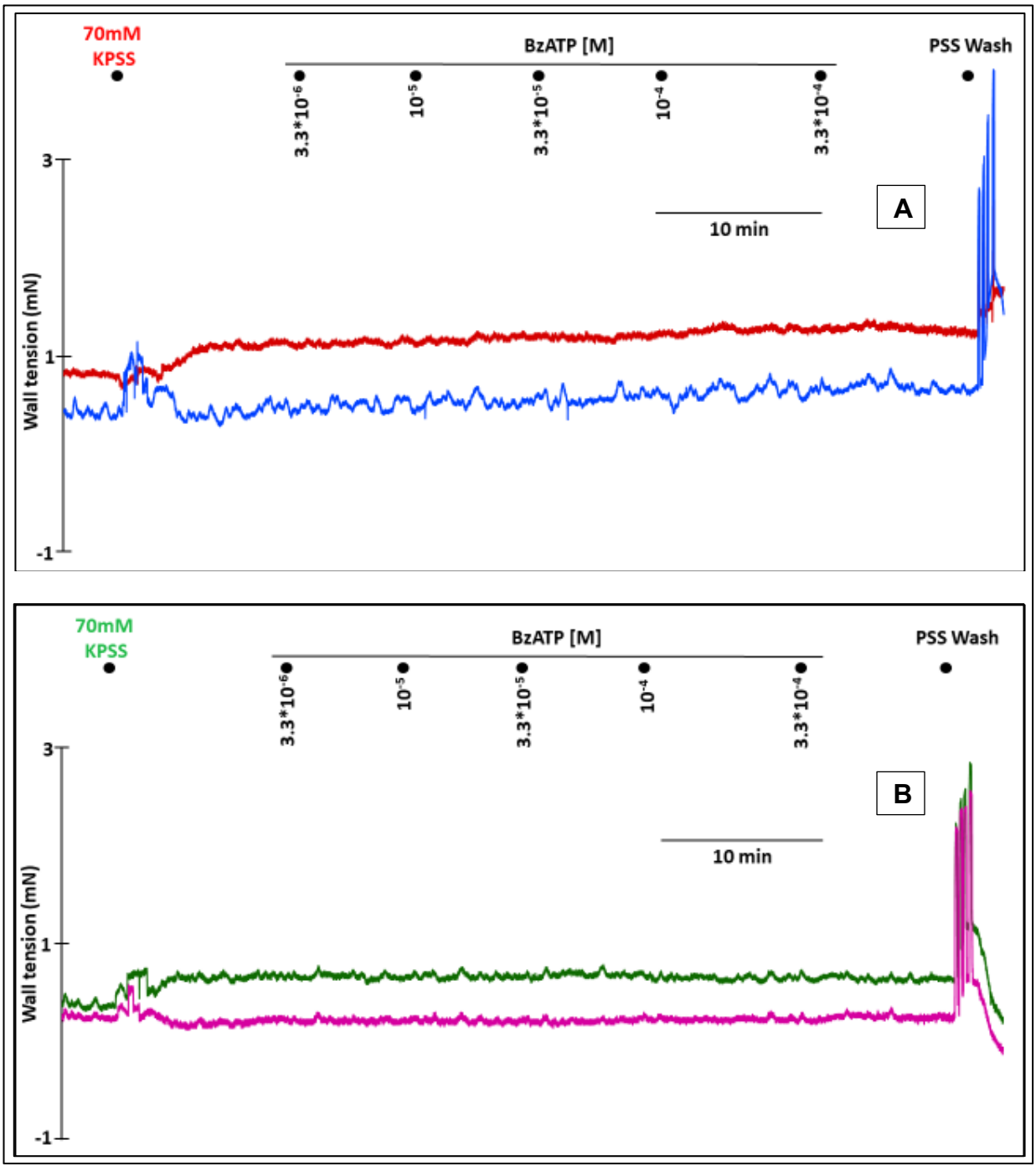


***Figure 137**. Vasoactive effects of BzATP initiated by isolated resistance CPA's in the absence and presence of 70mM KPSS originating from placental samples of two healthy patients (T2888 and T2889) **A**. Vasoactive effects of BzATP generated by isolated chorionic plate artery preparations (T2888) with internal diameters of 0.144mm (red trace) and 0.141mm (blue trace) **B**. BzATP-induced vasoconstriction effects originating from CPA's (T2889) with internal diameters of 0.190mm (green trace) and 0.144mm (purple trace). Black dots indicate drug additions to give indicated bath concentrations. Bar suggests the presence of the mentioned compound concentration to the corresponding matching colour force myograph trace (with the exception of black colour which applies to all traces) or physiological salt solution wash-out.*

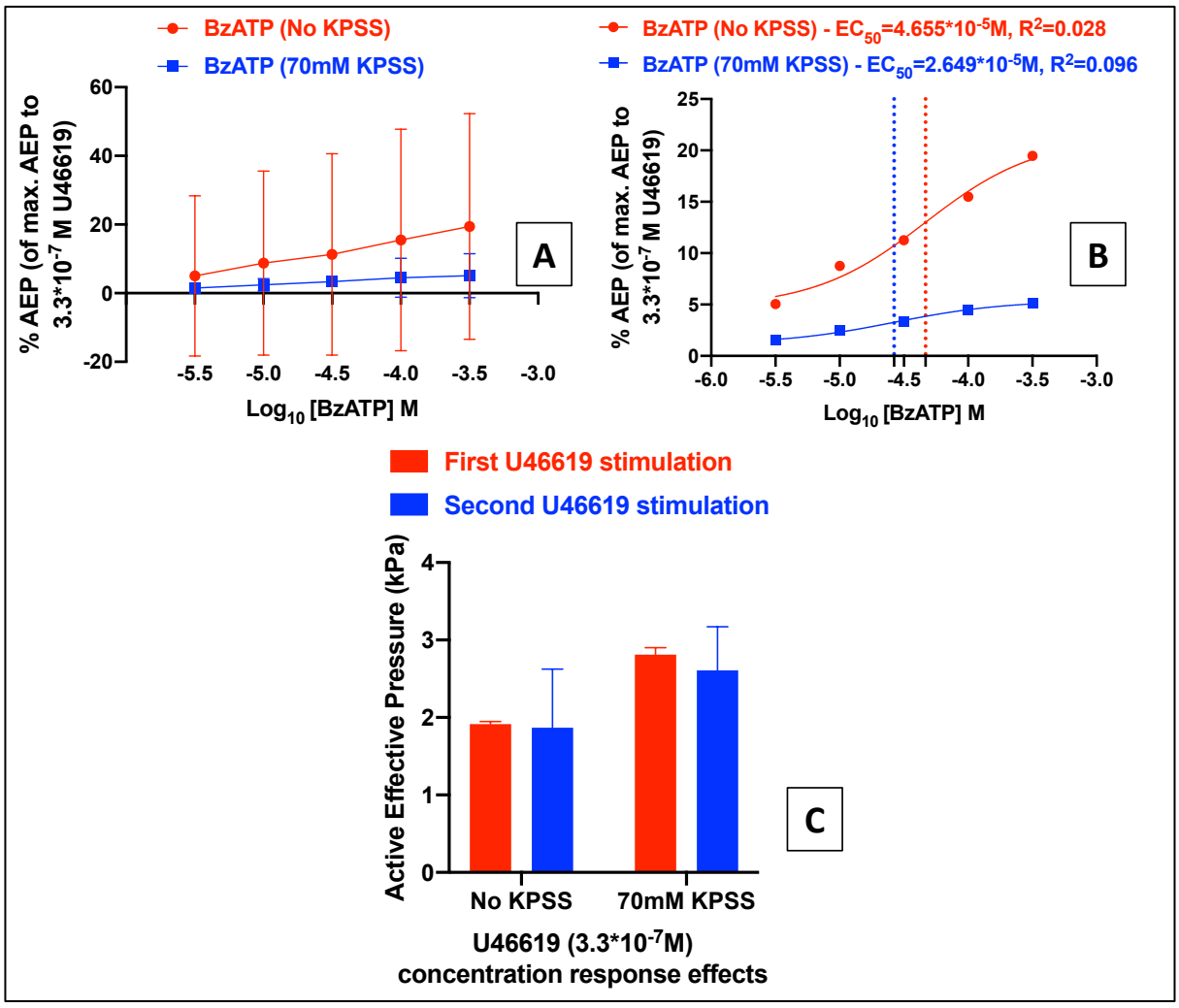


Figure 138. *Vasoactive effects of BzATP, U46619 and 70mM KPSS initiated by isolated resistance CPA's originating from placental samples of two healthy patients (T2888 and T2889)* ***A***. *Log concentration-effect curves elicited by BzATP in the absence and presence of 70mM KPSS. In this case, the preconstriction of CPA's with 70mM KPSS took place prior to BzATP stimulation. The active effective pressure elicited by 70mM KPSS has been subtracted from the maximal BzATP-induced vasoconstriction effects* ***B***. *Nonlinear regression fit (three parameter logistic equation) of log concentration-effect curve initiated by BzATP highlighting the calculated BzATP EC_{50} values (in the absence of 70mM KPSS – illustrated as a red vertical discontinued line and in the presence of 70mM KPSS – presented as a blue vertical discontinued line)* ***C***. *Vasoconstriction effects initiated via the exogenous application of U46619 ($3.3*10^{-7}$M) at the start (first challenge) and end (second challenge) of the wire myography experiment expressed as active effective pressure (kPa). Data are expressed as mean±SEM.*

4.4 Discussion

The processes in charge with the regulation of vasomotor tone and blood flow at the level of the human fetoplacental circulation have not been fully elucidated yet. Multiple studies have investigated the function of vasoactive mediators in the control of the human fetoplacental vascular tone via the methodology of whole perfused placental cotyledon [593–595] or small blood vessel myography studies to directly assess the contribution of stem villous arteries and chorionic plate veins or arteries [49,576,585,587]. Most investigations that have focused on small vessel myography studies have assessed the contribution of fetoplacental arteries in the control of the vascular tone. In this case, vasoconstriction has been shown using multiple compounds such as thromboxane-A_2 mimetic U46619 [588,590], vasopressin, oxytocin, angiotensin II, $PGF_{2\alpha}$ and circulating catecholamines for instance noradrenaline [576,590,591]. However, vasorelaxation has been particularly challenging to obtain with endothelium-dependent compounds for instance acetylcholine, histamine or bradykinin possessing particularly low vasodilating properties in chorionic plate arteries [576,585], even if vasodilation has been demonstrated in stem villous arteries under the exogenous application of PGI_2 [591] and histamine [586]. Moreover, a notable elevation in placental tone has also been shown with nitric oxide-inhibition in the perfused placental cotyledon [596]. A study by Learmont and Poston (1996) has demonstrated the relevance of flow at the level of the fetoplacental circulation via providing evidence of nitric oxide-regulated, flow-induced vasorelaxation of placental chorionic plate arteries [49]. Taking into account a possible involvement of chorionic plate arteries in the development of various placental malfunctions, a variety of pharmacological vasoactive modulators were investigated by assessing their vasocontractile or vasorelaxant capabilities using human placental blood vessel preparations originating

from placental samples of healthy or patients with various disorders. The well-known vasoconstrictor of chorionic plate arteries thromboxane A_2 mimetic U46619 gave rise to a reproducible and concentration-dependent contraction of the isolated superficial chorionic arteries as previously illustrated in multiple studies [53,523,576]. Initial wire myography studies have revealed a calculated U46619 EC_{50} value of $4.751*10^{-7}$M which was similar to other studies reporting a thromboxane A_2 agonist EC_{50} value of $1.2*10^{-7}$M [576].

An effective vasodilator of chorionic plate arteries is sodium nitroprusside which suggests that nitric oxide plays a crucial role in the regulation of the placental vasculature [59]. The current study has showed that the nitric oxide donor SNP (10^{-9}M to $3.3*10^{-9}$M) induced concentration-dependent relaxation in U46619-preconstricted CPA from a healthy patient, with a maximal vasodilation of 69.98% of the topmost U46619-preconstriction observed at an SNP concentration of $3.3*10^{-6}$M (SNP IC_{50} value of $4.717*10^{-8}$M). A similar vasorelaxation effect of CPA's to SNP of approximately 68% of the thromboxane A_2 mimetic standard was observed in another study [576]. A study by Mills *et al* (2005) has also provided evidence that SNP (10^{-9} – 10^{-4}M) significantly relaxed U46619-preconstricted chorionic plate arteries of both normal and fetal growth restriction pregnancy cases compared to time-matched control vessels (no SNP) [597]. Moreover, the SNP has been shown to cause vasodilation of stem villous arteries to about 50% of the preconstricted active effective pressure of U46619 (10^{-6}M) with an IC_{50} value of $7*10^{-6}$M which highlights the crucial role of nitric oxide for the regulation of the placental vasculature [482]. Another investigation by Gonzáles *et al* (1997) has presented evidence that SNP (10^{-8}M – 10^{-5}M) gave rise to concentration-dependent decline in tension in rings with endothelium of human chorionic arteries (EC_{50} value of $1.1±0.7*10^{-7}$M) and veins (EC_{50} value of

4.6±1.1*10^{-8}M) [598]. The same study has also investigated the vasodilatory effect of SNP in the same placental blood vessels of pre-eclamptic patients and found that the compound caused a concentration-dependent vasorelaxation response in chorionic plate artery (EC_{50} of 2.5±0.8*10^{-8}M) and chorionic plate vein (EC_{50} of 6.8±2.2*10^{-8}M) [598]. The current study confirms that SNP elicits vasorelaxation effects in isolated CPA's of healthy patients.

Another endothelium independent dilator tested was riluzole which is a sodium channel blocker, glutamate antagonist and potassium channel opener that is administered to patients with amyotrophic lateral sclerosis [599]. The compound acts on K_{2P}2.1 channel that is expressed in the vasculature of the human placenta. The current study suggests that riluzole does not elicit a reproducible notable vasorelaxation response in U46619 preconstricted CPA's originating from healthy patients with IC_{50} values of 1.442*10^{-5}M and 4.036*10^{-7}M. Furthermore, the compound did not elicit a substantial vasorelaxation effect in CPA's originating from placental samples of preeclamptic or intrauterine growth restriction patients. Most of these results contradict the published literature which suggests that the widely-used K_{2P}2.1 channel opener gives rise to an effective vasorelaxation of preconstricted arteries originating from healthy patients of approximately 83% [53]. Another study by Sander and colleagues (2019) has also suggested that riluzole causes significant vasorelaxation effects in preconstricted placental stem villous arteries originating from healthy patients of more than 60% of the preconstricted active effective pressure [482]. Further experiments have also assessed the U46619-induced vasoconstriction responses in the presence and absence of A740003 in isolated second and fourth order CPA's originating from healthy patients. The thromboxane A_2 mimetic-induced concentration response curves elicited by second order CPA's in the presence of

A740003 were notably rightward shifted, with a third U46619 stimulation in the absence of the P2X7 antagonist also resulting in a concentration response curve that was even further rightward displaced. These results show that A740003, DMSO or both compounds may cause a gradual loss in the potency of U46619-induced vasoconstriction effects potentially through a mechanism involving an inhibition of cytosolic phospholipase A_2 which in turn may supress the synthesis of arachidonic acid and ultimately lead to an inhibition of thromboxane A_2 synthase [366]. Additionally, in the case of fourth order CPA's, the U46619-induced vasoconstriction effects in the presence of A740003 gave rise to a leftward shifted concentration response curve. Here, a third thromboxane A_2 mimetic stimulation in the absence of the P2X7 receptor antagonist gave rise to a concentration response curve that was notably rightward shifted, suggesting a marked loss in the potency of U46619. These results potentially indicate a differential direct regulation of the fetoplacental blood flow between the second and fourth order chorionic plate arteries isolated from placental samples of healthy patients. A limitation of the results highlighting the vasoconstriction effect of U46619 elicited by the second and fourth order CPA's originating from healthy patients in the presence and absence of the P2X7 receptor antagonist A740003 is the lack of the reproducibility since the sample population included in the study was N=4 patients which further limits the interpretation of the acquired wire myography data. A study by Broegger *et al* (2016) has highlighted that the sensitivity of U46619 varies with inner diameter in human placental stem villous arteries [600]. This study showed a selective reduction in the sensitivity to thromboxane A_2 receptor stimulation with a decrease of the internal vascular diameter of stem villous arteries [600]. Furthermore, an investigation by Wareing and colleagues (2003) has highlighted that U46619 causes

vasoconstriction of isolated human placental chorionic plate veins of healthy patients [601].

However, since no DMSO vehicle control was carried out alongside experiments assessing the influence of the P2X7 receptor antagonist A740003 in U46619-induced vasoactive effects of isolated chorionic plate arteries, the desensitization effect following a second ATP stimulation does not imply an effect of A740003.

Adenosine 5'-triphosphate gave rise to spontaneous concentration-dependent vasoconstriction responses particularly in the absence of A740003 in both second and fourth order chorionic plate arteries originating from healthy patients. In the case of second order CPA's, the second ATP stimulation in the presence of A740003 initiated vasoconstriction responses below 50% of the initial nucleotide stimulation (undertaken in the absence of the P2X7 receptor antagonist). Similar vasoactive responses have also been documented from isolated fourth order CPA's characterised by a maximal vasoconstriction effect following the incubation with A740003 of less than 10% of the U46619 standard. Since a pronounced desensitization to ATP was seen when the nucleotide was added cumulatively characterised by transient and non-reproducible vasoactive responses, these results suggest that either A740003, DMSO or both compounds may contribute to the decrease in ATP-induced vasoactive responses as no DMSO vehicle control was undertaken alongside experiments assessing the vasomotor property of ATP in isolated resistance CPA's. Also, since the data highlighting the vasoactive effects of ATP before and after the incubation with A740003 initiated by second and fourth order CPA's was presented in the form of mean±SEM with the error bars possessing a high variation, undertaking sample size calculations may be advantageous in establishing that the study has the correct power to reject the null hypothesis [602]. A study by Read *et al* (1993) has highlighted that

human placental lobule perfusion with adenosine 5'-triphosphate and adenosine gave rise to a concentration-dependent decrease in the perfusion pressure when perfused into isolated placental lobules [475]. These observations started gradually with the vasodilator effects elicited after 20-30 minutes following the beginning of the perfusion with the nucleotides, with adenosine showing a notably less potent effect in decreasing the perfusion pressure compared to adenosine 5'-triphosphate which was noticed in all of the investigated placental specimens [475]. However, adenosine 5'-triphosphate gave rise to opposing responses [475]. The nucleotide primarily elicited concentration-dependent decreases in the perfusion pressure whereas in a few instances, ATP elicited concentration-dependent transient elevation in the pressure [475]. These results were found in further experiments which were characterised by an initial elevation followed by a drop in pressure [475]. The current study showed a similar vasoactive effect of ATP where the nucleotide initially gave rise to a vasoconstriction effect followed by vasodilatation in human placental chorionic plate arteries originating from healthy patients. A study by McCarthy *et al* (1994) has also highlighted that U46619 and endothelin-1 were potent vasoconstrictor compounds in these placental arteries, with the thromboxane A_2 mimetic giving rise to a contraction of 236.7% relative to the 125mM potassium-substituted physiologic salt solution standard [585]. The same study has also highlighted that angiotensin II, $PGF_{2\alpha}$ and PGE_2 also gave rise to a notable tension development [585]. In this case, the vasoconstriction effect elicited by chorionic plate arteries under the exogenous application of angiotensin II resulted in tachyphylaxis, a phenomenon where the tension reached a plateau phase and then returned to the baseline in spite of rising concentrations of the compound [585]. The same study has also showed that acetylcholine and bradykinin did not elicit notable vasorelaxation effects in chorionic plate arteries which have initially preconstricted with

U46619. However, in this case, histamine gave rise to a dose dependent relaxation of CPA's of circa 54.33% of the U46619 standard [585].

Further wire myography experiments have investigated the vasoactive properties of adenosine 5'-triphosphate in second order CPA's originating from healthy patients by constructing three cumulative concentration response curves and incubating the placental vessel preparations with A740003 either before the second (n=5 CPA's) or third (n=5 CPA's) ATP stimulation. After the exposure of CPA's with the P2X7 receptor antagonist, ATP-induced vasoactive responses corresponding to subsequent second and third nucleotide concentration response curves were particularly attenuated and displaced downwards. A comparable ATP-induced vasoactive effect was elicited following the second nucleotide stimulation of placental arteries in the absence of A740003 characterised by a notably decreased efficacy of the compound. Moreover, the third ATP stimulation in the presence of the P2X7 receptor antagonist elicited a similar concentration response curve that was notably displaced downwards. These results support the possibility of a desensitization effect taking place in the second order chorionic plate arteries following the acute exposure to cumulative concentrations of ATP starting with 10^{-5}M to 10^{-3}M, as the second nucleotide stimulation in the absence of A740003 elicited a distinct drop in the efficacy of the compound. A study by Valdecantos *et al* (2003) has also showed that adenosine 5'-triphosphate vasoconstricts chorionic arteries in a concentration-dependent manner and that the maximal contractions were close to 100% of the KCl standard with the exception of BzATP where the efficacy were approximately 50% [479]. The same study has also shown that following endothelium removal, ATP concentration curves were significantly attenuated [479]. An evaluation of the contractile response to adenosine 5'-triphosphate is difficult due to the transience of the vasoactive effect and the

desensitization response potentially of P2X receptors obtained from chorionic plate arteries of healthy patients. Furthermore, the possible coexistence of purinoceptors regulating vasorelaxation (P2Y and P1) and vasocontraction (P2X) responses to activation with adenosine 5'-triphosphate and different nucleotides support this difficulty. Although a decrease by approximately 40% was obtained from second order CPA's stimulated with A740003+ATP, since no vehicle control (DMSO) was carried out alongside experiments assessing the vasoactive effects of ATP in the presence of the P2X7 receptor antagonist, the desensitization effect could be due to either A740003, DMSO or to the transience of the response to ATP, therefore, the interpretation of the results in this case is particularly limited.

Similar results were obtained in the case of isolated resistance human chorionic plate arteries originating from healthy patients where the second ATP stimulation in the absence of A740003 gave rise to a significantly attenuated, flat concentration response curve suggesting a markedly low efficacy of the nucleotide. Furthermore, the third ATP stimulation in the presence of the P2X7 antagonist also elicited a flat concentration response curve that was even further displaced downwards characterised by nucleotide vasoactive effects taking place below the baseline corresponding to the U46619 standard. However, in the case of resistance CPA's which have been incubated with A740003 before the second ATP stimulation, the nucleotide gave rise to a concentration response curve that was also displaced downwards and almost flat. In this case, the nucleotide elicited a slightly higher efficacy compared to the second ATP stimulation in the absence of A740003, with a maximal spontaneous vasoconstriction response of more than 20% of the U46619 standard at a concentration of $3.3*10^{-3}$M. The third ATP stimulation in the absence of A740003 initiated substantially reduced spontaneous contractions of the isolated

placental arteries with a concentration response curve that was noticeably shifted downwards characterised by a low ATP efficacy. These results suggest that exogenous nucleotides such as ATP elicit potent but non-reproducible and transient contractions of the human placental chorionic plate arteries which is in agreement with previously published studies of perfused cotyledons from the human placenta [475,523]. A possible explanation to this phenomenon as suggested from a similar study published by Dobronyi *et al* (1997) [523] is that these chorionic plate arteries were exposed to adenosine 5'-triphosphate during delivery giving rise to desensitization.

The finding that adenosine 5'-triphosphate gave rise to a gradual run-down of transient responses from CPA's with increasing nucleotide cumulative concentrations in the presence and absence of A740003 may suggest that the nucleotide could become rapidly metabolised by ectonucleotidases from the isolated CPA's to adenosine which has been shown to contract CPA preparations close to 40% of 70mM KCl standard [473]. Considering the recognised variations in their current desensitization kinetics, recombinant P2X receptors are typically classified into 2 principal categories namely rapidly desensitizing (P2X1 and P2X3) and slowly desensitizing (P2X2, P2X4, P2X5, P2X6 and P2X7) purinoceptors [130]. Studies investigating the chimera subunits consisting of P2X1 and P2X2 or P2X3 subunits proposed that the fast desensitization necessitates interplay across 2 membrane spanning regions of receptor subunits [603]. Also, the long C-terminus of the P2X7 receptor has been proposed to account for the nondesensitizing characteristic of these ion channels during sequential activation [290]. Since ATP is a nucleotide which acts at all P2X receptors, this desensitization effect which took place after multiple exposures to ATP shown in the current study could be due to a direct or indirect attenuation in Ca^{2+} influx as it has been suggested in a study by Koshimizu *et al* (1999) where during

continuous exposure to agonist, current signals generated by recombinant P2X receptors are desensitised gradually [604]. Furthermore, these results which highlight the unusual nature of the properties of adenosine 5'-triphosphate in non-innervated CPA's could be due to the dephosphorylation of ATP to adenosine which may stimulate P1 receptors to cause vasodilation following the transient contractile response to the nucleotide where a constant concentration of ATP had been maintained.

The decrease in the vasoconstriction responses elicited by U46619 or ATP particularly in the absence of A740003 could be due to a desensitization effect taking place particularly in the case of ATP where it was not possible to elicit another concentration-response curve to the nucleotide for more than approximately 90 minutes following its initial challenge of CPA's as highlighted in chapter 4.3.8. This observation may imply that the chosen experimental protocol with regards to the cumulative concentration response curves was inappropriate to study the vasoactive effects of the thromboxane A_2-mimetic or the nucleotide in isolated resistance, second or fourth order CPA's originating from healthy patients.

Resistance chorionic plate arteries challenged with three consecutive additions of ATP gave rise to progressively reduced vasoconstriction effects in the case of both first and second nucleotide stimulations which have resulted in some cases to a total desensitization effect taking place. These results further complement a study published by Valdecantos and colleagues (2003) where the authors challenged superficial chorionic plate arteries with three consecutive applications of 91μM ATP which have resulted in a gradual decreased vasomotor response that attained 15% of its initial effect [479].

The progressive reductions in maximal vasoconstriction responses elicited by resistance CPA's were further investigated by elevating the resting basal tone of the blood vessel preparations using 30mM or 40mM KPSS followed by challenging the CPA's with ATP. The results have shown that a 30mM KPSS-induced preconstriction of CPA's increased the efficacy of the first ATP stimulation by more than 38% at a concentration of 10^{-3}M, which may suggest that a high extracellular potassium concentration could influence the ATP-induced vasoactive properties in placental blood vessel preparations originating from healthy patients. A limitation of these studies is the reproducibility of ATP induced vasoactive effects from CPA's, since a notable reduction in the ATP induced maximal vasoconstriction effect between the first and second nucleotide stimulation in the absence of 30mM KPSS ultimately resulting in a total desensitization took place (chapter 4.3.9) compared to the wire myography data highlighting the first and second ATP stimulation in the absence of 40mM KPSS where the concentration response curve of the nucleotide was almost flat and characterised by maximal vasoconstriction effects that plateaued at approximately 55% of the U46619 standard (chapter 4.3.11). Prior to the elevation of the resting basal tone with 30mM or 40mM KPSS, since the experimental conditions were the same as all CPA's were challenged with identical cumulative concentrations of ATP (10^{-3}M, $3.3*10^{-3}$M, 10^{-2}M; shown in the data as first and second ATP stimulation) and the vasomotor response from the placental arteries was notably different as shown in chapter 4.3.9 and 4.3.11, this study shows a decreased reproducibility in the vasomotor effect elicited by ATP in CPA's of healthy patients. A study by Abad *et al* (2003) has highlighted that the maximal response elicited by KCl in isolated human placental chorionic plate arteries was similar in blood vessels originating from vaginal deliveries (21.6±2 mN) and caesarean sections (19.6±2,9 mN) [605]. In spite of this, the

KCl EC_{50} value was decreased in chorionic plate arteries originating from vaginal deliveries (13.9±1.6mM) compared to blood vessels sourced from caesarean sections (23±1.8mM) [605]. The same study has also investigated the effect of gestational age on human chorionic vascular reactivity and highlighted that the maximal response to KCl was decreased in preterm chorionic plate arteries (9.8±1mN) compared to term arteries (21.6±2mN), with the KCl EC_{50} value in preterm blood vessels of 26±1.3mM and in term CPA's of 13.9±1.6mM [605]. However, the placental samples collected in the study performed by Abad and colleagues (2003) originated from caesarean deliveries undertaken under general anaesthesia and participants that delivered vaginally only used opioid analgesia [605].

A small proportion of isolated chorionic plate arteries have exhibited a phenomenon of vasomotion after the U46619 challenge characterised by a continuous cycle of vasoconstriction followed by vasorelaxation. This type of vasomotion has been characterised in an investigation published by Wareing and colleagues (2002), where approximately 56% of the chorionic plate vessels studied exhibited cyclical variations in the amount of tone under the initial exposure to arginine vasopressin at a concentration of 10^{-8}M [576].

A limitation of the current study is that reproducibility controls for instance DMSO solvent control was carried out only in the wire myography experiment assessing the vasoactive properties of riluzole, since the compound was prepared using dimethyl sulfoxide as vehicle control. However, no DMSO control experimental condition was undertaken alongside experiments assessing the function of A740003 in isolated chorionic plate artery preparations, hence the interpretation of the results involving the P2X7 receptor antagonist is notably limited.

In order to avoid desensitization to ATP, the chorionic plate arteries were preconstricted in a few experiments using 30mM, 40mM, 50mM or 70mM KPSS which gives a tone of approximately 20-25% of the maximal contraction. When a stable contraction was obtained (after circa 5-10minutes), a concentration response curve to ATP was undertaken. The precise mechanism by which KCl increases ATP contractions of human placental chorionic plate arteries has not been fully understood yet. Calcium sensitivity is mainly coordinated by myosin light chain (MLC) phosphorylation via changes in the action of MLC phosphatase [606] but could also be coordinated via changes in MLC kinase activity which implicates thin filament regulation and potentially a direct modulation via heat shock proteins of contractile proteins. The process involving KCl-induced contraction is caused by membrane depolarisation giving rise to Ca^{2+} entry via voltage-operated Ca^{2+} channels (VOCC) [607], stimulation of Ca^{2+}-dependent MLC kinase and elevation in MLC phosphorylation [608]. KCl is frequently utilised as a method to bypass G-protein coupled receptor activation and to stimulate smooth muscle by altering the K^+ equilibrium potential and maintaining the membrane potential above the resting status [609]. Continuous membrane depolarisation may preserve the intracellular calcium concentration and force above a basal stage through prolonged stimulation of Ca^{2+} entry via sensitive VOCC [610]. Since extracellular ATP has been shown to stimulate arachidonic acid (AA) release from aortic smooth muscle cells [611] (which causes a strong Ca^{2+} sensitisation in Ca^{2+} clamped smooth muscle [612]) and AA elevates RhoA kinase (ROK) activity by 5- to 6-times independently of RhoA [613] which regulates stress fiber and focal adhesion formation [614], the precontraction of placental CPA with KPSS may serve to augment ATP-induced vasoconstriction effects without involving GPCR

stimulation which has been shown to generate arachidonic acid as a cellular messenger [615].

Since BzATP is a relatively selective, though weakly potent compound acting at the P2X7 receptor with a reported EC_{50} value of 5μM at this purinergic receptor [146], the current study provides evidence that its exogenous application on isolated CPA's originating from healthy patients elicits a weak vasoconstriction response characterised by a particularly low efficacy of less than 25% of the U46619 standard. However, an elevation in the resting basal tone with 30mM KPSS followed by a BzATP cumulative concentration curve initiated a spontaneous vasoconstriction response from the isolated placental arteries that was less than 6% of the U46619 standard suggesting an overall decrease in the efficacy of the compound. An explanation of the lack of robust and reproducible responses to BzATP of isolated human placental chorionic plate arteries is the lack of involvement of the P2X7 receptor in the contractility of these blood vessels.

A study by Buvinic *et al* (2006) has highlighted that the $P2Y_1$ and $P2Y_2$ receptors are present along the human placental vasculature and showed an increased expression of 6- to 8-fold from the umbilical cord to the superficial chorionic blood vessels as well as the vasculature at the level of the internal placental cotyledons [481]. The authors have shown that the $P2Y_1$ receptor and $P2Y_2$ receptor are differentially distributed along the placental tree characterised by a change in distribution from the smooth muscle to the endothelium at the level of the cotyledon [481]. Also, the investigation by Buvinic and colleagues (2006) has highlighted that removal of the endothelial cell layer did not alter the expression of the $P2Y_1$ and $P2Y_2$ purinoceptors at the level of the umbilical vein or superficial chorionic plate vein or artery [481]. In this case, the authors have also presented data which showed a functional P2Y receptor-

mediated vascular reactivity via the $P2Y_1$ and $P2Y_2$ receptors through the stimulation of the chorionic plate arteries with 2-MeSADP (possessing a high selectivity for $P2Y_1$ receptor) and UTP (preferential affinity for the $P2Y_2$ receptor). The authors have shown that both compounds vasoconstricted chorionic plate artery preparations with 2-MeSADP being slightly less potent than UTP, with both nucleotides giving rise to a similar force of contraction [481]. A similar study by Wang *et al* (2015) has highlighted that ATP can also interact with $P2Y_2$ receptors on endothelial cells that is coupled with G_q and G_{11} proteins which further stimulates PECAM-1, VEGFR-2 triad and VE-Cadherin giving rise to AKT/Protein kinase B phosphorylation and nitric oxide liberation into the extracellular space [616].

A limitation of the current study is that the vasoactive responses of isolated chorionic plate arteries under the exogenic application of A740003, ATP and BzATP have not been investigated in blood vessel preparations with the endothelium removed to confirm the involvement of the smooth muscle towards the regulation of the placental blood flow.

As a result, ATP may act on both P2X and P2Y receptors by playing a crucial role in the regulation of the feto-placental blood flow, particularly at the level of the human placental superficial chorionic plate arteries where the nucleotide has been shown to possess a dual vasomotor action [481].

CHAPTER 5

ESTABLISHMENT OF AN *IN VITRO* MODEL OF HUMAN PLACENTAL CHORIONIC VESSEL

5.1 Introduction

The process of vascular paracellular permeability is tightly coordinated. The vasoactive regulators such as vascular endothelial growth factor (VEGF), thrombin or histamine have an intrinsic property to initiate and produce a short-term non-pathological elevation of vascular permeability, including phosphorylation and relocation of junctional adhesion molecules [617,618]. Disorders such as gestational or type 1 diabetes or diabetic retinopathy have been linked to an extended to a disproportionate vascular permeability that may happen as a result of an increase in junctional disruption and endothelial cell-cell overlap or a shift of the balance between pro- and anti-inflammatory markers [619]. A good instance is the early development of diabetic retinopathy in which the barrier separating blood and retina is harmed resulting in a persistent permeability. Following this initiation of events, elevated inflammation causes the disorder to progress to a more serious stage named proliferative diabetic retinopathy characterised by atypical angiogenesis, giving rise to the establishment of exceedingly permeable vasculature [620]. The link between highly-permeable vasculature and abnormal angiogenesis is usually found in other pathologies for instance solid cancers which typically comprise of cancer cells, lymphatic vessels, immune cells, blood and stromal cells, all connected together via a matrix [621–623]. In the placenta, abnormal angiogenesis is a feature of type 1 diabetes as it has been shown by Leach and colleagues (2009) [624]. Moreover, hypoxia has been suggested to play a key role in stimulating the synthesis of angiogenic markers for instance VEGF, which in turn promotes angiogenesis of structurally abnormal microvessels from both macroscopic and microscopic perspectives [625]. Other frequent instances of disorders characterised by abnormal vasculature include inflammatory conditions accompanied by atherosclerosis, but also more infrequent

disorders for instance age-related macular degeneration and benign tumors [625–627].. The disruption at the level of the fetal endothelial layer in the placenta gives rise to diminished junctional restrictiveness accompanied by a modified cleft size [628], elevated nutrient crossing time and an altered vascular permeability [119,126]. These disturbances ultimately affect the physiological solute transfer between the mother and fetus and result in a defective placental barrier role [484]. A perfusion study published by Leach and colleagues (2004) has highlighted that perfused term placental originating from type 1 diabetic patients possessed an elevated vascular leakage corresponding to more than 50% of blood vessels of the microvascular bed [97]. Furthermore, the same study suggested that the elevated leakage was strongly associated with phosphorylation of CD144, alterations of junctional proteins and increased VEGF protein expression. Similarly, other studies have shown that placental samples originating from gestational diabetic patients also possess a deficiency of junctional proteins [95,629].

The human placenta supports and protects the growing fetus whilst regulating the maternal physiology for the foetal benefit. This organ considered to be of fetal origin has an important barrier function and allows a particular nutrient exchange as well as oxygen uptake from the mother to the fetus [119]. An important placental structure contributing directly to its function is a multi-layered membranous arrangement comprising of the fetal capillary endothelium and the syncytiotrophoblast which are partitioned by a fine interstitium [630]. This functional barrier that delimitates the fetal circulation and the maternal intervillous zone is in charge with controlling the selectivity and rate of the placental transport. Abnormal alteration of this placental architecture and physiology is directly involved in many disorders associated with pregnancy for example intrauterine growth restriction, pre-eclampsia and diabetes.

Vascular permeability is defined as a pathophysiological process involving the flow of crucial fluids, solutes, cells and also proteins over an intact cell barrier under the influence of diverse stimuli. This process is responsible for the commencement and evolution of various disorders with a range of clinical manifestations [631]. Beside many stimuli that have been shown to influence permeability in particular cells for instance platelet activating factor, hypoxia and growth factors, vascular endothelial growth factor (VEGF) has been demonstrated to have a dominant property to initiate permeability in the perfused microvascular bed [119] as well as in a well-established endothelial cell monolayer [632,633]. In this case, *in vitro* models as a complimentary tool allow long term investigation of vascular permeability via enabling the control of a wide range of experimental variables and offering the possibility of quantitative analysis.

In order to understand permeability, initial studies have focused on quantifying the electrical impedance of cell barriers accompanied by the movement of radio-labelled compounds. A study performed by Hart and colleagues (1987) has showed the first application of transendothelial resistance (TER) measurements across the monolayer of brain endothelial cells for the purposes of studying cellular permeability [634]. Another study undertaken by Bowman and colleagues (1983) has presented the first measurement of ^{14}C-labelled sucrose trans-migration through an endothelial brain monolayer [635].

As vascular permeability is a key attribute of the blood vessels, different methodologies to investigate it have emerged over the last decade [169,636,637]. The earliest approaches to investigate and quantify vascular permeability have been based on *in vivo* assays for instance the miles assay [638] or using isolated blood vessels originating from various animals known as *ex vivo* assays [639]. As these models were particularly demanding to manipulate, it gave rise to the advancement of a new *in vitro*

model widely accepted as the transwell assay which is used to evaluate the permeability of an endothelial cell monolayer [640]. Novel studies focused on placental transport are primarily based on *in vitro* models using a transwell cell culture insert system which does not take into account the three-dimensional architecture of a blood vessel [641]. In spite of this, the transwell model has been broadly used for the purposes of establishing a monolayer of trophoblast cells for investigating their capability to transport various substances from the apical chamber to the basal chamber [127]. Following these advancements, existing transwell experiments do not take into account the stratification of the placental barrier in terms of syncitiotrophoblast, cytotrophoblast, basement membrane and fetal vessels by omitting the endothelial cell contribution to the barrier formation [642]. Moreover, a stagnant culture environment in these experiments does not take into consideration the constantly moving extracellular milieu of the human placenta *in vivo* which previously demonstrated to have an impact on cellular phenotypes in the case of placental barrier [643].

Even if these approaches based on electrical resistance may give rise to data describing an alteration in endothelial cell shape as well as barrier integrity, they offer a limited assessment of investigating the capability of certain proteins to cross the tight barrier formed by the endothelial cells and do not quantify permeability *per se*.

More recently, a significant development in terms of tissue engineering has been performed in order to create a more robust and complex *in vitro* blood vessel configuration. The current models of the vasculature have attempted to take into account the three-dimensional architecture of various microvessels and to facilitate the regulation of the cellular milieu [644]. Many blood vessel prototypes have been created by various groups with the help of human umbilical vein endothelial cells

(HUVECs) [645,646] or human dermal microvascular endothelial cells (HDMECs) [647,648]. The barrier permeability related to these vascular profiles has been tested to investigate the efficacy of monolayer tightness and to characterise the effect of stimulating permeability using inflammatory substances for example thrombin and histamine particularly in models of HDMEC [647]. Nonetheless, from the perspective of drug development, there are few studies which have developed assays for the purposes of assessing compounds which are able to support the physiological function of the barrier to correct the abnormalities of blood vessels by bringing them to a more physiological state thereby decreasing the evolution of various disorders.

Animals, in particular rodents may help to generate new data related to placental translocation of compounds or nanoparticles in a living organism or even to enhance the current knowledge about possible unfavourable consequences on their successors. In spite of this, the translation from animal to human subjects is particularly challenging because the placenta is widely considered as a species-specific organ [649,650]. As a result, indicative *ex vivo* and *in vitro* placenta architectures based on human tissue or cells are especially fundamental for preventing species-specific discrepancies. Alongside novel accessible translocation studies, *ex vivo* perfusion of term placental originating from human participants is widely regarded as the “gold standard” [651]. Complimentary *in vitro* experimental procedures that are widely used for instance cytotrophoblast cells which have been seeded on a permeable insert are more accessible to manipulate by taking into account trilayers for instance, “placenta on a chip”. These next generation *in vitro* models are potentially more suitable for an elevated throughput and are particularly relevant for investigating the mechanism of action of various compounds [652]. In spite of this, the above-

mentioned experimental design does not entirely simulate the physiological microenvironment of the placental barrier.

5.1.1 Molecular regulation of endothelial permeability

The endothelial paracellular permeability and monolayer integrity are tightly coordinated by junction adhesion mediators (JAM). These molecules are fundamental components of paracellular junctions encouraging similar cell types to communicate and elicit a complex connection arrangement in between adjacent cells [653]. Furthermore, the variation in expression of JAM differs depending on the characteristics and development of endothelial junctions. Also, tight junctions have inter-membrane adhesion mediators, claudins and occludin [654] while vascular endothelial cadherin is considered as an inter-membrane adhesion mediator belonging to endothelial adherens junctions [655]. These mediators may allow calcium-dependent typical cell-cell adhesions using their extracellular domains and their corresponding intracellular region enables interactions with other similar nearby junctions, as well as binding to peri-junctional proteins belonging to the cytoskeleton of the cell. Other important connecting mediators in charge with interactions related to adherens junctions are plakoglobin and β-catenin which are part of fully mature junctions [656]. Catenins are essential signalling factors especially non-junctional β-catenin which is involved in cell division [657]. Moreover, the intracellular domains of various adhesion factors have serine and tyrosine amino acid portions that cause them to be susceptible to phosphorylation events and cytoplasmic signalling pathways for instance tyrosine kinase interactions. The current configuration of adhesion factors enables stabilization corresponding to certain cell membrane parts supporting the control of endothelial cell polarity and morphology during closure and opening of various cell junctions [653,658].

Even if claudins support the arrangement of tight junctional filaments, on the other side, occludin is specifically involved in the adjustment of leakiness via assimilation with claudin-occupying threads. This mechanism acts as a crucial boundary in terms of the function of the permeability barrier in both endothelial and epithelial cells belonging to the blood-retinal and blood-brain barriers [659]. Following the discovery of the first tight junction linked to deposition proteins namely zonula occludens-1, more than thirty other factors have been characterised to be closely corelated to the cytosolic component of tight junctions. These may be classed in two groups peripherally correlated scaffolding proteins (for instance afadin, cingulin, ZO-1, ZO-2 and ZO-3) that anchor the membrane-spanning proteins and connect them to more cytosolic proteins and other signalling proteins for example Ras homolog gene family member A (RhoA), Ras effector 1 (Raf-1) and ZO-1 associated nucleic acid binding protein (ZONAB) which play a crucial role in the barrier construction and maintenance as well as gene transcription [660].

Since membrane spanning junctional mediators are closely associated with plasmalemma receptors involved in the regulation of growth factors responsible for pro-permeability and pro-angiogenesis for instance vascular endothelial growth factor, this proximity enables the junctional molecules to function as receptors for extracellular signalling. Moreover, VEGF was suggested to promote the phosphorylation of β-catenin, VE-cadherin, p120 and plakoglobin, giving rise to a raised endothelial cell infiltration and elevated the paracellular permeability as a result of loosening of cell-cell contacts [658,661]. A study by Groten *et al* (2010) has shown that VE-cadherin is expressed in the syncytiotrophoblast originating from human placental samples of healthy patients using immunohistochemistry [662]. Furthermore, the expression of VE-cadherin in cytotrophoblast cells has been investigated before [663].

Hydrophilic solutes of a similar molecular weight size to circulating proteins for instance alphafetoprotein (circa 60kDa) could translocate at the level of the human placenta via paracellular routes [664–666]. This paracellular diffusion is particularly important since it provides a crucial contribution to the unidirectional translocation of compounds from one side to the other of the human placenta [667,668]. Furthermore, the exchange barrier particularly in the third trimester of the gestation period has two cell layers namely the syncytiotrophoblast and the fetal capillary endothelium which is non-interrupted and at places delimitated by lateral intercellular junctions via which hydrophilic mediators could pass though even though for proteins with a molecular size similar to alphafetoprotein, the diffusion process may be reduced [123]. However, the syncytiotrophoblast is a true syncytium characterised by the absence of pronounced lateral intercellular junctions. As a result, this observation gave rise to controversy related to the physiological role of the paracellular routes at the level of the syncytiotrophoblast layer. In spite of this, multiple studies have showed that one such route may become established in regions of syncytial denudation which are characterised by a fibrin-type fibrinoid deposition [666,669]. Also, more than 70% of the unidirectional transport for instance of Ca^{2+} or Cl^{-} from the maternal to the fetal side of the placenta assessed using perfused human placental cotyledon takes place via paracellular diffusion [667,668]. Furthermore, VEGF has the ability to phosphorylate tight junctional molecules ZO-1 and occludin in a straightforward way with the help of protein kinase C [93]. Taking into consideration the human placenta, the regularity, location or proportion of tight junctions is relatively the same in most of the vasculature. On the other hand, junctional occupancy research has shown a variable expression of occludin corresponding to a favouring position in tight junctions belonging only to considerable conduit blood vessels [126]. Furthermore, the adherens junctions

belonging to the blood vessels where the placental exchange of nutrients and oxygen takes place i.e. the fetal capillaries contain an underdeveloped morphology with plakoglobin being replaced by β-catenin which interacts with the membrane spanning adhesion factor VE-cadherin. Also, the current fetal capillaries and the neighbouring trophoblast have elevated levels of angiogenic growth factors and their corresponding receptors that includes vascular endothelial growth factor and its equivalent receptors [125,670]. *Ex-vivo* perfusion research and *in vitro* investigations have highlighted that placental endothelial adhesion factors may be vulnerable to extrinsic inflammatory and angiogenic stimulation and also to the maternal nourishment condition [105,628,671,672].

An important role of endothelial cells is regulating the movement of flowing cells and plasma proteins from the lumen of the blood vessels towards the perivascular tissues. This activity is tightly coordinated by two cellular mechanisms namely paracellular and transcellular signalling pathways [673–676]. The paracellular process is controlled via opening of paracellular junctions or potentially through the readjustment of their organisation. On the other side, the transcellular method describes the flow of cytoplasmic factors via the cytosol of the endothelial cell facilitated via the activity of fenestrae or vesicular mechanisms. Lastly, alternative proteins located elsewhere around the endothelial cells could be partly responsible for the modulation of permeability. A good example of this regulation is PECAM-1 (platelet endothelial cell adhesion molecule 1) that may be phosphorylated by factors that elevate the permeability for example VEGF or even mechanical stimulation [661].

In the vasculature of adults, the smooth muscle cells are found in a contractile non-proliferating condition which supports the continuous interaction with endothelial cells [677,678]. The non-proliferating condition of the primary cells is supported by diffusible and connection reliant factors between the cells and their corresponding

extracellular matrix [679]. A good example of this phenomenon is angiopoietin 1 that is liberated into the extracellular space by vascular smooth muscle cells which interacts and stimulates tie2, a membrane spanning receptor tyrosine kinase primarily found on the membrane of endothelial cells. This process then stimulates akt (a cell survival kinase), ultimately promoting the support of vascular quiescence [680–682]. The endothelial cell – smooth muscle cell interplay is crucial for the duration of blood vessel synthesis. In this case, the smooth muscle cells recruited by endothelial cells [683] promote the establishment of the newly formed blood vessels via synthetising extracellular matrix. Further crucial factors that participate in the endothelial cell – smooth muscle cell interplay are transforming growth factor β [684], endothelial differentiation sphingolipid G-protein coupled receptor 1 [685] and vascular endothelial growth factor A [686]. As a result, the endothelial cell – smooth muscle cell interplay is vital for regulating the vascular tone and it's physiological function *in vivo*.

5.1.2 Investigating human feto-placental endothelial junction formation and barrier integrity using macromolecular permeability studies

The placenta originating from human subjects has been extensively studied for the purposes of describing its morphological structure from a macroscopic point of view to a cellular degree. A recent particular attention has been allocated for investigating the physiological and pathophysiological signalling pathways and aspects of placental permeability [687]. Although *in vivo* examinations taking place in human subjects have been restricted as a result of ethical controversy and limited access, the majority of current understanding of transplacental flux has been collected with the help of *in vitro* tests which have been based primarily on using placental

samples originating from third trimester of the pregnancy period. Despite the complicated and laborious methodologies used in these experiments, the knowledge acquired over the last decades highlights exclusively the overall action of the entire tissue representing the placental barrier [688]. More recently, a lot of configurations using various cell types have been established for the purposes of distinguishing certain inputs originating from the cells used to create the three-dimensional placental barrier [689]. Although many studies have investigated the uptake proportion as well as the signalling pathways involved in the establishment of the permeability especially in the syncytiotrophoblast, there is limited research data available detailing on the contribution of the feto-placental endothelium on the regulation of the placental barrier [690–692]. More recently, attention has been given to investigate the permeability characteristics of the human placenta with a particular focus on techniques for recognising membrane-embedded specific transporters particularly of glucose, fatty acids and amino-acids. Advancements in the knowledge of the class of transporters on both fetal and maternal surfaces of the syncytiotrophoblast are of an elevated importance when it comes to understanding the placental transport. Of an equal usefulness is determining the preponderance of each of the transporters on both surfaces in terms of number per cm^2, as well as the total surface of the placenta when it comes to various disorder cases. The majority of this knowledge has still not yet been identified [693].

In humans, the aspects of placental transport and the potential mechanisms involved have been particularly well investigated certainly in the case of the third trimester pregnancies. However, there are few well controlled quantitative studies undertaken in the first and early second trimester for the purposes of investigating placental barrier transport and permeability because of ethical controversy.

Although important progress has been noticed in the field of placental permeability and transport, there is still a tremendous amount of work that needs to be carried out in terms of investigating the function and anatomy of the placental barrier and moving studies to pre-clinical models. Moreover, more work needs to be undertaken in order to expand the current knowledge of the physiology influencing placental barrier in terms of syncytialization, oxygen microenvironment as well as multiple cell layers [694].

Novel *in vitro* models of placental permeability have an important aim to enhance the *in vivo* relevance by using supplementary suitable cell types in particular primary cells or fluidics for the purpose of simulating the exceptionally dynamic microenvironment of the human placenta. Huang and colleagues have managed to accomplish creating a confluent monolayer of primary human trophoblasts isolated from placental samples originating from healthy volunteers on a 0.4μm pore size transwell membrane [695]. However, the access to term placental samples could be restricted and the process of obtaining the primary trophoblast cells is expensive and time-consuming. Other studies have created new dynamic co-culture models involving micro and macro-fluidic approaches [630]. All models of co-cultures in terms of endothelial and trophoblastic cells have been seeded on various surfaces including denuded amniotic membranes, a microporous membrane or even on collagen membranes [630,692,696]. However, these models may only be of use for the purposes of transport studies of small substances because the membranes and scaffolds may create a major barrier to the free transmigration of larger molecules or nanoparticles. Overall, various improvement strategies in terms of co-cultures of primary cells accompanied by dynamic exposure are particularly promising however, more

optimisation of these models is required in order to achieve a suitable trans-location study for both small and large compounds as well as nanoparticles.

The motivation for this study was to develop a biological *in vitro* human chorionic vessel model that will mimic the *in vivo* structural architecture using primary placental chorionic plate artery smooth muscle cells (CPA-SMC) and human umbilical vein endothelial cells (HUVEC). Techniques involving co-culture of human cells have been successfully used for the purposes of creating multiple types of *in vitro* functional barriers for example pulmonary blood-gas barrier, eye and skin as well as blood-brain barrier [697–699]. In this case, establishing a reliable chorionic blood vessel model *in vitro* will contribute considerably to our knowledge of placental vascular function.

There are currently no commercially available human chorionic plate artery smooth muscle cells which could be used in order to establish a reliable chorionic vessel system *in vitro*. As a result, the development of an uncomplicated and cost-effective isolation technique for the purposes of obtaining the human chorionic plate artery smooth muscle cells, describing their phenotype and potentially using them in further *in vitro* experiments may be advantageous. These smooth muscle cells may possess an important value when it comes to investigating the signalling pathways involved in the regulation of vascular permeability, contractility as well as influencing the endothelial junction formation. With a complementary rationale, the phenotypic and functional signature of the smooth muscle cells was verified using immunocytochemistry and permeability studies.

In order to establish a reliable chorionic vessel system *in vitro*, initial validation studies had to be performed for establishing important aspects of the feto-placental barrier comprised from primary isolated CPA-SMC's and HUVEC cells. Some of these crucial aspects include the formulation of co-culture growth media, investigation of

primary cell capability to proliferate on transwell membrane inserts, optimisation of the proliferation period and seeding density of primary cells on inserts, timepoint following co-culture of primary cells at which the permeability study was undertaken and duration of permeability assays. All of these optimisation studies contributed greatly to the establishment of the *in vitro* model resembling the vascular wall of the chorionic plate arteries, which aimed to increase the current understanding of placental vascular function.

The efficacy of this optimised model was further tested by investigating the capacity of endothelial cell junction formation and barrier integrity. These aspects in terms of validation studies involved in the organisation of this *in vitro* co-culture system include the immunocytochemistry staining for smooth muscle cell specific marker α smooth muscle actin and endothelial cell inter-cellular junctional integrity marker VE-Cadherin, as well as assessing the barrier tightness which is mainly provided by HUVEC cells and regulated by CPA-SMC through the means of permeability assays.

Further validation experiments involved in the establishment of this co-culture system comprised of investigating the capability of CPA-SMC to adhere to the HUVEC monolayer and the optimisation of the immunocytochemistry protocol which involved secondary antibodies that were FITC conjugated.

Overall, a comprehensive characterisation of the cell signalling pathways taking place in the cellular constituents composing the *in vitro* placental barrier still needs to be addressed which will increase our understanding of maternal-fetal transport.

5.2 Hypothesis

The hypothesis of this study is that the co-culture of HUVEC cells with CPA-SMC cells will increase the barrier integrity compared to monoculture of HUVEC cells alone. Also, the immunophenotypic signature of the isolated CPA-SMC cells originating from placental samples of healthy and pregnancies complicated by gestational diabetes mellitus will be similar to the surface antigenic profiling characteristic of human multipotent mesenchymal stem cells.

The aims of this study were to:

- The first objective of this study was to fabricate an accurate and reproducible cell co-culture model using primary human umbilical vein endothelial cells (HUVEC) and freshly isolated chorionic plate artery smooth muscle cells (CPA-SMC).
- The second objective was to assess the efficacy of this co-culture model by evaluating its capacity of endothelial junction formation and barrier integrity.
- The third objective was to immunophenotype isolated CPA-SMC cells originating from placental samples of healthy and pregnancies complicated by gestational diabetes mellitus for cell surface markers that are typical of human multipotent mesenchymal stem cells.
- The fourth objective was to investigate the immunolocalization of α smooth muscle actin and VE-Cadherin in mono- and co-cultures of HUVEC and CPA-SMC using immunocytochemistry
- The fifth objective was to investigate the possibility of labelling the cellular membranes of HUVEC and CPA-SMC with PKH67 and PKH26

5.3 Results

The methods used in this results chapter have been described in chapter 2.14-2.16 and 2.19-2.22.

5.3.1 Human placenta chorionic plate artery smooth muscle cells can be isolated and grown to a high confluency using the tissue explant technique

In all cases of healthy, gestational diabetic mellitus or type 1 diabetic patients, the explant culture gave rise to a numerous homogenous population of smooth muscle cells. The CPA-SMC cells originating from placental samples of pregnancies complicated by gestational diabetic mellitus grew to confluence 2.8 times faster (approximately 10 days) compared to all other healthy volunteers (circa 28 days) measured between the point at which the CPA explant was seeded into the culture plate and obtaining a fully confluent flask. The smooth muscle cells showed signs of growth within the first week in the cell culture conditions as shown in chapter 5.3.1.1. At confluence the primary cells had a uniform morphology which could be described as elongated cells proliferating in parallel rows which is characteristic of smooth muscle cells. Moreover, another characteristic of these human placental cell cultures is the formation of overlapping sheets giving rise to ridges which are a typical growth sign for this cell type. The smooth muscle cell morphology also kept similar after passaging the cells multiple times. On the other side, another characteristic of these smooth muscle cells is the higher the passage the slower the proliferation rate, with cells not growing after p5. The morphology of CPA-SMC cells in coculture with HUVEC cells was characterised as spindle shape with SMC cells proliferating in multiple directions. The isolated CPA-SMC cells were positive for the myofilamentous protein

α-smooth muscle actin as shown in chapter 5.3.1.5. Also, a representative example of the spindle shaped morphology of smooth muscle cells in tissue culture conditions at confluence is presented in figure 139.

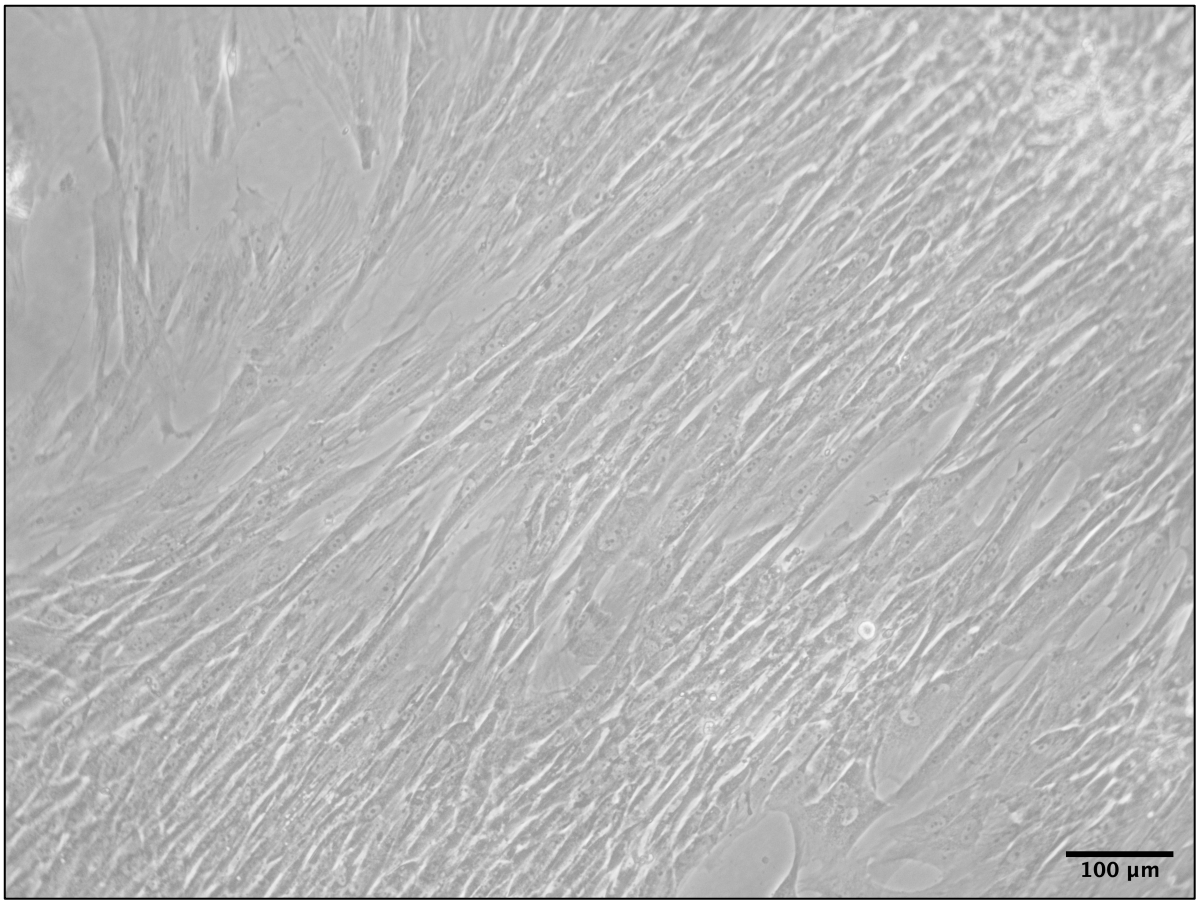


Figure 139. *This figure shows the spindle shaped morphology at confluence of the human term placenta chorionic plate artery smooth muscle cells originating from a healthy patient (N06022020, P0) resembling an elongated side-by-side rows appearance.*

5.3.1.1 Morphology and culture characteristics of chorionic plate artery smooth muscle cells

As the smooth muscle cells proliferated to reach a higher confluence, the cells gave rise to monolayers which at parts formed islets of sheets maintaining the same morphology of a hill and valley pattern. If the human smooth muscle cells were given the opportunity to further proliferate around the confluency period without passaging,

the generation of nodules was observed especially in the field of view with the highest cellular frequency. These nodules were composed of cellular waste and were enclosed by healthy smooth muscle cells.

The smooth muscle cells exhibited signs of growth within the first 7 days in culture conditions. The primary placental cells grew to confluence after 21-28 days, as gestational and type 1 diabetic cells grew faster (circa 10 days) compared to healthy cells. In all cases at the end of the exponential growth phase, the cell cultures resembled a similar morphology that may be described as spindle shaped cells positioned side-by-side often with long cytoplasmic projections connecting nearby cells as shown in figure 140. At parts, the cell culture showed the formation of stacked sheets which gave rise to the development of ridges. The cells maintained their morphology in all of the following sub-cultures after which, from passage 5 onwards, the proliferation rate decreased significantly, and the cell morphology showed a few large rounded senescent cells.

During the exponential growth phase between 7 and 21 days, there were many small high-proliferative cells located right next to the explant and other cells that were positioned further away from the explant which might be contact inhibited by long cellular processes. Other primary cells resembled a cobblestone-like shape close to the confluency period as shown in many of the representative figures in this chapter. These smooth muscle cells resemble phenotypic changes at low cell densities with a flat rectangular shape accompanied by small processes and rapidly became senescent. A large population of human placental CPA-SMC's cultures were spindle shaped, medium-sized even in areas comprising of cells with other morphology types for instance small cells with a cobblestone appearance or large cells which were often found in the primary explant culture.

Beside the typical hill and valley morphology, an important characteristic of these vascular smooth muscle cells especially after growing in culture conditions for more than 3 weeks was the presence of nodules (further characterised in chapter 5.3.1.3).

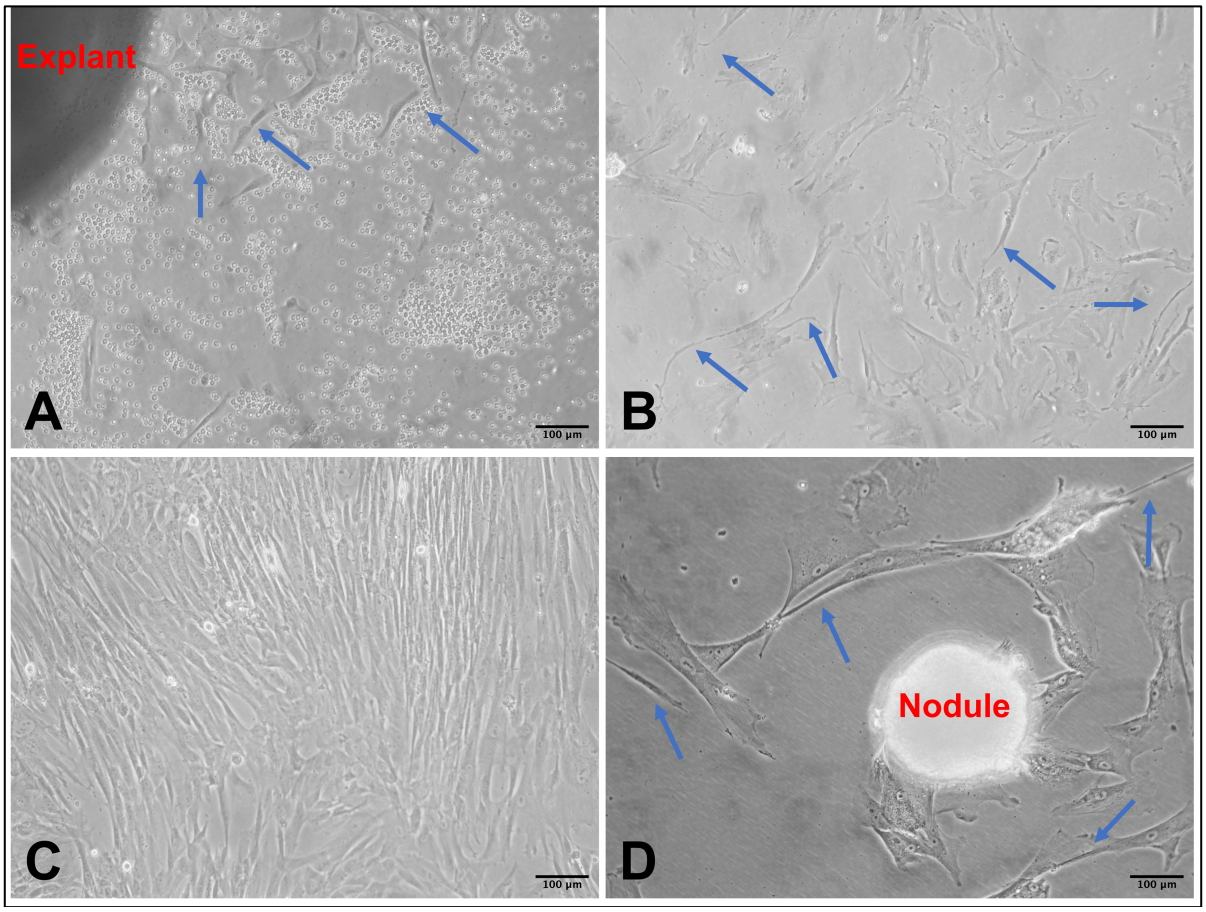


Figure 140. *This figure shows representative phase contrast images of the human placental chorionic plate artery smooth muscle cells in culture conditions originating from healthy patients.* ***A****. Cells from CPA explant can be observed after 6 days right next to the explant (N18072019) (blue arrows)* ***B.*** *Sub-confluent vascular smooth muscle cells at day 8 highlighting a typical spindle-shaped morphology which often possess long projections connecting nearby cells (N18072019) (blue arrows)* ***C****. Smooth muscle cells morphology at confluence after 19 days in culture environment resembling a parallel architecture (N06022020)* ***D****. Vascular smooth muscle cells at passage 2 after 57 days in culture conditions from the point of seeding the explants, highlighting a regular hills and valleys morphology with long projections (blue arrows) and the presence of nodules which is characteristic of smooth muscle cells after 30 days in culture (N18072019) (Scalebar 100µm).*

All human placenta chorionic plate artery smooth muscle cells originating from healthy patients resembled similar temporal changes in terms of morphology and proliferation characteristics during the isolation process.

Generally, the vascular smooth muscle cells isolated from the human placenta chorionic plate artery exhibited a ribbon shape accompanied by an oval-shaped nucleus possessing 2 or more nucleoli especially towards the full confluency and also the cytoplasm of these cells was particularly phase dense having a small number of visible inclusions.

Smooth muscle cells grew relatively slowly from the placental tissues and spread around the explant surrounding areas giving rise to uninucleate and binucleate cells. After 5 days in culture conditions, the human placenta smooth muscle cells started to reach each other and to become sub-confluent especially around the explant. On the other side, after sub-passaging the cells, SMC expanded in size and cell volume with a morphology characterised as polygonal cells.

5.3.1.2 Confluent cultures of human placenta chorionic plate artery smooth muscle cells present multiple formations of whirling arrangement foci in zones where the primary cells proliferate in singular sheets

The human placenta chorionic plate artery smooth muscle cells morphology at confluence resembled a few key characteristics such as spindle shaped cells growing in parallel which formed patches of sheets and ultimately gave rise to the generation of ridges. This in turn favoured the establishment of nodules positioned in areas where the SMC's grew in multiple sheets, typically in the adjacent peri-explant space. A further characterisation of confluent SMC proliferating in culture conditions was that

the cells never formed a tight monolayer, although at parts, especially after the majority of cells have migrated out from the explant, the parallel arrangement of smooth muscle cells gave rise to a sheet of cells tightly packed together.

After passaging the cells for the first time, the period between cell seeding and reaching a high confluence was relatively the same to the one between placing the chorionic plate artery explants on the culture plate and noticing the whirling effect of smooth muscle cells.

An important smooth muscle cell growth pattern which was mostly noticed when the cells became particularly confluent was the formation of a whirling arrangement. This effect has been noticed at multiple locations around the SMC primary cultures as shown in figure 141. The circular pattern was present only at sites where the smooth muscle cells were grouping in a singular sheet. As a point of view of timescale of SMC proliferation from explants, this whirling effect took place at the point of transition from a single sheet of cells to a nodular cell culture.

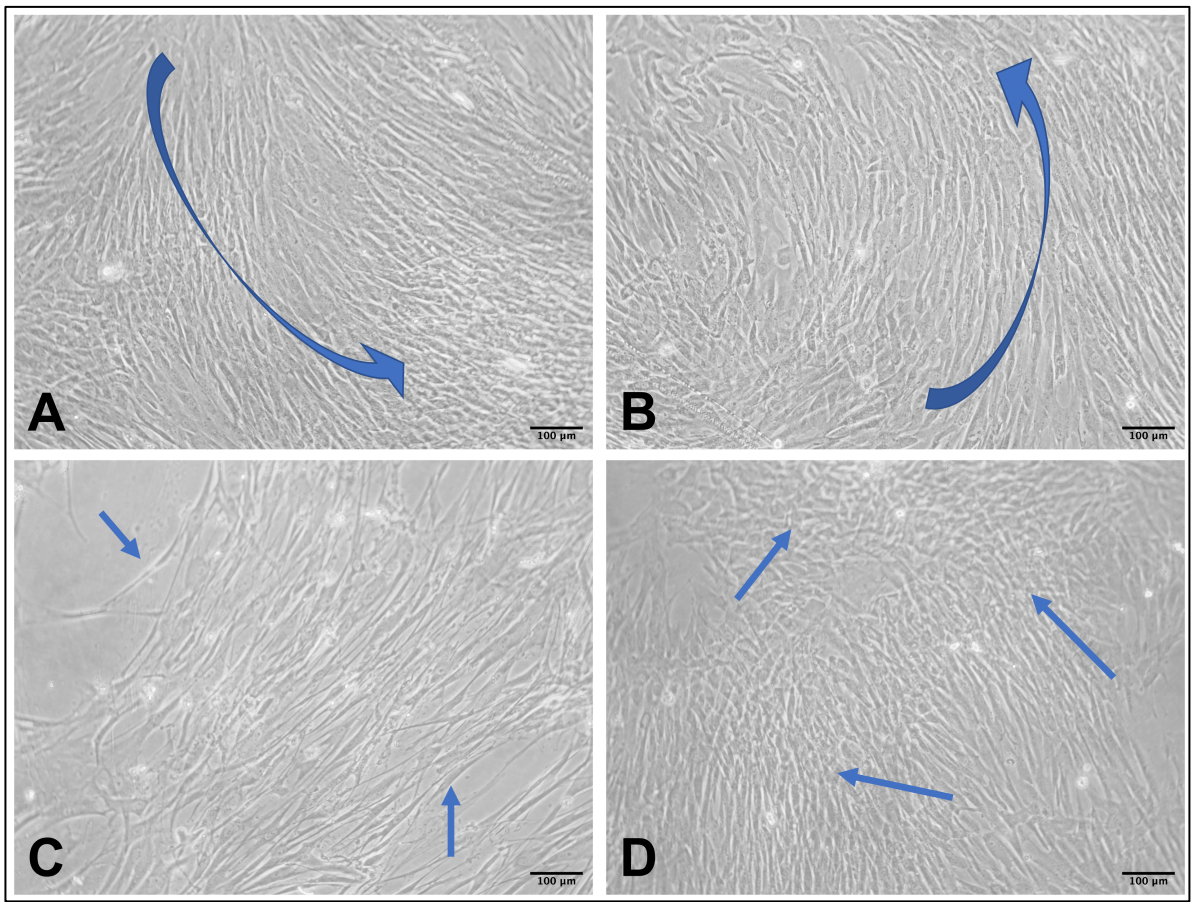


***Figure 141**. This figure describes the confluent arrangement pattern of the human chorionic plate artery smooth muscle cells originating from a healthy patient (N06022020) in different fields of view (10X) at day 19 after placing the placental explants in the culture plates. Scalebar 100µm. **A.** Representative example of a whirling effect of smooth muscle cells growth shown by the blue arrows **B.** Typical image highlighting the proliferation pattern resembling a circular appearance of the human smooth muscle cells (direction presented by curved arrow) **C.** Image showing the spindle-shaped morphology of smooth muscle cells with long projections connecting adjacent cells highlighted by arrows **D.** Appearance of confluent smooth muscle cells as stacked sheets (shown by arrows) which may further develop into ridges and ultimately into nodules.*

5.3.1.3 Human placenta chorionic plate artery smooth muscle cells gave rise to the formation of overlapping sheets of primary cells, generation of ridges and ultimately the development of nodular cultures

An important characteristic of human placenta chorionic plate artery smooth muscle cells cultures is the development of nodules after approximately 30 days in culture conditions as shown in figure 142, panels E-H. The cellular aggregation foci comprised of aggregates of cells that were circular in shape, with a diameter of approximately 250μm after 57 days in culture conditions as shown in figure 140 (panel D). This characteristic of vascular smooth muscle cells has been identified in all of the primary cell cultures. Although this property of nodule establishment is not exclusive for SMC's (as mesenchymal cells possessing osteoblastic characteristics could similarly give rise to nodules), it is a pivotal attribute that distinguishes human vascular smooth muscle cells from fibroblasts.

The nodules were not detached and stained for CD31 and a-SMA to confirm the presence of smooth muscle cells, endothelial cells or both.

The nodules were formed even in co-culture conditions using CPA-SMC's (N15072019, P3) and HUVEC cells (N21082019, P5) on sterile 12mm diameter transwell with 0.4μm pore size polyester membrane inserts as shown in figure 142, panels A-D, denoting that the formation of nodules was not affected by the presence of another cell type in the culture microenvironment. In the majority of cases, the nodules were of a similar size, with some being more phase dense than others.

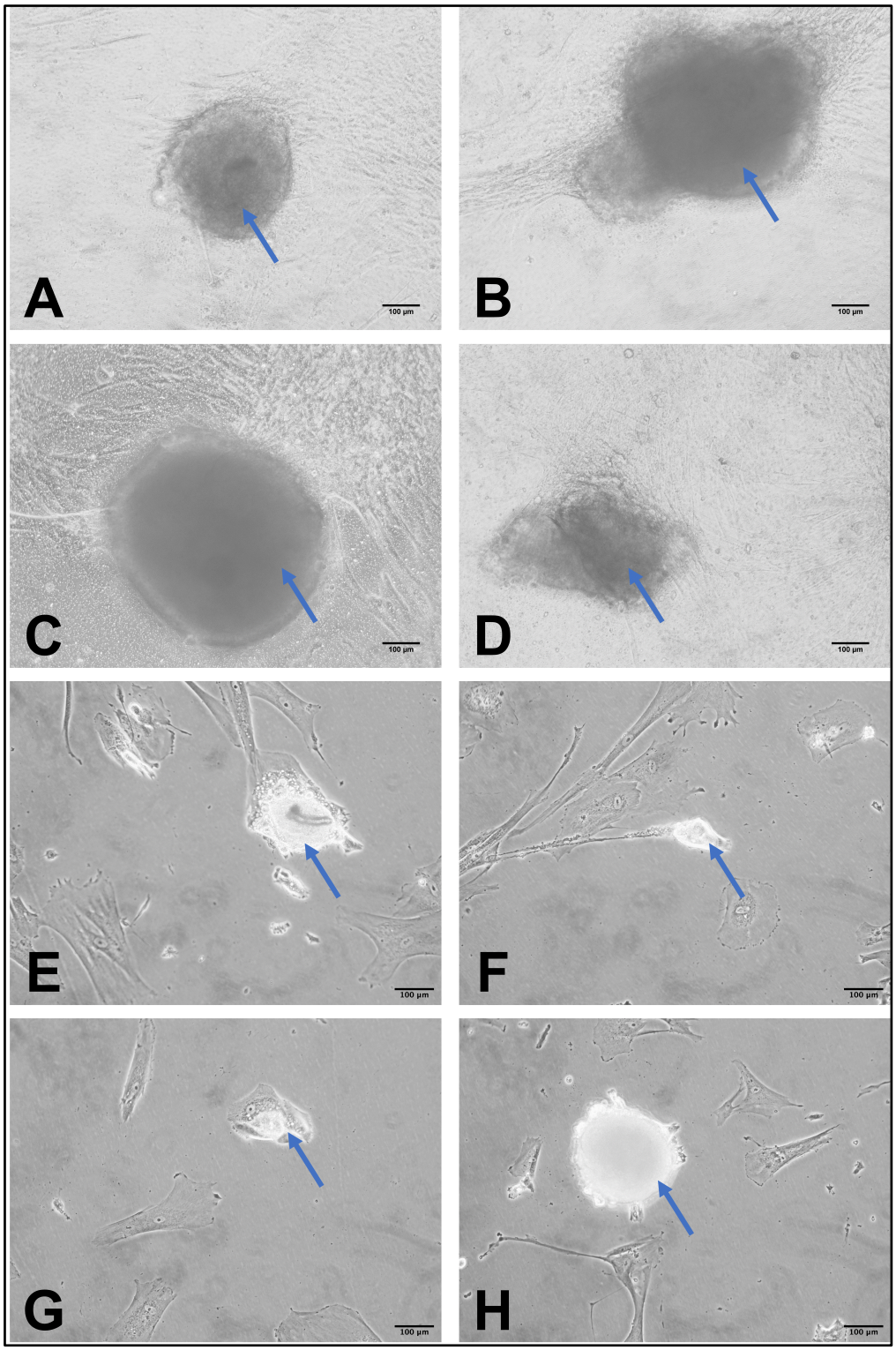


Figure 142. *This figure shows the morphology of nodule aggregates* ***(****panels* ***A-D)*** *with varying sizes growing on sterile 12mm diameter transwell with 0.4µm pore size polyester membrane inserts. Smooth muscle cells were seeded on inserts (day 0) and images were acquired at day 13.* ***A****. 1x10^4 SMC's (day 0) + 1% gelatin (day 11)* ***B****. 1x10^4 SMC's (day 0) + 1x10^4 HUVEC (day 11)* ***C****. 1x10^4 SMC's (day 0) only* ***D****. 1x10^4 SMC's (day 0) + 1% gelatin (day 11) + 1x10^4 HUVEC (day 11). Panels* ***E-H*** *highlight the early stages of nodule formation (blue arrow) in CPA-SMC cell cultures (N18072019) at P2 in T75 flask.* ***H****. Fully grown nodule. Scalebar 100µm.*

5.3.1.4 The population doubling time of primary isolated chorionic plate artery smooth muscle cells showed a decelerated proliferation rate in culture conditions

In the case of CPA-SMC's, the doubling time calculated using the data shown in table 28 expressed as mean ± standard deviation was 15.38±13.52 days (N=5 healthy patients).

Sample number	Passage number	Flask type	X_b	X_e	T	DT
N15072019	P1	T25	$5.29x10^5$	$1.16x10^6$	5	4.414
N21082019	P2	T75	$9.7x10^5$	$1.07x10^6$	5	35.32
N17092019	P1	T75	$1.26x10^6$	$3.06x10^6$	28	21.87
N18092019	P1	T75	$1.16x10^6$	$4.73x10^6$	41	12.73
N10072019	P1	T75	$1.23x10^6$	$3.6x10^6$	4	2.582

Table 28. *This table shows the human placenta chorionic plate artery smooth muscle cells doubling time (DT) with the corresponding sample and passage number, flask type, cell seeding (X_b), harvesting number (X_e) and incubation time (T).*

5.3.1.5 Human chorionic plate artery smooth muscle cell cultures revealed an uniform immunolocalization of α smooth muscle actin present on the microfilament bundles

Representative fluorescent images showing α-smooth muscle actin (green) immunolocalization in CPA-SMC's cultured on membrane inserts are presented in figure 143. All primary smooth muscle cells expressed the contractile protein α-smooth muscle actin on the microfilament bundles which were evenly distributed along the cytoplasmic compartment of the cells.

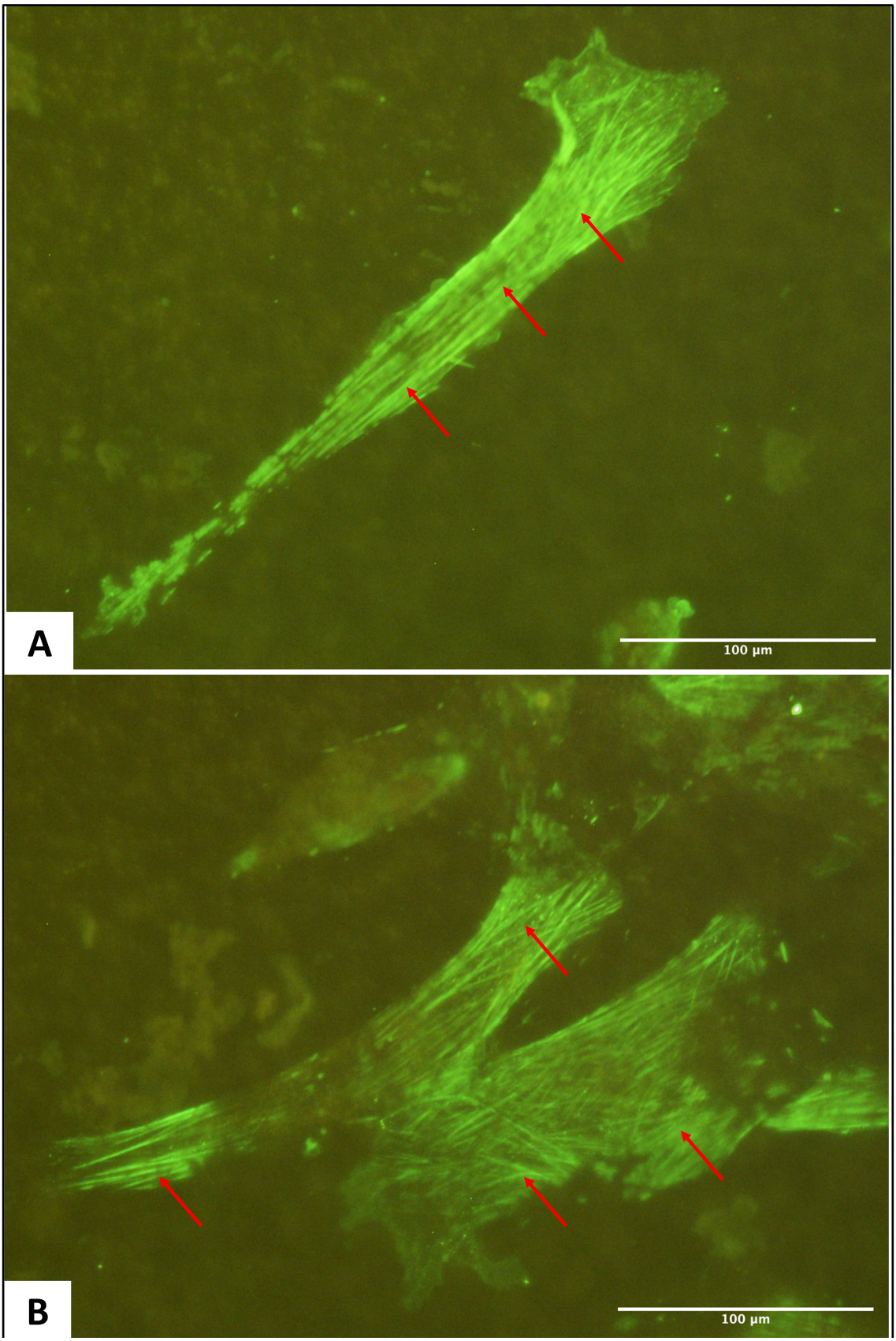


Figure 143. *This figure* ***(****panels* ***A-B)*** *shows the α-smooth muscle actin distribution (green) in CPA-SMC seeded on 0.4µm pore size polyester membrane insert at a density of 1x10^4 cells/1.12cm^2. Scalebar 100µm.*

5.3.1.6 Surface antigenic profiling of human placenta chorionic plate artery smooth muscle cells showed a particular similarity with the immunophenotypic signature characteristic of human multipotent mesenchymal stem cells

Immunophenotyping data using chorionic plate artery smooth muscle cells highlights the stem cell character of these isolated placental cells.

This study shows for the first time that the surface antigenic profiling of these CPA-SMC cells highlighted a positivity towards a specific population of adult mesenchymal stem cells markers. The chorionic plate artery smooth muscle cells originating from N=4 healthy patients were positive for CD73 (95.66±2.890%), CD90 (86.87±5.481%), CD105 (82.18±8.134%) and in terms of hMSC negative cocktail (CD34, CD11b, CD19, CD45 and HLA-DR), only 0.232±0.105% were positive for these cell surface markers relative to isotype control. On the other hand, immunophenotypic data of CPA-SMC's originating from N=4 gestational diabetic patients show a decrease in positivity for hMSC specific markers as follows: CD73 (93.68±0.949%), CD90 (65.91±5.745%), CD105 (67.37±8.064%) and hMSC negative cocktail (0.235±0.110%).

Figure 144 and figure 145 highlight the immunophenotypic data of all CPA-SMC originating from healthy and gestational diabetic patients in which the smooth muscle cells were stained with antibodies against surface specific receptors characteristic of mesenchymal stem cells. A Shapiro-Wilk test highlighted that all immunophenotype data corresponding to healthy and gestational diabetic patients was normally distributed. An unpaired, two-tailed T test with Welch's correction was carried out

between healthy and GDM patient subgroups separately in the case of CD73, CD90 and CD105 and highlighted a single statistically significant difference in the percentage of CD90 positive cells (*P=0.0386) as highlighted in figure 146.

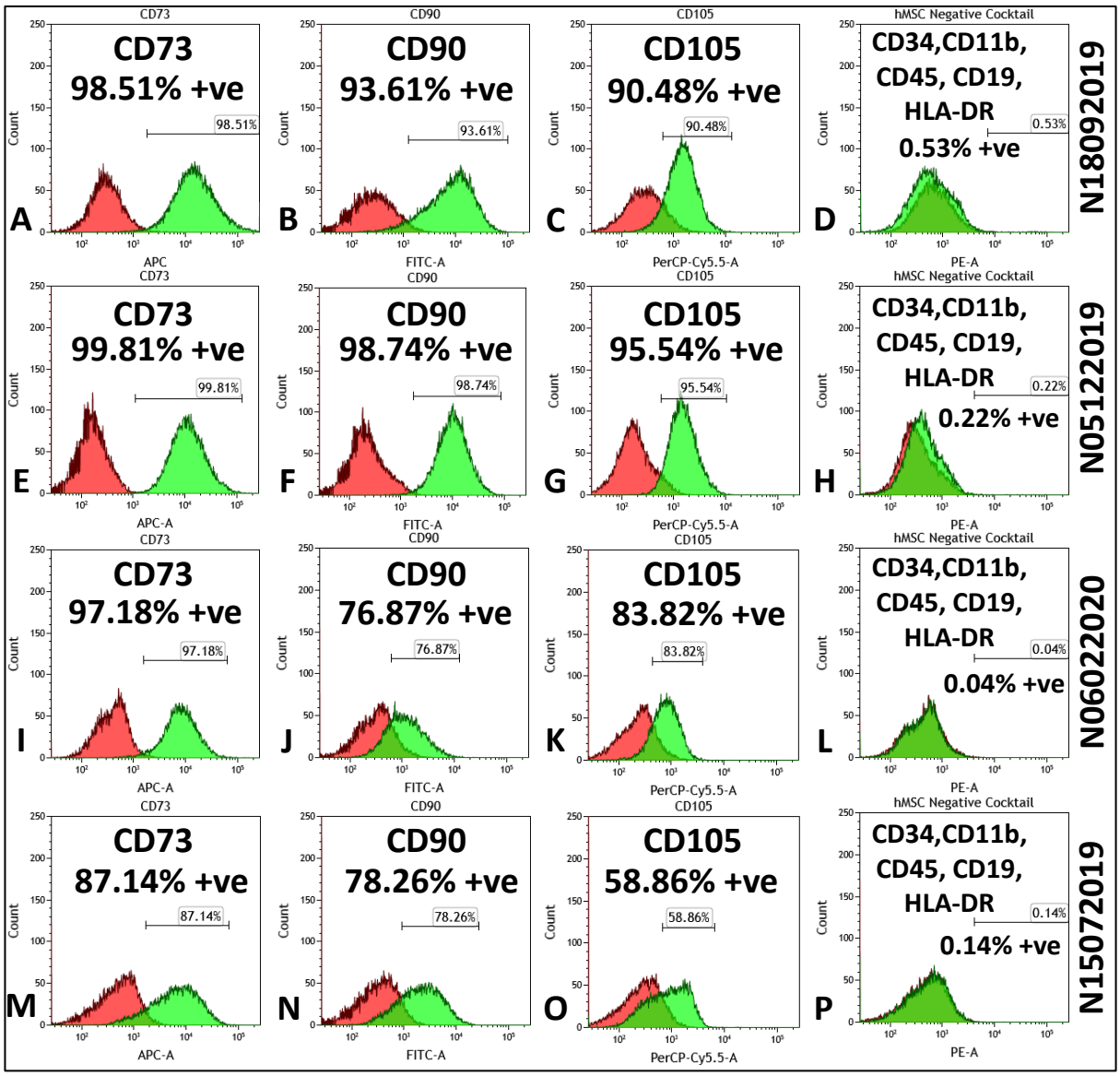


Figure 144. *This figure (panels **A-P**) highlights the immunophenotype data of human placenta chorionic plate artery smooth muscle cells originating from four healthy patients (N18092019, N05122019, N06022020 and N15072019). Flow cytometric analysis of the expression of cell surface markers showed that CPA-SMC's were positive for CD73 (95.66±2.890%), CD90 (86.87±5.481%) and CD105 (82.18±8.134%) and only 0.232±0.105% of the CPA-SMC population was positive for the hMSC negative cocktail markers (CD34, CD11b, CD19, CD45 and HLA-DR). CPA-SMC's were stained with antibodies against surface specific cellular markers as shown by the green histograms or an isotype matched monoclonal antibody as highlighted by the red histograms.*

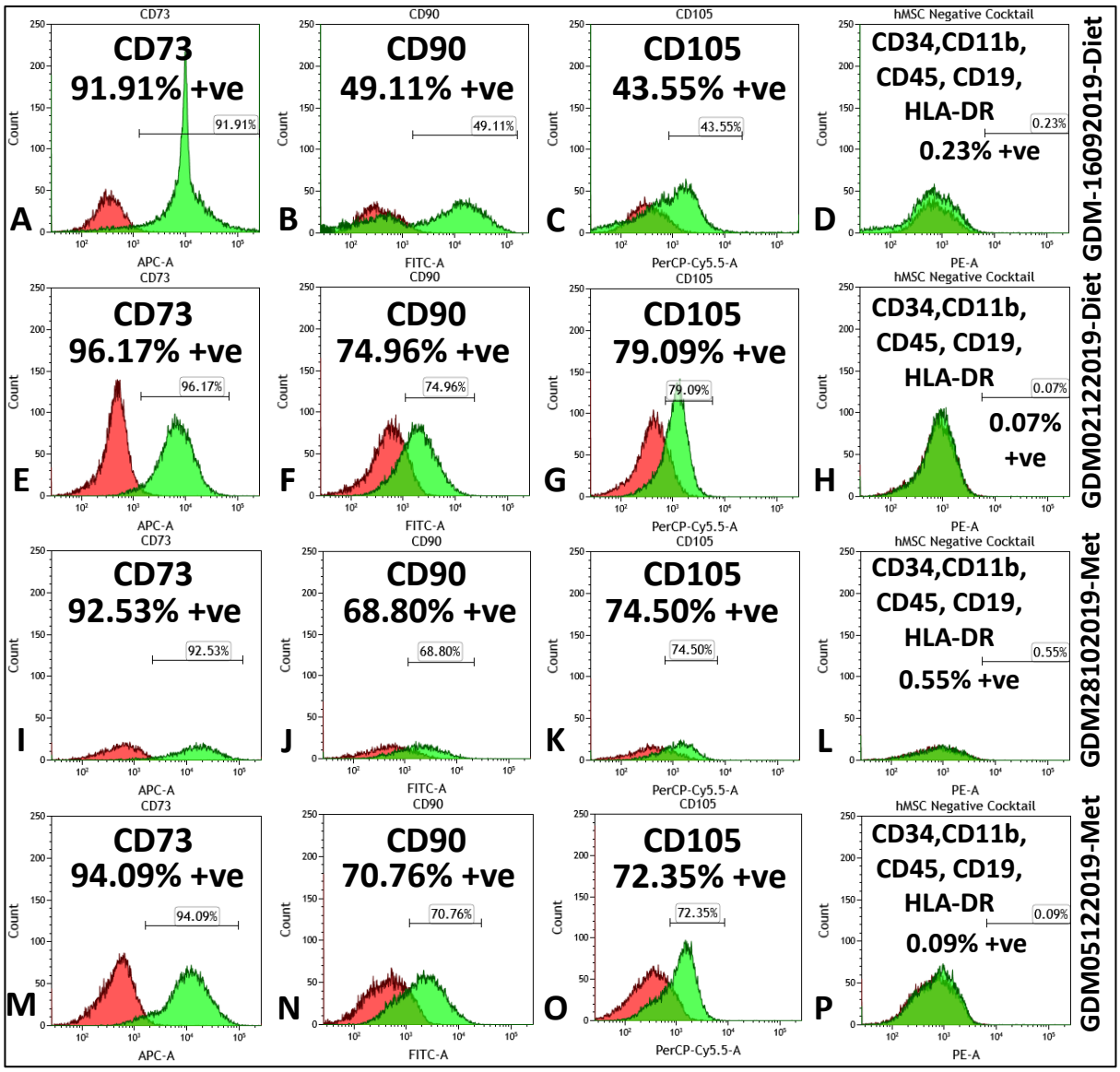


Figure 145. *This figure (panels **A-P**) highlights the immunophenotype data of human placenta chorionic plate artery smooth muscle cells originating from four gestational diabetic patients (GDM16092019-Diet, GDM02122019-Diet, GDM28102019-Metformin and GDM05122019-Metformin). Flow cytometric analysis of the expression of cell surface markers showed that CPA-SMC's were positive for CD73 (93.68±0.949%), CD90 (65.91±5.745%) and CD105 (67.37±8.064%) and only 0.235±0.110% of the CPA-SMC population was positive for the hMSC negative cocktail markers (CD34, CD11b, CD19, CD45 and HLA-DR). CPA-SMC's were stained with antibodies against surface specific cellular markers as shown by the green histograms or an isotype matched monoclonal antibody as highlighted by the red histograms.*

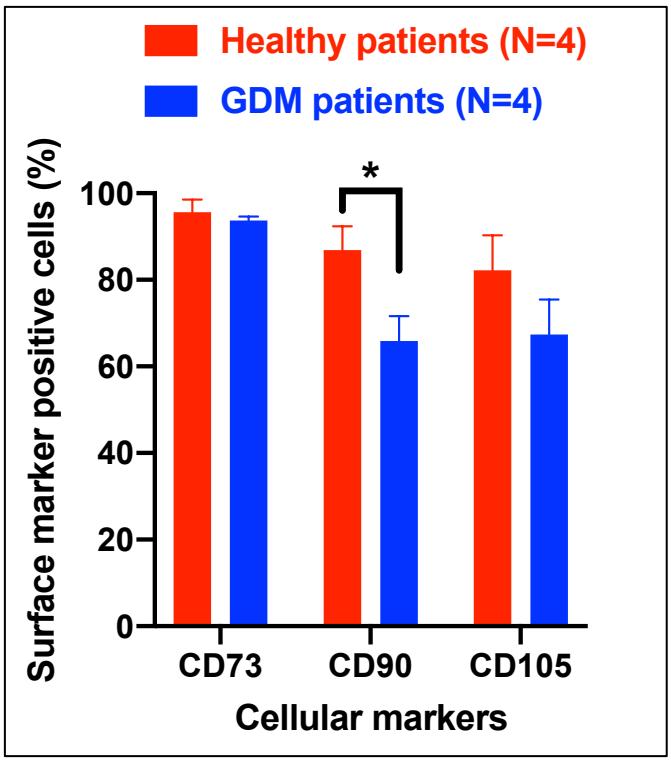


Figure 146. *This figure highlights the percentage of CPA-SMC cells that were positive for CD73, CD90 and CD105 originating from N=4 healthy patients (N18092019, N05122019, N06022020 and N15072019) and from N=4 gestational diabetic patients (GDM16092019-Diet, GDM02122019-Diet, GDM28102019-Metformin and GDM05122019-Metformin). Data are presented as mean ± SEM. *P≤0.05, **P≤0.01, ***P≤0.001, ****P≤0.0001.*

5.3.2 The morphology of human umbilical vein endothelial cells is characterised by a cobblestone appearance with dark large size nuclei inside the primary cells

The human umbilical vein endothelial cells resemble a homogenous cell population with a cobblestone appearance in culture conditions which is accompanied by generous size dark nuclei inside the cells (figure 147). Freshly isolated human umbilical vein endothelial cells comprised of many small-size slightly spindle-shaped clusters of cells which adhered to the 1% gelatin-coated T25 flasks in a period between 6-12 hours post seeding. On the following day after the HUVEC isolation took place, the cells proliferated at a high rate and established connections with adjacent adhered cells.

The primary endothelial cells gave rise to the formation of a monolayer comprising of heavily arranged evenly sized polygonal cells with a width ranging from 20-60μm at approximately 48 hours after the enzymatic digestion took place. This process was dependent on various factors such as the initial number of isolated viable cells placed in the 1% gelatinised flasks, the abundance of cells that have adhered to the plastic surface and potentially the growth environment. Representative examples of HUVEC cells at passage 3 in a 1% gelatin coated T75 flask originating from a healthy patient (N21082019) highlighting the morphology of the cells at both 10X and 20X magnifications are provided in figure 147. The morphology of many of the isolated endothelial cells can be characterised as hexagonal or polygonal with poorly defined borders that were hard to visualise and a small population exhibiting elongated shapes. The HUVEC cells did not form overlapping sheets of cells, nodules or ridges during the proliferation or even when the cells reached the confluency stage. As the

human umbilical vein endothelial cells cultures aged, the cells began to show signs of a more senescent heterogenous population with an unusual morphological appearance and elevated size.

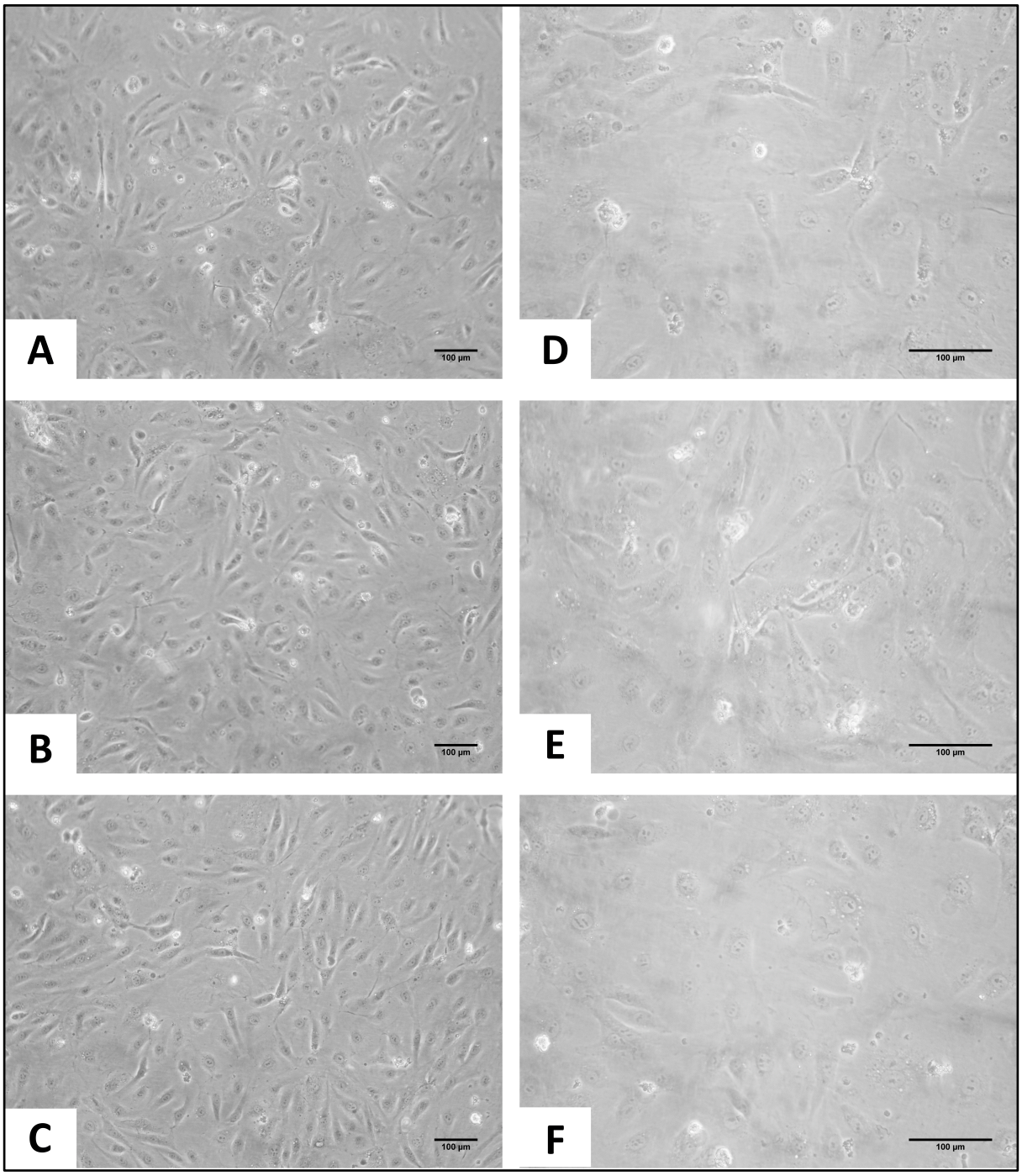


Figure 147. *This figure (panels **A-C**, 10X, panels **D-F**, 20X) shows the cuboidal morphological appearance of HUVEC cells in culture conditions at passage 3 originating from a healthy volunteer (N21082019). Scalebar 100µm.*

5.3.2.1 The population doubling time of isolated human umbilical vein endothelial cells suggests a highly proliferative rate in culture conditions

The human umbilical vein endothelial cells doubling time originating from 4 healthy volunteers as shown in table 29 expressed as mean ± standard deviation was 2.158±0.3893 days. This number highlights the high proliferation rate of these vascular cells, which is approximately 7.126 times higher than the doubling time of the chorionic plate artery smooth muscle cells.

Sample number	Passage number	Flask type	X_b	X_e	T	DT
N21082019	P1	T25	$1.06x10^6$	$3.16x10^6$	3	1.904
N10072019	P1	T75	$1.23x10^6$	$3.6x10^6$	4	2.582
N05122019	P1	T75	$2.1x10^6$	$6.83x10^6$	3	1.76
N12082019	P1	T25	$1.05x10^6$	$2.51x10^6$	3	2.386

Table 29. *This table shows the human umbilical vein endothelial cells doubling time (DT) originating from 4 healthy patients taking into consideration the cell seeding (X_b), harvesting number (X_e) and the incubation time (T).*

5.3.3 Isolated human placenta chorionic plate artery smooth muscle cells seeded at a density of $3x10^4$ cells on 6.5mm diameter 0.4µm pore size polycarbonate membrane inserts highlight a limited adhesion and proliferation capacity

Figure 148 highlights the appearance of $3x10^4$ chorionic plate artery smooth muscle cells just after seeding on 6.5mm diameter polycarbonate membrane inserts. As shown in figures 149 and 150, this trial study highlights that seeding $3x10^4$ SMC cells on the 0.4µm pore size polyester membrane facilitates the formation of

calcification nodules after 24 hours of primary cell culture in DMEM low glucose+10% (v/v) FBS+Penicillin/Streptomycin media. Figure 151 highlights the appearance of polycarbonate inserts without any cells seeded. As these nodules were typically formed by primary smooth muscle cells usually after 30 days in culture conditions, the current observations show that the cells were able to contribute significantly to the establishment of an apoptotic microenvironment if cultured at a high cell number relative to a limited growth surface area.

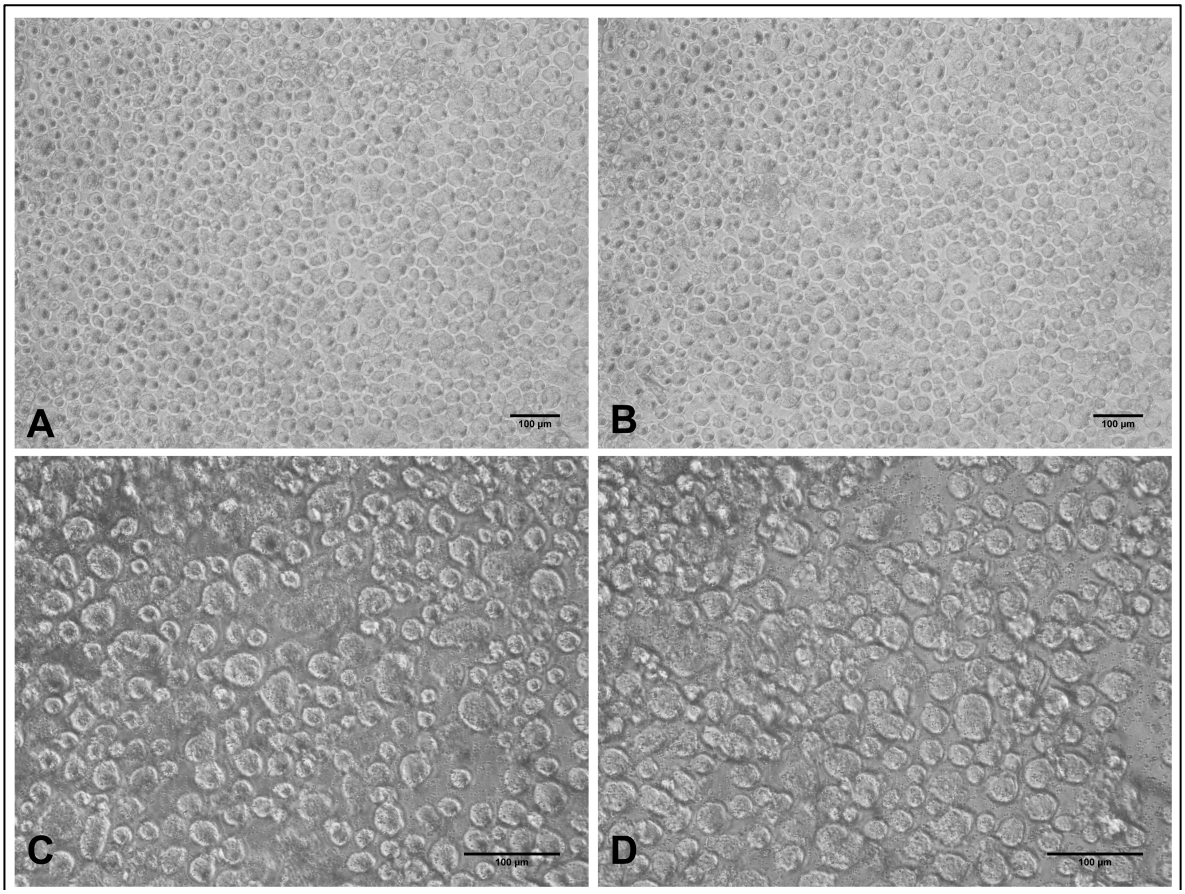


Figure 148. *This figure (panels **A-B** 10X, panels **C-D** 20X) shows the morphology of chorionic plate artery smooth muscle cells after seeding on the membrane insert. The cells appear circular in shape with a density of $3x10^4$ cells/$0.33cm^2$. Scalebar 100µm.*

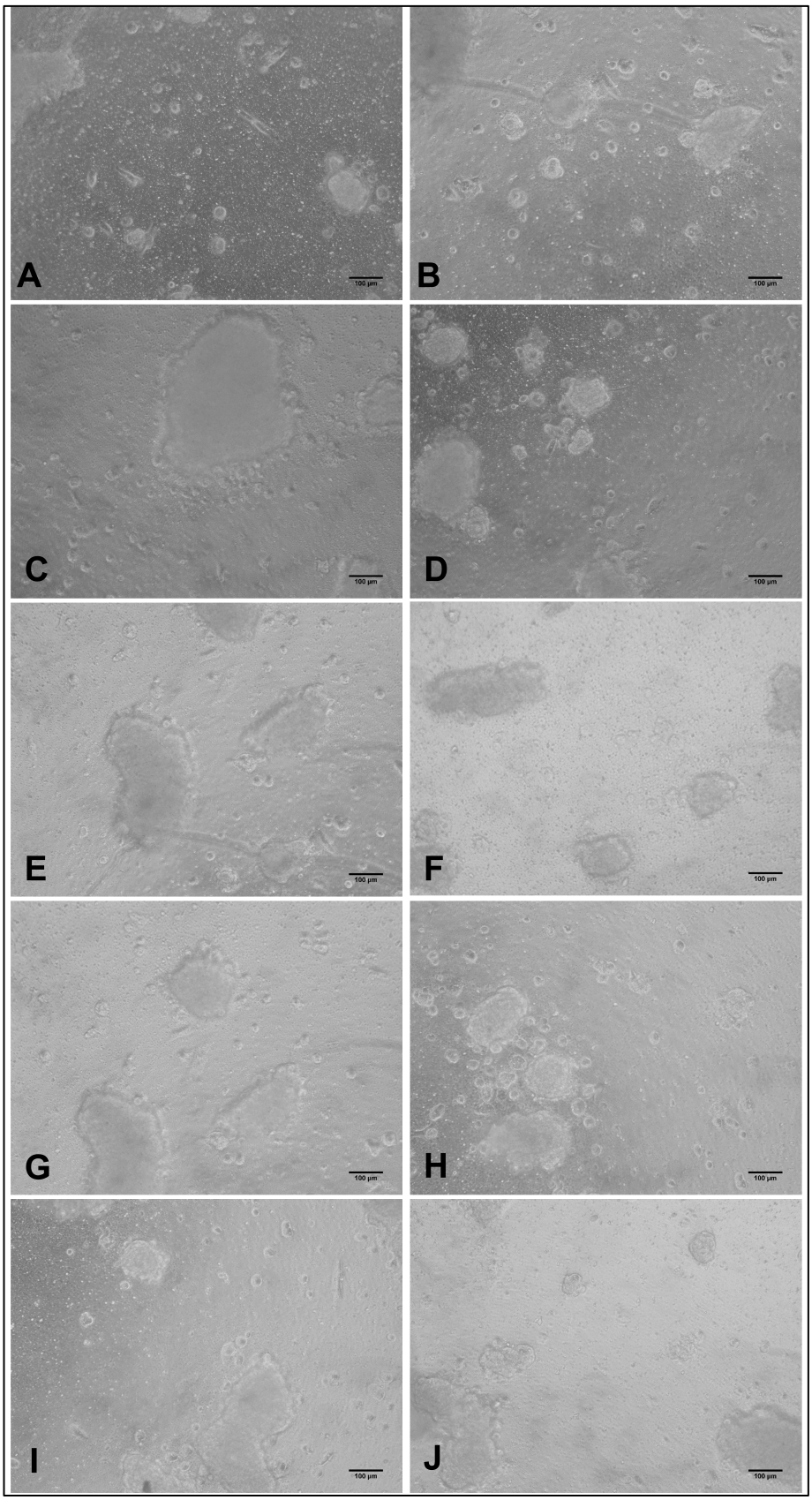


Figure 149. *This figure (panels **A-J**) shows the morphology of the smooth muscle cells (10X) at 24 hours after seeding on the polycarbonate membrane insert. Scalebar is 100µm.*

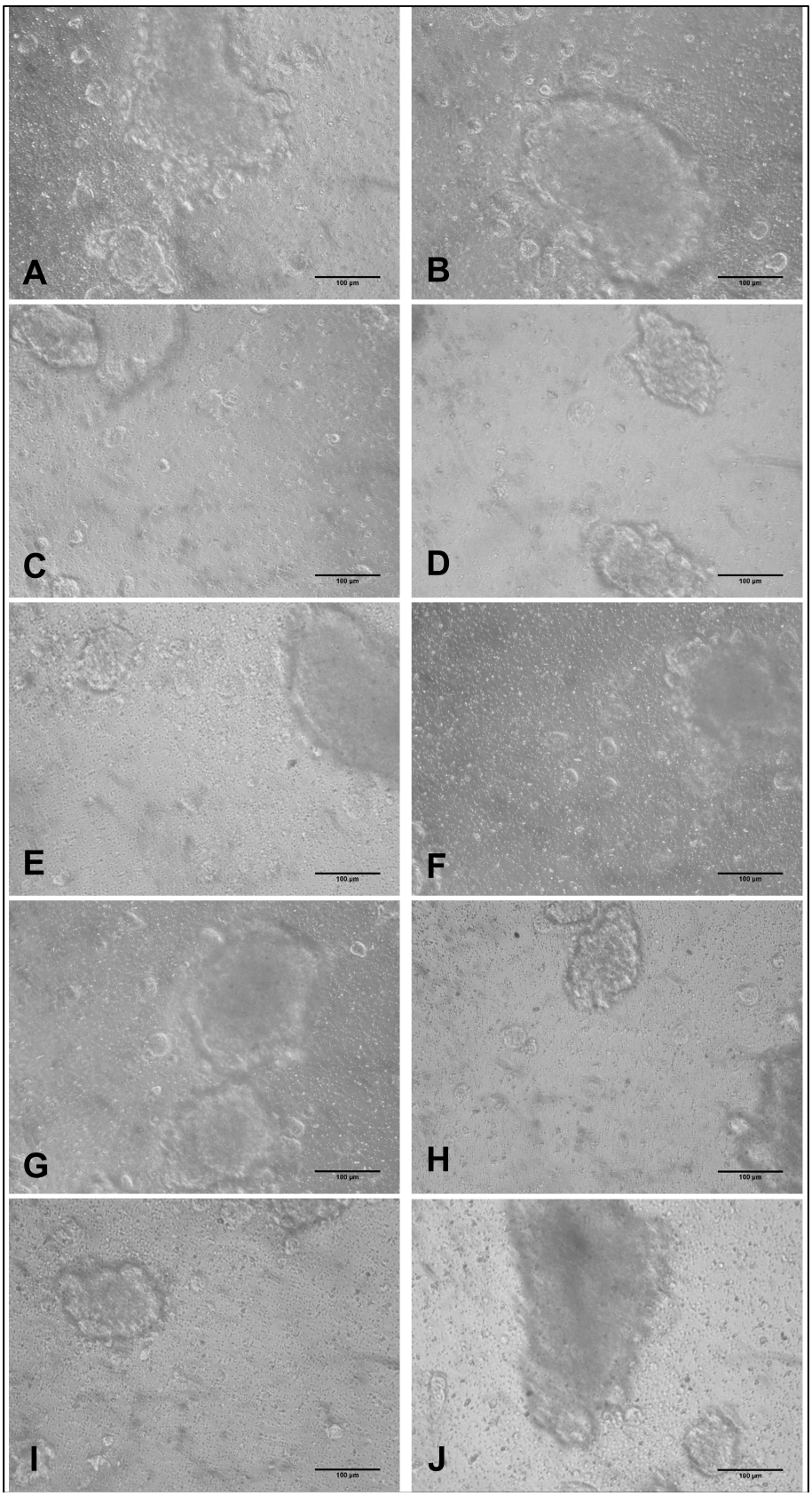


Figure 150. *This figure (panels **A-J**) shows the morphology of the smooth muscle cells (20X) at 24 hours after seeding on the polycarbonate membrane insert. Scalebar is 100µm.*

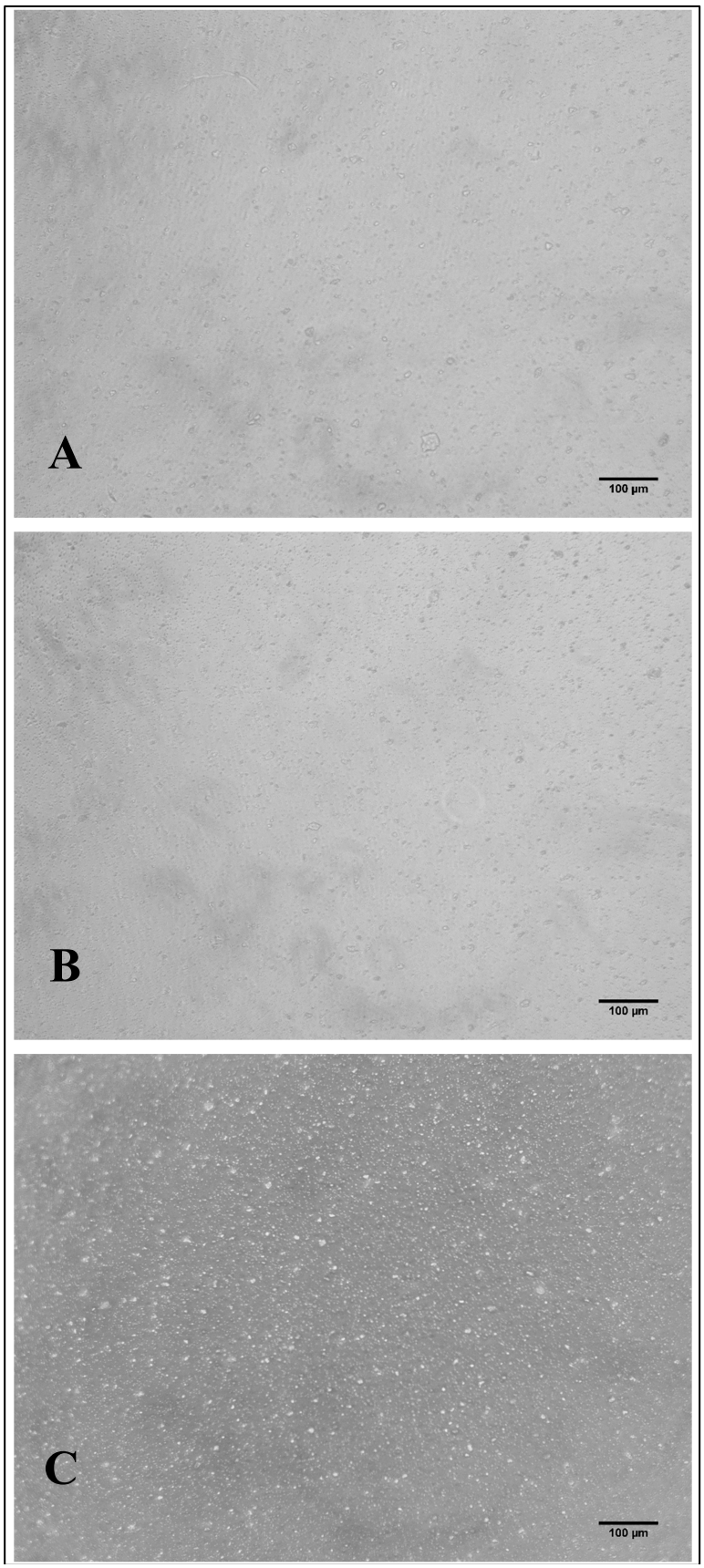


Figure 151. *This figure (panels **A-C**) shows the appearance of the polycarbonate inserts without any cells seeded (10X) as a media only control at 24 hours. Scalebar is 100µm.*

5.3.4 *In vitro* validation studies suggest that the cell seeding density of $1x10^4$ human placenta chorionic plate artery smooth muscle cells on 6.5mm diameter 0.4µm pore size polycarbonate membrane insert prevents the formation of nodular cultures for at least 48 hours

As shown from figures 152-156, the smooth muscle cells were able to adhere and proliferate on the inserts to the point of forming a disjointed sheet of cells. The primary cells were not able to fully cover the surface of the transwell inserts, not even at 120 hours post seeding. In some cases, specifically at 48 hours after seeding the cells (figure 154, panels M and P) where the SMC's were seeded at $1.5x10^4$ and $2x10^4$ cell density per transwell membrane insert, numerous nodules were formed.

Moreover, the images acquired at 120 hours post seeding as shown in figure 155 and figure 156 highlight that all CPA-SMC cell seeding densities gave rise to the formation of cellular aggregates.

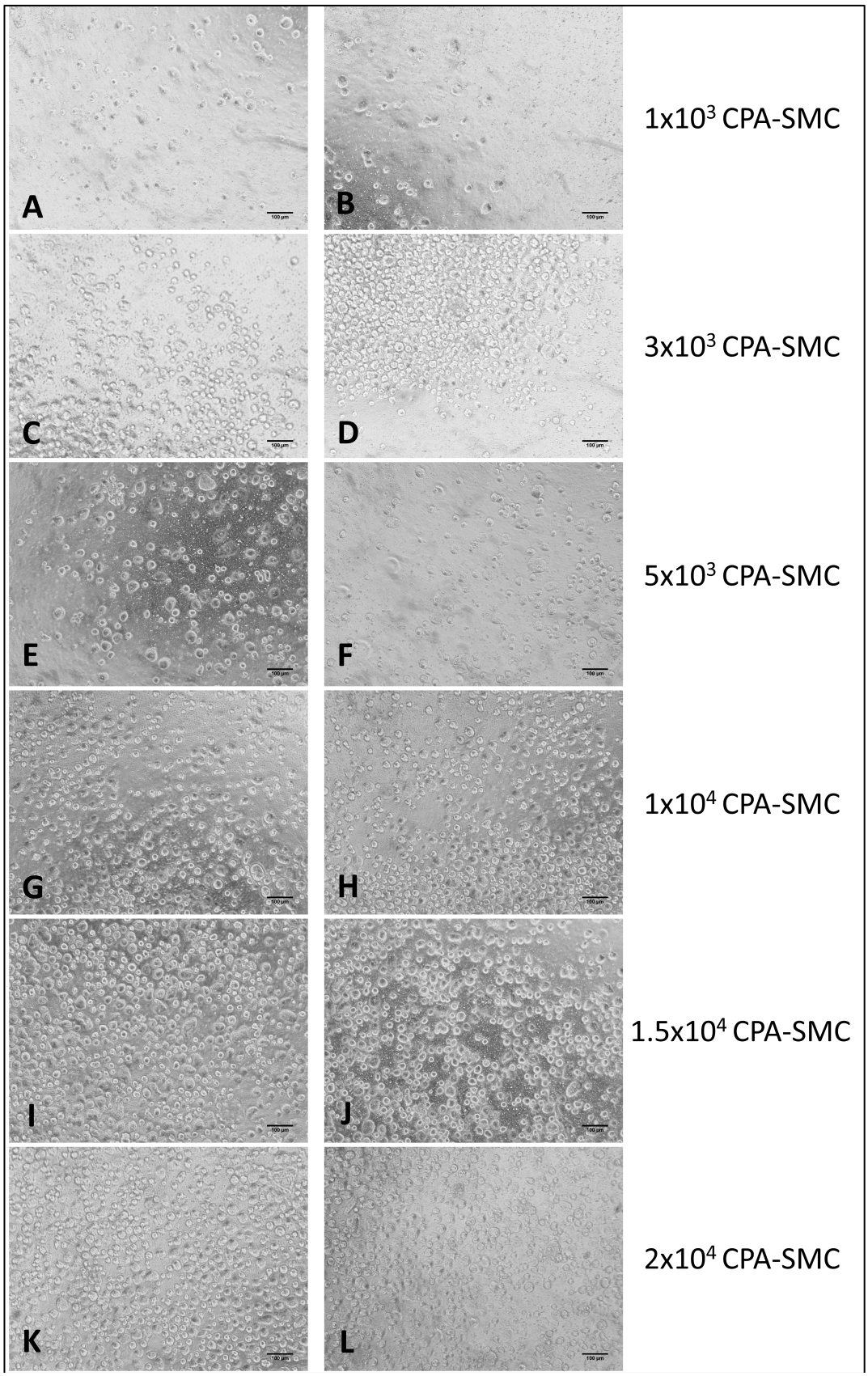


Figure 152. *This figure (panels **A-L**, 10X) shows the morphology of various cell densities of CPA-SMC right after seeding on the 0.4µm pore size polycarbonate membrane inserts (Scalebar 100µm).*

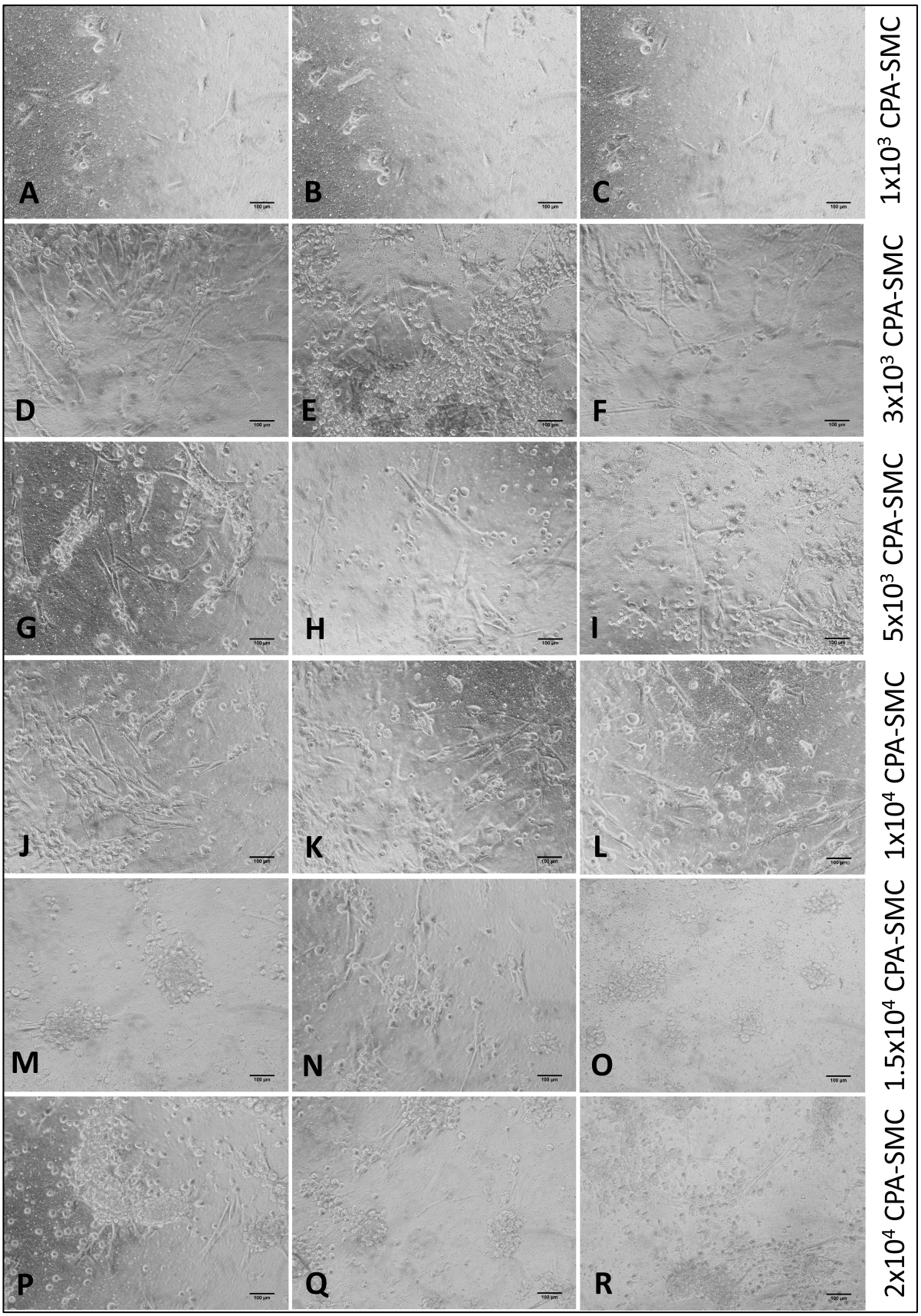


Figure 153. *This figure (panels **A-R**, 10X) shows the morphology of various cell densities of CPA-SMC at 24h post-seeding on the 0.4µm pore size polycarbonate membrane inserts (Scalebar 100µm).*

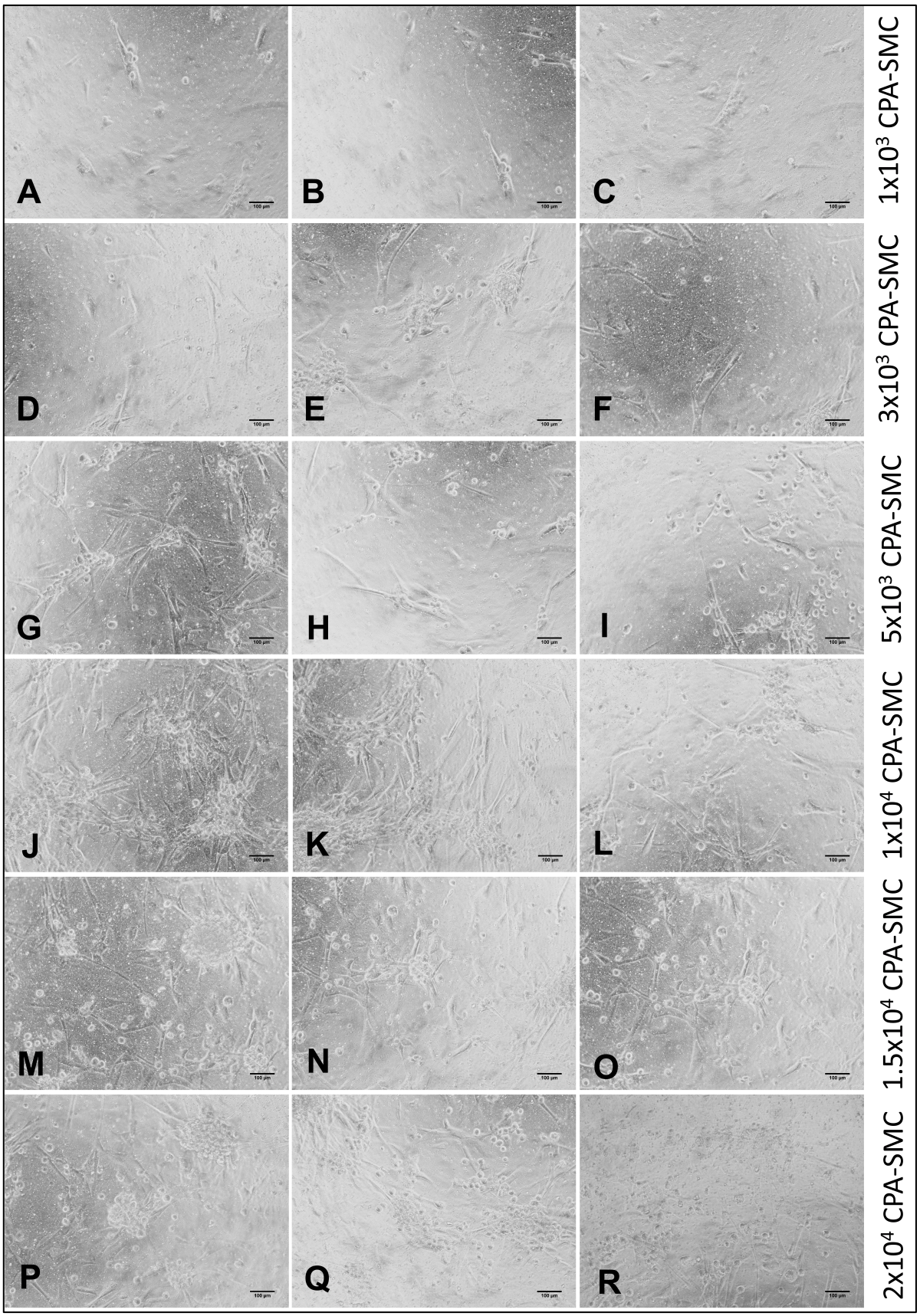


Figure 154. *This figure (panels **A-R**, 10X) shows the morphology of various cell densities of CPA-SMC at 48h post-seeding on the 0.4µm pore size polycarbonate membrane inserts (Scalebar 100µm).*

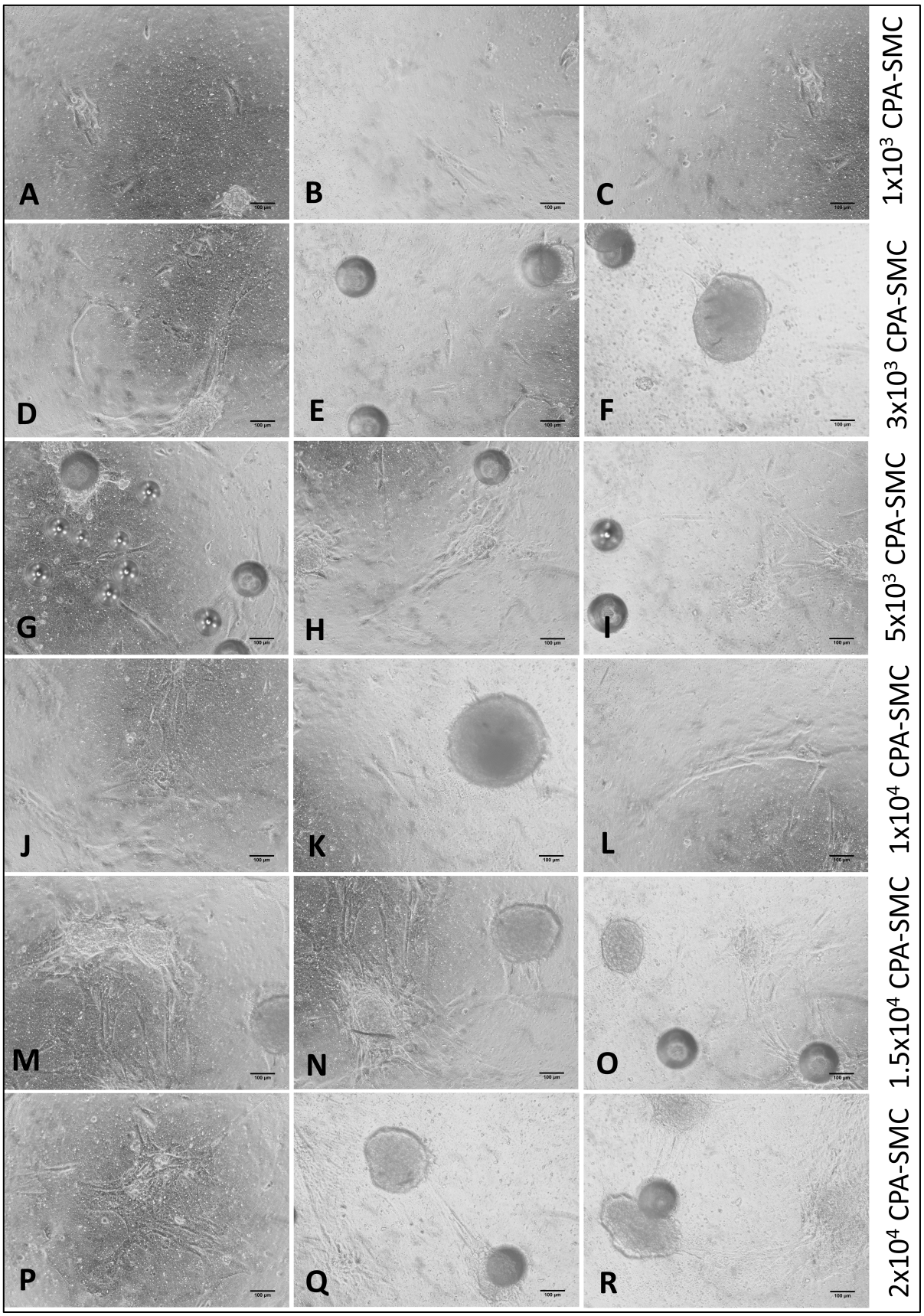


Figure 155. *This figure (panels **A-R**, 10X) shows the morphology of various cell densities of CPA-SMC at 120h post-seeding on the 0.4μm pore size polycarbonate membrane inserts (scalebar 100μm).*

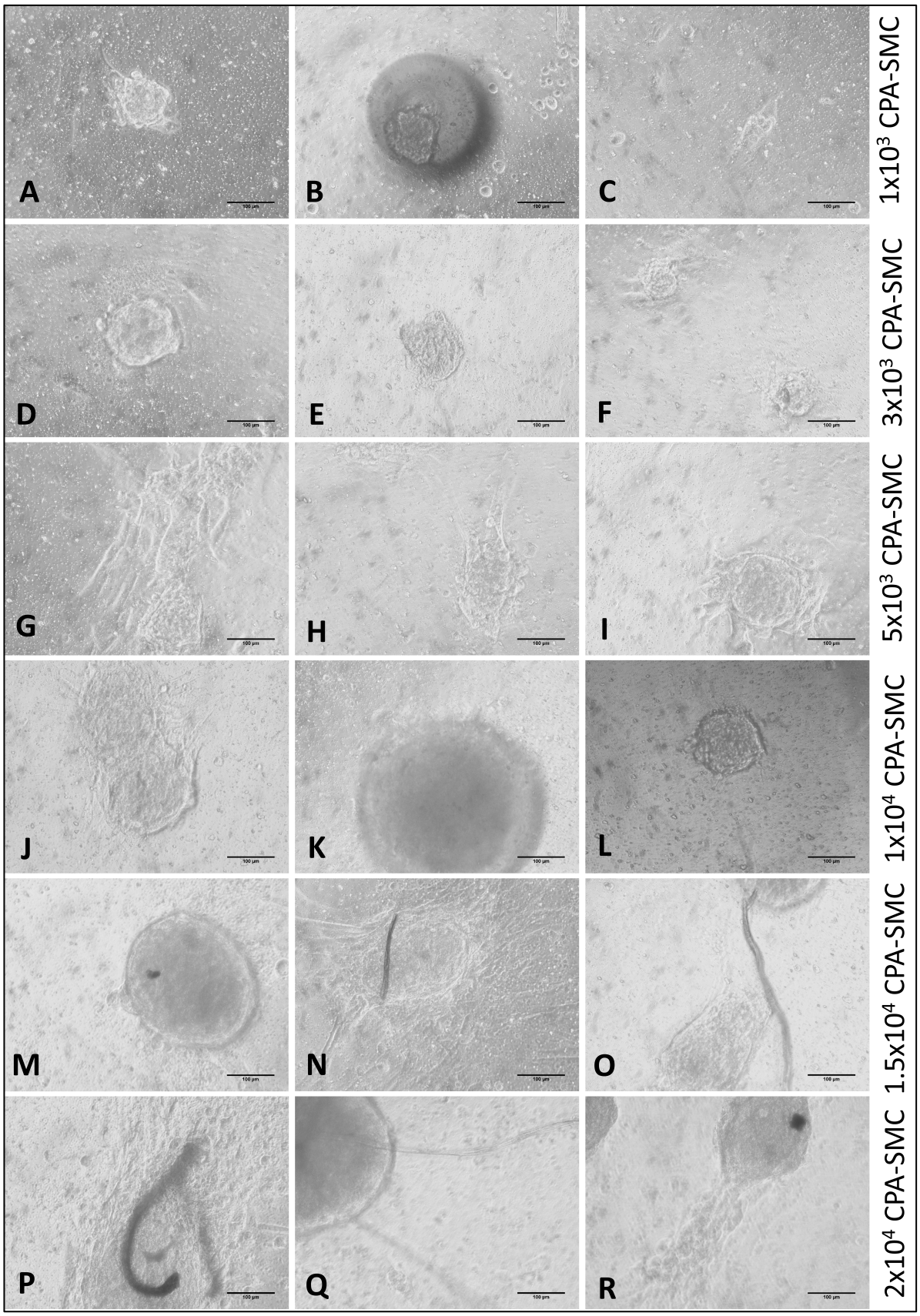


Figure 156. *This figure (panels **A-R**, 20X) shows the morphology of various cell densities of CPA-SMC at 120h post-seeding on the 0.4μm pore size polycarbonate membrane inserts (scalebar 100μm).*

As a result, the morphological image data from the previous *in vitro* CPA-SMC experiments has highlighted that the optimal cell seeding density of CPA-SMC's on 0.33cm^2 membrane inserts was 1x10^4 cells/transwell. Due to the fact that all cell seeding densities tested (1x10^3, 3x10^3, 5x10^3, 1x10^4, 1.5x10^4 and 2x10^4) of the primary smooth muscle cells on 6.5mm diameter polycarbonate membrane inserts gave rise to the formation of nodules after 5 days in culture conditions, an appropriate reliable period for culturing these cells on transwells was chosen to be up to 24 hours.

As shown from figure 153, panels J, K and L which correspond to a CPA-SMC cell seeding density of 1x10^4 cells per membrane insert, at the 24-hour timepoint, the physiological morphology of the primary cells was kept intact with the majority of cells resembling a spindle shape with no formation of nodular aggregates. Furthermore, most of the seeded primary cells showed signs of attachment to the polycarbonate inserts with very few cells floating in the SMC media (0.1mL) of the apical chamber.

5.3.5 Isolated human umbilical vein endothelial cells seeded at a density of 2x10^4 cells on 6.5mm diameter 0.4µm pore size polycarbonate membrane insert did attach and proliferate but did not form a monolayer for the first 48 hours in culture conditions

These primary cell morphological studies highlight that HUVEC were able to attach to the polycarbonate surface of the membrane inserts at all cell seeding densities as shown in figure 157. However, even if 2x10^4 seeded endothelial cells were left to proliferate for 48 hours in culture conditions, morphological data suggests that these cells were not able to form a tight monolayer in 2 days post seeding (figure 158, panel I).

CPA-SMC's were able to attach to both HUVEC and polycarbonate insert as there were few cells noticed in the culture media (figure 158, panels M-U) at the timepoint of 72 hours timepoint.

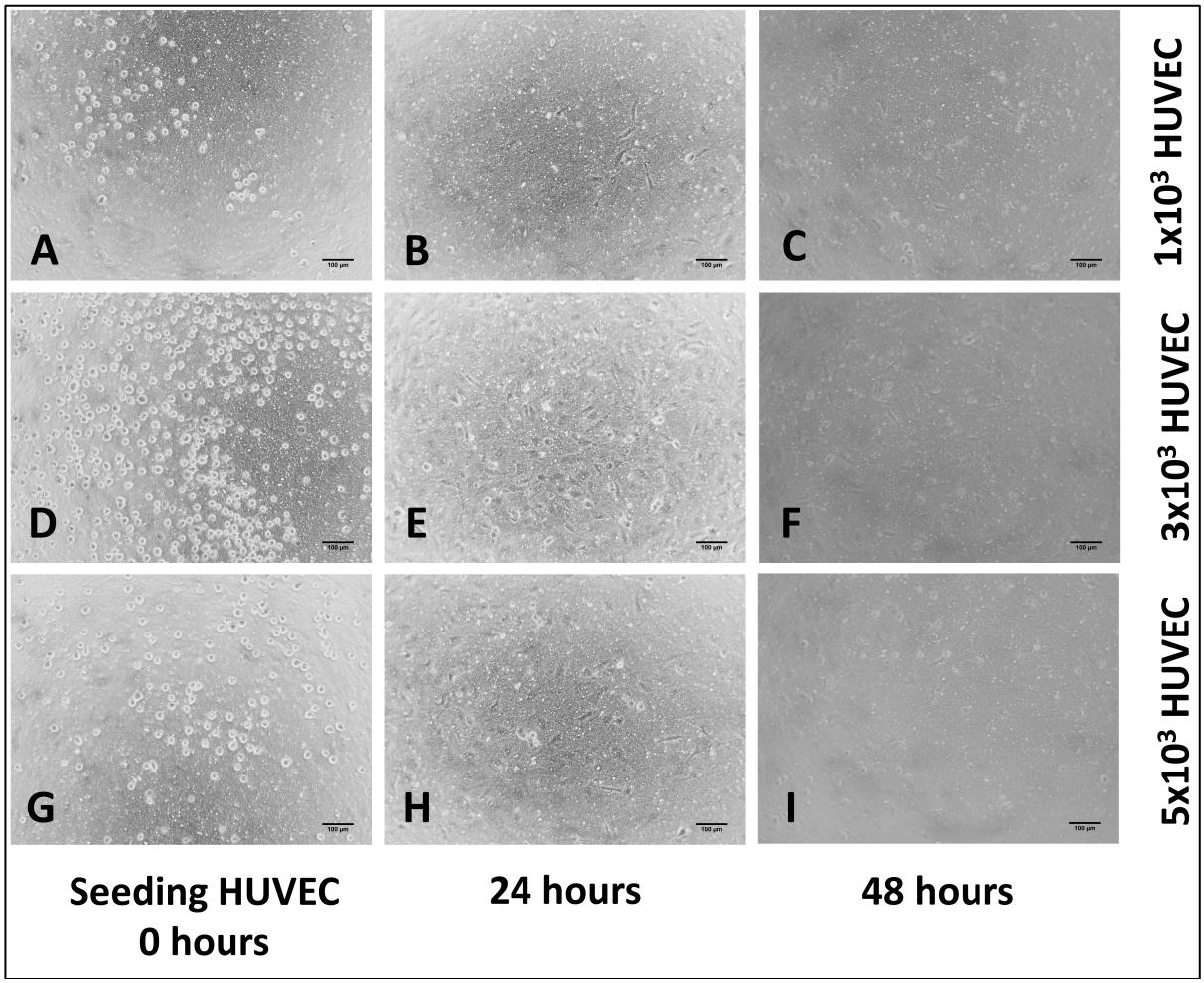


Figure 157. *This figure (panels **A-I**) highlights the morphology of HUVEC at 1x10^3, 3x10^3 and 5x10^3 cell seeding densities on 6.5mm diameter 0.4µm pore size polycarbonate membrane inserts just after seeding (0 hours), at 24 and 48 hours. At 24 hours there are clear signs of endothelial cell attachment to the insert especially at 3x10^3 and 5x10^3 cell seeding densities as shown in panels **E** and **H**. Panels **C, F** and **I** highlight that at 48 hours, none of the varying endothelial cell seeding densities gave rise to a confluent monolayer formed on the polycarbonate insert. This may suggest that the doubling time of HUVEC cells might be significantly greater than 2 days on the polycarbonate membranes. Scalebar 100µm.*

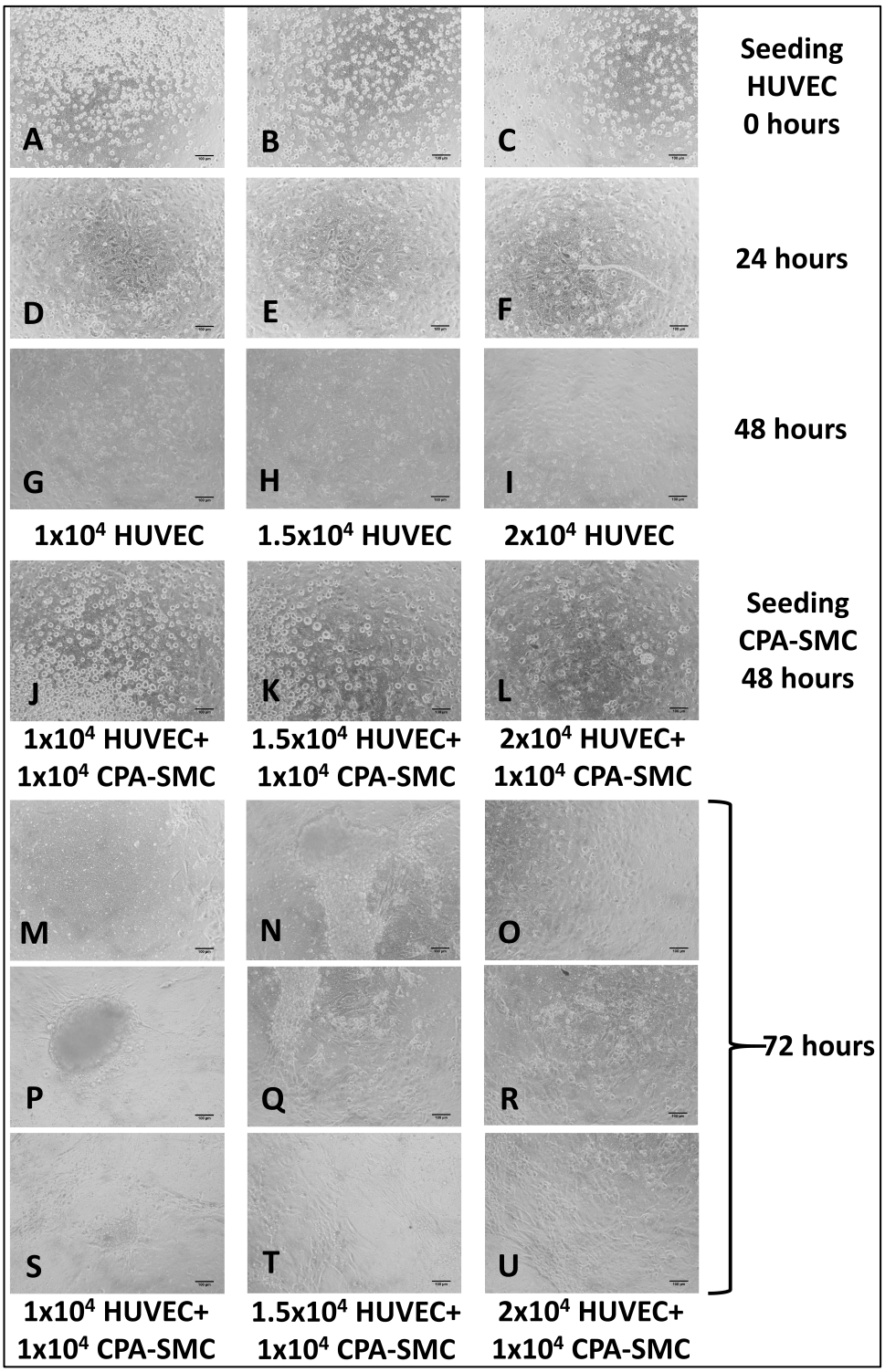


Figure 158. *This figure (panels **A-U**) highlights the morphology of HUVEC at 1x10⁴, 1.5x10⁴ and 2x10⁴ cell seeding densities on 6.5mm diameter 0.4µm pore size polycarbonate membrane inserts just after seeding (0 hours), 24, 48 and 72 hours. 1x10⁴ CPA-SMC's were seeded at the timepoint of 48 hours above adhered HUVEC cells as shown in panels **J, K** and **L** and left to grow for another 24 hours in co-culture. Further images were acquired at the timepoint of 72 hours with the co-cultured primary cells for the purposes of examining the morphology and monolayer forming capability of these cells. There were few signs of nodule formation as shown in panels **P, N** and **Q** at 72 hours. Scalebar 100µm.*

5.3.6 The cell seeding density of $1x10^5$ human umbilical vein endothelial cells on 12mm diameter 0.4µm pore size polyethylene terephthalate membrane insert did not give rise to the establishment of a monolayer after 48 hours in culture conditions

As shown in figure 159 (panels D-F), the results highlight that seeding $1x10^5$ human umbilical vein endothelial cells on 12mm diameter 0.4µm pore size polyethylene terephthalate (PET) membrane inserts did not facilitate the formation of a monolayer characterised by an endothelial cell cobblestone appearance. In this case, small signs of HUVEC attachment to the insert have been noticed, with an elevated number of floating cells in the apical chamber.

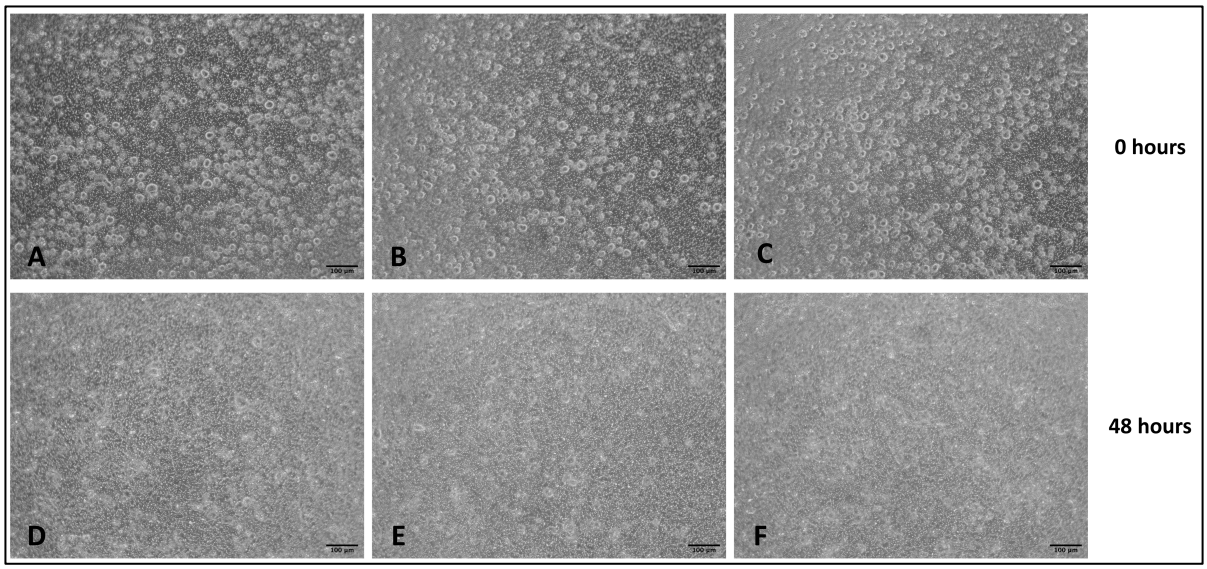


Figure 159. *This figure (panels **A-F**) shows the morphology of HUVEC cells seeded at a density of $1x10^5$ cells per 12mm diameter 0.4µm pore size polyethylene terephthalate membrane insert. Panels (**A-C**) highlight the appearance of the primary cells just after seeding on the insert and panels (**D-F**) denote the phenotype of the endothelial cells on the insert at 48 hours post seeding. Scalebar 100µm.*

5.3.7 Human placenta chorionic plate artery smooth muscle cells can survive and proliferate in complete endothelial cell media for at least 120 hours without significant changes in the primary cell morphology

The smooth muscle cells were able to survive in complete endothelial cell media for at least 48 hours without disturbing the tightly packed cells as highlighted in figure 160. At 120 hours of exposure of CPA-SMC to complete endothelial cell media, the primary cells started to show signs of senescence by disruption of the established sheets of cells as highlighted in figure 160, panels D, H, L, P and T.

Furthermore, the parallel pattern of closely arranged hill and valley CPA-SMC's changed significantly between 48 hours and 120 hours of culturing the human cells in complete endothelial cell media, as the cells became sparser by losing their tightly organised parallel growth appearance pattern. However, the morphology of CPA-SMC's remained similar with an elongated spindle shape with some cells possessing and sending projections towards adjacent primary cells.

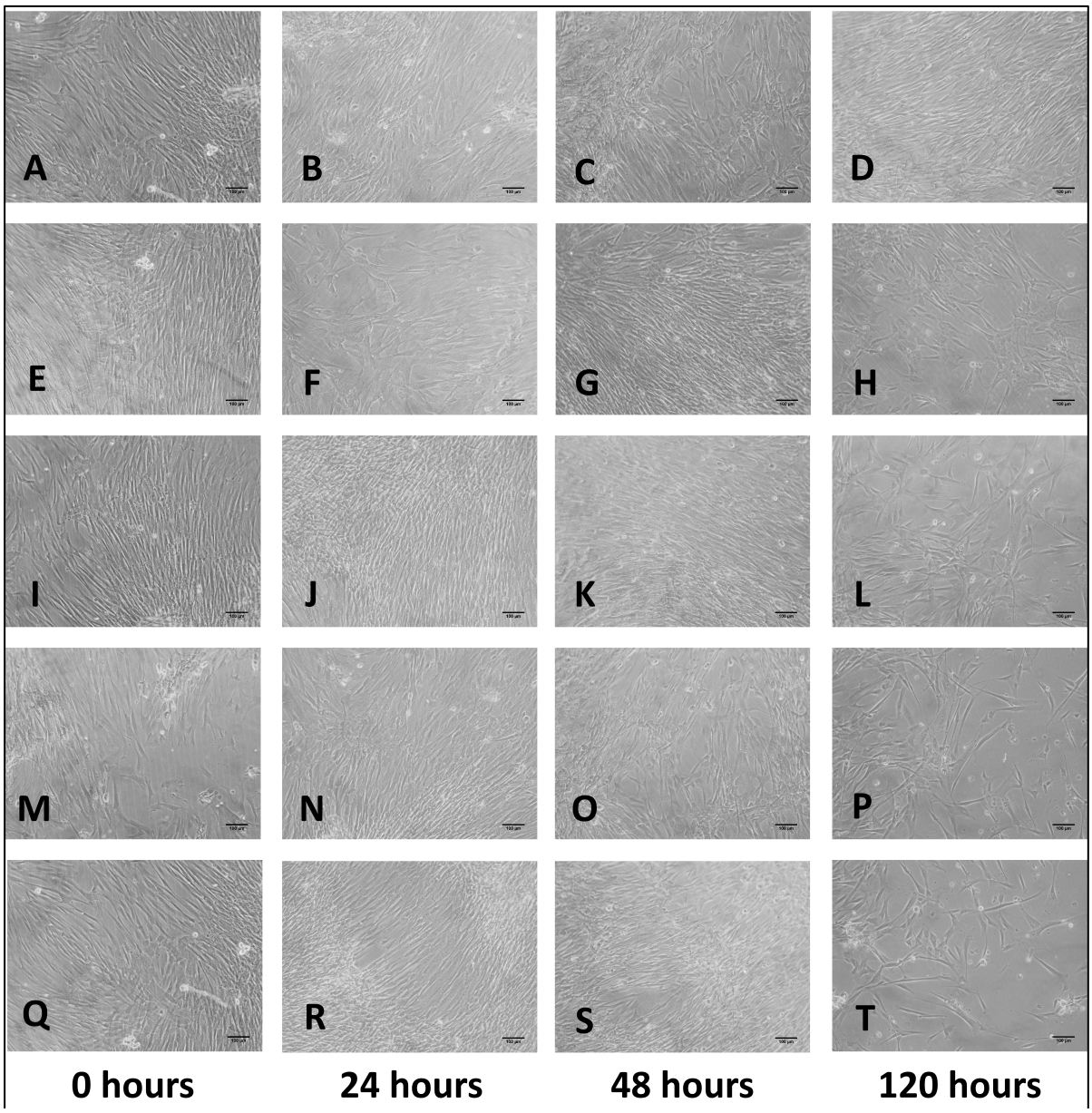


Figure 160. *This figure (panels **A-T**) shows the morphology of CPA-SMC's grown in complete endothelial cell media for 120 hours. Following chorionic explant removal and serum starvation for 24 hours the media was replaced with M199 supplemented with 20% (v/v) fetal bovine serum, heparin sodium salt (50µg/mL), endothelial cell growth factor supplement (75µg/mL), penicillin (100units/mL) and streptomycin (100µg/mL). Scalebar 100µm.*

5.3.8 Human umbilical vein endothelial cells seeded on transwell inserts showed a reduced staining for α smooth muscle actin compared to chorionic plate artery smooth muscle cells which was mainly immunolocalised on the plasma membrane

Following the permeability study, all eight *in vitro* mono- and co-culture preliminary conditions involving human placental chorionic plate artery smooth muscle cells and human umbilical vein endothelial cells seeded on transwell inserts were stained for the presence and localisation of α smooth muscle actin (α-SMA). CPA-SMC's (N15072019, P3) possessed uniform filamentous localisation of α smooth muscle actin as shown in figure 161. Immunofluorescence data shows that CPA-SMC's were large cells expressing α-SMA in the cytoskeleton of the primary cells. HUVEC cells (N21082019, P5) did not express α-SMA (Figure 161, panels D, H, L, P, T, Y) although at parts, a small number of endothelial cells were positively stained on the cellular border for the hallmark of mature myofibroblasts (Figure 162, panels D, H, L, P, S and V). Negative controls represented by omitting the primary antibody as highlighted in figure 162 (panels A, E, I, M, Q and T) for α-SMA had no staining in the co-culture of CPA-SMC and HUVEC cells although the primary cells were noticed adhered to the membrane insert. Similarly, there were small signs of background staining in the conditions with the absence of primary cells and 1% gelatin (Figure 162, panels B, F, J and N) and no signs immunostaining where only 1% gelatin was added to the membrane inserts (Figure 162, panels C, G, K, O, R and U). All fluorescent micrographs showing α-SMA immunolocalization in CPA-SMC and HUVEC

monolayers highlight that the protein was extensively expressed in stress fibers of smooth muscle cells.

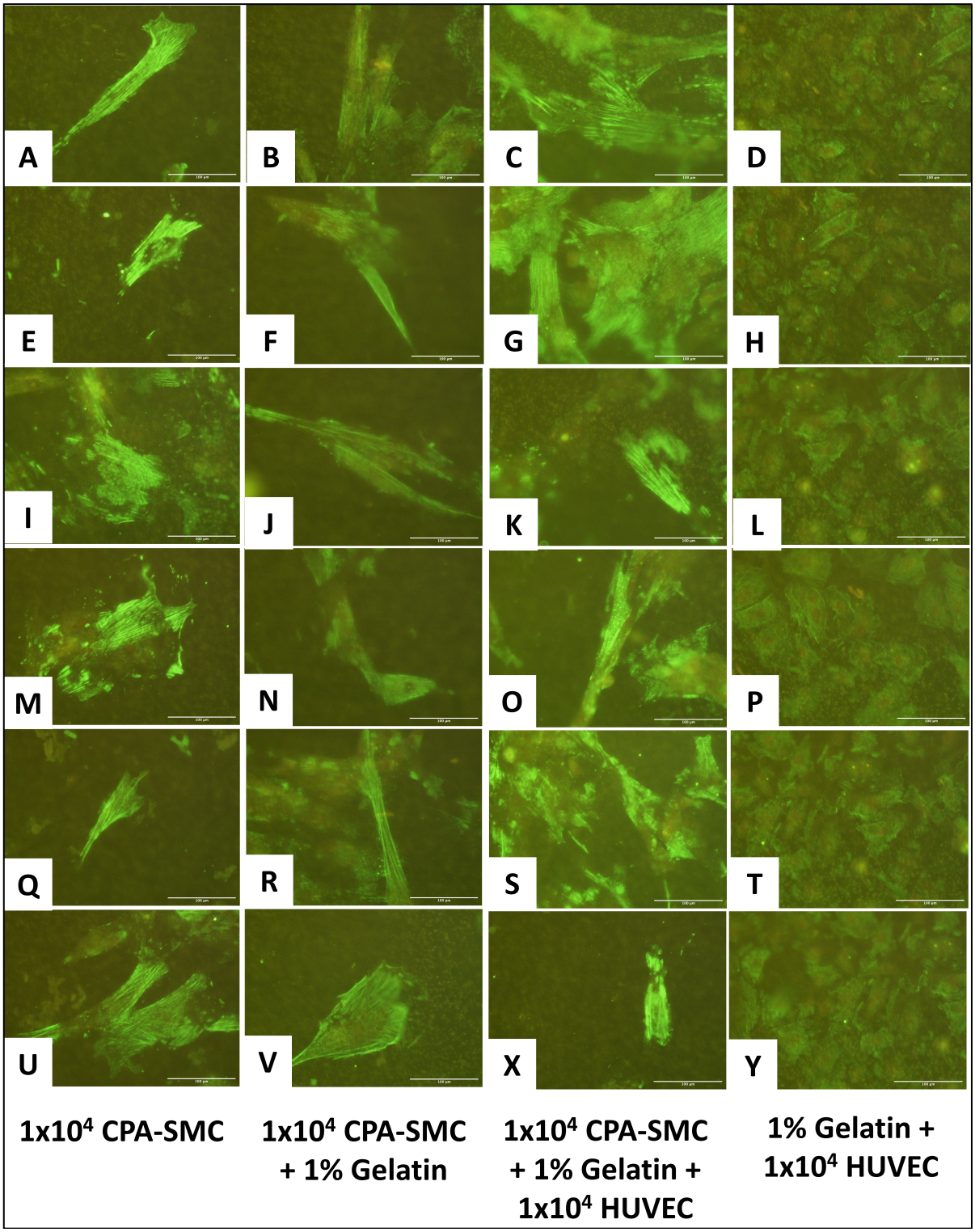


Figure 161. *This figure (panels **A-Y**) shows representative fluorescent micrographs of α smooth muscle actin immunolocalization in CPA-SMC and HUVEC cells in mono- or co-culture on 0.4μm pore size polyethylene terephthalate membrane inserts after the permeability assay was run. Scalebar 100μm.*

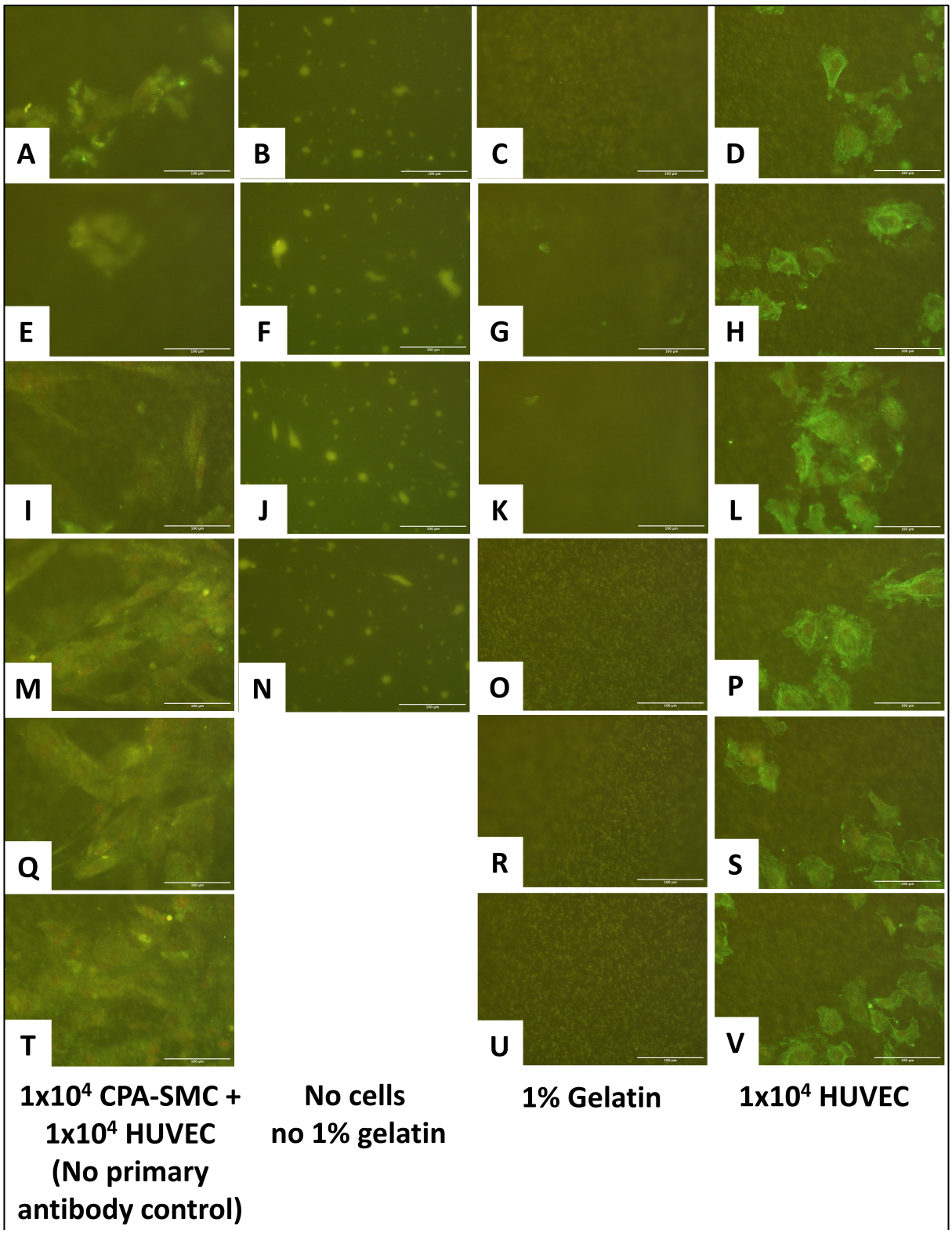


Figure 162. *This figure (panels **A-V**) highlights representative fluorescent micrographs for α smooth muscle actin immunolocalization in CPA-SMC and HUVEC cells seeded on 0.4μm pore size polyethylene terephthalate membrane inserts. Scalebar 100μm.*

5.3.9 There were no statistically significant differences in terms of tracer leakage levels between the coculture of human placenta chorionic plate artery smooth muscle cells with human umbilical vein endothelial cells and monoculture of primary endothelial cells at the same timepoints during the 120 minutes long permeability assay

Figure 163 highlights the cobblestone morphology of $6*10^4$ HUVEC cells originating from a healthy volunteer (N10072019) at passage 2 which have been cultured on transwell membrane inserts for 48 hours. This figure also shows that the HUVEC cells formed a confluent monolayer in the transwell inserts prior to the addition of CPA-SMC cells.

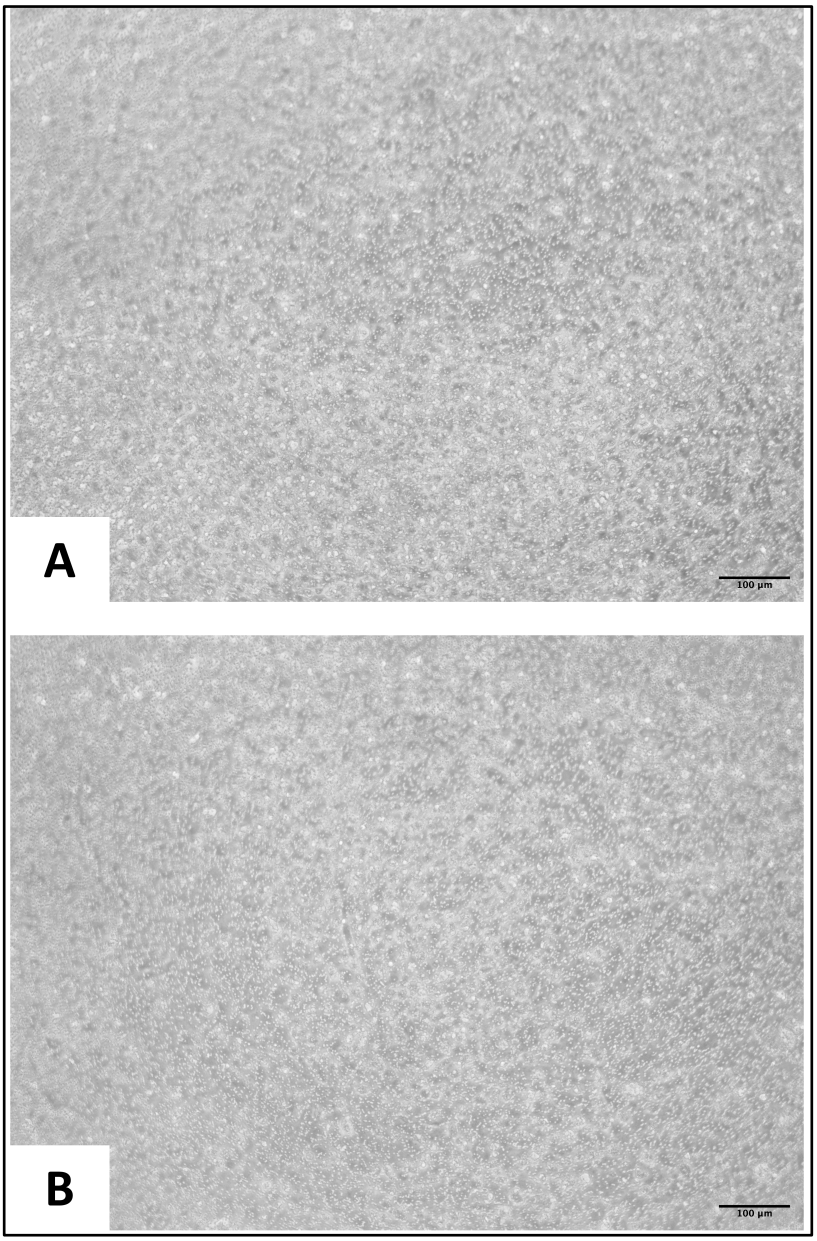


Figure 163. *This figure (**A-B**) shows the cobblestone morphology of 6*10^4 HUVEC cells originating from a healthy patient (N10072019) at passage 2 which have been cultured on transwell membrane inserts for 48 hours. In this case, the HUVEC cells formed a confluent monolayer in the transwells inserts prior to the addition of CPA-SMC cells. Scalebar 100µm.*

A Shapiro-Wilk test was used to evaluate the normal distribution of the permeability data which passed the normality test. A two-way ANOVA (****P<0.0001) with Geisser-Greenhouse correction (epsilon 0.6249) and Tukey's multiple comparison tests were performed between the control, mono- and co-culture experimental conditions at the same timepoints and showed that there were multiple statistically significant differences with P values highlighted in figure 164 and table 30. There were multiple statistically significant differences between 1%Gelatin and 1%Gelatin+HUVEC from 30 minutes until 120 minutes of the permeability assay with the highest difference at 60 minutes (****P<0.0001).

However, at the start of the assay (0 hours) there was no statistically significant difference (P=0.2048) between 1%Gelatin and 1%Gelatin+HUVEC experimental condition. In the case of comparing 1%gelatin with 1%gelatin+HUVEC+CPA-SMC, there were multiple significant gaps in terms of tracer leakage at all timepoints of the assay with a gradual decrease in significance from the beginning of the experiment towards the end (0 min ****P<0.0001, 30minutes ***P=0.0002, 60minutes ****P<0.0001, 90minutes **P=0.0019, 120 minutes *P=0.0121).

When the same statistical tests were conducted again between all permeability timepoints for each of the control, mono- and co-culture conditions, there were multiple statistically significant differences with P values highlighted in table 31. In all experimental conditions i.e. control, monoculture and coculture, there were multiple statistically significant differences of various degrees between all timepoints with the exception of 60 vs. 90 and 90 vs. 120 minutes. Additionally, in the 1% gelatin condition, further non-statistically significant timepoints were between 30 vs. 60 and 60 vs. 120 minutes.

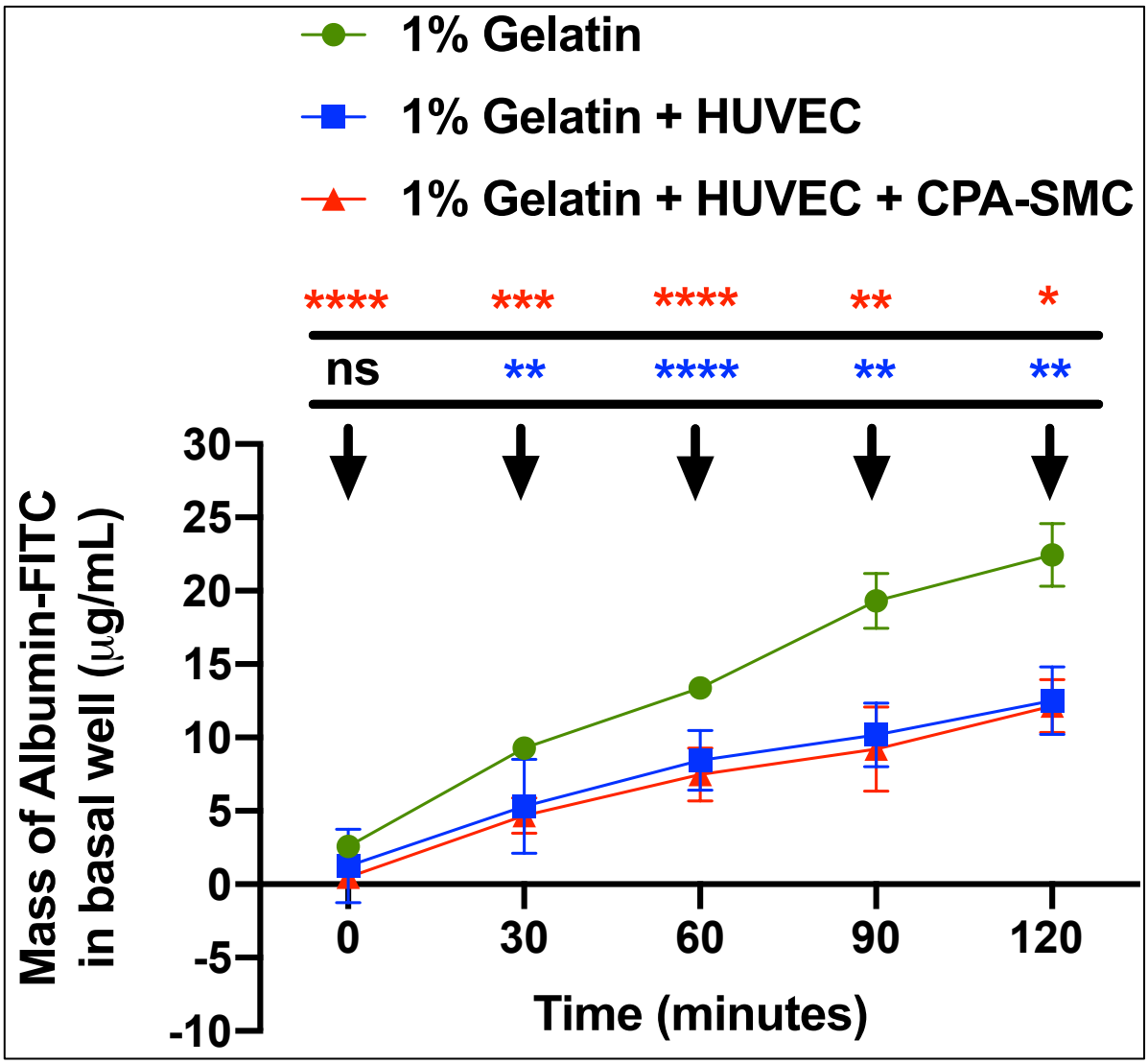


Figure 164. *This graph shows the accumulation of albumin-FITC over time in the basal compartment of the transwell system over a period of 2 hours involving control (1% gelatin), monoculture of HUVEC cells or co-culture of HUVEC with CPA-SMC cells on 1% gelatinised 12mm diameter 0.4µm pore polyethylene terephthalate membrane inserts. In total there were N=4 permeability experiments performed involving the isolation of human cells originating 7 different healthy patients. The permeability assay involving 1% gelatin condition was performed once in triplicate for the duration of 2 hours. In each assay undertaken, there were three inbuilt experimental repeats for each monoculture or co-culture conditions. Data are expressed as mean ± standard deviation. ns denotes not significant, blue stars highlight P value significance summary in control compared with monoculture condition, red stars suggest P value significance summary in control compared with coculture condition, black arrows link the P value significance summary to the corresponding timepoints, * P≤0.05, ** P≤0.01, *** P≤0.001, ****P≤0.0001.*

		Minutes				
		0	30	60	90	120
1% Gelatin vs. 1%Gelatin+HUVEC	Significance	No	Yes	Yes	Yes	Yes
	Summary	ns	**	****	**	**
	Adjusted P value	0.2048	0.0041	<0.0001	0.0062	0.009
1% Gelatin vs. 1% Gelatin+HUVEC +CPA-SMC	Significance	Yes	Yes	Yes	Yes	Yes
	Summary	****	***	****	**	*
	Adjusted P value	<0.0001	0.0002	<0.0001	0.0019	0.0121
1% Gelatin+HUVEC vs. 1%Gelatin+HUVEC +CPA-SMC	Significance	No	No	No	No	No
	Summary	ns	ns	ns	ns	ns
	Adjusted P value	0.5732	0.8061	0.4438	0.6332	0.8971

Table 30. *This table shows the results of Tukey's multiple comparisons test between the control, mono- and co-culture experimental conditions at the same timepoints related to the accumulation of albumin-FITC over time in the basal compartment of the transwell system highlighting the adjusted P values. ns denotes not significant, * P≤0.05, ** P≤0.01, *** P≤0.001, ****P≤0.0001.*

	1% Gelatin			1% Gelatin + HUVEC			1% Gelatin + HUVEC + CPA-SMC		
Minutes	**Significance**	**Summary**	**Adjusted P value**	**Significance**	**Summary**	**Adjusted P value**	**Significance**	**Summary**	**Adjusted P value**
0 vs. 30	Yes	*	0.0171	Yes	****	<0.0001	Yes	****	<0.0001
0 vs. 60	Yes	****	<0.0001	Yes	****	<0.0001	Yes	****	<0.0001
0 vs. 90	Yes	*	0.0158	Yes	****	<0.0001	Yes	****	<0.0001
0 vs. 120	Yes	*	0.014	Yes	****	<0.0001	Yes	****	<0.0001
30 vs. 60	No	ns	0.056	Yes	***	0.0007	Yes	****	<0.0001
30 vs. 90	Yes	*	0.015	Yes	**	0.0014	Yes	***	0.0006
30 vs. 120	Yes	*	0.0191	Yes	****	<0.0001	Yes	****	<0.0001
60 vs. 90	No	ns	0.1253	No	ns	0.3372	No	ns	0.444
60 vs. 120	No	ns	0.0548	Yes	**	0.0039	Yes	***	0.0002
90 vs. 120	No	ns	0.2671	No	ns	0.0735	No	ns	0.0861

Table 31. *This table shows the results of Tukey's multiple comparisons test with regards to the correlation between all permeability timepoints concerning each of the 1% Gelatin, 1%Gelatin+ HUVEC or 1%Gelatin+HUVEC+CPA-SMC experimental conditions. ns denotes not significant. * P≤0.05, ** P≤0.01, *** P≤0.001, ****P≤0.0001.*

5.3.10 Immunolocalization studies involving monocultures and cocultures of primary endothelial and smooth muscle cells showed VE-Cadherin staining as a thin or at parts thick uninterrupted or discontinuous line positioned at the paracellular overlapping regions between tightly arranged adjacent human umbilical vein endothelial cells

Figures 165-168 highlight 6 representative fluorescent images of the transwell membrane of each of the 1%gelatin, 1%gelatin+HUVEC and 1%gelatin+HUVEC+CPA-SMC experimental conditions showing VE-Cadherin (green) immunolocalization formed by human umbilical vein endothelial cell monolayers. Red arrows point towards the immunolocalisation of VE-Cadherin junctions in areas of cell-cell overlapping.

Due to the fact that the permeability tracer albumin was conjugated to fluorescein isothiocyanate and the secondary antibody used in the detection of VE-cadherin was also conjugated to FITC, many of the images acquired had a green non-specific background staining which might account for the albumin aggregates formed during the permeability study. However, this level of rounded patches of high brightness evenly distributed in the background of the micrographs taken was also detected in the control 1%gelatin only condition which further suggests that a small level of albumin-FITC might get trapped into the $4x10^6$ pores per cm^2 of the membrane inserts. VE-Cadherin was visualised as a thick line located between tightly packed adjacent HUVEC cells and also as an uninterrupted delicate line in the paracellular

overlapping locations of endothelial cells as highlighted in figures 166-168 by multiple red arrows in each of the images acquired.

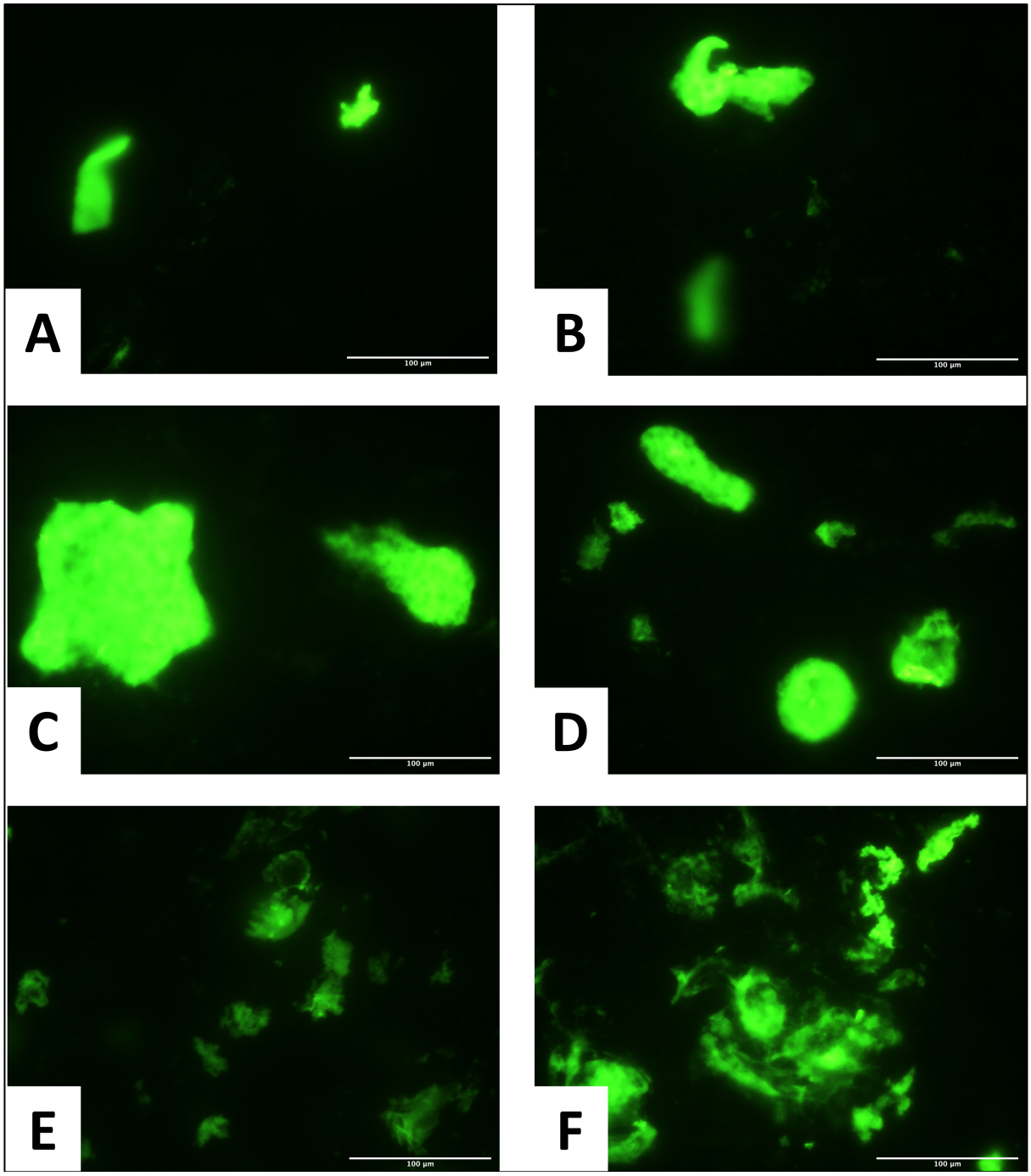


Figure 165. *This figure (panels **A-F**) highlights representative fluorescent images of VE-Cadherin (green) immunolocalisation in 1% gelatin experimental condition. Scalebar 100µm.*

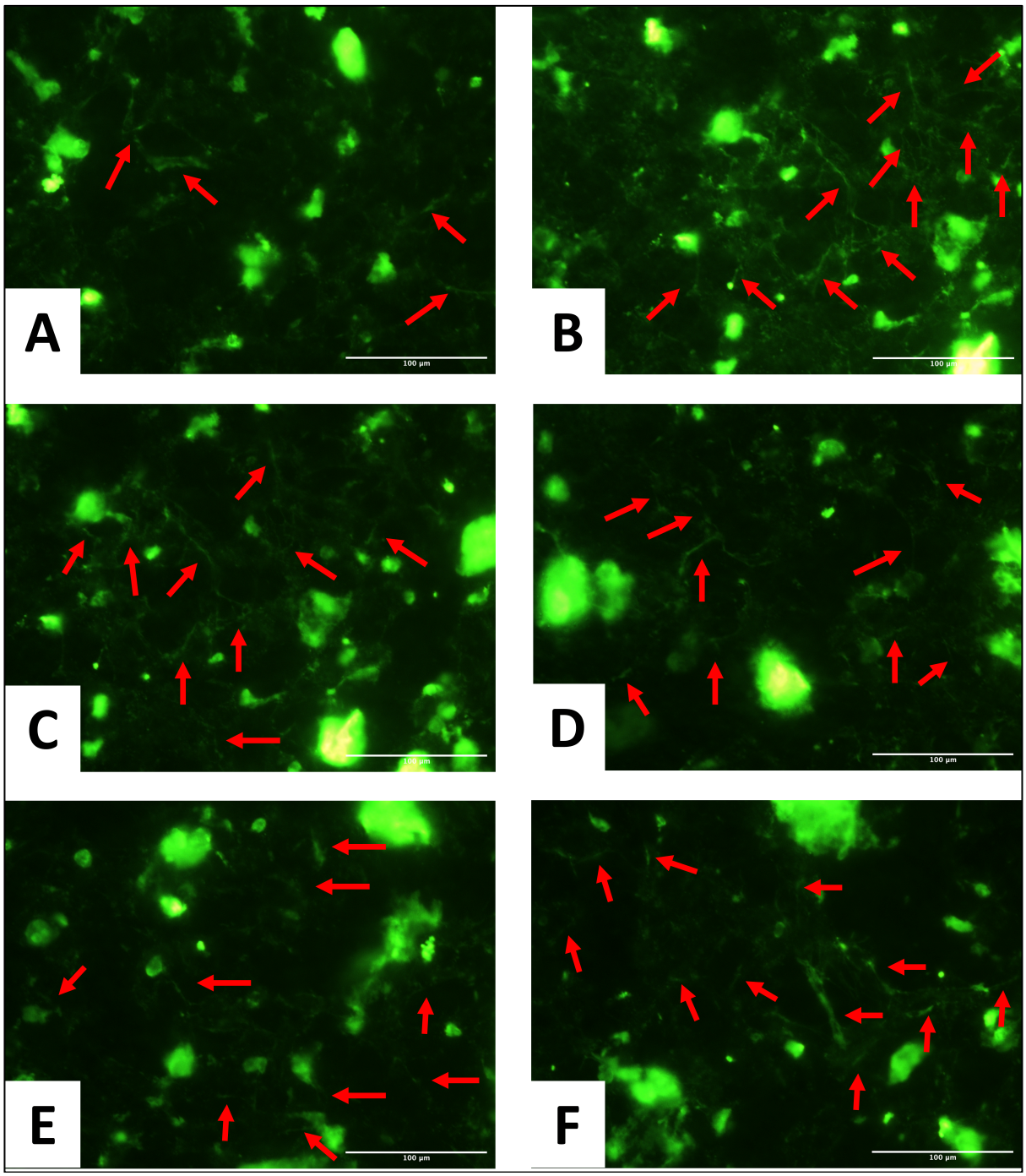


Figure 166. *This figure (panels **A-F**) comprises of representative fluorescent images of VE-Cadherin immunolocalisation (green) corresponding to 1%Gelatin+HUVEC experimental condition. VE-Cadherin was located at the paracellular overlapping regions of the HUVEC monolayer as a thick or at places delicate continuous or interrupted staining as highlighted by the red arrows in each of the images. Scalebar is 100µm.*

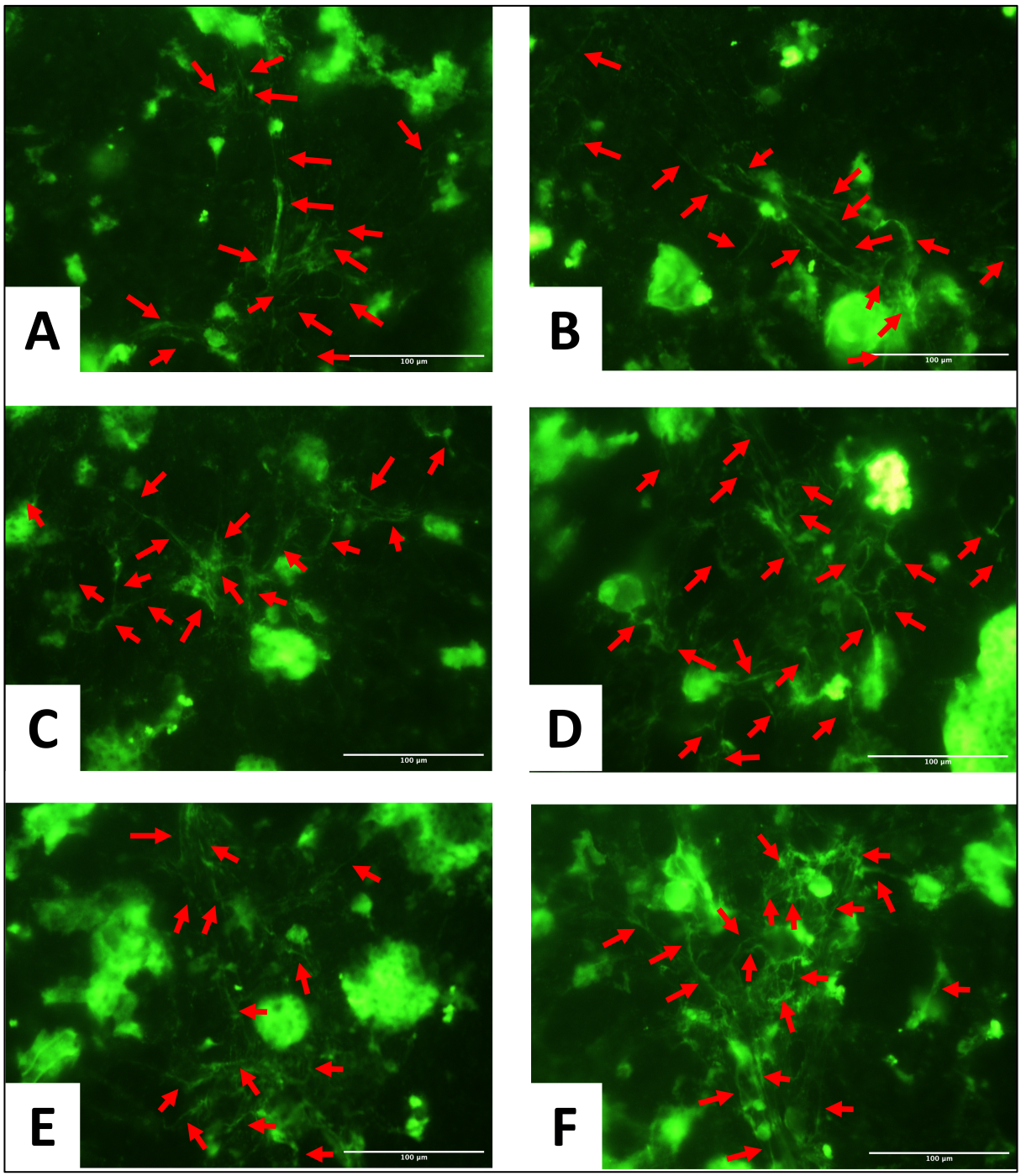


Figure 167. *This figure (panels **A-F**) comprises of representative fluorescent images of VE-Cadherin immunolocalisation (green) corresponding to 1%Gelatin+HUVEC+CPA-SMC experimental condition. VE-Cadherin was located at the paracellular overlapping regions of the HUVEC monolayer as a thick or at places delicate continuous or interrupted staining as highlighted by the red arrows in each of the images. Scalebar is 100µm.*

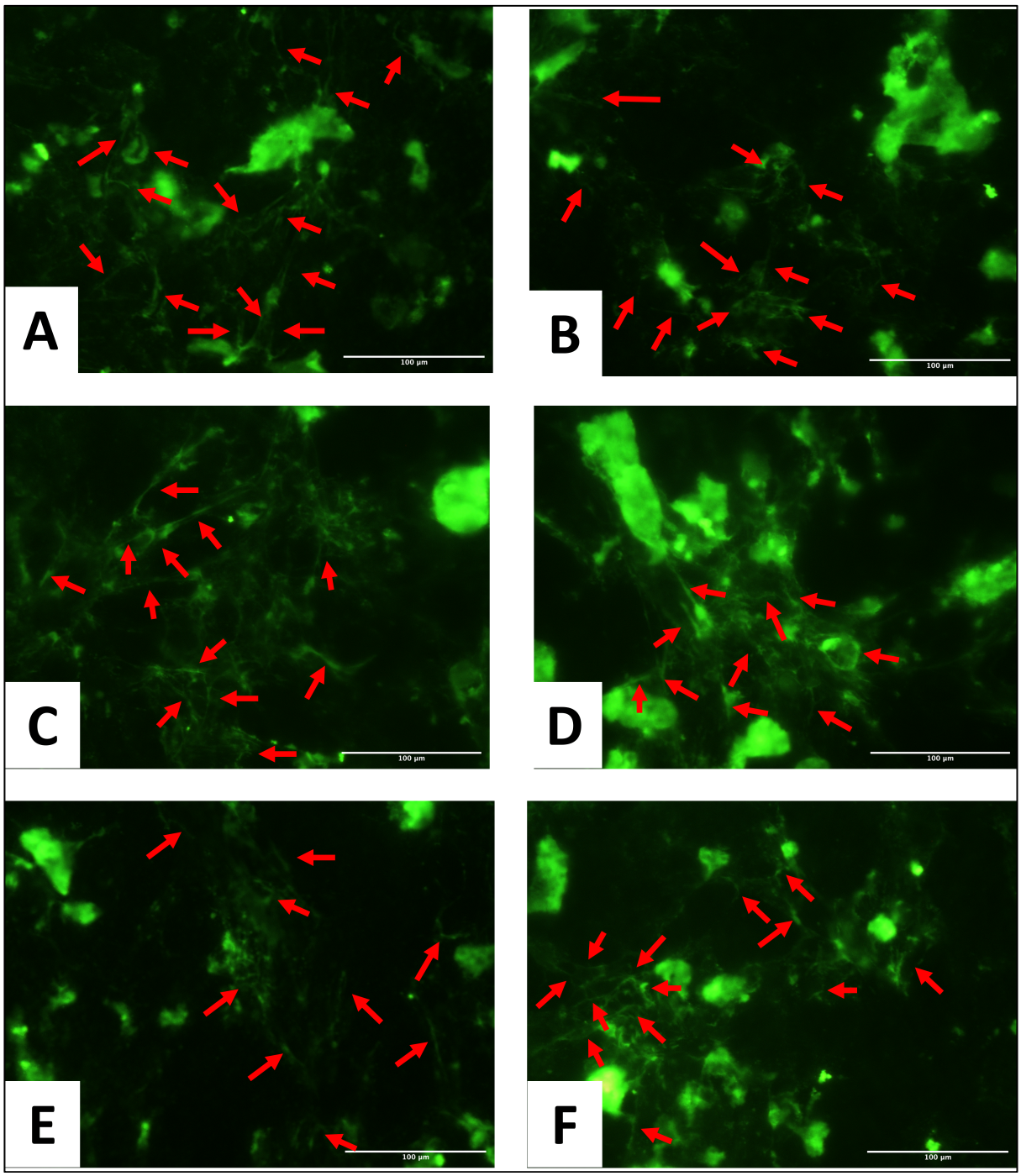


Figure 168. *This figure (panels **A-F**) comprises of representative no primary antibody control fluorescent images of VE-Cadherin immunolocalisation (green) corresponding to 1%Gelatin+HUVEC+CPA-SMC experimental condition. The non-specific binding of the secondary antibody (red arrows) was similar to the VE-Cadherin immunolabelling where the primary antibody against CD144 was present. Scalebar is 100µm.*

Immunofluorescence data highlights that in each of the three inbuilt experimental repeats (transwell assays) from the first permeability experiment of both 1% gelatin+HUVEC and 1%gelatin+HUVEC+CPA-SMC conditions, VE-Cadherin was immunolocalised at the level of the primary endothelial cell monolayer paracellular junctions as highlighted by the red arrows.

All transwell membrane inserts were again subjected to immunofluorescent investigation for the evaluation of VE-Cadherin junctional integrity and a potentially decreased formation of non-specific membrane bound albumin-FITC accumulations. Fluorescent images were acquired with all of the membrane inserts showing VE-Cadherin immunolocalisation in human umbilical vein endothelial cells monolayers and in co-culture with CPA-SMC as highlighted with red arrows in figures 170-172.

Although extensive washes of membrane inserts were performed prior to re-imaging the primary cells, the presence of albumin-FITC aggregates trapped in the 0.4μm pore size membranes was still noticeable in all of the micrographs acquired. VE-Cadherin was visualised as thick or delicate lines at the area of HUVEC paracellular junctions.

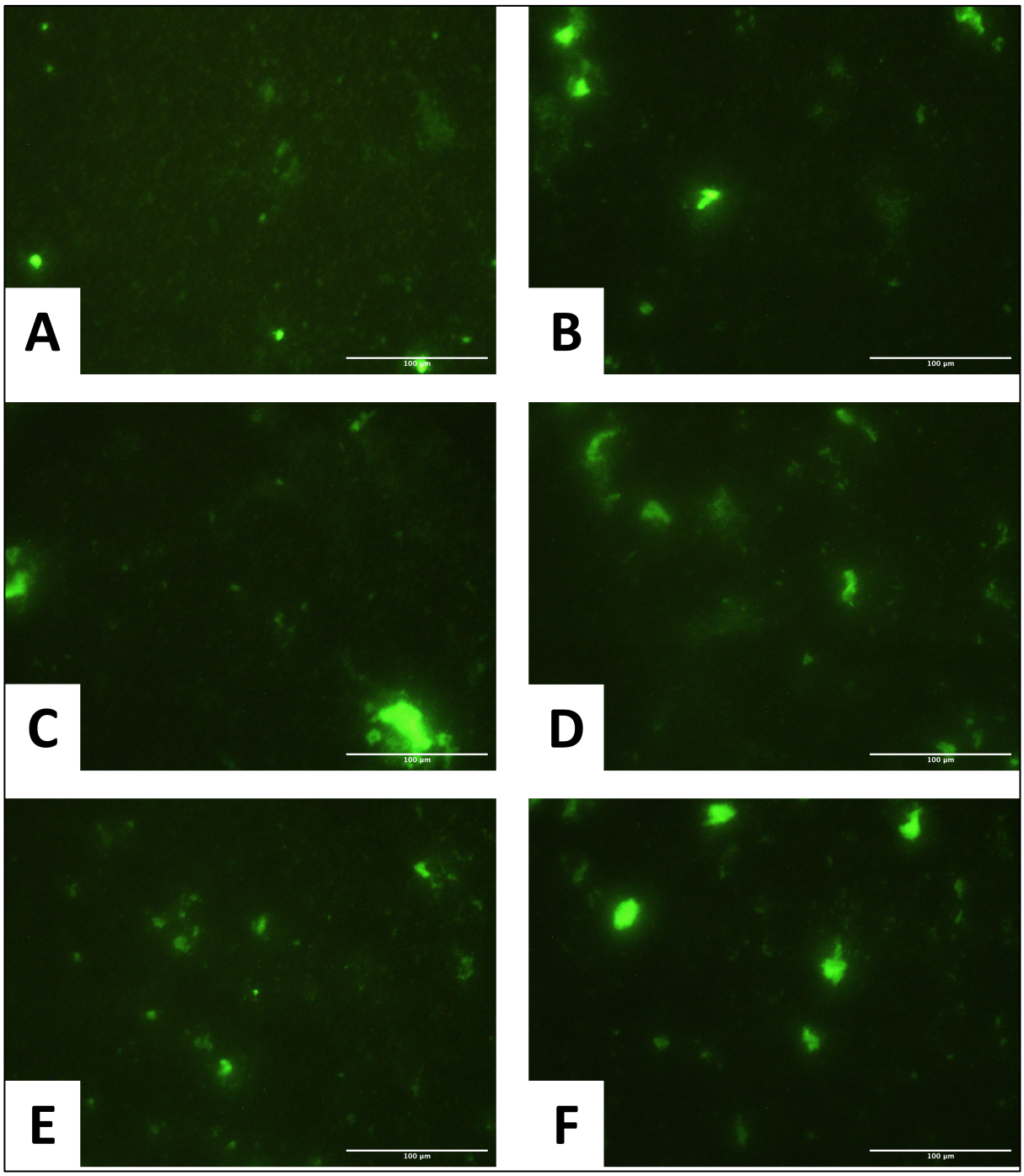


Figure 169. *This figure (panels **A-F**) highlights fluorescent images of VE-Cadherin (green) immunolocalisation in the re-washed 1% gelatin experimental condition. Scalebar 100µm.*

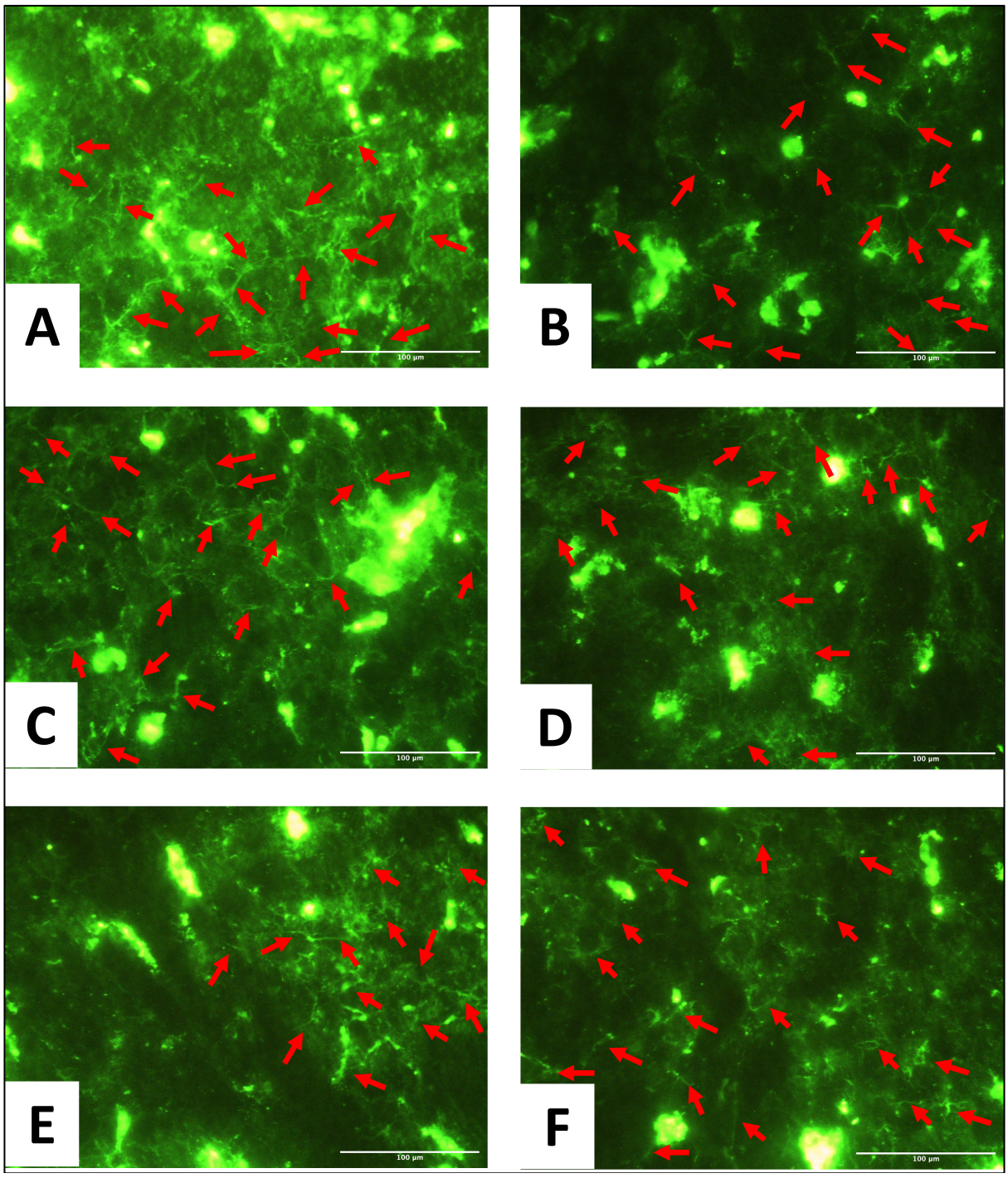


Figure 170. *This figure (panels **A-F**) comprises of representative fluorescent images of VE-Cadherin immunolocalisation (green) corresponding to the 1%Gelatin+HUVEC experimental condition following extensive washes of the transwell membrane insert. VE-Cadherin was located at the paracellular overlapping regions of the HUVEC monolayer as a thick or at places delicate continuous or interrupted staining as highlighted by the red arrows in each of the images. Scalebar is 100µm.*

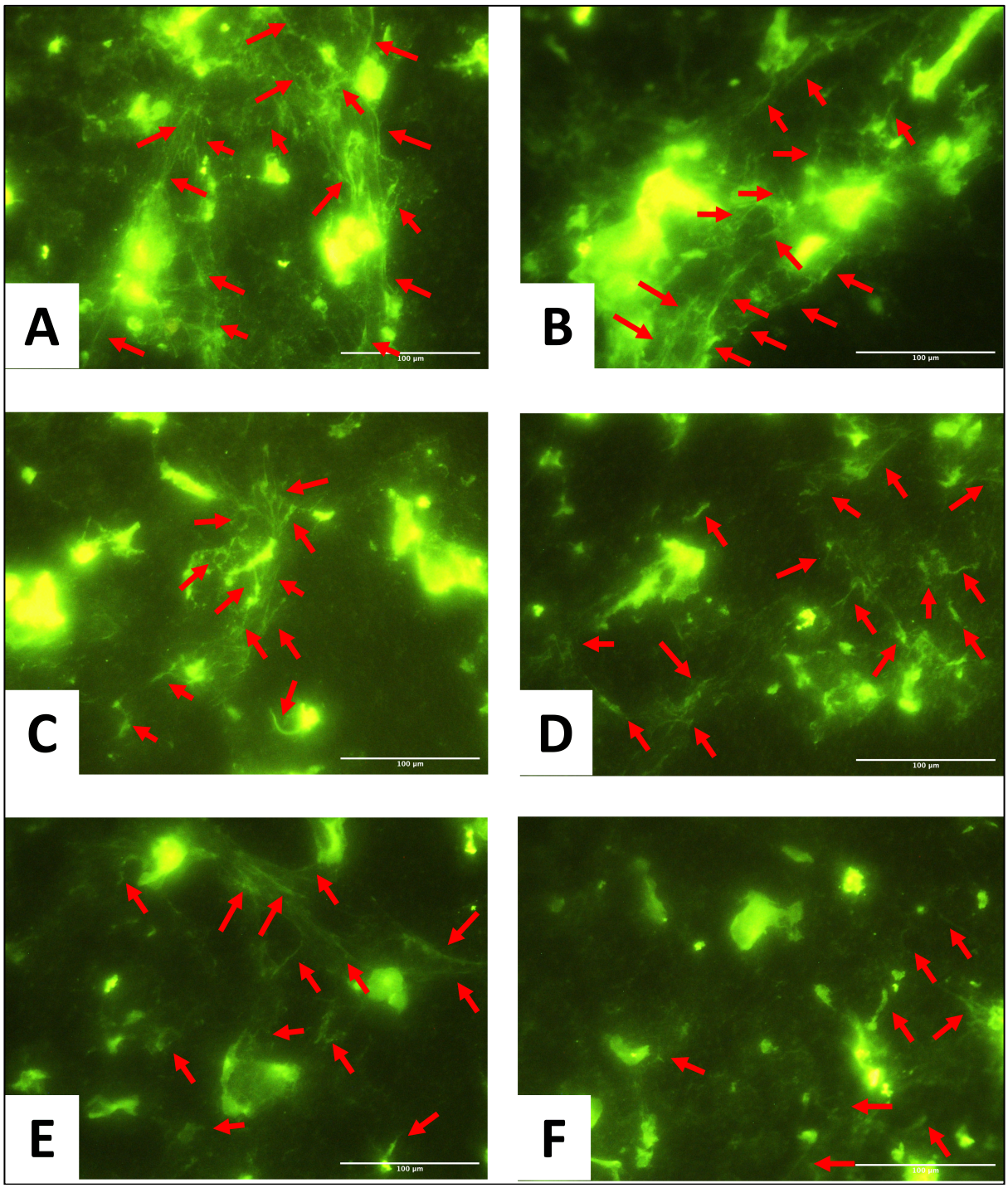


Figure 171. *This figure (panels **A-F**) comprises of representative fluorescent images of VE-Cadherin immunolocalisation (green) corresponding to the 1%Gelatin+HUVEC+CPA-SMC experimental condition following extensive washes of the transwell membrane insert. VE-Cadherin was located at the paracellular overlapping regions of the HUVEC monolayer as a thick or at places delicate continuous or interrupted staining as highlighted by the red arrows in each of the images. Scalebar is 100µm.*

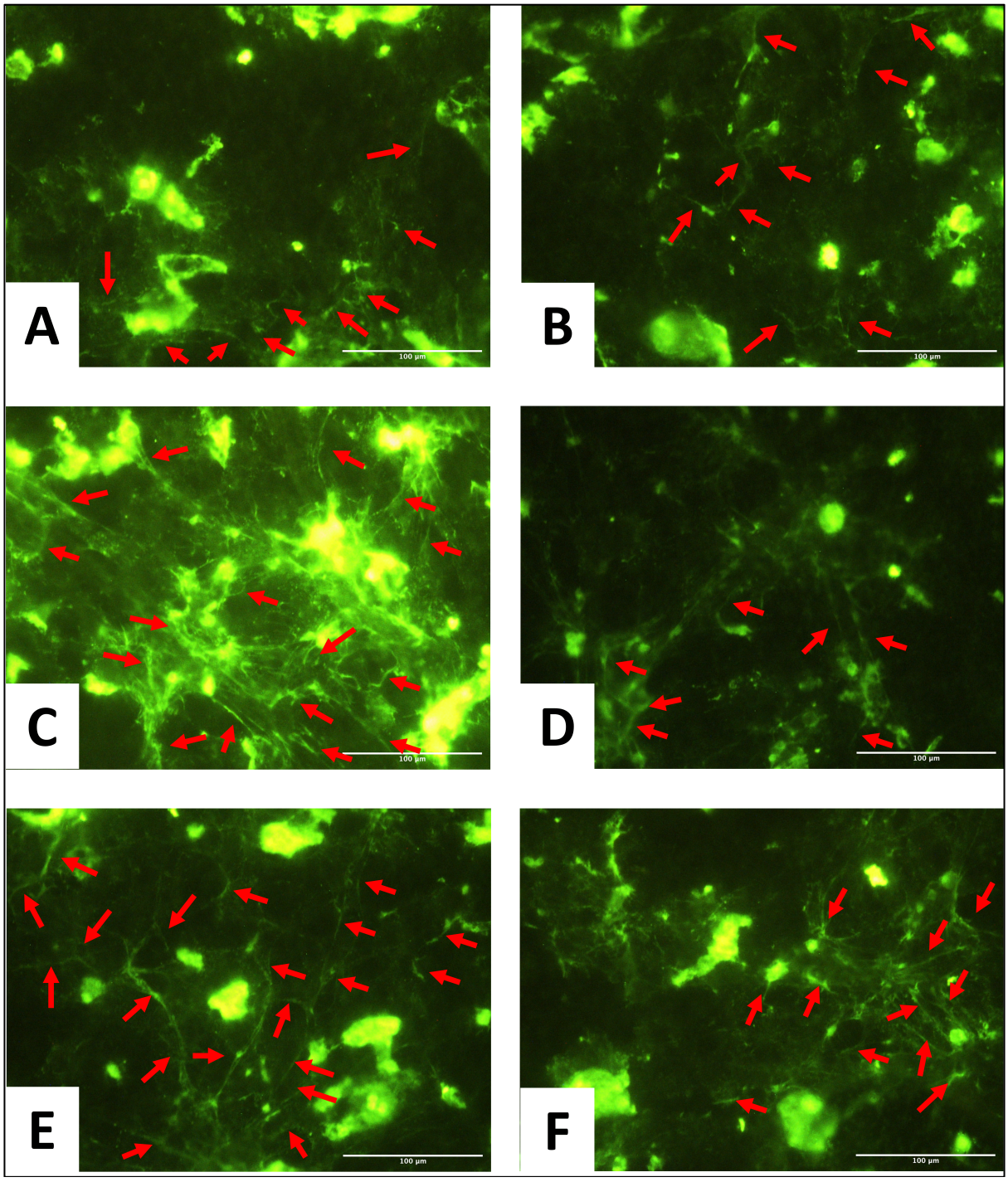


Figure 172. *This figure (panels **A-F**) comprises of representative no primary antibody control fluorescent images of VE-Cadherin immunolocalisation (green) corresponding to the 1%Gelatin+HUVEC+CPA-SMC experimental condition following extensive washes of the transwell membrane insert. Signs of non-specific binding of the secondary antibody (red arrows) were similar to VE-Cadherin immunolabelling where the primary antibody against CD144 was present. Scalebar is 100µm.*

Following extensive washes of all transwell membrane inserts for the purposes of reducing the non-specific background staining of membrane bound albumin-FITC tracer, immunofluorescent data of VE-Cadherin shown in figures 170-172 highlights that aggregates of the permeability tracer were still present evenly distributed in most of the images acquired. Also, as highlighted in figure 168 (before washes) and figure 172 (after washes) representing the 1%gelatin+HUVEC+CPA-SMC experimental condition, during the immunostaining for VE-Cadherin junctions, the primary antibody was replaced with 5% (v/v) normal human serum diluted in 0.1% (w/v) BSA/PBS to serve as a secondary antibody control. In this case, fluorescent micrographs show the presence of elongated green continuous lines of staining characteristic of VE-Cadherin as highlighted by the red arrows.

Red arrows highlight the VE-Cadherin immunolocalisation visualised as a prominent or delicate staining at the areas of paracellular endothelial cell overlap.

Following the second permeability experiment comprising of 1%gelatin+HUVEC and 1%gelatin+HUVEC+CPA-SMC culture conditions, a similar immunostaining protocol for VE-Cadherin junctions was performed with all transwell membrane inserts as highlighted in figures 173-174.

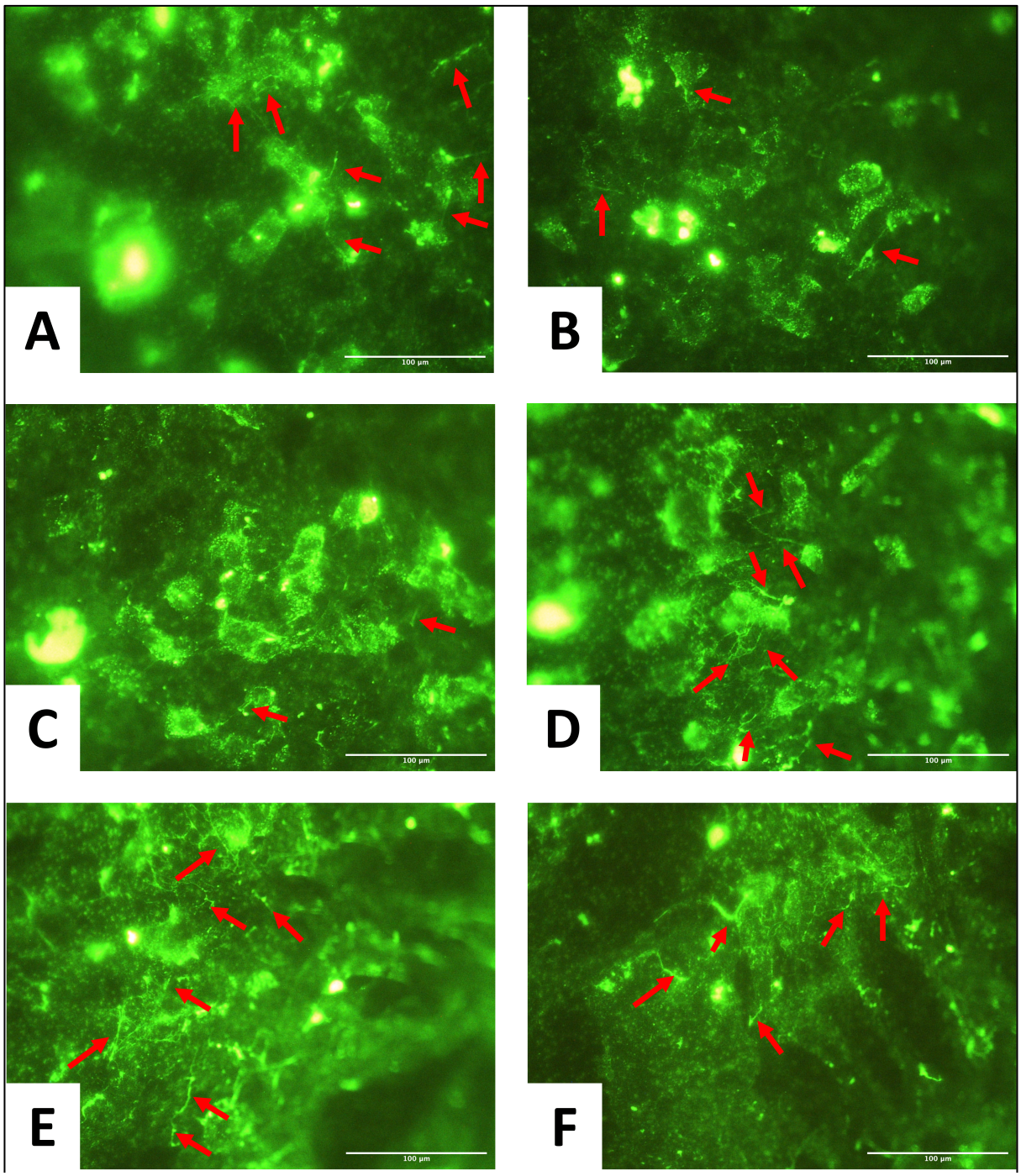


Figure 173. *This figure (panels **A-F**) comprises of representative fluorescent images of VE-Cadherin immunolocalisation (green) in the first replicate of the 1%Gelatin+HUVEC experimental condition. VE-Cadherin was located at the paracellular overlapping regions of the HUVEC monolayer as a thick or at places delicate continuous or interrupted staining as highlighted by the red arrows in each of the images. Scalebar is 100µm.*

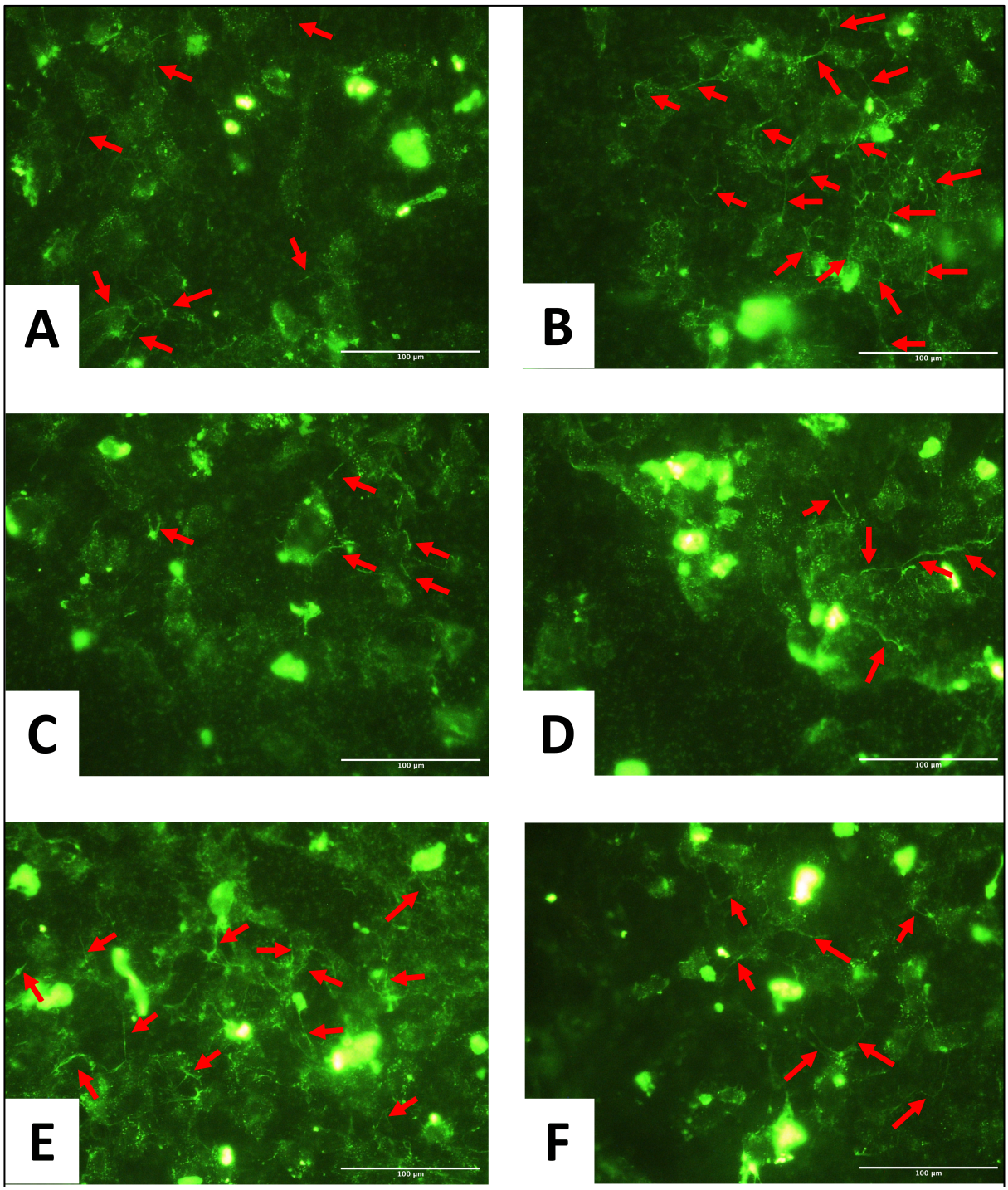


Figure 174. *This figure (panels **A-F**) comprises of representative fluorescent images of VE-Cadherin immunolocalisation (green) in the first replicate of the 1%Gelatin+HUVEC+SMC experimental condition. VE-Cadherin was located at the paracellular overlapping regions of the HUVEC monolayer as a thick or at places delicate continuous or interrupted staining as highlighted by the red arrows in each of the images. Scalebar is 100µm.*

In order to further investigate the origin of the non-specific background staining in the majority of all VE-Cadherin immunolocalization studies, one of the aims of the third and fourth permeability experiments was to replace the albumin-FITC tracer with unconjugated bovine serum albumin in the apical chamber of the transwell system at the same concentration of 1mg/mL.

In the case where only HUVEC cells were seeded on 1%gelatinised membrane inserts, some of the cells expressed α smooth muscle actin as highlighted in figures 175 and 176, panels A, D, G, J, M and P. In this experiment, there were very few signs of VE-Cadherin junctional staining both in monoculture and coculture of primary cells. However, there were no signs of non-specific background staining comprising of rounded shape evenly distributed bright spots as noticed in all fluorescent images of VE-Cadherin immunolocalization.

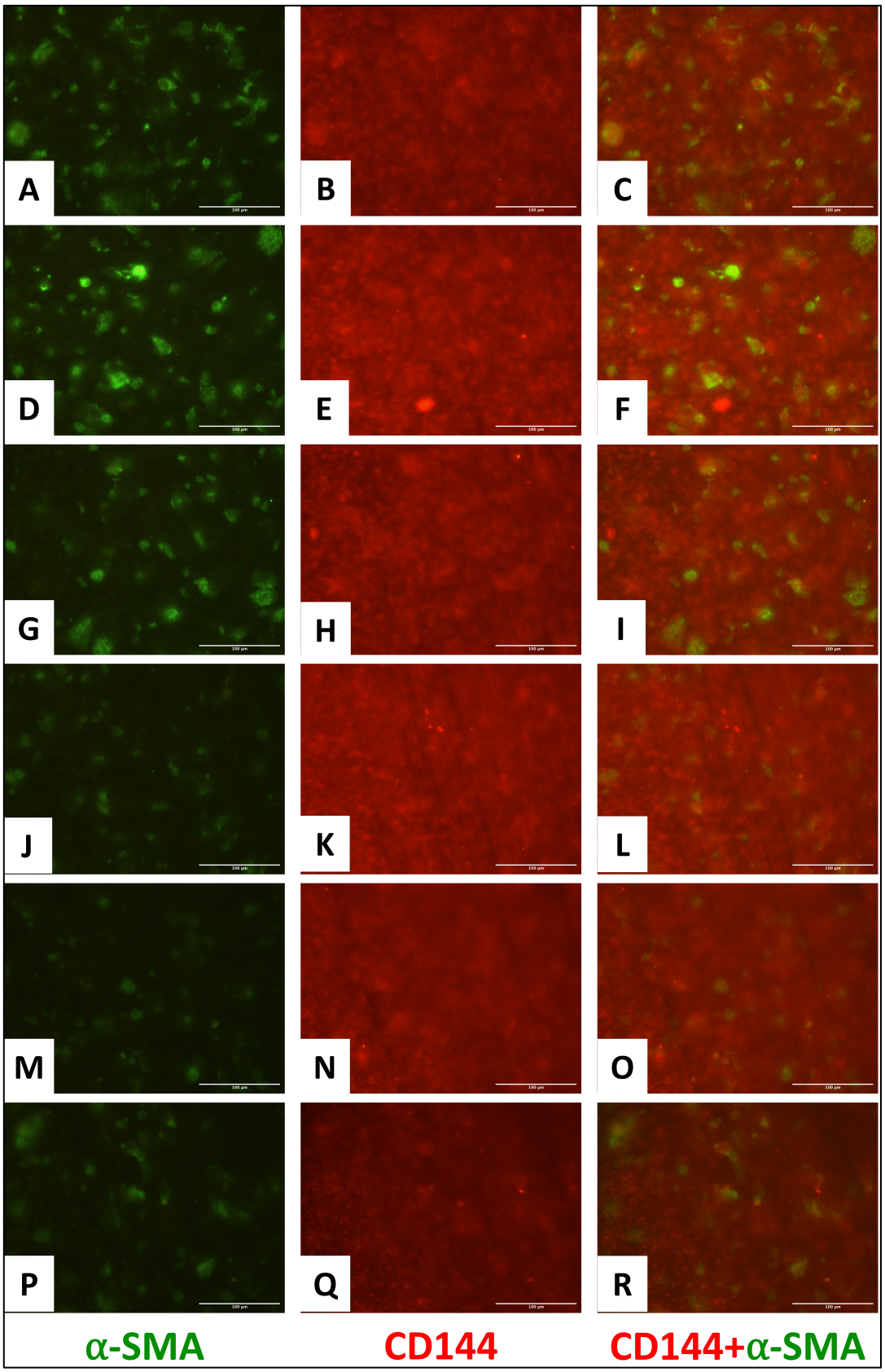


Figure 175. *This figure (**A-R**) shows representative micrographs of the immunolocalization of CD144 (red), α smooth muscle actin (α-SMA) - green and merged CD144+α-SMA in 1%gelatin+HUVEC cells seeded on 0.4μm pore size membrane inserts, where albumin-FITC was replaced with BSA. Scalebar 100μm.*

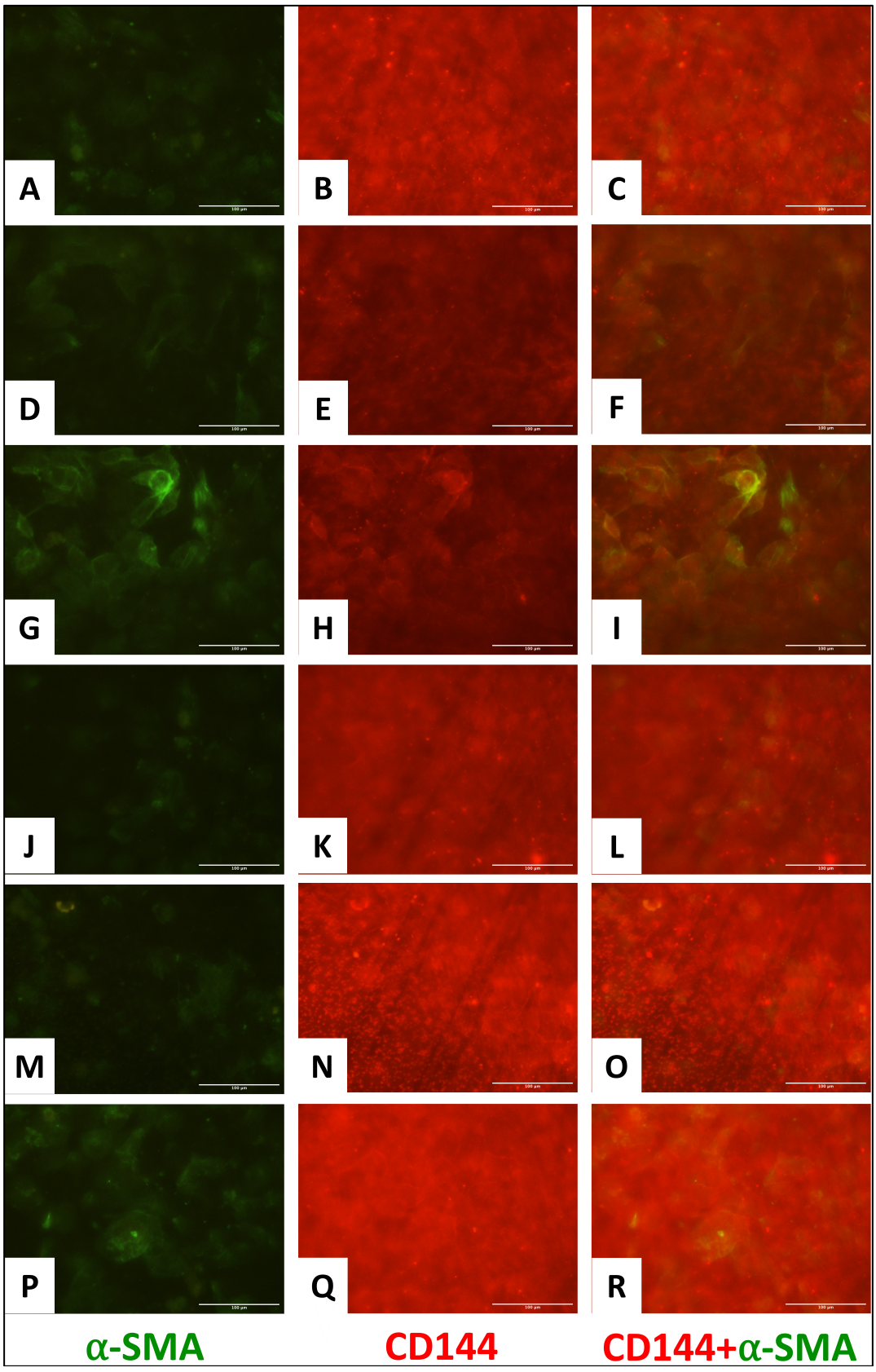


Figure 176. *This figure (**A-R**) shows representative micrographs of the immunolocalization of CD144 (red), α smooth muscle actin (α-SMA) - green and merged CD144+α-SMA in 1%gelatin+HUVEC+CPA-SMC cells seeded on 0.4μm pore size membrane inserts where albumin-FITC was replaced with BSA. Scalebar 100μm.*

5.3.11 Successful membrane labelling of human umbilical vein endothelial cells with PKH67 and human placenta chorionic plate artery smooth muscle cells with PKH26 revealed further potential opportunities of studying the trans-endothelial migration properties of smooth muscle cells across confluent primary endothelial cell monolayers

Fluorescent micrographs were acquired showing HUVEC (PKH-67 i.e. green) and CPA-SMC (PKH26 i.e. red) localisation on the membrane inserts as highlighted by figure 177 and figure 178. Figure 177 highlights that the immunolabelling of HUVEC cells with PKH67 was successful, as a considerable population of endothelial cells in each image stained green as shown in panels A, D, G, J, M, P. The characteristic morphology of HUVEC cells was also emphasized by the staining with PKH67, highlighting the cobblestone phenotype of these cells (figure 177, panels A, D, G, J, M and P; red arrows and figure 178, panels A, D, G, J, M and P; red arrows). Also, as there were no CPA-SMC cells seeded on these transwell inserts, there was no red staining with PKH26 highlighting the specificity of the experimental labelling procedure as shown in images B, E, H, K, N and Q. Figure 178 shows that when CPA-SMC cells were seeded above confluent HUVEC cells on the transwell membrane inserts, a red fluorescence signal was noticed highlighting the morphological appearance of smooth muscle cells as elongated with a spindle shape as presented in panels B, E, H, K, N and Q. This efficient method of double labelling of the cocultured primary cells may be useful for further *in vitro* complementary studies in terms of investigating the transendothelial migration properties of CPA-SMC across HUVEC monolayers

seeded on transwell membrane inserts with the help of confocal microscopy, live cell imaging and Z-stacks image acquisition.

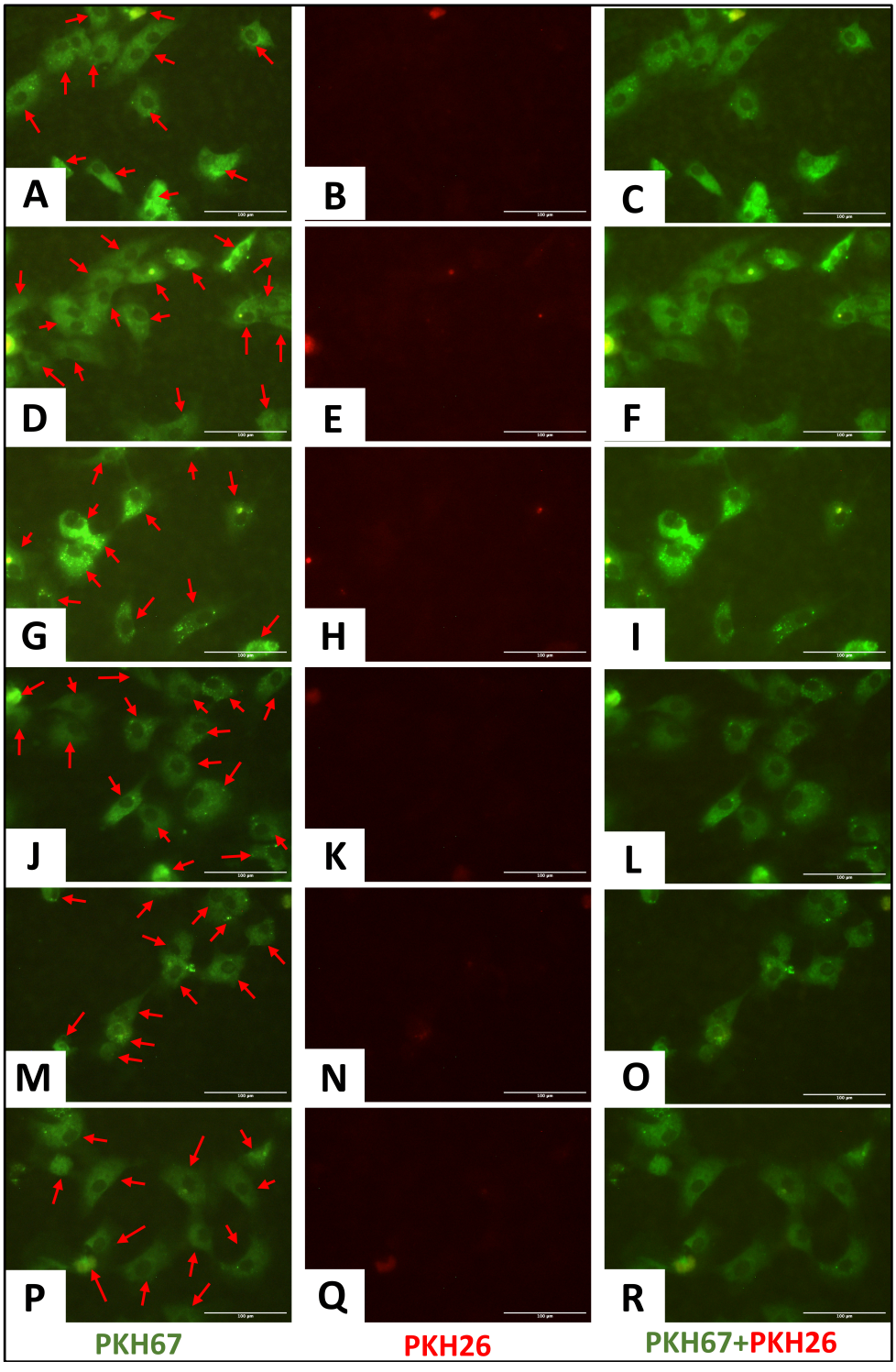


Figure 177. *This figure (panels **A-R**) highlights representative fluorescent micrographs of 1%gelatin+HUVEC condition in which HUVEC cells (N21082019, P3) were labelled with PKH67. Red arrows highlight the cobblestone appearance of HUVEC cells. In this case there were no CPA-SMC present in the transwell hence there is no red staining. Scalebar is 100μm.*

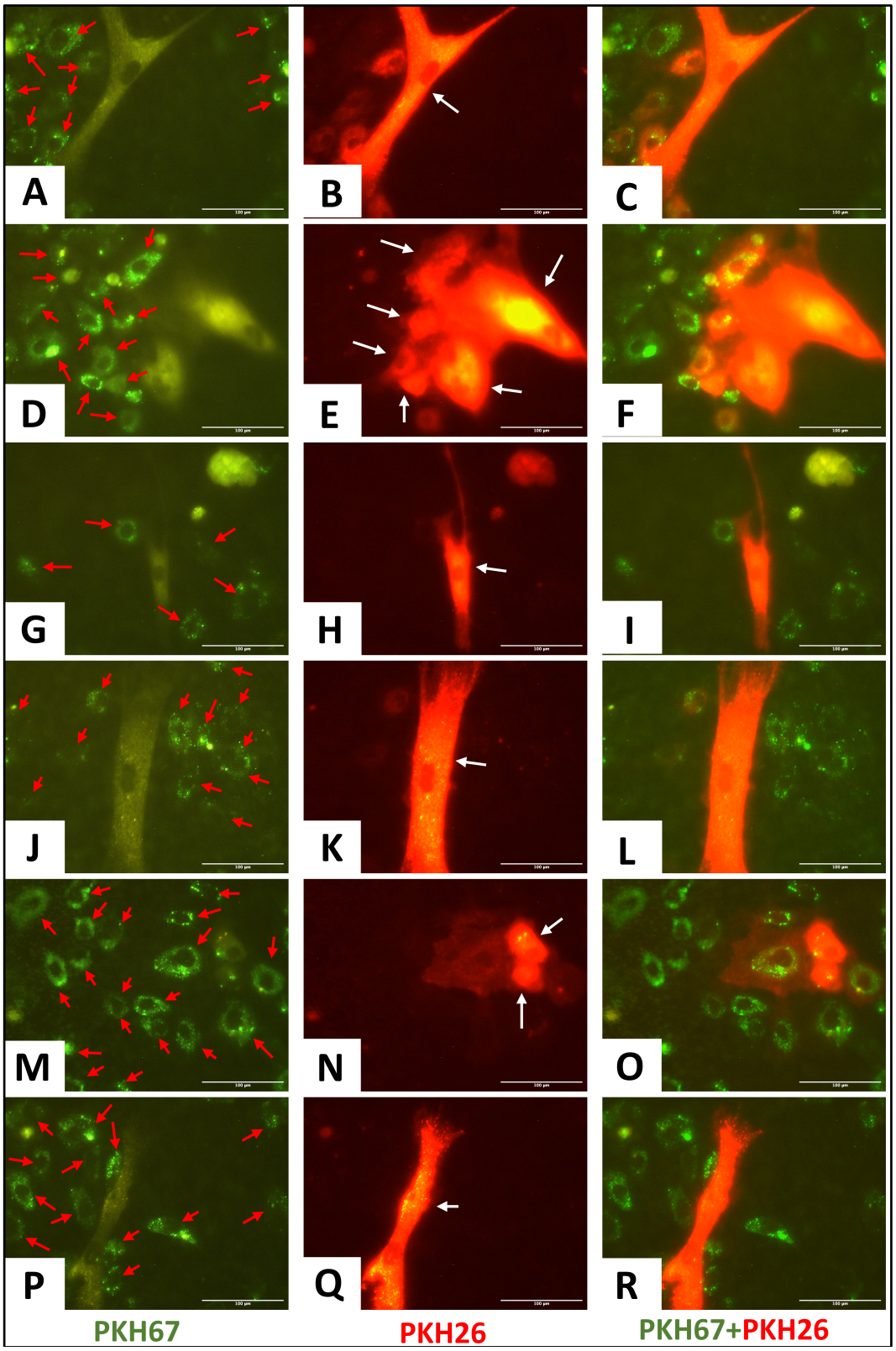


Figure 178. *This figure (panels **A-R**) highlights representative fluorescent micrographs of 1%gelatin+HUVEC+CPA-SMC condition in which HUVEC cells (N21082019, P3) were labelled with PKH67 and CPA-SMC cells (N18092019, P3) were labelled with PKH26. Red arrows highlight the cobblestone appearance of HUVEC cells. White arrows illustrate the hill and valley morphology of CPA-SMC cells. Scalebar is 100μm.*

5.4 Discussion

This study provides evidence of a functional *in vitro* model of a human chorionic vessel via the formation of a HUVEC monolayer on transwell membrane inserts for the duration of 48 hours post-seeding followed by the coculture of HUVEC with CPA-SMC cells for a further 26 hours prior to the start of the permeability assay. After the bilayer was obtained, a total of N=4 permeability assays were undertaken consisting of three experimental conditions (1%gelatin, 1%gelatin+HUVEC, 1%gelatin+HUVEC+CPA-SMC) which were repeated three times during each of the tracer leakage assays using isolated human placental primary cells originating from 7 healthy patients. Overall, under the conditions of the present study, the permeability data highlighted that CPA-SMC's do not significantly alter the tightness of the bilayer compared to monoculture of HUVEC cells during all timepoints of the tracer leakage assay. This finding suggests that there are no differences in endothelial paracellular barrier integrity between monoculture of HUVEC cells and coculture of HUVEC with CPA-SMC cells.

5.4.1 Isolation, culture and characterisation of human placenta chorionic plate artery smooth muscle cells

A similar arrangement of isolated human vascular smooth muscle cell cultures has been characterised before [700–702]. A study has highlighted that the phenomenon giving rise to the formation of nodules was also present in monocultures of isolated vascular smooth muscle cells originating from nonatherosclerotic areas of human aortas [703]. Moreover, the same study by Proudfoot and colleagues (1998) has highlighted that isolated human placental pericytes originating from placental villi also possessed the characteristic of nodule formation in primary pericyte cultures. Here,

the authors have suggested that the formation of nodules was characteristic of postconfluent cultures, giving rise to the precipitation of a mineralised matrix following one month in culture conditions, which was a requirement for calcification mainly represented by needle-like crystals and oval artefacts [703]. The current results may indicate that the isolated CPA-SMC cells could play an important role in promoting calcification potentially at an *in vivo* level. This pattern of closely arranged primary vascular smooth muscle cell cultures forming nodular aggregates has also been characterised by Björkerud and colleagues [702].

The current study evaluated that the CPA-SMC population doubling time was 15.38±13.52 days (mean ± S.D.). Here, the isolated primary smooth muscle cells have shown expression of α smooth muscle actin which was evenly distributed on the microfilament bundles. A similar morphology has been reported by Leik *et al* (2004) for CPA-SMC characterised by a ribbon shape and proliferated in a parallel arrangement [502]. α smooth muscle actin was found on the smooth muscle cells of chorionic plate arteries *in vivo* [501]. The morphology of isolated CPA-SMC cells by enzymatic digestion resembles the long oval shaped cells obtained in our study using the explant culture method [501].

A limitation of the methodology used in isolating the CPA-SMC cells is that the explant culture approach takes approximately 21-28 days until the primary smooth muscle cells originating from placental samples of healthy patients are sourced.

It is well recognised that maternal diabetes mellitus notably influences placental angiogenesis [704]. Although pregestational diabetes could alter the placental and fetal growth, the elevated blood glucose levels of gestational diabetes mellitus arise during the gestation period and clinically manifest only towards the end of the second trimester [704]. As a result, gestational diabetes mellitus could regulate the placental

metabolism especially during the advanced stages of the gestation period from the point of view of microvascular remodelling and angiogenesis [704]. In type 1 diabetes, the capillary surface area is elevated from the perspective of both increased ramifications of villous capillaries and lengthwise growth [102,103,705,706]. Complementary findings have also shown that in the case of placental samples originating from pregnancies complicated by gestational diabetes mellitus an elevation in the capillary ramification [707] and capillary surface area takes place [708]. In the case of type 1 diabetes, a 2-fold elevation in the number of redundant connections per villous was observed while in pregnancies complicated by gestational diabetes mellitus, a 1.8-fold increase of the same connections was reported [707,709]. From an angiogenesis point of view, these observations may explain the elevated proliferation of the isolated CPA-SMC cells *in vitro* originating from placental samples of pregnancies complicated by gestational diabetes mellitus or type 1 diabetes.

The surface antigenic profiling of CPA-SMC revealed that most isolated primary cells originating from placental samples of healthy and gestational diabetic patients were positive for mesenchymal stem cell markers CD73, CD90 and CD105, suggesting a potential involvement of these cells in tissue regeneration and also possessing an immunophenotypic signature similar to Wharton's Jelly Mesenchymal Stem Cells (WJ-MSC) [710]. These WJ-MSC cells are considered of an embryological state and represent the transition between embryonic and adult stem cells [710]. Furthermore, these primitive stem cells have been inducted to differentiate into chondrocytes [711], osteoblasts [712] and adipocytes [713] but also into cardiomyocytes and endothelial-like cells under the influence of certain conditions [714,715]. CD73 is a homodimeric enzyme with 5'-ectonucleotidase activity that dephosphorylates extracellular 5'-adenosine monophosphate to adenosine and phosphate [185]. The

enzyme exists in two forms: the first one is bound to the outer plasmalemma through glycosylphosphatidyl inositol [716] and the other soluble and free to circulate in blood [717]. CD90 is a 25-37 kDa glycosylphosphatidylinositol bound glycoprotein [718] that is known to be expressed in humans on fibroblasts, neural cells, early T and B lymphocytes, thymocytes, hematopoietic stem cells, endothelial cells, a few hematopoietic progenitors and <1% of peripheral blood T cells [719,720]. This cellular marker is involved in the regulation of cellular adhesion, T-cell activation [721], tumor growth, migration, neurite outgrowth, wound healing [722], fibrosis [723], fibrogenesis [724] and apoptosis [720]. Also, CD90 modulates cytoskeleton organisation, fibroblast focal adhesion and cell migration [725]. CD105 (endoglin) is a homodimeric cell membrane glycoprotein of 180kDa composed of disulphide-linked subunits of 95kDa [726] which participates in angiogenesis and is a dominant marker of neovascularization [727]. CD105 is particularly expressed on cellular lineages within the vascular system especially on endothelial cells [726,728], but also highly expressed on the syncytiotrophoblast layer of term placenta [729]. Since the morphology of CPA-SMC cells *in vitro* resembled a similar appearance to isolated Wharton's Jelly Mesenchymal Stem Cells (WJ-MSC) in terms of elongated spindle shape fibroblast-like cells [730], the confirmation that the smooth muscle cells are positive for CD73, CD90 and CD105 further suggests that the primary SMC cells may have originated from differentiated WJ-MSC cells, as it has been demonstrated that functional SMC cells can be derived from human MSC cells from the umbilical cord upon TGFβ1 stimulation *in vitro* [731]. The statistically significant decrease in the expression of CD90 identified in CPA-SMC cells originating from placental samples of gestational diabetic patients compared to healthy volunteers may suggest that the isolated primary cells could have been exposed to prolonged mechanical stress during the gestation period, since a study by

Wiesmann *et al* (2006) has shown that mechanical stimulation of cultured human MSC cells caused a marked decrease in CD90 expression compared to unstimulated stem cells [732]. Also, a study by Moraes *et al* (2016) has showed that a decrease in CD90 expression of mesenchymal stromal cells enhances their osteogenic and adipogenic differentiation *in vitro* which suggests that CD90 regulates the differentiation of MSC by acting as an obstacle in the pathway of differentiation commitment [733]. As a result, the decrease in CD90 expression in CPA-SMC cells originating from gestational diabetic patients may promote the potential dedifferentiation capability of the primary cells to a synthetic phenotype (especially in the case of cardiovascular pathologies [734]) which has been shown to participate in the formation of neointima by decreasing the expression of contractile proteins and elevating the migration, proliferation and the production of matrix protein [735].

5.4.2 Isolation, culture and characterisation of human umbilical vein endothelial cells

The current research provides further evidence that the well-established methodology of HUVEC cell isolation initially described by Jaffe and colleagues in 1973 remains the most advantageous approach to source and establish the human endothelial cell culture [504]. HUVEC cells showed a typical cobblestone monolayer appearance as highlighted in multiple *in vitro* investigations from our laboratory (chapter 5.3.2 and chapter 5.3.9) [119,483,736,737]. The doubling time of HUVEC cells was 2.158±0.3893 days (mean ± S.D.) which is similar to the published literature [738]. Bagley *et al* (2003) differentiated bone marrow progenitor cells and found them to have a similar doubling time to that seen in this study [738].

In our study, HUVEC cells demonstrated a diameter of 20 to 60μm in size. This agrees with a published study which also reports a broad size range of 30 to 50μm

wide [736]. The functionality of this pattern has not been elucidated yet. Moreover, HUVEC monolayers in culture and did not give rise to nodules (as observed with isolated primary smooth muscle cells) at all stages.

5.4.3 Permeability of CPA-SMC and HUVEC coculture model

These permeability studies are the first to show that the isolated human placenta chorionic plate artery smooth muscle cells do not induce significant changes in paracellular tracer leakage in human umbilical vein endothelial cell monolayers. There was a statistically significant difference between 1% gelatin and monoculture of HUVEC cells at 30, 60, 90 and 120 minutes of the permeability assay which suggests that the isolated endothelial cells were able to form a monolayer that restricted the passive leakage of albumin-FITC from the apical to the basal chamber of the transwell system. Similarly, a statistically significant difference was observed between 1% gelatin and coculture of HUVEC+CPA-SMC cells at all timepoints of the tracer leakage assay denoting that the established bilayer notably restricted the crossing of albumin-FITC from the apical to basal compartment.

The most important finding emerging from the permeability assays was that CPA-SMC cells neither tighten nor loosen the monolayer barrier formed by HUVEC cells for the duration of the entire tracer leakage investigation. These results suggest a limited capability of smooth muscle cells to significantly alter the integrity of paracellular junctions formed between adjacent HUVEC cells following the 26-hour period of *in vitro* coculture.

The cross-talks between endothelial cells and smooth muscle cells have been investigated to reproduce physiological [739], atherosclerotic blood vessel wall [740,741] or to induce angiogenesis [742]. There are multiple coculture models which have been

published where the smooth muscle cells and endothelial cells (EC's) were cultured on each side of membranes [743–746] or cultured on gels with EC's embedded which were composed of collagen or various polymers that incorporated SMC's [747,748], spheroid-bound smooth muscle cells or endothelial cells [749,750], coculture of EC right above SMC's [751,752] or even cells cultured next to each other [753,754]. Further studies have also assessed the potential interactions of EC's with SMC's using conditioned culture media [745,755] as an indirect method. The consensus appears to be that the co-cultures where ECs are in direct contact with SMCs provide the best model of mimicking the spatial arrangement of cells in arteries and the interaction between the two cell types.

Also, there is good evidence that the placental morphology and function is maintained following cotyledon perfusion for several hours as it has been shown for instance in a study by Eaton *et al* (1993) which has presented evidence of the first measurements of fetal villous microvascular permeability-surface area products originating from isolated lobules of healthy term human placental samples via a well-documented, multiple tracer dilution methodology [123]. In this case, the perfusate of both maternal and fetal circuits contained M199 tissue culture medium supplemented with 2.2g/L sodium bicarbonate, 100μM adenosine, 2mg/L cyanocobalamin, 8g/L dextran and in a few cases the perfusate also contained 5g/L bovine albumin [123]. Furthermore, another study by Leach *et al* (1991) which investigated the intracellular routing of immunoglobulin G in the human placenta also used an independent closed-circuit perfusion of the fetal villous circulation which contained a perfusate comprising of fetal blood and M199 medium supplemented with 19000 molecular weight dextran [756]. This investigation by Leach *et al* (1991) highlighted that at the level of the human placenta, maternal IgG binds to Fc gamma receptors on the syncytiotrophoblast and

takes a transcellular rather than paracellular route when crossing the fetal capillaries in order to reach the fetal blood [756]. In both studies, preparations were perfused for an initial stabilizing period of 20 minutes [123] or 30 minutes [756] for the purposes of restoring physiological placental function and structure after hypoxia and ischaemia related to the delivery of the human placenta [757,758].

The current human coculture model where the endothelial and smooth muscle cells are in direct contact reproduces the proliferation state and microenvironment of a placental chorionic blood vessel with an extracellular milieu that facilitates a short diffusion distance of cellular mediators between the primary cultured cells [759]. As the HUVEC and CPA-SMC cells were cultured in close vicinity to each other, the synthesis of extracellular matrix proteins may change. Although endothelial cells may infiltrate into gels composed of collagen and to give rise to networks *in vitro,* this architecture is not robust [759]. On the other side, if endothelial cells are cocultured with smooth muscle cells, the SMC's supress EC growth and the endothelial cells may give rise to the generation of capillaries and to produce collagen type IV [742]. In a study investigating the effects of mural cells in regulating vascular maturation, Evensen and colleagues have highlighted that the coculture of HUVEC with human pulmonary artery smooth muscle cells or mesenchymal stem cells gives rise to the formation of capillary-like structures [760]. In this context, capillary establishment was heavily reliant on the secretion of vascular endothelial growth factor from cultured smooth muscle cells. MSC's were able to mirror the effect caused by smooth muscle cells but the substitution of SMC's with fibroblasts prevents the generation of capillaries [739].

Furthermore, in humans, studies which have investigated the transplacental transport characteristics and their corresponding regulatory signalling pathways involved at the level of the placental barrier (comprising of endothelial cells, basal

membrane and syncytiotrphoblast) which separates the maternal and fetal circulation, especially during the first and early second trimester of the pregnancy period are very limited, if possible at all [692]. Moreover, there are few *in vivo* studies which have assessed the transplacental transport in humans due to ethical issues [761,762]. Also, as there are no *in vitro* studies which have established a functional model of a human chorionic vessel using isolated primary placental cells directly cocultured next to each other, the current study has addressed this gap into the literature by providing evidence of an optimised chorionic blood vessel model using primary cells isolated from term placental samples of healthy patients that may be suitable for translocation studies not only of small molecules but also of macromolecules and nanoparticles [651]. The coculture of different primary cell layers enables mechanistic assessments of their specific contribution on both permeability and translocation of compounds from the apical chamber to the basal chamber of the transwell system. The current multicellular model is reliable, cost-effective and thereby potentially more attractive for the pharmaceutical industry.

This study has intended to mimic the architecture of the human placenta chorionic plate artery using an *in vitro* approach by constructing a coculture model comprised of primary cells isolated from healthy patients. The current functional *in vitro* model of a human chorionic vessel comprised of the direct coculture of CPA-SMC and HUVEC cells in transwell inserts maintained a physiologically relevant representation of the smooth muscle cells and endothelial cells for 76 hours *in vitro* by recapitulating the spatial architecture of a placental chorionic vessel and allowing the physical and biochemical crosstalk between the two cocultured primary cells.

A study published in 2004 by Niwa and colleagues about the consequences of shear flow on the uptake of low-density lipoproteins (LDL) and acetylated (Ac-LDL) in

an *in vitro* monoculture and coculture model highlighted that the laminar flow resulted in an higher uptake of LDL and Ac-LDL by EC-SMC coculture compared to EC monoculture on its own [751]. Although this study is an example of endothelial cells cultured in direct contact with smooth muscle cells on 35mm-diameter dishes for the purposes of assessing the effects of sheer stress on mono- or co-cultured cells, in this case, the authors used commercially available endothelial and smooth muscle cells of a bovine origin [751].

Another example of EC-SMC coculture in which the cells were seeded on next to each other is an *in vitro* study undertaken by Wada and colleagues in 2000 which aimed to construct an arterial wall using aortic smooth muscle and endothelial cells isolated from rabbit [763]. In this case, the group focused on studying the transmigration capacity of isolated human peripheral monocytes across the co-cultured rabbit cells on transwell inserts using scanning electron and laser confocal microscopy [763]. Although the authors report that the number of monocytes that have transmigrated across the endothelial monolayer was particularly difficult to count, the confocal microscopic observation using three-dimensional and time-lapse imaging showed that endothelial cells and monocytes were able to be localised without any fixation [763].

In the context of assessing vascular permeability using primary isolated cells from placental samples, Wang and colleagues have published a study in 2004 investigating the effect of human placental trophoblast cells in regulating the elevated vascular leakage associated with preeclampsia [127]. On this occasion, the authors used an *in vitro* transwell system with isolated HUVEC cells seeded in the apical chamber in order to create a tight barrier and human placental trophoblast cells seeded in the basal chamber [127]. The results of this study showed that the endothelial junctions were susceptible targets of mediators synthetized by trophoblast cells and

cadherins were less vulnerable compared to occludin. Also, the developed disruption in paracellular contact in terms of junctions formed between adjacent cells was closely related to an elevation of the tracer leakage formed by the endothelial monolayer [127].

Due to the fact that the current permeability studies involved using albumin-FITC as tracer for studying the property of barrier integrity formed by isolated primary cells seeded on transwell membrane inserts, the visualisation of VE-Cadherin immunostaining of all cell cultures was made difficult as the secondary antibody was also FITC conjugated and the permeability tracer formed aggregates which strongly adhered to the 0.4µm pore size PET membranes. A recent study published in 2018 by Aengenheister and colleagues on the development of an advanced *in vitro* coculture model using BeWo b30 clone (human placental choriocarcinoma cell line) and HPEC-A2 cells (SV40 -transformed microvascular human placental venous endothelial cells) suggested that micro- or macrofluidic translocation investigations across established placental barriers are only relevant for small molecules [651]. In this context, the authors suggested that *in vitro* models assessing for instance glucose transport involving endothelial and trophoblastic cells seeded on denuded amniotic membrane, vitrified collagen membrane or poly-dimethylsiloxane (PDMS) scaffolds may form a significant barrier strongly influencing the free movement of larger substances or even nanoparticles [651]. A good example is fluorescein isothiocyanate – dextran (4.4kDa) which was considerably confined by the amnion layer in a study published by Levkovitz and colleagues in 2013 [692]. Another study by Cartwright and colleagues in 2012 has highlighted that decreased pore sizes could also predominantly prevent translocation of 37nm polystyrene nanoparticles [764]. In the case of poly-dimethylsiloxane microfluidic models used in translocation investigations, multiple studies have shown

that the devices may restrain small hydrophilic substances therefore preventing reproducible drug translocation observations [765–767].

A limitation of the current study is that the 2 hours long permeability assay was only undertaken following 26 hours of coculture of HUVEC with CPA-SMC cells which may limit the crosstalk between the two primary cell types in the formation of a tight blood vessel barrier. Also, another limitation of this investigation is that the effect of purinergic receptor agonists or antagonists such as ATP, BzATP or A740003 on the integrity of the formed barrier has not been assessed. Furthermore, the current *in vitro* coculture model lacks the highly dynamic microenvironment of the placental tissue since the primary cells were only cultured under static conditions.

5.4.4 Immunocytochemistry studies of endothelial junction formation in the mono- and co-culture of HUVEC with CPA-SMC cells

CD144 was visualised as a continuous or discontinuous thick or at parts thin line between tightly arranged adjacent human umbilical vein endothelial cells. The present study has not shown the continuous noninterrupted delicate lines as illustrated by Pang and colleagues (2017) which investigated the role of VEGF-A_{165}a, VEGF-A_{165}b and PIGF on junctional occupancy of CD144 and also tracer leakage in HUVEC monolayers formed on 6.5mm^2 diameter polyester membrane transwells [119]. With regards to immunolocalization studies, the authors found that in control HUVEC monolayers (vehicle treated), CD144 was visualised as a continuous consolidated staining in areas of paracellular overlap or at parts noninterrupted delicate lines in various adjacent endothelial cell-cell regions [119]. This study has also shown that in the vehicle treated HUVEC monolayers, VE-Cadherin was visualised as an interrupted

line or even at parts absent staining between paracellular endothelial overlap regions [119].

A further study published by Ebrahim and Leach in 2016 which investigated the transendothelial migration of isolated human umbilical mesenchymal stem cells through an established monolayer comprised of human uterine myometrial microvascular endothelial cells has shown that VE-Cadherin was also immunolocalised at the sites of paracellular endothelial cell borders as a non-interrupted line with a few areas showing a discontinuous staining [483]. Similar VE-Cadherin immunolocalization findings have also been published in another study by Wang and colleagues in 2004 which established a coculture model comprised of isolated HUVEC and trophoblast cells for the purposes of investigating the effects of trophoblast released mediators on the permeability of monolayers formed by endothelial cells [127]. In this case, the authors highlighted that CD144 was uniformly localised at the level of endothelial cell contact in both monoculture of HUVEC cells and coculture of HUVEC with trophoblast cells [127].

In another study published by Leach and colleagues in 2002, the immunolocalization of VE-Cadherin at a tissue level was investigated in isolated biopsies of first trimester placental samples and showed that CD144 was visualised in vascular profiles especially at the level of paracellular clefts between adjacent endothelial cells which formed part of blood vessels positioned under the trophoblast layer [125].

The current study also provides evidence that individual staining of the primary cells with PKH67 (green) in the case of HUVEC cells and PKH26 (red) of CPA-SMC's might be useful for further *in vitro* CPA-SMC trans-migration studies across established HUVEC monolayers. As the isolated CPA-SMC's have a phenotypic

signature similar to human umbilical Wharton's jelly mesenchymal stem cells (WJ-MSC's), the smooth muscle cells may possess a comparable exploratory behaviour in terms of inspecting endothelial cell-cell openings, as it has been suggested in the case of WJ-MSC's in a recent study published by Ebrahim and Leach in 2016 [483].

Due to the COVID-19 pandemic, the VE-Cadherin immunolocalization studies involving monoculture and coculture of primary endothelial and smooth muscle cells using a TRITC conjugated secondary antibody could not be performed. However, as presented earlier, even if multiple washes of the membranes were undertaken, a small level of albumin-FITC still remained adhered to the $4x10^6$ pores/cm^2 of the membrane inserts which resulted in the presence of multiple tracer aggregates.

5.5 Conclusions

In summary, this study provides novel evidence of the establishment of an *in vitro* model of a human placenta chorionic plate artery using isolated primary HUVEC and CPA-SMC cells. These investigations are the first to show that the co-culture of CPA-SMC cells with HUVEC did not significantly alter the vascular permeability compared to monoculture of HUVEC cells following a period of 26 hours in co-culture conditions. These results suggest that the CPA-SMC's were unable to induce a notable alteration in the vascular permeability levels of established HUVEC monolayers which may denote that during the coculture of both primary cell types, a limited EC-SMC cross talk took place. Further *in vitro* studies are necessary to fully understand the complicated interplay between isolated primary cells in co-culture conditions and to elucidate the potential involvement of multiple purinergic signalling pathways in the regulation of the human placental barrier function including the role of the P2X7 receptor in controlling the vascular permeability at the level of the chorionic plate arteries.

CHAPTER 6

GENERAL DISCUSSION

The human placenta plays a fundamental function in pregnancy as it comprises of the vascular network which is involved in the physiological exchange of nutrients and waste products between the developing fetus and the mother [576]. Despite this fundamental function, the regulation of the blood flow at the level of the fetoplacental vasculature has not been fully elucidated yet. A wide body of literature suggests that the fetoplacental and umbilical circulation do not possess any neuronal input [577], even if the umbilical artery has been demonstrated to retain a noticeable basal tone in the absence of vasoactive mediators [768].

The lack of autonomic innervation at the level of the fetoplacental vasculature denotes a potential involvement of the endothelial cells, circulating mediators or territorial paracrine factors in the regulation of the placental vascular resistance. Therefore, the current study aimed to investigate the purinergic signalling involvement in the regulation of the human placental vasculature by assessing the constrictor and dilatory responsiveness of decreased internal diameter arteries originating from the fetal interphase of the placenta.

The work from this study has determined the expression of multiple crucial purinergic signalling mediators in various placental tissues, and using wire myography, have established the possible function of these purinergic factors in regulating the blood flow at the level of the fetoplacental circulation.

The chorionic plate arteries studied in the current investigation are part of the principal regions of vascular resistance located on the fetal side of the human placenta. The fetoplacental arteries are also much less sensitive to vasoactive mediators that elicit potent effects in other blood vessels [61,769] and as a result, this unique characteristic of the human placental blood vessels contributes to an exclusive complexity in investigating the participation of the fetoplacental vasculature in

regulating the blood flow between the developing fetus and the pregnant mother. Expanding the current understanding of the physiological fetoplacental vascular reactivity to various circulating purinergic signalling mediators in healthy placental samples is a crucial necessity prior to obtaining a wider knowledge of the pathophysiology of preeclampsia, fetal growth restriction and gestational diabetes mellitus which are closely related to abnormal blood vessel perfusion levels.

The principal results that the P2X7 receptor is expressed at a protein level in CPA, SVA and trophoblast tissue could have far reaching implications. However, since the exogenic application of BzATP gave rise to vasoconstriction responses characterised by a particularly low efficacy of less than 25% of the U46619 standard, the absence of robust and reproducible responses from CPA's are due to the lack of involvement of the P2X7 receptor in regulating the contractility of these superficial human placental blood vessels.

The NLRP3 inflammasome was found to be expressed at a protein level in the second supernatant (cytosolic) fraction of SVA, fourth order CPA and choriodecidua tissue lysates using western blotting which has resulted in the detection of 4 isoforms at circa 79kDa, 107kDa, 171kDa and 222kDa. A study by Kummer *et al* (2007) has also found 2 isoforms of the multimeric protein using western blotting at approximately 75kDa and 130kDa in THP-1 and Jurkat cell lines [531]. Also, an investigation by Cheng *et al* (2019) has presented western blotting data using isolated primary trophoblast cells which have been cultured in hypoxia or normoxia conditions and detected an NLRP3 inflammasome protein product of the size of circa 100kDa which is approximately 7kDa below the approximately 107kDa isoform found in the current investigation [527].

The present investigation also provides novel evidence of the establishment of a scalable, reproducible and fast IgG immunodepletion method from the second pellet (membrane) and second supernatant (cytosolic) fraction of SVA, villous tissue and myometrium tissue lysates for the purposes of removing interfering immunoglobulin G from identifying less abundant protein targets at circa 50kDa. A good example from the current investigation of the usefulness of IgG immunodepletion from placental tissue lysates is the detection of pro-caspase-1 in the second supernatant fraction of SVA tissue lysates originating from healthy and preeclamptic patients which was found in the western blots at circa 47kDa. In this case, the identification of the biomarker would have not been possible without the removal of the heavy chain of IgG at circa 50kDa which could have partially obscured the detection of pro-caspase-1, since this protein is less abundantly expressed in stem villous arteries.

The present study has showed that the stimulation of human placental villous tissue with ATP, LPS+ATP and LPS+BzATP did not significantly alter the protein expression levels of the NLRP3 inflammasome compared to unstimulated tissue. However, a study by Maneta *et al* (2015) has found that LPS+BzATP stimulation of mononuclear cells isolated from maternal blood, cord blood and placental blood gave rise to a significant upregulation of IL-1β release compared to control [491]. Moreover, the same investigation presented flow cytometry data highlighting that the stimulation of cord blood mononuclear cells with LPS+BzATP gave rise to an upregulation of the multimeric protein compared to unstimulated primary cells [491].

The finding that no statistically significant differences in the protein expression levels of the P2X7 receptor, NLRP3 inflammasome and pro-caspase-1 were found in SVA tissue lysates originating from healthy and preeclamptic placental samples complements a study by Valdecantos *et al* (2003) which has found that the P2X7

receptor was expressed at an mRNA level in the smooth muscle of human chorionic blood vessels [479].

Moreover, the present study has showed that LPS+ATP stimulation of villous tissue, CPA and SVA gave rise to the highest release of IL-1β compared to control, ATP or LPS+BzATP stimulations of the same human placental tissue type. However, a study by Maneta *et al* (2015) has presented evidence that stimulated human mononuclear cells originating from cord blood, placental blood and maternal blood with LPS+BzATP elicits the highest IL-1β release compared to control, LPS or BzATP [491].

The current results have also presented evidence that the P2X7 receptor is expressed at the level of the syncytiotrophoblast layer, cytotrophoblast cells and fetal capillaries in isolated sections of human placental villous tissue originating from healthy and diet managed gestational diabetes mellitus patients. These novel results are of a particular importance especially in the case of pre-eclamptic patients where the extracellular adenosine 5'-triphosphate levels are particularly elevated at the level of the intervillous space [558] which could stimulate this purinoceptor located on the syncytiotrophoblast layer and therefore promote the assembly of the NLRP3 inflammasome, ultimately resulting in the release of IL-1β into the extracellular space.

The finding that the P2X7 receptor is expressed on isolated human placental chorionic plate artery smooth muscle cells originating from of healthy patients using immunocytochemistry complements a study by Valdecantos *et al* (2003) which has found that the P2X7 receptor is also expressed in chorionic plate arteries in the presence and absence of the endothelium and in chorionic plate veins at an mRNA level using RT-qPCR [479].

The mechanisms in charge with the adjustment of vasomotor tone and blood flow in the vasculature of the human placenta have not been fully elucidated yet. Multiple investigations have assessed the function of vasoactive compounds in the regulation of the fetoplacental vascular tone via small vessel myography studies using chorionic plate arteries or veins [576] and stem villous arteries [482] or using the methodology of perfused placental cotyledon [593]. In this case, most studies have focused on small vessel myography assessments using fetoplacental arteries to evaluate the contribution of these blood vessels in the control of vascular tone.

The current study has shown that the thromboxane A_2 mimetic U46619 elicited a reproducible and concentration-dependent vasoconstriction of the isolated chorionic plate arteries with an U46619 EC_{50} value of $1.2*10^{-7}$M as previously demonstrated in numerous investigations [53,482,576]. Other experiments from the current study have also assessed the U46619-induced vasoconstriction responses in the presence and absence of the P2X7 receptor antagonist A740003 using second and fourth order CPA's originating from healthy patients. In this case, U46619-induced concentration response curves elicited by the second order chorionic plate arteries in the presence of A740003 were notably rightward shifted which may indicate that A740003, DMSO or both compounds may cause a gradual loss in the potency of the thromboxane A_2 agonist-induced vasoconstriction effects, since one of the limitations of this study was that no vehicle control was undertaken to distinguish A740003 specific vasoactive responses.

The current study has also showed that adenosine 5'-triphosphate elicits spontaneous concentration-dependent vasoconstriction responses in the absence of A740003 in both second and fourth order CPA's originating from placental samples of healthy volunteers. Considering second order CPA's, the second adenosine 5'-

triphosphate stimulation in the presence of the P2X7 receptor antagonist gave rise to vasoconstriction responses below 50% of the initial ATP stimulation (without A740003), with fourth order CPA's showing a similar vasoconstriction effect of less than 10% of the U46619 standard. In this case, a notable desensitization to adenosine 5'-triphosphate took place after the nucleotide was added cumulatively described as transient and non-reproducible vasoactive responses from chorionic plate arteries of healthy patients which may suggest that A740003, DMSO or both compounds contribute to the decrease of ATP-induced vasoactive responses since a limitation of these studies was that no DMSO vehicle control was undertaken alongside experiments assessing the vasoactive role of the nucleotide. The current study complements an investigation by Read *et al* (1993) which presented evidence that human placental lobule perfusion with ATP and adenosine elicited a concentration-dependant decrease in the perfusion pressure when added into isolated placental lobules [475]. An investigation by Valdecantos *et al* (2003) has highlighted that adenosine 5'-triphosphate vasoconstricts chorionic plate arteries in a concentration-dependent manner, with the maximal vasoconstriction effects reaching almost 100% of the KCl standard [479]. An exception of this was BzATP with an E_{max} of 50.5% of the 70mM KCl standard [479]. Also, the same investigation has presented evidence that in endothelium denuded chorionic plate arteries, adenosine 5'-triphosphate concentration response curves were notably attenuated [479].

Similar results have also been obtained when isolated resistance human placental chorionic plate arteries were challenged with three ATP stimulations, with the second nucleotide stimulation in the absence of A740003 eliciting a significantly attenuated, flat concentration response curve which suggests a notable low efficacy of ATP. Moreover, the third nucleotide stimulation in the presence of A740003 gave

rise to a flat concentration response curve that was even further displaced downwards characterised by nucleotide vasoactive effects taking place below the baseline corresponding to U46619 standard. These results denote that adenosine 5'-triphosphate elicits potent but non-reproducible and transient contractions of the human placental chorionic plate arteries which is in agreement with previous studies of perfused cotyledons from the human placenta [475,523].

The current results have shown that adenosine 5'-triphosphate elicited a gradual run-down of transient responses from chorionic plate artery with increasing nucleotide cumulative concentrations in the presence and absence of the P2X7 receptor antagonist A740003. These results may denote that adenosine 5'-triphosphate may become rapidly metabolised by ectonucleotidases from isolated chorionic plate arteries to adenosine which has been shown to vasoconstrict CPA preparations close to 40% of the 70mM KCl standard [473].

The decrease in vasoconstriction responses generated by the thromboxane A_2 mimetic U46619 or adenosine 5'-triphosphate in the absence of the P2X7 receptor antagonist A740003 could be due to a desensitization effect taking place, particularly in the case of the nucleotide stimulation of CPA's where it was not possible to elicit another concentration-response curve for more than approximately 90 minutes following its initial challenge with ATP.

The present study has also demonstrated that resistance chorionic plate arteries challenged with three consecutive additions of adenosine 5'-triphosphate elicited progressively diminished vasoconstriction effects in the case of both first and second ATP challenges, which have resulted in a total desensitization effect taking place in a few of the functional studies undertaken. These results further complement an investigation by Valdecantos *et al* (2003) which has shown that superficial chorionic

plate arteries challenged with three consecutive applications of 91μM adenosine 5'-triphosphate elicited a progressively diminished vasomotor tone that attained 15% of its initial effect [479].

Although BzATP is a relatively selective though weakly potent compound acting at the P2X7 receptor (EC_{50} 5μM [146]), the present investigation provides evidence that its exogenous application on isolated human placental chorionic plate arteries of healthy patients gave rise to weak vasoconstriction responses described by a particularly decreased efficacy of less than 25% of the U46619 standard. An explanation of the lack of robust and reproducible vasoactive responses to BzATP of CPA's is the lack of involvement of the P2X7 receptor in the contractility of human placental chorionic plate arteries.

An investigation by Buvinic *et al* (2006) has presented evidence that the $P2Y_1$ and $P2Y_2$ receptors are expressed in the human placental vasculature and differentially distributed along the placental tree characterised by a change in expression from the smooth muscle to the endothelium at the level of the cotyledon [481]. The same study showed that removal of the endothelium from superficial chorionic plate artery or vein did not change the expression of both purinoceptors [481]. Furthermore, these authors have also shown a functional P2Y receptor-mediated vascular reactivity via the $P2Y_1$ and $P2Y_2$ receptors through the stimulation of CPA's with 2-MeSADP (possessing an elevated selectivity for $P2Y_1$ receptor) and UTP (preferential affinity for the $P2Y_2$ receptor) [481]. In this case, the same study showed that both compounds vasoconstricted chorionic plate artery preparations with 2-MeSADP being slightly less potent than UTP [481].

The current investigation also provided the first evidence that chorionic plate artery smooth muscle cells possess a phenotypic signature similar to mesenchymal

stem cells which could suggest that the primary cells may play a role in the regulation of vascular permeability of the chorionic plate arteries.

This study provides evidence of a functional *in vitro* model of a human chorionic vessel via the formation of a HUVEC monolayer on transwell membrane inserts for the duration of 48 hours post-seeding followed by the coculture of HUVEC with CPA-SMC cells for a further 26 hours prior to the commencement of the tracer leakage assay.

Under the conditions of the present study, the isolated smooth muscle cells did not significantly alter the monolayer barrier formed by the HUVEC cells for the entire duration of the permeability assay investigation suggesting that the primary cells possessed a limited capacity to affect the integrity of paracellular junctions formed between adjacent HUVEC cells.

The current study of the human coculture model where the endothelial and smooth muscle cells were in direct contact resembles the proliferation state and microenvironment of a human placental chorionic blood vessel by facilitating a diminished diffusion distance of cellular factors between the cultured HUVEC and CPA-SMC cells [759].

While progress has been made, there is still much work to be undertaken in the *in vitro* reconstruction of the anatomy and function of the human placental chorionic blood vessel system and to investigate the plethora of mediators that regulate its physiology for instance oxygen microenvironment and multiple cell layers.

Further work is required to obtain a better understanding of the involvement of purinergic signalling in the modulation of placental blood vessel contractility properties.

6.1 The most important findings of the current study

One of the most important finding of the present study is that no statistically significant differences were detected in stem villous artery relative protein expression levels of the P2X7 receptor, NLRP3 inflammasome and procaspase-1 between healthy and preeclamptic placental samples. Furthermore, another crucial finding from the current investigation is that GDM-Diet gave rise to a statistically significant downregulation in P2X7+CD31 double positive placental vascular profiles compared to healthy patients.

Another important result from the present study is that LPS+ATP stimulation of CPA, SVA and trophoblast tissue elicited a statistically significant difference in IL-1β release relative to control. Moreover, a crucial finding from the current investigation is that repeated cumulative additions of ATP gave rise to a progressively reduced vasomotor response in the presence and absence of the P2X7 receptor antagonist A740003. The 30mM KPSS-induced elevation in chorionic plate artery resting basal tone increased the efficacy of the first ATP stimulation by more than 38% at a nucleotide concentration of 10^{-3}M is also an important finding from the present investigation.

A further important result from the current investigation is that BzATP gave rise to a substantially reduced vasomotor effect from chorionic plate arteries characterised by an almost flat concentration response curve. Also, another crucial finding from the present investigation is that the surface antigenic profiling of human placenta chorionic plate artery smooth muscle cells showed a particular similarity with the immunophenotypic signature characteristic of human multipotent mesenchymal stem cells. Moreover, an important result from the current study is that no statistically significant differences in terms of tracer leakage levels were found between the

coculture of CPA-SMC with HUVEC and monoculture of primary endothelial cells at the same timepoints during the 120 minutes long permeability assay.

6.2 Limitations of the current study

A potential limitation of undertaking physiological studies using human placental villous tissue as in the current investigation by stimulating the explants with D-glucose for 4, 24 and 48 hours is that the syncytiotrophoblast undergoes non-interrupted renewal, shedding aged nuclei in the form of syncytial knots and incorporating fresh syncytiotrophoblast cells by fusion as it has been demonstrated in a study by Zhou and colleagues (2013) using isolated cytotrophoblast cells during the first 24-48 hours of culture conditions [546]. Furthermore, these authors have showed that the primary cytotrophoblast cells stained positive for CK7 and illustrated western blotting data highlighting that β-hCG protein expression levels increased during the first 24 and 48 hours *in vitro* [546]. Therefore, undertaking physiological studies using placental villous tissue during the first 48 hours following the isolation process could be sub-optimal.

Another important limitation of the current study is directly related to the western blotting data which illustrated the relative P2X7 receptor protein expression levels in isolated human placental villous tissue stimulated with D-glucose for 4, 24 and 48 hours, since a noticeable variability in the relative β-actin protein expression levels was detected across samples of the same placental villous tissue type. In this case, no optimisation in choosing a suitable loading control was undertaken and as a result, the selection of a different housekeeping protein that remains constant (relative to the total protein content) could be advantageous in the interpretation of the western blotting data.

Furthermore, a potential limitation of the western blotting data which presented the relative protein expression levels of the P2X7 receptor, NLRP3 inflammasome and pro-caspase-1 in isolated human SVA's was that two of the eight pre-eclamptic patients were also co-diagnosed with intrauterine growth restriction which is a confounder in the analysis of the data in terms of the association between pre-eclamptic patients and subjects co-diagnosed with pre-eclampsia and IUGR. Furthermore, another limitation of the western blotting studies is the absence of blocking peptide controls for the NLRP3 inflammasome and pro-caspase-1 since no blocking peptide could be sourced from the corresponding manufacturers.

A limitation of undertaking multiple comparison tests between the released levels of pro-inflammatory cytokines from CPA's, SVA's and placental villous tissue which have been stimulated with control, ATP, LPS+ATP and LPS+BzATP is the elevated statistical risk that a proportion of associations are false positives. Also, an important limitation of this study where the CPA, SVA and villous tissue was stimulated with control, ATP, LPS+ATP and LPS+BzATP was that no LPS control was undertaken alongside these experiments.

Another important limitation of the current study is that some of the western blotting, RT-qPCR, immunocytochemistry, pro-inflammatory cytokine and LDH measurement studies contained relatively few numbers of participants included, which could limit the interpretation of the data. Also, a limitation in the case of immunohistochemistry studies is that the P2X7 receptor expression was only investigated in isolated sections of chorionic plate arteries originating from two healthy patients which limits the interpretation of the acquired data.

A further limitation of the current study is that no negative or positive controls for the P2X7 receptor staining were undertaken alongside immunocytochemistry

experiments evaluating the immunolocalization of the purinergic receptor in smooth muscle cells which have been isolated from chorionic plate arteries.

Moreover, an important limitation of the present study is that no DMSO vehicle control was carried out alongside experiments evaluating the influence of A740003 in U46619-induced vasoactive effects and ATP-induced vasoactive effects elicited by chorionic plate arteries which further limits the interpretation of the wire myography data.

Another limitation of this study is that the vasoactive responses of isolated CPA preparations under the exogenic application of ATP, BzATP and A740003 have not been assessed in chorionic plate arteries with the endothelium removed to investigate the participation of the smooth muscle towards the regulation of the placental blood flow.

Also, a further limitation of the current study is that the isolation process of chorionic plate artery smooth muscle cells from healthy placental samples using the tissue explant culture method takes circa 21-28 days until the primary cells are sourced.

Another important limitation of the present study is that the two hours long tracer leakage assay was only undertaken following 26 hours of coculture of the primary placental cells which could limit the crosstalk between the CPA-SMC and HUVEC cells in the formation of a tight blood vessel barrier. The lack of investigating the effect of purinergic receptor agonists and antagonists for instance adenosine 5'-triphosphate, BzATP and A740003 on the integrity of the formed barrier is also considered a limitation of the current study.

Furthermore, the current *in vitro* coculture model using isolated human placental chorionic plate artery smooth muscle cells and human umbilical vein

endothelial cells lacks the highly dynamic microenvironment of the placental tissue since the two primary cell types were cultured under static conditions.

6.3 Future research

The individual methods used in the current study have been validated in chapters 3-5. However, the current research could be further complemented by assessing the vasoactive properties of various purinergic signalling mediators using the placental veins containing deoxygenated blood. Furthermore, the vasoactive properties of other non-hydrolysable ATP analogues should be tested on resistance chorionic plate arteries and veins to gain a better understanding of the involvement of other P2X and P2Y purinergic receptors in the regulation of the fetoplacental vasculature. Also, electrophysiology may be used to study single human chorionic plate artery smooth muscle cell responses to the exogenous addition of ATP and BzATP using the patch clamp technique of the whole cell. In this case, further information about the conductance of a single ion channel could be obtained by monitoring the intra- and extra-cellular movement of ions across the plasmalemma.

Moreover, the effects of ATP and BzATP on established cocultures of HUVEC and CPA-SMC cells should be tested to investigate the P2X receptor agonist capability to tighten or loosen the monolayer barrier formed by HUVEC cells using tracer leakage assays. Also, the mRNA expression of the P2X7 receptor, NLRP3 inflammasome and Caspase-1 should be assessed using CPA arteries for the purposes of correlating the mRNA levels with the expressed protein levels in both healthy and preeclamptic patients.

6.4 Conclusion

The current study provides evidence that the P2X7 receptor is expressed at the level of the human placental chorionic plate artery, stem villous artery and villous tissue originating from healthy patients and does not play a functional role in the contractility of the chorionic plate arteries since the exogenous challenge of CPA's with BzATP did not give rise to robust and reproducible vasoactive responses. Further *in vitro* studies are required in order to fully understand the participation of purinergic signalling into the modulation of the human placenta vasculature.

REFERENCES

[**1**] Anderson CM, Lopez F, Zhang H-Y, Pavlish K, Benoit JN. Reduced uteroplacental perfusion alters uterine arcuate artery function in the pregnant Sprague-Dawley rat. *Biol Reprod*. 2005;72(3):762–6. DOI:10.1095/biolreprod.104.036715

[**2**] Latendresse G, Founds S. The Fascinating and Complex Role of the Placenta in Pregnancy and Fetal Well-being. *J Midwifery Women's Heal* [Internet]. 2015/08/11. 2015;60(4):360–70. DOI:10.1111/jmwh.12344

[**3**] Stenqvist AC, Chen T, Hedlund M, Dimova T, Nagaeva O, Kjellberg L, et al. An efficient optimized method for isolation of villous trophoblast cells from human early pregnancy placenta suitable for functional and molecular studies. *Am J Reprod Immunol* [Internet]. 2008;60(1):33–42. DOI:10.1111/j.1600-0897.2008.00588.x

[**4**] Johnson MH. Essential Reproduction. 6th Editio. Chichester, UK: John Wiley & Sons, Ltd; 2007. 193, 212, 218, 220, 238–239 p.

[**5**] Benirschke K, Kaufmann P, Baergen RN. Pathology of the Human Placenta. 5th Editio. Springer Verlag New York; 2006. 10, 13–15 p. DOI:10.1007/b137920

[**6**] Genbacev O, Zhou Y, Ludlow JW, Fisher SJ. Regulation of Human Placental Development by Oxygen Tension. *Science (80-)* [Internet]. 1997 Sep 12 [cited 2020 Mar 22];277(5332):1669–72. DOI:10.1126/science.277.5332.1669

[**7**] Burton GJ, Fowden AL. The placenta: A multifaceted, transient organ [Internet]. Vol. 370, Philosophical Transactions of the Royal Society B: Biological Sciences. Royal Society of London; 2015 [cited 2020 Dec 15]. DOI:10.1098/rstb.2014.0066

[**8**] Gauster M, Huppertz B. The paradox of caspase 8 in human villous trophoblast fusion. *Placenta* [Internet]. 2010 Feb [cited 2020 Dec 15];31(2):82–8. DOI:10.1016/j.placenta.2009.12.007

[**9**] Rote NS, Wei BR, Xu C, Luo L. Caspase 8 and Human Villous Cytotrophoblast Differentiation. *Placenta* [Internet]. 2010 Feb [cited 2020 Dec 15];31(2):89–96. DOI:10.1016/j.placenta.2009.12.014

[**10**] Sadler TW. Langman's Medical Embryology. 12th editi. Lippincott Williams and Wilkins; 2012. 37–46 p.

[**11**] Knöfler M, Haider S, Saleh L, Pollheimer J, Gamage TKJB, James J. Human placenta and trophoblast development: key molecular mechanisms and model systems [Internet]. Vol. 76, Cellular and Molecular Life Sciences. Birkhauser Verlag AG; 2019 [cited 2020 Aug 22]. p. 3479–96. DOI:10.1007/s00018-019-03104-6

[**12**] Torres-Cuevas I, Parra-Llorca A, Sánchez-Illana A, Nuñez-Ramiro A, Kuligowski J, Cháfer-Pericás C, et al. Oxygen and oxidative stress in the perinatal period. Vol. 12, Redox Biology. Elsevier B.V.; 2017. p. 674–81. DOI:10.1016/j.redox.2017.03.011

[**13**] Huppertz B. Traditional and new routes of trophoblast invasion and their implications for pregnancy diseases [Internet]. Vol. 21, International Journal of Molecular Sciences. MDPI AG; 2020 [cited 2020 Aug 22]. DOI:10.3390/ijms21010289

[**14**] Turco MY, Moffett A. Development of the human placenta. *Dev* [Internet]. 2019 Nov 15 [cited 2020 Dec 15];146(22). DOI:10.1242/dev.163428

[**15**] Burton GJ, Jauniaux E. Development of the human placenta and fetal heart: Synergic or independent? *Front Physiol* [Internet]. 2018 Apr 12 [cited 2020 Dec 15];9(373). DOI:10.3389/fphys.2018.00373

[**16**] Pijnenborg R, Vercruysse L, Hanssens M. The Uterine Spiral Arteries In Human Pregnancy: Facts and Controversies [Internet]. Vol. 27, Placenta. Placenta; 2006 [cited 2020 Dec 15]. p. 939–58. DOI:10.1016/j.placenta.2005.12.006

[**17**] Whitley GSJ, Cartwright JE. Cellular and Molecular Regulation of Spiral Artery Remodelling: Lessons from the Cardiovascular Field. *Placenta* [Internet]. 2010 Jun [cited 2020 Dec 15];31(6):465–74. DOI:10.1016/j.placenta.2010.03.002

[**18**] Kam EPY, Gardner L, Loke YW, King A. The role of trophoblast in the physiological change in decidual spiral arteries. *Hum Reprod* [Internet]. 1999 [cited 2020 Dec 15];14(8):2131–8. DOI:10.1093/humrep/14.8.2131

[**19**] Harris LK. Review: Trophoblast-Vascular Cell Interactions in Early Pregnancy: How to Remodel a Vessel. *Placenta* [Internet]. 2010 Mar [cited 2020 Dec 15];31(SUPPL.). DOI:10.1016/j.placenta.2009.12.012

[**20**] Levine RJ, Maynard SE, Qian C, Lim K-H, England LJ, Yu KF, et al. Circulating Angiogenic Factors and the Risk of Preeclampsia. *N Engl J Med* [Internet]. 2004 Feb 12 [cited 2020 Dec 15];350(7):672–83. DOI:10.1056/nejmoa031884

[**21**] Salomon C, Yee SW, Mitchell MD, Rice GE. The Possible Role of Extravillous Trophoblast-Derived Exosomes on the Uterine Spiral Arterial Remodeling under Both Normal and Pathological Conditions [Internet]. Vol. 2014, BioMed Research International. Hindawi Publishing Corporation; 2014 [cited 2020 Aug 22]. p. 693157–693157. DOI:10.1155/2014/693157

[**22**] Burton GJ, Woods AW, Jauniaux E, Kingdom JCP. Rheological and Physiological Consequences of Conversion of the Maternal Spiral Arteries for Uteroplacental Blood Flow during Human Pregnancy. *Placenta* [Internet]. 2009 Jun [cited 2020 Dec 15];30(6):473–82. DOI:10.1016/j.placenta.2009.02.009

[**23**] Poston L. The control of blood flow to the placenta. *Exp Physiol*. 1997;82(2):377–87. DOI:10.1113/expphysiol.1997.sp004033

[**24**] Schiffer V, Evers L, de Haas S, Ghossein-Doha C, Al-Nasiry S, Spaanderman M. Spiral artery blood flow during pregnancy: a systematic review and meta-analysis. *BMC Pregnancy Childbirth* [Internet]. 2020 Dec 1 [cited 2020 Dec 15];20(1):680. DOI:10.1186/s12884-020-03150-0

[**25**] Chaddha V, Viero S, Huppertz B, Kingdom J. Developmental biology of the placenta and the origins of placental insufficiency. *Semin Fetal Neonatal Med* [Internet]. 2004;9(5):357–69. DOI:10.1016/j.siny.2004.03.006

[**26**] Kingdom J, Huppertz B, Seaward G, Kaufmann P. Development of the placental villous tree and its consequences for fetal growth. *Eur J Obstet Gynecol Reprod Biol* [Internet]. 2000;92(1):35–43. DOI:10.1016/S0301-2115(00)00423-1

[**27**] Abbas AE, Lester SJ, Connolly H. Pregnancy and the cardiovascular system. *Int J Cardiol*. 2005;98(2):179–89. DOI:10.1016/j.ijcard.2003.10.028

[**28**] Soma-Pillay P, Nelson-Piercy C, Tolppanen H, Mebazaa A. Physiological

changes in pregnancy. *Cardiovasc J Afr* [Internet]. 2016 Mar 1 [cited 2020 Aug 22];27(2):89–94. DOI:10.5830/CVJA-2016-021

[**29**] Humphries A, Mirjalili SA, Tarr GP, Thompson JMD, Stone P. The effect of supine positioning on maternal hemodynamics during late pregnancy. *J Matern neonatal Med Off J Eur Assoc Perinat Med Fed Asia Ocean Perinat Soc Int Soc Perinat Obstet*. 2019 Dec;32(23):3923–30. DOI:10.1080/14767058.2018.1478958

[**30**] Sanghavi M, Rutherford JD. Cardiovascular physiology of pregnancy. *Circulation* [Internet]. 2014 Sep 16 [cited 2020 Aug 22];130(12):1003–8. DOI:10.1161/CIRCULATIONAHA.114.009029

[**31**] Chapman AB, Abraham WT, Zamudio S, Coffin C, Merouani A, Young D, et al. Temporal relationships between hormonal and hemodynamic changes in early human pregnancy. *Kidney Int*. 1998 Dec;54(6):2056–63. DOI:10.1046/j.1523-1755.1998.00217.x

[**32**] Cheung KL, Lafayette RA. Renal physiology of pregnancy. *Adv Chronic Kidney Dis*. 2013 May;20(3):209–14. DOI:10.1053/j.ackd.2013.01.012

[**33**] Arroyo JA, Winn VD. Vasculogenesis and Angiogenesis in the IUGR Placenta. *Semin Perinatol*. 2008;32(3):172–7. DOI:10.1053/j.semperi.2008.02.006

[**34**] Ramaesh T, Logie JJ, Roseweir AK, Millar RP, Walker BR, Hadoke PWFF, et al. Kisspeptin-10 inhibits angiogenesis in human placental vessels ex vivo and endothelial cells in vitro. *Endocrinology* [Internet]. 2010;151(12):5927–34. DOI:10.1210/en.2010-0565

[**35**] Boura ALAA, Leitch IM, Read MA, Walters WAWW. The control of fetal vascular resistance in the human placenta. *Placenta* [Internet]. 1998 Jan [cited 2019 Aug 26];19:299–313. DOI:10.1016/S0143-4004(98)80021-0

[**36**] Ahmed A, Perkins J. Angiogenesis and intrauterine growth restriction. *Bailliere's Clin Obstet Gynaecol* [Internet]. 2000;14(6):981–98. DOI:10.1053/beog.2000.0139

[**37**] Velicky P, Kn??fler M, Pollheimer J rgen J rgen. Function and control of human invasive trophoblast subtypes: Intrinsic vs. maternal control. *Cell Adhes Migr* [Internet]. 2016;10(1–2):154–62. DOI:10.1080/19336918.2015.1089376

[**38**] Huppertz B, Weiss G, Moser G. Trophoblast invasion and oxygenation of the placenta: Measurements versus presumptions. *J Reprod Immunol*. 2014;101–102(1):74–9. DOI:10.1016/j.jri.2013.04.003

[**39**] Rubinchik-Stern M, Eyal S. Drug interactions at the human placenta: What is the evidence? *Front Pharmacol*. 2012;3(126). DOI:10.3389/fphar.2012.00126

[**40**] Huppertz B, Ghosh D, Sengupta J. An integrative view on the physiology of human early placental villi. *Prog Biophys Mol Biol*. 2014;114(1):33–48. DOI:10.1016/j.pbiomolbio.2013.11.007

[**41**] Johansson M, Jansson T, Pestov NB, Powell TL. Non-gastric H+/K+ ATPase is present in the microvillous membrane of the human placental syncytiotrophoblast. *Placenta*. 2004;25(6):505–11. DOI:10.1016/j.placenta.2003.11.008

[**42**] Marín R, Riquelme G, Godoy V, Díaz P, Abad C, Caires R, et al. Functional and

Structural Demonstration of the Presence of Ca-ATPase (PMCA) in Both Microvillous and Basal Plasma Membranes from Syncytiotrophoblast of Human Term Placenta. *Placenta*. 2008;29(8):671–9. DOI:10.1016/j.placenta.2008.06.003

[**43**] Desforges M, Lacey HA, Glazier JD, Greenwood SL, Mynett KJ, Speake PF, et al. SNAT4 isoform of system A amino acid transporter is expressed in human placenta. *Am J Physiol - Cell Physiol*. 2006;290(1):C305-12. DOI:10.1152/ajpcell.00258.2005

[**44**] Conner SD, Schmid SL. Regulated portals of entry into the cell. *Nature*. 2003;422(6927):37–44. DOI:10.1038/nature01451

[**45**] Malassine A, Alsat E, Besse C, Rebourcet R, Cedard L. Acetylated low density lipoprotein endocytosis by human syncytiotrophoblast in culture. *Placenta*. 1990;11(2):191–204. DOI:10.1016/S0143-4004(05)80180-8

[**46**] Fuchs R, Ellinger I. Endocytic and transcytotic processes in villous syncytiotrophoblast: Role in nutrient transport to the human fetus. Vol. 5, Traffic. Blackwell Munksgaard; 2004. p. 725–38. DOI:10.1111/j.1600-0854.2004.00221.x

[**47**] Cabrera L, Saavedra A, Rojas S, Cid M, Valenzuela C, Gallegos D, et al. Insulin induces relaxation and decreases hydrogen peroxide-induced vasoconstriction in human placental vascular bed in a mechanism mediated by calcium-activated potassium channels and L-arginine/nitric oxide pathways. *Front Physiol* [Internet]. 2016;7(NOV):1–13. DOI:10.3389/fphys.2016.00529

[**48**] Holcberg G, Sapir O, Hallak M, Alaa A, Shorok HY, David Y, et al. Selective vasodilator effect of magnesium sulfate in human placenta. *Am J Reprod Immunol* [Internet]. 2004;51(3):192–7. DOI:10.1111/j.1600-0897.2004.00115.x

[**49**] Learmont JG, Poston L. Nitric oxide is involved in flow-induced dilation of isolated human small fetoplacental arteries. *Am J Obs Gynecol* [Internet]. 1996;174(2):583–8. DOI:10.1016/S0002-9378(96)70432-5

[**50**] Corcoran JJ, Charnock JC, Martin J, Taggart MJ, Westwood M. Differential effect of insulin like growth factor-I on constriction of human uterine and placental arteries. *J Clin Endocrinol Metab* [Internet]. 2012;97(11):E2098-104. DOI:10.1210/jc.2012-1679

[**51**] Nugent JL, Wareing M, Palin V, Sibley CP, Baker PN, Ray DW, et al. Chronic glucocorticoid exposure potentiates placental chorionic plate artery constriction: Implications for aberrant fetoplacental vascular resistance in fetal growth restriction. *Endocrinology* [Internet]. 2013;154(2):876–87. DOI:10.1210/en.2012-1927

[**52**] Hayward CE, Higgins L, Cowley EJ, Greenwood SL, Mills TA, Sibley CP, et al. Chorionic plate arterial function is altered in maternal obesity. *Placenta* [Internet]. 2013;34(3):281–7. DOI:10.1016/j.placenta.2013.01.001

[**53**] Ali TY, Broughton Pipkin F, Khan RN, Torrens C, Pipkin FB, Khan RN. The Effect of pH and Ion Channel Modulators on Human Placental Arteries. *PLoS One* [Internet]. 2014 [cited 2017 Aug 31];9(12):1–21. DOI:10.1371/journal.pone.0114405

[**54**] Wareing M, Greenwood SL, Baker PN. Reactivity of human placental chorionic

plate vessels is modified by level of oxygenation: Differences between arteries and veins. *Placenta*. 2006;27(1):42–8. DOI:10.1016/j.placenta.2004.11.008

[**55**] Wareing M, Myers JE, O'Hara M, Kenny LC, Warren AY, Taggart MJ, et al. Effects of a phosphodiesterase-5 (PDE5) inhibitor on endothelium-dependent relaxation of myometrial small arteries. *Am J Obs Gynecol* [Internet]. 2004;190(5):1283–90. DOI:10.1016/j.ajog.2003.12.024

[**56**] Mazurek R, Dave JM, Chandran RR, Misra A, Sheikh AQ, Greif DM. Vascular Cells in Blood Vessel Wall Development and Disease. In: Advances in Pharmacology [Internet]. Academic Press Inc.; 2017 [cited 2020 Aug 22]. p. 323–50. DOI:10.1016/bs.apha.2016.08.001

[**57**] Greif DM, Kumar M, Lighthouse JK, Hum J, An A, Ding L, et al. Radial Construction of an Arterial Wall. *Dev Cell* [Internet]. 2012 Sep 11 [cited 2020 Aug 22];23(3):482–93. DOI:10.1016/j.devcel.2012.07.009

[**58**] Majesky MW, Dong XR, Hoglund V, Daum G, Mahoney WM. The adventitia: A progenitor cell niche for the vessel wall. *Cells Tissues Organs* [Internet]. 2011 Dec [cited 2020 Aug 22];195(1–2):73–81. DOI:10.1159/000331413

[**59**] Tropea T, Nihlen C, Weitzberg E, Lundberg JO, Wareing M, Greenwood SL, et al. Enhanced Nitrite-Mediated Relaxation of Placental Blood Vessels Exposed to Hypoxia Is Preserved in Pregnancies Complicated by Fetal Growth Restriction. *Int J Mol Sci*. 2021 Apr;22(9). DOI:10.3390/ijms22094500

[**60**] Krause BJ, Carrasco-Wong I, Caniuguir A, Carvajal J, Farías M, Casanello P. Endothelial eNOS/arginase imbalance contributes to vascular dysfunction in IUGR umbilical and placental vessels. *Placenta*. 2013 Jan;34(1):20–8. DOI:10.1016/j.placenta.2012.09.015

[**61**] Myatt L. Control of vascular resistance in the human placenta. *Placenta*. 1992;13(4):329–41. DOI:10.1016/0143-4004(92)90057-Z

[**62**] Feng X, Zhang Y, Zhang Y, Yang X, Man D, Lu L, et al. Prostaglandin I2 mediates weak vasodilatation in human placental microvessels. *Biol Reprod* [Internet]. 2020 Dec 1;103(6):1229–37. DOI:10.1093/biolre/ioaa156

[**63**] Hoeldtke NJ, Wagner RK, Calhoun BC, Hume RFJ. Vasodilatory response of fetoplacental vasculature to adrenomedullin after constriction with the thromboxane sympathomimetic U46619. *Am J Obstet Gynecol*. 2000 Dec;183(6):1573–8. DOI:10.1067/mob.2000.108071

[**64**] Holcberg G, Kossenjans W, Brewer A, Miodovnik M, Myatt L. Selective vasodilator effects of atrial natriuretic peptide in the human placental vasculature. *J Soc Gynecol Investig*. 1995;2(1):1–5.

[**65**] Kiernan MF, Barrie A, Szkolar J, Mills TA, Wareing M. Functional Evidence for Oxygen-Sensitive Voltage-Gated Potassium Channels in Human Placental Vasculature. *Placenta* [Internet]. 2010;31(6):553–5. DOI:10.1016/j.placenta.2010.03.009

[**66**] Bednov A, Espinoza J, Betancourt A, Vedernikov Y, Belfort M, Yallampalli C. L-arginine prevents hypoxia-induced vasoconstriction in dual-perfused human placental cotyledons. *Placenta* [Internet]. 2015;36(11):1254–9. DOI:10.1016/j.placenta.2015.08.012

[**67**] Mills TA, Taggart MJ, Greenwood SL, Baker PN, Wareing M. Histamine-Induced Contraction and Relaxation of Placental Chorionic Plate Arteries. *Placenta* [Internet]. 2007;28(11–12):1158–64. DOI:10.1016/j.placenta.2007.05.008

[**68**] Byrne BM, Howard RB, Morrow RJ, Whiteley KJ, Adamson SL. Role of the L-arginine nitric oxide pathway in hypoxic fetoplacental vasoconstriction. *Placenta*. 1997;18(8):627–34. DOI:10.1016/S0143-4004(97)90003-5

[**69**] Hampl V, Bíbová J, Stranák Z, Wu X, Michelakis ED, Hashimoto K, et al. Hypoxic fetoplacental vasoconstriction in humans is mediated by potassium channel inhibition. *Am J Physiol Hear Circ Physiol* [Internet]. 2002;283(6):H2440-9. DOI:10.1152/ajpheart.01033.2001

[**70**] McIntyre HD, Catalano P, Zhang C, Desoye G, Mathiesen ER, Damm P. Gestational diabetes mellitus. *Nat Rev Dis Prim*. 2019 Jul;5(1):47. DOI:10.1038/s41572-019-0098-8

[**71**] Hedderson MM, Darbinian JA, Quesenberry CP, Ferrara A. Pregravid cardiometabolic risk profile and risk for gestational diabetes mellitus. *Am J Obstet Gynecol*. 2011 Jul;205(1):55.e1-7. DOI:10.1016/j.ajog.2011.03.037

[**72**] Carpenter MW, Coustan DR. Criteria for screening tests for gestational diabetes. *Am J Obstet Gynecol* [Internet]. 1982;144(7):768–73. DOI:https://doi.org/10.1016/0002-9378(82)90349-0

[**73**] Gunderson EP. Gestational diabetes and nutritional recommendations. *Curr Diab Rep*. 2004 Oct;4(5):377–86. DOI:10.1007/s11892-004-0041-5

[**74**] Chiswick C, Reynolds RM, Denison F, Drake AJ, Forbes S, Newby DE, et al. Effect of metformin on maternal and fetal outcomes in obese pregnant women (EMPOWaR): a randomised, double-blind, placebo-controlled trial. *lancet Diabetes Endocrinol*. 2015 Oct;3(10):778–86. DOI:10.1016/S2213-8587(15)00219-3

[**75**] Kurtzhals LL, Nørgaard SK, Secher AL, Nichum VL, Ronneby H, Tabor A, et al. The impact of restricted gestational weight gain by dietary intervention on fetal growth in women with gestational diabetes mellitus. *Diabetologia*. 2018 Dec;61(12):2528–38. DOI:10.1007/s00125-018-4736-6

[**76**] Landon MB, Rice MM, Varner MW, Casey BM, Reddy UM, Wapner RJ, et al. Mild gestational diabetes mellitus and long-term child health. *Diabetes Care*. 2015 Mar;38(3):445–52. DOI:10.2337/dc14-2159

[**77**] Kim C. Maternal outcomes and follow-up after gestational diabetes mellitus. *Diabet Med*. 2014 Mar;31(3):292–301. DOI:10.1111/dme.12382

[**78**] Haas DM, Benjamin T, Sawyer R, Quinney SK. Short-term tocolytics for preterm delivery - current perspectives. *Int J Womens Health* [Internet]. 2014 Mar 27;6:343–9. DOI:10.2147/IJWH.S44048

[**79**] Walsh SW, Wang Y, Killian A. AA-2414, an antioxidant and thromboxane receptor blocker, completely inhibits peroxide-induced vasoconstriction in the human placenta. *J Pharmacol Exp Ther*. 1999;290(1):220–6.

[**80**] Kovac CM, Howard BC, Pierce BT, Hoeldtke NJ, Calhoun BC, Napolitano PG. Fetoplacental vascular tone is modified by magnesium sulfate in the preeclamptic ex vivo human placental cotyledon. *Am J Obs Gynecol* [Internet].

2003;189(3):839–42. DOI:10.1067/S0002-9378(03)00851-2

[**81**] Mäkikallio K, Kaukola T, Tuimala J, Kingsmore SF, Hallman M, Ojaniemi M. Umbilical artery chemokine CCL16 is associated with preterm preeclampsia and fetal growth restriction. *Cytokine* [Internet]. 2012;60(2):377–84. DOI:10.1016/j.cyto.2012.07.008

[**82**] Balan A, Szaingurten-Solodkin I, Swissa SS, Feinshtein V, Huleihel M, Holcberg G, et al. The effects of pravastatin on the normal human placenta: Lessons from ex-vivo models. *PLoS One*. 2017;12(2):1–17. DOI:10.1371/journal.pone.0172174

[**83**] Valente AM, Economy KE. Preeclampsia. *Circulation*. 2013;128(17):344–5. DOI:10.1161/CIRCULATIONAHA.113.003858

[**84**] Spaans F, Melgert BN, Chiang C, Borghuis T, Klok PA, De Vos P, et al. Extracellular ATP decreases trophoblast invasion, spiral artery remodeling and immune cells in the mesometrial triangle in pregnant rats. *Placenta* [Internet]. 2014/06/24. 2014;35(8):587–95. DOI:10.1016/j.placenta.2014.05.013

[**85**] Spaans F, De Vos P, Bakker WW, Van Goor H, Faas MM. Danger signals from ATP and adenosine in pregnancy and preeclampsia. *Hypertension*. 2014;63(6):1154–60. DOI:10.1161/HYPERTENSIONAHA.114.03240

[**86**] Kohli S, Ranjan S, Hoffmann J, Kashif M, Daniel EA, Al-Dabet MM, et al. Maternal extracellular vesicles and platelets promote preeclampsia via inflammasome activation in trophoblasts. *Blood* [Internet]. 2016/10/30. 2016;128(17):2153–64. DOI:10.1182/blood-2016-03-705434

[**87**] Kohli S, Isermann B. Placental hemostasis and sterile inflammation: New insights into gestational vascular disease. *Thromb Res* [Internet]. 2017/03/07. 2017 Mar [cited 2019 Jan 24];151 Suppl:S30-s33. DOI:10.1016/s0049-3848(17)30063-4

[**88**] Sargent IL, Germain SJ, Sacks GP, Kumar S, Redman CW. Trophoblast deportation and the maternal inflammatory response in pre-eclampsia. *J Reprod Immunol*. 2003/08/05. 2003;59(2):153–60.

[**89**] Sargent IL, Borzychowski AM, Redman CW. NK cells and human pregnancy--an inflammatory view. *Trends Immunol*. 2006/07/18. 2006;27(9):399–404. DOI:10.1016/j.it.2006.06.009

[**90**] Peyter AC, Delhaes F, Baud D, Vial Y, Diaceri G, Menétrey S, et al. Intrauterine growth restriction is associated with structural alterations in human umbilical cord and decreased nitric oxide-induced relaxation of umbilical vein. *Placenta* [Internet]. 2014;35(11):891–9. DOI:10.1016/j.placenta.2014.08.090

[**91**] Jones S, Bischof H, Lang I, Desoye G, Greenwood SL, Johnstone ED, et al. Dysregulated flow-mediated vasodilatation in the human placenta in fetal growth restriction. *J Physiol* [Internet]. 2015 [cited 2019 Jul 21];593(14):3077–92. DOI:10.1113/JP270495

[**92**] Antonetti DA, Barber AJ, Khin S, Lieth E, Tarbell JM, Gardner TW. Vascular permeability in experimental diabetes is associated with reduced endothelial occludin content. Vascular endothelial growth factor decreases occludin in retinal endothelial cells. *Diabetes*. 1998;47(12):1953–9. DOI:10.2337/diabetes.47.12.1953

[**93**] Harhaj NS, Felinski EA, Wolpert EB, Sundstrom JM, Gardner TW, Antonetti DA. VEGF activation of protein kinase C stimulates occludin phosphorylation and contributes to endothelial permeability. *Investig Ophthalmol Vis Sci*. 2006;47(11):5106–15. DOI:10.1167/iovs.06-0322

[**94**] Giebel SJ, Menicucci G, McGuire PG, Das A. Matrix metalloproteinases in early diabetic retinopathy and their role in alternation of the blood-retinal barrier. *Lab Investig*. 2005;85(5):597–607. DOI:10.1038/labinvest.3700251

[**95**] Babawale MO, Lovat S, Mayhew TM, Lammiman MJ, James DK, Leach L. Effects of gestational diabetes on junctional adhesion molecules in human term placental vasculature. *Diabetologia*. 2000;43(9):1185–96. DOI:10.1007/s001250051511

[**96**] Navaratna D, McGuire PG, Menicucci G, Das A. Proteolytic degradation of VE-cadherin alters the blood-retinal barrier in diabetes. *Diabetes*. 2007;56(9):2380–7. DOI:10.2337/db06-1694

[**97**] Leach L, Gray C, Staton S, Babawale MO, Gruchy A, Foster C, et al. Vascular endothelial cadherin and β-catenin in human fetoplacental vessels of pregnancies complicated by Type 1 diabetes: Associations with angiogenesis and perturbed barrier function. *Diabetologia*. 2004;47(4):695–709. DOI:10.1007/s00125-004-1341-7

[**98**] Aiello LP, Arrigg PG, Shah ST, Keyt BA, Avery RL, Jampel HD, et al. Vascular Endothelial Growth Factor in Ocular Fluid of Patients with Diabetic Retinopathy and Other Retinal Disorders. *N Engl J Med*. 1994;331(22):1480–7. DOI:10.1056/NEJM199412013312203

[**99**] Cooper ME, Vranes D, Youssef S, Stacker SA, Cox AJ, Rizkalla B, et al. Increased renal expression of vascular endothelial growth factor (VEGF) and its receptor VEGFR-2 in experimental diabetes. *Diabetes*. 1999;48(11):2229–39. DOI:10.2337/diabetes.48.11.2229

[**100**] Liu F, Xia M, Xu A. Expression of VEGF, iNOS, and eNOS is increased in cochlea of diabetic rat. *Acta Otolaryngol*. 2008;128(11):1178–86. DOI:10.1080/00016480801901774

[**101**] Teasdale F. Histomorphometry of the human placenta in class B diabetes mellitus. *Placenta*. 1983;4(1):1–12. DOI:10.1016/S0143-4004(83)80012-5

[**102**] Mayhew T. Enhanced fetoplacental angiogenesis in pre-gestational diabetes mellitus: The extra growth is exclusively longitudinal and not accompanied by microvascular remodelling. *Diabetologia*. 2002;45(10):1434–9. DOI:10.1007/s00125-002-0927-1

[**103**] Jauniaux E, Burton GJ. Villous histomorphometry and placental bed biopsy investigation in type I diabetic pregnancies. *Placenta*. 2006;27(4–5):468–74. DOI:10.1016/j.placenta.2005.04.010

[**104**] Wright TJ, Leach L, Shaw PE, Jones P. Dynamics of vascular endothelial-cadherin and β-catenin localization by vascular endothelial growth factor-induced angiogenesis in human umbilical vein cells. *Exp Cell Res*. 2002;280(2):159–68. DOI:10.1006/excr.2002.5636

[**105**] Dye J, Lawrence L, Linge C, Leach L, Firth JA, Clark P. Distinct Patterns of Microvascular Endothelial Cell Morphology Are Determined by Extracellular

Matrix Composition. *Endothelium*. 2004;11:151–67. DOI:10.1080/10623320490512093

[**106**] Sweet IR, Gilbert M, Maloney E, Hockenbery DM, Schwartz MW, Kim F. Endothelial inflammation induced by excess glucose is associated with cytosolic glucose 6-phosphate but not increased mitochondrial respiration. *Diabetologia*. 2009;52(5):921–31. DOI:10.1007/s00125-009-1272-4

[**107**] Yang Z, Laubach VE, French BA, Kron IL. Acute hyperglycemia enhances oxidative stress and exacerbates myocardial infarction by activating nicotinamide adenine dinucleotide phosphate oxidase during reperfusion. *J Thorac Cardiovasc Surg*. 2009;137(3):723–9. DOI:10.1016/j.jtcvs.2008.08.056

[**108**] Ettelaie C, Su S, Li C, Collier MEW. Tissue factor-containing microparticles released from mesangial cells in response to high glucose and AGE induce tube formation in microvascular cells. *Microvasc Res*. 2008;76(3):152–60. DOI:10.1016/j.mvr.2008.07.007

[**109**] Ejaz S. Importance of pericytes and mechanisms of pericyte loss during diabetes retinopathy. *Diabetes, Obes Metab*. 2008;10(1):53–63. DOI:10.1111/j.1463-1326.2007.00795.x

[**110**] Boden G, Vaidyula VR, Homko C, Cheung P, Rao AK. Circulating tissue factor procoagulant activity and thrombin generation in patients with type 2 diabetes: Effects of insulin and glucose. *J Clin Endocrinol Metab*. 2007;92(11):4352–8. DOI:10.1210/jc.2007-0933

[**111**] Singh VP, Le B, Khode R, Baker KM, Kumar R. Intracellular angiotensin II production in diabetic rats is correlated with cardiomyocyte apoptosis, oxidative stress, and cardiac fibrosis. *Diabetes*. 2008;57(12):3297–306. DOI:10.2337/db08-0805

[**112**] Kwaan HC. Changes in blood coagulation, platelet function, and plasminogen-plasmin system in diabetes. *Diabetes*. 1992;41(SUPPL. 2):32–5. DOI:10.2337/diab.41.2.s32

[**113**] Kario K, Matsuo T, Kobayashi H, Matsuo M, Sakata T, Miyata T. Activation of tissue factor-induced coagulation and endothelial cell dysfunction in non-insulin-dependent diabetic patients with microalbuminuria. *Arterioscler Thromb Vasc Biol*. 1995;15(8):1114–20. DOI:10.1161/01.ATV.15.8.1114

[**114**] Chiarelli F, Cipollone F, Romano F, Tumini S, Costantini F, Di Ricco L, et al. Increased circulating nitric oxide in young patinets with type 1 diabetes and persistent microalbuminuria: Relation to glomerular hyperfiltration. *Diabetes*. 2000;49(7):1258–63. DOI:10.2337/diabetes.49.7.1258

[**115**] Sung SH, Ziyadeh FN, Wang A, Pyagay PE, Kanwar YS, Chen S. Blockade of vascular endothelial growth factor signaling ameliorates diabetic albuminuria in mice. *J Am Soc Nephrol*. 2006;17(11):3093–104. DOI:10.1681/ASN.2006010064

[**116**] Desoye G, Hahn T, Hartmann M, Blaschitz A, Dohr G, Kohnen G, et al. Insulin receptors in syncytitrophoblast and fetal endothelium of human placenta. Immunohistochemical evidence for developmental changes in distribution pattern. *Histochemistry*. 1994;101(4):277–85. DOI:10.1007/BF00315915

[**117**] Hiden U, Glitzner E, Hartmann M, Desoye G. Insulin and the IGF system in the

human placenta of normal and diabetic pregnancies. *J Anat*. 2009;215(1):60–8. DOI:10.1111/j.1469-7580.2008.01035.x

[**118**] Su EJ. Role of the fetoplacental endothelium in fetal growth restriction with abnormal umbilical artery Doppler velocimetry. *Am J Obs Gynecol* [Internet]. 2015;213(4):S123–30. DOI:10.1016/j.ajog.2015.06.038

[**119**] Pang V, Bates DO, Leach L. Regulation of human feto-placental endothelial barrier integrity by vascular endothelial growth factors: Competitive interplay between VEGF-A165a, VEGF-A165b, PIGF and VE-cadherin. *Clin Sci*. 2017;131(23):2763–75. DOI:10.1042/CS20171252

[**120**] Kaufmann P. Basic Morphology of the Fetal and Maternal Circuits in the Human Placenta. In: Contributions to Gynecology and Obstetrics. Karger Publishers; 1985. p. 5–17. DOI:10.1159/000410663

[**121**] Reynolds F, Knott C. Pharmacokinetics in pregnancy and placental drug transfer. *Oxf Rev Reprod Biol*. 1989;11:389–449.

[**122**] Firth JA, Leach L. Structure and permeability in human placental capillaries. *Placenta*. 1997;18:205–13. DOI:10.1016/s0143-4004(97)80090-2

[**123**] Eaton BM, Leach L, Firth JA. Permeability of the fetal villous microvasculature in the isolated perfused term human placenta. *J Physiol*. 1993;463(1):141–55. DOI:10.1113/jphysiol.1993.sp019588

[**124**] Wessel F, Winderlich M, Holm M, Frye M, Rivera-Galdos R, Vockel M, et al. Leukocyte extravasation and vascular permeability are each controlled in vivo by different tyrosine residues of VE-cadherin. *Nat Immunol*. 2014;15(3):223–30. DOI:10.1038/ni.2824

[**125**] Leach L, Babawale MO, Anderson M, Lammiman M. Vasculogenesis, angiogenesis and the molecular organisation of endothelial junctions in the early human placenta. *J Vasc Res*. 2002;39(3):246–59. DOI:10.1159/000063690

[**126**] Leach L, Lammiman MJ, Babawale MO, Hobson SA, Bromilou B, Lovat S, et al. Molecular organization of tight and adherens junctions in the human placental vascular tree. *Placenta*. 2000;21(5–6):547–57. DOI:10.1053/plac.2000.0541

[**127**] Wang Y, Lewis DF, Gu Y, Zhang Y, Alexander JS, Granger DN. Placental Trophoblast-Derived Factors Diminish Endothelial Barrier Function. *J Clin Endocrinol Metab*. 2004;89(5):2421–8. DOI:10.1210/jc.2003-031707

[**128**] Bates DO, MacMillan PP, Manjaly JG, Qiu Y, Hudson SJ, Bevan HS, et al. The endogenous anti-angiogenic family of splice variants of VEGF, VEGF xxxb, are down-regulated in pre-eclamptic placentae at term. *Clin Sci*. 2006;110(5):575–85. DOI:10.1042/CS20050292

[**129**] Burnstock G. Purinergic Nerves. *Pharmacol Rev* [Internet]. 1972 [cited 2021 Sep 19];24(3):509–81. Available from: https://pubmed.ncbi.nlm.nih.gov/4404211/

[**130**] Ralevic V, Burnstock G. Receptors for purines and pyrimidines. *Pharmacol Rev*. 1998;50(3):413–92. DOI:10.1007/978-3-642-28863-0_5

[**131**] G B. Purine and pyrimidine receptors. *Cell Mol Life Sci* [Internet]. 2007 Jun [cited 2021 Sep 19];64(12):1471–83. DOI:10.1007/S00018-007-6497-0

[**132**] Burnstock G, Knight GE. Cellular distribution and functions of P2 receptor

subtypes in different systems. *Int Rev Cytol*. 2004;240:31–304. DOI:10.1016/S0074-7696(04)40002-3

[**133**] Burnstock G. Short- and long-term (trophic) purinergic signalling. *Philos Trans R Soc B Biol Sci* [Internet]. 2016 Aug 5 [cited 2021 Sep 19];371(1700). DOI:10.1098/RSTB.2015.0422

[**134**] Borea PA, Gessi S, Merighi S, Varani K. Adenosine as a Multi-Signalling Guardian Angel in Human Diseases: When, Where and How Does it Exert its Protective Effects? *Trends Pharmacol Sci*. 2016 Jun;37(6):419–34. DOI:10.1016/j.tips.2016.02.006

[**135**] Sattin A, Rall TW. The effect of adenosine and adenine nucleotides on the cyclic adenosine 3', 5'-phosphate content of guinea pig cerebral cortex slices. *Mol Pharmacol*. 1970 Jan;6(1):13–23.

[**136**] Fredholm BB, IJzerman AP, Jacobson KA, Linden J, Müller CE. International Union of Basic and Clinical Pharmacology. LXXXI. Nomenclature and Classification of Adenosine Receptors—An Update. *Pharmacol Rev* [Internet]. 2011 Mar 1 [cited 2021 Sep 17];63(1):1–34. DOI:10.1124/PR.110.003285

[**137**] Peleli M, Fredholm BB, Sobrevia L, Carlström M. Pharmacological targeting of adenosine receptor signaling. *Mol Aspects Med*. 2017 Jun;55:4–8. DOI:10.1016/j.mam.2016.12.002

[**138**] Fredholm BB, Arslan G, Halldner L, Kull B, Schulte G, Wasserman W. Structure and function of adenosine receptors and their genes. *Naunyn Schmiedebergs Arch Pharmacol*. 2000 Nov;362(4–5):364–74. DOI:10.1007/s002100000313

[**139**] Fredholm BB, IJzerman AP, Jacobson KA, Klotz KN, Linden J. International Union of Pharmacology. XXV. Nomenclature and classification of adenosine receptors. *Pharmacol Rev*. 2001 Dec;53(4):527–52.

[**140**] Aghaei M, Panjehpour M, Karami-Tehrani F, Salami S. Molecular mechanisms of A3 adenosine receptor-induced G1 cell cycle arrest and apoptosis in androgen-dependent and independent prostate cancer cell lines: involvement of intrinsic pathway. *J Cancer Res Clin Oncol*. 2011 Oct;137(10):1511–23. DOI:10.1007/s00432-011-1031-z

[**141**] Borea PA, Gessi S, Merighi S, Vincenzi F, Varani K. Pharmacology of Adenosine Receptors: The State of the Art. *https://doi.org/101152/physrev000492017* [Internet]. 2018 May 31 [cited 2021 Sep 17];98(3):1591–625. DOI:10.1152/PHYSREV.00049.2017

[**142**] Ralevic V, Dunn WR. Purinergic transmission in blood vessels. *Aut Neurosci* [Internet]. 2015;191:48–66. DOI:10.1016/j.autneu.2015.04.007

[**143**] McCarthy AE, Yoshioka C, Mansoor SE. Full-Length P2X7 Structures Reveal How Palmitoylation Prevents Channel Desensitization. *Cell*. 2019 Oct 17;179(3):659-670.e13. DOI:10.1016/J.CELL.2019.09.017

[**144**] Jacobson KA, Müller CE. Medicinal chemistry of adenosine, P2Y and P2X receptors. *Neuropharmacology*. 2016 May;104:31–49. DOI:10.1016/j.neuropharm.2015.12.001

[**145**] Lambertucci C, Dal Ben D, Buccioni M, Marucci G, Thomas A, Volpini R. Medicinal chemistry of P2X receptors: agonists and orthosteric antagonists.

Curr Med Chem. 2015;22(7):915–28. DOI:10.2174/0929867321666141215093513

[**146**] Illes P, Müller CE, Jacobson KA, Grutter T, Nicke A, Fountain SJ, et al. Update of P2X receptor properties and their pharmacology: IUPHAR Review 30. *Br J Pharmacol* [Internet]. 2021 Feb 1 [cited 2021 Sep 17];178(3):489–514. DOI:10.1111/BPH.15299

[**147**] Dal Ben D, Buccioni M, Lambertucci C, Marucci G, Spinaci A, Marchenkova A, et al. Investigation on 2',3'-O-Substituted ATP Derivatives and Analogs as Novel P2X3 Receptor Antagonists. *ACS Med Chem Lett* [Internet]. 2018 Dec 26;10(4):493–8. DOI:10.1021/acsmedchemlett.8b00524

[**148**] Obrecht AS, Urban N, Schaefer M, Röse A, Kless A, Meents JE, et al. Identification of aurintricarboxylic acid as a potent allosteric antagonist of P2X1 and P2X3 receptors. *Neuropharmacology*. 2019 Nov;158:107749. DOI:10.1016/j.neuropharm.2019.107749

[**149**] Khakh BS, Proctor WR, Dunwiddie T V., Labarca C, Lester HA. Allosteric Control of Gating and Kinetics at P2X4Receptor Channels. *J Neurosci* [Internet]. 1999 Sep 1 [cited 2021 Sep 21];19(17):7289–99. DOI:10.1523/JNEUROSCI.19-17-07289.1999

[**150**] A P, SD S. Mechanism of ivermectin facilitation of human P2X4 receptor channels. *J Gen Physiol* [Internet]. 2004 Mar [cited 2021 Sep 21];123(3):281–93. DOI:10.1085/JGP.200308986

[**151**] Nörenberg W, Sobottka H, Hempel C, Plötz T, Fischer W, Schmalzing G, et al. Positive allosteric modulation by ivermectin of human but not murine P2X7 receptors. *Br J Pharmacol*. 2012 Sep;167(1):48–66. DOI:10.1111/j.1476-5381.2012.01987.x

[**152**] Jacobson KA, Kim YC, Wildman SS, Mohanram A, Harden TK, Boyer JL, et al. A pyridoxine cyclic phosphate and its 6-azoaryl derivative selectively potentiate and antagonize activation of P2X1 receptors. *J Med Chem*. 1998 Jun;41(13):2201–6. DOI:10.1021/jm980183o

[**153**] Baqi Y, Hausmann R, Rosefort C, Rettinger J, Schmalzing G, Müller CE. Discovery of potent competitive antagonists and positive modulators of the P2X2 receptor. *J Med Chem*. 2011 Feb;54(3):817–30. DOI:10.1021/jm1012193

[**154**] Jacobson KA, Delicado EG, Gachet C, Kennedy C, von Kügelgen I, Li B, et al. Update of P2Y receptor pharmacology: IUPHAR Review 27. *Br J Pharmacol*. 2020 Jun 1;177(11):2413–33. DOI:10.1111/BPH.15005

[**155**] Rafehi M, Müller CE. Tools and drugs for uracil nucleotide-activated P2Y receptors. *Pharmacol Ther*. 2018 Oct;190:24–80. DOI:10.1016/j.pharmthera.2018.04.002

[**156**] Fredriksson R, Schiöth HB. The repertoire of G-protein-coupled receptors in fully sequenced genomes. *Mol Pharmacol*. 2005 May;67(5):1414–25. DOI:10.1124/mol.104.009001

[**157**] Nishimura A, Sunggip C, Oda S, Numaga-Tomita T, Tsuda M, Nishida M. Purinergic P2Y receptors: Molecular diversity and implications for treatment of cardiovascular diseases. *Pharmacol Ther*. 2017 Dec 1;180:113–28. DOI:10.1016/J.PHARMTHERA.2017.06.010

[**158**] Gao Z-G, Jacobson KA. Distinct Signaling Patterns of Allosteric Antagonism at the P2Y1 Receptor. *Mol Pharmacol* [Internet]. 2017 Nov 1 [cited 2021 Sep 24];92(5):613. DOI:10.1124/MOL.117.109660

[**159**] Miras-Portugal MT, Queipo MJ, Gil-Redondo JC, Ortega F, Gómez-Villafuertes R, Gualix J, et al. P2 receptor interaction and signalling cascades in neuroprotection. *Brain Res Bull*. 2019 Sep;151:74–83. DOI:10.1016/j.brainresbull.2018.12.012

[**160**] Zhang D, Gao Z-G, Zhang K, Kiselev E, Crane S, Wang J, et al. Two disparate ligand-binding sites in the human P2Y1 receptor. *Nature*. 2015 Apr;520(7547):317–21. DOI:10.1038/nature14287

[**161**] Zhang J, Zhang K, Gao Z-G, Paoletta S, Zhang D, Han GW, et al. Agonist-bound structure of the human P2Y12 receptor. *Nature*. 2014 May;509(7498):119–22. DOI:10.1038/nature13288

[**162**] Zhang K, Zhang J, Gao Z-G, Zhang D, Zhu L, Han GW, et al. Structure of the human P2Y12 receptor in complex with an antithrombotic drug. *Nature*. 2014 May;509(7498):115–8. DOI:10.1038/nature13083

[**163**] Burnstock G. Do some nerve cells release more than one transmitter? [Internet]. Vol. 1, Neuroscience. Neuroscience; 1976 [cited 2020 Jul 15]. p. 239–48. DOI:10.1016/0306-4522(76)90054-3

[**164**] Furchgott RF. The Role of Endothelium in the Responses of Vascular Smooth Muscle to Drugs. *Annu Rev Pharmacol Toxicol* [Internet]. 1984 Apr [cited 2020 Jul 15];24(1):175–97. DOI:10.1146/annurev.pa.24.040184.001135

[**165**] Burnstock G. Local control of blood pressure by purines. *Blood Vessels* [Internet]. 1987 [cited 2020 Jul 15];24(3):156–60. DOI:10.1159/000158691

[**166**] Burnstock G. Sympathetic purinergic transmission in small blood vessels. *Trends Pharmacol Sci* [Internet]. 1988 [cited 2020 Jul 15];9(4):116–7. DOI:10.1016/0165-6147(88)90185-X

[**167**] Burnstock G. Vascular control by purines with emphasis on the coronary system. *Eur Heart J*. 1989 Nov;10 Suppl F:15–21. DOI:10.1093/eurheartj/10.suppl_f.15

[**168**] Burnstock G. Local mechanisms of blood flow control by perivascular nerves and endothelium. *J Hypertens Suppl Off J Int Soc Hypertens*. 1990 Dec;8(7):S95-106.

[**169**] Bersini S, Yazdi IK, Talò G, Shin SR, Moretti M, Khademhosseini A. Cell-microenvironment interactions and architectures in microvascular systems. *Biotechnol Adv*. 2016;34(6):1113–30. DOI:10.1016/j.biotechadv.2016.07.002

[**170**] Atkinson CL, Lewis NCS, Carter HH, Thijssen DHJ, Ainslie PN, Green DJ. Impact of sympathetic nervous system activity on post-exercise flow-mediated dilatation in humans. *J Physiol*. 2015 Dec;593(23):5145–56. DOI:10.1113/JP270946

[**171**] Hong K-S, Lee M-G. Endothelial Ca(2+) signaling-dependent vasodilation through transient receptor potential channels. *Korean J Physiol Pharmacol* [Internet]. 2020 Jul 1;24(4):287–98. DOI:10.4196/kjpp.2020.24.4.287

[**172**] Begandt D, Good ME, Keller AS, DeLalio LJ, Rowley C, Isakson BE, et al.

Pannexin channel and connexin hemichannel expression in vascular function and inflammation. *BMC Cell Biol*. 2017 Jan;18(Suppl 1):2. DOI:10.1186/s12860-016-0119-3

[**173**] Burnstock G. Vessel tone and remodeling. *Nat Med* [Internet]. 2006;12(1):16–7. DOI:10.1038/nm0106-16

[**174**] Su C. Extracellular Functions of Nucleotides in Heart and Blood Vessels. *Annu Rev Physiol* [Internet]. 1985 Oct [cited 2020 Jul 15];47(1):665–76. DOI:10.1146/annurev.ph.47.030185.003313

[**175**] Burnstock G, Kennedy C. Is there a basis for distinguishing two types of P2-purinoceptor? *Gen Pharmacol*. 1985;16(5):433–40. DOI:10.1016/0306-3623(85)90001-1

[**176**] Pearson JD, Gordon JL. P2 purinoceptors in the blood vessel wall. *Biochem Pharmacol* [Internet]. 1989 Dec 1 [cited 2020 Jul 15];38(23):4157–63. DOI:10.1016/0006-2952(89)90509-1

[**177**] Bodin P, Bailey D, Burnstock G. Increased flow-induced ATP release from isolated vascular endothelial cells but not smooth muscle cells. *Br J Pharmacol*. 1991 May;103(1):1203–5. DOI:10.1111/j.1476-5381.1991.tb12324.x

[**178**] Bodin P, Burnstock G. Evidence that release of adenosine triphosphate from endothelial cells during increased shear stress is vesicular. *J Cardiovasc Pharmacol*. 2001 Dec;38(6):900–8. DOI:10.1097/00005344-200112000-00012

[**179**] Vessey KA, Ho T, Jobling AI, Wang AY, Fletcher EL. Fluorescent Labeling and Quantification of Vesicular ATP Release Using Live Cell Imaging. *Methods Mol Biol*. 2020;2041:209–21. DOI:10.1007/978-1-4939-9717-6_15

[**180**] Lim To WK, Kumar P, Marshall JM. Hypoxia is an effective stimulus for vesicular release of ATP from human umbilical vein endothelial cells. *Placenta*. 2015 Jul;36(7):759–66. DOI:10.1016/j.placenta.2015.04.005

[**181**] Faigle M, Seessle J, Zug S, El Kasmi KC, Eltzschig HK. ATP release from vascular endothelia occurs across Cx43 hemichannels and is attenuated during hypoxia. *PLoS One* [Internet]. 2008 Jul 30;3(7):e2801–e2801. DOI:10.1371/journal.pone.0002801

[**182**] Kameritsch P, Pogoda K. The Role of Connexin 43 and Pannexin 1 During Acute Inflammation. *Front Physiol*. 2020;11:594097. DOI:10.3389/fphys.2020.594097

[**183**] Dosch M, Zindel J, Jebbawi F, Melin N, Sanchez-Taltavull D, Stroka D, et al. Connexin-43-dependent ATP release mediates macrophage activation during sepsis. *Elife*. 2019 Feb;8. DOI:10.7554/eLife.42670

[**184**] Yegutkin GG. Nucleotide- and nucleoside-converting ectoenzymes: Important modulators of purinergic signalling cascade. Vol. 1783, Biochimica et Biophysica Acta - Molecular Cell Research. Elsevier; 2008. p. 673–94. DOI:10.1016/j.bbamcr.2008.01.024

[**185**] Zimmermann H, Zebisch M, Sträter N. Cellular function and molecular structure of ecto-nucleotidases. *Purinergic Signal*. 2012 Sep;8(3):437–502. DOI:10.1007/s11302-012-9309-4

[**186**] Kepp O, Loos F, Liu P, Kroemer G. Extracellular nucleosides and nucleotides as immunomodulators. *Immunol Rev*. 2017 Nov;280(1):83–92.

DOI:10.1111/imr.12571

[**187**] Giuliani AL, Sarti AC, Di Virgilio F. Extracellular nucleotides and nucleosides as signalling molecules. *Immunol Lett*. 2019 Jan;205:16–24. DOI:10.1016/j.imlet.2018.11.006

[**188**] Dou L, Chen Y-F, Cowan PJ, Chen X-P. Extracellular ATP signaling and clinical relevance. *Clin Immunol*. 2018 Mar;188:67–73. DOI:10.1016/j.clim.2017.12.006

[**189**] Strassheim D, Verin A, Batori R, Nijmeh H, Burns N, Kovacs-Kasa A, et al. P2Y Purinergic Receptors, Endothelial Dysfunction, and Cardiovascular Diseases. *Int J Mol Sci*. 2020 Sep;21(18). DOI:10.3390/ijms21186855

[**190**] Burnstock G, Ralevic V. Purinergic signaling and blood vessels in health and disease. *Pharmacol Rev* [Internet]. 2013/12/18. 2014 [cited 2019 Mar 1];66(1):102–92. DOI:10.1124/pr.113.008029

[**191**] Burnstock G. Purinergic Signalling and Endothelium. *Curr Vasc Pharmacol*. 2016;14(2):130–45. DOI:10.2174/1570161114666151202204948

[**192**] Burnstock G. Purinergic regulation of vascular tone and remodelling. *Auton Autacoid Pharmacol*. 2009 Jul;29(3):63–72. DOI:10.1111/j.1474-8673.2009.00435.x

[**193**] Van Coevorden A, Boeynaems JM. Physiological concentrations of ADP stimulate the release of prostacyclin from bovine aortic endothelial cells. *Prostaglandins*. 1984 Apr;27(4):615–26. DOI:10.1016/0090-6980(84)90097-2

[**194**] Bogle RG, Coade SB, Moncada S, Pearson JD, Mann GE. Bradykinin and ATP stimulate L-arginine uptake and nitric oxide release in vascular endothelial cells. *Biochem Biophys Res Commun*. 1991 Oct;180(2):926–32. DOI:10.1016/s0006-291x(05)81154-4

[**195**] Kelm M, Feelisch M, Deussen A, Strauer BE, Schrader J. Release of endothelium derived nitric oxide in relation to pressure and flow. *Cardiovasc Res*. 1991 Oct;25(10):831–6. DOI:10.1093/cvr/25.10.831

[**196**] Nava E, Llorens S. The paracrine control of vascular motion. A historical perspective. *Pharmacol Res*. 2016 Nov;113(Pt A):125–45. DOI:10.1016/j.phrs.2016.08.003

[**197**] Bodin P, Burnstock G. ATP-stimulated release of ATP by human endothelial cells. *J Cardiovasc Pharmacol*. 1996 Jun;27(6):872–5. DOI:10.1097/00005344-199606000-00015

[**198**] BURNSTOCK G. Release of vasoactive substances from endothelial cells by shear stress and purinergic mechanosensory transduction. *J Anat* [Internet]. 1999 Apr [cited 2020 Jul 16];194(3):335–42. DOI:10.1046/j.1469-7580.1999.19430335.x

[**199**] Yamamoto K, Imamura H, Ando J. Shear stress augments mitochondrial ATP generation that triggers ATP release and Ca(2+) signaling in vascular endothelial cells. *Am J Physiol Heart Circ Physiol*. 2018 Nov;315(5):H1477–85. DOI:10.1152/ajpheart.00204.2018

[**200**] Schwiebert LM, Rice WC, Kudlow BA, Taylor AL, Schwiebert EM. Extracellular ATP signaling and P2X nucleotide receptors in monolayers of primary human vascular endothelial cells. *Am J Physiol Cell Physiol*. 2002 Feb;282(2):C289-

301. DOI:10.1152/ajpcell.01387.2000

[**201**] LeRoy EC, Ager A, Gordon JL. Effects of neutrophil elastase and other proteases on porcine aortic endothelial prostaglandin I2 production, adenine nucleotide release, and responses to vasoactive agents. *J Clin Invest* [Internet]. 1984 [cited 2020 Jul 16];74(3):1003–10. DOI:10.1172/JCI111467

[**202**] Sathanoori R, Rosi F, Gu BJ, Wiley JS, Müller CE, Olde B, et al. Shear stress modulates endothelial KLF2 through activation of P2X4. *Purinergic Signal*. 2015 Mar;11(1):139–53. DOI:10.1007/s11302-014-9442-3

[**203**] Dosch M, Gerber J, Jebbawi F, Beldi G. Mechanisms of ATP Release by Inflammatory Cells. *Int J Mol Sci*. 2018 Apr;19(4). DOI:10.3390/ijms19041222

[**204**] Lohman AW, Billaud M, Isakson BE. Mechanisms of ATP release and signalling in the blood vessel wall. *Cardiovasc Res*. 2012 Aug;95(3):269–80. DOI:10.1093/cvr/cvs187

[**205**] Lohman AW, Billaud M, Straub AC, Johnstone SR, Best AK, Lee M, et al. Expression of pannexin isoforms in the systemic murine arterial network. *J Vasc Res*. 2012;49(5):405–16. DOI:10.1159/000338758

[**206**] Yamamoto K, Furuya K, Nakamura M, Kobatake E, Sokabe M, Ando J. Visualization of flow-induced ATP release and triggering of Ca2+ waves at caveolae in vascular endothelial cells. *J Cell Sci*. 2011 Oct;124(Pt 20):3477–83. DOI:10.1242/jcs.087221

[**207**] Tölle M, Jankowski V, Schuchardt M, Wiedon A, Huang T, Hub F, et al. Adenosine 5'-tetraphosphate is a highly potent purinergic endothelium-derived vasoconstrictor. *Circ Res*. 2008 Nov;103(10):1100–8. DOI:10.1161/CIRCRESAHA.108.177865

[**208**] Lang JA, Krajek AC, Smaller KA. Evidence for a functional vasoconstrictor role for ATP in the human cutaneous microvasculature. *Exp Physiol*. 2017 Jun;102(6):684–93. DOI:10.1113/EP086231

[**209**] Jankowski V, Tölle M, Vanholder R, Schönfelder G, van der Giet M, Henning L, et al. Uridine adenosine tetraphosphate: a novel endothelium- derived vasoconstrictive factor. *Nat Med*. 2005 Feb;11(2):223–7. DOI:10.1038/nm1188

[**210**] Niemelä J, Henttinen T, Yegutkin GG, Airas L, Kujari A-M, Rajala P, et al. IFN-alpha induced adenosine production on the endothelium: a mechanism mediated by CD73 (ecto-5'-nucleotidase) up-regulation. *J Immunol*. 2004 Feb;172(3):1646–53. DOI:10.4049/jimmunol.172.3.1646

[**211**] Grünewald JK, Ridley AJ. CD73 represses pro-inflammatory responses in human endothelial cells. *J Inflamm (Lond)*. 2010 Feb;7(1):10. DOI:10.1186/1476-9255-7-10

[**212**] Sollevi A, Fredholm BB. Influence of adenosine on the vascular responses to sympathetic nerve stimulation in the canine subcutaneous adipose tissue. *Acta Physiol Scand*. 1983/09/01. 1983;119(1):15–24. DOI:10.1111/j.1748-1716.1983.tb07300.x

[**213**] Sparks H V., Gorman MW. Adenosine in the Local Regulation of Blood Flow: Current Controversies. In: Topics and Perspectives in Adenosine Research [Internet]. Springer Berlin Heidelberg; 1987 [cited 2020 Jul 16]. p. 406–15.

DOI:10.1007/978-3-642-45619-0_33

[**214**] Tabrizchi R, Bedi S. Pharmacology of adenosine receptors in the vasculature. *Pharmacol Ther*. 2001/12/01. 2001;91(2):133–47. DOI:10.1016/S0163-7258(01)00152-8

[**215**] Li J m, Fenton RA, Wheeler HB, Powell CC, Peyton BD, Cutler BS, et al. Adenosine A2a receptors increase arterial endothelial cell nitric oxide. *J Surg Res*. 1998 Dec;80(2):357–64. DOI:10.1006/jsre.1998.5439

[**216**] Smits P, Williams SB, Lipson DE, Banitt P, Rongen GA, Creager MA. Endothelial release of nitric oxide contributes to the vasodilator effect of adenosine in humans. *Circulation*. 1995 Oct;92(8):2135–41. DOI:10.1161/01.cir.92.8.2135

[**217**] Iwamoto T, Umemura S, Toya Y, Uchibori T, Kogi K, Takagi N, et al. Identification of adenosine A2 receptor-cAMP system in human aortic endothelial cells. *Biochem Biophys Res Commun*. 1994 Mar;199(2):905–10. DOI:10.1006/bbrc.1994.1314

[**218**] Auchampach JA. Adenosine receptors and angiogenesis. *Circ Res* [Internet]. 2007 Nov [cited 2020 Jul 16];101(11):1075–7. DOI:10.1161/CIRCRESAHA.107.165761

[**219**] Feoktistov I, Goldstein AE, Ryzhov S, Zeng D, Belardinelli L, Voyno-Yasenetskaya T, et al. Differential expression of adenosine receptors in human endothelial cells: role of A2B receptors in angiogenic factor regulation. *Circ Res*. 2002 Mar;90(5):531–8. DOI:10.1161/01.res.0000012203.21416.14

[**220**] Takagi H, King GL, Robinson GS, Ferrara N, Aiello LP. Adenosine mediates hypoxic induction of vascular endothelial growth factor in retinal pericytes and endothelial cells. *Invest Ophthalmol Vis Sci*. 1996 Oct;37(11):2165–76.

[**221**] Grant MB, Tarnuzzer RW, Caballero S, Ozeck MJ, Davis MI, Spoerri PE, et al. Adenosine receptor activation induces vascular endothelial growth factor in human retinal endothelial cells. *Circ Res*. 1999 Oct;85(8):699–706. DOI:10.1161/01.res.85.8.699

[**222**] Feoktistov I, Ryzhov S, Goldstein AE, Biaggioni I. Mast cell-mediated stimulation of angiogenesis: cooperative interaction between A2B and A3 adenosine receptors. *Circ Res*. 2003 Mar;92(5):485–92. DOI:10.1161/01.RES.0000061572.10929.2D

[**223**] Wiktorowska-Owczarek A, Namiecinska M, Balcerczyk A, Nowak JZ. Human micro- and macrovessel-derived endothelial cells: a comparative study on the effects of adrenaline and a selective adenosine A2-type receptor agonist under normoxic and hypoxic conditions. *Pharmacol Rep*. 2007;59(6):800–6.

[**224**] Deguchi H, Takeya H, Urano H, Gabazza EC, Zhou H, Suzuki K. Adenosine regulates tissue factor expression on endothelial cells. *Thromb Res*. 1998 Jul;91(2):57–64. DOI:10.1016/s0049-3848(98)00045-0

[**225**] Bahreyni A, Avan A, Shabani M, Ryzhikov M, Fiuji H, Soleimanpour S, et al. Therapeutic potential of A2 adenosine receptor pharmacological regulators in the treatment of cardiovascular diseases, recent progress, and prospective. *J Cell Physiol*. 2019 Feb;234(2):1295–9. DOI:10.1002/jcp.27161

[**226**] Nguyen DK, Montesinos MC, Williams AJ, Kelly M, Cronstein BN. Th1 cytokines regulate adenosine receptors and their downstream signaling elements in human microvascular endothelial cells. *J Immunol*. 2003 Oct;171(8):3991–8. DOI:10.4049/jimmunol.171.8.3991

[**227**] Faas MM, Saez T, de Vos P. Extracellular ATP and adenosine: The Yin and Yang in immune responses? *Mol Asp Med* [Internet]. 2017/01/18. 2017;55:9–19. DOI:10.1016/j.mam.2017.01.002

[**228**] Thakur S, Du J, Hourani S, Ledent C, Li J-M. Inactivation of adenosine A2A receptor attenuates basal and angiotensin II-induced ROS production by Nox2 in endothelial cells. *J Biol Chem*. 2010 Dec;285(51):40104–13. DOI:10.1074/jbc.M110.184606

[**229**] Henttinen T, Jalkanen S, Yegutkin GG. Adherent leukocytes prevent adenosine formation and impair endothelial barrier function by Ecto-5'-nucleotidase/CD73-dependent mechanism. *J Biol Chem*. 2003 Jul;278(27):24888–95. DOI:10.1074/jbc.M300779200

[**230**] Zukowska P, Kutryb-Zajac B, Toczek M, Smolenski RT, Slominska EM. The role of ecto-5'-nucleotidase in endothelial dysfunction and vascular pathologies. *Pharmacol Rep*. 2015 Aug;67(4):675–81. DOI:10.1016/j.pharep.2015.05.002

[**231**] Devaux Y, Bousquenaud M, Rolland-Turner M, Maskali F, Zhang L, Marie P, et al. Systems-based investigation of the effects of adenosine on endothelial progenitor cells. *Cardiovasc Res*. 2012 Mar 15;S15–S15.

[**232**] Fernandez P, Jara C, Aguilera V, Caviedes L, Diaz F, Radojkovic C, et al. Adenosine A 2A and A 3 receptors are involved in the human endothelial progenitor cells migration. *J Cardiovasc Pharmacol*. 2012 May;59(5):397–404. DOI:10.1097/FJC.0b013e3182471d14

[**233**] Rolland-Turner M, Goretti E, Bousquenaud M, Léonard F, Nicolas C, Zhang L, et al. Adenosine Stimulates the Migration of Human Endothelial Progenitor Cells. Role ofCXCR4 and MicroRNA-150. *PLoS One* [Internet]. 2013 Jan 16 [cited 2020 Jul 17];8(1). DOI:10.1371/journal.pone.0054135

[**234**] Ray FR, Huang W, Slater M, Barden JA. Purinergic receptor distribution in endothelial cells in blood vessels: a basis for selection of coronary artery grafts. *Atherosclerosis*. 2002 May;162(1):55–61. DOI:10.1016/s0021-9150(01)00681-5

[**235**] Wang L, Karlsson L, Moses S, Hultgårdh-Nilsson A, Andersson M, Borna C, et al. P2 receptor expression profiles in human vascular smooth muscle and endothelial cells. *J Cardiovasc Pharmacol*. 2002 Dec;40(6):841–53. DOI:10.1097/00005344-200212000-00005

[**236**] Musa H, Tellez JO, Chandler NJ, Greener ID, Maczewski M, Mackiewicz U, et al. P2 purinergic receptor mRNA in rat and human sinoatrial node and other heart regions. *Naunyn Schmiedebergs Arch Pharmacol*. 2009 Jun;379(6):541–9. DOI:10.1007/s00210-009-0403-2

[**237**] Kanellopoulos JM, Almeida-da-Silva CLC, Rüütel Boudinot S, Ojcius DM. Structural and Functional Features of the P2X4 Receptor: An Immunological Perspective [Internet]. Vol. 12, Frontiers in Immunology . 2021. p. 852. Available from: https://www.frontiersin.org/article/10.3389/fimmu.2021.645834

[**238**] Glass R, Loesch A, Bodin P, Burnstock G. P2X4 and P2X6 receptors associate with VE-cadherin in human endothelial cells. *Cell Mol Life Sci*. 2002 May;59(5):870–81. DOI:10.1007/s00018-002-8474-y

[**239**] Yamamoto K, Sokabe T, Matsumoto T, Yoshimura K, Shibata M, Ohura N, et al. Impaired flow-dependent control of vascular tone and remodeling in P2X4-deficient mice. *Nat Med*. 2006 Jan;12(1):133–7. DOI:10.1038/nm1338

[**240**] Kessler S, Clauss WG, Fronius M. Laminar shear stress modulates the activity of heterologously expressed P2X(4) receptors. *Biochim Biophys Acta*. 2011 Oct;1808(10):2488–95. DOI:10.1016/j.bbamem.2011.07.010

[**241**] Yamamoto K, Korenaga R, Kamiya A, Ando J. Fluid Shear Stress Activates Ca $^{2+}$ Influx Into Human Endothelial Cells via P2X4 Purinoceptors. *Circ Res* [Internet]. 2000 Sep 1 [cited 2020 Jul 17];87(5):385–91. DOI:10.1161/01.RES.87.5.385

[**242**] Kaczmarek-Hájek K, Lörinczi E, Hausmann R, Nicke A. Molecular and functional properties of P2X receptors--recent progress and persisting challenges. *Purinergic Signal* [Internet]. 2012/05/01. 2012 Sep;8(3):375–417. DOI:10.1007/s11302-012-9314-7

[**243**] Glas R, Sauter NS, Schulthess FT, Shu L, Oberholzer J, Maedler K. Purinergic P2X7 receptors regulate secretion of interleukin-1 receptor antagonist and beta cell function and survival. *Diabetologia*. 2009;52(8):1579–88. DOI:10.1007/s00125-009-1349-0

[**244**] Beaucage KL, Xiao A, Pollmann SI, Grol MW, Beach RJ, Holdsworth DW, et al. Loss of P2X7 nucleotide receptor function leads to abnormal fat distribution in mice. *Purinergic Signal*. 2014;10(2):291–304. DOI:10.1007/s11302-013-9388-x

[**245**] Raqeeb A, Sheng J, Ao N, Braun AP. Purinergic P2Y2 receptors mediate rapid Ca2+ mobilization, membrane hyperpolarization and nitric oxide production in human vascular endothelial cells. *Cell Calcium*. 2011 Apr 1;49(4):240–8. DOI:10.1016/j.ceca.2011.02.008

[**246**] Korenaga R, Yamamoto K, Ohura N, Sokabe T, Kamiya A, Ando J. Sp1-mediated downregulation of P2X4 receptor gene transcription in endothelial cells exposed to shear stress. *Am J Physiol Heart Circ Physiol*. 2001 May;280(5):H2214-21. DOI:10.1152/ajpheart.2001.280.5.H2214

[**247**] Wilson HL, Varcoe RW, Stokes L, Holland KL, Francis SE, Dower SK, et al. P2X receptor characterization and IL-1/IL-1Ra release from human endothelial cells. *Br J Pharmacol*. 2007 May 12;151(1):96–108. DOI:10.1038/sj.bjp.0707213

[**248**] Tang Y, Matsuoka I, Ono T, Inoue K, Kimura J. Selective up-regulation of P2X4-receptor gene expression by interferon-gamma in vascular endothelial cells. *J Pharmacol Sci*. 2008 Aug;107(4):419–27. DOI:10.1254/jphs.08073fp

[**249**] Gil-Redondo JC, Iturri J, Ortega F, Pérez-Sen R, Weber A, Miras-Portugal MT, et al. Nucleotides-Induced Changes in the Mechanical Properties of Living Endothelial Cells and Astrocytes, Analyzed by Atomic Force Microscopy. *Int J Mol Sci*. 2021 Jan;22(2). DOI:10.3390/ijms22020624

[**250**] Wei W-L, He H, Guan Y-Y. Characteristic of Cl? current induced by ATP in bovine aortic endothelial cells. *Drug Dev Res* [Internet]. 2003 Jan 1 [cited 2020 Jul 18];58(1):53–6. DOI:10.1002/ddr.10129

[**251**] Mokhtar SS, Rasool AHG. Role of endothelium-dependent hyperpolarisation and prostacyclin in diabetes. *Malays J Med Sci*. 2015;22(2):8–17.

[**252**] Radziwon-Balicka A, Lesyk G, Back V, Fong T, Loredo-Calderon EL, Dong B, et al. Differential eNOS-signalling by platelet subpopulations regulates adhesion and aggregation. *Cardiovasc Res* [Internet]. 2017 Dec 1;113(14):1719–31. DOI:10.1093/cvr/cvx179

[**253**] Palmer DS, Aye MT, Ganz PR, Halpenny M, Hashemi S. Adenosine nucleotides and serotonin stimulate von Willebrand factor release from cultured human endothelial cells. *Thromb Haemost*. 1994 Jul;72(1):132–9.

[**254**] Vischer UM, Wollheim CB. Purine nucleotides induce regulated secretion of von Willebrand factor: involvement of cytosolic Ca2+ and cyclic adenosine monophosphate-dependent signaling in endothelial exocytosis. *Blood*. 1998 Jan;91(1):118–27.

[**255**] Randi AM, Smith KE, Castaman G. von Willebrand factor regulation of blood vessel formation. *Blood* [Internet]. 2018/06/04. 2018 Jul 12;132(2):132–40. DOI:10.1182/blood-2018-01-769018

[**256**] Ding L, Ma W, Littmann T, Camp R, Shen J. The P2Y(2) nucleotide receptor mediates tissue factor expression in human coronary artery endothelial cells. *J Biol Chem*. 2011 Jul;286(30):27027–38. DOI:10.1074/jbc.M111.235176

[**257**] Liu Y, Zhang L, Wang C, Roy S, Shen J. Purinergic P2Y2 Receptor Control of Tissue Factor Transcription in Human Coronary Artery Endothelial Cells: NEW AP-1 TRANSCRIPTION FACTOR SITE AND NEGATIVE REGULATOR. *J Biol Chem* [Internet]. 2015/12/02. 2016 Jan 22;291(4):1553–63. DOI:10.1074/jbc.M115.681163

[**258**] Gachet C. P2 receptors, platelet function and pharmacological implications. *Thromb Haemost*. 2008 Mar;99(3):466–72. DOI:10.1160/TH07-11-0673

[**259**] Hechler B, Gachet C. P2 receptors and platelet function. *Purinergic Signal* [Internet]. 2011 Sep [cited 2020 Jul 18];7(3):293–303. DOI:10.1007/s11302-011-9247-6

[**260**] Neubauer K, Zieger B. Endothelial cells and coagulation. *Cell Tissue Res* [Internet]. 2021; DOI:10.1007/s00441-021-03471-2

[**261**] Greenberg HZE, Shi J, Jahan KS, Martinucci MC, Gilbert SJ, Vanessa Ho W-S, et al. Stimulation of calcium-sensing receptors induces endothelium-dependent vasorelaxations via nitric oxide production and activation of IKCa channels. *Vascul Pharmacol*. 2016 May;80:75–84. DOI:10.1016/j.vph.2016.01.001

[**262**] Carling D. AMPK signalling in health and disease. *Curr Opin Cell Biol*. 2017 Apr;45:31–7. DOI:10.1016/j.ceb.2017.01.005

[**263**] Herzig S, Shaw RJ. AMPK: guardian of metabolism and mitochondrial homeostasis. *Nat Rev Mol Cell Biol*. 2018 Feb;19(2):121–35. DOI:10.1038/nrm.2017.95

[**264**] da Silva CG, Jarzyna R, Specht A, Kaczmarek E. Extracellular nucleotides and adenosine independently activate AMP-activated protein kinase in endothelial cells: involvement of P2 receptors and adenosine transporters. *Circ Res*. 2006 Mar;98(5):e39-47. DOI:10.1161/01.RES.0000215436.92414.1d

[**265**] Purkiss JR, Boarder MR. Stimulation of phosphatidate synthesis in endothelial cells in response to P2-receptor activation. Evidence for phospholipase C and phospholipase D involvement, phosphatidate and diacylglycerol interconversion and the role of protein kinase C. *Biochem J*. 1992 Oct;287 (Pt 1(Pt 1):31–6. DOI:10.1042/bj2870031

[**266**] da Silva CG, Specht A, Wegiel B, Ferran C, Kaczmarek E. Mechanism of purinergic activation of endothelial nitric oxide synthase in endothelial cells. *Circulation*. 2009 Feb;119(6):871–9. DOI:10.1161/CIRCULATIONAHA.108.764571

[**267**] HARTEL F, RODEWALD C, ASLAM M, GUNDUZ D, HAFER L, NEUMANN J, et al. Extracellular ATP induces assembly and activation of the myosin light chain phosphatase complex in endothelial cells☆. *Cardiovasc Res* [Internet]. 2007 Jun 1 [cited 2020 Jul 19];74(3):487–96. DOI:10.1016/j.cardiores.2007.02.013

[**268**] Umapathy NS, Zemskov EA, Gonzales J, Gorshkov BA, Sridhar S, Chakraborty T, et al. Extracellular β-nicotinamide adenine dinucleotide (β-NAD) promotes the endothelial cell barrier integrity via PKA- and EPAC1/Rac1-dependent actin cytoskeleton rearrangement. *J Cell Physiol* [Internet]. 2010 Apr 1 [cited 2020 Jul 19];223(1):215–23. DOI:10.1002/jcp.22029

[**269**] Simon J, Filippov AK, Göransson S, Wong YH, Frelin C, Michel AD, et al. Characterization and channel coupling of the P2Y(12) nucleotide receptor of brain capillary endothelial cells. *J Biol Chem*. 2002 Aug;277(35):31390–400. DOI:10.1074/jbc.M110714200

[**270**] Rauch BH, Rosenkranz AC, Ermler S, Böhm A, Driessen J, Fischer JW, et al. Regulation of functionally active P2Y12 ADP receptors by thrombin in human smooth muscle cells and the presence of P2Y12 in carotid artery lesions. *Arterioscler Thromb Vasc Biol*. 2010 Dec;30(12):2434–42. DOI:10.1161/ATVBAHA.110.213702

[**271**] Inoue T, Node K. Molecular basis of restenosis and novel issues of drug-eluting stents. *Circ J*. 2009 Apr;73(4):615–21. DOI:10.1253/circj.cj-09-0059

[**272**] Owens GK, Kumar MS, Wamhoff BR. Molecular regulation of vascular smooth muscle cell differentiation in development and disease. Vol. 84, Physiological Reviews. 2004. p. 767–801. DOI:10.1152/physrev.00041.2003

[**273**] Govindan S, Taylor EJA, Taylor CW. Ca(2+) signalling by P2Y receptors in cultured rat aortic smooth muscle cells. *Br J Pharmacol* [Internet]. 2010 Aug;160(8):1953–62. DOI:10.1111/j.1476-5381.2010.00763.x

[**274**] Carty DM, Delles C, Dominiczak AF. Preeclampsia and future maternal health. *J Hypertens*. 2010 Jul;28(7):1349–55. DOI:10.1097/HJH.0b013e32833a39d0

[**275**] Fouyet S, Olivier E, Leproux P, Dutot M, Rat P. Bisphenol A, Bisphenol F, and Bisphenol S: The Bad and the Ugly. Where Is the Good? *Life (Basel, Switzerland)*. 2021 Apr;11(4). DOI:10.3390/life11040314

[**276**] Tsimis ME, Lei J, Rosenzweig JM, Arif H, Shabi Y, Alshehri W, et al. P2X7 receptor blockade prevents preterm birth and perinatal brain injury in a mouse model of intrauterine inflammation. *Biol Reprod* [Internet]. 2017/10/19. 2017;97(2):230–9. DOI:10.1093/biolre/iox081

[**277**] Roberts VHJJ, Greenwood SL, Elliott AC, Sibley CP, Waters LH. Purinergic receptors in human placenta: evidence for functionally active P2X4, P2X7, P2Y2, and P2Y6. *Am J Physiol Regul Integr Comp Physiol*. 2006;290(5):1374–86. DOI:10.1152/ajpregu.00612.2005.

[**278**] Barakonyi A, Miko E, Szereday L, Polgar PD, Nemeth T, Szekeres-Bartho J, et al. Cell death mechanisms and potentially cytotoxic natural immune cells in human pregnancies complicated by preeclampsia. *Reprod Sci*. 2014 Feb;21(2):155–66. DOI:10.1177/1933719113497288

[**279**] Shirasuna K, Karasawa T, Takahashi M. Role of the NLRP3 Inflammasome in Preeclampsia. *Front Endocrinol (Lausanne)* [Internet]. 2020 Feb 25;11:80. DOI:10.3389/fendo.2020.00080

[**280**] Dubyak GR. Signal transduction by P2-purinergic receptors for extracellular ATP. *Am J Respir Cell Mol Biol*. 1991 Apr;4(4):295–300. DOI:10.1165/ajrcmb/4.4.295

[**281**] Cai WQ, Dikranian K, Bodin P, Turmaine M, Burnstock G. Colocalization of vasoactive substances in the endothelial cells of human umbilical vessels. *Cell Tissue Res* [Internet]. 1993 Dec [cited 2019 Aug 25];274(3):533–8. DOI:10.1007/BF00314550

[**282**] Bours MJ, Swennen EL, Di Virgilio F, Cronstein BN, Dagnelie PC. Adenosine 5'-triphosphate and adenosine as endogenous signaling molecules in immunity and inflammation. *Pharmacol Ther*. 2006/06/21. 2006;112(2):358–404. DOI:10.1016/j.pharmthera.2005.04.013

[**283**] Bodin P, Burnstock G. Increased release of ATP from endothelial cells during acute inflammation. *Inflamm Res Off J Eur Histamine Res Soc . [et al]*. 1998 Aug;47(8):351–4. DOI:10.1007/s000110050341

[**284**] Mariathasan S, Weiss DS, Newton K, McBride J, O'Rourke K, Roose-Girma M, et al. Cryopyrin activates the inflammasome in response to toxins and ATP. *Nature*. 2006 Mar;440(7081):228–32. DOI:10.1038/nature04515

[**285**] Warren AY, Harvey L, Shaw RW, Khan RN. Interleukin-1 Secretion From Cord Blood Mononuclear Cells In Vitro Involves P2X7 Receptor Activation. *Reprod Sci* [Internet]. 2008;15(2):189–94. DOI:10.1177/1933719107310710

[**286**] Kahlenberg JM, Lundberg KC, Kertesy SB, Qu Y, Dubyak GR. Potentiation of caspase-1 activation by the P2X7 receptor is dependent on TLR signals and requires NF-kappaB-driven protein synthesis. *J Immunol*. 2005 Dec;175(11):7611–22. DOI:10.4049/jimmunol.175.11.7611

[**287**] Coddou C, Yan Z, Obsil T, Huidobro-Toro JP, Stojilkovic SS. Activation and regulation of purinergic P2X receptor channels. *Pharmacol Rev*. 2011 Sep;63(3):641–83. DOI:10.1124/pr.110.003129

[**288**] Sluyter R. The P2X7 Receptor. *Adv Exp Med Biol*. 2017;1051:17–53. DOI:10.1007/5584_2017_59

[**289**] Pegoraro A, De Marchi E, Adinolfi E. P2X7 Variants in Oncogenesis. *Cells*. 2021 Jan;10(1). DOI:10.3390/cells10010189

[**290**] Surprenant A, Rassendren F, Kawashima E, North RA, Buell G. The cytolytic P2Z receptor for extracellular ATP identified as a P2X receptor (P2X7). *Science*.

1996 May;272(5262):735–8. DOI:10.1126/science.272.5262.735

[**291**] Rassendren F, Buell GN, Virginio C, Collo G, North RA, Surprenant A. The permeabilizing ATP receptor, P2X7. Cloning and expression of a human cDNA. *J Biol Chem*. 1997 Feb;272(9):5482–6. DOI:10.1074/jbc.272.9.5482

[**292**] Illes P. P2X7 Receptors Amplify CNS Damage in Neurodegenerative Diseases. *Int J Mol Sci*. 2020 Aug;21(17). DOI:10.3390/ijms21175996

[**293**] Steinberg TH, Silverstein SC. Extracellular ATP4- promotes cation fluxes in the J774 mouse macrophage cell line. *J Biol Chem* [Internet]. 1987 Mar 5 [cited 2020 Aug 5];262(7):3118–22. Available from: http://www.ncbi.nlm.nih.gov/pubmed/2950094

[**294**] Chessell IP, Simon J, Hibell AD, Michel AD, Barnard EA, Humphrey PP. Cloning and functional characterisation of the mouse P2X7 receptor. *FEBS Lett*. 1998 Nov;439(1–2):26–30. DOI:10.1016/s0014-5793(98)01332-5

[**295**] Karasawa A, Michalski K, Mikhelzon P, Kawate T. The P2X7 receptor forms a dye-permeable pore independent of its intracellular domain but dependent on membrane lipid composition. *Elife*. 2017 Sep;6. DOI:10.7554/eLife.31186

[**296**] Linden J, Koch-Nolte F, Dahl G. Purine Release, Metabolism, and Signaling in the Inflammatory Response. *Annu Rev Immunol*. 2019 Apr;37:325–47. DOI:10.1146/annurev-immunol-051116-052406

[**297**] Lenertz LY, Gavala ML, Zhu Y, Bertics PJ. Transcriptional control mechanisms associated with the nucleotide receptor P2X7, a critical regulator of immunologic, osteogenic, and neurologic functions [Internet]. Vol. 50, Immunologic Research. NIH Public Access; 2011 [cited 2020 Aug 5]. p. 22–38. DOI:10.1007/s12026-011-8203-4

[**298**] Grassi F, De Ponte Conti B. The P2X7 Receptor in Tumor Immunity. *Front cell Dev Biol* [Internet]. 2021 Jun 22;9:694831. DOI:10.3389/fcell.2021.694831

[**299**] Andrejew R, Oliveira-Giacomelli Á, Ribeiro DE, Glaser T, Arnaud-Sampaio VF, Lameu C, et al. The P2X7 Receptor: Central Hub of Brain Diseases. *Front Mol Neurosci* [Internet]. 2020 Jul 31;13:124. DOI:10.3389/fnmol.2020.00124

[**300**] Li M, Yang C, Wang Y, Song W, Jia L, Peng X, et al. The Expression of P2X7 Receptor on Th1, Th17, and Regulatory T Cells in Patients with Systemic Lupus Erythematosus or Rheumatoid Arthritis and Its Correlations with Active Disease. *J Immunol*. 2020 Oct;205(7):1752–62. DOI:10.4049/jimmunol.2000222

[**301**] Jørgensen NR. The purinergic P2X7 ion channel receptor-a “repair” receptor in bone. *Curr Opin Immunol*. 2018 Jun;52:32–8. DOI:10.1016/j.coi.2018.03.016

[**302**] Gentile D, Natale M, Lazzerini PE, Capecchi PL, Laghi-Pasini F. The role of P2X7 receptors in tissue fibrosis: a brief review. *Purinergic Signal* [Internet]. 2015/08/29. 2015 Dec;11(4):435–40. DOI:10.1007/s11302-015-9466-3

[**303**] Sperlagh B, Vizi ES, Wirkner K, Illes P. P2X7 receptors in the nervous system. *Prog Neurobiol* [Internet]. 2006;78(6):327–46. DOI:10.1016/j.pneurobio.2006.03.007

[**304**] Zhao Y-F, Tang Y, Illes P. Astrocytic and Oligodendrocytic P2X7 Receptors Determine Neuronal Functions in the CNS. *Front Mol Neurosci* [Internet]. 2021 Feb 9;14:641570. DOI:10.3389/fnmol.2021.641570

[**305**] Wiley JS, Sluyter R, Gu BJ, Stokes L, Fuller SJ. The human P2X7 receptor and its role in innate immunity. *Tissue Antigens*. 2011 Nov;78(5):321–32. DOI:10.1111/j.1399-0039.2011.01780.x

[**306**] Kaczmarek-Hajek K, Zhang J, Kopp R, Grosche A, Rissiek B, Saul A, et al. Re-evaluation of neuronal P2X7 expression using novel mouse models and a P2X7-specific nanobody. *Elife* [Internet]. 2018 Aug 3;7:e36217. DOI:10.7554/eLife.36217

[**307**] Cario-Toumaniantz C, Loirand G, Ladoux A, Pacaud P. P2X7 receptor activation-induced contraction and lysis in human saphenous vein smooth muscle. *Circ Res* [Internet]. 1998/08/01. 1998 Jul 27 [cited 2019 Aug 25];83(2):196–203. DOI:10.1161/01.RES.83.2.196

[**308**] Lewis CJ, Evans RJ. P2X receptor immunoreactivity in different arteries from the femoral, pulmonary, cerebral, coronary and renal circulations. *J Vasc Res*. 2001;38(4):332–40. DOI:10.1159/000051064

[**309**] Piscopiello M, Sessa M, Anzalone N, Castellano R, Maisano F, Ferrero E, et al. P2X7 receptor is expressed in human vessels and might play a role in atherosclerosis. *Int J Cardiol*. 2013;168(3):2863–6. DOI:10.1016/j.ijcard.2013.03.084

[**310**] Clapp C, Diaz-Lezama N, Adan-Castro E, Ramirez-Hernandez G, Moreno-Carranza B, Sarti AC, et al. Pharmacological blockade of the P2X7 receptor reverses retinal damage in a rat model of type 1 diabetes. *Acta Diabetol*. 2019 Sep;56(9):1031–6. DOI:10.1007/s00592-019-01343-4

[**311**] Portillo J-AC, Lopez Corcino Y, Dubyak GR, Kern TS, Matsuyama S, Subauste CS. Ligation of CD40 in Human Müller Cells Induces P2X7 Receptor-Dependent Death of Retinal Endothelial Cells. *Invest Ophthalmol Vis Sci* [Internet]. 2016 Nov 1;57(14):6278–86. DOI:10.1167/iovs.16-20301

[**312**] Luo W, Feldman D, McCallister R, Brophy C, Cheung-Flynn J. P2X7R antagonism after subfailure overstretch injury of blood vessels reverses vasomotor dysfunction and prevents apoptosis. *Purinergic Signal* [Internet]. 2017/09/13. 2017 Dec;13(4):579–90. DOI:10.1007/s11302-017-9585-0

[**313**] Menzies RI, Howarth AR, Unwin RJ, Tam FWK, Mullins JJ, Bailey MA. Inhibition of the purinergic P2X7 receptor improves renal perfusion in angiotensin-II-infused rats. *Kidney Int*. 2015 Nov;88(5):1079–87. DOI:10.1038/ki.2015.182

[**314**] Franco M, Bautista-Pérez R, Cano-Martínez A, Pacheco U, Santamaría J, Del Valle Mondragón L, et al. Physiopathological implications of P2X(1) and P2X(7) receptors in regulation of glomerular hemodynamics in angiotensin II-induced hypertension. *Am J Physiol Renal Physiol*. 2017 Jul;313(1):F9–19. DOI:10.1152/ajprenal.00663.2016

[**315**] Kawamura H, Sugiyama T, Wu DM, Kobayashi M, Yamanishi S, Katsumura K, et al. ATP: a vasoactive signal in the pericyte-containing microvasculature of the rat retina. *J Physiol*. 2003 Sep;551(Pt 3):787–99. DOI:10.1113/jphysiol.2003.047977

[**316**] Mahdi A, Jiao T, Tratsiakovich Y, Yang J, Östenson C-G, Pernow J, et al. Altered Purinergic Receptor Sensitivity in Type 2 Diabetes-Associated Endothelial Dysfunction and Up_4A-Mediated Vascular Contraction. *Int J Mol Sci* [Internet].

2018 Dec 7;19(12):3942. DOI:10.3390/ijms19123942

[**317**] Komalavilas P, Luo W, Guth CM, Jolayemi O, Bartelson RI, Cheung-Flynn J, et al. Vascular surgical stretch injury leads to activation of P2X7 receptors and impaired endothelial function. Kanellopoulos J, editor. *PLoS One* [Internet]. 2017 Nov 14 [cited 2020 Mar 30];12(11):e0188069. DOI:10.1371/journal.pone.0188069

[**318**] Oliveira SDDS, Coutinho-Silva R, Silva CLM. Endothelial P2X7 receptors' expression is reduced by schistosomiasis. *Purinergic Signal* [Internet]. 2012/09/18. 2013 Mar;9(1):81–9. DOI:10.1007/s11302-012-9332-5

[**319**] Chiao CW, Tostes RC, Webb RC. P2X7 receptor activation amplifies lipopolysaccharide-induced vascular hyporeactivity via interleukin-1 beta release. *J Pharmacol Exp Ther* [Internet]. 2008/06/19. 2008;326(3):864–70. DOI:10.1124/jpet.107.135350

[**320**] Chiao C-W, da Silva-Santos JE, Giachini FR, Tostes RC, Su M-J, Webb RC. P2X7 receptor activation contributes to an initial upstream mechanism of lipopolysaccharide-induced vascular dysfunction. *Clin Sci (Lond)* [Internet]. 2013;125(3):131–41. DOI:10.1042/CS20120479

[**321**] Roberts VHJ, Waters LH, Powell T. Purinergic Receptor Expression and Activation in First Trimester and Term Human Placenta. *Placenta* [Internet]. 2007 Apr [cited 2020 Jul 4];28(4):339–47. DOI:10.1016/j.placenta.2006.04.007

[**322**] Martínez-Cuesta MÁ, Blanch-Ruiz MA, Ortega-Luna R, Sánchez-López A, Álvarez Á. Structural and Functional Basis for Understanding the Biological Significance of P2X7 Receptor. *Int J Mol Sci*. 2020 Nov;21(22). DOI:10.3390/ijms21228454

[**323**] Calzaferri F, Narros-Fernández P, de Pascual R, de Diego AMG, Nicke A, Egea J, et al. Synthesis and Pharmacological Evaluation of Novel Non-nucleotide Purine Derivatives as P2X7 Antagonists for the Treatment of Neuroinflammation. *J Med Chem*. 2021 Feb;64(4):2272–90. DOI:10.1021/acs.jmedchem.0c02145

[**324**] Robinson LE, Shridar M, Smith P, Murrell-Lagnado RD. Plasma membrane cholesterol as a regulator of human and rodent P2X7 receptor activation and sensitization. *J Biol Chem*. 2014 Nov;289(46):31983–94. DOI:10.1074/jbc.M114.574699

[**325**] Garré JM, Yang G, Bukauskas FF, Bennett MVL. FGF-1 Triggers Pannexin-1 Hemichannel Opening in Spinal Astrocytes of Rodents and Promotes Inflammatory Responses in Acute Spinal Cord Slices. *J Neurosci*. 2016 Apr;36(17):4785–801. DOI:10.1523/JNEUROSCI.4195-15.2016

[**326**] Virginio C, MacKenzie A, Rassendren FA, North RA, Surprenant A. Pore dilation of neuronal P2X receptor channels. *Nat Neurosci* [Internet]. 1999 Apr [cited 2020 Aug 6];2(4):315–21. DOI:10.1038/7225

[**327**] Thompson RJ, Jackson MF, Olah ME, Rungta RL, Hines DJ, Beazely MA, et al. Activation of pannexin-1 hemichannels augments aberrant bursting in the hippocampus. *Science (80-)* [Internet]. 2008 Dec 5 [cited 2020 Aug 6];322(5907):1555–9. DOI:10.1126/science.1165209

[**328**] Di Virgilio F, Schmalzing G, Markwardt F. The Elusive P2X7 Macropore. *Trends*

Cell Biol [Internet]. 2018;28(5):392–404. DOI:10.1016/j.tcb.2018.01.005

[**329**] Ugur M, Ugur Ö. A mechanism-based approach to P2X7 receptor action [Internet]. Vol. 95, Molecular Pharmacology. American Society for Pharmacology and Experimental Therapy; 2019 [cited 2020 Mar 30]. p. 442–50. DOI:10.1124/mol.118.115022

[**330**] Smart ML, Gu B, Panchal RG, Wiley J, Cromer B, Williams DA, et al. P2X7 receptor cell surface expression and cytolytic pore formation are regulated by a distal C-terminal region. *J Biol Chem*. 2003 Mar;278(10):8853–60. DOI:10.1074/jbc.M211094200

[**331**] Pelegrin P, Surprenant A. Pannexin-1 mediates large pore formation and interleukin-1β release by the ATP-gated P2X7 receptor. *EMBO J* [Internet]. 2006 Nov 1 [cited 2020 Aug 6];25(21):5071–82. DOI:10.1038/sj.emboj.7601378

[**332**] Qu Y, Misaghi S, Newton K, Gilmour LL, Louie S, Cupp JE, et al. Pannexin-1 is required for ATP release during apoptosis but not for inflammasome activation. *J Immunol*. 2011 Jun;186(11):6553–61. DOI:10.4049/jimmunol.1100478

[**333**] Alberto AVP, Faria RX, Couto CGC, Ferreira LGB, Souza CAM, Teixeira PCN, et al. Is pannexin the pore associated with the P2X7 receptor? *Naunyn Schmiedebergs Arch Pharmacol*. 2013 Sep;386(9):775–87. DOI:10.1007/s00210-013-0868-x

[**334**] Bhaskaracharya A, Dao-Ung P, Jalilian I, Spildrejorde M, Skarratt KK, Fuller SJ, et al. Probenecid Blocks Human P2X7 Receptor-Induced Dye Uptake via a Pannexin-1 Independent Mechanism. Barnes S, editor. *PLoS One* [Internet]. 2014 Mar 26 [cited 2020 Aug 6];9(3):e93058. DOI:10.1371/journal.pone.0093058

[**335**] Yan Z, Li S, Liang Z, Tomić M, Stojilkovic SS. The P2X 7 receptor channel pore dilates under physiological ion conditions. *J Gen Physiol* [Internet]. 2008 Nov [cited 2020 Aug 6];132(5):563–73. DOI:10.1085/jgp.200810059

[**336**] Khadra A, Tomić M, Yan Z, Zemkova H, Sherman A, Stojilkovic SS. Dual gating mechanism and function of P2X7 receptor channels. *Biophys J*. 2013 Jun 18;104(12):2612–21. DOI:10.1016/j.bpj.2013.05.006

[**337**] Nicke A. Homotrimeric complexes are the dominant assembly state of native P2X7 subunits. *Biochem Biophys Res Commun*. 2008 Dec;377(3):803–8. DOI:10.1016/j.bbrc.2008.10.042

[**338**] Jiang LH, Baldwin JM, Roger S, Baldwin SA. Insights into the molecular mechanisms underlying mammalian P2X7 receptor functions and contributions in diseases, revealed by structural modeling and single nucleotide polymorphisms [Internet]. Vol. 4 MAY, Frontiers in Pharmacology. Frontiers; 2013 [cited 2020 Aug 6]. p. 55. DOI:10.3389/fphar.2013.00055

[**339**] Gusic M, Benndorf K, Sattler C. Dissecting activation steps in P2X7 receptors. *Biochem Biophys Res Commun* [Internet]. 2021;569:112–7. DOI:https://doi.org/10.1016/j.bbrc.2021.06.101

[**340**] Riedel T, Lozinsky I, Schmalzing G, Markwardt F. Kinetics of P2X7 receptor-operated single channels currents. *Biophys J*. 2007 Apr;92(7):2377–91. DOI:10.1529/biophysj.106.091413

[**341**] Pelegrin P, Barroso-Gutierrez C, Surprenant A. P2X7 receptor differentially couples to distinct release pathways for IL-1beta in mouse macrophage. *J Immunol*. 2008 Jun;180(11):7147–57. DOI:10.4049/jimmunol.180.11.7147

[**342**] Wilson HL, Francis SE, Dower SK, Crossman DC. Secretion of intracellular IL-1 receptor antagonist (type 1) is dependent on P2X7 receptor activation. *J Immunol*. 2004 Jul;173(2):1202–8. DOI:10.4049/jimmunol.173.2.1202

[**343**] Martin U, Scholler J, Gurgel J, Renshaw B, Sims JE, Gabel CA. Externalization of the leaderless cytokine IL-1F6 occurs in response to lipopolysaccharide/ATP activation of transduced bone marrow macrophages. *J Immunol*. 2009 Sep;183(6):4021–30. DOI:10.4049/jimmunol.0803301

[**344**] Muñoz-Planillo R, Kuffa P, Martínez-Colón G, Smith BL, Rajendiran TM, Núñez G. K+ Efflux Is the Common Trigger of NLRP3 Inflammasome Activation by Bacterial Toxins and Particulate Matter. *Immunity* [Internet]. 2013 Jun 27 [cited 2020 Aug 6];38(6):1142–53. DOI:10.1016/j.immuni.2013.05.016

[**345**] Lenertz LY, Gavala ML, Hill LM, Bertics PJ. Cell signaling via the P2X7 nucleotide receptor: Linkage to ROS production, gene transcription, and receptor trafficking. *Purinergic Signal* [Internet]. 2009 [cited 2020 Aug 6];5(2):175–87. DOI:10.1007/s11302-009-9133-7

[**346**] Moore SF, MacKenzie AB. NADPH Oxidase NOX2 Mediates Rapid Cellular Oxidation following ATP Stimulation of Endotoxin-Primed Macrophages. *J Immunol* [Internet]. 2009 Sep 1 [cited 2020 Aug 6];183(5):3302–8. DOI:10.4049/jimmunol.0900394

[**347**] Apolloni S, Parisi C, Pesaresi MG, Rossi S, Carrì MT, Cozzolino M, et al. The NADPH oxidase pathway is dysregulated by the P2X7 receptor in the SOD1-G93A microglia model of amyotrophic lateral sclerosis. *J Immunol*. 2013 May;190(10):5187–95. DOI:10.4049/jimmunol.1203262

[**348**] Bartlett R, Yerbury JJ, Sluyter R. P2X7 Receptor Activation Induces Reactive Oxygen Species Formation and Cell Death in Murine EOC13 Microglia. Wei S-J, editor. *Mediators Inflamm* [Internet]. 2013;2013:271813. DOI:10.1155/2013/271813

[**349**] Seil M, Fontanils U, Etxebarria IG, Pochet S, Garcia-Marcos M, Marino A, et al. Pharmacological evidence for the stimulation of NADPH oxidase by P2X7 receptors in mouse submandibular glands. *Purinergic Signal* [Internet]. 2008 [cited 2020 Aug 6];4(4):347–55. DOI:10.1007/s11302-008-9118-y

[**350**] Wang B, Sluyter R. P2X7 receptor activation induces reactive oxygen species formation in erythroid cells. *Purinergic Signal*. 2013 Mar;9(1):101–12. DOI:10.1007/s11302-012-9335-2

[**351**] Munoz FM, Gao R, Tian Y, Henstenburg BA, Barrett JE, Hu H. Neuronal P2X7 receptor-induced reactive oxygen species production contributes to nociceptive behavior in mice. *Sci Rep* [Internet]. 2017;7(1):3539. DOI:10.1038/s41598-017-03813-7

[**352**] Nakahira K, Haspel JA, Rathinam VAK, Lee SJ, Dolinay T, Lam HC, et al. Autophagy proteins regulate innate immune responses by inhibiting the release of mitochondrial DNA mediated by the NALP3 inflammasome. *Nat Immunol* [Internet]. 2011 Mar [cited 2020 Aug 6];12(3):222–30. DOI:10.1038/ni.1980

[**353**] Wilkaniec A, Cieślik M, Murawska E, Babiec L, Gąssowska-Dobrowolska M, Pałasz E, et al. P2X7 Receptor is Involved in Mitochondrial Dysfunction Induced by Extracellular Alpha Synuclein in Neuroblastoma SH-SY5Y Cells. Vol. 21, International Journal of Molecular Sciences . 2020. DOI:10.3390/ijms21113959

[**354**] Tschopp J. Mitochondria: Sovereign of inflammation? *Eur J Immunol*. 2011 May;41(5):1196–202. DOI:10.1002/eji.201141436

[**355**] Qu Y, Dubyak GR. P2X7 receptors regulate multiple types of membrane trafficking responses and non-classical secretion pathways. *Purinergic Signal*. 2009 Jun;5(2):163–73. DOI:10.1007/s11302-009-9132-8

[**356**] Di Virgilio F, Dal Ben D, Sarti AC, Giuliani AL, Falzoni S. The P2X7 Receptor in Infection and Inflammation [Internet]. Vol. 47, Immunity. Cell Press; 2017 [cited 2020 Aug 7]. p. 15–31. DOI:10.1016/j.immuni.2017.06.020

[**357**] Pupovac A, Foster CM, Sluyter R. Human P2X7 receptor activation induces the rapid shedding of CXCL16. *Biochem Biophys Res Commun*. 2013 Mar;432(4):626–31. DOI:10.1016/j.bbrc.2013.01.134

[**358**] Lin C, Ren S, Zhang L, Jin H, Sun J, Zuo Y. Extracellular ATP induces CD44 shedding from macrophage-like P388D1 cells via the P2X7 receptor. *Hematol Oncol*. 2012 Jun;30(2):70–5. DOI:10.1002/hon.1008

[**359**] Delarasse C, Auger R, Gonnord P, Fontaine B, Kanellopoulos JM. The purinergic receptor P2X7 triggers alpha-secretase-dependent processing of the amyloid precursor protein. *J Biol Chem*. 2011 Jan;286(4):2596–606. DOI:10.1074/jbc.M110.200618

[**360**] Garbers C, Jänner N, Chalaris A, Moss ML, Floss DM, Meyer D, et al. Species specificity of ADAM10 and ADAM17 proteins in interleukin-6 (IL-6) trans-signaling and novel role of ADAM10 in inducible IL-6 receptor shedding. *J Biol Chem* [Internet]. 2011 Apr 29 [cited 2020 Aug 6];286(17):14804–11. DOI:10.1074/jbc.M111.229393

[**361**] Gu B, Bendall LJ, Wiley JS. Adenosine triphosphate-induced shedding of CD23 and L-selectin (CD62L) from lymphocytes is mediated by the same receptor but different metalloproteases. *Blood*. 1998 Aug;92(3):946–51.

[**362**] Moon H, Na H-Y, Chong KH, Kim TJ. P2X7 receptor-dependent ATP-induced shedding of CD27 in mouse lymphocytes. *Immunol Lett*. 2006 Jan;102(1):98–105. DOI:10.1016/j.imlet.2005.08.004

[**363**] Kopp R, Krautloher A, Ramírez-Fernández A, Nicke A. P2X7 Interactions and Signaling – Making Head or Tail of It [Internet]. Vol. 12, Frontiers in Molecular Neuroscience . 2019. p. 183. Available from: https://www.frontiersin.org/article/10.3389/fnmol.2019.00183

[**364**] Barberà-Cremades M, Baroja-Mazo A, Gomez AI, Machado F, Di Virgilio F, Pelegrín P. P2X7 receptor-stimulation causes fever via PGE2 and IL-1β release. *FASEB J Off Publ Fed Am Soc Exp Biol*. 2012 Jul;26(7):2951–62. DOI:10.1096/fj.12-205765

[**365**] Bartlett R, Stokes L, Sluyter R. The P2X7 receptor channel: recent developments and the use of P2X7 antagonists in models of disease. *Pharmacol Rev*. 2014/06/15. 2014;66(3):638–75. DOI:10.1124/pr.113.008003

[**366**] Andrei C, Margiocco P, Poggi A, Lotti L V, Torrisi MR, Rubartelli A. Phospholipases C and A2 control lysosome-mediated IL-1 beta secretion: Implications for inflammatory processes. *Proc Natl Acad Sci U S A*. 2004 Jun;101(26):9745–50. DOI:10.1073/pnas.0308558101

[**367**] El Ouaaliti M, Seil M, Dehaye JP. Activation of calcium-insensitive phospholipase A2 (iPLA 2) by P2X7 receptors in murine peritoneal macrophages. *Prostaglandins Other Lipid Mediat*. 2012 Dec 1;99(3–4):116–23. DOI:10.1016/j.prostaglandins.2012.09.005

[**368**] Bernier LP, Ase AR, Séguéla P. P2X receptor channels in chronic pain pathways. *Br J Pharmacol*. 2018;175(12):2219–30. DOI:10.1111/bph.13957

[**369**] Shokoples BG, Paradis P, Schiffrin EL. P2X7 Receptors; An Untapped Target for the Management of Cardiovascular Disease. *Arterioscler Thromb Vasc Biol*. 2021;41(1):186–99. DOI:10.1161/ATVBAHA.120.315116

[**370**] Giuliani AL, Sarti AC, Falzoni S, Di Virgilio F. The P2X7 Receptor-Interleukin-1 Liaison. *Front Pharmacol* [Internet]. 2017 Mar 16;8:123. DOI:10.3389/fphar.2017.00123

[**371**] Hadadi E, Zhang B, Baidžajevas K, Yusof N, Puan KJ, Ong SM, et al. Differential IL-1β secretion by monocyte subsets is regulated by Hsp27 through modulating mRNA stability. *Sci Rep*. 2016 Dec;6:39035. DOI:10.1038/srep39035

[**372**] Ainscough JS, Gerberick GF, Kimber I, Dearman RJ. Interleukin-1β Processing Is Dependent on a Calcium-mediated Interaction with Calmodulin. *J Biol Chem*. 2015 Dec;290(52):31151–61. DOI:10.1074/jbc.M115.680694

[**373**] Di Virgilio F. The therapeutic potential of modifying inflammasomes and NOD-like receptors. *Pharmacol Rev*. 2013 Jul;65(3):872–905. DOI:10.1124/pr.112.006171

[**374**] de Torre-Minguela C, Barberà-Cremades M, Gómez AI, Martín-Sánchez F, Pelegrín P. Macrophage activation and polarization modify P2X7 receptor secretome influencing the inflammatory process. *Sci Rep*. 2016 Mar;6:22586. DOI:10.1038/srep22586

[**375**] Franceschini A, Capece M, Chiozzi P, Falzoni S, Sanz JM, Sarti AC, et al. The P2X7 receptor directly interacts with the NLRP3 inflammasome scaffold protein. *FASEB J Off Publ Fed Am Soc Exp Biol*. 2015 Jun;29(6):2450–61. DOI:10.1096/fj.14-268714

[**376**] Srinivasula SM, Poyet J-L, Razmara M, Datta P, Zhang Z, Alnemri ES. The PYRIN-CARD protein ASC is an activating adaptor for caspase-1. *J Biol Chem*. 2002 Jun;277(24):21119–22. DOI:10.1074/jbc.C200179200

[**377**] Sharma D, Kanneganti T-D. The cell biology of inflammasomes: Mechanisms of inflammasome activation and regulation. *J Cell Biol* [Internet]. 2016 Jun 20;213(6):617–29. DOI:10.1083/jcb.201602089

[**378**] Zheng D, Liwinski T, Elinav E. Inflammasome activation and regulation: toward a better understanding of complex mechanisms. *Cell Discov* [Internet]. 2020;6(1):36. DOI:10.1038/s41421-020-0167-x

[**379**] Martinon F, Burns K, Tschopp J. The inflammasome: a molecular platform triggering activation of inflammatory caspases and processing of proIL-beta. *Mol*

Cell. 2002/08/23. 2002;10(2):417–26.

[**380**] Fenini G, Karakaya T, Hennig P, Di Filippo M, Beer H-D. The NLRP1 Inflammasome in Human Skin and Beyond. Vol. 21, International Journal of Molecular Sciences . 2020. DOI:10.3390/ijms21134788

[**381**] Finger JN, Lich JD, Dare LC, Cook MN, Brown KK, Duraiswami C, et al. Autolytic proteolysis within the function to find domain (FIIND) is required for NLRP1 inflammasome activity. *J Biol Chem*. 2012 Jul;287(30):25030–7. DOI:10.1074/jbc.M112.378323

[**382**] Mariathasan S, Hewton K, Monack DM, Vucic D, French DM, Lee WP, et al. Differential activation of the inflammasome by caspase-1 adaptors ASC and Ipaf. *Nature* [Internet]. 2004 Jul 8 [cited 2020 Aug 7];430(6996):213–8. DOI:10.1038/nature02664

[**383**] Bauer R, Rauch I. The NAIP/NLRC4 inflammasome in infection and pathology. *Mol Aspects Med*. 2020 Dec;76:100863. DOI:10.1016/j.mam.2020.100863

[**384**] Amer A, Franchi L, Kanneganti T-D, Body-Malapel M, Ozören N, Brady G, et al. Regulation of Legionella phagosome maturation and infection through flagellin and host Ipaf. *J Biol Chem*. 2006 Nov;281(46):35217–23. DOI:10.1074/jbc.M604933200

[**385**] Miao EA, Alpuche-Aranda CM, Dors M, Clark AE, Bader MW, Miller SI, et al. Cytoplasmic flagellin activates caspase-1 and secretion of interleukin 1beta via Ipaf. *Nat Immunol*. 2006 Jun;7(6):569–75. DOI:10.1038/ni1344

[**386**] Franchi L, Amer A, Body-Malapel M, Kanneganti T-D, Ozören N, Jagirdar R, et al. Cytosolic flagellin requires Ipaf for activation of caspase-1 and interleukin 1beta in salmonella-infected macrophages. *Nat Immunol*. 2006 Jun;7(6):576–82. DOI:10.1038/ni1346

[**387**] Suzuki T, Franchi L, Toma C, Ashida H, Ogawa M, Yoshikawa Y, et al. Differential Regulation of Caspase-1 Activation, Pyroptosis, and Autophagy via Ipaf and ASC in Shigella-Infected Macrophages. Ramakrishnan L, editor. *PLoS Pathog* [Internet]. 2007 Aug 10 [cited 2020 Aug 7];3(8):e111. DOI:10.1371/journal.ppat.0030111

[**388**] Craven RR, Gao X, Allen IC, Gris D, Bubeck Wardenburg J, McElvania-Tekippe E, et al. Staphylococcus aureus alpha-hemolysin activates the NLRP3-inflammasome in human and mouse monocytic cells. *PLoS One*. 2009 Oct;4(10):e7446. DOI:10.1371/journal.pone.0007446

[**389**] Zhou R, Tardivel A, Thorens B, Choi I, Tschopp J. Thioredoxin-interacting protein links oxidative stress to inflammasome activation. *Nat Immunol* [Internet]. 2010 Feb 20 [cited 2020 Aug 7];11(2):136–40. DOI:10.1038/ni.1831

[**390**] Martinon F, Pétrilli V, Mayor A, Tardivel A, Tschopp J. Gout-associated uric acid crystals activate the NALP3 inflammasome. *Nature* [Internet]. 2006 Mar 11 [cited 2019 Feb 11];440(7081):237–41. DOI:10.1038/nature04516

[**391**] Ding S, Xu S, Ma Y, Liu G, Jang H, Fang J. Modulatory mechanisms of the NLRP3 inflammasomes in diabetes. *Biomolecules*. 2019;9(12). DOI:10.3390/biom9120850

[**392**] Biasizzo M, Kopitar-Jerala N. Interplay Between NLRP3 Inflammasome and

Autophagy. *Front Immunol*. 2020;11:591803. DOI:10.3389/fimmu.2020.591803

[**393**] Fernandes-Alnemri T, Yu JW, Datta P, Wu J, Alnemri ES. AIM2 activates the inflammasome and cell death in response to cytoplasmic DNA. *Nature* [Internet]. 2009 Mar 26 [cited 2020 Aug 7];458(7237):509–13. DOI:10.1038/nature07710

[**394**] Bürckstümmer T, Baumann C, Blüml S, Dixit E, Dürnberger G, Jahn H, et al. An orthogonal proteomic-genomic screen identifies AIM2 as a cytoplasmic DNA sensor for the inflammasome. *Nat Immunol* [Internet]. 2009 Jan 21 [cited 2020 Aug 7];10(3):266–72. DOI:10.1038/ni.1702

[**395**] Morrone SR, Matyszewski M, Yu X, Delannoy M, Egelman EH, Sohn J. Assembly-driven activation of the AIM2 foreign-dsDNA sensor provides a polymerization template for downstream ASC. *Nat Commun* [Internet]. 2015 Jul 22;6:7827. DOI:10.1038/ncomms8827

[**396**] Rathinam VAK, Jiang Z, Waggoner SN, Sharma S, Cole LE, Waggoner L, et al. The AIM2 inflammasome is essential for host defense against cytosolic bacteria and DNA viruses. *Nat Immunol* [Internet]. 2010 May [cited 2020 Aug 7];11(5):395–402. DOI:10.1038/ni.1864

[**397**] Hornung V, Ablasser A, Charrel-Dennis M, Bauernfeind F, Horvath G, Caffrey DR, et al. AIM2 recognizes cytosolic dsDNA and forms a caspase-1-activating inflammasome with ASC. *Nature*. 2009 Mar;458(7237):514–8. DOI:10.1038/nature07725

[**398**] Sharma BR, Karki R, Kanneganti T-D. Role of AIM2 inflammasome in inflammatory diseases, cancer and infection. *Eur J Immunol*. 2019 Nov;49(11):1998–2011. DOI:10.1002/eji.201848070

[**399**] Martinon F, Burns K, Tschopp J. The Inflammasome: A molecular platform triggering activation of inflammatory caspases and processing of proIL-β. *Mol Cell*. 2002;10(2):417–26. DOI:10.1016/S1097-2765(02)00599-3

[**400**] Schroder K, Tschopp J. The Inflammasomes. Vol. 140, Cell. Cell Press; 2010. p. 821–32. DOI:10.1016/j.cell.2010.01.040

[**401**] Xu Z, Zhou Y, Liu M, Ma H, Sun L, Zahid A, et al. Homotypic CARD-CARD interaction is critical for the activation of NLRP1 inflammasome. *Cell Death Dis* [Internet]. 2021;12(1):57. DOI:10.1038/s41419-020-03342-8

[**402**] Martinon F, Tschopp J. Inflammatory caspases and inflammasomes: master switches of inflammation. *Cell Death Differ*. 2007 Jan;14(1):10–22. DOI:10.1038/sj.cdd.4402038

[**403**] Lu A, Magupalli VG, Ruan J, Yin Q, Atianand MK, Vos MR, et al. Unified polymerization mechanism for the assembly of asc-dependent inflammasomes. *Cell* [Internet]. 2014 Mar 13 [cited 2020 Aug 8];156(6):1193–206. DOI:10.1016/j.cell.2014.02.008

[**404**] Guo H, Callaway JB, Ting JP. Inflammasomes: mechanism of action, role in disease, and therapeutics. *Nat Med* [Internet]. 2015/06/30. 2015;21(7):677–87. DOI:10.1038/nm.3893

[**405**] Pontillo A, Girardelli M, Agostinis C, Masat E, Bulla R, Crovella S. Bacterial LPS differently modulates inflammasome gene expression and IL-1β secretion in trophoblast cells, decidual stromal cells, and decidual endothelial cells. *Reprod*

Sci. 2013 May;20(5):563–6. DOI:10.1177/1933719112459240

[**406**] Hoang M, Potter JA, Gysler SM, Han CS, Guller S, Norwitz ER, et al. Human fetal membranes generate distinct cytokine profiles in response to bacterial Toll-like receptor and nod-like receptor agonists. *Biol Reprod*. 2014 Feb;90(2):39. DOI:10.1095/biolreprod.113.115428

[**407**] Lappas M. Caspase-1 activation is increased with human labour in foetal membranes and myometrium and mediates infection-induced interleukin-1β secretion. *Am J Reprod Immunol*. 2014 Feb;71(2):189–201. DOI:10.1111/aji.12174

[**408**] Zhu J, Ma C, Zhu L, Li J, Peng F, Huang L, et al. A role for the NLRC4 inflammasome in premature rupture of membrane. *PLoS One* [Internet]. 2020 Aug 24;15(8):e0237847–e0237847. DOI:10.1371/journal.pone.0237847

[**409**] Cicko S, Köhler TC, Ayata CK, Müller T, Ehrat N, Meyer A, et al. Extracellular ATP is a danger signal activating P2X7 Receptor in a LPS mediated inflammation (ARDS/ALI). *Oncotarget*. 2018;9(55):30635–48. DOI:10.18632/oncotarget.25761

[**410**] Yegutkin G, Bodin P, Burnstock G. Effect of shear stress on the release of soluble ecto-enzymes ATPase and 5'-nucleotidase along with endogenous ATP from vascular endothelial cells. *Br J Pharmacol* [Internet]. 2000 [cited 2020 Aug 8];129(5):921–6. DOI:10.1038/sj.bjp.0703136

[**411**] Pedersen S, Pedersen SF, Nilius B, Lambert IH, Hoffmann EK. Mechanical stress induces release of ATP from Ehrlich ascites tumor cells. *Biochim Biophys Acta - Biomembr*. 1999 Jan 12;1416(1–2):271–84. DOI:10.1016/S0005-2736(98)00228-4

[**412**] Urabe S, Miyoshi H, Fujiwara H, Yamaoka K, Kudo Y. Enhanced expression of P2X4 and P2X7 purinergic receptors in the myometrium of pregnant rats in preterm delivery models. *Reprod Sci*. 2009;16(12):1186–92. DOI:10.1177/1933719109344630

[**413**] Jo EK, Kim JK, Shin DM, Sasakawa C. Molecular mechanisms regulating NLRP3 inflammasome activation. *Cell Mol Immunol* [Internet]. 2015/11/10. 2016;13(2):148–59. DOI:10.1038/cmi.2015.95

[**414**] Khan RN, Hay DP. A clear and present danger: Inflammasomes DAMPing down disorders of pregnancy. *Hum Reprod Update*. 2015;21(3):388–405. DOI:10.1093/humupd/dmu059

[**415**] Kelley N, Jeltema D, Duan Y, He Y. The NLRP3 Inflammasome: An Overview of Mechanisms of Activation and Regulation. *Int J Mol Sci* [Internet]. 2019 Jul 6;20(13):3328. DOI:10.3390/ijms20133328

[**416**] Yang Y, Wang H, Kouadir M, Song H, Shi F. Recent advances in the mechanisms of NLRP3 inflammasome activation and its inhibitors. *Cell Death Dis* [Internet]. 2019;10(2):128. DOI:10.1038/s41419-019-1413-8

[**417**] Bianchi ME. DAMPs, PAMPs and alarmins: all we need to know about danger. *J Leukoc Biol* [Internet]. 2006/10/13. 2007;81(1):1–5. DOI:10.1189/jlb.0306164

[**418**] Gallucci S, Matzinger P. Danger signals: SOS to the immune system. Vol. 13, Current Opinion in Immunology. Elsevier Ltd; 2001. p. 114–9.

DOI:10.1016/S0952-7915(00)00191-6

[**419**] Kono H, Rock KL. How dying cells alert the immune system to danger [Internet]. Vol. 8, Nature Reviews Immunology. Nature Publishing Group; 2008 [cited 2020 Aug 10]. p. 279–89. DOI:10.1038/nri2215

[**420**] Chen GY, Nuñez G, Nunez G. Sterile inflammation: sensing and reacting to damage. *Nat Rev Immunol* [Internet]. 2010/11/23. 2010;10(12):826–37. DOI:10.1038/nri2873

[**421**] Gong T, Liu L, Jiang W, Zhou R. DAMP-sensing receptors in sterile inflammation and inflammatory diseases. *Nat Rev Immunol* [Internet]. 2020;20(2):95–112. DOI:10.1038/s41577-019-0215-7

[**422**] Dostert C, Pétrilli V, Van Bruggen R, Steele C, Mossman BT, Tschopp J. Innate immune activation through Nalp3 inflammasome sensing of asbestos and silica. *Science (80-)* [Internet]. 2008 May 2 [cited 2020 Aug 9];320(5876):674–7. DOI:10.1126/science.1156995

[**423**] Hornung V, Bauernfeind F, Halle A, Samstad EO, Kono H, Rock KL, et al. Silica crystals and aluminum salts activate the NALP3 inflammasome through phagosomal destabilization. *Nat Immunol* [Internet]. 2008 Aug 11 [cited 2020 Aug 9];9(8):847–56. DOI:10.1038/ni.1631

[**424**] Eisenbarth SC, Colegio OR, O'Connor W, Sutterwala FS, Flavell RA. Crucial role for the Nalp3 inflammasome in the immunostimulatory properties of aluminium adjuvants. *Nature*. 2008 Jun;453(7198):1122–6. DOI:10.1038/nature06939

[**425**] Duewell P, Kono H, Rayner KJ, Sirois CM, Vladimer G, Bauernfeind FG, et al. NLRP3 inflammasomes are required for atherogenesis and activated by cholesterol crystals. *Nature* [Internet]. 2010 Apr 29 [cited 2020 Aug 9];464(7293):1357–61. DOI:10.1038/nature08938

[**426**] Babelova A, Moreth K, Tsalastra-Greul W, Zeng-Brouwers J, Eickelberg O, Young MF, et al. Biglycan, a danger signal that activates the NLRP3 inflammasome via toll-like and P2X receptors. *J Biol Chem*. 2009 Sep;284(36):24035–48. DOI:10.1074/jbc.M109.014266

[**427**] Halle A, Hornung V, Petzold GC, Stewart CR, Monks BG, Reinheckel T, et al. The NALP3 inflammasome is involved in the innate immune response to amyloid-beta. *Nat Immunol*. 2008 Aug;9(8):857–65. DOI:10.1038/ni.1636

[**428**] Agresti A, Bianchi ME. HMGB proteins and gene expression. Vol. 13, Current Opinion in Genetics and Development. Elsevier Ltd; 2003. p. 170–8. DOI:10.1016/S0959-437X(03)00023-6

[**429**] Müller S, Ronfani L, Bianchi ME. Regulated expression and subcellular localization of HMGB1, a chromatin protein with a cytokine function. *J Intern Med*. 2004 Mar;255(3):332–43. DOI:10.1111/j.1365-2796.2003.01296.x

[**430**] Foell D, Wittkowski H, Vogl T, Roth J. S100 proteins expressed in phagocytes: a novel group of damage-associated molecular pattern molecules. *J Leukoc Biol*. 2007 Jan;81(1):28–37. DOI:10.1189/jlb.0306170

[**431**] Zhou Z, Yamamoto Y, Sugai F, Yoshida K, Kishima Y, Sumi H, et al. Hepatoma-derived growth factor is a neurotrophic factor harbored in the nucleus. *J Biol*

Chem. 2004 Jun;279(26):27320–6. DOI:10.1074/jbc.M308650200

[**432**] Sedlmaier A, Wernert N, Gallitzendörfer R, Abouzied MM, Gieselmann V, Franken S. Overexpression of hepatoma-derived growth factor in melanocytes does not lead to oncogenic transformation. *BMC Cancer* [Internet]. 2011 Oct 20 [cited 2020 Aug 10];11(1):457. DOI:10.1186/1471-2407-11-457

[**433**] Schmitt E, Gehrmann M, Brunet M, Multhoff G, Garrido C. Intracellular and extracellular functions of heat shock proteins: repercussions in cancer therapy. *J Leukoc Biol*. 2007 Jan;81(1):15–27. DOI:10.1189/jlb.0306167

[**434**] Dubey A, Prajapati KS, Swamy M, Pachauri V. Heat shock proteins: A therapeutic target worth to consider. *Vet World* [Internet]. 2015 [cited 2020 Aug 10];8(1):46–51. DOI:10.14202/vetworld.2015.46-51

[**435**] Cassel SL, Joly S, Sutterwala FS. The NLRP3 inflammasome: A sensor of immune danger signals. Vol. 21, Seminars in Immunology. Academic Press; 2009. p. 194–8. DOI:10.1016/j.smim.2009.05.002

[**436**] Pan Y-G, Huang M-T, Sekar P, Huang D-Y, Lin W-W, Hsieh S-L. Decoy Receptor 3 Inhibits Monosodium Urate-Induced NLRP3 Inflammasome Activation via Reduction of Reactive Oxygen Species Production and Lysosomal Rupture [Internet]. Vol. 12, Frontiers in Immunology . 2021. p. 392. Available from: https://www.frontiersin.org/article/10.3389/fimmu.2021.638676

[**437**] Pelegrin P, Surprenant A. Pannexin-1 couples to maitotoxin- and nigericin-induced interleukin-1beta release through a dye uptake-independent pathway. *J Biol Chem*. 2007 Jan;282(4):2386–94. DOI:10.1074/jbc.M610351200

[**438**] Xu Z, Chen Z-M, Wu X, Zhang L, Cao Y, Zhou P. Distinct Molecular Mechanisms Underlying Potassium Efflux for NLRP3 Inflammasome Activation. *Front Immunol* [Internet]. 2020 Dec 7;11:609441. DOI:10.3389/fimmu.2020.609441

[**439**] Piippo N, Korhonen E, Hytti M, Kinnunen K, Kaarniranta K, Kauppinen A. Oxidative Stress is the Principal Contributor to Inflammasome Activation in Retinal Pigment Epithelium Cells with Defunct Proteasomes and Autophagy. *Cell Physiol Biochem Int J Exp Cell Physiol Biochem Pharmacol*. 2018;49(1):359–67. DOI:10.1159/000492886

[**440**] Deets KA, Vance RE. Inflammasomes and adaptive immune responses. *Nat Immunol* [Internet]. 2021;22(4):412–22. DOI:10.1038/s41590-021-00869-6

[**441**] Coutinho-Silva R, Savio LEB. Purinergic signalling in host innate immune defence against intracellular pathogens. *Biochem Pharmacol* [Internet]. 2021;187:114405. DOI:https://doi.org/10.1016/j.bcp.2021.114405

[**442**] Praetorius HA, Leipziger J. ATP release from non-excitable cells [Internet]. Vol. 5, Purinergic Signalling. Springer; 2009 [cited 2020 Aug 9]. p. 433–46. DOI:10.1007/s11302-009-9146-2

[**443**] Lazarowski ER, Boucher RC, Harden TK. Constitutive release of ATP and evidence for major contribution of ecto-nucleotide pyrophosphatase and nucleoside diphosphokinase to extracellular nucleotide concentrations. *J Biol Chem* [Internet]. 2000/07/27. 2000;275(40):31061–8. DOI:10.1074/jbc.M003255200

[**444**] Di Virgilio F, Sarti AC, Coutinho-Silva R. Purinergic signaling, DAMPs, and

inflammation. *Am J Physiol Physiol* [Internet]. 2020 Mar 11;318(5):C832–5. DOI:10.1152/ajpcell.00053.2020

[**445**] Iyer SS, Pulskens WP, Sadler JJ, Butter LM, Teske GJ, Ulland TK, et al. Necrotic cells trigger a sterile inflammatory response through the Nlrp3 inflammasome. *Proc Natl Acad Sci U S A* [Internet]. 2009 Dec 1 [cited 2020 Aug 9];106(48):20388–93. DOI:10.1073/pnas.0908698106

[**446**] Amores-Iniesta J, Barberà-Cremades M, Martínez CM, Pons JA, Revilla-Nuin B, Martínez-Alarcón L, et al. Extracellular ATP Activates the NLRP3 Inflammasome and Is an Early Danger Signal of Skin Allograft Rejection. *Cell Rep*. 2017 Dec;21(12):3414–26. DOI:10.1016/j.celrep.2017.11.079

[**447**] Riteau N, Baron L, Villeret B, Guillou N, Savigny F, Ryffel B, et al. ATP release and purinergic signaling: a common pathway for particle-mediated inflammasome activation. *Cell Death Dis* [Internet]. 2012/10/13. 2012;3(10):e403. DOI:10.1038/cddis.2012.144

[**448**] Medzhitov R, Janeway CJ. The Toll receptor family and microbial recognition. *Trends Microbiol*. 2000 Oct;8(10):452–6. DOI:10.1016/s0966-842x(00)01845-x

[**449**] Takeda K, Akira S. Toll-like receptors in innate immunity. *Int Immunol*. 2005 Jan;17(1):1–14. DOI:10.1093/intimm/dxh186

[**450**] Amarante-Mendes GP, Adjemian S, Branco LM, Zanetti LC, Weinlich R, Bortoluci KR. Pattern Recognition Receptors and the Host Cell Death Molecular Machinery [Internet]. Vol. 9, Frontiers in Immunology . 2018. p. 2379. Available from: https://www.frontiersin.org/article/10.3389/fimmu.2018.02379

[**451**] Janeway CAJ, Medzhitov R. Innate immune recognition. *Annu Rev Immunol*. 2002;20:197–216. DOI:10.1146/annurev.immunol.20.083001.084359

[**452**] Li D, Wu M. Pattern recognition receptors in health and diseases. *Signal Transduct Target Ther* [Internet]. 2021;6(1):291. DOI:10.1038/s41392-021-00687-0

[**453**] Medzhitov R, Preston-Hurlburt P, Janeway CA. A human homologue of the Drosophila toll protein signals activation of adaptive immunity. *Nature* [Internet]. 1997 [cited 2020 Aug 9];388(6640):394–7. DOI:10.1038/41131

[**454**] Schwandner R, Dziarski R, Wesche H, Rothe M, Kirschning CJ. Peptidoglycan- and lipoteichoic acid-induced cell activation is mediated by toll-like receptor 2. *J Biol Chem*. 1999 Jun;274(25):17406–9. DOI:10.1074/jbc.274.25.17406

[**455**] Hayashi F, Smith KD, Ozinsky A, Hawn TR, Yi EC, Goodlett DR, et al. The innate immune response to bacterial flagellin is mediated by Toll-like receptor 5. *Nature* [Internet]. 2001 Apr 26 [cited 2020 Aug 9];410(6832):1099–103. DOI:10.1038/35074106

[**456**] Hemmi H, Takeuchi O, Kawai T, Kaisho T, Sato S, Sanjo H, et al. A Toll-like receptor recognizes bacterial DNA. *Nature* [Internet]. 2000 Dec 7 [cited 2020 Aug 9];408(6813):740–5. DOI:10.1038/35047123

[**457**] Liu T, Zhang L, Joo D, Sun S-C. NF-κB signaling in inflammation. *Signal Transduct Target Ther* [Internet]. 2017/07/14. 2017;2:17023. DOI:10.1038/sigtrans.2017.23

[**458**] Martinon F, Tschopp J. NLRs join TLRs as innate sensors of pathogens. *Trends*

Immunol. 2005 Aug;26(8):447–54. DOI:10.1016/j.it.2005.06.004

[**459**] Franchi L, McDonald C, Kanneganti T-D, Amer A, Núñez G. Nucleotide-binding oligomerization domain-like receptors: intracellular pattern recognition molecules for pathogen detection and host defense. *J Immunol*. 2006 Sep;177(6):3507–13. DOI:10.4049/jimmunol.177.6.3507

[**460**] Wang X, Yi F. The Nucleotide Oligomerization Domain-Like Receptors in Kidney Injury. *Kidney Dis (Basel, Switzerland)*. 2016 Apr;2(1):28–36. DOI:10.1159/000444736

[**461**] Ting JP-Y, Lovering RC, Alnemri ES, Bertin J, Boss JM, Davis BK, et al. The NLR gene family: a standard nomenclature. *Immunity*. 2008 Mar;28(3):285–7. DOI:10.1016/j.immuni.2008.02.005

[**462**] Tschopp J, Martinon F, Burns K. NALPs: A novel protein family involved in inflammation [Internet]. Vol. 4, Nature Reviews Molecular Cell Biology. Nature Publishing Group; 2003 [cited 2020 Aug 10]. p. 95–104. DOI:10.1038/nrm1019

[**463**] Kim YK, Shin JS, Nahm MH. NOD-Like Receptors in Infection, Immunity, and Diseases. *Yonsei Med J* [Internet]. 2016 Jan;57(1):5–14. DOI:10.3349/ymj.2016.57.1.5

[**464**] Chatuphonprasert W, Jarukamjorn K, Ellinger I. Physiology and Pathophysiology of Steroid Biosynthesis, Transport and Metabolism in the Human Placenta [Internet]. Vol. 9, Frontiers in Pharmacology . 2018. p. 1027. Available from: https://www.frontiersin.org/article/10.3389/fphar.2018.01027

[**465**] Yoneyama Y, Suzuki S, Sawa R, Otsubo Y, Power GG, Araki T. Plasma adenosine levels increase in women with normal pregnancies. *Am J Obstet Gynecol*. 2000 May 1;182(5):1200–3. DOI:10.1067/mob.2000.104832

[**466**] León D, Albasanz JL, Ruíz MA, Martín M. Chronic caffeine or theophylline intake during pregnancy inhibits A1 receptor function in the rat brain. *Neuroscience*. 2005 Jan 1;131(2):481–9. DOI:10.1016/j.neuroscience.2004.11.028

[**467**] Monteiro JP, Alves MG, Oliveira PF, Silva BM. Structure-Bioactivity Relationships of Methylxanthines: Trying to Make Sense of All the Promises and the Drawbacks. *Molecules* [Internet]. 2016 Jul 27;21(8):974. DOI:10.3390/molecules21080974

[**468**] Fox IH, Kurpis L. Binding characteristics of an adenosine receptor in human placenta. *J Biol Chem* [Internet]. 1983 Jun 10;258(11):6952–5. Available from: http://www.jbc.org/content/258/11/6952.abstract

[**469**] Acevedo CG, Rojas S, Ramirez M, Bravo I. Transport and metabolism of adenosine in the perfused human placenta. *Placenta*. 1995 Oct 1;16(7):611–22. DOI:10.1016/0143-4004(95)90030-6

[**470**] Wheeler CP, Yudilevich DL. Transport and metabolism of adenosine in the perfused guinea-pig placenta. *J Physiol* [Internet]. 1988 Nov 1 [cited 2020 Aug 10];405(1):511–26. DOI:10.1113/jphysiol.1988.sp017345

[**471**] Reviriego J, Alonso MJ, Ibañez C, Marín J. Action of adenosine and characterization of adenosine receptors in human placental vasculature. *Gen Pharmacol*. 1990;21(2):227–33. DOI:10.1016/0306-3623(90)90906-3

[**472**] Reid DL, Davidson SR, Phernetton TM, Rankin JH. Adenosine causes a

biphasic response in the ovine fetal placental vasculature. *J Dev Physiol* [Internet]. 1990 Apr [cited 2019 Aug 25];13(4):237–40. Available from: http://www.ncbi.nlm.nih.gov/pubmed/2277187

[**473**] Donoso MV, Lopez R, Miranda R, Briones R, Huidobro-Toro JP, López R, et al. A2B adenosine receptor mediates human chorionic vasoconstriction and signals through arachidonic acid cascade. *Am J Physiol - Hear Circ Physiol* [Internet]. 2005 May [cited 2019 Jul 13];288(5 57-5):2439–49. DOI:10.1152/ajpheart.00548.2004

[**474**] MAGUIRE MH, KITAGAWA H, HOSOKAWA T, HOWARD RB. ATP and Adenosine. *Ann N Y Acad Sci* [Internet]. 1990 Dec 1 [cited 2020 Aug 10];603(1 Biological Ac):443–4. DOI:10.1111/j.1749-6632.1990.tb37698.x

[**475**] Read MA, Boura ALAA, Walters WAWW. Vascular actions of purines in the foetal circulation of the human placenta. *Br J Pharmacol* [Internet]. 1993 Sep [cited 2019 Aug 25];110(1):454–60. DOI:10.1111/j.1476-5381.1993.tb13832.x

[**476**] Malek A, Miller RK, Mattison DR, Ceckler T, Panigel M, di Sant'Agnese PA, et al. Continuous measurement of ATP by 31P-NMR in term human dually perfused placenta in vitro: response to ischemia. *J Appl Physiol* [Internet]. 1995 May 1 [cited 2020 Aug 12];78(5):1778–86. DOI:10.1152/jappl.1995.78.5.1778

[**477**] Petit A, Bélisle S. Stimulation of intracellular calcium concentration by adenosine triphosphate and uridine 5′-triphosphate in human term placental cells: Evidence for purinergic receptors. *J Clin Endocrinol Metab* [Internet]. 1995 Jun [cited 2020 Mar 28];80(6):1809–15. DOI:10.1210/jcem.80.6.7775628

[**478**] Ralevic V, Burrell S, Kingdom J, Burnstock G. Characterization of P2 receptors for purine and pyrimidine nucleotides in human placental cotyledons. *Br J Pharmacol*. 1997;121(6):1121–6. DOI:10.1038/sj.bjp.0701262

[**479**] Valdecantos P, Briones R, Moya P, Germain A, Huidobro-Toro JP. Pharmacological Identification of P2X1, P2X4 and P2X7 Nucleotide Receptors in the Smooth Muscles of Human Umbilical Cord and Chorionic Blood Vessels. *Placenta*. 2003;24(1):17–26. DOI:10.1053/plac.2002.0862

[**480**] Roberts VHJ, Waters LH, Powell T. Purinergic Receptor Expression and Activation in First Trimester and Term Human Placenta. *Placenta*. 2007;28(4):339–47. DOI:10.1016/j.placenta.2006.04.007

[**481**] Buvinic S, Poblete MI, Donoso MV, Delpiano AM, Briones R, Miranda R, et al. P2Y1 and P2Y2 receptor distribution varies along the human placental vascular tree: Role of nucleotides in vascular tone regulation. *J Physiol* [Internet]. 2006 Jun 1 [cited 2019 Mar 1];573(2):427–43. DOI:10.1113/jphysiol.2006.105882

[**482**] Sander KN, Ali TY, Warren AY, Hay DP, Broughton Pipkin F, Barrett DA, et al. Pharmacological profile of vascular activity of human stem villous arteries. *Placenta*. 2019 Dec 1;88:12–9. DOI:10.1016/j.placenta.2019.09.009

[**483**] Ebrahim NA, Leach L. Transendothelial migration of human umbilical mesenchymal stem cells across uterine endothelial monolayers: Junctional dynamics and putative mechanisms. *Placenta*. 2016;48:87–98. DOI:10.1016/j.placenta.2016.10.014

[**484**] Villota SD, Toledo-Rodriguez M, Leach L. Compromised barrier integrity of human feto-placental vessels from gestational diabetic pregnancies is related to

downregulation of occludin expression. *Diabetologia* [Internet]. 2021 Jan 1 [cited 2021 Jan 20];64(1):195–210. DOI:10.1007/s00125-020-05290-6

[**485**] Afshar Y, Dong J, Zhao P, Li L, Wang S, Zhang RY, et al. Circulating trophoblast cell clusters for early detection of placenta accreta spectrum disorders. *Nat Commun*. 2021 Aug;12(1):4408. DOI:10.1038/s41467-021-24627-2

[**486**] Parchem JG, Brock CO, Chen H-Y, Kalluri R, Barton JR, Sibai BM. Placental Growth Factor and the Risk of Adverse Neonatal and Maternal Outcomes. *Obstet Gynecol*. 2020 Mar;135(3):665–73. DOI:10.1097/AOG.0000000000003694

[**487**] Zhu L, Lu J, Huang W, Zhao J, Li M, Zhuang H, et al. A modified suture technique for the treatment of patients with pernicious placenta previa and placenta accreta spectrum: a case series. *Ann Transl Med* [Internet]. 2021 Jul;9(14):1140. DOI:10.21037/atm-21-2318

[**488**] Razak AA, Leach L, Ralevic V. Impaired vasocontractile responses to adenosine in chorionic vessels of human term placenta from pregnant women with pre-existing and gestational diabetes. *Diabetes Vasc Dis Res* [Internet]. 2018 Nov 1 [cited 2021 Jan 21];15(6):528–40. DOI:10.1177/1479164118790904

[**489**] Pearson T, Zhang J, Arya P, Warren AY, Ortori C, Fakis A, et al. Measurement of vasoactive metabolites (hydroxyeicosatetraenoic and epoxyeicosatrienoic acids) in uterine tissues of normal and compromised human pregnancy. *J Hypertens*. 2010 Dec;28(12):2429–37. DOI:10.1097/HJH.0b013e32833e86aa

[**490**] Pearson T, Warren AY, Barrett DA, Khan RN. Detection of EETs and HETE-generating cytochrome P-450 enzymes and the effects of their metabolites on myometrial and vascular function. *Am J Physiol Endocrinol Metab*. 2009 Sep;297(3):E647-56. DOI:10.1152/ajpendo.00227.2009

[**491**] Maneta E, Warren AY, Hay DP, Khan RN. Caspase-1-mediated cytokine release from gestational tissues, placental, and cord blood. *Front Physiol*. 2015;6(JUN):1–10. DOI:10.3389/fphys.2015.00186

[**492**] Donnelly-Roberts DL, Namovic MT, Han P, Jarvis MF. Mammalian P2X7 receptor pharmacology: comparison of recombinant mouse, rat and human P2X7 receptors. *Br J Pharmacol* [Internet]. 2009/06/22. 2009 Aug;157(7):1203–14. DOI:10.1111/j.1476-5381.2009.00233.x

[**493**] Savio LEBB, de Andrade Mello P, da Silva CG, Coutinho-Silva R, Mello P de A, da Silva CG, et al. The P2X7 Receptor in Inflammatory Diseases: Angel or Demon? *Front Pharmacol*. 2018;9(FEB):52. DOI:10.3389/fphar.2018.00052

[**494**] Young MT, Pelegrin P, Surprenant A. Amino acid residues in the P2X7 receptor that mediate differential sensitivity to ATP and BzATP. *Mol Pharmacol*. 2007 Jan;71(1):92–100. DOI:10.1124/mol.106.030163

[**495**] Allsopp RC, Dayl S, Schmid R, Evans RJ. Unique residues in the ATP gated human P2X7 receptor define a novel allosteric binding pocket for the selective antagonist AZ10606120. *Sci Rep* [Internet]. 2017;7(1):725. DOI:10.1038/s41598-017-00732-5

[**496**] Ofinran O, Bose U, Hay D, Abdul S, Tufatelli C, Khan R. Selection of suitable reference genes for gene expression studies in normal human ovarian tissues,

borderline ovarian tumours and ovarian cancer. *Mol Med Rep*. 2016 Dec;14(6):5725–31. DOI:10.3892/mmr.2016.5933

[**497**] Koenen TB, Stienstra R, van Tits LJ, de Graaf J, Stalenhoef AFH, Joosten LAB, et al. Hyperglycemia activates caspase-1 and TXNIP-mediated IL-1beta transcription in human adipose tissue. *Diabetes*. 2011 Feb;60(2):517–24. DOI:10.2337/db10-0266

[**498**] Al-Khyatt W, Tufarelli C, Khan R, Iftikhar SY. Selective oestrogen receptor antagonists inhibit oesophageal cancer cell proliferation in vitro. *BMC Cancer* [Internet]. 2018;18(1):121. DOI:10.1186/s12885-018-4030-5

[**499**] Patel SK, Jackson L, Warren AY, Arya P, Shaw RW, Khan RN. A role for two-pore potassium (K2P) channels in endometrial epithelial function. *J Cell Mol Med* [Internet]. 2013/01/11. 2013 Jan;17(1):134–46. DOI:10.1111/j.1582-4934.2012.01656.x

[**500**] Chanrachakul B, Broughton Pipkin F, Khan RN. Contribution of coupling between human myometrial beta2-adrenoreceptor and the BK(Ca) channel to uterine quiescence. *Am J Physiol Cell Physiol*. 2004 Dec;287(6):C1747-52. DOI:10.1152/ajpcell.00236.2004

[**501**] Brereton MF, Wareing M, Jones RL, Greenwood SL. Characterisation of K+ Channels in Human Fetoplacental Vascular Smooth Muscle Cells. *PLoS One*. 2013;8(2). DOI:10.1371/journal.pone.0057451

[**502**] Leik CE, Willey A, Graham MF, Walsh SW. Isolation and Culture of Arterial Smooth Muscle Cells from Human Placenta. *Hypertension*. 2004;43(4):837–40. DOI:10.1161/01.HYP.0000119191.33112.9c

[**503**] Ebrahim NA, Leach L. Temporal studies into attachment, VE-cadherin perturbation, and paracellular migration of human umbilical mesenchymal stem cells across umbilical vein endothelial monolayers. *Stem Cells Dev* [Internet]. 2014/12/10. 2015 Feb 15;24(4):426–36. DOI:10.1089/scd.2014.0207

[**504**] Jaffe EA, Nachman RL, Becker CG, Minick CR. Culture of human endothelial cells derived from umbilical veins. Identification by morphologic and immunologic criteria. *J Clin Invest* [Internet]. 1973 [cited 2021 Jan 19];52(11):2745–56. DOI:10.1172/JCI107470

[**505**] Marin V, Kaplanski G, Grès S, Farnarier C, Bongrand P. Endothelial cell culture: protocol to obtain and cultivate human umbilical endothelial cells. *J Immunol Methods*. 2001 Aug 1;254(1–2):183–90. DOI:10.1016/S0022-1759(01)00408-2

[**506**] Solini A, Novak I. Role of the P2X7 receptor in the pathogenesis of type 2 diabetes and its microvascular complications. Vol. 47, Current Opinion in Pharmacology. Elsevier Ltd; 2019. p. 75–81. DOI:10.1016/j.coph.2019.02.009

[**507**] Burnstock G, Knight GE. The potential of P2X7 receptors as a therapeutic target, including inflammation and tumour progression. *Purinergic Signal*. 2018;14(1). DOI:10.1007/s11302-017-9593-0

[**508**] Adinolfi E, Giuliani AL, De Marchi E, Pegoraro A, Orioli E, Di Virgilio F. The P2X7 receptor: A main player in inflammation. *Biochem Pharmacol*. 2018;151:234–44. DOI:10.1016/j.bcp.2017.12.021

[**509**] Di Virgilio F, Sarti AC, Grassi F. Modulation of innate and adaptive immunity by

P2X ion channels. *Curr Opin Immunol*. 2018;52:51–9. DOI:10.1016/j.coi.2018.03.026

[**510**] DeFronzo RA, Ferrannini E, Groop L, Henry RR, Herman WH, Holst JJ, et al. Type 2 diabetes mellitus. *Nat Rev Dis Prim*. 2015;1(July):1–23. DOI:10.1038/nrdp.2015.19

[**511**] Uresti-Rivera EE, García-Jacobo RE, Méndez-Cabañas JA, Gaytan-Medina LE, Cortez-Espinosa N, Portales-Pérez DP, et al. The presence of the 1068 G>A variant of P2X7 receptors is associated to an increase in IL-1Ra levels, insulin secretion and pancreatic β-cell function but not with glycemic control in type 2 diabetes patients. *Gene*. 2018;652:1–6. DOI:10.1016/j.gene.2018.01.084

[**512**] Tozzi M, Larsen AT, Lange SC, Giannuzzo A, Andersen MN, Novak I. The P2X7 receptor and pannexin-1 are involved in glucose-induced autocrine regulation in β-cells. *Sci Rep*. 2018;8(1):1–15. DOI:10.1038/s41598-018-27281-9

[**513**] Stachon P, Heidenreich A, Merz J, Hilgendorf I, Wolf D, Willecke F, et al. P2X7 Deficiency Blocks Lesional Inflammasome Activity and Ameliorates Atherosclerosis in Mice. *Circulation*. 2017;135(25):2524–33. DOI:10.1161/CIRCULATIONAHA.117.027400

[**514**] Portillo JAC, Corcino YL, Miao Y, Tang J, Sheibani N, Kern TS, et al. CD40 in retinal müller cells induces P2X7-dependent cytokine expression in macrophages/microglia in diabetic mice and development of early experimental diabetic retinopathy. *Diabetes*. 2017;66(2):483–93. DOI:10.2337/db16-0051

[**515**] Giacovazzo G, Apolloni S, Coccurello R. Loss of P2X7 receptor function dampens whole body energy expenditure and fatty acid oxidation. *Purinergic Signal*. 2018;14(3):299–305. DOI:10.1007/s11302-018-9610-y

[**516**] Blasetti Fantauzzi C, Menini S, Iacobini C, Rossi C, Santini E, Solini A, et al. Deficiency of the Purinergic Receptor 2X7 Attenuates Nonalcoholic Steatohepatitis Induced by High-Fat Diet: Possible Role of the NLRP3 Inflammasome. *Oxid Med Cell Longev*. 2017;2017:8962458. DOI:10.1155/2017/8962458

[**517**] Solini A, Menini S, Rossi C, Ricci C, Santini E, Blasetti Fantauzzi C, et al. The purinergic 2X7 receptor participates in renal inflammation and injury induced by high-fat diet: Possible role of NLRP3 inflammasome activation. *J Pathol*. 2013;231(3):342–53. DOI:10.1002/path.4237

[**518**] Vieira FS, Nanini HF, Takiya CM, Coutinho-Silva R. P2X7 receptor knockout prevents streptozotocin-induced type 1 diabetes in mice. *Mol Cell Endocrinol*. 2016;419:148–57. DOI:10.1016/j.mce.2015.10.008

[**519**] Liu W, Ao Q, Guo Q, He W, Peng L, Jiang J, et al. miR-9 Mediates CALHM1-Activated ATP-P2X7R Signal in Painful Diabetic Neuropathy Rats. *Mol Neurobiol*. 2017;54(2):922–9. DOI:10.1007/s12035-016-9700-1

[**520**] Seref-Ferlengez Z, Maung S, Schaffler MB, Spray DC, Suadicani SO, Thi MM. P2X7R-Panx1 Complex Impairs Bone Mechanosignaling under High Glucose Levels Associated with Type-1 Diabetes. Genetos DC, editor. *PLoS One*. 2016;11(5):e0155107. DOI:10.1371/journal.pone.0155107

[**521**] Novak I, Solini A. P2X receptor-ion channels in the inflammatory response in adipose tissue and pancreas — potential triggers in onset of type 2 diabetes?

Curr Opin Immunol. 2018;52:1–7. DOI:10.1016/j.coi.2018.02.002

[**522**] Burnstock G. Purinergic signalling in the reproductive system in health and disease. *Purinergic Signal* [Internet]. 2013/11/26. 2014;10(1):157–87. DOI:10.1007/s11302-013-9399-7

[**523**] Dobronyi I, Hung KS, Satchell DG, Maguire MH. Evidence for a novel P2X purinoceptor in human placental chorionic surface arteries. *Eur J Pharmacol* [Internet]. 1997 Feb 5 [cited 2019 Aug 25];320(1):61–4. DOI:10.1016/s0014-2999(96)00967-3

[**524**] von Versen-Höynck F, Rajakumar A, Bainbridge SA, Gallaher MJ, Roberts JM, Powers RW. Human Placental Adenosine Receptor Expression is Elevated in Preeclampsia and Hypoxia Increases Expression of the A2A Receptor. *Placenta* [Internet]. 2009;30(5):434–42. DOI:10.1016/j.placenta.2009.02.004

[**525**] Roberts VHJ, Webster RP, Brockman DE, Pitzer BA, Myatt L. Post-Translational Modifications of the P2X4 Purinergic Receptor Subtype in the Human Placenta are Altered in Preeclampsia. *Placenta*. 2007;28(4):270–7. DOI:10.1016/j.placenta.2006.04.008

[**526**] Bryant AH, Bevan RJ, Spencer-Harty S, Scott LM, Jones RH, Thornton CA. Expression and function of NOD-like receptors by human term gestation-associated tissues. *Placenta* [Internet]. 2017/10/01. 2017;58:25–32. DOI:10.1016/j.placenta.2017.07.017

[**527**] Cheng S-B, Nakashima A, Huber WJ, Davis S, Banerjee S, Huang Z, et al. Pyroptosis is a critical inflammatory pathway in the placenta from early onset preeclampsia and in human trophoblasts exposed to hypoxia and endoplasmic reticulum stressors. *Cell Death Dis* [Internet]. 2019;10(12):927. DOI:10.1038/s41419-019-2162-4

[**528**] Stødle GS, Silva GB, Tangerås LH, Gierman LM, Nervik I, Dahlberg UE, et al. Placental inflammation in pre-eclampsia by Nod-like receptor protein (NLRP)3 inflammasome activation in trophoblasts. *Clin Exp Immunol* [Internet]. 2018/04/23. 2018 Jul;193(1):84–94. DOI:10.1111/cei.13130

[**529**] Yang Y, Li J, Han T-L, Zhou X, Qi H, Baker PN, et al. Endoplasmic reticulum stress may activate NLRP3 inflammasomes via TXNIP in preeclampsia. *Cell Tissue Res*. 2020 Mar;379(3):589–99. DOI:10.1007/s00441-019-03104-9

[**530**] Coutinho-Silva R, Persechini PM. P2Z purinoceptor-associated pores induced by extracellular ATP in macrophages and J774 cells. *Am J Physiol - Cell Physiol* [Internet]. 1997 [cited 2021 Mar 15];273(6 42-6). DOI:10.1152/ajpcell.1997.273.6.c1793

[**531**] Kummer JA, Broekhuizen R, Everett H, Agostini L, Kuijk L, Martinon F, et al. Inflammasome components NALP 1 and 3 show distinct but separate expression profiles in human tissues suggesting a site-specific role in the inflammatory response. *J Histochem Cytochem* [Internet]. 2007 May [cited 2021 Mar 15];55(5):443–52. DOI:10.1369/jhc.6A7101.2006

[**532**] Zahid A, Li B, Kombe AJK, Jin T, Tao J. Pharmacological Inhibitors of the NLRP3 Inflammasome [Internet]. Vol. 10, Frontiers in Immunology . 2019. p. 2538. Available from: https://www.frontiersin.org/article/10.3389/fimmu.2019.02538

[**533**] Groslambert M, Py BF. Spotlight on the NLRP3 inflammasome pathway. *J Inflamm Res*. 2018;11:359–74. DOI:10.2147/JIR.S141220

[**534**] Kirley TL, Norman AB. Unfolding of IgG domains detected by non-reducing SDS-PAGE. *Biochem Biophys Res Commun* [Internet]. 2018/06/23. 2018 Sep 5;503(2):944–9. DOI:10.1016/j.bbrc.2018.06.100

[**535**] Lee PY, Osman J, Low TY, Jamal R. Plasma/serum proteomics: depletion strategies for reducing high-abundance proteins for biomarker discovery. *Bioanalysis*. 2019 Oct;11(19):1799–812. DOI:10.4155/bio-2019-0145

[**536**] Green JP, Souilhol C, Xanthis I, Martinez-Campesino L, Bowden NP, Evans PC, et al. Atheroprone flow activates inflammation via endothelial ATP-dependent P2X7-p38 signalling. *Cardiovasc Res* [Internet]. 2017/11/11. 2018;114(2):324–35. DOI:10.1093/cvr/cvx213

[**537**] Milner P, Bodin P, Loesch A, Burnstock G. Rapid release of endothelin and ATP from isolated aortic endothelial cells exposed to increased flow. *Biochem Biophys Res Commun*. 1990 Jul;170(2):649–56. DOI:10.1016/0006-291x(90)92141-l

[**538**] Robson SC, Kaczmarek E, Siegel JB, Candinas D, Koziak K, Millan M, et al. Loss of ATP diphosphohydrolase activity with endothelial cell activation. *J Exp Med*. 1997 Jan;185(1):153–63. DOI:10.1084/jem.185.1.153

[**539**] Sathanoori R, Swärd K, Olde B, Erlinge D. The ATP receptors P2X7 and P2X4 modulate high glucose and palmitate-induced inflammatory responses in endothelial cells. *PLoS One*. 2015;10(5):1–24. DOI:10.1371/journal.pone.0125111

[**540**] Solini A, Chiozzi P, Falzoni S, Morelli A, Fellin R, Di Virgilio F. High glucose modulates P2X7 receptor-mediated function in human primary fibroblasts. *Diabetologia* [Internet]. 2000;43(10):1248–56. DOI:10.1007/s001250051520

[**541**] Gonnord P, Delarasse C, Auger R, Benihoud K, Prigent M, Cuif MH, et al. Palmitoylation of the P2X7 receptor, an ATP-gated channel, controls its expression and association with lipid rafts. *FASEB J Off Publ Fed Am Soc Exp Biol*. 2009 Mar;23(3):795–805. DOI:10.1096/fj.08-114637

[**542**] Hung S-CC, Choi CH, Said-Sadier N, Johnson L, Atanasova KR, Sellami H, et al. P2X(4) Assembles with P2X(7) and Pannexin-1 in Gingival Epithelial Cells and Modulates ATP-induced Reactive Oxygen Species Production and Inflammasome Activation. *PLoS One* [Internet]. 2013/08/13. 2013;8(7):e70210. DOI:10.1371/journal.pone.0070210

[**543**] Wang D, Wang H, Gao H, Zhang H, Zhang H, Wang Q, et al. P2X7 receptor mediates NLRP3 inflammasome activation in depression and diabetes [Internet]. Vol. 10, Cell and Bioscience. BioMed Central Ltd.; 2020 [cited 2020 Mar 30]. p. 28. DOI:10.1186/s13578-020-00388-1

[**544**] Alfadhli EM. Gestational diabetes mellitus. *Saudi Med J* [Internet]. 2015 Apr;36(4):399–406. DOI:10.15537/smj.2015.4.10307

[**545**] Katsarou A, Gudbjörnsdottir S, Rawshani A, Dabelea D, Bonifacio E, Anderson BJ, et al. Type 1 diabetes mellitus. *Nat Rev Dis Prim*. 2017 Mar;3:17016. DOI:10.1038/nrdp.2017.16

[**546**] Zhou Z, Zhang Q, Lu X, Wang R, Wang H, Wang Y-L, et al. The proprotein convertase furin is required for trophoblast syncytialization. *Cell Death Dis* [Internet]. 2013;4(4):e593–e593. DOI:10.1038/cddis.2013.106

[**547**] Tack CJ, Stienstra R, Joosten LAB, Netea MG. Inflammation links excess fat to insulin resistance: the role of the interleukin-1 family. *Immunol Rev*. 2012 Sep;249(1):239–52. DOI:10.1111/j.1600-065X.2012.01145.x

[**548**] Maedler K, Sergeev P, Ris F, Oberholzer J, Joller-Jemelka HI, Spinas GA, et al. Glucose-induced β cell production of IL-1β contributes to glucotoxicity in human pancreatic islets. *J Clin Invest*. 2002;110(6):851–60. DOI:10.1172/jci15318

[**549**] Minn AH, Hafele C, Shalev A. Thioredoxin-interacting protein is stimulated by glucose through a carbohydrate response element and induces beta-cell apoptosis. *Endocrinology*. 2005 May;146(5):2397–405. DOI:10.1210/en.2004-1378

[**550**] Böni-Schnetzler M, Thorne J, Parnaud G, Marselli L, Ehses JA, Kerr-Conte J, et al. Increased interleukin (IL)-1beta messenger ribonucleic acid expression in beta -cells of individuals with type 2 diabetes and regulation of IL-1beta in human islets by glucose and autostimulation. *J Clin Endocrinol Metab*. 2008 Oct;93(10):4065–74. DOI:10.1210/jc.2008-0396

[**551**] Van Wilpe S, Koornstra R, Den Brok M, De Groot JW, Blank C, De Vries J, et al. Lactate dehydrogenase: a marker of diminished antitumor immunity. *Oncoimmunology*. 2020;9(1):1731942. DOI:10.1080/2162402X.2020.1731942

[**552**] Menyhart O, Weltz B, Győrffy B. MultipleTesting.com: A tool for life science researchers for multiple hypothesis testing correction. *PLoS One* [Internet]. 2021 Jun 9;16(6):e0245824–e0245824. DOI:10.1371/journal.pone.0245824

[**553**] Gudipaty L, Humphreys BD, Buell G, Dubyak GR. Regulation of P2X(7) nucleotide receptor function in human monocytes by extracellular ions and receptor density. *Am J Physiol Cell Physiol*. 2001 Apr;280(4):C943-53. DOI:10.1152/ajpcell.2001.280.4.C943

[**554**] Maneta E, Warren AY, Hay DP, Khan RN. Caspase-1-mediated cytokine release from gestational tissues, placental, and cord blood. *Front Physiol* [Internet]. 2015/07/15. 2015;6:186. DOI:10.3389/fphys.2015.00186

[**555**] Rodrigues AM, Bergamaschi CT, Fernandes MJS, Paredes-Gamero EJ, Buri M V, Ferreira AT, et al. P2X(7) receptor in the kidneys of diabetic rats submitted to aerobic training or to N-acetylcysteine supplementation [corrected]. *PLoS One*. 2014;9(6):e97452. DOI:10.1371/journal.pone.0097452

[**556**] Menzies RI, Tam FW, Unwin RJ, Bailey MA. Purinergic signaling in kidney disease. *Kidney Int*. 2017 Feb;91(2):315–23. DOI:10.1016/j.kint.2016.08.029

[**557**] Solini A, Chiozzi P, Morelli A, Adinolfi E, Rizzo R, Baricordi OR, et al. Enhanced P2X7 activity in human fibroblasts from diabetic patients: a possible pathogenetic mechanism for vascular damage in diabetes. *Arterioscler Thromb Vasc Biol*. 2004 Jul;24(7):1240–5. DOI:10.1161/01.ATV.0000133193.11078.c0

[**558**] Bakker WW, Donker RB, Timmer A, van Pampus MG, van Son WJ, Aarnoudse JG, et al. Plasma hemopexin activity in pregnancy and preeclampsia. *Hypertens Pregnancy* [Internet]. 2007/05/01. 2007;26(2):227–39. DOI:10.1080/10641950701274896

[**559**] North RA. Molecular physiology of P2X receptors. *Physiol Rev*. 2002 Oct;82(4):1013–67. DOI:10.1152/physrev.00015.2002

[**560**] Erb L, Lustig KD, Ahmed AH, Gonzalez FA, Weisman GA. Covalent incorporation of 3'-O-(4-benzoyl)benzoyl-ATP into a P2 purinoceptor in transformed mouse fibroblasts. *J Biol Chem*. 1990 May;265(13):7424–31.

[**561**] Honore P, Donnelly-Roberts D, Namovic MT, Hsieh G, Zhu CZ, Mikusa JP, et al. A-740003 [N-(1-{[(cyanoimino)(5-quinolinylamino) methyl]amino}-2,2-dimethylpropyl)-2-(3,4-dimethoxyphenyl)acetamide], a novel and selective P2X7 receptor antagonist, dose-dependently reduces neuropathic pain in the rat. *J Pharmacol Exp Ther*. 2006 Dec;319(3):1376–85. DOI:10.1124/jpet.106.111559

[**562**] Agrawal A, Kruse LS, Vangsted AJ, Gartland A, Jørgensen NR. Human P2X7 Receptor Causes Cycle Arrest in RPMI-8226 Myeloma Cells to Alter the Interaction with Osteoblasts and Osteoclasts. *Cells*. 2020 Oct;9(11). DOI:10.3390/cells9112341

[**563**] Abbracchio MP, Burnstock G. Purinoceptors: are there families of P2X and P2Y purinoceptors? *Pharmacol Ther*. 1994;64(3):445–75. DOI:10.1016/0163-7258(94)00048-4

[**564**] Burnstock G. Purine-mediated signalling in pain and visceral perception. *Trends Pharmacol Sci* [Internet]. 2001 Apr 1 [cited 2020 Dec 17];22(4):182–8. DOI:10.1016/S0165-6147(00)01643-6

[**565**] North RA, Surprenant A. Pharmacology of Cloned P2X Receptors. *Annu Rev Pharmacol Toxicol*. 2000 Apr;40(1):563–80. DOI:10.1146/annurev.pharmtox.40.1.563

[**566**] Bo X, Fischer B, Maillard M, Jacobson KA, Burnstock G. Comparative studies on the affinities of ATP derivatives for P2X-purinoceptors in rat urinary bladder. *Br J Pharmacol* [Internet]. 1994 [cited 2020 Dec 17];112(4):1151–9. DOI:10.1111/j.1476-5381.1994.tb13204.x

[**567**] Choi RCY, Man MLS, Ling KKY, Ip NY, Simon J, Barnard EA, et al. Expression of the P2Y1 nucleotide receptor in chick muscle: Its functional role in the regulation of acetylcholinesterase and acetylcholine receptor. *J Neurosci* [Internet]. 2001 Dec 1 [cited 2020 Dec 17];21(23):9224–34. DOI:10.1523/jneurosci.21-23-09224.2001

[**568**] Dranoff JA, Masyuk AI, Kruglov EA, LaRusso NF, Nathanson MH. Polarized expression and function of P2Y ATP receptors in rat bile duct epithelia. *Am J Physiol - Gastrointest Liver Physiol* [Internet]. 2001 [cited 2020 Dec 17];281(4 44-4). DOI:10.1152/ajpgi.2001.281.4.g1059

[**569**] Jin J, Daniel JL, Kunapuli SP. Molecular basis for ADP-induced platelet activation: II. The P2Y1 receptor mediates ADP-induced intracellular calcium mobilization and shape change in platelets. *J Biol Chem* [Internet]. 1998 Jan 23 [cited 2020 Dec 17];273(4):2030–4. DOI:10.1074/jbc.273.4.2030

[**570**] Hollopeter G, Jantzen HM, Vincent D, Li G, England L, Ramakrishnan V, et al. Identification of the platelet ADP receptor targeted by antithrombotic drugs. *Nature* [Internet]. 2001 Jan 11 [cited 2020 Dec 17];409(6817):202–7. DOI:10.1038/35051599

[**571**] Foster CJ, Prosser DM, Agans JM, Zhai Y, Smith MD, Lachowicz JE, et al. Molecular identification and characterization of the platelet ADP receptor targeted by thienopyridine antithrombotic drugs. *J Clin Invest* [Internet]. 2001 [cited 2020 Dec 17];107(12):1591–8. DOI:10.1172/JCI12242

[**572**] Bo X, Burnstock G. Distribution of [3H]α,β –methylene ATP binding sites in rat brain and spinal cord. *Neuroreport* [Internet]. 1994 [cited 2020 Dec 17];5(13):1601–4. DOI:10.1097/00001756-199408150-00015

[**573**] Soto F, Garcia-Guzman M, Karschin C, Stühmer W. Cloning and tissue distribution of a novel P2X receptor from rat brain. *Biochem Biophys Res Commun*. 1996 Jun 14;223(2):456–60. DOI:10.1006/bbrc.1996.0915

[**574**] Mulvany MJ, Aalkjaer C. Structure and function of small arteries. Vol. 70, Physiological Reviews. 1990. p. 921–61. DOI:10.1152/physrev.1990.70.4.921

[**575**] Dubyak GR, el-Moatassim C. Signal transduction via P2-purinergic receptors for extracellular ATP and other nucleotides. *Am J Physiol*. 1993 Sep;265(3 Pt 1):C577-606. DOI:10.1152/ajpcell.1993.265.3.C577

[**576**] Wareing M, Crocker IP, Warren AY, Taggart MJ, Baker PN. Characterization of small arteries isolated from the human placental chorionic plate. *Placenta* [Internet]. 2002 May [cited 2019 Aug 25];23(5):400–9. DOI:10.1053/plac.2002.0825

[**577**] Fox SB, Khong TY. Lack of innervation of human umbilical cord. An immunohistological and histochemical study. *Placenta* [Internet]. 1990 [cited 2020 Dec 19];11(1):59–62. DOI:10.1016/S0143-4004(05)80443-6

[**578**] Poston L. The control of blood flow to the placenta. *Exp Physiol* [Internet]. 1997 [cited 2020 Jul 8];82(2):377–87. DOI:10.1113/expphysiol.1997.sp004033

[**579**] Clozel M, Fischli W. Human cultured endothelial cells do secrete endothelin-1. *J Cardiovasc Pharmacol* [Internet]. 1989 [cited 2020 Dec 19];13:S229–31. DOI:10.1097/00005344-198900135-00068

[**580**] Van de Voorde J, Vanderstichele H, Leusen I. Release of endothelium-derived relaxing factor from human umbilical vessels. *Circ Res* [Internet]. 1987 Apr [cited 2020 Dec 19];60(4):517–22. DOI:10.1161/01.RES.60.4.517

[**581**] Chaudhuri G, Buga GM, Gold ME, Wood KS, Ignarro LJ. Characterization and actions of human umbilical endothelium derived relaxing factor. *Br J Pharmacol* [Internet]. 1991 [cited 2020 Dec 19];102(2):331–6. DOI:10.1111/j.1476-5381.1991.tb12174.x

[**582**] Gude NM, King RG, Brennecke SP. Role of endothelium-derived nitric oxide in maintenance of low fetal vascular resistance in placenta [Internet]. Vol. 336, The Lancet. Lancet; 1990 [cited 2020 Dec 19]. p. 1589–90. DOI:10.1016/0140-6736(90)93374-X

[**583**] Myatt L, Brewer AS, Brockman DE. The comparative effects of big endothelin-1, endothelin-1, and endothelin-3 in the human fetal-placental circulation. *Am J Obstet Gynecol* [Internet]. 1992 Dec [cited 2019 Aug 26];167(6):1651–6. DOI:10.1016/0002-9378(92)91756-Z

[**584**] Parisi VM, Walsh SW. Fetal vascular responses to prostacyclin. *Am J Obstet Gynecol* [Internet]. 1989 Apr [cited 2019 Aug 26];160(4):871–6; discussion 876-

8. DOI:10.1016/0002-9378(89)90303-7

[**585**] McCarthy AL, Woolfson RG, Evans BJ, Davies DR, Raju SK, Poston L. Functional characteristics of small placental arteries. *Am J Obstet Gynecol*. 1994;170(3):945–51. DOI:10.1016/S0002-9378(94)70311-6

[**586**] Sabry S, Mondon F, Ferré F, Dinh-Xuan AT. In vitro contractile and relaxant responses of human resistance placental stem villi arteries of healthy parturients: role of endothelium. *Fundam Clin Pharmacol* [Internet]. 1995 [cited 2019 Aug 26];9(1):46–51. Available from: http://www.ncbi.nlm.nih.gov/pubmed/7768487

[**587**] Kwek K, Read MA, Khong TY, Bisits AT, Walters WAW. Vasoactive effects of 8-epi-prostaglandin F2α in isolated human placental conduit and resistance blood vessels in vitro. *Placenta* [Internet]. 2001 Jul [cited 2019 Aug 26];22(6):526–33. DOI:10.1053/plac.2001.0690

[**588**] Skajaa K, Svane D, Andersson KE, Forman A. Effects of magnesium and isradipine on contractile activation induced by the thromboxane A2 analog U46619 in human uteroplacental arteries in term pregnancy. *Am J Obstet Gynecol*. 1990 Oct 1;163(4 PART 1):1323–33. DOI:10.1016/0002-9378(90)90714-I

[**589**] Svane D, Skajaa K, Andersson KE, Forman A. Effects of the thromboxane-receptor antagonists AH 23848 and BM 13.177 on human uteroplacental arteries. *Obstet Gynecol* [Internet]. 1992 Aug 1 [cited 2020 Dec 19];80(2):234–40. Available from: https://europepmc.org/article/med/1386150

[**590**] Allen J, Forman A, Maigaard S, Jespersen LT, Andersson KE. Effect of endogenous vasoconstrictors on maternal intramyometrial and fetal stem villous arteries in pre-eclampsia. *J Hypertens* [Internet]. 1989 [cited 2020 Dec 19];7(7):529–36. DOI:10.1097/00004872-198907000-00004

[**591**] Maigaard S, Forman A, Andersson KE. Digoxin inhibition of relaxation induced by prostacyclin and vasoactive intestinal polypeptide in small human placental arteries. *Placenta* [Internet]. 1985 [cited 2020 Dec 19];6(5):435–43. DOI:10.1016/S0143-4004(85)80021-7

[**592**] Westfall DP, Todorov LD, Mihaylova-Todorova ST. ATP as a cotransmitter in sympathetic nerves and its inactivation by releasable enzymes. *J Pharmacol Exp Ther*. 2002 Nov 1;303(2):439–44. DOI:10.1124/jpet.102.035113

[**593**] Amarnani S, Sangrat B, Chaudhuri G. Effects of selected endothelium-dependent vasodilators on fetoplacental vasculature: physiological implications. *Am J Physiol Circ Physiol* [Internet]. 1999 Aug 1;277(2):H842–7. DOI:10.1152/ajpheart.1999.277.2.H842

[**594**] Hoeldtke NJ, Napolitano PG, Moore KH, Calhoun BC, Hume RFJ. Fetoplacental vascular tone during fetal circuit acidosis and acidosis with hypoxia in the ex vivo perfused human placental cotyledon. *Am J Obstet Gynecol*. 1997 Nov;177(5):1088–92. DOI:10.1016/s0002-9378(97)70020-6

[**595**] Boura ALA, Walters WAW, Read MA, Leitch IM. Autacoids and Control of Human Placental Blood Flow. *Clin Exp Pharmacol Physiol* [Internet]. 1994 Oct [cited 2019 Aug 26];21(10):737–48. DOI:10.1111/j.1440-1681.1994.tb02441.x

[**596**] King RG, Gude NM, Di Iulio JL, Brennecke SP. Regulation of human placental

fetal vessel tone: role of nitric oxide. *Reprod Fertil Dev*. 1995;7(6):1407–11. DOI:10.1071/rd9951407

[**597**] Mills TA, Wareing M, Bugg GJ, Greenwood SL, Baker PN. Chorionic plate artery function and Doppler indices in normal pregnancy and intrauterine growth restriction. *Eur J Clin Invest*. 2005 Dec;35(12):758–64. DOI:10.1111/j.1365-2362.2005.01577.x

[**598**] González C, Cruz MA, Gallardo V, Miguel P, Carrasco G. Relative potency of nitrovasodilators on human placental vessels from normal and preeclamptic pregnancies. *Gynecol Obstet Invest*. 1997;43(4):219–24. DOI:10.1159/000291861

[**599**] Cadaveira-Mosquera A, Ribeiro SJ, Reboreda A, Pérez M, Lamas JA. Activation of TREK currents by the neuroprotective agent riluzole in mouse sympathetic neurons. *J Neurosci* [Internet]. 2011 Jan 26 [cited 2021 Jan 9];31(4):1375–85. DOI:10.1523/JNEUROSCI.2791-10.2011

[**600**] Broegger T, Andersson KE, Aalkjaer C, Forman A, Boedtkjer DB. Sensitivity to the thromboxane A2 analog U46619 varies with inner diameter in human stem villous arteries. *Placenta*. 2016 Mar 1;39:111–5. DOI:10.1016/j.placenta.2016.01.017

[**601**] Wareing M, Greenwood SL, Taggart MJ, Baker PN. Vasoactive responses of veins isolated from the human placental chorionic plate. *Placenta*. 2003 Aug;24(7):790–6. DOI:10.1016/s0143-4004(03)00108-5

[**602**] O'Keeffe AG, Ambler G, Barber JA. Sample size calculations based on a difference in medians for positively skewed outcomes in health care studies. *BMC Med Res Methodol* [Internet]. 2017;17(1):157. DOI:10.1186/s12874-017-0426-1

[**603**] Werner P, Seward EP, Buell GN, North RA. Domains of P2X receptors involved in desensitization. *Proc Natl Acad Sci* [Internet]. 1996 Dec 24;93(26):15485 LP – 15490. DOI:10.1073/pnas.93.26.15485

[**604**] Koshimizu T, Koshimizu M, Stojilkovic SS. Contributions of the C-terminal Domain to the Control of P2X Receptor Desensitization *. *J Biol Chem* [Internet]. 1999 Dec 31;274(53):37651–7. DOI:10.1074/jbc.274.53.37651

[**605**] Abad A, Estañ L, Morales-Olivas FJ, Serra V. Reactivity of isolated human chorionic vessels: analysis of some influencing variables. *Can J Physiol Pharmacol*. 2003 Dec;81(12):1147–51. DOI:10.1139/y03-119

[**606**] Kitazawa T, Masuo M, Somlyo AP. G protein-mediated inhibition of myosin light-chain phosphatase in vascular smooth muscle. *Proc Natl Acad Sci U S A* [Internet]. 1991 Oct 15;88(20):9307–10. DOI:10.1073/pnas.88.20.9307

[**607**] Ganitkevich V Y a, Isenberg G. Depolarization-mediated intracellular calcium transients in isolated smooth muscle cells of guinea-pig urinary bladder. *J Physiol*. 1991 Apr;435:187–205. DOI:10.1113/jphysiol.1991.sp018505

[**608**] Driska SP, Aksoy MO, Murphy RA. Myosin light chain phosphorylation associated with contraction in arterial smooth muscle. *Am J Physiol*. 1981 May;240(5):C222-33. DOI:10.1152/ajpcell.1981.240.5.C222

[**609**] Ratz PH, Berg KM, Urban NH, Miner AS. Regulation of smooth muscle calcium

sensitivity: KCl as a calcium-sensitizing stimulus. *Am J Physiol Cell Physiol*. 2005 Apr;288(4):C769-83. DOI:10.1152/ajpcell.00529.2004

[**610**] Himpens B, Somlyo AP. Free-calcium and force transients during depolarization and pharmacomechanical coupling in guinea-pig smooth muscle. *J Physiol*. 1988 Jan;395:507–30. DOI:10.1113/jphysiol.1988.sp016932

[**611**] Shinoda J, Suzuki A, Oiso Y, Kozawa O. Involvement of phosphatidylcholine hydrolysis by phospholipase D in extracellular ATP-induced arachidonic acid release in aortic smooth muscle cells. *Arterioscler Thromb Vasc Biol*. 1997 Feb;17(2):295–9. DOI:10.1161/01.atv.17.2.295

[**612**] Araki S, Ito M, Kureishi Y, Feng J, Machida H, Isaka N, et al. Arachidonic acid-induced Ca2+ sensitization of smooth muscle contraction through activation of Rho-kinase. *Pflugers Arch*. 2001 Feb;441(5):596–603. DOI:10.1007/s004240000462

[**613**] Feng J, Ito M, Kureishi Y, Ichikawa K, Amano M, Isaka N, et al. Rho-associated kinase of chicken gizzard smooth muscle. *J Biol Chem*. 1999 Feb;274(6):3744–52. DOI:10.1074/jbc.274.6.3744

[**614**] Leung T, Manser E, Tan L, Lim L. A novel serine/threonine kinase binding the Ras-related RhoA GTPase which translocates the kinase to peripheral membranes. *J Biol Chem*. 1995 Dec;270(49):29051–4. DOI:10.1074/jbc.270.49.29051

[**615**] Gong MC, Kinter MT, Somlyo A V, Somlyo AP. Arachidonic acid and diacylglycerol release associated with inhibition of myosin light chain dephosphorylation in rabbit smooth muscle. *J Physiol* [Internet]. 1995 Jul 1;486 (Pt 1(Pt 1):113–22. DOI:10.1113/jphysiol.1995.sp020795

[**616**] Wang S, Iring A, Strilic B, Albarrán Juárez J, Kaur H, Troidl K, et al. $P2Y_2$ and Gq/G_{11} control blood pressure by mediating endothelial mechanotransduction. *J Clin Invest*. 2015 Aug;125(8):3077–86. DOI:10.1172/JCI81067

[**617**] Rabiet M-J, Plantier J-L, Rival Y, Genoux Y, Lampugnani M-G, Dejana E. Thrombin-Induced Increase in Endothelial Permeability Is Associated With Changes in Cell-to-Cell Junction Organization. *Arterioscler Thromb Vasc Biol*. 1996;16(3):488–96. DOI:10.1161/01.ATV.16.3.488

[**618**] Claesson-Welsh L. Vascular permeability - The essentials. *Ups J Med Sci*. 2015;120(3):135–43. DOI:10.3109/03009734.2015.1064501

[**619**] Weis SM. Vascular permeability in cardiovascular disease and cancer. *Curr Opin Hematol*. 2008;15(3):243–9. DOI:10.1097/MOH.0b013e3282f97d86

[**620**] Antonetti DA, Klein R, Gardner TW. Diabetic retinopathy. *N Engl J Med*. 2012;366(13):1227–39. DOI:10.1056/NEJMra1005073

[**621**] Folkman J. Angiogenesis: an organizing principle for drug discovery? *Nat Rev Drug Discov*. 2007;6(4):273–86. DOI:10.1038/nrd2115

[**622**] Hanahan D, Weinberg RA. Hallmarks of cancer: The next generation. *Cell*. 2011;144(5):646–74. DOI:10.1016/j.cell.2011.02.013

[**623**] Carmeliet P, Jain RK. Angiogenesis in cancer and other diseases. *Nature*. 2000;407(6801):249–57. DOI:10.1038/35025220

[**624**] Leach L, Taylor A, Sciota F. Vascular dysfunction in the diabetic placenta:

causes and consequences. *J Anat*. 2009;215:69–76. DOI:10.1111/j.1469-7580.2009.01098.x

[**625**] Goel S, Duda DG, Xu L, Munn LL, Boucher Y, Fukumura D, et al. Normalization of the vasculature for treatment of cancer and other diseases. *Physiol Rev*. 2011;91(3):1071–121. DOI:10.1152/physrev.00038.2010

[**626**] Nakajima M, Cooney MJ, Tu AH, Kwang Yul Chang, Cao J, Ando A, et al. Normalization of retinal vascular permeability in experimental diabetes with genistein. *Investig Ophthalmol Vis Sci* [Internet]. 2001 [cited 2020 Apr 12];42(9):2110–4. Available from: http://www.ncbi.nlm.nih.gov/pubmed/11481279

[**627**] Carmeliet P, Jain RK. Principles and mechanisms of vessel normalization for cancer and other angiogenic diseases. *Nat Rev Drug Discov*. 2011;10(6):417–27. DOI:10.1038/nrd3455

[**628**] Leach L, Eaton BM, Westcott EDA, Firth JA. Effect of histamine on endothelial permeability and structure and adhesion molecules of the paracellular junctions of perfused human placental microvessels. *Microvasc Res*. 1995;50(3):323–37. DOI:10.1006/mvre.1995.1062

[**629**] Baumüller S, Lehnen H, Schmitz J, Fimmers R, Müller AM. The impact of Insulin treatment on the expression of vascular endothelial cadherin and beta-catenin in human fetoplacental vessels. *Pediatr Dev Pathol* [Internet]. 2015 Jan 1 [cited 2021 Jan 22];18(1):17–23. DOI:10.2350/13-11-1400-OA.1

[**630**] Blundell C, Tess ER, Schanzer ASR, Coutifaris C, Su EJ, Parry S, et al. A microphysiological model of the human placental barrier. *Lab Chip*. 2016;16(16):3065–73. DOI:10.1039/c6lc00259e

[**631**] Chandra A, Barillas S, Suliman A, Angle N. A novel fluorescence-based cellular permeability assay. *J Biochem Biophys Methods*. 2007;70(3):329–33. DOI:10.1016/j.jbbm.2006.07.002

[**632**] Roberts WG, Palade GE. Increased microvascular permeability and endothelial fenestration induced by vascular endothelial growth factor. *J Cell Sci* [Internet]. 1995 [cited 2020 Apr 12];108(6):2369 LP – 2379. Available from: http://jcs.biologists.org/content/108/6/2369.abstract

[**633**] Farmer PJ, Girardot D, Lepage A, Regoli D, Sirois P. Inhibition of prostaglandin G/H synthase unveils a potent effect of platelet activating factor on the permeability of bovine aortic endothelial cells to albumin. *Inflammation*. 2002;26(6):253–8. DOI:10.1023/A:1021477316559

[**634**] Hart MN, Van Dyk LF, Moore SA, Shasby MD, Cancilla PA. Differential opening of the brain endothelial barrier following neutralization of the endothelial luminal anionic charge in vitro. *J Neuropathol Exp Neurol*. 1987;46(2):141–53. DOI:10.1097/00005072-198703000-00003

[**635**] Bowman PD, Ennis SR, Rarey KE, Lorris Betz A, Goldstein GW. Brain microvessel endothelial cells in tissue culture: A model for study of blood-brain barrier permeability. *Ann Neurol*. 1983;14(4):396–402. DOI:10.1002/ana.410140403

[**636**] Auger FA, Gibot L, Lacroix D. The Pivotal Role of Vascularization in Tissue Engineering. *Annu Rev Biomed Eng*. 2013;15(1):177–200.

DOI:10.1146/annurev-bioeng-071812-152428

[**637**] Hasan A, Paul A, Vrana NE, Zhao X, Memic A, Hwang YS, et al. Microfluidic techniques for development of 3D vascularized tissue. *Biomaterials*. 2014;35(26):7308–25. DOI:10.1016/j.biomaterials.2014.04.091

[**638**] Miles AA, Miles EM. Vascular reactions to histamine, histamine-liberator and leukotaxine in the skin of guinea-pigs. *J Physiol*. 1952;118(2):228–57. DOI:10.1113/jphysiol.1952.sp004789

[**639**] Yuan Y, Chilian WM, Granger HJ, Zawieja DC. Permeability to albumin in isolated coronary venules. *Am J Physiol*. 1993;265(2 Pt 2):H543-52. DOI:10.1152/ajpheart.1993.265.2.H543

[**640**] Siflinger-Birnboim A, del Vecchio PJ, Cooper JA, Blumenstock FA, Shepard JM, Malik AB. Molecular sieving characteristics of the cultured endothelial monolayer. *J Cell Physiol*. 1987;132(1):111–7. DOI:10.1002/jcp.1041320115

[**641**] Sastry BVR. Techniques to study human placental transport. *Adv Drug Deliv Rev*. 1999;38(1):17–39. DOI:10.1016/S0169-409X(99)00004-6

[**642**] Elad D, Levkovitz R, Jaffa AJ, Desoye G, Hod M. Have We Neglected the Role of Fetal Endothelium in Transplacental Transport? *Traffic*. 2014;15(1):122–6. DOI:10.1111/tra.12130

[**643**] Miura S, Sato K, Kato-Negishi M, Teshima T, Takeuchi S. Fluid shear triggers microvilli formation via mechanosensitive activation of TRPV6. *Nat Commun*. 2015;6:8871. DOI:10.1038/ncomms9871

[**644**] Bogorad MI, DeStefano J, Karlsson J, Wong AD, Gerecht S, Searson PC. Review: In vitro microvessel models. *Lab Chip*. 2015;15(22):4242–55. DOI:10.1039/c5lc00832h

[**645**] Baker BM, Trappmann B, Stapleton SC, Toro E, Chen CS. Microfluidics embedded within extracellular matrix to define vascular architectures and pattern diffusive gradients. *Lab Chip*. 2013;13(16):3246–52. DOI:10.1039/c3lc50493j

[**646**] Kim S, Lee H, Chung M, Jeon NL. Engineering of functional, perfusable 3D microvascular networks on a chip. *Lab Chip*. 2013;13(8):1489–500. DOI:10.1039/c3lc41320a

[**647**] Chrobak KM, Potter DR, Tien J. Formation of perfused, functional microvascular tubes in vitro. *Microvasc Res*. 2006;71(3):185–96. DOI:10.1016/j.mvr.2006.02.005

[**648**] Wong KHK, Truslow JG, Tien J. The role of cyclic AMP in normalizing the function of engineered human blood microvessels in microfluidic collagen gels. *Biomaterials*. 2010;31(17):4706–14. DOI:10.1016/j.biomaterials.2010.02.041

[**649**] Schmidt A, Morales-Prieto DM, Pastuschek J, Fröhlich K, Markert UR. Only humans have human placentas: Molecular differences between mice and humans. *J Reprod Immunol*. 2015;108:65–71. DOI:10.1016/j.jri.2015.03.001

[**650**] Hougaard KS, Campagnolo L, Chavatte-Palmer P, Tarrade A, Rousseau-Ralliard D, Valentino S, et al. A perspective on the developmental toxicity of inhaled nanoparticles. *Reprod Toxicol*. 2015;56:118–40. DOI:10.1016/j.reprotox.2015.05.015

[**651**] Aengenheister L, Keevend K, Muoth C, Schönenberger R, Diener L, Wick P, et al. An advanced human in vitro co-culture model for translocation studies across the placental barrier. *Sci Rep*. 2018;8(1):1–12. DOI:10.1038/s41598-018-23410-6

[**652**] Hamilton RD, Leach L. Isolation and properties of an in vitro human outer blood-retinal barrier model. *Methods Mol Biol*. 2011;686:401–16. DOI:10.1007/978-1-60761-938-3_20

[**653**] Bazzoni G, Dejana E. Endothelial cell-to-cell junctions: Molecular organization and role in vascular homeostasis. *Physiol Rev*. 2004;84(3):869–901. DOI:10.1152/physrev.00035.2003

[**654**] Tsukita S, Furuse M. Occludin and claudins in tight-junction strands: Leading or supporting players? *Trends Cell Biol*. 1999;9(7):268–73. DOI:10.1016/S0962-8924(99)01578-0

[**655**] Lampugnani MG, Resnati M, Raiteri M, Pigott R, Pisacane A, Houen G, et al. A novel endothelial-specific membrane protein is a marker of cell-cell contacts. *J Cell Biol*. 1992;118(6):1511–22. DOI:10.1083/jcb.118.6.1511

[**656**] Caveda L, Martìn-Padura I, Navarro P, Breviario F, Corada M, Gulino D, et al. Inhibition of cultured cell growth by vascular endothelial cadherin (cadherin-5/VE-cadherin). *J Clin Invest*. 1996;98(4):886–93. DOI:10.1172/JCI118870

[**657**] Conacci-Sorrell M, Zhurinsky J, Ben-Ze'ev A. The cadherin-catenin adhesion system in signaling and cancer. *J Clin Invest*. 2002;109(8):987–91. DOI:10.1172/jci15429

[**658**] Vestweber D. VE-cadherin: The major endothelial adhesion molecule controlling cellular junctions and blood vessel formation. *Arterioscler Thromb Vasc Biol*. 2008;28(2):223–32. DOI:10.1161/ATVBAHA.107.158014

[**659**] Förster C. Tight junctions and the modulation of barrier function in disease. *Histochem Cell Biol*. 2008;130(1):55–70. DOI:10.1007/s00418-008-0424-9

[**660**] Schneeberger EE, Lynch RD. The tight junction: A multifunctional complex. *Am J Physiol - Cell Physiol*. 2004;286(6 55-6):C1213-28. DOI:10.1152/ajpcell.00558.2003

[**661**] Esser S, Lampugnani MG, Corada M, Dejana E, Risau W. Vascular endothelial growth factor induces VE-cadherin tyrosine phosphorylation in endothelial cells. *J Cell Sci* [Internet]. 1998 [cited 2020 Apr 17];111(Pt 13):1853–65. Available from: https://jcs.biologists.org/content/111/13/1853

[**662**] Groten T, Gebhard N, Kreienberg R, Schleussner E, Reister F, Huppertz B. Differential expression of VE-cadherin and VEGFR2 in placental syncytiotrophoblast during preeclampsia - New perspectives to explain the pathophysiology. *Placenta*. 2010 Apr;31(4):339–43. DOI:10.1016/j.placenta.2010.01.014

[**663**] Bulla R, Villa A, Bossi F, Cassetti A, Radillo O, Spessotto P, et al. VE-cadherin is a critical molecule for trophoblast-endothelial cell interaction in decidual spiral arteries. *Exp Cell Res*. 2005 Feb;303(1):101–13. DOI:10.1016/j.yexcr.2004.09.015

[**664**] Bain MD, Copas DK, Landon MJ, Stacey TE. In vivo permeability of the human

placenta to inulin and mannitol. *J Physiol* [Internet]. 1988 May;399:313–9. DOI:10.1113/jphysiol.1988.sp017082

[**665**] Bain MD, Copas DK, Taylor A, Landon MJ, Stacey TE. Permeability of the human placenta in vivo to four non-metabolized hydrophilic molecules. *J Physiol* [Internet]. 1990 Dec;431:505–13. DOI:10.1113/jphysiol.1990.sp018343

[**666**] Edwards D, Jones CJ, Sibley CP, Nelson DM. Paracellular permeability pathways in the human placenta: a quantitative and morphological study of maternal-fetal transfer of horseradish peroxidase. *Placenta*. 1993;14(1):63–73. DOI:10.1016/s0143-4004(05)80249-8

[**667**] Doughty IM, Glazier JD, Greenwood SL, Boyd RD, Sibley CP. Mechanisms of maternofetal chloride transfer across the human placenta perfused in vitro. *Am J Physiol*. 1996 Dec;271(6 Pt 2):R1701-6. DOI:10.1152/ajpregu.1996.271.6.R1701

[**668**] Stulc J, Stulcová B, Smíd M, Sach I. Parallel mechanisms of Ca++ transfer across the perfused human placental cotyledon. *Am J Obstet Gynecol*. 1994 Jan;170(1 Pt 1):162–7. DOI:10.1016/s0002-9378(94)70403-1

[**669**] Brownbill P, Edwards D, Jones C, Mahendran D, Owen D, Sibley C, et al. Mechanisms of alphafetoprotein transfer in the perfused human placental cotyledon from uncomplicated pregnancy. *J Clin Invest*. 1995 Nov;96(5):2220–6. DOI:10.1172/JCI118277

[**670**] Demir R, Kayisli UA, Cayli S, Huppertz B. Sequential Steps During Vasculogenesis and Angiogenesis in the Very Early Human Placenta. *Placenta*. 2006;27(6–7):535–9. DOI:10.1016/j.placenta.2005.05.011

[**671**] Dye JF, Leach L, Clark P, Firth JA. Cyclic AMP and acidic fibroblast growth factor have opposing effects on tight and adherens junctions in microvascular endothelial cells in vitro. *Microvasc Res*. 2001;62(2):94–113. DOI:10.1006/mvre.2001.2333

[**672**] Rutland CS, Latunde-Dada AO, Thorpe A, Plant R, Langley-Evans S, Leach L. Effect of Gestational Nutrition on Vascular Integrity in the Murine Placenta. *Placenta*. 2007;28(7):734–42. DOI:10.1016/j.placenta.2006.07.001

[**673**] Dvorak AM, Kohn S, Morgan ES, Fox P, Nagy JA, Dvorak HF. The vesiculo-vacuolar organelle (VVO): A distinct endothelial cell structure that provides a transcellular pathway for macromolecular extravasation. *J Leukoc Biol*. 1996;59(1):100–15. DOI:10.1002/jlb.59.1.100

[**674**] Feng D, Nagy JA, Hipp J, Dvorak HF, Dvorak AM. Vesiculo-vacuolar organelles and the regulation of venule permeability to macromolecules by vascular permeability factor, histamine, and serotonin. *J Exp Med*. 1996;183(5):1981–6. DOI:10.1084/jem.183.5.1981

[**675**] Michel CC, Curry FE. Microvascular permeability. *Physiol Rev*. 1999;79(3):703–61. DOI:10.1152/physrev.1999.79.3.703

[**676**] Stevens T, Garcia JGN, Shasby DM, Bhattacharya J, Malik AB. Mechanisms regulating endothelial cell barrier function. *Am J Physiol - Lung Cell Mol Physiol*. 2000;279(3 23-3). DOI:10.1152/ajplung.2000.279.3.l419

[**677**] Canham PB, Finlay HM, Dixon JG, Boughner DR, Chen A. Measurements from

light and polarised light microscopy of human coronary arteries fixed at distending pressure. *Cardiovasc Res*. 1989 Nov;23(11):973–82. DOI:10.1093/cvr/23.11.973

[**678**] Gasser TC, Ogden RW, Holzapfel GA. Hyperelastic modelling of arterial layers with distributed collagen fibre orientations. *J R Soc Interface*. 2006 Feb;3(6):15–35. DOI:10.1098/rsif.2005.0073

[**679**] Lilly B. We have contact: endothelial cell-smooth muscle cell interactions. *Physiology (Bethesda)*. 2014 Jul;29(4):234–41. DOI:10.1152/physiol.00047.2013

[**680**] Davis S, Aldrich TH, Jones PF, Acheson A, Compton DL, Jain V, et al. Isolation of angiopoietin-1, a ligand for the TIE2 receptor, by secretion-trap expression cloning. *Cell*. 1996 Dec;87(7):1161–9. DOI:10.1016/s0092-8674(00)81812-7

[**681**] Papapetropoulos A, García-Cardeña G, Dengler TJ, Maisonpierre PC, Yancopoulos GD, Sessa WC. Direct actions of angiopoietin-1 on human endothelium: evidence for network stabilization, cell survival, and interaction with other angiogenic growth factors. *Lab Invest*. 1999 Feb;79(2):213–23.

[**682**] Fukuhara S, Sako K, Noda K, Zhang J, Minami M, Mochizuki N. Angiopoietin-1/Tie2 receptor signaling in vascular quiescence and angiogenesis. *Histol Histopathol*. 2010 Mar;25(3):387–96. DOI:10.14670/HH-25.387

[**683**] Hellström M, Kalén M, Lindahl P, Abramsson A, Betsholtz C. Role of PDGF-B and PDGFR-beta in recruitment of vascular smooth muscle cells and pericytes during embryonic blood vessel formation in the mouse. *Development*. 1999 Jun;126(14):3047–55.

[**684**] Pepper MS. Transforming growth factor-beta: vasculogenesis, angiogenesis, and vessel wall integrity. *Cytokine Growth Factor Rev*. 1997 Mar;8(1):21–43. DOI:10.1016/s1359-6101(96)00048-2

[**685**] Liu Y, Wada R, Yamashita T, Mi Y, Deng CX, Hobson JP, et al. Edg-1, the G protein-coupled receptor for sphingosine-1-phosphate, is essential for vascular maturation. *J Clin Invest*. 2000 Oct;106(8):951–61. DOI:10.1172/JCI10905

[**686**] Hoeben A, Landuyt B, Highley MS, Wildiers H, Van Oosterom AT, De Bruijn EA. Vascular endothelial growth factor and angiogenesis. *Pharmacol Rev*. 2004 Dec;56(4):549–80. DOI:10.1124/pr.56.4.3

[**687**] Desoye G, Mouzon SH. The Human Placenta in Gestational Diabetes Mellitus. *Diabetes Care*. 2007;30(Supplement 2):S120–6. DOI:10.2337/DC07-S203

[**688**] Mathiesen L, Mose T, Mørck TJ, Nielsen JKS, Nielsen LK, Maroun LL, et al. Quality assessment of a placental perfusion protocol. *Reprod Toxicol*. 2010;30(1):138–46. DOI:10.1016/j.reprotox.2010.01.006

[**689**] Myllynen P, Vähäkangas K. Placental transfer and metabolism: an overview of the experimental models utilizing human placental tissue. *Toxicol In Vitro*. 2013;27(1):507–12. DOI:10.1016/j.tiv.2012.08.027

[**690**] Haggarty P. Fatty Acid Supply to the Human Fetus. *Annu Rev Nutr*. 2010;30(1):237–55. DOI:10.1146/annurev.nutr.012809.104742

[**691**] Lager S, Powell TL. Regulation of nutrient transport across the placenta. *J Pregnancy*. 2012;2012:179827. DOI:10.1155/2012/179827

[**692**] Levkovitz R, Zaretsky U, Gordon Z, Jaffa AJ, Elad D. In vitro simulation of placental transport: Part I. Biological model of the placental barrier. *Placenta*. 2013;34(8):699–707. DOI:10.1016/j.placenta.2013.03.014

[**693**] Battaglia FC. Placental transport: a function of permeability and perfusion. *Am J Clin Nutr*. 2007;85(2):591S-597S. DOI:10.1093/ajcn/85.2.591S

[**694**] Wong MK, Li EW, Adam M, Selvaganapathy PR, Raha S. Establishment of an in vitro placental barrier model cultured under physiologically relevant oxygen levels. *Mol Hum Reprod*. 2020;26(5):353–65. DOI:10.1093/molehr/gaaa018

[**695**] Huang X, Lüthi M, Ontsouka EC, Kallol S, Baumann MU, Surbek D V., et al. Establishment of a confluent monolayer model with human primary trophoblast cells. *Mol Hum Reprod*. 2016;22(6):442–56. DOI:10.1093/molehr/gaw018

[**696**] Lee JS, Romero R, Han YM, Kim HC, Kim CJ, Hong JS, et al. Placenta-on-A-chip: A novel platform to study the biology of the human placenta. *J Matern Neonatal Med*. 2016;29(7):1046–54. DOI:10.3109/14767058.2015.1038518

[**697**] Ma SH, Lepak LA, Hussain RJ, Shain W, Shuler ML. An endothelial and astrocyte co-culture model of the blood-brain barrier utilizing an ultra-thin, nanofabricated silicon nitride membrane. *Lab Chip*. 2005;5(1):74–85. DOI:10.1039/b405713a

[**698**] Dai NT, Yeh MK, Liu DD, Adams EF, Chiang CH, Yen CY, et al. A co-cultured skin model based on cell support membranes. *Biochem Biophys Res Commun*. 2005;329(3):905–8. DOI:10.1016/j.bbrc.2005.02.059

[**699**] Hermanns MI, Unger RE, Kehe K, Peters K, Kirkpatrick CJ. Lung epithelial cell lines in coculture with human pulmonary microvascular endothelial cells: Development of an alveolo-capillary barrier in vitro. *Lab Investig*. 2004;84(6):736–52. DOI:10.1038/labinvest.3700081

[**700**] Gimbrone MA, Cotran RS. Human vascular smooth muscle in culture. Growth and ultrastructure. *Lab Invest* [Internet]. 1975;33(1):16—27. Available from: https://pubmed.ncbi.nlm.nih.gov/167231/

[**701**] Björkerud S. Agglomeration to nodules modulates human arterial smooth muscle cells to distinct postinjury phenotype via foam cell transition. *Am J Pathol* [Internet]. 1987 [cited 2020 May 2];127(3):485–98. Available from: https://www.ncbi.nlm.nih.gov/pmc/articles/PMC1899762/

[**702**] Bjorkerud S, Bjorkerud B, Joelsson M. Structural organization of reconstituted human arterial smooth muscle tissue. *Arterioscler Thromb*. 1994;14(4):644–51. DOI:10.1161/01.atv.14.4.644

[**703**] Proudfoot D, Skepper JN, Shanahan CM, Weissberg PL. Calcification of human vascular cells in vitro is correlated with high levels of matrix Gla protein and low levels of osteopontin expression. *Arterioscler Thromb Vasc Biol*. 1998;18(3):379–88. DOI:10.1161/01.ATV.18.3.379

[**704**] Cvitic S, Desoye G, Hiden U. Glucose, insulin, and oxygen interplay in placental hypervascularisation in diabetes mellitus. *Biomed Res Int*. 2014;2014:145846. DOI:10.1155/2014/145846

[**705**] Nelson SM, Coan PM, Burton GJ, Lindsay RS. Placental structure in type 1 diabetes: relation to fetal insulin, leptin, and IGF-I. *Diabetes*. 2009

Nov;58(11):2634–41. DOI:10.2337/db09-0739

[**706**] Mayhew TM, Sørensen FB, Klebe JG, Jackson MR. Growth and maturation of villi in placentae from well-controlled diabetic women. *Placenta*. 1994 Jan;15(1):57–65. DOI:10.1016/s0143-4004(05)80236-x

[**707**] Jirkovská M, Kubínová L, Janácek J, Moravcová M, Krejcí V, Karen P. Topological properties and spatial organization of villous capillaries in normal and diabetic placentas. *J Vasc Res*. 2002;39(3):268–78. DOI:10.1159/000063692

[**708**] Teasdale F. Histomorphometry of the human placenta in class C diabetes mellitus. *Placenta*. 1985;6(1):69–81. DOI:10.1016/S0143-4004(85)80034-5

[**709**] Jirkovská M, Kučera T, Kaláb J, Jadrníček M, Niedobová V, Janáček J, et al. The branching pattern of villous capillaries and structural changes of placental terminal villi in type 1 diabetes mellitus. *Placenta*. 2012 May;33(5):343–51. DOI:10.1016/j.placenta.2012.01.014

[**710**] Pu L, Meng M, Wu J, Zhang J, Hou Z, Gao H, et al. Compared to the amniotic membrane, Wharton's jelly may be a more suitable source of mesenchymal stem cells for cardiovascular tissue engineering and clinical regeneration. *Stem Cell Res Ther* [Internet]. 2017 Mar 21 [cited 2021 Feb 13];8(1):72. DOI:10.1186/s13287-017-0501-x

[**711**] Esposito M, Lucariello A, Costanzo C, Fiumarella A, Giannini A, Riccardi G, et al. Differentiation of Human Umbilical Cord-derived Mesenchymal Stem Cells, WJ-MSCs, into Chondrogenic Cells in the Presence of Pulsed Electromagnetic Fields. *In Vivo*. 2013 Jul 1;27:495–500.

[**712**] Baba K, Yamazaki Y, Ikemoto S, Aoyagi K, Takeda A, Uchinuma E. Osteogenic potential of human umbilical cord-derived mesenchymal stromal cells cultured with umbilical cord blood-derived autoserum. *J Cranio-Maxillofacial Surg*. 2012 Dec 1;40(8):768–72. DOI:10.1016/j.jcms.2012.02.006

[**713**] Hsieh JY, Fu YS, Chang SJ, Tsuang YH, Wang HW. Functional module analysis reveals differential osteogenic and stemness potentials in human mesenchymal stem cells from bone marrow and Wharton's Jelly of umbilical cord. *Stem Cells Dev* [Internet]. 2010 Dec 1 [cited 2021 Feb 13];19(12):1895–910. DOI:10.1089/scd.2009.0485

[**714**] Wang H-S, Hung S-C, Peng S-T, Huang C-C, Wei H-M, Guo Y-J, et al. Mesenchymal Stem Cells in the Wharton's Jelly of the Human Umbilical Cord. *Stem Cells* [Internet]. 2004 Dec [cited 2021 Feb 13];22(7):1330–7. DOI:10.1634/stemcells.2004-0013

[**715**] Chen MY, Lie PC, Li ZL, Wei X. Endothelial differentiation of Wharton's jelly-derived mesenchymal stem cells in comparison with bone marrow-derived mesenchymal stem cells. *Exp Hematol* [Internet]. 2009 May [cited 2021 Feb 13];37(5):629–40. DOI:10.1016/j.exphem.2009.02.003

[**716**] Hunsucker SA, Mitchell BS, Spychala J. The 5'-nucleotidases as regulators of nucleotide and drug metabolism. *Pharmacol Ther*. 2005 Jul;107(1):1–30. DOI:10.1016/j.pharmthera.2005.01.003

[**717**] Maksimow M, Kyhälä L, Nieminen A, Kylänpää L, Aalto K, Elima K, et al. Early prediction of persistent organ failure by soluble CD73 in patients with acute

pancreatitis*. *Crit Care Med*. 2014 Dec;42(12):2556–64. DOI:10.1097/CCM.0000000000000550

[**718**] Williams AF, Gagnon J. Neuronal cell Thy-1 glycoprotein: homology with immunoglobulin. *Science*. 1982 May;216(4547):696–703. DOI:10.1126/science.6177036

[**719**] Blair A, Hogge DE, Ailles LE, Lansdorp PM, Sutherland HJ. Lack of expression of Thy-1 (CD90) on acute myeloid leukemia cells with long-term proliferative ability in vitro and in vivo. *Blood*. 1997 May;89(9):3104–12.

[**720**] Rege TA, Hagood JS. Thy-1 as a regulator of cell-cell and cell-matrix interactions in axon regeneration, apoptosis, adhesion, migration, cancer, and fibrosis. *FASEB J Off Publ Fed Am Soc Exp Biol*. 2006 Jun;20(8):1045–54. DOI:10.1096/fj.05-5460rev

[**721**] Barboni E, Gormley AM, Pliego Rivero FB, Vidal M, Morris RJ. Activation of T lymphocytes by cross-linking of glycophospholipid-anchored Thy-1 mobilizes separate pools of intracellular second messengers to those induced by the antigen-receptor/CD3 complex. *Immunology*. 1991 Apr;72(4):457–63.

[**722**] Saalbach A, Aneregg U, Bruns M, Schnabel E, Herrmann K, Haustein UF. Novel fibroblast-specific monoclonal antibodies: properties and specificities. *J Invest Dermatol*. 1996 Jun;106(6):1314–9. DOI:10.1111/1523-1747.ep12349035

[**723**] Fries KM, Blieden T, Looney RJ, Sempowski GD, Silvera MR, Willis RA, et al. Evidence of fibroblast heterogeneity and the role of fibroblast subpopulations in fibrosis. *Clin Immunol Immunopathol*. 1994 Sep;72(3):283–92. DOI:10.1006/clin.1994.1144

[**724**] Hagood JS, Prabhakaran P, Kumbla P, Salazar L, MacEwen MW, Barker TH, et al. Loss of fibroblast Thy-1 expression correlates with lung fibrogenesis. *Am J Pathol*. 2005 Aug;167(2):365–79. DOI:10.1016/S0002-9440(10)62982-3

[**725**] Barker TH, Grenett HE, MacEwen MW, Tilden SG, Fuller GM, Settleman J, et al. Thy-1 regulates fibroblast focal adhesions, cytoskeletal organization and migration through modulation of p190 RhoGAP and Rho GTPase activity. *Exp Cell Res*. 2004 May;295(2):488–96. DOI:10.1016/j.yexcr.2004.01.026

[**726**] Gougos A, Letarte M. Identification of a human endothelial cell antigen with monoclonal antibody 44G4 produced against a pre-B leukemic cell line. *J Immunol*. 1988 Sep;141(6):1925–33.

[**727**] Fonsatti E, Sigalotti L, Arslan P, Altomonte M, Maio M. Emerging role of endoglin (CD105) as a marker of angiogenesis with clinical potential in human malignancies. *Curr Cancer Drug Targets*. 2003 Dec;3(6):427–32. DOI:10.2174/1568009033481741

[**728**] Burrows FJ, Derbyshire EJ, Tazzari PL, Amlot P, Gazdar AF, King SW, et al. Up-regulation of endoglin on vascular endothelial cells in human solid tumors: implications for diagnosis and therapy. *Clin cancer Res an Off J Am Assoc Cancer Res*. 1995 Dec;1(12):1623–34.

[**729**] Wang JM, Kumar S, Pye D, van Agthoven AJ, Krupinski J, Hunter RD. A monoclonal antibody detects heterogeneity in vascular endothelium of tumours and normal tissues. *Int J cancer*. 1993 May;54(3):363–70. DOI:10.1002/ijc.2910540303

[**730**] Ali H, Al-Yatama MK, Abu-Farha M, Behbehani K, Al Madhoun A. Multi-lineage differentiation of human umbilical cord Wharton's Jelly Mesenchymal Stromal Cells mediates changes in the expression profile of stemness markers. *PLoS One* [Internet]. 2015 Apr 7;10(4):e0122465–e0122465. DOI:10.1371/journal.pone.0122465

[**731**] Gu W, Hong X, Le Bras A, Nowak WN, Issa Bhaloo S, Deng J, et al. Smooth muscle cells differentiated from mesenchymal stem cells are regulated by microRNAs and suitable for vascular tissue grafts. *J Biol Chem* [Internet]. 2018/04/11. 2018 May 25;293(21):8089–102. DOI:10.1074/jbc.RA118.001739

[**732**] Wiesmann A, Bühring H-J, Mentrup C, Wiesmann H-P. Decreased CD90 expression in human mesenchymal stem cells by applying mechanical stimulation. *Head Face Med* [Internet]. 2006 Mar 31;2:8. DOI:10.1186/1746-160X-2-8

[**733**] Moraes DA, Sibov TT, Pavon LF, Alvim PQ, Bonadio RS, Da Silva JR, et al. A reduction in CD90 (THY-1) expression results in increased differentiation of mesenchymal stromal cells. *Stem Cell Res Ther* [Internet]. 2016;7(1):97. DOI:10.1186/s13287-016-0359-3

[**734**] Owens GK. Molecular control of vascular smooth muscle cell differentiation and phenotypic plasticity. *Novartis Found Symp*. 2007;283:173-174,238-241. DOI:10.1002/9780470319413.ch14

[**735**] Yoshida T, Kaestner KH, Owens GK. Conditional deletion of Krüppel-like factor 4 delays downregulation of smooth muscle cell differentiation markers but accelerates neointimal formation following vascular injury. *Circ Res*. 2008 Jun;102(12):1548–57. DOI:10.1161/CIRCRESAHA.108.176974

[**736**] Bala K, Ambwani K, Gohil NK. Effect of different mitogens and serum concentration on HUVEC morphology and characteristics: Implication on use of higher passage cells. *Tissue Cell*. 2011;43(4):216–22. DOI:10.1016/j.tice.2011.03.004

[**737**] Jiménez N, Krouwer VJD, Post JA. A new, rapid and reproducible method to obtain high quality endothelium in vitro. *Cytotechnology*. 2013;65(1):1–14. DOI:10.1007/s10616-012-9459-9

[**738**] Bagley RG, Walter-Yohrling J, Cao X, Weber W, Simons B, Cook BP, et al. Endothelial precursor cells as a model of tumor endothelium: Characterization and comparison with mature endothelial cells. *Cancer Res*. 2003;63(18):5866–73.

[**739**] Wallace CS, Champion JC, Truskey GA. Adhesion and function of human endothelial cells co-cultured on smooth muscle cells. *Ann Biomed Eng*. 2007;35(3):375–86. DOI:10.1007/s10439-006-9230-5

[**740**] Chiu JJ, Chen LJ, Chen CN, Lee PL, Lee CI. A model for studying the effect of shear stress on interactions between vascular endothelial cells and smooth muscle cells. *J Biomech*. 2004;37(4):531–9. DOI:10.1016/j.jbiomech.2003.08.012

[**741**] Chiu JJ, Chen LJ, Chang SF, Lee PL, Lee CI, Tsai MC, et al. Shear stress inhibits smooth muscle cell-induced inflammatory gene expression in endothelial cells: Role of NF-κB. *Arterioscler Thromb Vasc Biol*.

2005;25(5):963–9. DOI:10.1161/01.ATV.0000159703.43374.19

[**742**] Evensen L, Micklem DR, Blois A, Berge SV, Aarsaether N, Littlewood-Evans A, et al. Mural cell associated VEGF is required for organotypic vessel formation. *PLoS One*. 2009;4(6). DOI:10.1371/journal.pone.0005798

[**743**] Chiu JJ, Chen LJ, Lee PL, Lee CI, Lo LW, Usami S, et al. Shear stress inhibits adhesion molecule expression in vascular endothelial cells induced by coculture with smooth muscle cells. *Blood*. 2003;101(7):2667–74. DOI:10.1182/blood-2002-08-2560

[**744**] Rainger GE, Stone P, Morland CM, Nash GB. A novel system for investigating the ability of smooth muscle cells and fibroblasts to regulate adhesion of flowing leukocytes to endothelial cells. *J Immunol Methods*. 2001;255(1–2):73–82. DOI:10.1016/S0022-1759(01)00427-6

[**745**] Fillinger MF, Sampson LN, Cronenwett JL, Powell RJ, Wagner RJ. Coculture of endothelial cells and smooth muscle cells in bilayer and conditioned media models. *J Surg Res*. 1997;67(2):169–78. DOI:10.1006/jsre.1996.4978

[**746**] Nackman GB, Bech FR, Fillinger MF, Wagner RJ, Cronenwett JL. Endothelial cells modulate smooth muscle cell morphology by inhibition of transforming growth factor-beta1 activation. *Surgery*. 1996;120(2):418–26. DOI:10.1016/S0039-6060(96)80318-7

[**747**] van Buul-Wortelboer MF, Brinkman HJM, Dingemans KP, De Groot PG, van Aken WG, van Mourik JA. Reconstitution of the vascular wall in vitro. A novel model to study interactions between endothelial and smooth muscle cells. *Exp Cell Res*. 1986;162(1):151–8. DOI:10.1016/0014-4827(86)90433-7

[**748**] Ziegler T, Alexander RW, Nerem RM. An endothelial cell-smooth muscle cell co-culture model for use in the investigation of flow effects on vascular biology. *Ann Biomed Eng*. 1995;23(3):216–25. DOI:10.1007/BF02584424

[**749**] Davies PF, Truskey GA, Warren HB, O'Connor SE, Eisenhaure BH. Metabolic cooperation between vascular endothelial cells and smooth muscle cells in co-culture: Changes in low density lipoprotein metabolism. *J Cell Biol*. 1985;101(3):871–9. DOI:10.1083/jcb.101.3.871

[**750**] KORFF T, KIMMINA S, MARTINY-BARON G, AUGUSTIN HG. Blood vessel maturation in a 3-dimensional spheroidal coculture model: direct contact with smooth muscle cells regulates endothelial cell quiescence and abrogates VEGF responsiveness. *FASEB J*. 2001;15(2):447–57. DOI:10.1096/fj.00-0139com

[**751**] Niwa K, Kado T, Sakai J, Karino T. The effects of a shear flow on the uptake of LDL and acetylated LDL by an EC monoculture and an EC-SMC coculture. *Ann Biomed Eng*. 2004;32(4):537–43. DOI:10.1023/B:ABME.0000019173.79939.54

[**752**] Wada Y, Sugiyama A, Kohro T, Kobayashi M, Takeya M, Naito M, et al. In vitro Model of Atherosclerosis Using Coculture of Arterial Wall Cells and Macrophage. Vol. 41, Yonsei Medical Journal. 2000. p. 740–55. DOI:10.3349/ymj.2000.41.6.740

[**753**] Hirschi KK, Rohovsky SA, D'Amore PA. PDGF, TGF-β, and heterotypic cell-cell interactions mediate endothelial cell-induced recruitment of 10T1/2 cells and their differentiation to a smooth muscle fate. *J Cell Biol*. 1998;141(3):805–14. DOI:10.1083/jcb.141.3.805

[**754**] Powell RJ, Bhargava J, Basson MD, Sumpio BE. Coculture conditions alter endothelial modulation of TGF-β1 activation and smooth muscle growth morphology. *Am J Physiol - Hear Circ Physiol*. 1998;274(2 43-2). DOI:10.1152/ajpheart.1998.274.2.h642

[**755**] Zhang JC, Ruan QR, Paucz L, Fabry A, Binder BR, Wojta J. Stimulation of tissue factor expression in human microvascular and macrovascular endothelial cells by cultured vascular smooth muscle cells in vitro. *J Vasc Res*. 1999;36(2):126–32. DOI:10.1159/000025635

[**756**] Leach L, Eaton BM, Firth JA, Contractor SF. Immunocytochemical and labelled tracer approaches to uptake and intracellular routing of immunoglobulin-G (IgG) in the human placenta. *Histochem J*. 1991 Oct;23(10):444–9. DOI:10.1007/BF01041374

[**757**] Bloxam DL, Bullen BE. Condition and performance of the perfused human placental cotyledon. *Am J Obstet Gynecol* [Internet]. 1986;155(2):382–8. DOI:https://doi.org/10.1016/0002-9378(86)90835-5

[**758**] Leach L, Firth JA. Fine structure of the paracellular junctions of terminal villous capillaries in the perfused human placenta. *Cell Tissue Res*. 1992;268(3):447–52. DOI:10.1007/bf00319151

[**759**] Truskey GA. Endothelial vascular smooth muscle cell coculture assay for high throughput screening assays to identify antiangiogenic and other therapeutic molecules. *Int J High Throughput Screen*. 2010;2010(1):171. DOI:10.2147/ijhts.s13459

[**760**] Evensen L, Micklem DR, Blois A, Berge SV, Aarsaether N, Littlewood-Evans A, et al. Mural cell associated VEGF is required for organotypic vessel formation. *PLoS One*. 2009;4(6). DOI:10.1371/journal.pone.0005798

[**761**] Knipp GT, Audus KL, Soares MJ. Nutrient transport across the placenta. *Adv Drug Deliv Rev*. 1999 Jun;38(1):41–58. DOI:10.1016/s0169-409x(99)00005-8

[**762**] Ala-Kokko TI, Myllynen P, Vähäkangas K. Ex vivo perfusion of the human placental cotyledon: implications for anesthetic pharmacology. *Int J Obstet Anesth* [Internet]. 2000;9(1):26–38. DOI:https://doi.org/10.1054/ijoa.1999.0312

[**763**] Wada Y, Sugiyama A, Kohro T, Kobayashi M, Takeya M, Naito M, et al. In vitro Model of Atherosclerosis Using Coculture of Arterial Wall Cells and Macrophage. *Yonsei Med J*. 2000;41(6):740–55. DOI:10.3349/ymj.2000.41.6.740

[**764**] Cartwright L, Poulsen MS, Nielsen HM, Pojana G, Knudsen LE, Saunders M, et al. In vitro placental model optimization for nanoparticle transport studies. *Int J Nanomedicine*. 2012;7:497–510. DOI:10.2147/IJN.S26601

[**765**] van Meer BJ, de Vries H, Firth KSA, van Weerd J, Tertoolen LGJ, Karperien HBJ, et al. Small molecule absorption by PDMS in the context of drug response bioassays. *Biochem Biophys Res Commun*. 2017;482(2):323–8. DOI:10.1016/j.bbrc.2016.11.062

[**766**] Toepke MW, Beebe DJ. PDMS absorption of small molecules and consequences in microfluidic applications. Vol. 6, Lab on a Chip. Royal Society of Chemistry; 2006. p. 1484–6. DOI:10.1039/b612140c

[**767**] Wang JD, Douville NJ, Takayama S, Elsayed M. Quantitative analysis of molecular absorption into PDMS microfluidic channels. *Ann Biomed Eng*. 2012;40(9):1862–73. DOI:10.1007/s10439-012-0562-z

[**768**] Wylam ME, Samsel RW, Schumacker PT, Umans JG. Extracellular calcium and intrinsic tone in the human umbilical artery. *J Pharmacol Exp Ther* [Internet]. 1993 Sep [cited 2019 Aug 26];266(3):1475–81. Available from: http://www.ncbi.nlm.nih.gov/pubmed/8371151

[**769**] McCarthy AL, Woolfson RG, Raju SK, Poston L. Abnormal endothelial cell function of resistance arteries from women with preeclampsia. *Am J Obs Gynecol* [Internet]. 1993/04/01. 1993;168(4):1323–30. Available from: https://www.ajog.org/article/0002-9378(93)90389-Z/pdf

[**770**] Zhang Y, Zhang Y, Li H, Jia X, Zhang X, Xia Y, et al. Increased expression of P2X7 receptor in peripheral blood mononuclear cells correlates with clinical severity and serum levels of Th17-related cytokines in patients with myasthenia gravis. *Clin Neurol Neurosurg* [Internet]. 2017;157:88–94. DOI:https://doi.org/10.1016/j.clineuro.2017.04.012

APPENDICES

APPENDIX 1: Patient Information Sheet

University of Nottingham
UK | CHINA | MALAYSIA

Derby Teaching Hospitals NHS
NHS Foundation Trust

Patient Information Sheet (V5.0; 08/06/18)

Studies of human pregnancy and preterm birth

You are being invited to take part in a research study of the University of Nottingham being carried out in Derby. Before you decide it is important for you to understand why the research is being done and what it will involve. Please take time to read the following information carefully. Talk to others about the study if you wish.

1. What is the purpose of the study?
The switch from pregnancy to labour and how the uterus contracts for delivery is not understood. In some cases, labour may begin too early when the baby is not ready to be born (preterm). Preterm birth is delivery occurring before 37 completed weeks of pregnancy and affects about 8% of all pregnancies in the UK. Preterm labour is a factor in approximately 40% of all preterm deliveries. Two other pregnancy-specific disorders preeclampsia (high blood pressure with protein in the urine) and intrauterine growth restriction (IUGR), where babies are born small for their size, may also lead to preterm birth To date, there are still no effective drugs to treat preterm birth due to preterm labour nor any reliable markers that allow these disorders to be monitored throughout pregnancy.

Here at the Royal Derby Hospital, we are carrying out research into term and preterm birth with the aim of improving our understanding of the causes of preterm birth. We hope that new information from our studies will pave the way for the future development of new drugs and new ways designed to reduce the incidence of preterm delivery. The three projects we are involved with are as follows:
Project 1: Inflammation in pregnancy: The uterus produces many important proteins which play a role in pregnancy and labour. It is thought that infection or inflammation of the female reproductive tract may activate the process of labour too early by causing uterine contractions through molecules produced by the placenta and cord blood.
Project 2: Lipid-protein interactions in the pregnant human uterus. In recent years, there has been great interest in how certain fats affect pregnancy. We are studying how these fats (also known as lipids) present in the uterus (womb) influence labour. In addition, we know that the location of these lipids within cells may also indirectly activate pathways that control the production of proteins in the uterus
Project 3: Vascular problems in pregnancy: During pregnancy, blood flow to the baby provides food and oxygen essential to baby's growth and development. In some 10% of cases, poor blood flow to the placenta (afterbirth) may mean that the baby does not develop or grow properly, a condition known as intra-uterine growth restriction, (IUGR). In addition, 1-2% of pregnancies result in preeclampsia, a leading cause of high blood pressure in pregnancy, which may endanger both mother's and baby's health if left undiagnosed. The aim of our project is to study the properties of the blood vessels in the uterus and placentae of women with preeclampsia or a growth-restricted pregnancy to identify whether blood vessel function is changed in these disorders compared with vessels of women with a normal pregnancy.

2. Why have you been invited? We are recruiting patients from four different groups. You have been chosen as somebody who falls into one of the four following groups: (a) normal non-labouring, term pregnancy (b) labouring pregnancy, or you have been diagnosed with (c) a growth-restricted pregnancy, (d) preeclampsia. The 'normal pregnancy' group is a control group and including patients from this group will allow us to compare normal versus potentially difficult pregnancies. The groups will be divided further into term or preterm. We are recruiting patients for all three projects and it is likely that your tissue and cord blood samples will be used for any one of these 3 projects. We aim to recruit 2650 women for this study. There will be no direct benefit to you from this study but your participation may significantly aid our understanding of pregnancy and birth thus enabling us to make advances in the field of female and fetal health.

3. Do I have to take part? No. It is up to you to decide whether or not to take part. If you do, you will be given this information sheet to keep and be asked to sign a consent form.
You are still free to withdraw at any time and without giving a reason. A decision to withdraw at any time, or a decision not to take part, will not affect the standard of care you receive. Any stored tissue samples that can still be identified as yours will be destroyed if you wish.

4. What will happen to me if I take part? Should you decide to take part, if you will be undergoing a caesarean section, you may be asked to provide a myometrial (uterine muscle) biopsy which will be taken at caesarean section from the site of the operation. The biopsy is ~2g in weight and the size of a thumb tip. We will also ask you if we can take your placenta for research. We may also take from the placenta after delivery. In the case of a normal delivery, we will ask you to consider providing a placental and cord blood sample only after your baby has been delivered. Cord blood samples collected will not be available for any clinical needs such as subsequent treatment of your baby or

RNK-V5/MUPPPS 08/06/18

other investigations. All samples will be taken after delivery of the baby. There is no further follow-up in relation to our study. This investigation is laboratory-based therefore samples will be taken to the lab and analysed using a variety of experimental techniques.
We would also wish to store any unused tissue and blood samples obtained from you for future unspecified research. Samples will only be used for studies approved by a research ethics committee. If however, you change your mind later about having your tissues stored for future research, then you can withdraw at any time without providing a reason. This should be done by contacting the Chief Investigator (contact details at bottom of this sheet).

5. **What are the other possible disadvantages and risks of taking part?** There is minimal risk from taking the muscle biopsy over and above that associated with the caesarean section. Taking the sample at caesarean section will not harm your baby, nor prolong the operation and will not affect the normal healing of your uterus. Nor will there be any effect on the structure or function of your uterus afterwards, your future fertility or any risk to baby as the biopsy will be taken after delivery of your baby. If it is felt by the clinician in charge of your care that taking a muscle biopsy is not appropriate, the sample will not be taken. Your wellbeing and that of your baby is paramount. There is no risk to you or your baby from the use of placental samples.

6. **What are the possible benefits of taking part?** There is no direct benefit to you or your baby in taking part in this study. However the information obtained from using your muscle biopsy and placenta may enable us to identify possible new pathways that will improve our understanding of uterine function

7. **What happens when the research study stops?** The data collected will be analyzed and prepared for scientific publication. We would hope to expand the study to understand more about the functions of the human uterus in normal and abnormal conditions. Participants will not be identified in any report, presentation or publication.

8. **Will my taking part in the study be kept confidential?** We will follow ethical and legal practice and all information about you will be handled in confidence. If you join the study, we will use information collected from you and your medical records during the course of the research. This information will be kept **strictly confidential**, stored in a secure and locked office, and on a password protected database at the University of Nottingham. Under UK Data Protection laws the University is the Data Controller (legally responsible for the data security) and the Chief Investigator of this study (named above) is the Data Custodian (manages access to the data). This means we are responsible for looking after your information and using it properly. Your rights to access, change or move your information are limited as we need to manage your information in specific ways to comply with certain laws and for the research to be reliable and accurate. To safeguard your rights we will use the minimum personally – identifiable information possible. You can find out more about how we use your information and to read our privacy notice at: https://www.nottingham.ac.uk/utilities/privacy.aspx.
The data collected for the study will be looked at and stored by authorised persons from the University of Nottingham who are organising the research. They may also be looked at by authorised people from regulatory organisations to check that the study is being carried out correctly. All will have a duty of confidentiality to you as a research participant and we will do our best to meet this duty.
Where possible information about you which leaves the Royal Derby Hospital site will have your name and address removed and a unique code will be used so that you cannot be recognised from it. However sometimes we need to ensure that we can recognise you to link the research data with your medical records so in these instances we will need to know your name and date of birth.

9. **Who is organising and funding the research?** This study is being funded through various sources including the Biotechnology and Biological Sciences Research Council, the British Heart Foundation and the University of Nottingham. The research is sponsored by the University of Nottingham.

10. **Who has reviewed the study?** All research in the NHS is looked at by independent group of people, called a Research Ethics Committee, to protect your interests. This study has been reviewed and given favourable opinion by Derbyshire Research Ethics Committee.

Complaints: If you have a concern about any aspect of this study, you should ask to speak with the researchers who will do their best to answer your questions (Professor Raheela Khan 01332 724664; raheela.khan@nottingham.ac.uk). If you remain unhappy and wish to complain formally, you can do this through the NHS Complaints Procedure or PALs. Details can be obtained from the Royal Derby Hospital.

Contact for Further Information:
Professor Raheela N Khan 01332 724664; bleep 1208; email: raheela.khan@nottingham.ac.uk.
For more information on the research of the group: http:\\www.nottingham.ac.uk/mhs/gem/research/og.php

Thank you for taking the time to read this and for taking part in this study.

RNK-V5/MUPPPS 08/06/18

The University of Nottingham
UNITED KINGDOM · CHINA · MALAYSIA

Nottingham University Hospitals NHS
NHS Trust

Participant Information Sheet
Final version 5.0: 01 Oct.15

Title of Study: Laboratory studies of structure and function of the placenta after birth

Name of Researcher(s): Dr Lopa Leach

We would like to invite you to take part in our research study. Before you decide we would like you to understand why the research is being done and what it would involve for you. One of our team will go through the information sheet with you and answer any questions you have. Talk to others about the study if you wish. Ask us if there is anything that is not clear.

Purpose of study
We are asking for your permission to carry out studies of your placenta (afterbirth) with attached membranes and cord after your delivery.

Normally, once the baby has been delivered and the umbilical cord clamped and cut, the placenta and attached membranes and cord are thrown away. Instead we want to carry out detailed studies in the laboratory into whether the blood vessels present in normal placenta is similar to that seen in placenta from diabetic or pre-eclamptic pregnancies. Both diabetes and pre-eclampsia are diseases that can affect the baby throughout pregnancy.

If the placenta, which separates the mothers blood from the babies is different in structure and permeability from normal placenta then we can start planning strategies which can help alleviate the problem.

Over the next five years we wish to look at placenta from normal, diabetic and pre-eclamptic pregnancies after the baby has been delivered.

In the laboratory we will study the endothelial cells lining the blood vessels in the placenta by using a perfusion model which allows us to perfuse blood vessels in the placenta and by taking out the cells and growing them in culture. Specifically we will look at molecules which help endothelial cells stick together, regulate how leaky the vessels are and which help new blood vessels grow. Any differences in the behaviour of these molecules in the three study groups will help us understand how/why things can go wrong.

The study has the approval of the Nottingham 2 Ethics Committee (OG010101).

Why have I been chosen?
Since all the work is done in the laboratory, and we need time to make all the solutions, we are taking placentae and umbilical cord from Elective Caesarean Sections only. We can then plan to do experiments immediately after the section. Your consultant, and your notes, has advised/informed us that your afterbirth is suitable for our study.

Do I have to agree?
No. It is up to you to decide whether you agree that we may study your discarded placenta and umbilical cord. If you do decide to agree you will be given this information sheet to keep and be asked to sign a consent form. If you decide to agree you are still free to withdraw at any time and without giving a reason. This will not affect the standard of care you receive.

As stated before we want to take away your afterbirth, which is normally thrown away, to the laboratory to perform these studies. After the laboratory analyses, the tissue and endothelial cells will be destroyed.

What will happen to me if I take part?
We do not want you to do anything different from what you are doing now. This is a laboratory study, using your afterbirth. There are no side effects for you or your baby. There are no risks involved for you or your baby.

What are the possible benefits of agreeing?
There are no intended clinical benefits to you from taking part in this trial.

Will my participation be kept confidential?
All information which is collected about you during the course of the research will be kept strictly confidential. Any information about you which leaves the hospital/surgery will have your name and address removed so that you cannot be recognised from it.

What will happen to the results of this research study?
Results from this study will be published in scientific journals and presented in scientific conferences and may form part of a students PhD. However, as stated before you will not be identified in any report/publication.

Who is organising and funding the research?
This is research led by Dr L Leach. Dr Leach is an Associate Professor of Vascular Biology, School of Life Sciences, Faculty of Medicine, University of Nottingham. We have full permission of the clinical director Professor Jim Thornton, Division of Obstetrics and Gynaecology, to retrieve the placenta and cord from the labour ward and theatre at QMC and City Hospital. The project is being funded by the University of Nottingham and the British Heart Foundation.

Who has reviewed the study?
All research in the NHS is looked at by independent group of people, called a Research Ethics Committee, to protect your interests. This study has been reviewed and given favourable opinion by Nottingham 2 Research Ethics Committee Ref. OG010101.

Contact for further information:

Dr L Leach, School of Life Sciences, E Floor Medical School, Queens Medical Centre, Nottingham NG7 2UH. Tel 0115 823 0175; Fax 0115 823 0142. Email lopa.leach@nottingham.ac.uk.

Professor Jim Thornton, Professor of Obstetrics and Gynaecology. Division of Obstetrics and Gynaecology, Maternity Department, City Hospital, Hucknall Road, Nottingham. NG5 1PB. Tel +44 (0)115 82 31889. Fax +44 (0)115 82 31908. email: jim.thornton@nottingham.ac.uk
www.igreens.org.uk

Thank you very much in anticipation for your permission.

Patient must be given a copy of the information sheet and a signed consent form to keep. A copy of signed consent should be placed in the clinical notes.

Appendix 2: Consent form: Pregnancy

University of Nottingham
UK | CHINA | MALAYSIA

Derby Teaching Hospitals NHS
NHS Foundation Trust

CONSENT FORM: Pregnancy
(Version 5MUPPS – 06/2018)

Title of Study: Studies of human pregnancy and preterm birth

REC ref: 09/H0401/90

Name of Researcher: Professor Raheela Khan

Name of Participant: _____ **Please initial box**

1. I confirm that I have read and understand the information sheet version number 5 dated 06/2018 for the above study and have had the opportunity to ask questions. ☐

2. I understand that my participation is voluntary and that I am free to withdraw at any time, without giving any reason, and without my medical care or legal rights being affected. I understand that should I withdraw then the information collected so far cannot be erased and that this information may still be used in the project analysis. ☐

3. I understand that relevant sections of my medical notes and data collected in the study may be looked at by authorised individuals from the University of Nottingham, the research group and regulatory authorities where it is relevant to my taking part in this study. I give permission for these individuals to have access to these records and to collect, store, analyse and publish information obtained from my participation in this study. I understand that my personal details will be kept confidential. ☐

4. I understand and agree to a myometrial ☐ placental ☐ and cord blood sample to be taken for research investigations. ☐

5. I agree to the storage of uterine, placental and cord blood samples for any future, as yet, unspecified research studies relating to the study of pregnancy and pregnancy related disorders. ☐
NB: Cord blood samples collected will not be available for any clinical needs such as subsequent treatment of your baby or other investigations.

6. I agree to take part in the above study. ☐

Name of Participant	Date	Signature
Name of Person taking consent (if different from Principal Investigator)	Date	Signature
Name of Principal Investigator	Date	Signature

3 copies: 1 for participant, 1 for the project notes and 1 for the medical notes

RNKV5 PTB Consent Form

The University of Nottingham
UNITED KINGDOM · CHINA · MALAYSIA

Nottingham University Hospitals NHS
NHS Trust

(Form to be printed on local headed paper)

CONSENT FORM
(Final version 4.0: 01 Oct.15)

Title of Study: Laboratory studies of structure and function of the placenta after birth

REC ref: OG010101

Name of Researcher: Dr Lopa Leach

Name of Participant:

Please initial box

1. I confirm that I have read and understand the information sheet version number 5.0 dated 01 Oct. 15 for the above study and have had the opportunity to ask questions. ☐
2. I understand that my participation is voluntary and that I am free to withdraw at any time, without giving any reason, and without my medical care or legal rights being affected. I understand that should I withdraw then the information collected so far cannot be erased and that this information may still be used in the project analysis. ☐
3. I understand that relevant sections of my medical notes and data collected in the study may be looked at by authorised individuals from the University of Nottingham, the research group and regulatory authorities where it is relevant to my taking part in this study. I give permission for these individuals to have access to these records and to collect, store, analyse and publish information obtained from my participation in this study. I understand that my personal details will be kept confidential. ☐
4. I understand and agree that the placenta and umbilical cord will be taken for laboratory analyses of the blood vessels and growth of cells lining the vessels. ☐
5. I agree to take part in the above study. ☐

Name of Participant	Date	Signature
Name of Person taking consent	Date	Signature

3 copies: 1 for participant, 1 for the project notes and 1 for the medical notes

Appendix 3: Case report form (CRF)

Case Report Form (CRF)

Study ID:

Date:

Gestational age: ..... weeks + ... days

Parity: ..... Pre PET

Pre DM

Gravida: .....

Booking Ht

Wt

BMI

Smoking:

Medication: Yes ☐ No ☐

If yes, Aspirin ☐ Clexane ☐ Metformin ☐ Insulin ☐

Others .....

Complications:

PET ☐

DM ☐

Retinopathy ☐

Nephropathy ☐

Essential hypertension ☐

Birth weight:

Gender of the baby:

Gestation:

HC (Centile):

Appendix 4: Details of the research study – poster format

Structure and Function of the term placenta and cord in normal pregnancies and those complicated by Pre-eclampsia, GDM & Diabetes & Type 1 Diabetes.

University of Nottingham
UK | CHINA | MALAYSIA

What are we doing?

We are carrying out detailed studies in the laboratory on whether the blood vessels present in normal placenta function similar to those in placenta from pregnancies complicated by pre-eclampsia, gestational diabetes (GDM) or type 1 diabetic (T1DM) pregnancies.

What do we need?

We need freshly delivered placenta with attached membranes and long cord (clamped) from Elective Caesarean Sections only. We need to take the tissue away as quickly as possible to the lab to start our cannulation and perfusion of vessels and isolation of cells to ensure that the tissue/cells are viable and retain physiological function. We will have consented the mother and her designated midwife will also be informed that consent has occurred. We have ethical approval and funding for these research projects (British Heart Foundation, BBSRC, Anatomical Society, University of Nottingham).

How can you, the invaluable theatre staff, help?

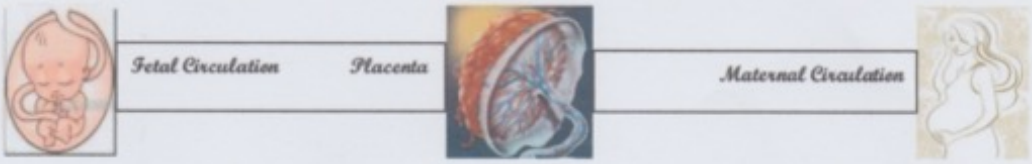
Please call us (numbers below) as soon as the placenta is delivered or when surgeons start the procedure. We will come down and wait. We can check the placenta or wait until the midwives have done so. We need minimum blood loss from the placenta circuit (thus cord needs to be left clamped, and we need placenta from Sections).

Research outcomes

The research so far has revealed valuable data on differences in permeability, angiogenesis, vascular maturity and re-modelling, vascular tone, nutrient transfer. This is paving the way for new therapeutic approaches and your help is always acknowledged in our papers. We are very grateful for the ease and timeliness of placenta retrieval you provide.

Please call any one of us below:

Shukla Rani Das	07466963562
Samar Salem	07383183825
Maria Haig	07412344793
Professor (Assoc) Lopa Leach	01158230175 (Team Leader).



Appendix 5: Solution compositions

4% (w/v) paraformaldehyde

4g PFA dissolved in distilled water at 60^0C, pH 7.4.

DMEM

500mL tissue culture medium supplemented with 10% (v/v) heat inactivated fetal bovine serum, 100 units/mL penicillin and 100µg/mL streptomycin

HBSS

500mL HBSS supplemented with 5mL of 1M HEPES and 5mL of penicillin and streptomycin (100X)

Homogenisation buffer for tissue

Sucrose (300mM), Tris base (25mM), ethylenediaminetetraacetic acid (EDTA) (1mM), monothioglycerol (10mM), tween 20 (0.1%), 1/500 protease inhibitors and 1/100 phosphatase inhibitors (Sigma-Aldrich, Poole, UK) at a pH of 7.4

Homogenisation buffer for primary cells

Sucrose (320mM), Tris base (10mM), KCl (50mM), EDTA (1mM), Igepal (0.5%), 1/500 protease inhibitors and 1/100 phosphatase inhibitors, pH 7.8

Immunoprecipitation buffer

Tris base (50mM), NaCl (150mM), EDTA (1mM), ethylene glycol tetraacetic acid (EGTA) (0.2mM) SDS (0.1%), Sodium Deoxycholate (0.3%), 1/500 protease inhibitors and 1/100 phosphatase inhibitors, pH 7.5

Physiological salt solution

119mM NaCl, 4.69mM KCl, 2.4mM $MgSO_4$, 25mM $NaHCO_3$, 1.17mM KH_2PO_4, 6.05mM D-Glucose, 3.2mM $CaCl_2$, pH 7.4

60mM High Potassium physiological salt solution

63.7mM NaCl, 60mM KCl, 2.4mM $MgSO_4$, 25mM $NaHCO_3$, 1.17mM KH_2PO_4, 6.05mM D-Glucose, 3.2mM $CaCl_2$, pH 7.4

123mM High Potassium physiological salt solution

123.69mM KCl, 2.4mM $MgSO_4$, 25mM $NaHCO_3$, 1.17mM KH_2PO_4, 6.05mM D-Glucose, 3.2mM $CaCl_2$, pH 7.4

1% (w/v) gelatin

5g gelatin in 500mL distilled water

1% (w/v) collagenase type II

1g collagenase type II in 10mL Medium 199 supplemented with 100U/mL penicillin and 100µg/mL streptomycin to obtain a 10% (w/v) collagenase type II, aliquoted into 10x1mL Eppendorf tubes and frozen at -20^{0}C prior to use. When required, 1x1mL collagenase type II Eppendorf tube was defrosted and added to 9 mL of warm Medium 199 supplemented with 100U/mL penicillin and 100µg/mL streptomycin to obtain a 1% (w/v) collagenase type II solution

10% Ammonium Persulfate (AP)

0.1g Ammonium persulfate in 1mL distilled water

Laemmli buffer

50µL β-Mercaptoethanol in 950µL sample loading buffer (BioRad, 161-0747)

Appendix 6: Demographic and clinical information worksheet

Placenta sample number	Type of patient and treatment	Maternal age (years)	Gestational weeks	BMI	Ethnicity	Parity	Gravida	Neonatal birth weight (kg)	Sex of offspring	Head circumference (cm)	Placenta weight (g)	Individual Birthweight Centile
N10072019	Healthy	37	39weeks+2days		Romanian		2	3.38	Female	33.5	689	70.11
N12072019B	Healthy	26	37weeks	31		0	1		Female		660	
N15072019	Healthy											
N18072019	Healthy		39weeks+3days	20.1	British	1	2	3.675	Female	35.5		87.89
N12082019	Healthy											
N21082019	Healthy	35	39weeks+3days	37	White British	1	3	3.775	Female			91.79
N17092019	Healthy		39 weeks+4days		White	0	1		Female			
N18092019	Healthy	34			Bangladesh	1	2		Female			
N15102019	Healthy	33	39weeks+1day		White British	0	1	3.28	Male	36		51.92
N11112019a	Healthy	37	39weeks	22	White British	1	1	3.465	Male	36	575	70.73
N11112019b	Healthy		41weeks+1day	26	White British	1	3	3.37	Male	37	582	34.29
N05122019	Healthy	42	39weeks	19	British	0	1	3.43	Female	35	507	77.16
N16012020	Healthy	27	39weeks+2days	45	White British	1	3	3.71	Female	35	554	90.19
N23012020	Healthy	26	39weeks+4days	26		0	1	3.88	Male	39	740	90.17
N27012020A	Healthy	36	39weeks+1day	27				3.68	Male	37.5	458	83.88
N27012020B	Healthy	25						3.065	Male		578	
N04022020	Healthy	38	39weeks+5days	24	Pakistani	1	3	3.35	Male	35	592	50.56
N06022020	Healthy	31	39weeks	28	White British	1	3		Female		616	
N19022020	Healthy	36	39weeks+5days	32	White British	0	1	3.73	Female	35	505	88.61
N20022020	Healthy	33	39weeks	18.55		2	3	3.55	Female	36	749	84.71
N05032020	Healthy	35	39weeks+3days	25	White British	1	3	3.61	Male	35	473	76.85
GDM-12082019-Diet	GDM on diet	41	37weeks+1day	32	Pakistani	2	6	1.805	Male	32	508	0.4
GDM-16092019-Diet	GDM on diet	21	39weeks+5days	32.5	White British	0	1	4.195	Female	39.5	909	98.52
GDM-02122019-Diet	GDM on diet	22		43	Turkish	0	1				446	
GDM-10122019-Diet	GDM on diet	38	39weeks+1days	36	Pakistani	2	3	4.755	Male		661	99.87
GDM-09012020-Diet	GDM on diet	39	39weeks+2days	25	Indian	1	3	3.43	Female	36		74.14
GDM-14022020-Diet	GDM on diet	31	37weeks+2days	16	Indian	1	2	2.34	Male	32	369	6.31
GDM-20022020-Diet	GDM on diet	46	38weeks	25		2	4	3.445	Female	34	646	87.41
GDM-26072019-Insulin, Metformin	GDM on insulin and metformin		39weeks	34	Ukrainian	1	2	3.74	Female	35	674	92.64
GDM-03022020-Insulin, Metformin	GDM on insulin and metformin	32	38 weeks+2days	35		0	1	3.98	Male	38	740	97.7
GDM-28102019-Metformin	GDM on metformin	31	39weeks+1day	24	White British	1	3	3.92	Female	35	737	96.31
GDM-05122019-Metformin	GDM on metformin	36	39weeks	28	Pakistani	1	4	2.25	Male	30	405	0.81
GDM-16012020-Diet+Metformin	GDM on metformin	40	39weeks+4days	29	Nigerian	2	3	3.285	Male	35	584	46.13
T1D23102019	T1D on insulin	32	36weeks+6days	47	White British	1	2	4.21	Male	37		99.72

T3012	Healthy	Maternal Age 34 years, G2, P1, 39weeks+3days, Male Fetus, 3510g
T3023	Healthy	Maternal Age 26 years, G2, P1, 39weeks, Female fetus, 3690g
T3024	Healthy	Maternal Age 29 years, P0
T3027	Healthy	Maternal Age 34 years, G3, P2, 37weeks+1day, Male Fetus, 4080g
T2878	Healthy	Maternal Age 28 years, P1
T2879	Healthy	Maternal Age 40 years
T2880	Healthy	Maternal Age 44, P0, G2, 39weeks + 3 days Male fetus, 4180g
T2881	Healthy	Maternal Age 28 years, G3, P2, 39weeks+2days, Male fetus, 3430g
T2884	Healthy	Maternal Age 40 years, G4, P2, 36 weeks, Male fetus, 2920g, placenta Previa
T2885	Healthy	Maternal Age 29 years, G4, P2, 38weeks+3days, Male fetus, 4100g
T2886	Healthy	Maternal Age 38 years, G2, P1, 39weeks+1day, Female fetus, 2910g, Breech
T2887	Healthy	Maternal Age 27 years, G3, P1, 38weeks+3days, Female fetus, 3250g, Breech
T2888	Healthy	Maternal Age 38 years, G2, P1, 39weeks+2days, Female fetus, 4150g
T2889	Healthy	Maternal Age 30 years, 37weeks+6days, Increased BMI, Male Fetus, 3960g
T2890	Healthy	Maternal Age 21 years, G2, P1, 39weeks, Male fetus, 3530g
T2891	Healthy	Maternal Age 33 years, G1, P0, 39weeks+2days, Male fetus, 3350g
T2892	Healthy	Maternal Age 17 years, G1, P0, 39weeks+1day, Group B Streptococcus on HVS, Female fetus, 3130g
T2893	Healthy	Maternal Age 29 years, G2, P1, 39weeks+2days, Male fetus, 3630g
T2959	Healthy	Maternal Age 32 years, G1, P0, Male Fetus, 3510g, Placenta Previa
T2960	Healthy	Maternal Age 30 years, G1, P0, Female Fetus, 3580g
T2956	Healthy	Maternal Age 36 years, G4, P2, 39 weeks, Male Fetus, 4000g
T2957	Healthy	Maternal Age 32 years, P1, Male fetus, 4200g, Low Pregnancy assosiated plasma protein A
T3025	Healthy	Maternal Age 27 years, G1, P0, 38 weeks+2 Days, Obstetric cholestasis, Male Fetus, 3690g
T3026	Healthy	Maternal Age 29 years, G2, P1, 39 weeks + 3 days, Male fetus, 4340g
T3027	Healthy	Maternal Age 34 years, G3, P1, 37weeks + 1 day, Male Fetus, 4080g
MB220	Healthy	Maternal Age 31 years, G1, P0, 36weeks+3 days, Female Fetus, 2930g
MB227	Healthy	Maternal Age 24 years, G1, P0, 36 weeks, Male fetus, 2700g
T738	Preeclamptic	Maternal Age 24 years, 34weeks+6 days, P1, Breech

T829	Healthy	Maternal Age 31 years, G2, P1, 39weeks+3 days, Female fetus
T840	Healthy	Maternal Age 29 years
T853	Preeclamptic	Maternal Age 30 years, G3, P1, 33weeks+1 day, BMI 37, Blood pressure 186/91, Proteinuria +++, Blurry vision, Swollen face, previous preeclamptic caesarean section
T860	Preeclamptic	Maternal Age 36 years, Blood Pressure 140/100, Protein +, Labetalol, Nifedipine, 38weeks+4 days, uncomplicated blood test
T910	Healthy	Maternal age 28 years, G2, P1, 39weeks, BMI 35
T927	Healthy	Maternal age 22 years, G2, P1
T928	Healthy	Maternal Age 36 years, G2, P1, Breech
T952	Healthy	Maternal Age 29 years, G4, P3, 39 weeks, BMI 24, breech
T962	Healthy	Maternal Age 29, G2, P1, 39weeks + 1 day, Breech
T994	Preeclamptic	Maternal Age 25 years, 34weeks+6 days, IUGR, blood pressure 141/90, Proteinuria 2+, Increased alanine transaminase, decreased platelets
T997	Preeclamptic	Maternal Age 29 years, G1, P0, 34 weeks+4day, Blood pressure 141/91, Occasional Headache, Proteinuria 2+, leg edema, no epigastric pain, no visual disturbance, uncomplicated blood test
T1145	Preeclamptic	Maternal age 33 years, 36 weeks, G1, P0, BMI 41, blood pressure 142/88, Proteinuria 2+, Visual disturbance, Epigastric pain, labetolol, nifedipine
T1269	Preeclamptic	Maternal Age 34 years, 34 weeks+6days, P2, IUGR, Proteinuria 3+, Blood pressure 136/84, mild edema, decreased platelets
T1469	Healthy	Maternal Age 39 years, G4, P1, 39weeks
T1609	Preeclamptic	Maternal Age 24 years, Proteinuria ++
T1964	Healthy	Maternal Age 38 years
T1992	Healthy	Maternal Age 27 years, P2
T2025	Healthy	Maternal Age 25 years, G2, P1, 39weeks
T2041	Healthy	Maternal Age 37 years
T2087	Healthy	Maternal Age 37 years, G4, P3, 39 weeks, Female Fetus, 2590g
T2817	Healthy	Maternal Age 33 years, G7, P2, 39weeks+2days, BMI 38, Male Fetus, 39weeks+2days
T2818	Healthy	Maternal Age 39 years, G4, P3, 38weeks+1day, Male 2760g
T2823	Healthy	Maternal Age 34 years, G4, P1, 36 weeks+4 days, oligohydramnios, Female fetus, 2240g
T2895	Healthy	Maternal Age 33 years, G2, P1, 39weeks+1day, Male Fetus, 3660g
T2929	Healthy	Maternal Age 20 years, G2, P1, 39weeks+2days, Male Fetus, 3690g
T2930	Healthy	Maternal Age 39 years, G2, P1, 39weeks+1day, Female Fetus, 3930g
T2942	Healthy	Maternal Age 31 years, G3, P1, 39 weeks, Male fetus, 3120g
T2944	Healthy	Maternal Age 32 years, G2, P1, 39weeks+6days
T2945	Healthy	Maternal Age 26 years, G2, P1, 39weeks+6days, Male Fetus, 3300g

T2946	Healthy	Maternal Age 36 years, G2, P3, 39weeks+2 days, Female Fetus, 2810g
T2970	Healthy	Maternal Age 28 years, G6, P1, 39weeks, Male fetus, 3410g
T2971	Healthy	Maternal Age 35 years, G2, P1, 39 weeks, Male fetus, 3300g
T2972	Healthy	Maternal Age 28 years, P4, G5, Male Fetus, 4050g
T2979	GDM-Metformin	Maternal Age 30 years, G3, P1, 39 weeks+1day, Male Fetus, 4210g
T2614	Healthy	Maternal Age 21 years, G3, P1, 38weeks, DCDA Tweens, Breech, Male fetus, 2720g, Male fetus 3190
T2615	Healthy	Maternal Age 29 years, G2, P1, 39weeks+3 days, Female Fetus, 3860g
T2616	Healthy	Maternal Age 33 years, G3, P2, 39weeks+3 days, Female fetus, 2920g
T2662	Healthy	Maternal Age 34 years, G2, P1, 39weeks+1day, Female Fetus, 4130g
T2665	Healthy	Maternal Age 27 years, G7, P6, 37weeks+4days, Male fetus, 3150g
T2788	Healthy	Maternal Age 28 years, G3, P2, 39weeks, Female Fetus, 4040g
T2789	Healthy	Maternal Age 26 years, G2, P1, 40weeks+2days, Male fetus, 4540g
T2650	Healthy	Maternal Age 27 years, G2, P0, 37 weeks, DCDA tweens, Male fetus, 2550g, Male fetus, 3000g
T2651	Healthy	Maternal Age 30 years, G2, P1, 40weeks+2days, Male fetus, 3460g
T2654	Healthy	Maternal Age 34 years, G1, P0, 39weeks+4days, Female Fetus, 3310g
T2655	Healthy	Maternal Age 31 years, G3, P1, 38weeks+3days, Male fetus, 3610g
T2995	GDM-Metformin	Maternal Age 36 years, G2, P1, 39weeks+2days, Female Fetus 3400g
T2648	Healthy	Maternal Age 30 years, G2, P1, 39weeks, Female fetus, 2109g
T2649	Healthy	Maternal Age 33 years, G2, P1, 39weeks, Male fetus, 4320g
T2810	Healthy	Maternal Age 34 years, G2, P1, 40 weeks, Female Fetus, 3990g
T2813	Healthy	Maternal Age 22 yaers, P1
T2812	Healthy	Maternal Age 34 years, G2, P1, 40 weeks, Male Fetus, 3630g
T2814	Healthy	Maternal Age 34 years, G3, P2, 39weeks+5days, Female fetus, 3960g
T2894	IUGR	Maternal Age 37 years, G3, P2, 38weeks, Female Fetus, 2940g
T2831	Healthy	Maternal Age 28 years, G2, P3, 39weeks+5days, Female Fetus, 3110g
T2837	Healthy	Maternal Age 49 years, G3, P0, 38weeks, Male fetus, 3040g
T2841	Healthy	Maternal Age 37 years, G2, P1, 39weeks+5days, Female fetus, 4110g
T2843	GDM-Metformin	Maternal Age 37 years, G1, P0, 39weeks+2days, Female fetus, 3520g

T2846	Healthy	Maternal Age 25 years, G1, P0, 39weeks+2days, Female fetus, 3830g
T2857	Healthy	Maternal Age 32 years, G5, P4, 38weeks+1day, Female Fetus, 2790g
T2856	Healthy	Maternal Age 34 years, G2, P0, 38weeks, oligohydramnios, breech, Male fetus, 2620g
T2855	Healthy	Maternal Age 22 years, G1, P0, Breech, 39weeks, Male Fetus, 2790g
T2858	Healthy	Maternal Age 36 years, G3, P2, 37weeks+5days, Female fetus, 3180g
T2861	GDM-Insulin	Maternal Age 38 years, G3, P1, polyhydramnios, BMI 45, 36 weeks
T2824	GDM-Insulin	Maternal Age 35 years, G7, P1, 39 weeks, Female Fetus, 3690g
T2828	Healthy	Maternal Age 24 years, G3, P2, 39 weeks, Female fetus, 3950g
T2826	Healthy	Maternal Age 32 years, G2, P1, 39weeks, Male fetus, 3950g
T2827	Healthy	Maternal Age 32 years, G1, P0, Breech, 39 weeks, Male fetus, 3090g
T2809	Healthy	Maternal Age 36 years, G2, P1, 40 weeks, Female Fetus, 3990g
T2815	IUGR	Maternal Age 27 years, G2, P0, Breech, 37weeks+1day, oligohydramnios, Male fetus, 2470g
T2825	Healthy	Maternal Age 35 years, G3, P2, 39weeks, Male Fetus, 3000g
T2863	Healthy	Maternal Age 34 years, G3, P2, 39weeks+4days, Female Fetus, 3390g
T2865	Healthy	Maternal Age 29 years, G3, P2, 39weeks+3days, female fetus, 3390g
T2866	Healthy	Maternal Age 33 years, G3, P2, 39weeks+3days, Male fetus, 3260g
T2872	Healthy	Maternal Age 43 years, G5, P4, 38weeks+4days, Male fetus, 2770g
T2873	Healthy	Maternal Age 32 years, G9, P3, Male fetus, 3980g
T2859	Healthy	Maternal Age 35 years, G2, P1, 39 weeks, female fetus, 3740g
T2860	Healthy	Maternal Age 35 years, G2, P1, 39weeks+1day, Female Fetus, 2240g
T2862	GDM	Maternal Age 33 years, G3, P2, 39weeks+2days, Male fetus, 3490g
T2874	Healthy	Maternal Age 35 years, G5, P2, 37weeks, Male Fetus, 3070g
T2875	Healthy	Maternal Age 31 years, G2, P1, 39weeks+5days, Male fetus, 4100g
T2775	Healthy	Maternal Age 35 years, G2, P1, 39weeks+1day, Female fetus, 3880g
T2697	Healthy	Maternal Age 21 years, G2, P1, 37 years, Tweens DCDA, Female Fetus 2240g, Male Fetus, 2630g
T2770	GDM-Metformin	Maternal Age 30 years, G4, P1, 38weeks+1day, Proteinuria ++, hyperthyroid, Female Fetus, 2880g

T2716	Haelthy	Maternal Age 34 years, G2, P1, 39weeks+2days, Male Fetus, 4900g
T2768	Healthy	Maternal Age 36 years, G5, P1, 39 weeks, Male Fetus, 3960g
T2771	GDM	Maternal Age 32 years, G4, P1, 39weeks+5days, Male Fetus, 4000g
T2776	Healthy	Maternal Age 28 years, G5, P3, 39weeks, Female fetus, 3280g, BMI32
T2778	GDM-Metformin	Maternal Age 34 years, G3, P1, 39weeks+2days, female Fetus, 4110g
T2780	Type 2 GDM	Maternal Age 34 years, G12, P2, 37weeks+1day, Female Fetus, 2660g
T2769	Healthy	Maternal Age 39 years, G3, P1, 39weeks+1day, Male fetus, 3230g
T2805	GDM-Metformin	Maternal Age 35 years, G2, P1, 39weeks+2days, Male fetus, 3420g
T2806	Healthy	Maternal Age 29 years, G2, P0, BMI20, 39weeks+1day, Male fetus, 4170g
T2686	IUGR	Maternal Age 40 years, oligohydramnios, 37weeks+2days
T2718	Preeclamptic	Maternal Age 35 years, P0, Proteinuria ++, 39weeks+1day, Male fetus, 3950g

Appendix 7: Handcasting polyacrylamide gels

Resolving gel (10%)

4.1mL Distilled water, 3.3mL 30% Acrylamide, 2.5mL resolving gel buffer (Tris Base pH 8.8), 100µL 10% SDS, 100µL ammonium persulfate, 4µL TEMED

Resolving gel (15%)

3.53mL Distilled water, 7.5mL 30% Acrylamide, 3.75mL resolving gel buffer (Tris Base pH 8.8), 150µL 10% SDS, 75µL ammonium persulfate, 7.5µL TEMED

Resolving gel (7%)

5.1mL Distilled water, 2.33mL 30% Acrylamide, 2.5mL resolving gel buffer (Tris Base pH 8.8), 100µL 10% SDS, 100µL ammonium persulfate, 4µL TEMED

Stacking gel (4%)

3.4mL Distilled water, 0.85mL 30% Acrylamide, 0.625mL resolving gel buffer (Tris Base pH 6.8), 50µL 10% SDS, 50µL ammonium persulfate, 5µL TEMED

Electrophoresis buffer

1.51g Tris, 94g Glycine, 50mL 10% SDS dissolved in 1L distilled water

Transfer buffer

24mM Tris base, 80mM glycine, 20% methanol

Tris Buffered Saline (TBS)

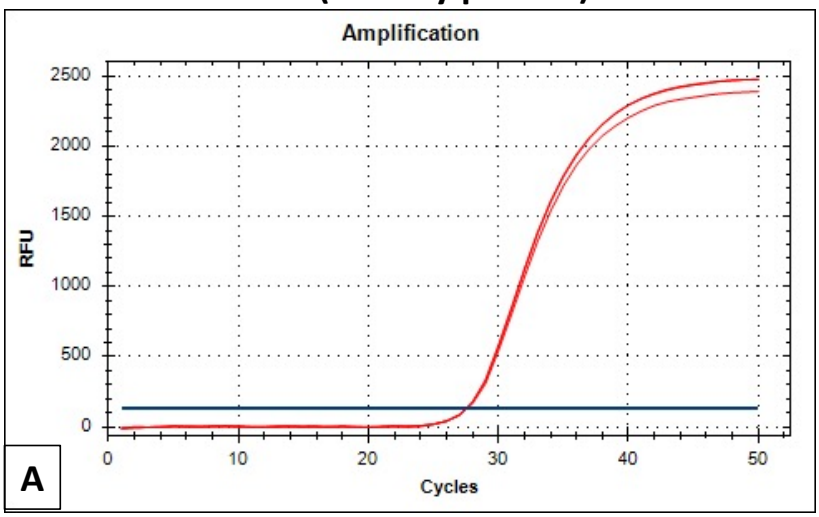
12.11g Tris base, 146.1g NaCl dissolved in 5L distilled water, pH 7.4

TBS-Tween (TBS-T) 0.1% (v/v)

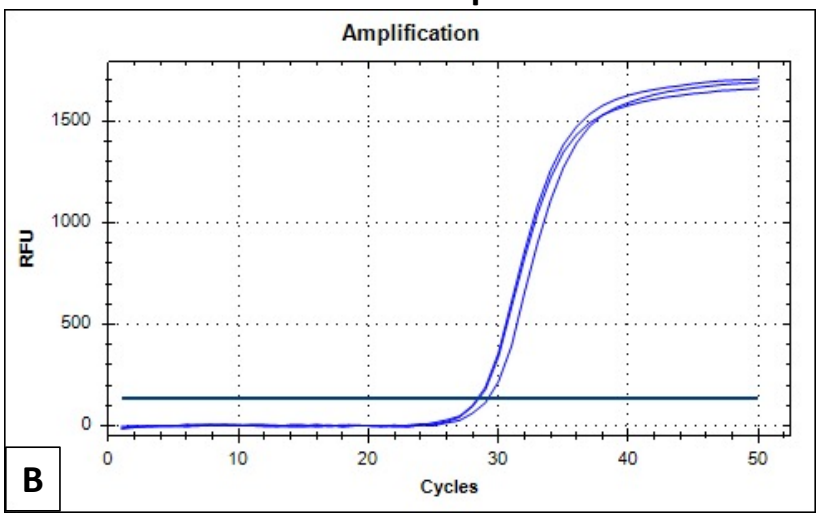
1L TBS, 1mL Tween-20

Appendix 8: RT-qPCR amplification plots

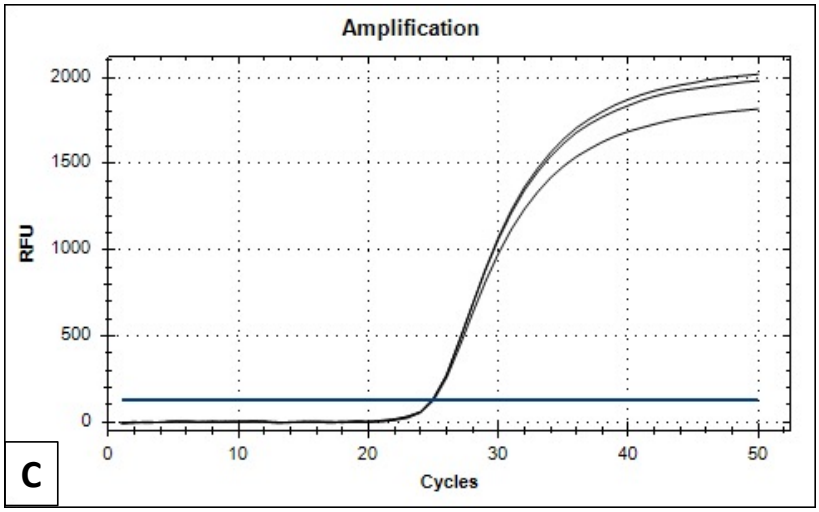
T910 (healthy patient)



P2RX7 Receptor



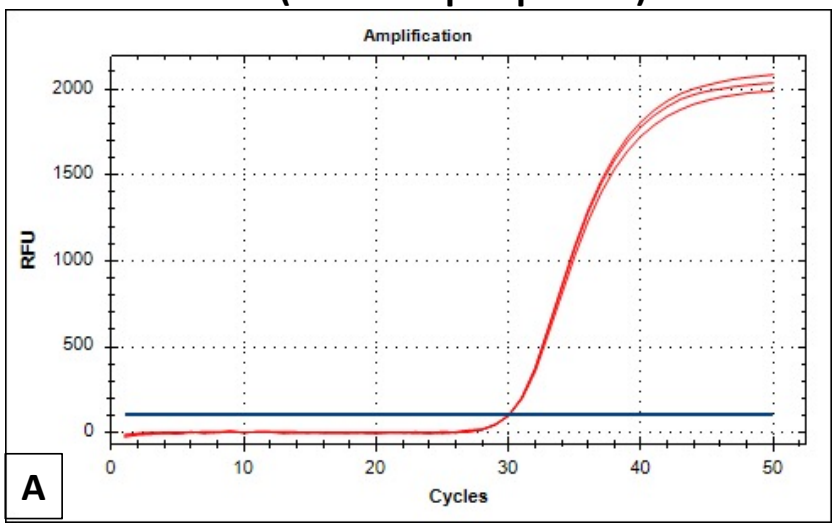
NLRP3 inflammasome



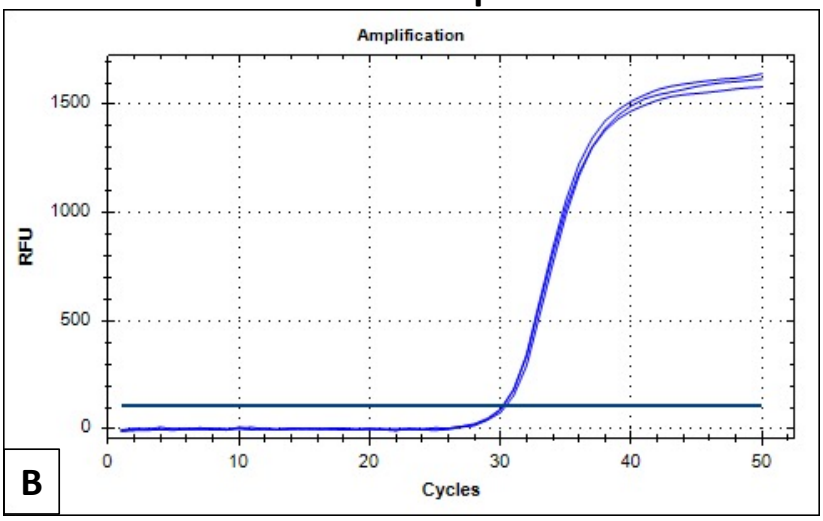
Caspase-1

Figure I. *This figure (**A-C**) shows the amplification plot of real time polymerase chain reaction data.*

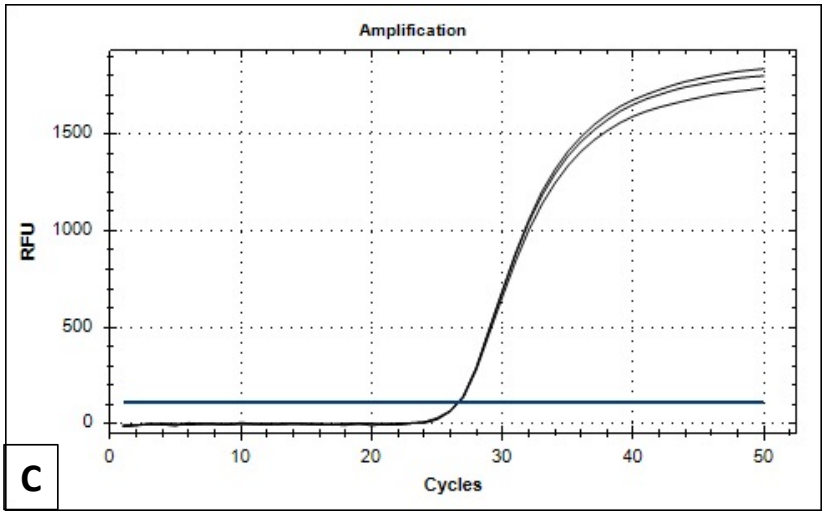
T738 (Preeclamptic patient)



P2RX7 Receptor



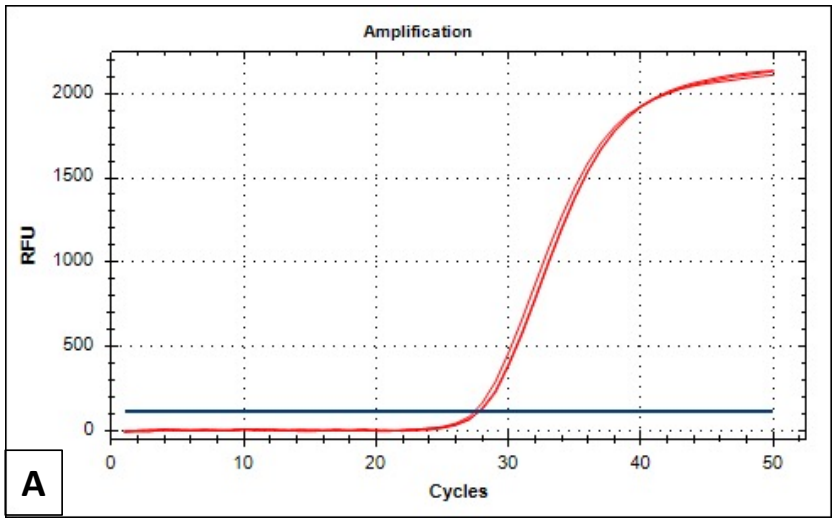
NLRP3 inflammasome



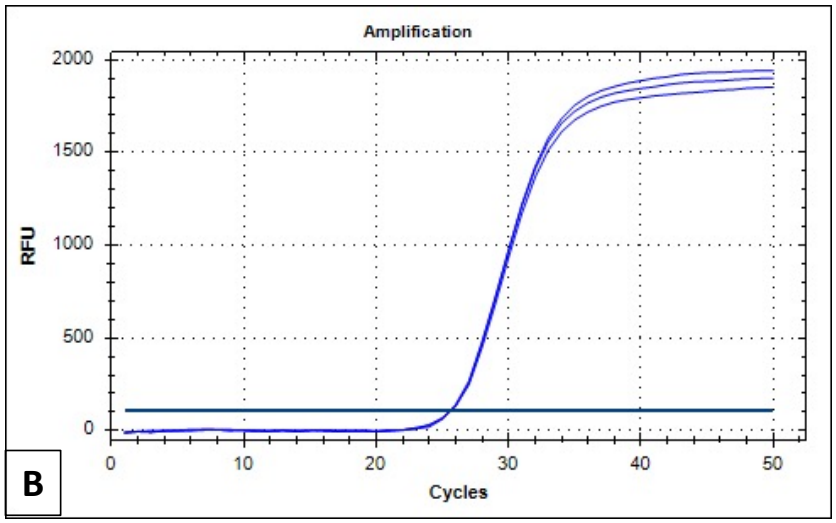
Caspase-1

Figure II. *This figure (**A-C**) shows the amplification plot of real time polymerase chain reaction data.*

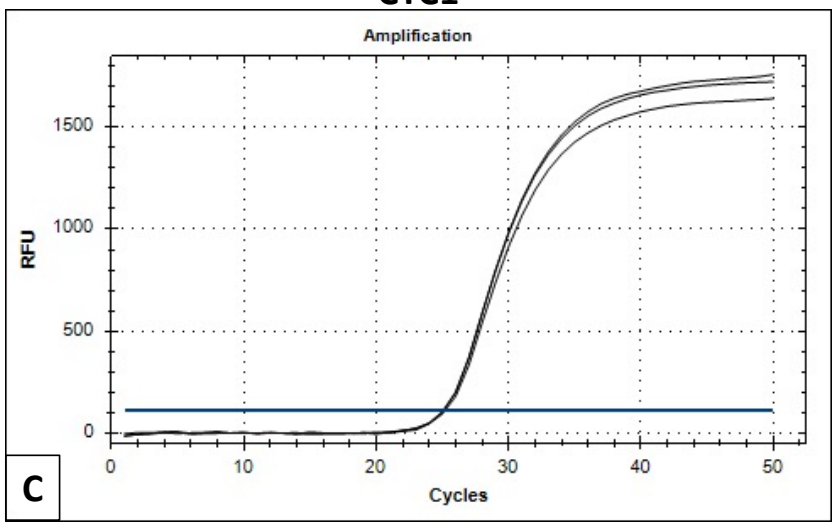
T853 (Preeclamptic patient)



HPRT1



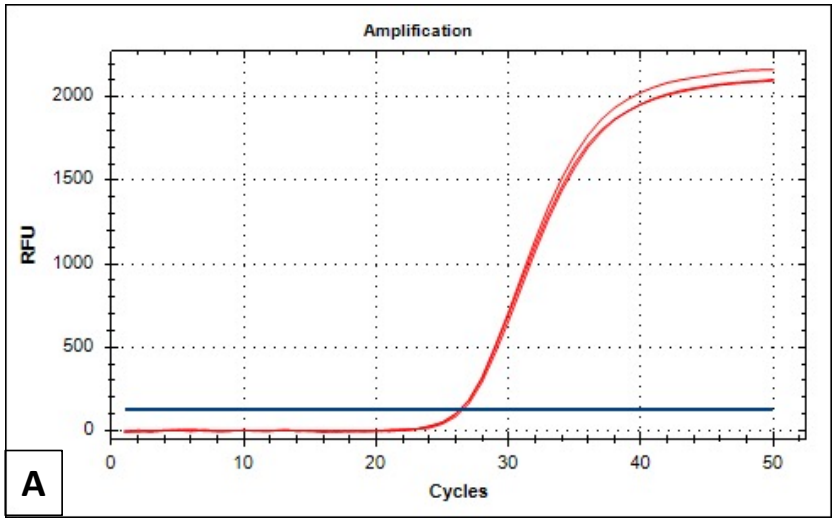
CYC1



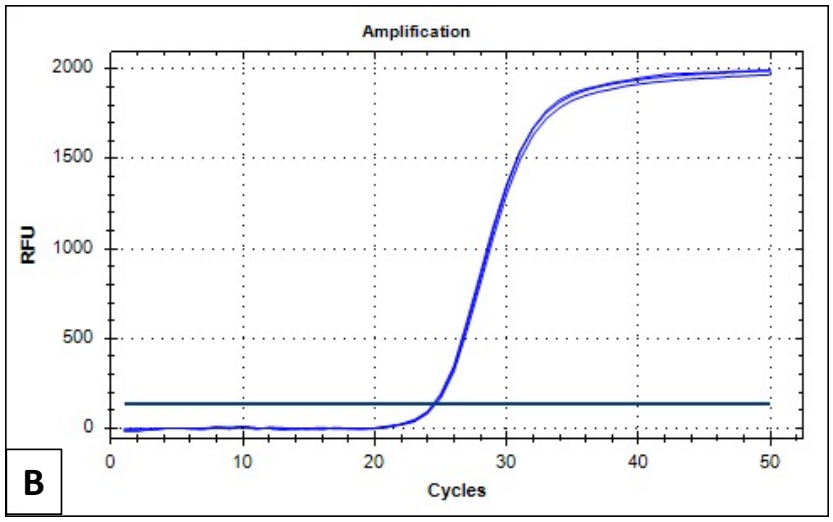
TOP1

Figure III. *This figure (**A-C**) shows the amplification plot of real time polymerase chain reaction data.*

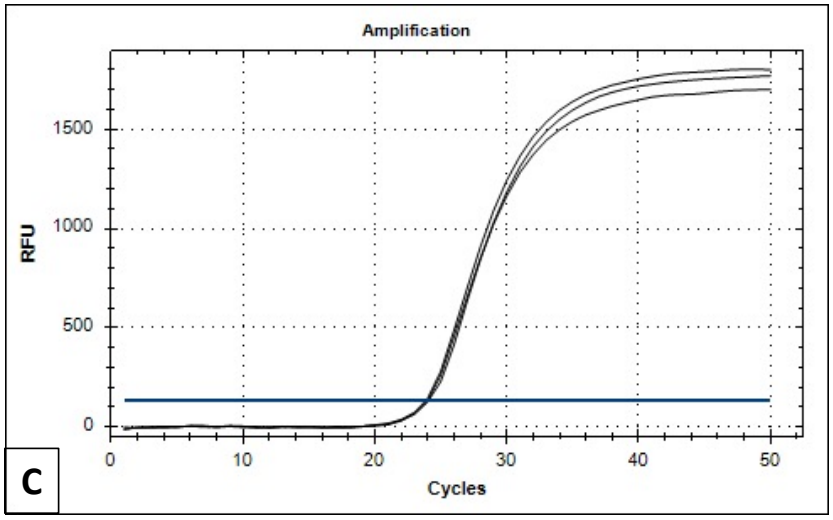
T910 (Healthy patient)



HPRT1



CYC1



TOP1

Figure IV. *This figure (**A-C**) shows the amplification plot of real time polymerase chain reaction data.*

Appendix 9: Immunohistochemistry and immunophenotyping

Surface antigenic profiling of human placenta chorionic plate artery smooth muscle cells originating from a type 1 diabetic patient

The isolated human placenta chorionic plate artery smooth muscle cells originating from a type 1 diabetic patient (T1D23102019) possessed an immunophenotypic profile characteristic of human mesenchymal stem cells as follows: CD73 (75.06% of cells were positive), CD90 (65.58% positive cells), CD105 (51.13% positive cells) and only 0.59% of cells were positive for CD34, CD11b, CD45, CD19 and HLA-DR. The flow cytometry data of CPA-SMC cells are presented in figure V (highlighting the percentage of positive cells) and figure VI (detailing the no antibody control and isotype control).

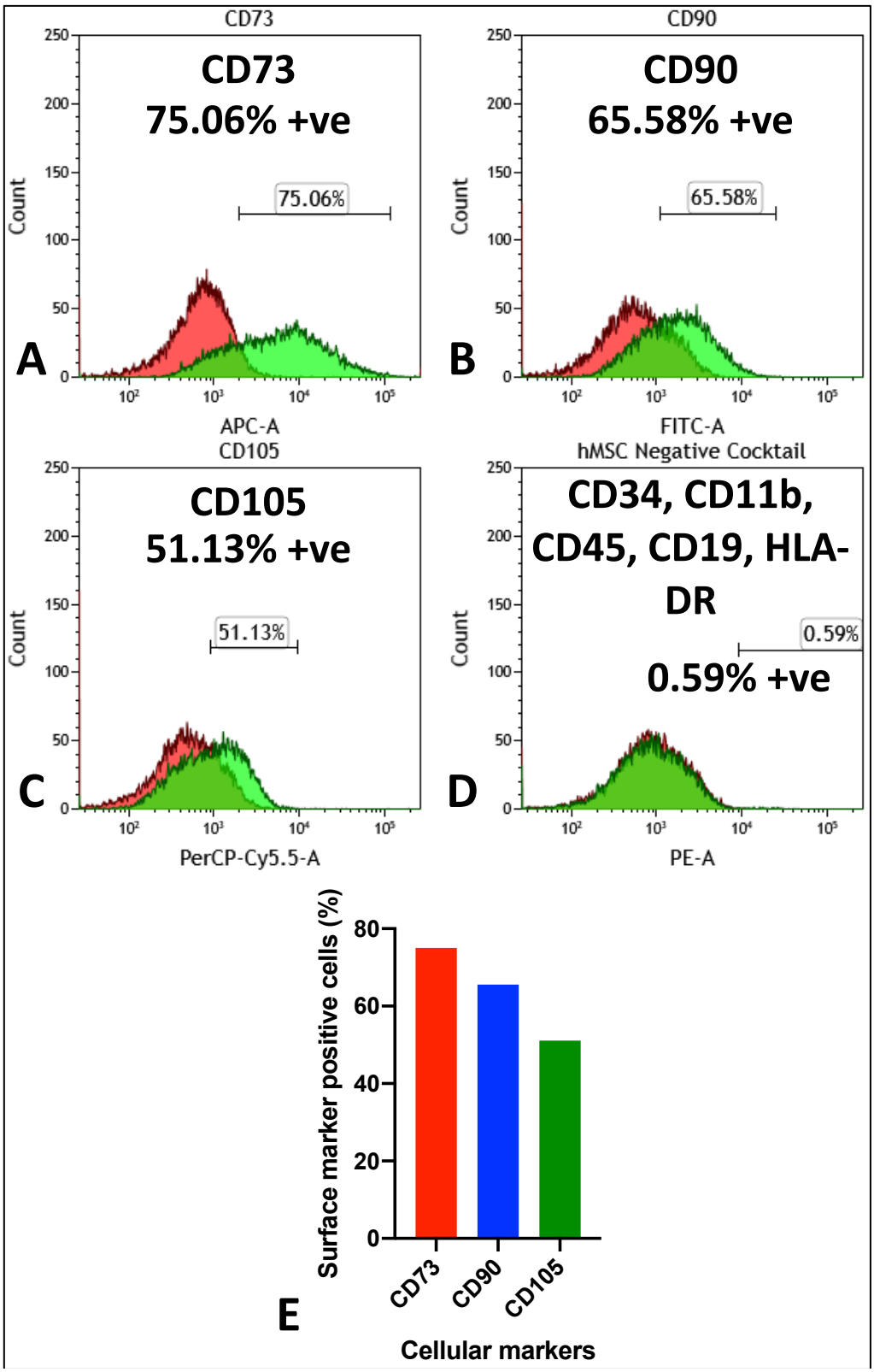


Figure V. *This figure (panels **A-E**) highlights the immunophenotype data of human placenta chorionic plate artery smooth muscle cells originating from a type 1 diabetic patient (T1D23102019). CPA-SMC's were stained with antibodies against surface specific cellular markers as shown by the green histograms or an isotype matched monoclonal antibody as highlighted by the red histograms. Panel **E** highlights the percentage of CPA-SMC cells that were positive for CD73, CD90 and CD105.*

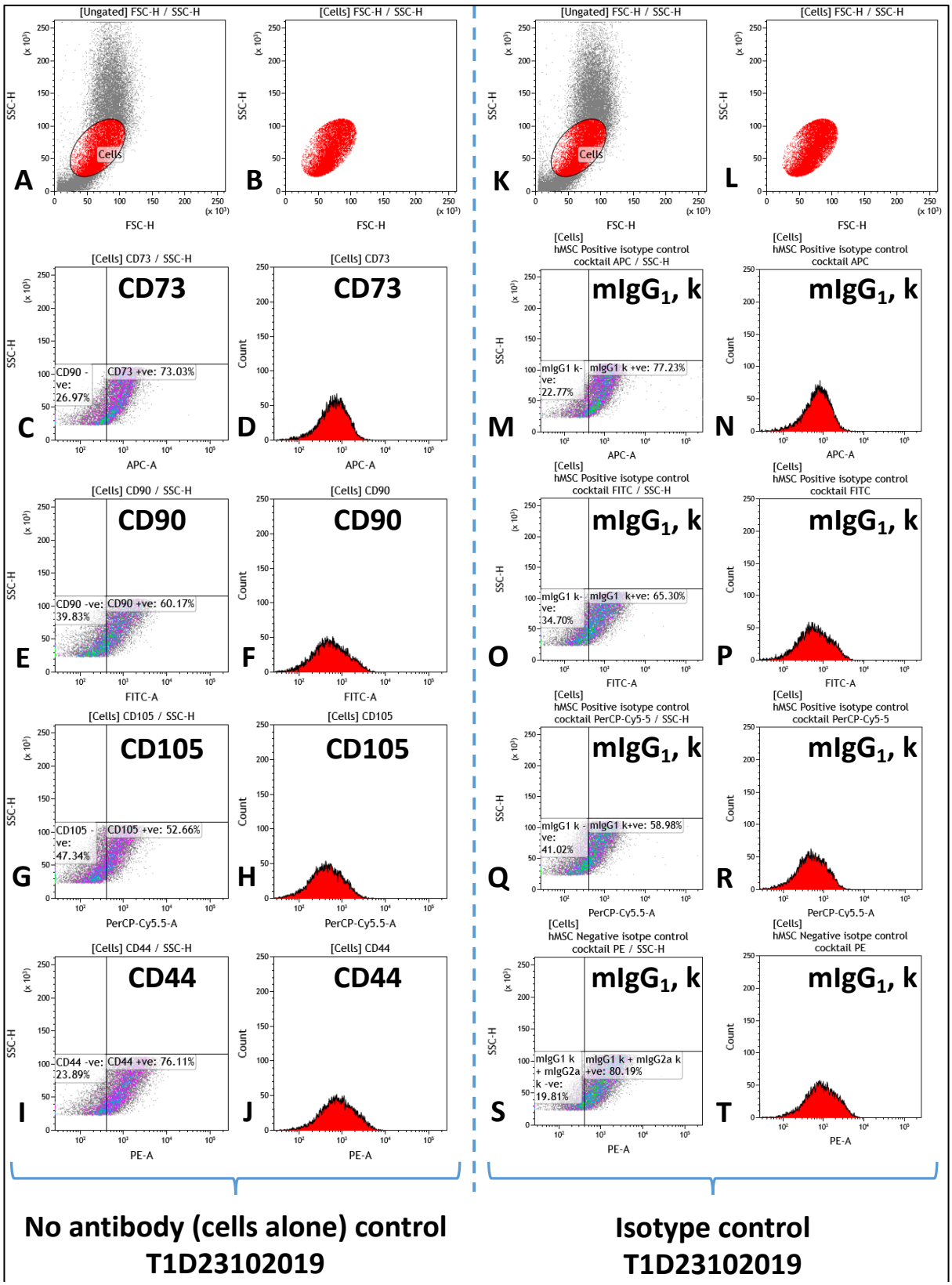


Figure VI. *This figure highlights representative scatter plots and histograms of no primary antibody (cells alone) control (panels **A-J**) and isotype control (panels **K-T**) in the immunophenotyping of CPA-SMC originating from a type 1 diabetic patient (T1D23102019).*

Immunohistochemical expression of the P2X7 receptor in isolated sections of human placental villous tissue highlighted that the syncytiotrophoblast and fetal blood vessels stained positive for the purinergic receptor

Figures VII-X highlight representative fluorescence micrographs of P2X7 (green) and CD31 (red) immunolocalization in human placental villous tissue originating from metformin (GDM05122019-Metformin), diet+metformin (GDM16012020-Diet+Metformin) and insulin+metformin (GDM03022020-Insulin+Metformin) managed gestational diabetic patients as well as from a type 1 diabetic patient (T1D23102019). The P2X7 receptor expression at the level of the syncytiotrophoblast was highlighted with red arrows and the immunolocalization of the ATP receptor on cytotrophoblasts was signposted with yellow arrows. Representative CD31 positive fetal vascular profiles were labelled with a white asterisk. The fetal vascular profiles which were double positive for P2X7+CD31 were labelled with white arrows. Figure XI highlights the percentage of placental vascular profiles that were positive or negative for P2X7, positive for CD31 and double positive for P2X7+CD31 (panel A), as well as the fluorescence intensity levels of P2X7 receptor positive syncytiotrophoblast profiles (panel B).

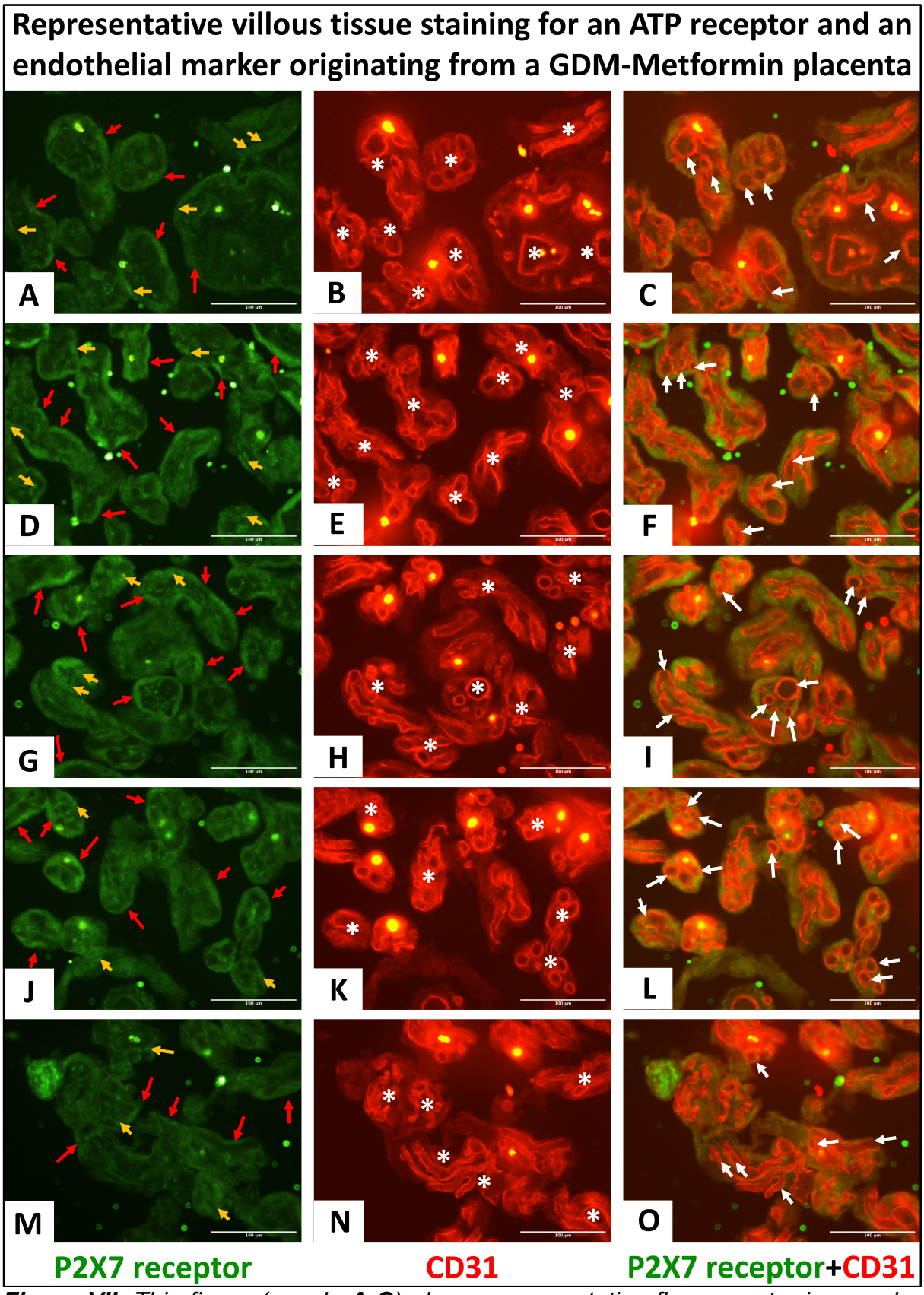


Figure VII. *This figure (panels **A-O**) shows representative fluorescent micrographs highlighting P2X7 (green), CD31 (red) and P2X7+CD31 (merged) immunolocalization in placental villous tissue originating from a placenta sample of a metformin managed gestational diabetic patient (GDM-Metformin 05122019). Scalebar 100µm.*

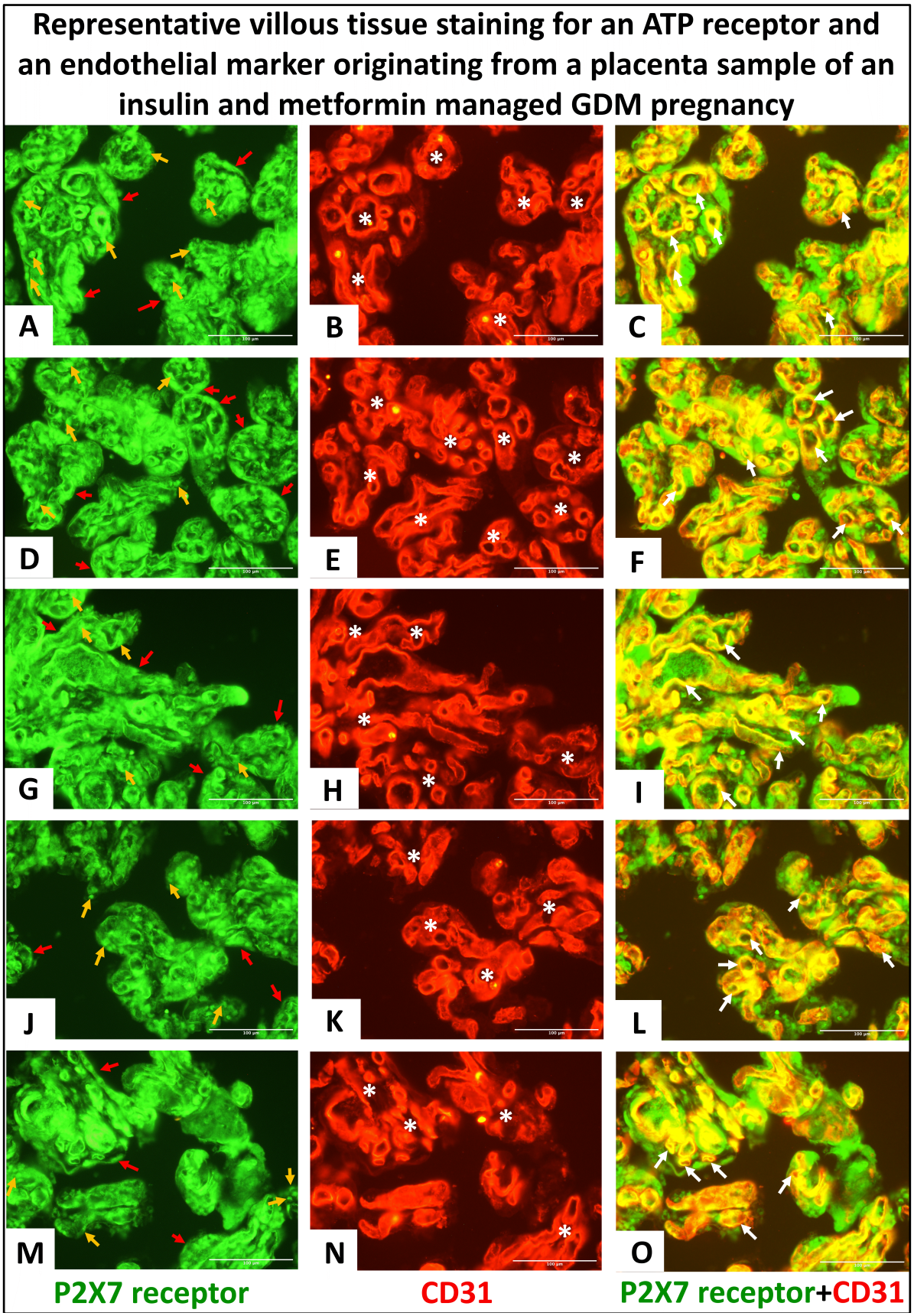


Figure VIII. *This figure (panels **A-O**) shows representative fluorescent micrographs highlighting P2X7 (green), CD31 (red) and P2X7+CD31 (merged) immunolocalization in placental villous tissue originating from an insulin and metformin managed gestational diabetic patient (GDM03022020-Insulin+Metformin). Scalebar 100μm.*

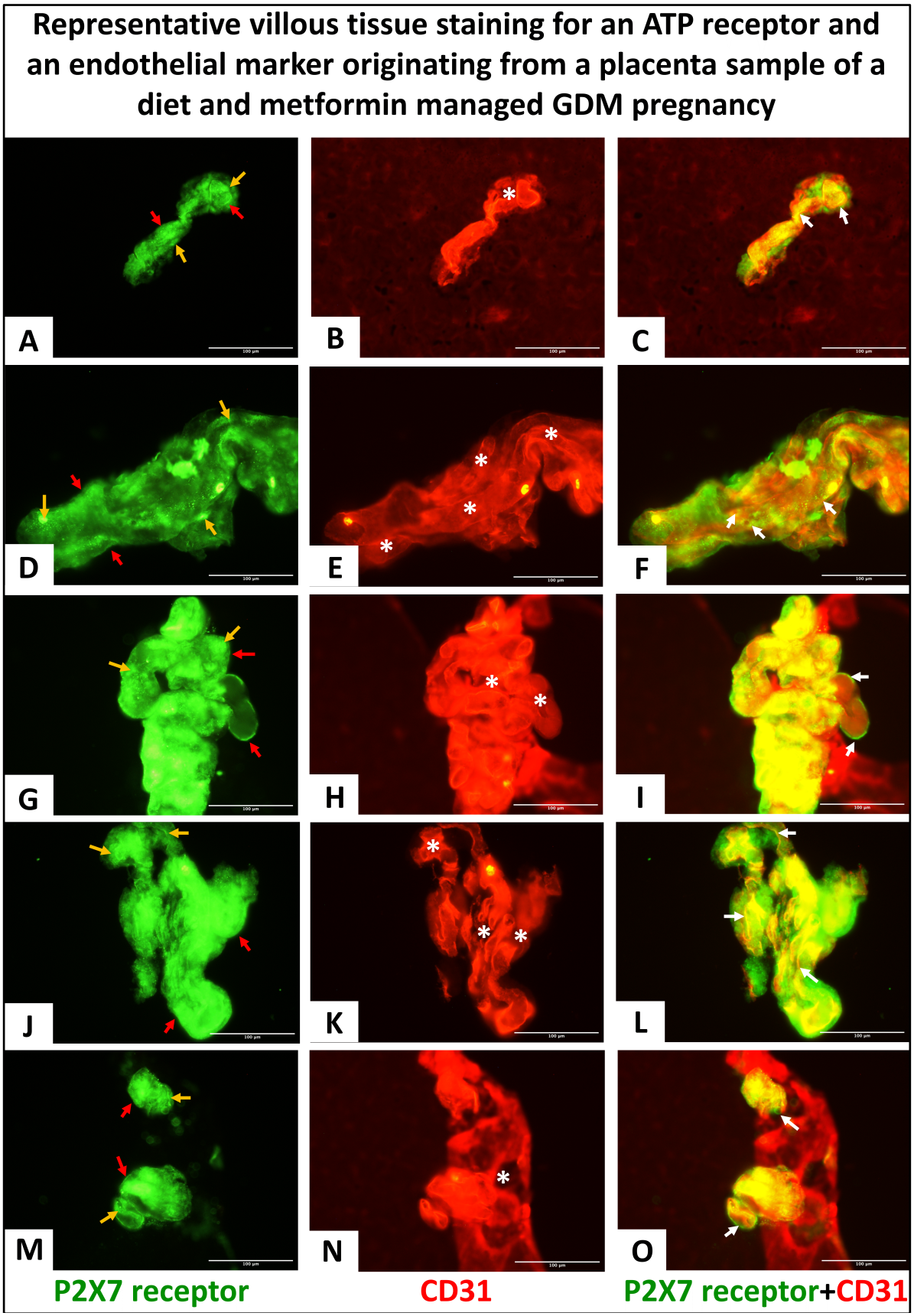


Figure IX. *This figure (panels **A-O**) shows representative fluorescent micrographs highlighting P2X7 (green), CD31 (red) and P2X7+CD31 (merged) immunolocalization in placental villous tissue originating from a diet and metformin managed gestational diabetic patient (GDM16012020-Diet+Metformin). Scalebar 100μm.*

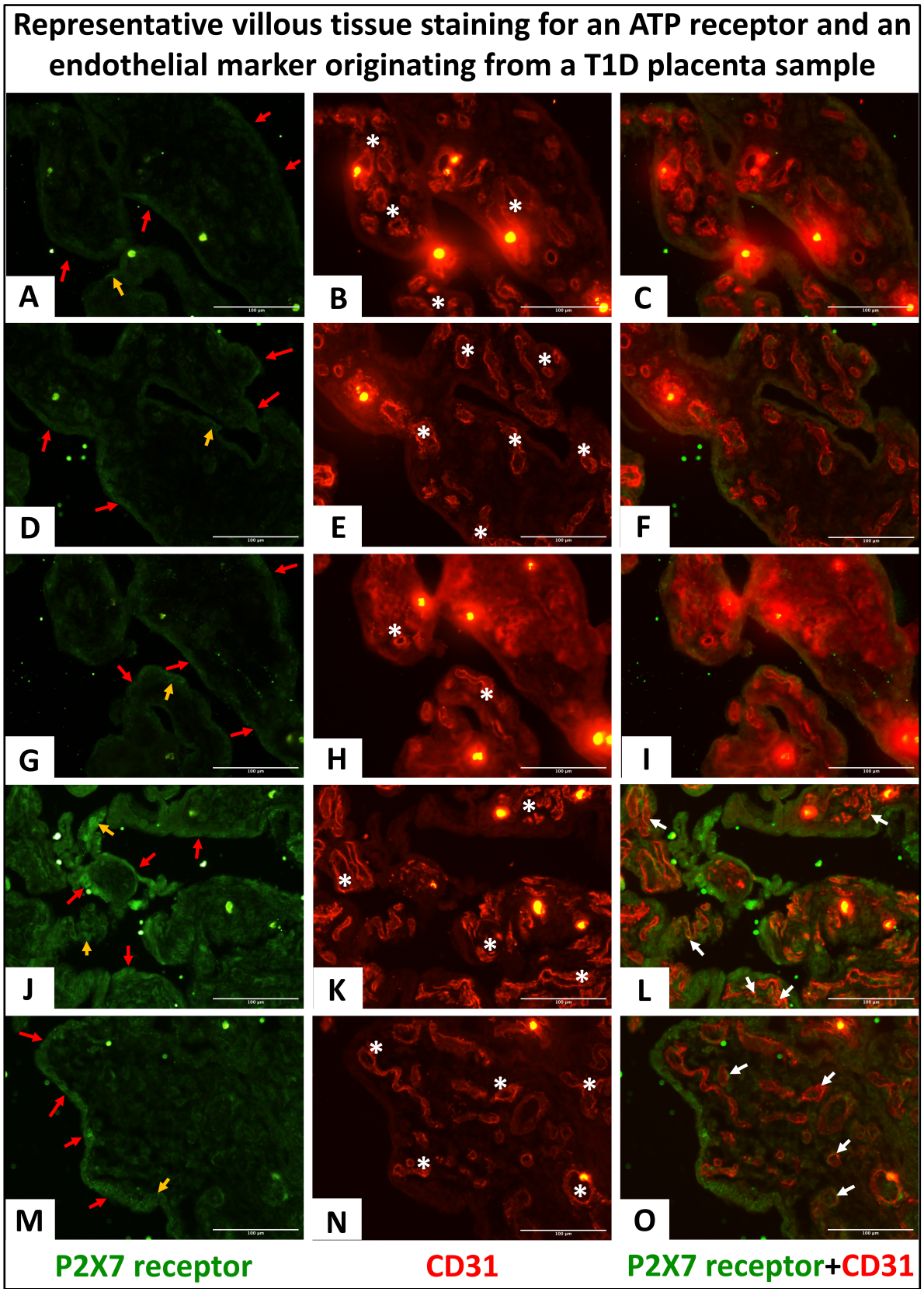


***Figure X**. This figure (panels **A-O**) shows representative fluorescent micrographs highlighting P2X7 (green), CD31 (red) and P2X7+CD31 (merged) immunolocalization in placental villous tissue originating from a type 1 diabetic patient (T1D23102019). Scalebar 100µm.*

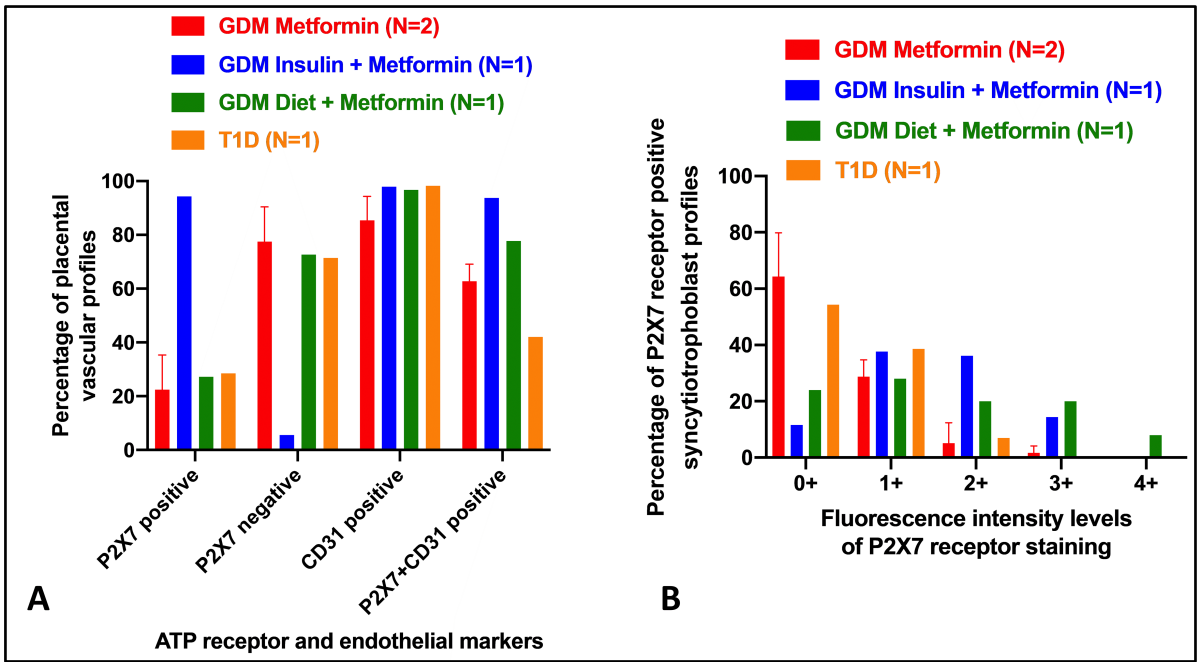


Figure XI A. *This graph shows the percentage of placental vascular profiles that were positive or negative for P2X7, positive for CD31 and double positive for P2X7+CD31* ***B.*** *This graph shows the percentage of P2X7 receptor positive syncytiotrophoblast profiles according to the fluorescence intensity levels of the P2X7 receptor staining in placental villous tissue. The placental villous tissue samples originated from an insulin+metformin (GDM03022020-Insulin+Metformin) and a diet+metformin (GDM16012020-Diet+Metformin) managed gestational diabetic patient as well as a type 1 diabetic patient (T1D23102019).*

Appendix 10: Western blotting

The P2X7 receptor expression in second supernatant of human trophoblast tissue, second and fourth order chorionic plate artery, stem villous artery, choriodecidua, myometrium and peripheral blood mononuclear cells

PBMC cells were used as a positive control for the P2X7 receptor since the primary cells have been demonstrated to express the purinergic receptor at and mRNA and protein level by Zhang *et al* (2017) [770].

P2X7 receptor products were detected in a western blot at a molecular weight of approximately 90kDa in the second supernatant of trophoblast, SVA, fourth and second order CPA tissue lysates originating from a placenta sample of a healthy patient as presented in figure XII. In this case, the trophoblast and fourth order CPA tissue lysates possessed similar relative P2X7 receptor protein expression levels (figure XII, panel D). The ponceau S staining of the nitrocellulose membrane presented in figure XII, panel C demonstrates equal protein loading.

However, a weak signal of detected bands corresponding to the P2X7 receptor was identified in two western blots at approximately 83kDa (figure XIII) and 73kDa (figure XIV) using the second supernatant of SVA, choriodecidua and fourth order CPA tissue lysates originating from three placental samples of healthy patients. Here, the fourth order CPA possessed the highest purinergic receptor protein expression level compared to SVA and choriodecidua (figure XIII, panel D and figure XIV, panel D). A Shapiro-Wilk test of the relative P2X7 receptor levels presented in figure IX highlighted that all data was normally distributed with the exception of fourth order CPA (*P=0.0426). No statistically significant differences of relative P2X7 receptor protein expression levels normalised to β-Actin illustrated in figure XIII were found between all tissue types using a Kruskal-Wallis test (P=0.9929) and Dunn's multiple comparison tests. The relative P2X7 receptor protein expression levels shown in the western blot

presented in figure XIV were subjected to a Shapiro-Wilk test which highlighted that all data was normally distributed. No statistically significant differences of the relative P2X7 receptor protein expression levels (figure XIV) were found across all tissue types using a Brown-Forsythe ANOVA test (P=0.4150) and Dunnett's T3 multiple comparisons test. Furthermore, a strong signal was detected at circa 215kDa, 108kDa, 58kDa and 50kDa (figure XIII) in the P2X7 receptor immunoblot which was due to the non-specific binding of the P2X7 receptor secondary antibody (rabbit anti-goat IgG H&L alkaline phosphatase, Abcam, Ab97097) as suggested from the immunoblot presented in figure XIV, panel E. Similar strong signals were identified in the P2X7 receptor western blot presented in figure XIV at approximately 168kDa, 93kDa, 55kDa and 46kDa. The ponceau S staining presented in figure XIII (panel C) and figure XIV (panel C and F) highlight equal protein loading.

Figure XV (panel A) highlights the relative P2X7 receptor protein expression levels in 10-60µg of total protein loaded per well (second supernatant) of fourth order CPA lysates originating from a placenta sample of a healthy patient. In this case, no protein bands corresponding to the purinergic receptor were detected in the western blot. A strong signal was observed in the P2X7 receptor western blot presented in figure XV (panel A) possessing a molecular weight of approximately 49kDa which was due to the non-specific binding of the P2X7 receptor secondary antibody as indicated from the immunoblot presented in figure XIV, panel E. Furthermore, the densitometric analysis of β-Actin protein levels illustrated in figure XV (panel E) presents the span of the signal intensities which show a linear connection between the quantity of protein present on the nitrocellulose membrane and the signal intensity measured by the detector. The optimal amount of total protein western blot load per well for the purposes of semi-quantifying β-Actin (loading control) levels falling within the linear

detection range was between 20-40µg per well (figure XV, panel E). In this case, the ponceau S staining presented in figure XV showed a successful transfer of the resolved proteins from the 10% polyacrylamide gels to the nitrocellulose membranes.

The P2X7 receptor protein expression in 40-60µg of total protein per well (second supernatant) of PBMC lysate originating from the maternal blood of a healthy patient is presented in figure XVI. In this case, two dilutions of the P2X7 receptor primary antibody were tested (1:500 and 1:200) and no bands were detected in both western blots (figure XVI, panel C and D). The densitometric analyses of β-Actin protein expression levels are also presented in figure XVI panels E and F highlighting the levels of the signal intensity against the amount of total protein loaded (40-60µg).

Figure XVII (panel C) highlights the relative P2X7 receptor protein expression levels in the second supernatant of PBMC, myometrium and choriodecidua tissue lysates. Here, a weak signal was detected at approximately 73kDa and 121kDa which disappeared when the anti-P2X7 receptor primary antibody was preabsorbed with the corresponding blocking peptide as highlighted in figure XVII, panel D. Moreover, a strong signal was observed at approximately 49kDa in the P2X7 receptor western blot (figure XVII, panel C) and also at approximately 51kDa in the P2X7 receptor with blocking peptide western blot (figure XVII, panel D) which was due to the non-specific binding of the P2X7 receptor primary antibody as shown in chapter 3.3.2. The ponceau S staining presented in figure XVII (panel A) shows that the resolved proteins were successfully transferred from the 10% polyacrylamide gel to the nitrocellulose membrane.

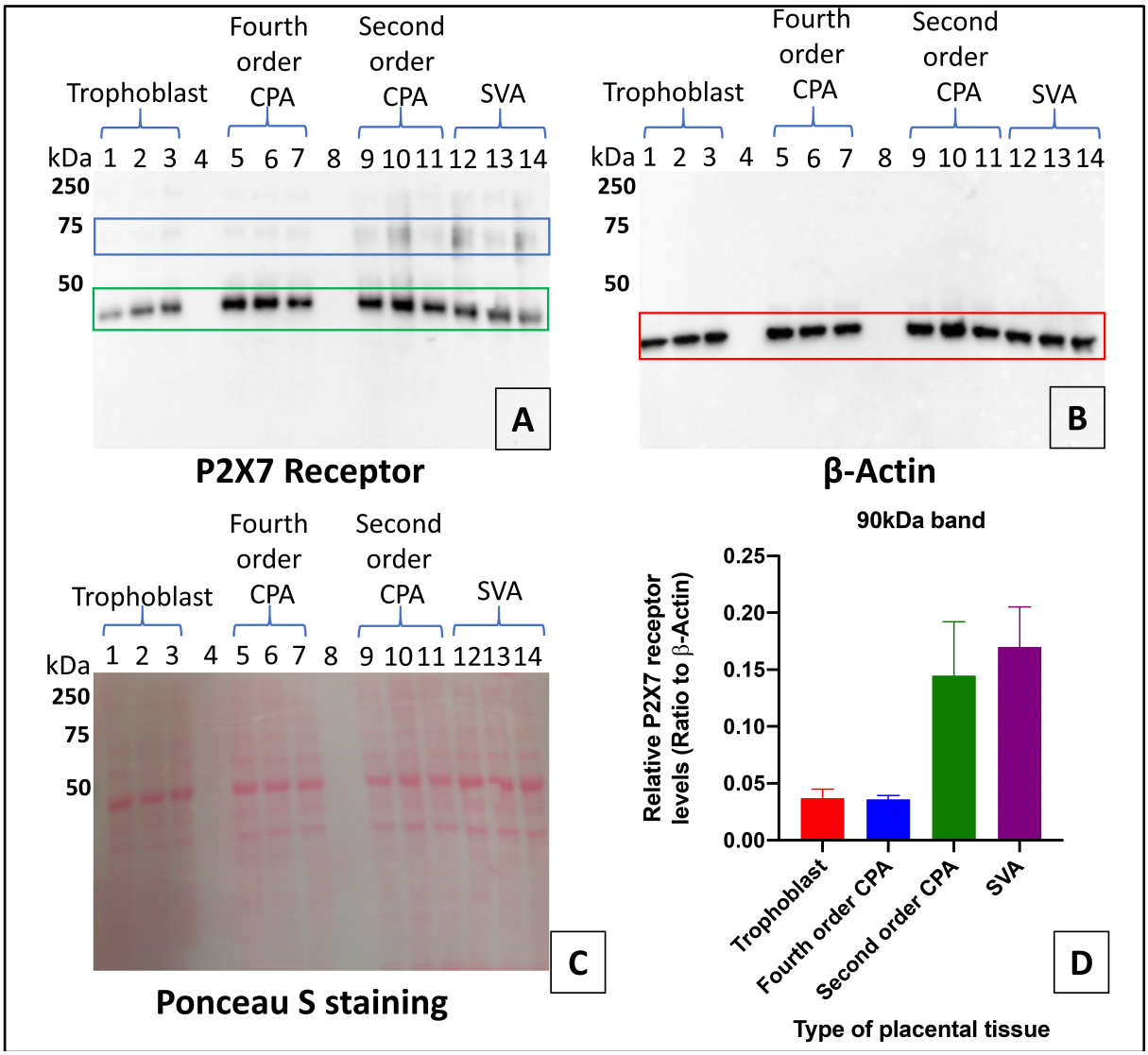


Figure XII. *This figure shows the P2X7 receptor protein expression levels (panel **A**, blue box) in the second supernatant of trophoblast tissue (lanes 1-3), fourth order chorionic plate artery (CPA) (lanes 5-7), second order CPA (lanes 9-11) and stem villous artery (SVA) (lanes 12-14) lysates originating from a placenta sample of a healthy patient (T2807). The protein bands highlighted with the green box denote non-specific binding of the secondary antibody. No tissue lysate was loaded in lanes 4 and 8. **B**. The immunoblot was stripped and then reblotted with β actin for loading control (red box) **C**. Ponceau S staining of the western blot nitrocellulose membrane prior to immunoblotting for the P2X7 receptor **D**. Relative P2X7 receptor protein expression levels in each lane normalised to its individual β actin expression. Data are expressed as mean ± SEM. Each well was loaded with 40μg of total protein. Antibodies used: P2X7 primary antibody (goat polyclonal IgG, Santa Cruz, SC-15200) at a dilution of 1:500, P2X7 secondary antibody (rabbit anti-goat IgG H&L alkaline phosphatase, Abcam, Ab97097) at a dilution of 1:25000, β actin primary antibody (rabbit polyclonal IgG, Abcam, Ab8227) at a dilution of 1:2500 and β actin secondary antibody (Anti-rabbit IgG (whole molecule), F(ab')$_2$, fragment – alkaline phosphatase antibody produced in goat – Sigma, A3937) at a dilution of 1:30000. In this case, the proteins were resolved using a 15 well 10% Mini-Protean TGX precast gel (Bio-Rad, 4561036).*

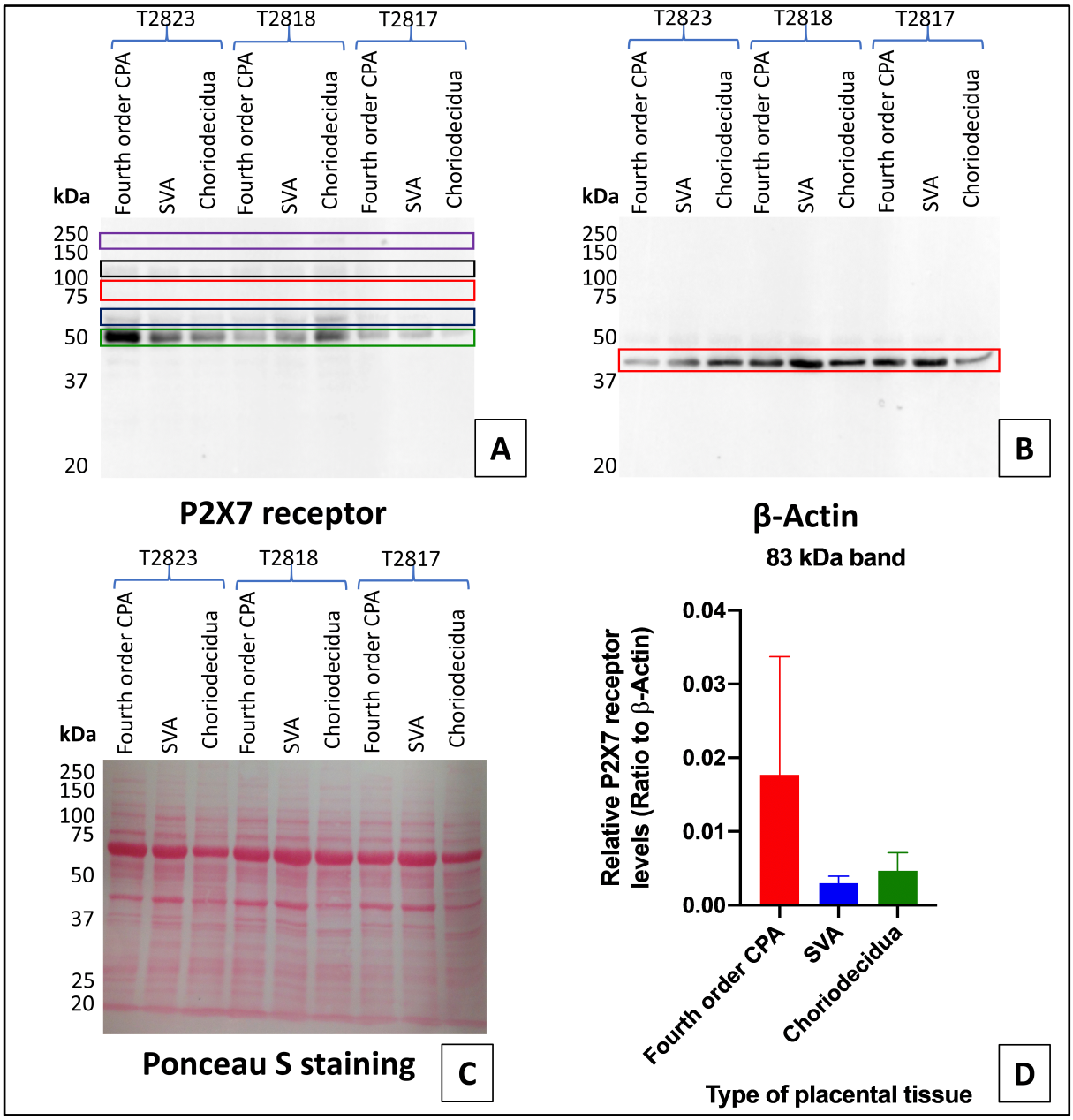


Figure XIII. *This figure shows the P2X7 receptor expression (panel **A**, red box) in second supernatant of fourth order CPA, SVA and choriodecidua lysates originating from three placental samples of healthy patients (T2823, T2818 and T2817). The protein bands highlighted with violet (215kDa), black (108kDa), blue (58kDa) and green (50kDa) boxes denote non-specific binding of the secondary antibody **B**. The immunoblot was stripped and then reblotted with β actin for loading control (red box) **C**. Ponceau S staining of the nitrocellulose membrane prior to the commencement of immunoblotting for the P2X7 receptor **D**. Relative P2X7 receptor levels normalised to β actin. Data are expressed as mean ± SEM. Each well was loaded with 40μg of total protein. Antibodies used: P2X7 primary antibody (goat polyclonal IgG, Santa Cruz SC-15200) at a dilution of 1:500, P2X7 secondary antibody (rabbit anti-goat IgG H&L alkaline phosphatase, Abcam Ab97097) at a dilution of 1:25000, β actin primary antibody (rabbit polyclonal IgG, Abcam Ab8227) at a dilution of 1:2500 and β actin secondary antibody (Anti-rabbit IgG (whole molecule), F(ab')$_2$, fragment – alkaline phosphatase antibody produced in goat – Sigma A3937) at a dilution of 1:30000.*

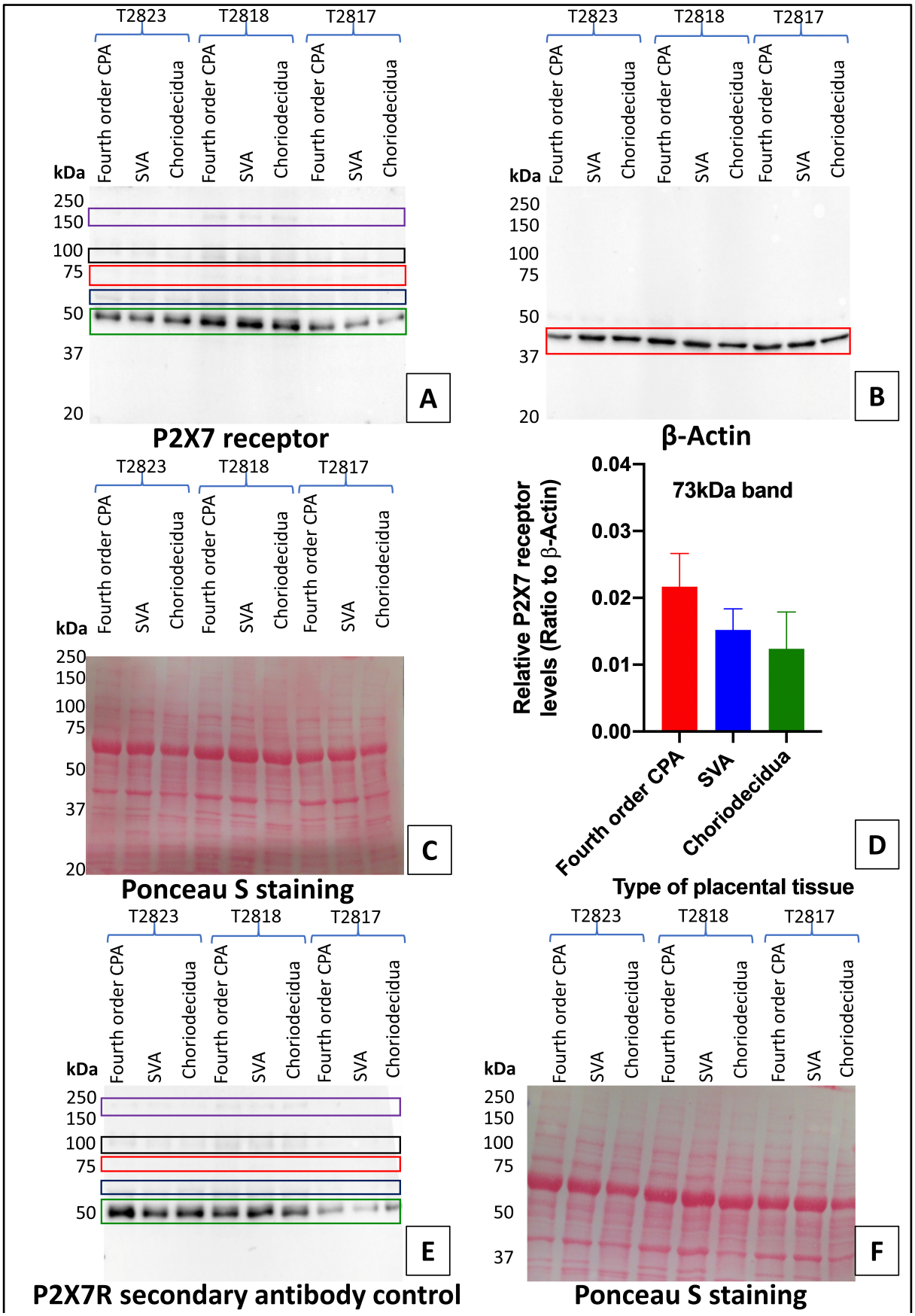


Figure XIV. *This figure shows the P2X7 receptor protein expression levels (panel **A**, red box, approximately 83kDa) from a repeated western blotting experiment using the*

second supernatant of fourth order CPA, SVA and choriodecidua tissue lysates originating from three placental samples of healthy patients (T2823, T2818 and T2817). The protein bands highlighted with violet (approximately 168kDa), black (circa 93kDa), blue (relatively 55kDa) and green (around 46kDa) boxes denote non-specific binding of the secondary antibody ***B****. The immunoblot was stripped and then reblotted with β actin for loading control (red box)* ***C****. Ponceau S staining of the nitrocellulose membrane prior to immunoblotting for the P2X7 receptor* ***D****. Relative P2X7 receptor protein expression levels normalised to β actin. Data are expressed as mean ± SEM* ***E****. Immunoblot highlighting the P2X7 receptor secondary antibody control where the primary antibody corresponding to the purinergic receptor has been replaced with 3% marvel. Red box denotes no protein bands were present at approximately 73kDa. The protein bands highlighted with violet (200kDa), black (98kDa), blue (60kDa) and green (50kDa) boxes denote non-specific binding of the secondary antibody* ***F****. Ponceau S staining of the nitrocellulose membrane corresponding to the P2X7 receptor secondary antibody control. Each well was loaded with 40µg of total protein. Antibodies used: P2X7 primary antibody (goat polyclonal IgG, Santa Cruz, SC-15200) at a dilution of 1:500, P2X7 secondary antibody (rabbit anti-goat IgG H&L alkaline phosphatase, Abcam, Ab97097) at a dilution of 1:25000, β actin primary antibody (rabbit polyclonal IgG, Abcam, Ab8227) at a dilution of 1:2500 and β actin secondary antibody (Anti-rabbit IgG (whole molecule), F(ab')$_2$, fragment – alkaline phosphatase antibody produced in goat – Sigma, A3937) at a dilution of 1:30000.*

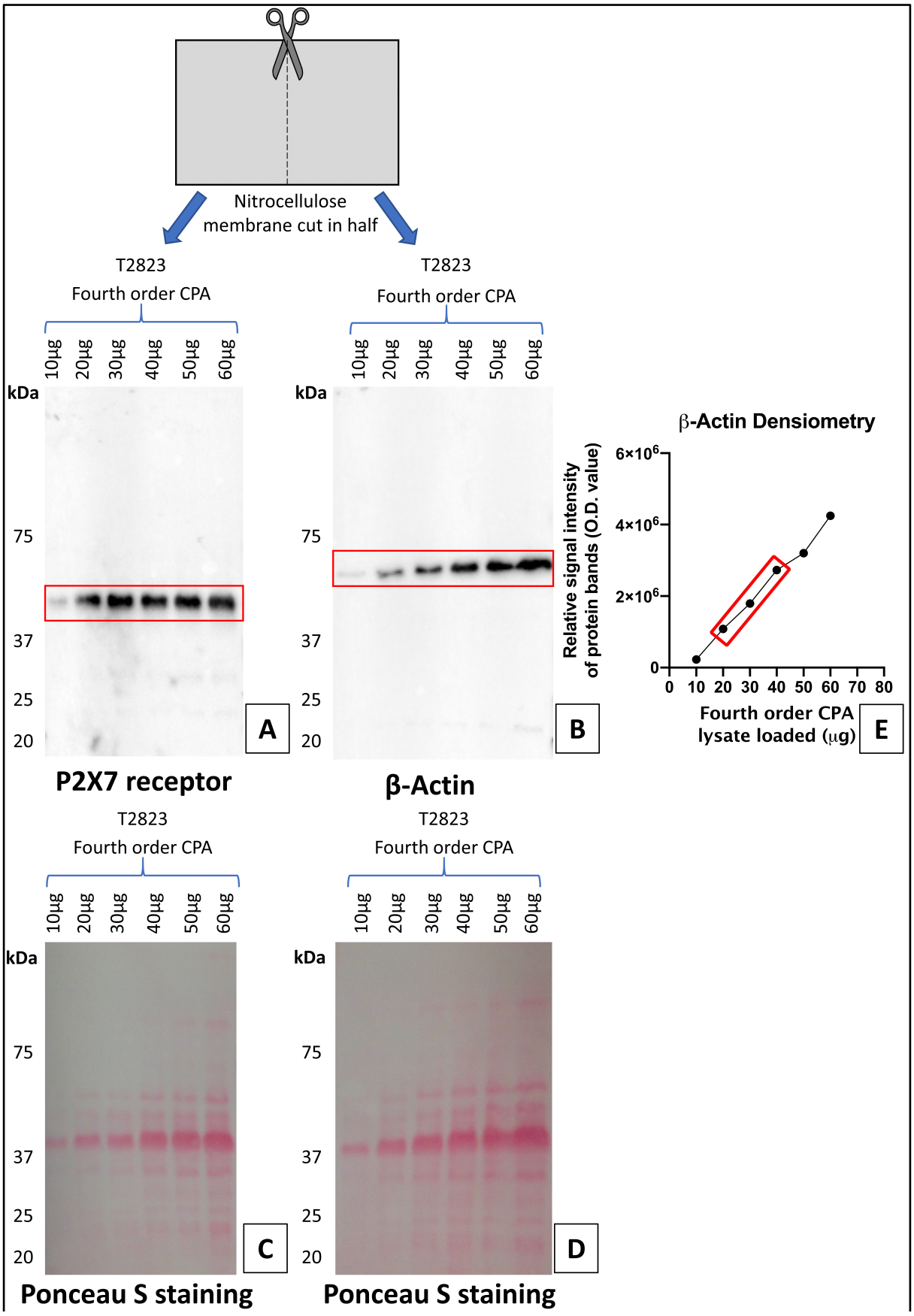


Figure XV. *This figure shows the P2X7 receptor protein expression levels in the second supernatant of fourth order chorionic plate artery lysate originating from a*

placenta sample of a healthy patient (T2823) ***A****. Western blot of chorionic plate artery homogenate with 10-60μg of total protein loaded per well probing for the P2X7 receptor. Red box (approximately 49kDa) denotes non-specific binding of the secondary antibody* ***B****. Adjacent western blot of CPA homogenate with 10-60μg of total protein loaded per well probing for β actin (red box)* ***C****. Ponceau S staining of nitrocellulose membrane prior to immunoblotting for the P2X7 receptor* ***D****. Ponceau S staining of adjacent nitrocellulose membrane prior to immunoblotting for β actin* ***E****. Graph highlighting the relative signal intensity of β actin protein bands using total protein (10-60μg/well) originating from the second supernatant of the CPA lysate. Red box highlights the optimal load (20-40μg total protein/well) for loading control protein detection. Antibodies used: P2X7 primary antibody (goat polyclonal IgG, Santa Cruz, SC-15200) at a dilution of 1:500, P2X7 secondary antibody (rabbit anti-goat IgG H&L alkaline phosphatase, Abcam, Ab97097) at a dilution of 1:25000, β actin primary antibody (rabbit polyclonal IgG, Abcam, Ab8227) at a dilution of 1:2500 and β actin secondary antibody (Anti-rabbit IgG (whole molecule), F(ab')$_2$, fragment – alkaline phosphatase antibody produced in goat – Sigma, A3937) at a dilution of 1:30000. In this case, the resolved proteins were transferred on to the nitrocellulose membrane for a period of 90 minutes.*

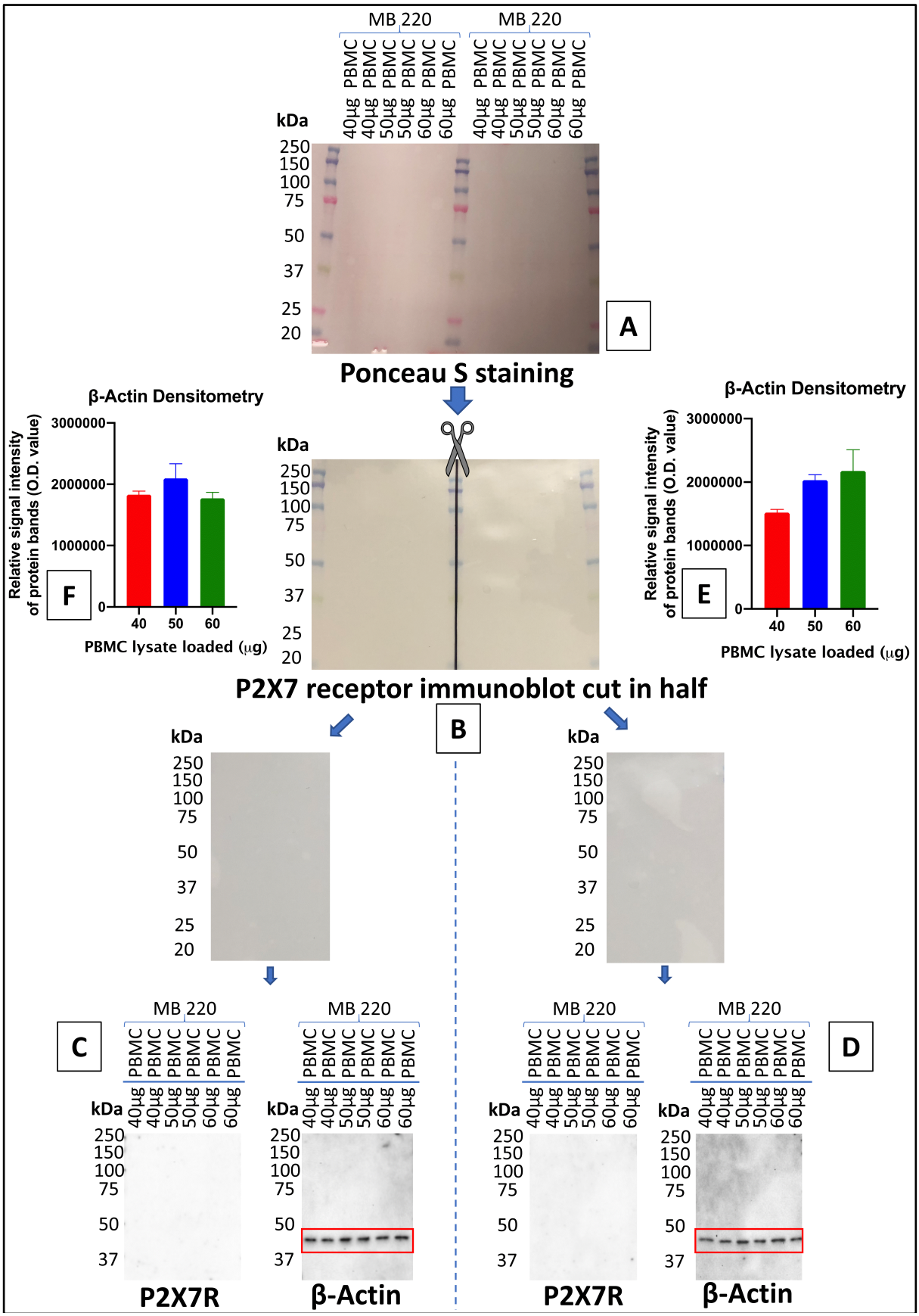


Figure XVI. *This figure shows the P2X7 receptor protein expression levels in the second supernatant of isolated peripheral blood mononuclear cells (PBMC) lysates*

originating from the maternal blood (MB) of a healthy patient (MB220). Both immunoblot segments were then stripped and reblotted with β actin for loading control (red box, panel C and D). Here, the total protein loaded ranged from 40-60μg per well ***A****. Ponceau S staining of western blot nitrocellulose membrane prior to immunoblotting for the P2X7 receptor* ***B****. The immunoblot was then cut into two strips* ***C****. P2X7 receptor protein expression levels in PMBC accompanied by the corresponding β actin levels. The P2X7 receptor primary antibody dilution used in this case was 1:500* ***D****. P2X7 receptor protein expression levels in PMBC with the matched β actin levels. Here, the P2X7 receptor primary antibody dilution used was 1:200* ***E****. Graph highlighting the relative signal intensity of β actin protein bands corresponding to the P2X7 receptor immunoblot presented in panel D* ***F****. Graph showing the relative signal intensity of β actin protein bands related to the P2X7 receptor immunoblot presented in panel C. Data are expressed as mean ± SEM. Antibodies used: P2X7 primary antibody (goat polyclonal IgG, Santa Cruz, SC-15200), P2X7 secondary antibody (rabbit anti-goat IgG H&L alkaline phosphatase, Abcam, Ab97097) at a dilution of 1:25000, β actin primary antibody (rabbit polyclonal IgG, Abcam, Ab8227) at a dilution of 1:2500 and β actin secondary antibody (Polyclonal goat anti rabbit immunoglobulins alkaline phosphatase, Dako, D0487) at a dilution of 1:1000. In this case, the PBMC homogenisation buffer was supplemented with a protease inhibitor buffer sourced from Roche (cOmplete Mini protease inhibitor cocktail, 4693124001). O.D. denotes optical density.*

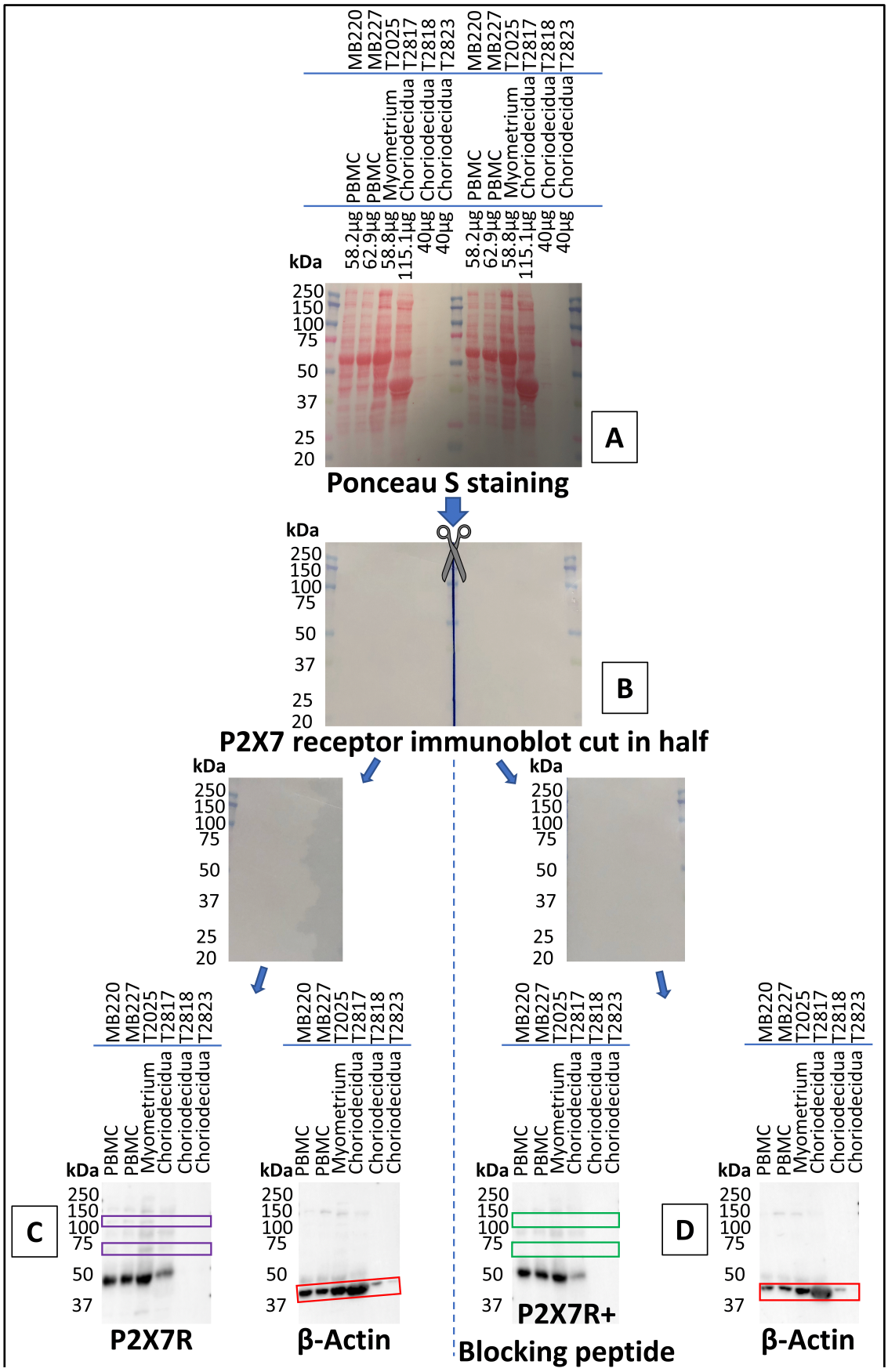


Figure XVII. *This figure highlights the P2X7 receptor protein expression levels (121kDa and 73kDa, violet boxes, panel C) in second supernatant of peripheral blood*

mononuclear cells (PBMC) originating from the maternal blood (MB) of two healthy patients (MB220 and MB227), myometrium (healthy patient T2025) and choriodecidua obtained from the placental samples of three healthy patients (T2817, T2818 and T2823). Myometrium was used as a positive control for the P2X7 receptor. Both immunoblot segments were then stripped and reblotted with β actin for loading control (red box, panel C and D). Here, the gel was loaded with the maximal total protein amount (i.e. neat extracted protein diluted 1:1 with 2X laemmli sample buffer + β-Mercaptoethanol) as presented on panel A, with the exception of choriodecidua samples originating from 2 healthy patients (T2818 and T2823) where 40µg of total protein was loaded ***A****. Ponceau S staining of western blot nitrocellulose membrane prior to immunoblotting for the P2X7 receptor* ***B****. The immunoblot was then cut into two strips* ***C****. P2X7 receptor protein expression levels (violet boxes) accompanied by the corresponding β actin levels (red box). The P2X7 receptor primary antibody dilution used in this case was 1:600* ***D****. Immunoblot highlighting the absence of the corresponding P2X7 receptor band (green boxes). In this case the anti-P2X7 receptor antibody was pre-absorbed with the matching blocking peptide. The corresponding β actin levels are also presented (red box). Antibodies used: P2X7 primary antibody (Rabbit polyclonal IgG, Alomone Labs, APR-004), P2X7 secondary antibody (Polyclonal goat anti rabbit immunoglobulins alkaline phosphatase, Dako, D0487) at a dilution of 1:1000, β actin primary antibody (rabbit polyclonal IgG, Abcam, Ab8227) at a dilution of 1:2500 and β actin secondary antibody (Polyclonal goat anti rabbit immunoglobulins alkaline phosphatase, Dako, D0487) at a dilution of 1:1000.*

Appendix 11: Wire myography

The vasoactive effects of riluzole in isolated CPA's collected from a human placenta sample originating from a preeclamptic patient are presented in the wire myography trace highlighted in figure XVIII. The $K_{2P}2.1$ channel opener gave rise to a diminished vasorelaxation effect taking place particularly at concentrations of 10^{-5} and $3.3*10^{-5}$M compared to time matched control as highlighted by the black arrows in figure XVIII. An initial concentration-response curve of the thromboxane A_2 mimetic U46619 (10^{-10}M to $3.3*10^{-6}$M) was constructed and used to determine the EC_{80} concentration of U46619. Prior to the exogenous application of riluzole, all CPA's were preconstricted with U46619 ($3.3*10^{-7}$M; approximate EC_{80}). In this case, riluzole did not induce a notable vasorelaxation effect compared to time matched controls at the same timepoints.

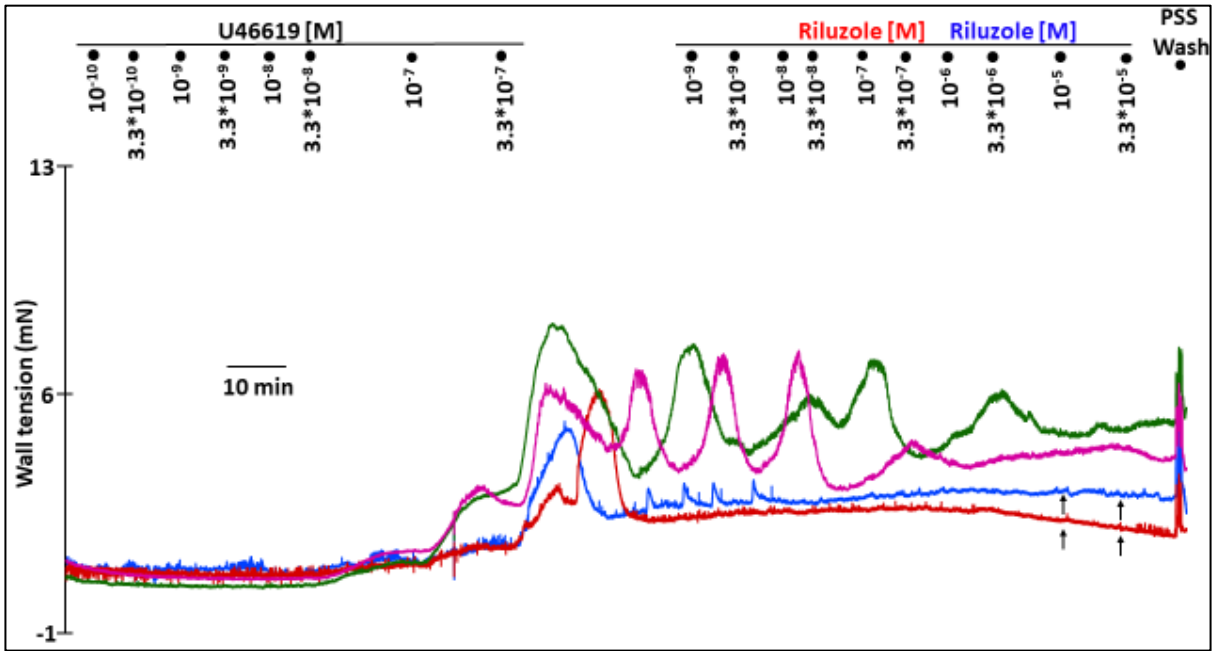


Figure XVIII. *Wire myography trace highlighting the vasoactive effects of riluzole in isolated chorionic plate arteries originating from a placenta sample of a preeclamptic patient (T2718). Following preconstruction with U46619, the green and purple recordings correspond to the time matched control (no drugs added). In this case, all CPA's were preconstricted with a U46619 concentration of $3.3*10^{-7}$M (approximate EC_{80}). Back arrows indicate a notable CPA vasorelaxation effect taking place under the exogenous addition of riluzole, particularly at cumulative concentrations of 10^{-5}M*

*and 3.3*10^{-5}M. Internal diameters of CPA's were as follows: red trace 0.230mm, blue trace 0.277mm, green trace 0.322mm and purple trace 0.297mm. Black dots indicate drug additions to give indicated bath concentrations. Bar indicates the presence of the mentioned compound to the corresponding matching colour force myograph trace (with the exception of black colour which applies to all traces i.e. U46619) or physiological salt solution wash-out.*

Further preliminary wire myography data has also assessed the vasoactive properties of ATP using the same nucleotide cumulative concentrations between second and fourth order isolated CPA's originating from a metformin managed gestational diabetic patient as highlighted in figure XIX. The ATP-induced vasoconstriction effects corresponding to the second nucleotide stimulation (following incubation with A740003) were notably decreased compared to the first ATP stimulation (before CPA exposure to A740003) in the case of the second order CPA as shown in figure XX. A similar decrease in ATP-induced vasoconstriction responses was found in the case of the fourth order CPA, with the second ATP stimulation giving rise to a vasoactive effect taking place below the baseline of the first nucleotide stimulation. The internal diameter of the second order CPA was 0.441mm and the fourth order CPA was 0.251mm.

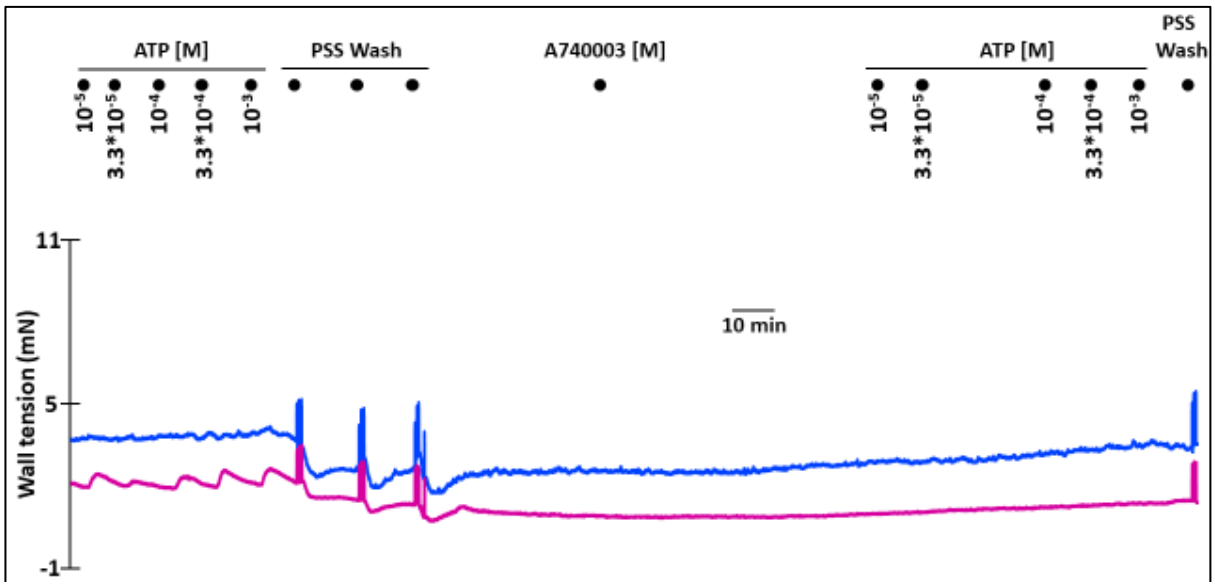


Figure XIX. *Wire myography trace highlighting adenosine 5'-triphosphate-induced vasoconstriction responses in the absence and presence of A740003 using isolated second (blue trace) and fourth (purple trace) order CPA's originating from a metformin managed gestational diabetic patient (T2770). The internal diameter of the second order CPA was 0.441mm (red trace) and fourth order CPA was 0.251mm (violet trace). Black dots indicate drug additions to give indicated bath concentrations. Bar suggests the presence of the mentioned compound or physiological salt solution wash-out.*

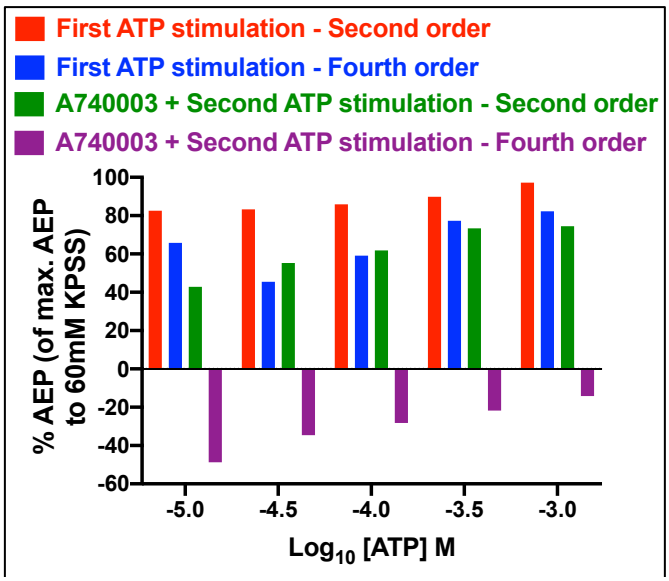


Figure XX*. Log concentration-effect responses elicited by ATP in isolated second and fourth order CPA's originating from a metformin managed gestational diabetic patient (T2770) expressed as percentage active effective pressure (AEP) of maximal AEP to 60mM KPSS.*

Repeated ATP cumulative concentration curves in the presence and absence of A740003 elicited a gradual run-down of vasoactive responses in CPA's isolated from a human placenta sample of an insulin managed gestational diabetic patient

The vasoactive effects of ATP were also assessed in the presence and absence of A740003 using resistance CPA's originating from a placenta sample of an insulin managed gestational diabetic patient as shown in the wire myography trace presented in figure XXI. Adenosine 5'-triphosphate gave rise to a concentration dependent vasoconstriction effect especially between 10^{-5}M to 10^{-3}M in the case of the first ATP stimulation as highlighted in figure XXII, panel A. Following the incubation with the P2X7 receptor antagonist, the second and third ATP stimulation were notably displaced downwards with maximal vasoconstriction evoked not reaching more than 20% of the U46619 standard. The calculated ATP EC_{50} values were as follows: $1.947*10^{-4}$M corresponding to first ATP stimulation, $2.065*10^{-4}$M related to A740003 + second ATP stimulation and $5.239*10^{-5}$M matching the third ATP stimulation as highlighted in figure XXII, panel B. On the other hand, the second (without A740003 incubation) and third (with A740003 incubation) ATP stimulations gave rise to concentration response curves that were particularly flat, with the vasoactive effects taking place under the first ATP stimulation baseline as illustrated in figure XXII, panels C and D. In this case, the calculated ATP EC_{50} value was $2.241*10^{-3}$M corresponding to the second ATP stimulation as presented in figure XXII, panel D. An unpaired two-tailed T-test with Welch's correction highlighted no statistically significant differences in terms of the maximal vasoconstriction elicited between U46619 ($3.3*10^{-7}$M; undertaken at the beginning of the wire myography experiment) and 123mM KPSS (carried out at the end of the functional study) (P=0.8105) as illustrated in figure XXII, panel E.

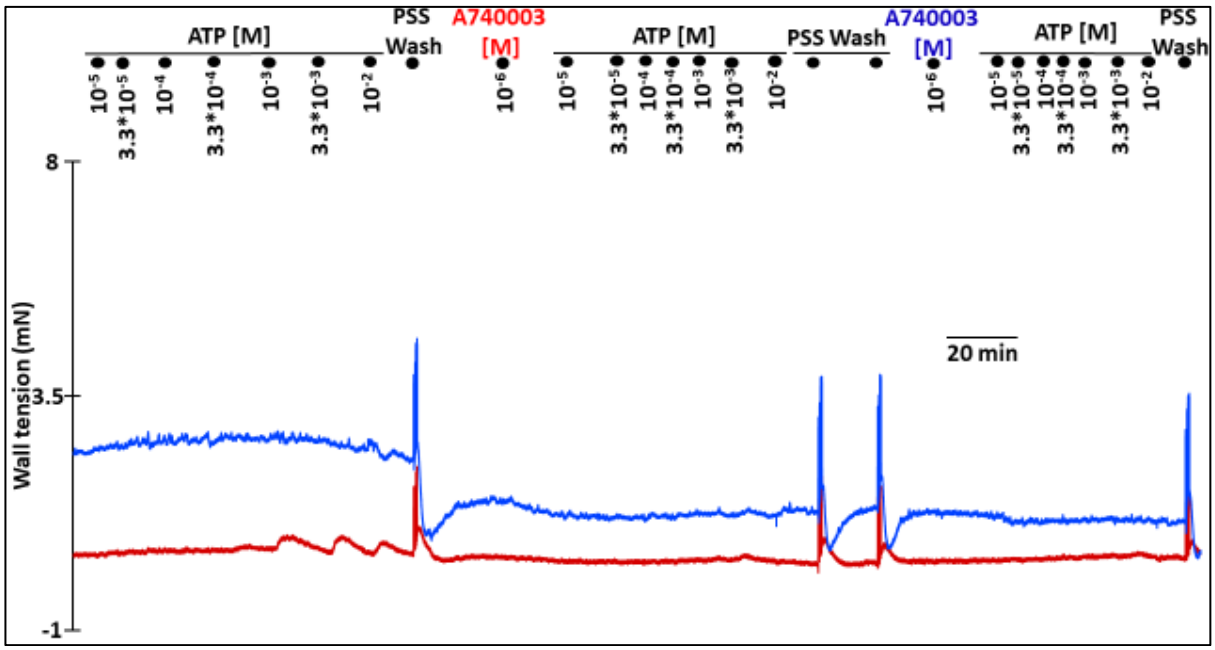


Figure XXI. *Wire myography trace highlighting ATP-induced vasoconstriction responses in the absence and presence of A740003 using isolated resistance CPA's originating from a placenta sample of an insulin managed gestational diabetic patient (T2814). Internal diameter of CPA's was 0.109mm (red trace) and 0.138mm (blue trace). Black dots indicate drug additions to give indicated bath concentrations. Bar suggests the presence of the mentioned compound to the corresponding matching colour force myograph trace (with the exception of black colour which applies to all traces) or physiological salt solution wash-out.*

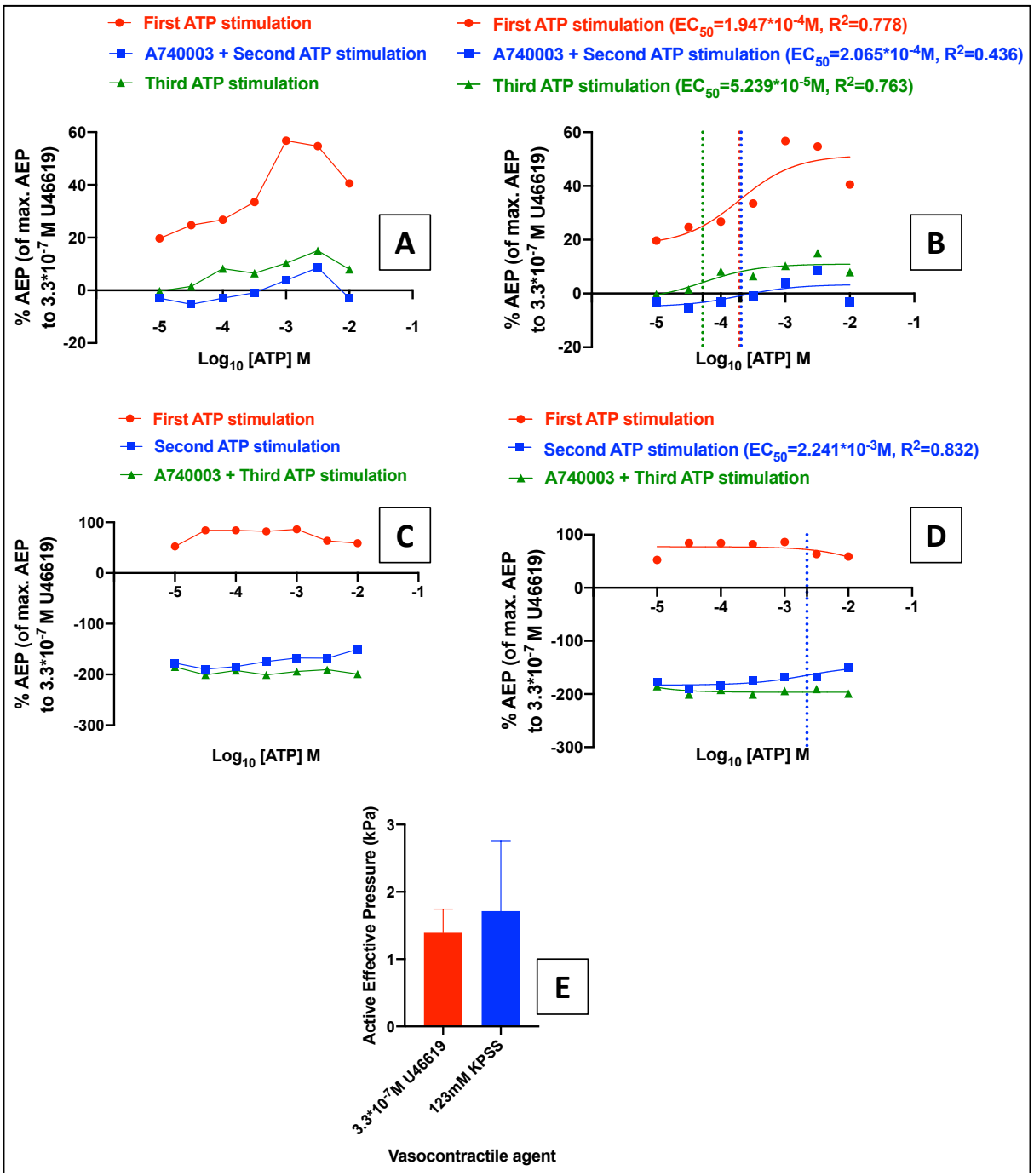


Figure XXII. *Vasoactive effects of ATP before and after the incubation with A740003 initiated by isolated resistance CPA's originating from a placenta sample of an insulin managed gestational diabetic patient (T2814)* ***A****. Log concentration-effect curves elicited by ATP prior and following the incubation with A740003. In this case, the CPA's were incubated with the P2X7 receptor antagonist before the second ATP stimulation* ***B****. Nonlinear regression fit (three parameter logistic equation) of log concentration-effect curve initiated by ATP highlighting the calculated ATP EC_{50} values (first ATP stimulation – illustrated as a red vertical discontinued line, A740003+ second ATP stimulation – presented as a blue vertical discontinued line, third ATP stimulation – shown as a green vertical discontinued line). In this case, the CPA's were incubated with the P2X7 receptor antagonist before the second ATP stimulation* ***C****. Log concentration-effect curves elicited by ATP prior and following the incubation with*

A740003. In this case, the CPA's were incubated with the P2X7 receptor antagonist before the third ATP stimulation ***D****. Nonlinear regression fit (three parameter logistic equation) of log concentration-effect curve initiated by ATP highlighting the calculated ATP* EC_{50} *value (second ATP stimulation – illustrated as a blue vertical discontinued line). Here, the CPA's were incubated with the P2X7 receptor antagonist before the third ATP stimulation.* ***E****. Vasoconstriction effects initiated by the exogenous application of U46619 (*$3.3*10^{-7}$*M) and 123mM KPSS by resistance CPA's expressed as active effective pressure (kPa). *P≤0.05, **P≤0.01, ***P≤0.001, ****P≤0.0001; Data are expressed as mean±SEM.*

The spontaneous maximal vasocontractile responses initiated by chorionic plate arteries under the exogenous ATP exposure in the presence and absence of A740003 were notably attenuated in repeated cumulative concentration curves

The vascular effects of adenosine 5'-triphosphate on isolated resistance CPA's originating from an insulin managed gestational diabetic patient were further tested using three cumulative concentrations of the nucleotide (10^{-3}M, $3.3*10^{-3}$M and 10^{-2}M) in the absence and presence of the P2X7 receptor antagonist A740003 as highlighted by the wire myography traces presented in figure XXIII, panels A and B. The first ATP stimulation gave rise to a progressively reduced vasomotor effect which resulted in a maximal vasoconstriction response that was less than 20% of the U46619 standard at the cumulative concentration of 10^{-2}M as illustrated in figure XXIV, panels A and B. The second and third ATP stimulations of the placental arteries (without the exposure to A740003) gave rise to notably attenuated concentration response curves which were displaced downwards, flat and characterised by vasoconstriction effects below 1% of the U46619 standard denoting a marked loss in the efficacy of the nucleotide as highlighted in figure XXIV, panel A. Furthermore, CPA preparations incubated with A740003 before the second ATP stimulation also gave rise to adenosine 5'-triphosphate-induced contractions that were notably reduced by more than 80% in the case of the second and third ATP stimulations as highlighted by figure XXIV, panel B. In this case, the ATP concentration response curves were also flat with weak or diminished responses to increasing concentrations of the nucleotide. Figure XXIV,

panel C also highlights U46619-induced vasoconstriction effects at the start of the wire myography experiment (first U46619 stimulation) and end of the functional study (second U46619 stimulation) in arteries which have been either incubated or not incubated with A740003. A two-way ANOVA test (****P<0.0001) with Geisser-Greenhouse correction (epsilon 0.7587) and Tukey's multiple comparison tests were undertaken at the same ATP concentrations between all of the cumulative concentration response curves and highlighted multiple statistically significant differences at 10^{-3}M between the first ATP stimulation vs. second ATP stimulation (*P=0.0241) and also between the first ATP stimulation and third ATP stimulation (*P=0.0302) and at 10^{-2}M between second and third ATP stimulation (*P=0.0213) (figure XXIV, panel A). Also, the same test was undertaken again separately between all of the cumulative concentrations of the nucleotide in all ATP concentration response curves which revealed a statistically significant difference between 10^{-3}M and $3.3*10^{-3}$M corresponding to the first ATP stimulation (*P=0.0211). The same test has also revealed a statistically significant difference between 10^{-3}M and 10^{-2}M corresponding to the first ATP stimulation just before the incubation of the CPA's with A740003 (*P=0.420) as highlighted in figure XXIV, panel B.

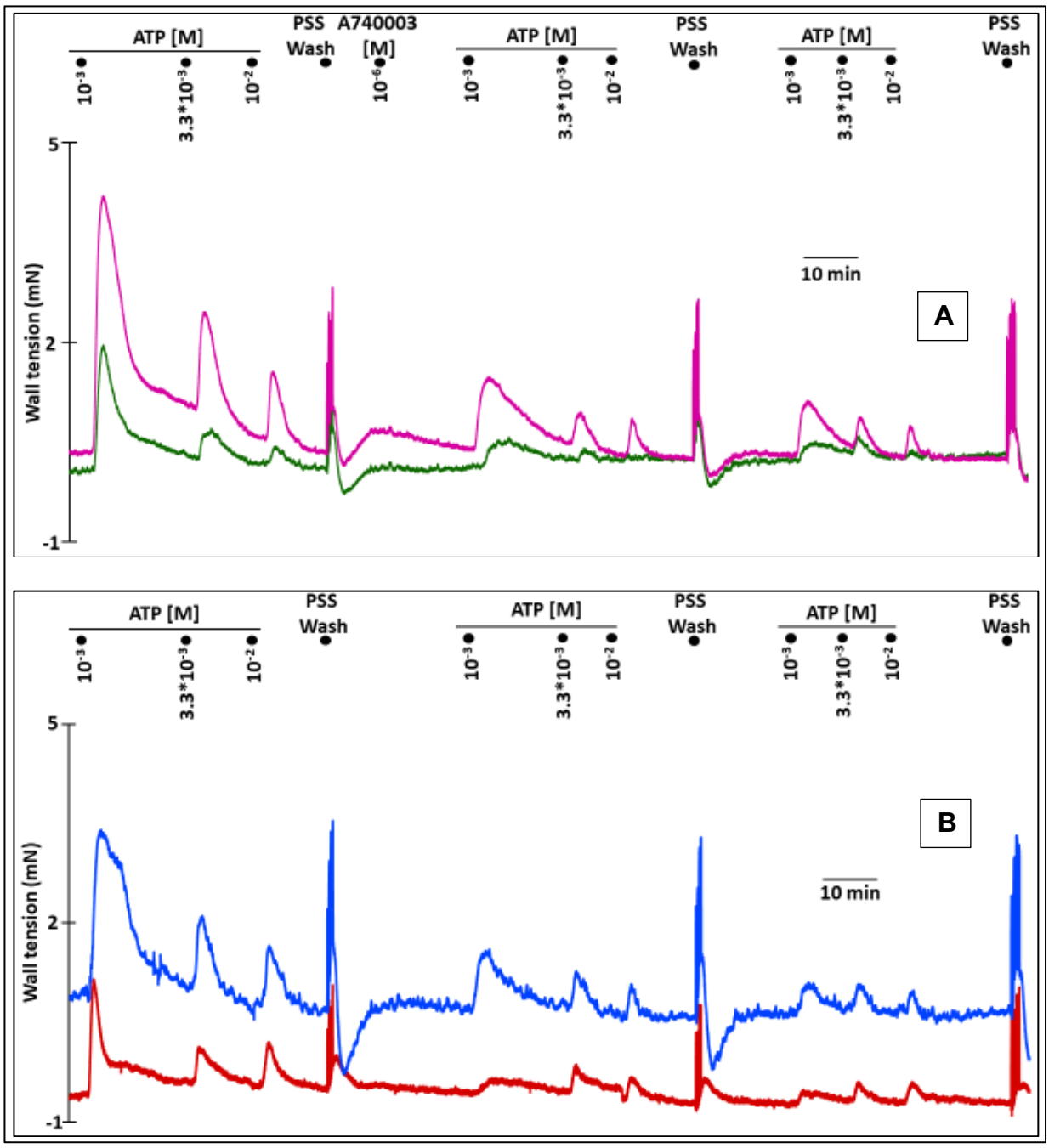


Figure XXIII. *Wire myography traces highlighting ATP-induced vasoconstriction responses in the absence and presence of A740003 using isolated resistance CPA's originating from an insulin managed gestational diabetic patient (T2824)* ***A****. Typical vasoactive effects of ATP generated before and after the incubation with A740003 by isolated chorionic plate artery preparations. Internal diameter of CPA's was 0.159mm (green trace) and 0.170mm (purple trace)* ***B****. Conventional ATP-induced vasoconstriction effects elicited by chorionic plate arteries. Internal diameter CPA's was 0.113mm (red trace) and 0.181mm (blue trace). Black dots indicate drug additions to give indicated bath concentrations. Bar suggests the presence of the mentioned compound or physiological salt solution wash-out.*

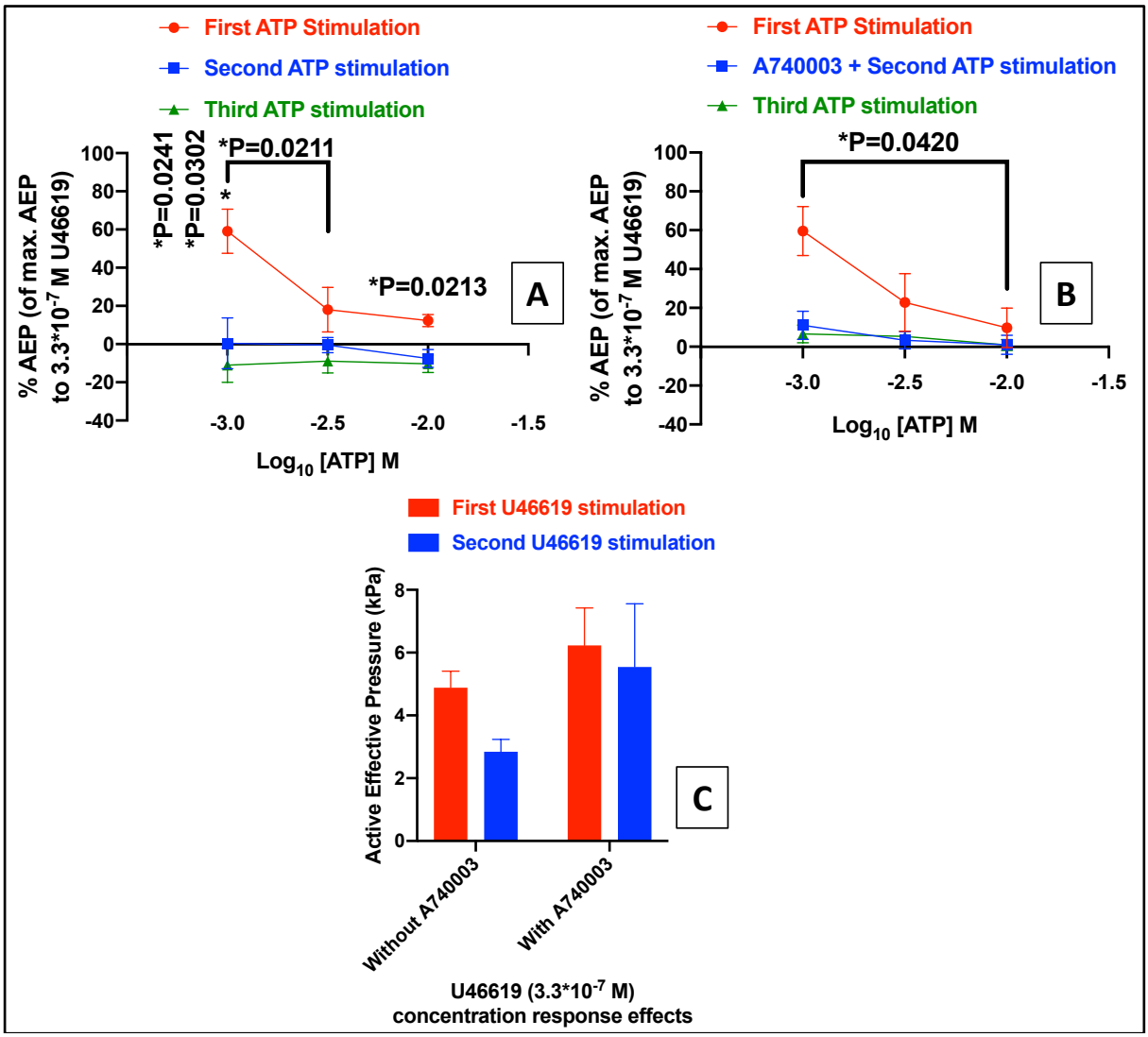


Figure XXIV. *Vasoactive effects of ATP before and after the incubation with A740003 initiated by isolated resistance CPA's originating from a placenta sample of an insulin managed gestational diabetic patient (T2824)* ***A***. *Log concentration-effect curves elicited by ATP* ***B***. *Log concentration-effect curves elicited by ATP prior and following the incubation with A740003. In this case, the CPA's were incubated with the P2X7 receptor antagonist before the second ATP stimulation* ***C***. *Vasoconstriction effects initiated via the exogenous application of U46619 ($3.3*10^{-7}$M) by resistance CPA's (that have been exposed or not exposed to A740003) at the start (first stimulation) and end (second stimulation) of the wire myography experiment expressed as active effective pressure (kPa). *P≤0.05, **P≤0.01, ***P≤0.001, ****P≤0.0001; Data are expressed as mean±SEM.*

Appendix 12: HUVEC and CPA-SMC permeability assay

A permeability study highlighted that the coculture of CPA-SMC with HUVEC does not appear to alter the barrier tightness compared to monoculture of HUVEC cells between 120 and 180 minutes of the tracer leakage assay

Figure XXV highlights the accumulation of albumin-FITC over 180 minutes in the basal compartment of the transwell system by taking into account monoculture of HUVEC and coculture of HUVEC with CPA-SMC on 1% gelatinised membrane inserts.

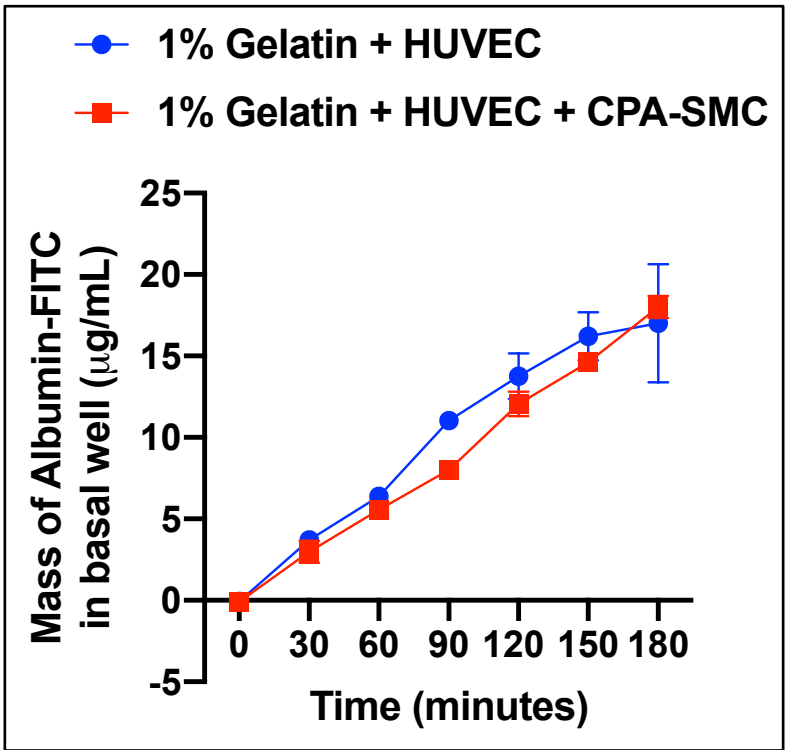


Figure XXV. *This graph highlights the accumulation of albumin-FITC over time in the basal compartment of the transwell system over a period of 3 hours involving monoculture of HUVEC cells or co-culture of HUVEC with CPA-SMC cells on 1% gelatinised 12mm diameter 0.4µm pore size polyethylene terephthalate membrane inserts. In this second permeability assay undertaken, there were three inbuilt experimental repeats for each of the monoculture or co-culture conditions. Data are expressed as mean ± standard deviation.*